ISSN 1122-8628

TERRA ANTARTICA
AN ANTARCTIC EARTH SCIENCE JOURNAL

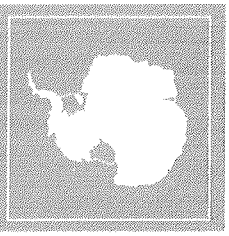

Volume 5, Number 1 - 1998

Initial Report on CRP-1, Cape Roberts Project, Antarctica

GUEST EDITORS

Peter J. Barrett, Chris Fielding, Sherwood W. Wise

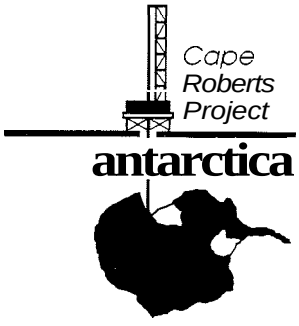

TERRA ANTARTICA
AN ANTARCTIC TERRE SCIENCE JOURNAL

INITIAL REPORT ON CRP-1, CAPE ROBERTS PROJECT, ANTARCTICA

CONTENTS

Page

Foreword - P.J. Barrett & C.A. Ricci V

Cape Roberts Project Personnel VII

Background to CRP-1, Cape Roberts Project, Antarctica

Cape Roberts Science Team

Introduction 1

Regional Setting 3

Drill-Site Observation 6

Sea-Ice Observations

Coring History

Core Properties 11

Fracture Arrays

Physical Properties

Estimated Depth to Base of V3

Stratigraphic Summary 19

Correlation of Seismic Reflectors with CRP-1 20

Techniques 22

Palynology Processing

Palaeomagnetic Laboratory

Core Management and Sampling

Quaternary Strata in CRP-1, Cape Roberts Project, Antarctica

Cape Roberts Science Team

Lithostratigraphy 31

Introduction

Facies Analysis

Description of Sequence

Sequence Stratigraphic Interpretation

Sedimentology 34

Introduction

X-Radiography and Sedimentological Features

Clast Variability

Clast Shape

Description and Interpretation of the Carbonate-Rich Unit

Petrology 42

Introduction

Basement Clasts

Clay Mineralogy

Sand Grains and Provenance

Palaeontology 49

Introduction

Diatoms

Foraminifera

Macrofossils

Calcareous Nannofossils

Palynology

Miocene Strata in CRP-1, Cape Roberts Project, Antarctica

Cape Roberts Science Team

Lithostratigraphy 63
Introduction
Facies Analysis
Description of Sequence
Sequence Stratigraphic Interpretation
Sedimentology 73
Introduction
X-Radiography and Sedimentological Features
Clast Variability
Clast Fabric
Clast Shape
Petrology 79
Introduction
Basement Clasts
Clay Mineralogy
X-Ray Mineralogy
Organic Geochemistry and Diagenesis
Sand Grains and Provenance
Palaeontology 93
Introduction
Diatoms
Foraminifera
Macrofossils
Calcareous Nannofossils
Palynology
Palaeomagnetism and Mineral Magnetic Properties 113

Summary of Results from CRP-1, Cape Roberts Project, Antarctica

Cape Roberts Science Team

Introduction 125
Drilling History 126
Lithostratigraphy 127
Petrology 127
Palaeontology 128
Age Model and Correlation to the Magnetic Polarity Time Scale (MPTS) 130
Seismic Correlations to the Victoria Land Basin, and Core Physical Properties 132
Palaeoenvironmental Interpretation 132
Quaternary Environments and Depositional Hystory 134
Miocene Environments and Depositional Hystory 135
Conclusions 136
Future Plans 137

Appendix 1
Core Recovery Log 139

Appendix 2
1:20 Core Logs 141

Appendix 3
Core Box Images 177

Foreword

This volume is the first of several special issues of *Terra Antartica* to present the results of the Cape Roberts Project, in which the Antarctic programmes of Australia, Germany, Italy, New Zealand, UK and USA are collaborating to take a series of cores off the Antarctic coast from a drilling rig set on the fast sea-ice to investigate climatic and tectonic history of the region (Barrett & Davey, 1992; International Steeling Committee, 1994). Although this first season of drilling was curtailed at a depth of 148 mbsf (metres below sea floor) by an unusual storm-generated ice break-out, the core recovered represents a significant advance for geological understanding in the region, both with new facies and with early Neogene ages from the presumed Paleogene sequence. Down hole conditions were also more difficult than expected and improvements arc being sought for the drilling system to deal with these. But not the least of the challenges was for the Cape Roberts Science Team of 50 scientific technical and support staff, meeting in early October for the first time, to process, describe, sample and analyse the core and complete their first report by mid November and within 3 weeks of completion of the drill hole. We thank all of those who took part in the project for their commitment to its success and for achieving this season as much as the Antarctic would allow. We look forward in late 1998 to the next Cape Roberts special issue, the Scientific Report, with a more detailed analysis of the results of the 1997 drilling, and to the next drilling season.

We are grateful for the support of the national Antarctic programmes of Australia, Great Britain, Germany, Italy, New Zealand and the United States for making this project possible, and in accommodating the delays brought about by ice conditions in the Antarctic. We thank Gillian Wratt and Antarctica New Zealand for coordinating the logistics of the project and Jim Cowie as Project Manager for maintaining a difficult operation on a sound and secure footing despite the challenges of the Antarctic environment. We also thank Scott Borg and the US National Science Foundation for making available the Crary Science & Engineering Center at McMurdo Station so that the scientific studies reported here could be carried out immediately after the drilling. Finally we gratefully acknowledge the editorial role taken by Chris Fielding and Woody Wise in helping complete this volume.

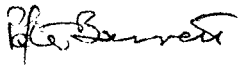

Peter J. Barrett

Carlo Alberto Ricci

November 1997

REFERENCES

Barrett P.J. & Davey F.J., 1992. Cape Roberts Project Workshop Report. *Royal Society of New Zealand, Miscellaneous Series*, **23**, 38 **p.**

International Steering Committee, 1994. Cape Roberts Project - coring for Antarctic tectonic and climatic history. *EOS*, **75**(1), 2-3.

Cape Roberts Project Personnel

INTERNATIONAL STEERING COMMITTEE

Professor Maria Bianca Cita
Dipartimento di Scienze della Terra
Università degli Studi di Milano
Via L. Mangiagalli 34, I 20133 Milano
ITALY
e-mail: cita@imiucca.csi.unimi.it

Dr Fred Davey
Institute of Geological & Nuclear Sciences Ltd
P O Box 1320
Kelburn, Wellington
NEW ZEALAND
e-mail: f.davey@gns.cri.nz

Dr Franz Tessensohn
Bundesanstalt fur Geowissenschaften und Rohstoffe
Stilleweg 2, D-3000 Hannover 51
GERMANY
e-mail: Franz.Tessensohn@bgr.de

Dr Mike Thomson
British Antarctic Survey
High Cross, Madingley Road, Cambridge CB3 0ET
UNITED KINGDOM
e-mail: m.thomson@bas.ac.uk

Professor Peter N. Webb
Department of Geological Sciences
Ohio State University
Columbus Ohio 43210
UNITED STATES OF AMERICA
e-mail: pnwebb@magnus.acs.ohio-state.edu

Dr Ken Woolfe
Department of Geology
James Cook University
Townesville Q4811
AUSTRALIA
e-mail: ken.woolfe@jcu.edu.au

OPERATIONS/LOGISTICS MANAGEMENT GROUP

Ms Gillian Wratt (Convener)
Antarctica NZ
Private Bag 4745
Christchurch
NEW ZEALAND

Mr Erick Chiang
Office of Polar Programs
National Science Foundation
4201 Wilson Boulevard
Arlington, Virginia 22230
UNITED STATES OF AMERICA

Mr Jack Sayers
Antarctic Division
Channel Highway
Kingston, Tasmania
AUSTRALIA

Dr Dougal Goodman
British Antarctic Survey
High Cross Madingley Road
Cambridge CB3 OET
UNITED KINGDOM

Sr Mario Zucchelli
ENEA
Via Anguillarese, 3301 - Roma
0010 Roma AD
ITALY

Dr Max Tilzer
Alfred-Wegener-Institut
Postfach 12 01 81
27516 Bremerhaven
GERMANY

SCIENCE PARTICIPANTS

Professor Peter J. Barrett
Chief Scientist
School of Earth Sciences
Victoria University of Wellington
P O Box 600, Wellington
NEW ZEALAND
e-mail: Peter.Barrett@vuw.ac.nz

Professor Peter N. Webb
Crary Lab Science Leader
Byrd Polar Research Centre
Ohio State University
Columbus Ohio 43210
UNITED STATES OF AMERICA
e-mail: pnwebb@magnus.acs.ohio-state.edu

Ms Jo Anderson
Core Processing Technician
School of Earth Sciences
Victoria University of Wellington
P O Box 600, Wellington
NEW ZEALAND
c-mail: jo.anderson@vuw.ac.nz

Dr Pietro Armienti
Petrologist
Dipartimento di Scienze della Terra
Universitii degli Studi di Pisa
via Santa Maria 53,56126 Pisa
ITALY
e-mail: armienti@dst.unipi.it

Mr Cliff Atkins
Core Processing Technician/Sedimentologist
School of Earth Sciences
Victoria University of Wellington
P O Box 600, Wellington
NEW ZEALAND
e-mail: cliff.atkins@vuw.ac..nz

Mr Steven Bohaty
Micropalaeontology Technician
Department of Geosciences
University of Nebraska - Lincoln
Lincoln, Nebraska 68588-0340
UNITED STATES OF AMERICA
e-mail: sbohaty@unlgradl.unl.edu

Ms Sonia Bryce
Core Processing Technician
Department of Geology
James Cook University
Townsville Q 4811
AUSTRALIA
e-mail: sonya.bryce@jcu.edu.au

Dr Michele Claps
Sedimentologist
Dipartimento di Geologia e Paleontologia
Universitii degli Studi di Ferrara
Corso Ercole I d'Este 32, 44100 Ferrara
ITALY
e-mail: cli@dns.unife.it

Mr Matt Curren
Core Curator
Antarctic Marine Geology Research Facility
Department of Geology, Florida State University
Tallahassee, Florida 32306-4100
UNITED STATES OF AMERICA
e-mail: curator@geomag.gly.fsu.edu

Dr Fred J. Davey
Marine Geophysicist
Institut of Geological and Nuclear Sciences
P O Box 1320, Wellington
NEW ZEALAND
e-mail: f.davey@gns.cri.nz

Dr Laura De Santis
Sedimentologist/Geophysicist
Osscrvatorio Geofisico Sperimentale
Borgo Grotta Gigante
C.P. 2011 - 34016 Trieste
ITALY
e-mail: ldesantis@ogs.trieste.it

Dr Werner Ehrmann
Sedimentologist
Martin-Luther-Universitat
Institut fur Geologische Wissenschaften
Domstrasse 5, D-06108 Halle
GERMANY
e-mail: ehrmann@geologie.uni-halle.de

Dr Chris Fielding
Sedimentologist
Department of Earth Sciences
University of Queensland
Brisbane, QLD 4072
AUSTRALIA
e-mail: chrisf@earthsciences.uq.edu.au

Dr Fabio Florindo
Palaeomagnetist
Istituto Nazionale di Geofisica
Via di Vigna Murata 605,00143 Roma
ITALY
e-mail:florindo@nettuno.ingrm.it
FLORINDO@ing750.ingrm.it

Dr Michael Hambrey
Sedimentologist
Institute of Geography & Earth Sciences
University of Wales
Aberystwyth, Ceredigion, SY23 3DB
UNITED KINGDOM
e-mail: mjh@aber.ac.uk

Dr Michael Hannah
Palynologist
School of Earth Sciences
Victoria University of Wellington
P O Box 600, Wellington
NEW ZEALAND
e-mail: michael.hannah@vuw.ac.nz

Professor David M. Harwood
Palaeontologist (siliceous microfossils)
Department of Geosciences
University of Nebraska - Lincoln
Lincoln, Nebraska 68588-0340
UNITED STATES OF AMERICA
e-mail: dharwood@unlinfo.unl.edu

Dr Stuart Henrys
Marine Geophysicist
Institute of Geological & Nuclear Sciences
P O Box 1320, Kelburn, Wellington
NEW ZEALAND
e-mail: s.henrys@gns.cri.nz

Mr Ferdinand Hoelscher
Downhole Logging Technician
Bundesanstalt fur Geowisscnschaften
Stilleweg 2, D-3000 Hannover 51
GERMANY

Dr John A. Howe
Sedimentologist
British Antarctic Survey
High Cross, Madingley Road
Cambridge CB3 0ET
UNITED KINGDOM
e-mail: j.howe@bas.ac.uk

Professor Richard Jarrard
Downhole Logging Specialist
Department of Geology & Geophysics
University of Utah
Salt Lake City, Utah
UNITED STATES OF AMERICA
e-mail: rich@westlog.utah.edu

Professor Richard Kettler
Organic Geochemist
Department of Geosciences
University of Nebraska - Lincoln
Lincoln, Nebraska 68588-0340
UNITED STATES OF AMERICA
e-mail: rkettler@unlinfo.unl.edu

Ms Sherry Kooyman
Graphic Artist
4005 Carmel View Rd., No. 70
San Diego, California 92130
UNITED STATES OF AMERICA
e-mail: sherry@sd.znet.com

Conrad Kopsch
Physical Properties Technician
Alfred-Wegener-Institut
Postfach 12 01 81,27516 Bremerhaven
GERMANY

Professor Lawrence Krissek
Sedimentologist
Department of Geological Sciences
Ohio State University
Columbus Ohio 43210
UNITED STATES OF AMERICA
e-mail: krissek@mps.ohio-state.edu

Dr Mark Lavelle
Sedimentologist
British Antarctic Survey
High Cross, Madingley Road, Cambridge CB3 0ET
UNITED KINGDOM
e-mail: rn.lavelle@bas.ac.uk

Ms Elisabeth Levac
Photography Technician
Department of Geology and Geophysics
Louisiana State University
Baton Rouge, Louisiana 70803
UNITED STATES OF AMERICA
c-mail: elevac@tiger.lsu.edu

Dr Frank Niessen
Physical Properties Specialist
Alfred-Wegener-Institut
Postfach 12 01 81,27516 Bremerhaven
GERMANY
e-mail: fniessen@awi-bremerhaven.de

Ms Sandra Passchier
Micropalaeontology Technician
Byrd Polar Research Centre
Ohio State University
Columbus Ohio 43210
UNITED STATES OF AMERICA
e-mail: passchier.1@osu.edu

Mr Timothy Paulsen
Core Scanning Technician
Byrd Polar Research Center
Ohio State University
Columbus, Ohio 43210
UNITED STATES OF AMERICA
e-mail: paulsen.9@osu.edu

Professor Ross D. Powell
Sedimentologist
Department of Geology
Northern Illinois University
DeKalb, Illinois, 60115
UNITED STATES OF AMERICA
e-mail: ross@geol.niu.edu

Mr Alex Pyne
Sea Ice Specialist
School of Earth Sciences
Victoria University of Wellington
P O Box 600, Wellington
NEW ZEALAND
e-mail: alex.pyne@vuw.ac.nz

Dr Ghodrat Rafat
Core Scanning Technician
DMT - GeoTec
Franz-Fischer-Weg 61, D-45307 Essen
GERMANY
e-mail: rafat@geotec.dmt-fp.cubis.de

Dr Ian J. Raine
Palaeontologist (terrestrial palynomorphs)
Institute of Geological & Nuclear Sciences
P O Box 30 368, Lower Hutt
NEW ZEALAND
e-mail: i.raine@gns.cri.nz

Dr Andrew P. Roberts
Palaeomagnetist
Department of Oceanography, University of Southampton
Southampton Oceanography Centre
European Way, Southampton S014 3ZH
UNITED KINGDOM
e-mail: arob@mail.soc.soton.ac

Dr Leonardo Sagnotti
Palaeomagnetist
Istituto Nazionale di Geofisica
Via di Vigna Murata 605,00143 Roma
ITALY
e-mail: sagnotti@marte.ingrm.it

Ms Sonia Sandroni
Editorial Assistant
Dipartimento di Scienze della Terra
Universith degli Studi di Siena
via delle Cerchia 3,53100 Siena
ITALY
e-mail: terranta@dst.unisi.it

Mr Erich Scholz
Downhole Logging Technician
Department of Geology & Geophysics
University of Utah
Salt Lake City, Utah
UNITED STATES OF AMERICA

Mr John Simes
Palynology technician
Institute of Geological & Nuclear Sciences
P O Box 30 368, Lower Hutt
NEW ZEALAND
e-mail: j.simes@gns.cri.nz

Dr John Smellie
Petrologist
British Antarctic Survey
High Cross, Madingley Road
Cambridge CB3 OET
UNITED KINGDOM
e-mail: j.smellie@bas.ac.uk

Dr Percy Strong
Palaeontologist (foraminifera)
Institute of Geological & Nuclear Sciences
P O Box 30 368, Lower Hutt
NEW ZEALAND
e-mail: p.strong@gns.cri.nz

Mr Michael Tabecki
Rock Section Technician
British Antarctic Survey
High Cross, Madingley Road, Cambridge CB3 OET
UNITED KINGDOM
e-mail: mgta@bas.ac.uk

Dr Franco M. Talarico
Petrologist
Dipartimento di Scienze della Terra
Università degli Studi di Siena
via delle Cerchia 3, 53100 Siena
ITALY
e-mail: talaf@dst.unisi.it

Dr Marco Taviani
Palaeontologist (macrofossils)
Istituto di Geologia Marina, CNR
via Gobetti 101, I-40129 Bologna
ITALY
e-mail: taviani@boigm2.igm.bo.cnr.it

Professor Kenneth L. Verosub
Palaeomagnetist
Department of Geology
University of California
Davis, California 95616
UNITED STATES OF AMERICA
e-mail: verosub@geology.ucdavis.edu

Dr Giuliana Villa
Palaeontologist (calcareous nannofossils)
Dipartimento di Scienze della Terra
Università degli Studi di Parma
Viale delle Scienze 78, 43100 Parma
ITALY
e-mail: geol01@ipruniv.cce.unipr.it

Dr Gary S. Wilson
Palaeomagnetist
Byrd Polar Research Center
Ohio State University
Columbus, Ohio 43210
UNITED STATES OF AMERICA
e-mail: wilsongs@lion.mps.ohio-state.edu

Professor Terry Wilson
Structural Geologist
Byrd Polar Research Center
Ohio State University
Columbus, Ohio 43210
UNITED STATES OF AMERICA
e-mail: twilson@mps.ohio-state.edu

Professor Sherwood W. Wise, Jr.
Paleontologist (calcareous nannofossils)
Department of Geology, 4100
Florida State University
Tallahassee, Florida 32306
UNITED STATES OF AMERICA
e-mail: wise@geomag.gly.fsu.edu

Dr Tom Wonik
Downhole Logging Specialist
Bundesanstalt für Geowissenschaften
Stilleweg 2, D-3000 Hannover 51
GERMANY
e-mail: wonik@bgr.de

Dr Ken Woolfe
Sedimentologist
Department of Geology
James Cook University
Townsville Q 4811
AUSTRALIA
e-mail: ken.woolfe@jcu.edu.au

Professor John H. Wrenn
Palynologist
Department of Geology and Geophysics
Center for Excellence in Palynology
Louisiana State University
Baton Rouge, Louisiana 70803
UNITED STATES OF AMERICA
e-mail: glwrenn@lsuvm.sncc.lsu.edu

PROJECTSTAFF

Mr Jim Cowie
Project Manager
Antarctica NZ
Private Bag 4745
Christchurch
NEW ZEALAND
e-mail: j.cowie@antarcticanz.govt.nz

Mr Alex Pyne
Science Support Manager
School of Earth Sciences
Victoria University of Wellington
P O Box 600, Wellington
NEW ZEALAND
e-mail: alex.pyne@vuw.ac.nz

Mr Pat Cooper
Drilling Manager
Rapid Creek, Waimangaroa
Westport
NEW ZEALAND

Mr John Alexander
Cape Roberts Liaison Officer
P O Box 314
Queenstown
NEW ZEALAND

WINFLY TEAM

Alex Pyne	Science Support Manager
Cliff Atkins	Core Processing technician
Murray Knox	Plant Operator
Brent Palmer	Paramedic/GD
Brian Reid	Electrician
Jeremy (JR) Ridgen	Mechanic
Peter Sinclair	Carpenter
Richard Struthers	Carpenter/Field Assistant

CAMP SUPPORT

Dennis Skinner	Chef

DRILLERS

Pat Cooper	Drilling Supervisor
John Marcussen	Driller
Tom Rae	Driller
Frank Tansey	Driller
Michael Avey	Assistant Driller
Chris Collie	Assistant Driller
David Eaton	Assistant Driller
Todd Symons	Assistant Driller
Brent Wallis	Assistant Driller
Sam Woodford	Assistant Driller
Leon Holloway	Drilling consultant

Terra Antartica
1998, 5(1), 1-30

Background to CRP-1, Cape Roberts Project, Antarctica

CAPE ROBERTS SCIENCE TEAM*

Abstract - The first hole of the Cape Roberts Project, CRP-1, was chilled in October, 1997, to a depth of 148 metres below the sea floor (mbsf) before being terminated unexpectedly by the loss of fast sea-ice seaward of the rig following a severe storm. The site lies in 150 m of water at 77.008°S and 163.755°E, 16 km off Cape Roberts. This part of the report outlines the geologic setting, a gently tilted sequence near the margin of the Victoria Land Basin, and describes the history of the growth of sea ice, which provided the drilling platform, as well as the history of the drilling itself. Core recovery was around 77% in soft and brittle strata to 100 m and 98% below that.

The sequence was found to comprise a Quaternary glacigenic interval down to 43.55 mbsf and below this an early Miocene interval that was also glacigenic. Core properties that were studied include fracture patterns, porosity, sonic velocity and magnetic susceptibility. Velocity in particular was useful in relating the cored sequence to the regional seismic stratigraphy. A preliminary assessment suggests that the bottom of the hole is 15 m short of the boundary between seismic sequences V3 and V4.

Analytical facilities new to the Antarctic and used for processing samples for the project are described here and include a bench top palynological processing system and a palaeomagnetic laboratory. The core management and sampling system, which recorded over 2 000 samples, is also outlined.

INTRODUCTION

The Cape Roberts Project is a co-operative drilling project between the Antarctic programmes of Australia, Germany, Italy, New Zealand, UK and USA. The aim is to obtain continuous core through strata from 30 Ma in age back to perhaps as much as 100 Ma in age beneath the western side of McMurdo Sound, Antarctica, in order to study the tectonic and climatic history of the region. It is named after Cape Roberts, the staging point for the offshore drilling and a small promontory 125 km north west of McMurdo Station and Scott Base (Fig. 1).

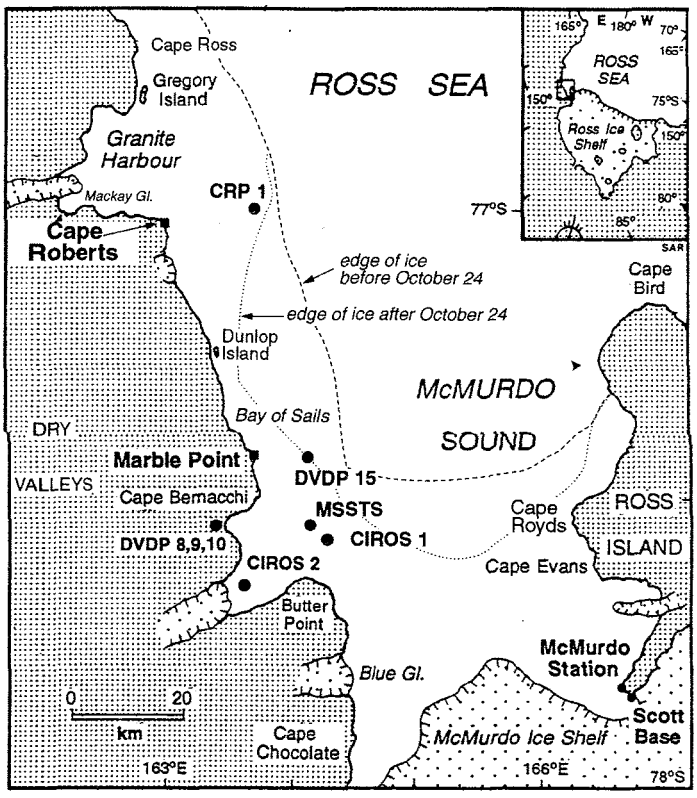

Fig. 1 - Map of the south west corner of the Ross Sea, showing the locations of Cape Roberts, CRP-1 and other drill sites in the area, and McMurdo Station1 Scott Base, the main staging point for the project. The edge of the fast ice before and after the October 24 break-out is also shown.

* J. Anderson, P. Armienti, C. Atkins, P. Barrett, S. Bohaty, S. Bryce, M. Claps, M. Curran, F.J. Davey, L. De Santis, W. Ehrmann, F. Florindo, C. Fielding, M. Hambrey, M. Hannah, D.M. Harwood, S. Henrys, F. Hoelscher, J.A. Howe, R. Jarrard, R. Kettler, S. Kooyman, C. Kopsch, L. Krissek, M. Lavelle, E. Levac, F. Niessen, S. Passchier, T. Paulsen, R. Powell, A. Pyne, G. Rafat, I.J. Raine, A.P. Roberts, L. Sagnotti, S. Sandroni, E. Scholz, J. Simes, J. Smellie, P. Strong, M. Tabecki, F.M. Talarico, M. Taviani, K.L. Verosub, G. Villa, P.N. Webb, G.S. Wilson, T. Wilson, S.W. Wise, T. Wonik, K. Woolfe, J.H. Wrenn.

The project is designed to address two major questions:

- did ice sheets grow and decay on Antarctica, with attendant changes in global sea level, prior to the earliest Oligocene 34 Ma ago, when it is widely believed the first extensive ice formed on the continent?
- at what time did the continent begin to rift to form the Ross Sea and the Transantarctic Mountains?

Implicit in the objectives is the significant contribution to be made through age- and rock-type calibration for the 40 000 km of seismic surveys in the Western Ross Sea by coring the strata off Cape Roberts.

The strata to be cored form a seaward-dipping sequence 10 to 15 km off Cape Roberts and seaward of the boundary between the Transantarctic Mountains (TAM) block and the Victoria Land Basin (VLB) (Fig.2). Seismic surveys of the basin have traced 3 sequences into the 2000+ m of strata off Cape Roberts (V3, V4 and V5 – Fig. 3). Correlation with the CIROS-1 hole 70 km to the south indicated that most of the strata are more than 30 million years old (Barrett et al., 1995; Barteket al., 1996). The Cape Roberts Project aims to core 1200 or more m of this sequence by drilling at least three holes ranging in depth from 400 to 700 m and overlapping so as to ensure a continuous stratigraphic record.

This *Initial Report,* and a companion *Scientific Report* to be published later this year, provide results from the first drilling season. After some uncertainties following a year's postponement due to the late development of fast sea ice in 1996 and a series of winter ice break-outs this year, the ice was thought likely to be thick enough in the drill-site area to safely support the drilling system. A decision was taken to send the advance party to Scott Base on the August "WINFLY" operation to establish a land mute to Cape Roberts and locate the first drill site. The party arrived at Scott Base on August 25, and, after some challenging route-finding around the edge of the McMurdo Ice Shelf, reached Cape Roberts on August 30 Observations of sea-ice character and thickness led to the selection of site 1 on the southern of three possible transect lines indicated in the Science Plan (Barrett, 1997, Fig. 3.5) as the location for the first drill site - CRP-1.

CRP-1 was terminated prematurely after 7 days of coring when a large section of the fast sea-ice broke out after an unexpectedly fierce storm on October 23-24, leaving the rig vulnerable to further break-outs. Nevertheless, significant core had been recovered from both the Quaternary cover beds and the older part of the section to a depth of 147 metres below the sea floor (mbsf), and forms the subject of this report. Basic data for the hole are summarised in table 1, and the depth and range of ages encountered are shown in figure 3 in the context of the 3 sites planned for the project.

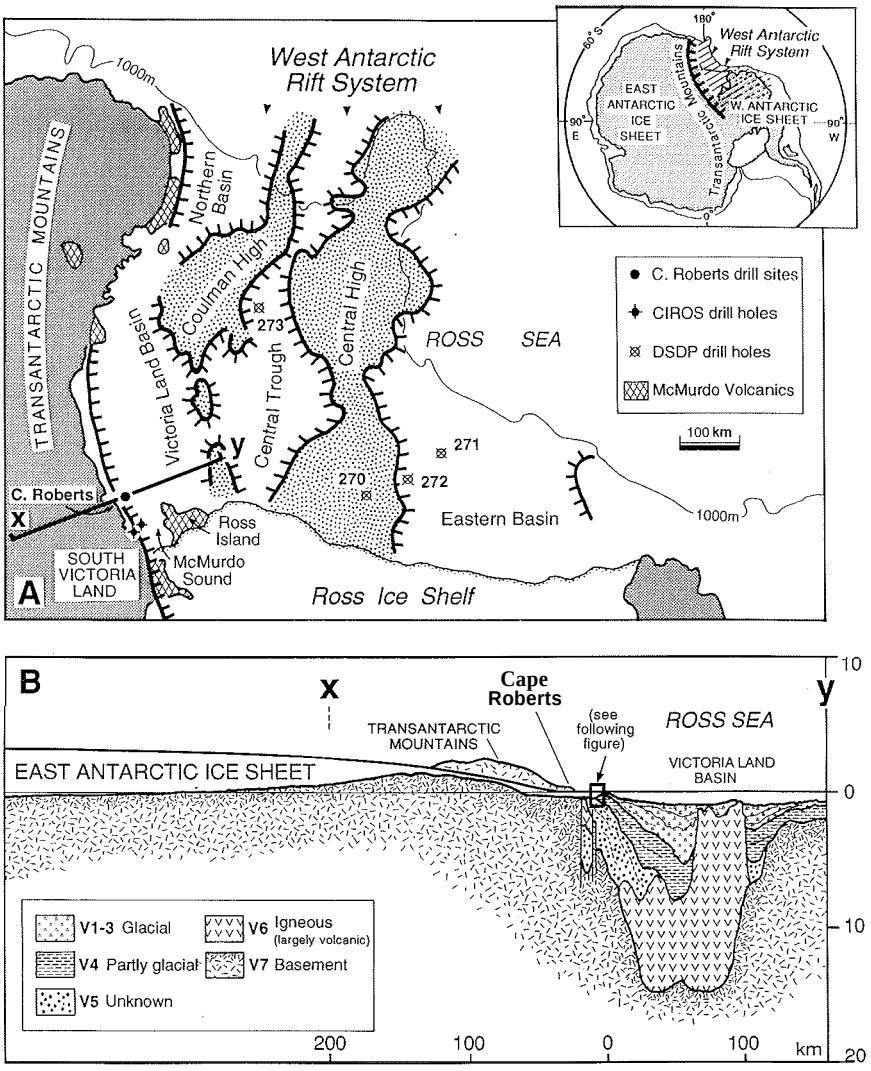

Fig. 2 - Map of Ross continental shelf (A) and cross-section through the edge of the east Antarctic Rift System (B), showing the location of Cape Roberts with respect to the East Antarctic Ice Sheet, the Transantarctic Mountains and the Victoria Land Basin. The location of figure 3, with the 3 planned drill sites off Cape Roberts, is also shown.

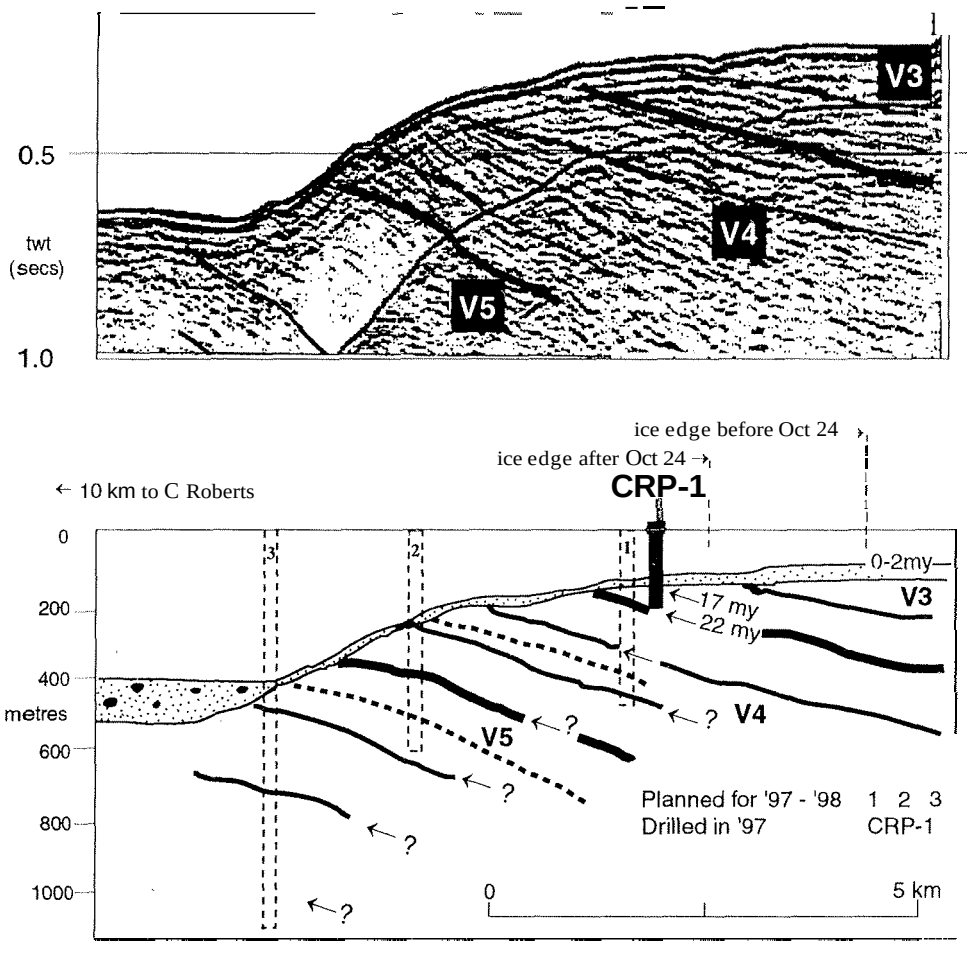

Figure 3 - Geological section based on seismic data from NBP96-89 (adapted from Fig. 3.5by S.A. Henrys in Barrett, 1997), showing CRP-1 and the ages obtained by the Cape Roberts Science Team (see Quaternary and Miocene Strata, this volume).

Tab. *1* -Site data for CRP-l.

Position	16 km ENE of Cape Roberts
Latitude	77.008° S
Longitude	163.755° E
Water depth	153.50 m
Sea ice thickness	1.60 m
First core	1:30 am, 17 October 1997
Last core	2:00 am, 24 October 1997
Cored interval	132.06 m
Core recovered	113.32 m
Recovery	86%
Depth to bottom of hole	147.69 mbsf
Age and lithology of oldest strata	22-24 Ma. Mudstone with scattered pebbles

The report is organised as 4 related articles:

1 - *Background to CRP-1.* This section includes information on geological context for drillhole, coring and sea-ice observations, core properties and an overview of the core. It also includes core recovery data (Appendix 1), core logs on a scale of 1:20 (Appendix 2) and scanned images of the core face after splitting (Appendix 3).

2 - *Quaternary strata.* These are about twice as thick as expected, and contain an unusual carbonate facies.

3 - *Miocene strata.* Although these are part of the dipping "target" sequence, they are around 8 my younger than we expected from seismic correlation from the CIROS-1 drillhole 70 km to the south. However the CRP-1 core provides a new window on the period from 17 to 22 Ma in this region.

4 - *Summary of results.* This provides a preliminary age model for the core and interpretations on glacial advance and retreat over the site in early Quaternary and Miocene time.

REGIONAL SETTING

GEOLOGICAL SETTING

McMurdo Sound lies at the southwestern end of the Ross Sea, between the Transantarctic Mountains of South Victoria Land and the recent (*5* Ma) volcanic Ross Island (Fig. 4). It coincides with the southwestern end of the Victoria Land Basin (VLB), one of four major extensional basins forming the Ross Sea continental shelf (Houtz & Davey, 1973; Davey, 1981,1983; Hinz & Block, 1984; Cooper et al., 1987,1994). The VLB is a complex structure, extending from Ross Island to Terra Nova Bay, and comprising a major basin up to 14 km deep in the west separated from a subbasin, in the east by a volcaniczone, the Terror Rift, which apparently continues into Ross Island. Ross Island may be expected to be underlain by several kms of sedimentary rocks (Cooper & Davey, 1987; Melhuish et al., 1995). In this region the TAM forms the western margin of the VLB and the deformational history of the two are probably directly related. Two main crustal thinning events have formed the basins of the Ross Sea but they are not well constrained in time. The first, an essentially non-magmatic rifting event over most of the Ross Sea, is probably related to the break-up of Gondawana in this region (late Mesozoic). The second event was associated with volcanic activity and

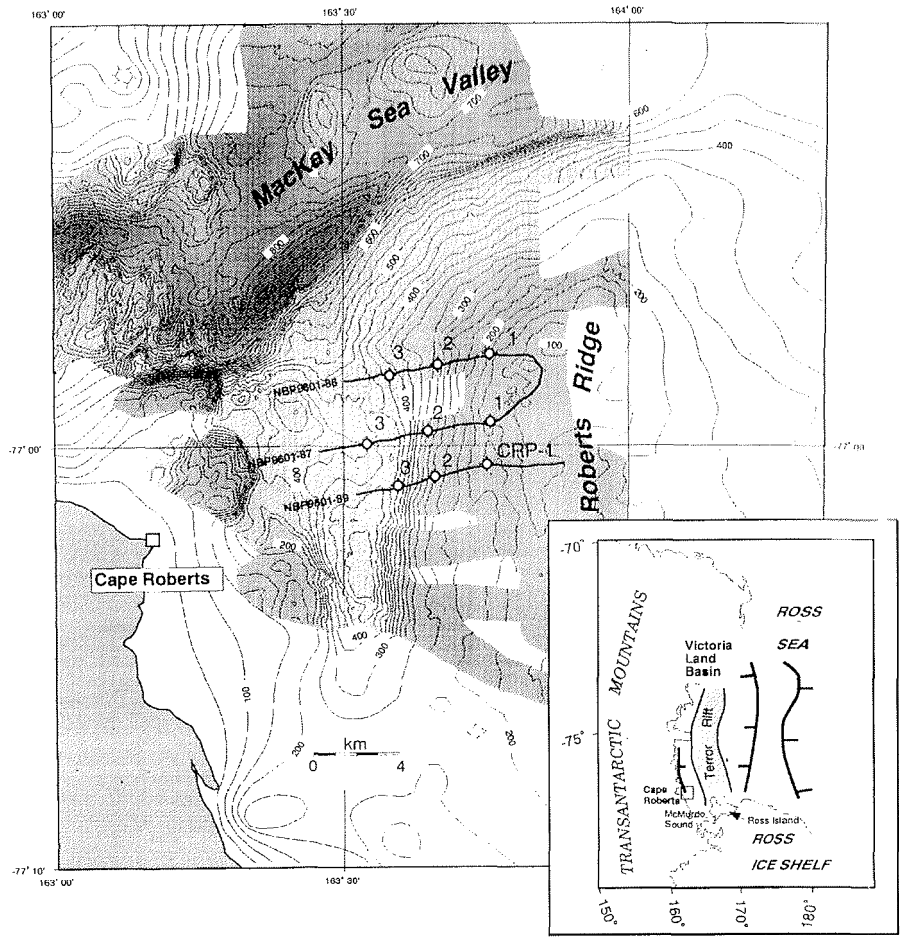

Fig. 4 - Location (inset) and bathymetry of the Cape Roberts Project survey area. Swath bathymetry is shown, with contours interpolated from other single track data where swath data were not available. Contours are at *25* m intervals over the swath area, and 50 m elsewhere. The seismic profile in figure *5* is along the line NBP9601-89. Drill-site options (sites 1, *2,* 3 on NBP lines 86, 87 and 89) and the drill site CRP-1 are marked.

localised in the VLB, and an Eocene and younger age has been proposed (Cooper et al., 1987,1991).

The main structural trend is north-south, with major normal faulting forming half grabens in basement and terminating in the overlying sedimentary section. Cenozoic faulting cuts through the sedimentary section and, in places, reaches the sea floor. Late Cenozoic structural trends have been mapped also transverse to these features (Cooper et al., 1994).

The planned Cape Roberts drill sites are located on an offshore bathymetric rise, Roberts Ridge, in northern McMurdo Sound, about 10 to 20 km east of Cape Roberts on the southern entrance of Granite Harbour (Figs. 1 & 4). This bathymetric high rises from about 500 m depth in the west to within 100 m of sea level. To the south, Roberts Ridge broadens into a shallow-coastal platform 200 m below sea level in western McMurdo Sound. Glacial advances have truncated Roberts Ridge to the north and west exposing the older east-dipping strata of the VLB close to the sea floor (Fig. *5).* A thick stratigraphic section through strata of the VLB can therefore be sampled by a series of shallow drillholes stepping down the western flank of Roberts Ridge.

The sedimentary geology beneath McMurdo Sound comprises strata that dip gently east from the western shelf of McMurdo Sound and apparently under Ross Island. These same strata crop out on western Roberts Ridge, where they were first observed in 1980 (D. Bennett, unpublished manuscript). Subsequent multichannel seismic measurements from R N SP LEE and R/V OGS-EXPLORA demonstrated that the units could be traced into the lower (deeper) sedimentary sequences of the VLB (Cooper et al., 1987; Brancolini et al., 1994). Several seismic surveys have defined the major seismostratigraphic units throughout the Victoria Land Basin (Cooper & Davey, 1987; Brancolini et al., 1995; Barrett et al., 1995; Bartek et al., 1996). The stratigraphy, ages and facies (based on CIROS-1 correlation) from these studies are summarized in table 2. The major seismic units, V1 through V7, used in this paper follow the stratigraphy of Cooper & Davey (1987). Drilling in southern McMurdo Sound (MSSTS-1 and CIROS-1) sampled rocks back to Eocene in age. They indicated very limited ice distribution in the Eocene and early Oligocene, and grounded ice in the late Oligocene and early Miocene (Barrett, 1986, 1989), but the onset of glaciation in the region has not been sampled. Correlation of these drilling results with the Cape Roberts sequences (Barrett et al., 1995; Bartek et al., 1996) suggested that the latter sequences are the same and older in age and may therefore contain a record of the onset of Antarctic glaciation. Sampling these lower units will also provide information on the age and evolution of the VLB and uplift history of the adjacent TAM.

BATHYMETRY

Bathymetric-data coverage over Roberts Ridge has significantly improved with the advent of multibeam

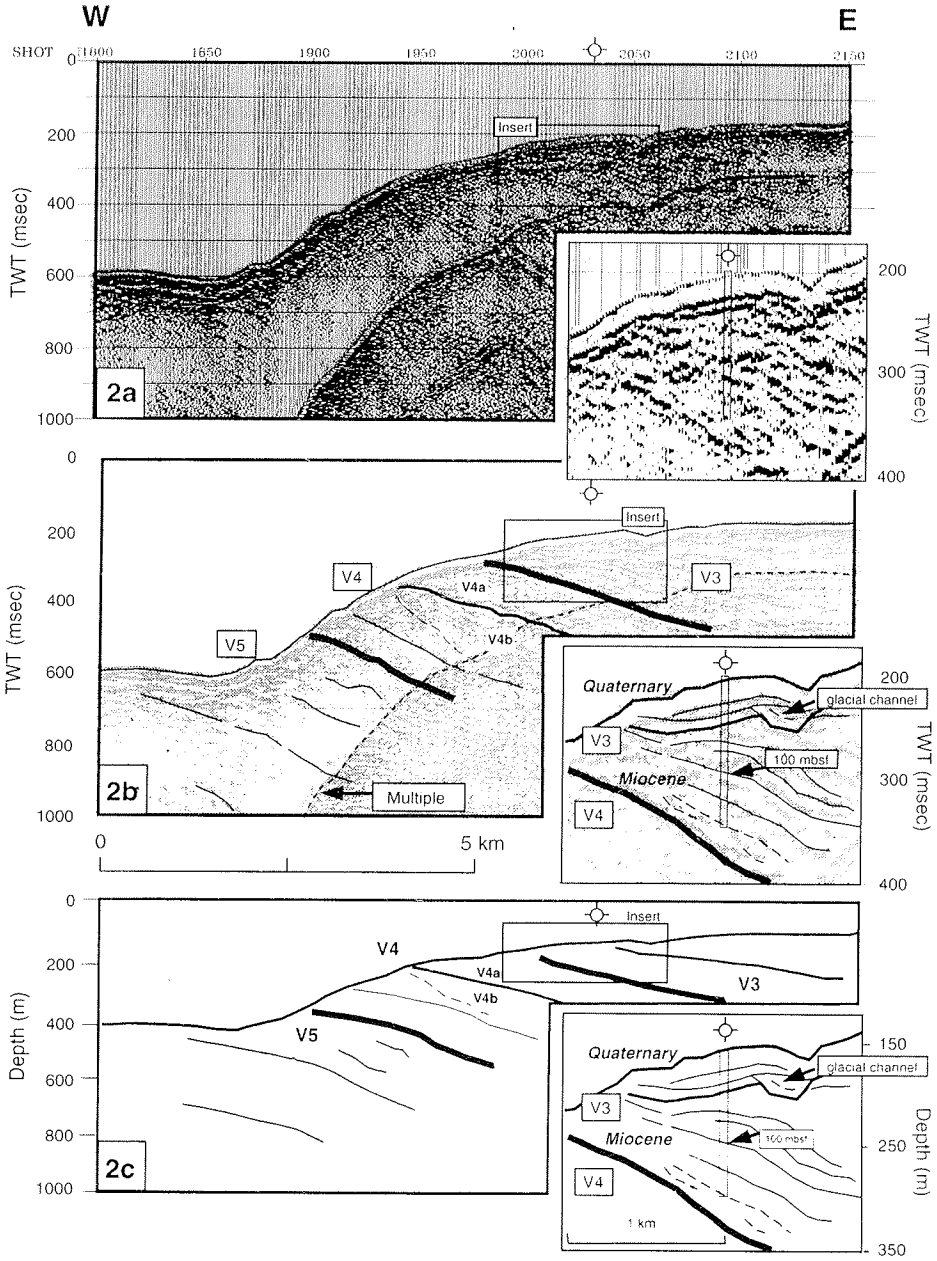

Fig. 5 - Seismic record for line NBP 9601-89 (*a*), with interpretation of the stratigraphic Units V3, V4 and V5 in terms of two-way travel time (*b*) and depth (*c*). Insets provide detail of the record over the CRP-1 site. Note the broad shallow scour channels near the sea floor.

Tab. 2 - Seismic stratigraphy of the Victoria Land Basin (after Cooper et al., 1987). Modified to take into account seismic correlation of the Cape Roberts sequence with CIROS-1, and the revision of the age of the lower part of the hole (Hannah et al., in press).

	Thickness (km)	Velocity (km/sec)	Age	Lithology
V1	< 1.2	1.7 - 2.3	mid Pliocene	Glacial marine sediments
V2	0.2 - 1.3	2.1 - 2.9	mid Miocene to Pliocene	Glacial marine sediments
V3	0.3 - 2.5	2.7 - 4.1	late Oligocene to early Miocene	Glacial marine sediments
V4 a	< 1	4.0 - 4.9	early Oligocene and Eocene	Marine sediments?
b	< 0.5		Eocene and older	
V5	< 8	4.5 - 5.6	Cretaceous to early Paleogene	Marine sediments?
V6	< 8		Paleogene - Recent	Basaltic volcanics
V7		5.0 - 7.4	Precambrian - mid Paleozoic	Basement

techniques. The bathymetric map (Fig. 4) for the sea floor east of Cape Roberts is largely based on multibeam data collected over most of the area of the map by the R/V NATHANIEL B. PALMER, using a Seabeam 2112 multibeam sonar survey system in February 1996. The few areas not covered by the multibeam data were filled in with other data sets. The data sets merge well with discrepancies of less than 20 m in general. The compiled bathymetry shows the steep slopes of northern and western parts of Roberts Ridge, which we infer were caused by glacial erosion controlled by the structures forming the 900-m-deep Mackay Sea Valley and by coast-parallel faulting associated with the Transantarctic Mountain Front. A tectonic influence on the Mackay Sea Valley is suggested

by the observation that it forms the northern limit of Roberts Ridge. The Cape Roberts basin (Hamilton et al., 1997), west of northern Roberts Ridge, is up to 500 m deep and dies away to the south of Cape Roberts. The drill site CRP-1 is located on the western side of Roberts Ridge at a depth of 150 m (Fig. 4).

AEROMAGNETIC DATA

An aeromagnetic survey was carried out by the German-Italian Aeromagnetic Research in Antarctica (GITARA) project in 1994 (Bozzo et al., in press) across the Roberts Ridge region in response to a report of a large positive magnetic anomaly just west of the northern Roberts Ridge, from which Behrendt et al. (1987) inferred a submarine volcano. The GITARA aeromagnetic study (500 m line spacing, 125 m altitude) greatly improved the definition of the magnetic anomalies and the bodies causing them, and suggested that the bodies are more likely to be fragments of stratiform basic igneous bodies. Although the modelled bodies came close to the sea floor, this occurs well (more than a kilometre vertically and horizontally) to the west of the most western proposed drill site. The outline, at a depth of 1 km, of the magnetic bodies, is shown in figure 5.

SEISMIC REFLECTION DATA

The coverage of seismic profiles is now adequate to trace boundaries of the major seismic units over the area east of Cape Roberts. Only the older seismic Units (V3, V4, V5) have been identified in the Cape Roberts region, as V1 and V2 have been largely eroded away here (Fig. 5). V4 has been further subdivided into Units V4a and V4b on the basis of an angular unconformity between the two sub-units in this region (Barrett et al., 1995; Hamilton et al., 1997), but we have not subdivided the unit in figure 6. V3 and V4 can be further sub-divided on the single channel seismic data, with, for example, at least 6 sequences recognised in V3 in some places (Henrys et al., 1994; Bartek et al., 1996). However, track-line coverage is not sufficient to resolve them across the whole area, and they have not been delineated in this report.

The distribution of major seismostratigraphic units is shown in figure 6a and b, along with the primary seismic tracks (SP LEE (1984), EXPLORA (1990), POLAR DUKE (1990), and PALMER (1996)) across Roberts Ridge. The stratigraphic sequences were correlated and mapped on the basis of lateral continuity and seismic character. The strata are found to strike consistently just west of north and to dip gently east with dips rising from 2.5° for the upper part of the section to around 5° for the lower part, based on sea-floor outcrop of the units. Dips on Units V5 and V4b increase to the south, with Units V3 and V4a onlapping V4b and pinching out to the west against V4b and the sea floor. V5 and V4b gradually thicken towards the east.

The sedimentary section off Cape Roberts is bounded on its western margin by a major, steeply dipping, north trending fault about 5 km offshore, upthrown to the west and bringing basement rocks to the sea floor (V7 of Cooper & Davey, 1987). These rocks are most likely to be granitoid bodies similar to the exposed rocks around Granite Harbour. Faulting in the sedimentary section is generally sub-parallel to the Transantarctic Mountain Front (NNE) or to the Mackay Glacier trough (ENE) and is apparently mostly normal in character.

Unit V5, the presumed oldest sedimentary seismic unit in the area (Tab. 2), is of unknown age and lithology. It rises from deep in the Victorian Land Basin to reach the sea floor from 12 to 5 km east of Cape Roberts, where it is truncated by a north-trending fault. V5 is estimated to reach a thickness of between 2 and 5 km (Cooper et al., 1987). Its likely age lies between 105 and 55 Ma; lithologies could include either or both shallow-marine or terrestrial facies (see Barrett et al., 1995, for discussion and comparisons with possible New Zealand counterparts).

Unit V4 is presumed, from correlative strata at CIROS-1, to be largely marine mudstone of Eocene-early Oligocene age, although, as discussed by Barrett et al. (1995), the base of CIROS-1 may not coincide with the base of V4 and the lower part of the unit may be older. It crops out on the west flank of the ridge 20 km off Cape Roberts, curving eastward into the Mackay Sea Valley in response to valley bathymetry. Structure contours on the base of V4 indicate a planar surface dipping gently just north of east. Isopachs constructed for V4 (Fig. 6b) show that it thickens eastward at around 100 m/km. Its thickness varies little from south to north.

Unit V3 is the youngest of the exposed strata of the Victoria Land Basin in the mapped area. The sequence underlies Roberts Ridge and the area to the east with a maximum thickness of a little over 200 m attained for V3 just east of the ridge crest. On the basis of seismic correlation with the CIROS-1 drillhole and its similar position relative to the Transantarctic Mountains, V3 was inferred to comprise alternating diamictite, shallow-marine mudstone and sandstone of late Oligocene to early Miocene age, as in the CIROS-1 drillhole, and records many advances of east Antarctic ice beyond the mountains and into the basin. Scour channels, presumably of glacial origin, are evident in the shallow part of the seismic profiles of this unit.

DRILL-SITE OBSERVATIONS

SEA-ICE OBSERVATIONS

Each winter a fringe of fast sea-ice (abbreviated to "fast ice") forms around the southern and western margins of McMurdo Sound, and extends north along the Victoria Land coast past Cape Roberts (Fig. 1). The fast ice was first used as a drilling platform in 1974 for DVDP-15, and then subsequently in 1979 (MSSTS-l), in 1984 (CIROS-2) and 1986 (CIROS-1). Both practical experience and theoretical calculations indicate that a minimum safe ice thickness for supporting the drilling system for a period of several weeks is 1.5 m (Pyne, 1986). In most years this is achieved in mid-late September. The ice grows through October to a maximum of between 1.7 and 2.0 m but begins to lose strength as it becomes isothermal when temperatures rise to around -5°C, typically in late November. This provides a "drilling window" for setting

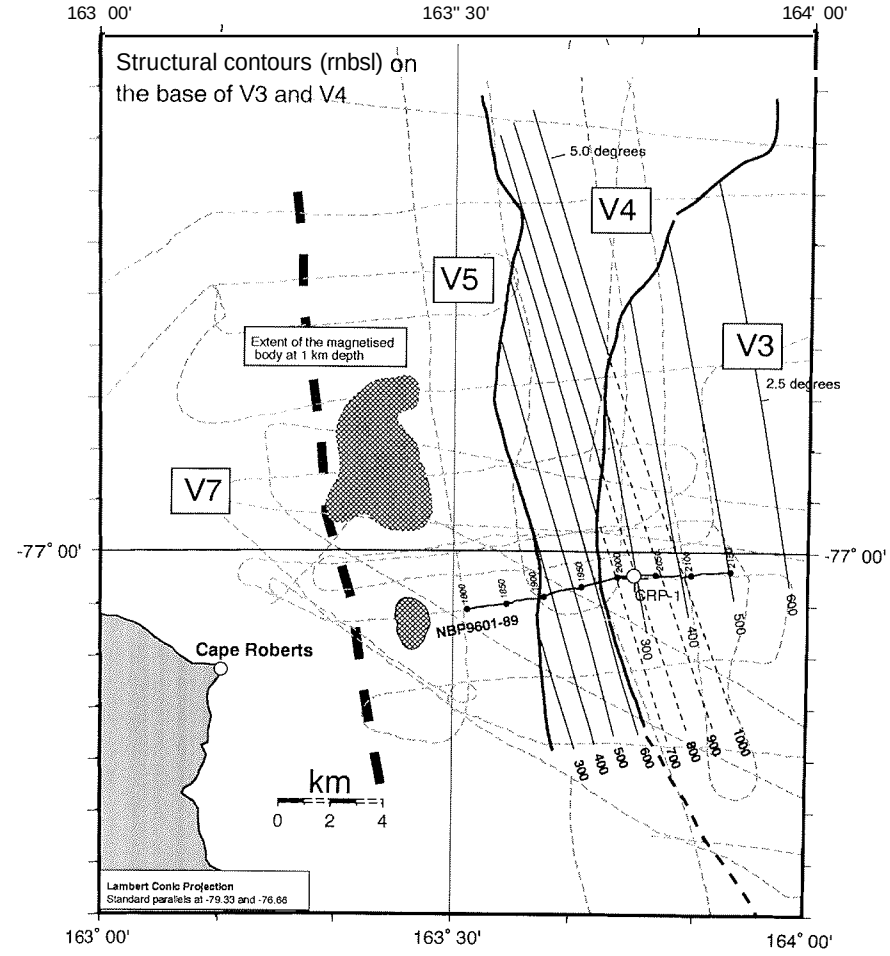

Fig. 6 - Map of the area off Cape Roberts, showing the distribution of the sedimentary sequences (V3, V4, V5) beneath the Quaternary cover beds there.
a) Ship's tracks (dotted) and structure contours on the base of V3 and V4.

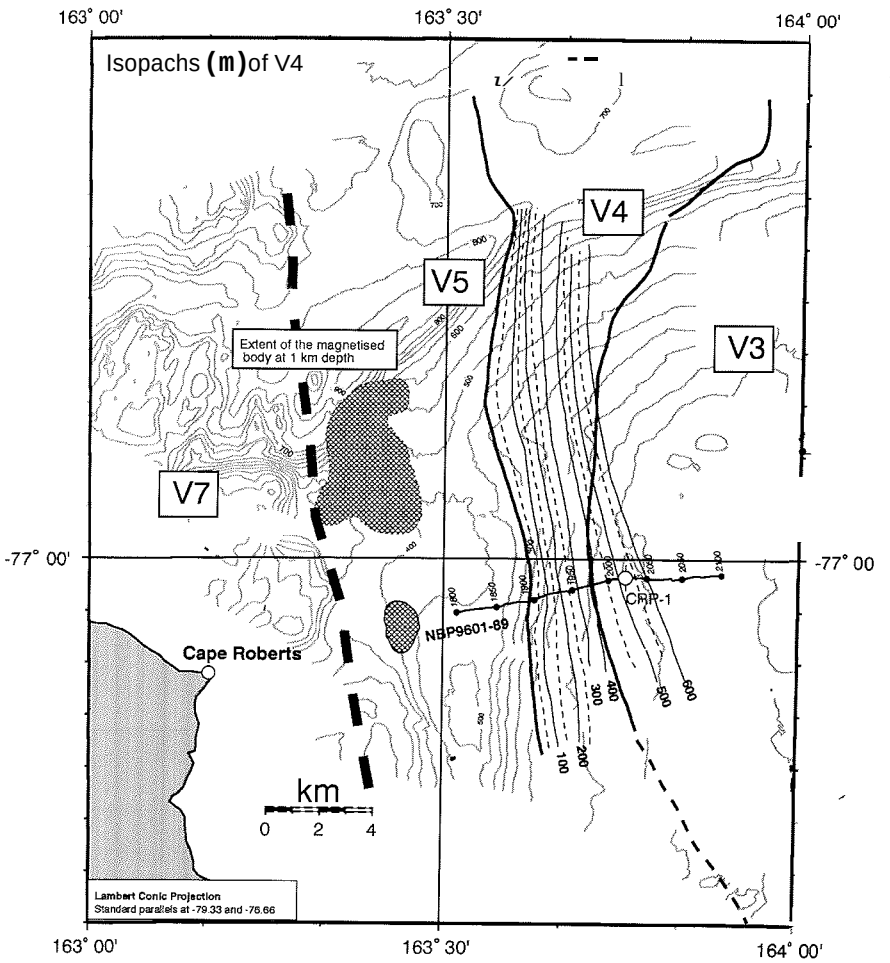

b) Bathymetry (dotted lines) and isopachs for V4 (both in metres) off Cape Roberts.

up, coring and removing the rig from the beginning of October to late November, a period of about 50 days.

Monitoring of sea-ice conditions for ensuring the safety of the drilling system can be divided into two phases; a preparatory phase and an operational phase. The preparatory phase involves satellite monitoring of the extent of the sea-ice with polar-orbiting AVHRR and DMSP imagery, which have a resolution of 1.10 and 0.55 km respectively. These images were made available after processing from ASA headquarters in Denver within a few days of capture. The AVHRR/DMSP images were interpreted regularly by the Science Support Manager from the end of May, and in 1997 the ice edge was well established by early July, but previous large storms in May and June had blown out ice in southern McMurdo Sound. A storm in mid-July moved out a large section of the ice fringe, but it remained in large fragments which refroze in the area of the proposed drill site. The edge that developed at this time continued until August 11, when a southerly storm blew out the ice again in the southern past of the sound, leaving the ice off Cape Roberts still fast but exposed (Fig. 7a). In the two weeks that followed to the end of August, calm cold weather allowed the fringe to re-establish itself.

The last step in the preparatory phase was for the advance party led by Alex Pyne (see Cape Roberts Project Personnel - WINFLY team) to find a route across the sea ice to Cape Roberts, locate the three sites alone, the southern transect (Fig. 4), and determine ice thicknesses From these measurements on August 29, it was projected that the ice thickness at site 1 would exceed 1.5 m. It was then decided that the setting up of the camp and drill site should proceed.

Measurements in the operational phase included ice thickness growth data (Tab. 3), lateral movement of the ice as measured by GPS (Tab. 4) and depression of the ice from the loading by the drilling system, recorded as elevation of the surface of the sea-ice above sea level (also called "freeboard", Tab. 5). Ice thickness exceeded the 1.5 m minimum requirement at all three sites by late September and continued to thicken to 1.7 m in early October. After this, little change took place due to unseasonally warm weather. Lateral-seaward movement of the fast ice at all 3 sites was quite fast in September (0.5 m/day) but reduced to 0.14 m/day during the drilling peiiod in October (Tab. 4) This resulted in a total movement of 3.3 m for CRP-1, well within the specified 26 m lateral movement tolerance of the drilling system for a hole in 150 m of water. The "freeboard" of around 50 mm in the last week of drilling (Tab. 5) was expected to diminish with time, but was considered adequate for a further two weeks of drilling.

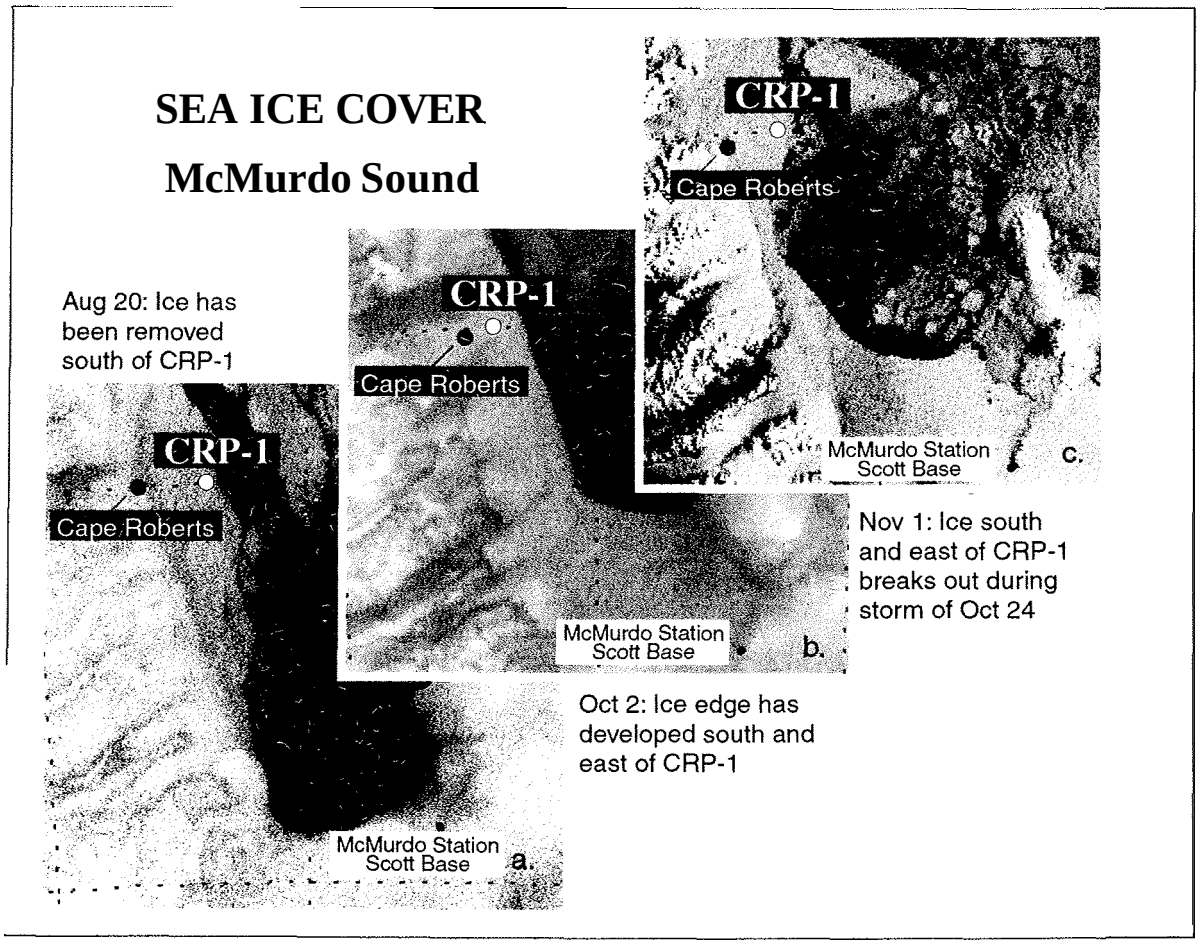

Fig. 7- DMSP satellite images of western McMurdo Sound showing the locations of CRP-1, and of Cape Roberts Camp (CRC), at the southern entrance to Granite Harbour. a) Image from August 20. The sea-ice fringe that had formed around McMurdo Sound has been blown north by gales on August 11, but the ice in the area of the drill site remains intact. b) Image of October 2. The sea-ice fringe has formed again to its normal position in southern and western McMurdo Sound, lasting until the storm of October 24. *c)* Image of November 1. A "bite" has been taken out of the ice edge south of the drill site by swells from the east following the storm of October 24, leaving the drill site at risk.

However, it could have been a significant point of concern after that. A further analysis of these data, along with weather data from these and past years will appear in the *Scientific Report* for CRP-1.

Distance to the edge of the fast ice (marked by an iceberg 4.9 km east of the site) was also checked every few days, and did not change measurably through the set up and drilling period. In addition regular checks were made on the route to the drill site to monitor possible development of cracks in the ice. The well known "Cape Roberts crack", which forms each year running NNW-SSE about 2 km off Cape Roberts, had grown to a typical width of around 10 in, with ice thickness ranging from 70 cm at the edge to a few cm of open water in the middle. Nevertheless it could be crossed, with bridging, by 22 tonne crawler tractor 8 kilometres to the north and 11 kilometres to the south of Cape Roberts. No other cracks were identified, but several small cracks in the local Cape Roberts area were often crossed without bridging and larger frozen cracks of thinner ice were seen in the offshore ice. We conclude that until the storm of October 23-24, fast-ice behaviour lay well within the limits set for safe drilling operation.

The storm of October 23-24 was unusual both in the severity of the winds (exceeding 50 knots at Cape Roberts), and in the swell that propagated through the ice from the open waters of the Ross Sea. The swell was detected early on October 23 by the drilling team and the Science Support Manager, the project's sea-ice adviser. The maximum-safe limit for vertical-ice movement by swells with a period of 10-12 second had been set at 30 mm, based on advice from Dr. Tim Haskell, sea-ice physicist. This limit was exceeded in the early hours of October 24. After securing the drill site the personnel returned to Cape Roberts. After the storm, the fast ice had broken out to within 1 km of the rig (Fig. 7c), well below the accepted safe limit of 5 km. As a consequence of the exposure to possible future storms and the premature weakening of the fast ice by temperatures around 7°C warmer then average, the drill-site equipment was taken to Cape Roberts and plans for further drilling abandoned for this season.

CORING HISTORY

The various elements of the drilling system and camp were on site by the end of October 4 and the rig assembled and in position by October 5. On October 6 two sea-ice holes were drilled for the video hut and drill rig. The sea riser was then lowered on its first full deployment with both rigid and inflatable floats (Fig. 8), and set into the sea floor on October 12. This took a little longer than planned due to technical problems. The riser was then under-reamed to a depth of 16 mbsf through a mixture of mud, sand and cobbles and onto a 46-cm thick boulder of what was later found to be dolerite. It was cemented in and tension adjusted with the inflatable floats.

Coring began late on October 16 with the H drill string (core size 61 mm), the first core (of grout with the top 3 cm of a dolerite boulder at the bottom) coming onto the rig floor at 1:30 a.m. on October 17. Coring proceeded steadily but with difficulties encountered in

Tab. 3 -Measurements of ice thickness through time for the three proposed drill sites on the southern transect of the Cape Roberts Project (Fig. 4). Satellite images indicate that the ice cover began to form around July 1.

Position	Lat	Long	1 Jul (cm)	31 Aug (cm)	9 Sep (cm)	29 Sep (cm)	10 Oct (cm)	11 Nov (cm)
DS3-1	77.0079	163.7482	0	128	145	158	171	171
DS3-2	77.0088	163.6496	0	125	142	154		171
DS3-3	77.0152	163.5877	0	124	146	158		169

Tab. 4 - GPS measurements of the movement of each of the proposed drill sites on transect 3 (southern) as well as the actual site for CRP-1.

Site	Lat (degrees)	Long (degrees)	18 Sep (m)	29 Sep (m)	11 Oct (m)	18 Oct (m)	20 Oct (m)	1 Nov (m)	4 Nov (m)	7 Nov (m)	Ice Movement Rate* (m/day)	Dir (° true)
CRP-1	77.0076	163.7552			0.00	0.92	1.41	2.82	3.03	3.83	0.14	60°
DS 3-1	77.0079	163.7482	0.00	5.72	9.07	10.08	9.97				0.20	77°
DS3-2	77.0088	163.6496	0.00	5.21				11.65	11.83		0.18	72°
DS3-3	77.0152	163.5877	0.00	4.33				11.04	11.49		0.19	70°

* rate based on the following periods: CRP-1 Oct 11 - Nov 7; DS 3-1 Sep 29 - Oct 20; DS 3-2 Sep 29 - Nov 4; DS 3-3 Sep 29 - Nov 4.

Tab. 5 - Freeboard measurements (in mm) of water level below the sea-ice surface at CRP-1.

Date	Oct 3	Oct 6	Oct 16	Oct 18	Oct 19	Oct 23	Oct 25	Oct 25
Notes (see below)	a	b				c	d	e
Drill Hole Freeboard	160	100	60	55	45	40	-10	120
Video Hole Freeboard	160	100	50	40	50	40	0	120

Notes: a. Estimate of the sea-ice surface freeboard one day prior to loading the Drill Site; b. Estimate of the freeboard in the Drill and Video holes immediately after final positioning of the drill rig; c. Measured freeboard @ 1108 NZDST at the begining of the October 23-24 storm; d. Estimate of the freeboard after the storm with large snow drifts around the rig; e. Estimate of the freeboard after the site is completely cleared.

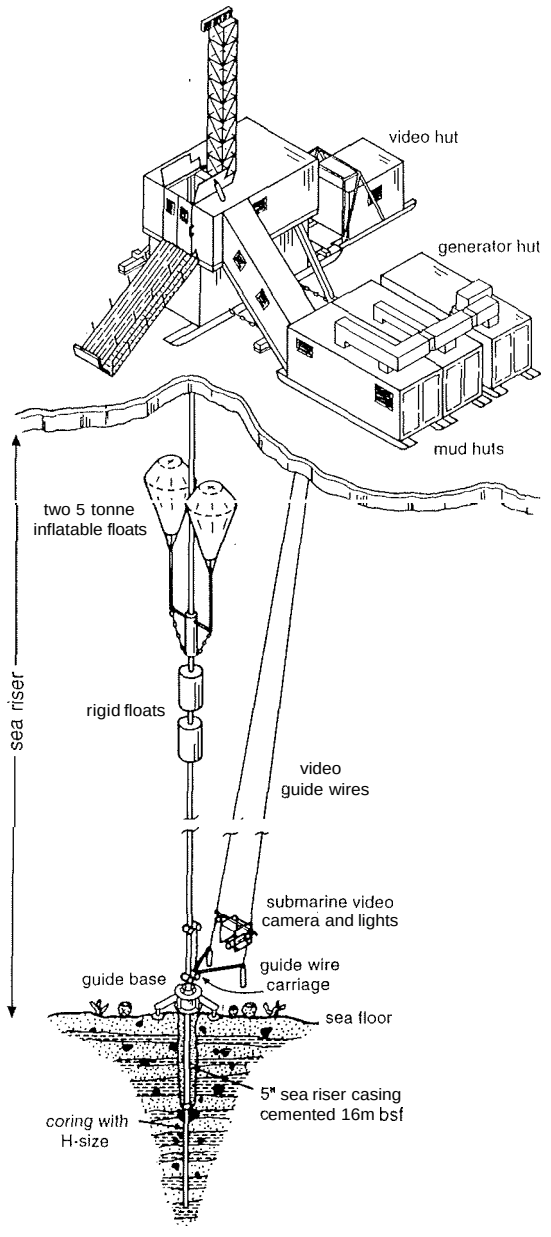

Fig. 8 - Drilling system used for CRP-1. The sea riser comprises 5" OD casing set 16 m into the sea floor, cemented and then over tensioned with inflatable floats. It was designed to support the rotating drill string and to withstand lateral movement of the sea-ice and currents, which reach up to 35 *cm/sec* at this site. The mud hut is for mixing, conditioning and extracting drill cuttings from the drilling fluid. The video hut holds the winch, monitor and control system for the submarine video camera system. This runs on guide wires from the surface to the sea floor and allows the drill-site team to view all parts of the sea riser for operational, safety and environmental reasons.

recovering soft pebbly sand and maintaining hole stability. The softness of much of thesediment required relatively short core runs to achieve reasonable recovery and high mud weights and viscosities were used to maintain hole stability. Unstable down-hole conditions persisted well below the 20 m or so expected. In fact they extended below the Quaternary sediments (base at 43.5 mbsf) and into the Miocene sequence as a consequence of both brecciation and some soft sand layers. This condition led to almost total loss of drilling fluid at a rate of 5 tonnes/day, hard to sustain without resupply for more than a few days. These difficulties continued down to 100 mbsf with down-hole progress averaging around 16 m/day and recovery around 77%.

Late on October 21 drilling conditions became firm as pebbly mudstone and then diamictite were encountered Rate of progress increased to 20 m/day and recovery to 98%, but the near total loss of drilling fluid continued through theinterval above 100 m. There was also a thin but potent interval of loose sand between 114 and 117 mbsf that rose 8 m in the hole after the inner tube was retrieved. Nevertheless the formation was considered competent, and by the evening of October 23 it had been decided to case and cement in the H rod at the depth then reached (148 mbsf) and to continue the hole with N rod (45 mm core diameter). This would preclude down-hole logging, to this level, but it was clear from the mud loss and the washing needed on several occasions to get the inner tube back to the bottom of the hole that withdrawing the drill pipe to above 120 mbsf would lead inevitably to collapse and loss of the hole.

During the day of October 23 the drillsite team noted movement between the tensioned sea riser anchored into the sea floor and the drill rig on the floating sea-ice platform. This movement was attributed to sea swell travelling through the sea-ice platform. It ranged from short period (10-12 seconds) to less regular longer periods of 25+ seconds and was accompanied by increasingwinds. Later during this shift and into the following "night" shift the larger long period movement caused uneven bit pressures during coring and obvious fracturing of the recovered core. The Science Support Manager advised that the maximum safe limit for vertical ice movement was 30 mm for the short period movement (see Sea-Ice Observations section). Measurements were taken regularly, and in the early morning of the 24th, with swellsconsistentl y exceeding the limit and high winds prevailing, the Science Support Manager advised that personnel should be evacuated from the rig. The storm continued through the day, but a party was able to reach the rig for refueling in winds exceeding 50 knots.

On the morning of October 25, the storm had abated, and the weather was clear and calm. A helicopter reconnaissance by the Project Manager and Science Support Manager revealed that extensive fast ice had broken out to the east and south of the drill site, leaving the rig within 1 km of the new ice edge. Plans were then made for immediate recovery of the rig and other equipment at the site. Before the recovery operation began, the drill team was able to tag the bottom of the hole and rotate the drill string, indicating that the hole was still in good condition. Almost all of the equipment was back at Cape Roberts within 24 hours. The sea riser was also recovered in subsequent days, apart from the sea-floor guide base and 18-m section cemented into the sea floor.

This account is essentially a lay summary of events for this *Initial Report*. For a technical and authoritative account the reader is referred to the Drilling Manager's Report to the Cape Roberts Project Manager, Antarctica New Zealand. Matters relating to the sea ice are addressed in more detail in the Science Support Manager's Report, and in an article to be prepared for the *Scientific Report.*

CORE PROPERTIES

FRACTURE ARRAYS IN THE CRP-1 CORE

Introduction

Complementary studies of fractures in the core and in the borehole walls were designed to determine the stress field history, including the contemporary stress directions, associated with rifting along the structural boundary between the Transantarctic Mountains and the adjacent Victoria Land rift basin at Cape Roberts. This boundary appeals to have been reactivated during the multiple rift phases which occurred within Antarctica during progressive breakup of the Gondwana supercontinent, although age constraints on the timing of structural movements are few. A well-dated structural record of the kinematic and dynamic history along the Transantarctic Mountains Front can be obtained from fracture analysis of strata cored by the Cape Roberts Project, potentially spanning the major part of the rift history. Because rocks of suitable age are not exposed on outcrop in Antarctica, an age-controlled post-Jurassic fracture record can only be obtained from drilling the basin strata.

For the CRP-1 drillhole, only the core fracture studies were completed. Fracture logging of core was used to map natural fractures yielding kinematic and palaeostress information and to identify any induced fractures that may reflect the in *situ* stress field. Natural fractures are those present in the rock prior to drilling and intersected during coring. Induced fractures form in response to drilling- or coring-related perturbations of the stress field, or due to subsequent handling of the core. Fractures were abundant throughout the CRP-1 core, averaging 5 fractures/m. Although surface kinematic/dynamic indicators were sparse, these data together with morphologic and geometric characteristics of the core fractures allow us to make a preliminary interpretation of key fracture types. Natural microfault and fracture arrays and clastic dykes are present. Induced fractures include petal and petal-centreline fractures, potentially indicative of in *situ* contemporary stress directions, disc fractures, and subhorizontal fractures formed due to sea swell-related influences on the drilling process (see Coring History section).

Fracture Study Procedures

The whole core prior to splitting was systematically logged for fractures, which were numbered sequentially downward from core top. Depths to the top and base of each fracture were recorded. Fracture attitudes (dip and dip direction) were measured with respect to an arbitrarily placed red line scribed along the length of the core. Logging included observations on fracture morphology, fracture surface features, and fracture terminations, cross-cutting and abutting relations. Features of special interest were photographed or scanned. Procedures for logging fractures in cores and criteria used for distinguishing natural and induced fractures generally followed Kulander et al. (1990).

Initial plans called for scanning the circumference of the entire core using the CoreScan® equipment leased from DMT, Germany. The CoreScan® obtains digital images by rotating the whole core on rollers, scanning segments up to 33 cm in length, and digitally joining these segments into 'unrolled' core images a maximum of 100 cm in length. The 1 m coie scans were then digitally joined into core runs using the Corelog® software provided by DMT. Due to the poor induration of coie material, it was not possible to do whole-core scanning of most of the interval 16-95 mbsf. The subsequent coie interval 95-147 mbsf was scanned with the exception of highly fractured intervals, resulting in multiple short gaps in the whole-core scan records. The slabbed face of the entire working half of the core was also scanned after placement in the core boxes. Note that, due to evacuation of the drillsite lab with processed coie material, the archive half of the core had to be scanned for Boxes 35, 36, and 37.

The fracture measurements made on the core were entered into DMT's Teclog® software to generate plots of fracture attitude, type (where known), and fracture density. In addition, a utility in the Corelog® software was used to digitize structures from the 'uniolled' whole-core scans and to produce plots of fracture attitude and type *vs.* depth for each core iun. These plots were used to check hand-measured orientations and to identify additional, handling-induced fracture planes.

In CRP-1, the instability of some sections of the borehole precluded using an orienting tool (designed by Alex Pyne at Victoria University of Wellington) to directly orient core runs. Borehole instability and the early termination of drilling prevented downhole logging with dipmeter and borehole televiewer tools. Fracture mapping from these oriented downhole log records would have been used to orient the cores by matching borehole wall and core fractures *(cf.* Nelson et al., 1987); in particular, matching the borehole televiewer images of the borehole walls with the whole-core scan images provides a robust method of core orientation *(e.g.,* Schmitz et al., 1989; Weber, 1994). In the absence of these data, several means of determining core orientation are being explored. In some segments of core it was possible to obtain direct measurements on bedding and/or cross-bedding, and these can be oriented to match seismically-determined regional dip. Where successive core runs fit together, sections of core up to ~10 m in length can be oriented from bedding dip direction. Additional data on bedding dip will be obtained from the whole-core and slabbed-core scan records and used to orient larger intervals of the core. Core sections lacking bedding may be oriented by matching distinct fracture sets with consistent orientations with oriented core runs. This approach may constrain the general orientation of most of the core. In addition, it may be possible to use palaeomagnetic inclination vectors to orient portions of the core. Until these further analyses are carried out, however, the fracture data presented represents orientation only with respect to an "arbitrary north" defined by the red scribe line, which differs between core runs.

Fracture Distribution and Density

Fractures occurred in all portions of the core except for unlithified sand intervals. Fracture density, plotted as fractures/m, is shown in figure 9. Note that breaks in the histogram with no fractures reflect intervals where no core was recovered. Fracture densities in the Quaternary section average 1.5 fractures/m and range from 1-2 fractures/m. In the Miocene section, fracture densities range from 1-15 fractures/m and average about 6 fractureslm. The marked increase in fracture density across the contact between Quaternary and Miocene strata is only partly attributable to increased induration, as much of the upper Miocene section is also quite poorly indurated, and it appears that the Miocene interval has been more intensely deformed. Although fracture density varies between lithologic units, suggestive of mechanical differences between rock types and/or induration, our preliminary comparison of fracture density vs. lithology does not reveal any consistent relations at this whole-core scale. The marked increase in fracture density near the base of the core coincides with a major storm period when the vertical oscillation of the drill bit due to the sea swell was repeatedly breaking the core.

Fracture Types

Unambiguous natural fractures in the CRP-1 core include microfaults which offset bedding, vein fill, and clastic dykes. Probable natural fracture sets have been inferred based on geometry and a very sparse set of fracture surface features. The absence of well-developed surface features likely reflects the poorly indurated nature and medium/coarse grain size of much of the core material, since delicate sin face features are best developed in highly indurated, fine-grained materials *(e.g.,* Kulander et al, 1979).

In the CRP-1 core, microfaults occur in 2 distinct intervals of well-laminated sandstone at 65-70 mbsf and 109-116 mbsf. With one exception, the faults have normal offset of bedding. At around 66 mbsf a well-developed set of conjugate normal microfaults is present (Fig. 10) Fault dips range between 55 and 70 degiees and the faults have curved, listric profiles. Bedding offsets range from 2-6 mm.

Clastic dykes occur in the core at 133.30 and 139.05 mbsf The dykes injected diamictite, are made of sand, are planar with sharp boundaries, and have a thickness of approximately 1-2 cm. Both dykes dip at 77 degrees (Fig. 11). Indentation of lonestones into the dyke margins due to compaction attests to the soft state of the material during and after injection of the sand dykes. A vein occurs at 112 mbsf with a pull-apart opening across the surface of 1-3 mm and a fill that appears to be fine clastic material(?)

Fractuie surfaces with moderate to steep dips between –45-80 degrees are common in the CRP-1 fracture array

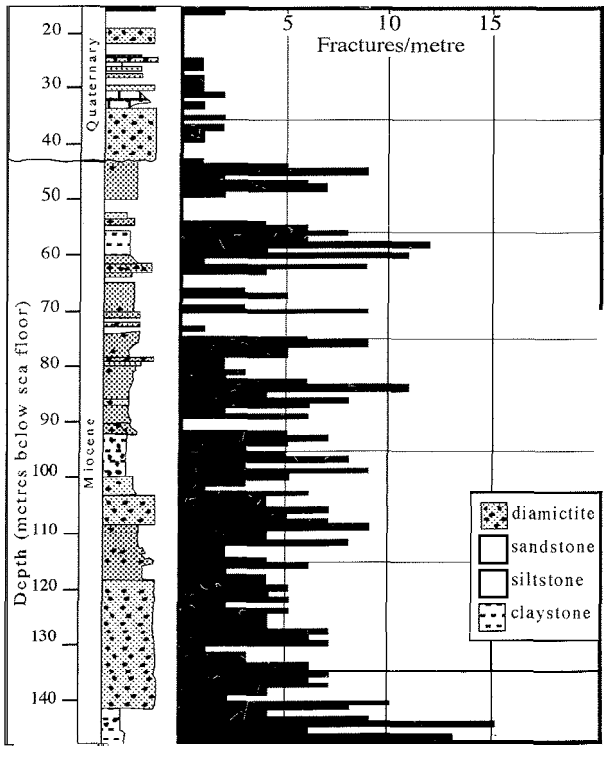

Fig. 9 - Fracture density plot showing the number of fractures per metre with relation to depth and lithologic and age boundaries within the CRP-1 core. Note the increase in fracture density across the Quaternary/ Miocene boundary and also at the bottom of the CRP-1 core where fractures were induced during drilling due to the influence of the sea swell from a storm. Stratigraphic column modified from figure 18.

Fig. *10* - Corescan® image of conjugate normal microfaults within sandstone in slabbed CRP-1 core at 66 mbsf. Horizontal width of core is 6.1 centimetres and vertical length is 18.5 centimetres.

Fig. 11 - Corescan® image of a high-angle clastic dyke on the 'unrolled' circumference of the ("RI'-1 core from 139.05 to 139.22 mbsf. While dashed lines mark planar dyke margins. The steeply-dipping dyke appears as a high-amplitude sine wave on the 'unrolled' core surface. The arrow points to compaction-related indentation of a lonestone into the dike margin.

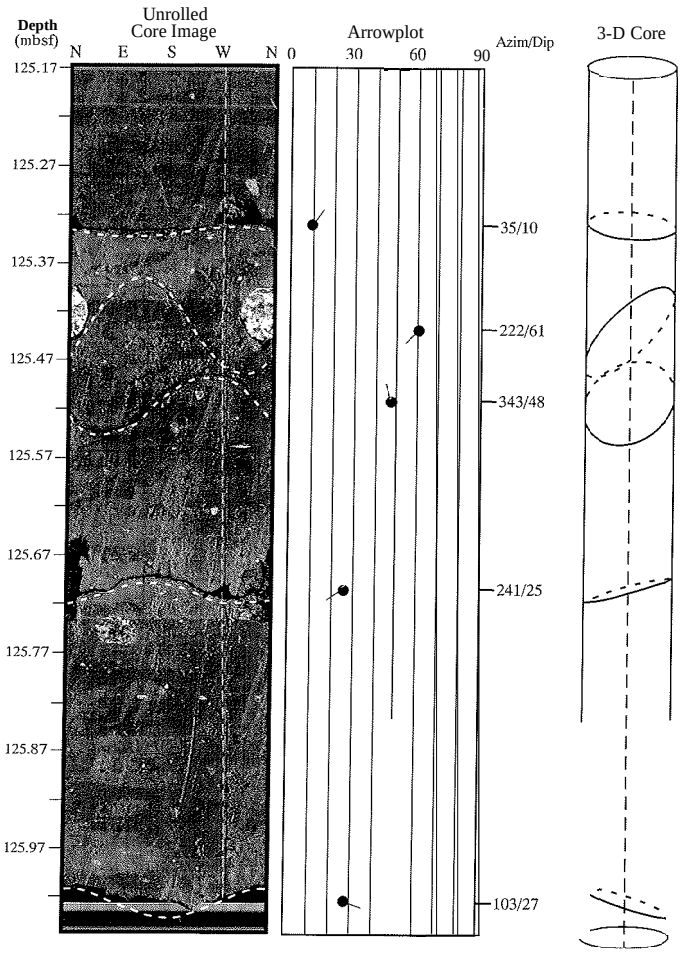

Fig. 12 - Corescan® image and Corelog® structural plot of a typical fractured interval in CRP-1 core, containing populations of subhorizontal/low angle and moderately dipping fractures (marked by dashed white lines on 'unrolled' core surface image). The vertical line on the core image is the scribe line defining an arbitrary 'north'referencelineforfractureattitudemeasurements. The 'tails' in the arrowplot show fracture dip direction with respect to this reference line and this line is shown as the vertical, dashed reference line in the '3-D Core' plot.

(Fig. 12). Such dips are atypical of fractures induced by stresses related to drilling, coring and handling. Several factors arc consistent with these fractures being pre-existing fracture planes. Based on this evidence and their apparent incompatibility with induced fracture geometries, we tentatively interpret them as natural fractures.

Avariety ofdrilling-, coring- and handling-related stresses can cause fractures and these breaks can have characteristic patterns related to in situ stress conditions. Several distinct types of fractures in the CRP-1 core were definitely or very likely induced during drilling and coring.

Petal and petal-centreline fractures form in response to stress induced beneath the advancing drill bit, thus originate outside of the core boundaries and have curved forms that follow the induced stress trajectories (Kulander et al., 1990). Curviplanar fractures that terminate within the core occur at 29.65 mbsf within the Quaternary section and throughout the Miocene strata to the base of the CRP-1 core. Although these fractures lack the distinctive surface plumes and arrest lines reported by Kulander et al. (1990), the fact that they curve into the core margin (Fig. 13) and terminate within the core shows that they are induced fractures. The distinctive curviplanar form and the position of the steep 'centreline' portion following the vertical core axis (Fig. 13) are diagnostic characteristics of petal-centreline fractures (Lorenz et al., 1990). Theincrease in occurrence of fractures with petal-centreline morphology during storm periods when sea swell and resultant vertical motion caused variation in drill bit weight at the base of the borehole is consistent with the genesis of petal-centreline fractures (Kulander et al., 1990; Lorenz et al., 1990).

Disc fractures are fractures normal to the core axis that generally form in regions of high horizontal stresses. Subhorizontal to low-angle (<30 degree dip) fractures are very abundant in the CRP-1 core (Fig. 12). Many of these fractures were lined with drilling mud or associated with microfractured rubble zones probably induced by drilling, indicating that they are either natural fractures or induced during

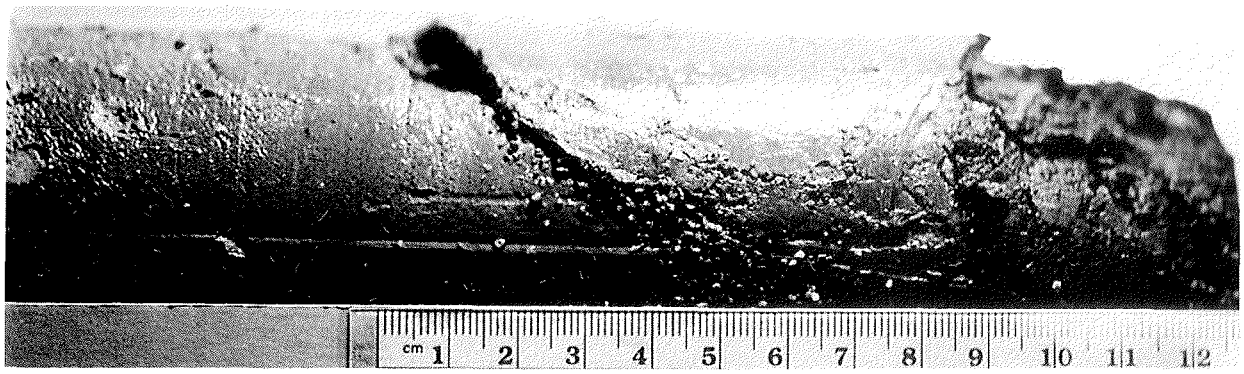

Fig. 13 - Photograph of a petal-centreline fracture at 29.7 mbsf within the Quaternary section of the CRP-1 core. Note diagnostic curvature inward and down-core axis from core margin. Horizontal length of core is 17.5 centimetres.

drilling or coring when drilling mud had access to the fracture planes. One such fracture had an origin point on the fracture surface indicating nucleation at a lonestone, proving an induced, tensile fracture origin. Low-angle fractures followed bedding or cross-laminae in many cases. A proportion of the subhorizontal/low-angle fracture set may represent disc fractures, in part localized by bedding anisotropies.

Another population of subhorizontal fractures formed due to vertical motion of the drill string, when the drill bit rose and 'plucked' a segment of core from the base of the borehole. Subsequent spinning of the core segment as the drill bit re-engaged is shown by the exquisitely developed circular lines and grooves on these fracture surfaces (Fig. 14). The marked increase in fracture density near the base of the cored interval (Fig. 9) is due to the development of these fractures during the storm that resulted in the early termination of drilling.

Handling-induced fractures of many varieties developed during core processing and transport. Some such fractures mimic the geometry of the fractures previously described and may have nucleated on incipient drilling- or coring-induced fractures that had not propagated completely through the core. Much of the fracturing visible in the boxed core was due to collapse of round core in the flat trays as the boxes flexed during transport.

Fig. 14 - Photograph of the surface of a typical drilling-induced, horizontal fracture that developed near the base of the CRP-1 core (144.2 mbsf). The core was broken and spun due to sea swell-induced vertical motion of the drill bit, resulting in the finely etched circular grooves and striae. Core is 6.1 cm in diameter.

Brecciation of Core Material

In addition to the discrete fracture planes that occur throughout the core, significant portions of the core material have a brecciated texture indicating another mode of deformation of the section. Weakly developed brecciation first appears in the Quaternary(?) section at approximately 40 mbsf. The uppermost section of Miocene strata is extensively brecciated, down to approximately 50 mbsf. Additional brecciated intervals from 10-80 cm thick occur sporadically down to about 84 mbsf. Brecciated textures have not yet been studied in detail, but some characteristics can be summarized at this point. Most of the breccia is characterized by a 'jigsaw puzzle' fabric in which little or no motion has occurred between clasts (Fig. 15). Clast shapes range from sharply angular to subrounded and clasts themselves are all the same material as the surrounding in situ rock. Irregular, but generally steeply inclined, zones of brecciation occur in which the microcrack network is filled with pale, fine-grained material. Lack of clast transport, of any extraformational clasts, and of any sign of shearing such as striae or slickensides, suggest that these are not tectonic breccias associated with faulting. Instead, an in *situ* brecciation process, perhaps related to hydrofracturing of the core under elevated pore fluid pressure conditions, seems a more likely genesis for the brecciated intervals.

Interpretation of Fractures and Stress Regimes

Detailed interpretation of the types of deformation and stress regime(s) associated with the fracture populations in the CRP-1 core must await further data that will allow orientation of all or parts of the core. However, several important points can be made at this stage.

The microfault arrays have a conjugate geometry and offset sense which demonstrate a vertical maximum compressive stress during deformation, and this deformation regime must be younger than ~18.5-20.5 Ma. The high-angle clastic dykes in the core are also consistent

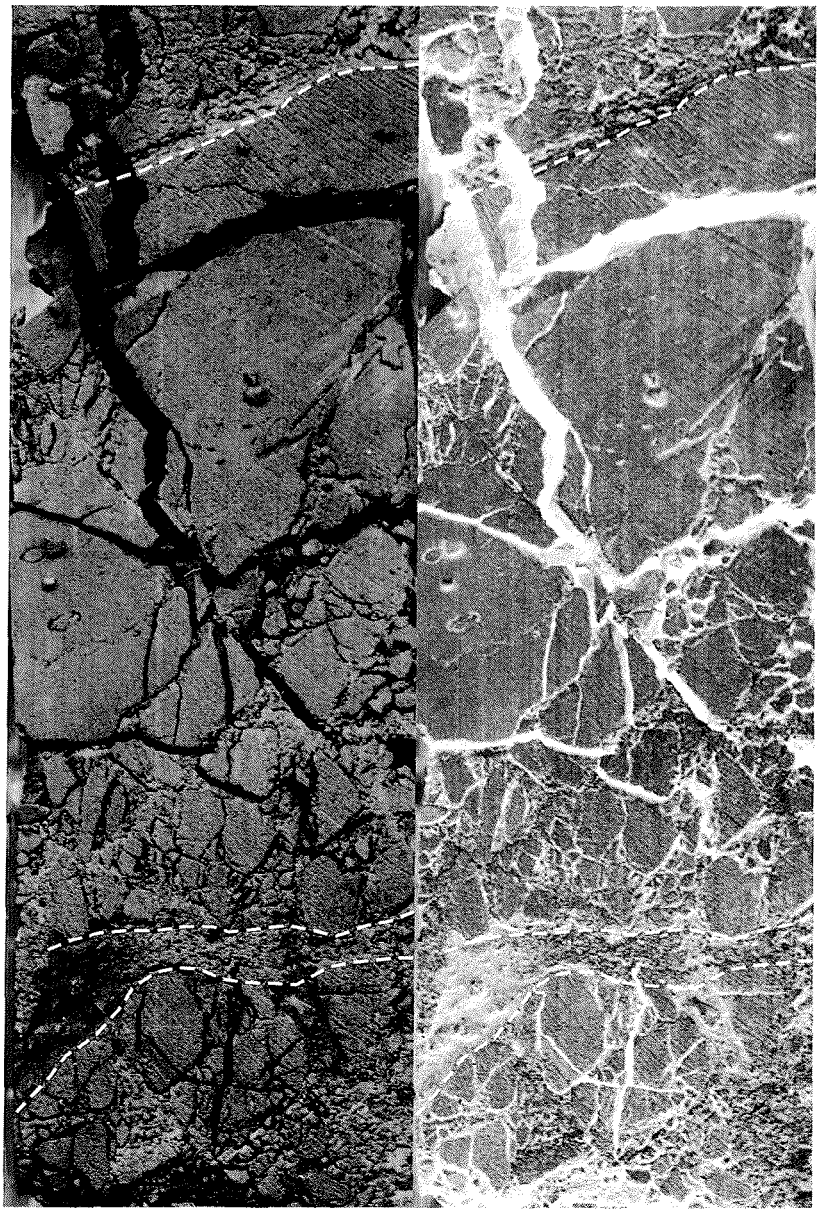

Fig. 15 - Corescan® image of brecciation textures in slabbed CRP-1 core at 50.00 to 59.10 mbsf. The right-hand image is a negative image of the left-hand side, emphasizing the 'jigsaw puzzle' fit of the fragments and minimal relative movement between clasts. White dashed lines outline deformed surfaces (bedding?) marked by changes in clast size in the brecciated material.

with this stress orientation. A stress regime with vertical maximum compressive stress is characteristic of a continental rift regime and these structures may reflect tectonic deformation of the Cape Roberts region. Alternatively, aglacial load may have imposed thevertical compression responsible for these structures.

The mode of formation of breccias within the core needs to be further investigated. If brecciation proves to be related to hydrofracturing, high fluid pressures in a subglacial environment may be a likely setting for deformation. This in turn may provide constraints on the deformation regime responsible for development of faults and fractures throughout the core.

The presence of petal-centreline fractures is very significant, as this fracture type may mark the orientation of the in *situ* stress field, having strikes that parallel the regional maximum horizontal stress direction (Plumb & Cox, 1987; Lorenz et al., 1990). The petal-centreline fractures in the CRP-1 core occur in strata of both Quaternary and Miocene age and are clearly neotectonic, induced fracture sets. This demonstrates that, when core orientation is available, it will be possible to place the first constraints on the contemporary stress regime along the Transantarctic Mountains Front.

PHYSICAL PROPERTIES

Methods

Drill Site laboratory work for CRP-1 included non-destructive, near-continuous determinations of Wet Bulk Density (WBD), P-wave velocity and magnetic susceptibility in 2 cm intervals. The Multi Sensor Core Logger (MSCL, Geotek Ltd., UK) was used to measure core temperature, core diameter, P-wave travel time, gamma-ray attenuation and magnetic susceptibility.

Magnetic susceptibility was measured in terms of SI units (m, kg, J). Data are corrected for loop-sensor and core diameter as follows:

magnetic susceptibility (10^{-5} SI) =
measured value (10^{-5} SI) / K-re1

K-re1 is a sensor-specific correction calculated from the diameter of the core over the diameter of the loop sensor according to the correction instructions for the Bartington MS2 sensor systems (Tab. 6).

P-wave velocities were calculated from the core diameter and travel time after subtraction of the travel time through the transducer caps (P-wave travel time offset, Tab. 6). The arrival time of the P-wave pulse is detected using the second zero-crossing of the received waveform. Resulting P-wave velocities are normalized to 20°C using the core temperature logs.

The gamma detector is calibrated using aluminum, carbon and nylon of known densities. Quantification of Wet Bulk Densities was carried out according to the following formula:

$$WBD = a + b * (1/-p* d) * \ln (I/Io)$$

a, b: system-specific variables to correct for count-rate dependent errors as described by Weber et al. (1997);
d: core diameter;
μ: specific attenuation coefficient for gamma rays;
ln (I/Io): natural logarithm of the ratio of attenuated (sample) over nonattenuated (air) gamma counts per second.

Porosity is calculated from the WBD as follows:

$$POR = (dg - WBD) / (dg - dw)$$

dg: grain density = 2.65 g cm^{-3};
dw: pore-water density = 1.024 g cm^{-3}.

The technical specifications of the MSCL system are summarized in table 6.

Stratigraphy Based on Physical Properties

Based on the results of the whole-core logging, there are six major units in the CRP-1 core. These units are defined in terms of both the level and scatter of amplitudes of magnetic susceptibility, P-wave velocity and porosity Magnetic susceptibilities range on a large scale from nearly 1 to more than 1 000 (10^{-5} SI, Fig. 16) so that the data are plotted on a logarithmic scale. The log of P-wave velocity is discontinuous because no results were obtained in fractured and unconsolidated sections of the core.

Unit *PP1*, which extends from the top of the core to 31.89 mbsf, is defined by relatively high magnetic susceptibility, low P-wave velocities and, on average, porosities well above 0.5. There is a relatively large degree of scatter observed in the data, in particular in the porosity log. This includes a few exceptional data points of very low porosity. The unit also includes a large boulder of dolerite located at the top of the core, which is characterized by high magnetic susceptibility (up to 790), P-wavevelocity near 6 000 ms^{-1} and a porosity of 0.

Unit PP2 (31.89 to 63.20 mbsf) exhibits lower magnetic susceptibilities (mostly below 100), P-wave velocities between 1500 and 2000 ms^{-1} and relatively high porosities similar to Unit PP1. Porosities peak in the middle part of the Unit PP2 at nearly 0.8 where no P-wave results were achieved. The entire unit is characterized by the highest degree of scatter in the physical properties data of the entire CRP-1 core. The boundaries at the top and bottom of Unit PP2 are sharp.

Unit PP3 (63.20 to 92.19 mbsf) is defined by the lowest magnetic susceptibilities measured in the core. P-wave velocity is well above 2 000 ms^{-1} and porosity gradually decreases from about 0.5 to 0.35. Also, there is remarkably little scatter in the data as compared to the units above. The physical property logs appear to be cyclic in both the magnetic susceptibility and porosity logs.

Unit PP4 (92.19 to 103.41 mbsf) is characterized by a sharp increase of magnetic susceptibility at the top of the unit to more than 100 (10^{-5} SI), whereas the general pattern of P-wave velocity and porosity remains similar to the overlying Unit PP3.

Unit PP5 (103.41 to 141.60 mbsf) is defined by a relatively sharp downcore increase of P-wave velocities to values well above 3 000 ms^{-1} and a decrease of porosity to 0.2.

Tab. 6 - Specifications for Multi-Sensor-Core Logger MSCL-25.

P-wave Velocity and Core Diameter	
Transducer diameter	5 cm (7.5 cm including transducer caps)
Transmitter pulse frequency	500 kHz
Transmitted pulse repetition rate:	1 kHz
Received pulse resolution	50 ns
P-wave travel-time offset	21.85 μs
Wet Bulk Density	
Gamma ray source	Cs-137
Source activity	356 MBq
Source energy	0.662 MeV
Collimator diameter	5 mm
Gamma detector	Scintillation Counter (John Count Scientific Ltd.)
Magnetic Susceptibility	
Loop sensor type	MS-2B (Bartington Ltd.)
Loop sensor diameter	S cm
Alternating field frequency	0.565 kHz
Magnetic field intensity	approx. SO A/m RMS
Loop sensor correction coefficient K-re1	1.45

Similar to the above Units PP3 and PP4, the downcore variation of all three physical parameters appears somewhat cyclicalthough Unit PP5 is characterized by an increase in data scatter compared to the overlying unit. In particular, there is a relatively high amount of scattered data points indicating very high magnetic susceptibility (>1 000 10^{-5} SI), P-wave velocity (>6 000 ms^{-1}) and very low porosity (<0.2) in some narrow intervals of Unit PP5. Also, between about 108 and 115 mbsf and near the bottom of Unit PP5 there are two layers of relatively high porosity (>0.4).

Unit PP6 (141.60 to 147.69 mbsf) exhibits a significant downcorc gradient back to higher porosities (up to about 0.55) and lower P-wave velocities (2 000 ms^{-1}). Magnetic susceptibility scatters between 10 and 100. The physical properties of Unit PP6 appear to be somewhat similar to that of Unit PP4, although the magnetic susceptibility is lower in PP6.

Discussion

All unit boundaries of the physical properties match boundaries in the lithostratigraphy. The lower boundary of PP1 coincides with the boundary between lithostratigraphic Units 2.3 and 3.1. The base of PP2 correlates with the boundary between 5.3 and 5.4. Unit PP4 is equivalent to 5.8 in the lithostratigraphy. The unit boundary of PP5 to PP6 is linked to the transition from lithostratigrahic Units 6.3 to 7.1.

In general, it appears that the higher degree of scatter in the physical property data is mostly observed in units containing diamicts. In particular, large lonestones cause high to very high P-wave velocities and very lowporosities. Major units of diamictites such as the lithostratigraphic Units 2.1, 4.1, 6.1 and 6.3 are all characterized by a high degree of data scatter. Lonestones are much less abundant in the middle (Units 5.1 to 5.8) and the lowermost part of the core (Unit 7.1), where a lower degree of data scatter is observed in the physical properties. This would imply that the degree of data scatter, particularly in the P-wave and porosity logs, is a reflection of distance from the ice margin as interpreted from the sedimentological evidence (see Quaternary and Miocene Strata, this volume -section on Facies Analysis). The physical property Units PP1 and PP2 as well as PP5 would then be more proximal glaciomarine, and Units PP3, PP4 and PP6 more distal glaciomarine.

It is interesting to note, however, that there is no significant change in the physical properties at the major unconformity in the core, which is located at about 43.55 mbsf in the upper part of Unit PP2. This may be at least partly explained by the fact that the physical property data in Unit PP2 are more strongly affected by poor core quality than in other parts of the core. Major parts of this section are fractured or unconsolidated. This also caused the large gaps in the P-wave log because no P-wave signal was recorded. In particular, the very high porosities in Unit PP2 of more than 0.7 are unlikely for unconsolidated sands observed at that depth. This may be explained in terms of artifacts from the drilling operation such as mixing of the sands with the suspended drilling mud. It is, therefore, likely that the physical properties in the lower part of Unit PP2 have been somewhat altered. Thus, the

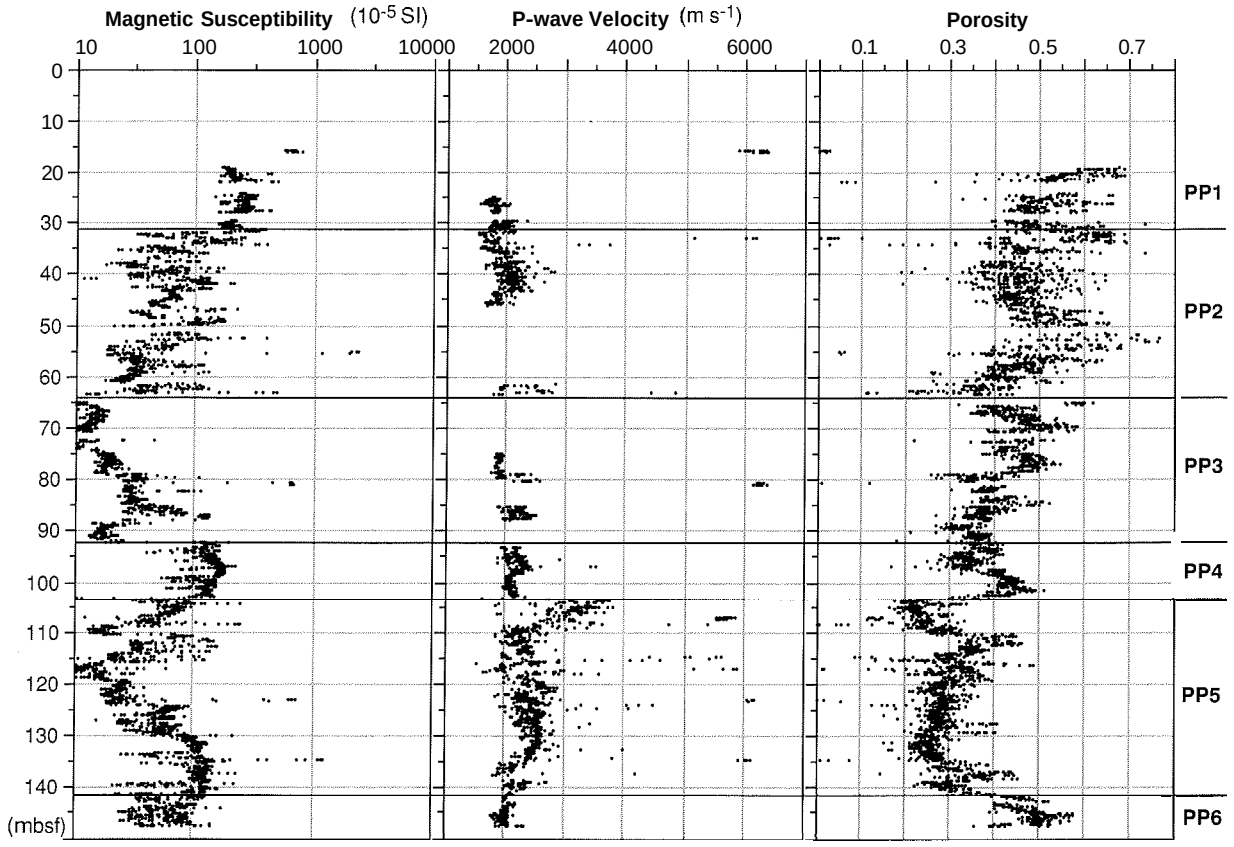

Fig. 16 - Logs of whole-core physical properties and physical property Units PP1 to PP5 in core CRF-1

unconformity between the lithostratigraphic Units 4.1 and 5.1 may be masked in the dataset.

On the other hand, there is a very good coincidence between the increase in magnetic susceptibility and the increase in volcanic debris in the core (see Miocene Strata, this volume - section on Sand Grains and Provenance) above the lower boundary of Unit PP2, which suggests major changes in the geological record controlled by changes in the palaeo-environment rather than artifacts at this boundary. In marine sediments, changes in susceptibility are normally controlled by variation in the content of magnetite. Magnetite has a significantly higher susceptibility ($k = +10^{-2}$) than most common minerals (-10^{-6} to $+10^{-6}$) and is more abundant in volcanic rocks and ashes. Higher magnetic susceptibilities in the upper part of the core (Units PP1 and PP2) may then reflect higher volcanic activity and, subsequently, deposition of volcanic debris at the drillsite superimposed on variation of marine and glaciomarine sedimentation.

In terms of the acoustic behaviour of the rocks, there are two major boundaries seen in the physical property logs. (i) The steep gradient of downcore increase of P-wave velocity combined with a decrease in porosity defines a strong change in acoustic impedance at the top of the diamictite at about 103 mbsf. If resolved in seismic profiles this horizon will create a relatively strong reflector. (ii) A similar strong, but reverse, gradient in porosity and P-wave velocity is seen at the transition between the mudstones of lithostratigraphic Unit 7.1 (PP6) and the overlying diamictite of Unit 6.3 (PP5). The resulting impedance contrast would imply seismic reflection with strong negative peaks in the wavelets, if the mudstone unit is thick enough to be resolved in seismic sections.

In summary, there is a lot of coincidence between the physical properties and other results from the CRP-1 core Major changes in the lithology can be traced using the physical properties. Magnetic susceptibility seems to Insignificantly influenced by the content of volcanically derived material. These correlations will be clarified after additional corrections are applied to the data during final data processing. These include calibration of the whole core data using results from plug samples, correction for overburden pressure release, correction of possible errors in the detection of P-wave travel time-onsets, corrections for detector drift and temperature effects on the magnetic susceptibility and correction for drift of the gamma detector.

ESTIMATED DEPTH TO BASE OF V3

Measurements of P-wave velocities were used to calculate a two-way travel time log for the CRP-1 core site (Fig. 17) in order to estimate the base of the V3 seismic unit. Unrealistic data points, probably caused by poor core quality, were removed from the P-wave velocity log. However, there may still be some errors in the data because, for very low amplitude levels on the receiver side, the Geotek system has difficulties detecting the arrival time of the P-wave pulse correctly. This error may be up to +/- 20% for some data points if the detection is affected by a negative or positive offset of one wavelength on the received P-wavelet. It is assumed, however, that this error would largely smooth out, if the 2-way travel time is calculated for each individual depth interval between 2 data points and then summed up (Fig. 17). For larger gaps in the data set, the P-wave velocity was estimated on the basis of the average velocities measured in the underlying or overlying units.

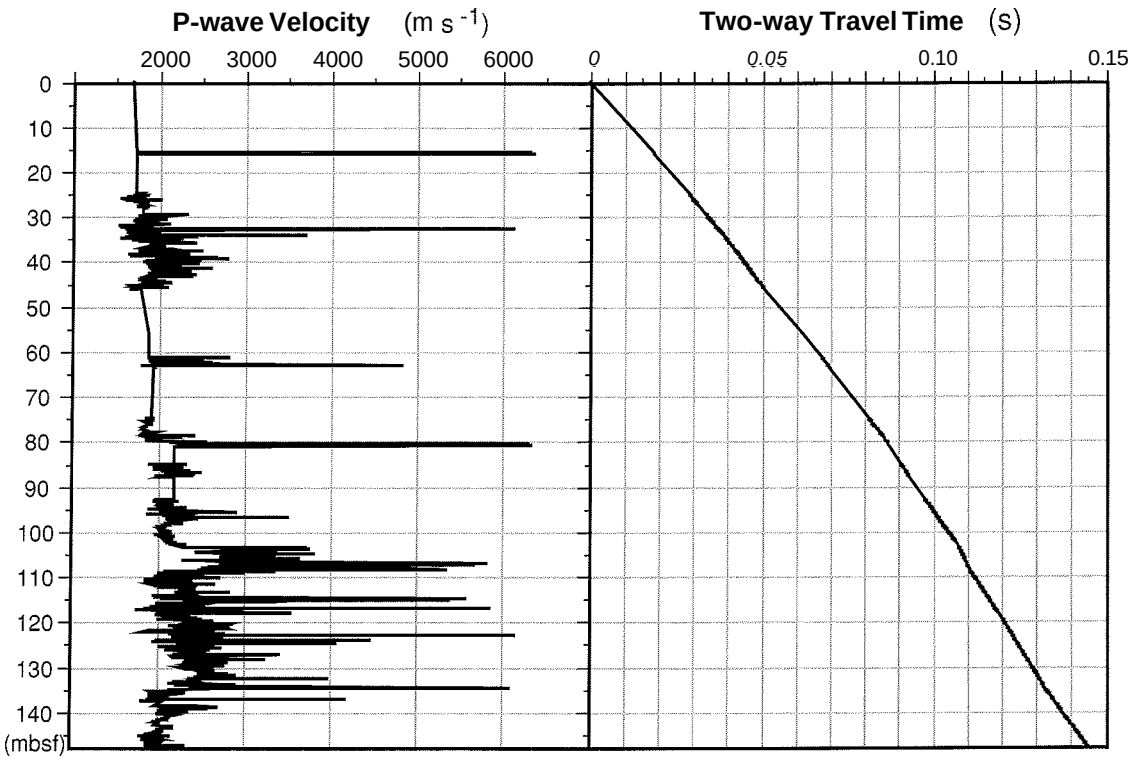

Fig. 17 - Continuous P-wave log (left) used to calculate the two-way travel-time sum log (right) of the CRP-1 core.

For the total length of the core, a two-way travel time of nearly 0.15 s is determined. The two major reflections, which are suggested from the impedance contrast of the physical properties record to be at 103 and 140 mbsf (the transition from lithostratigraphic Units 5.8 to 6.1 and from Units 6.3 to 7.1), reveal two-way travel times of 0.107 and 0.137 s, respectively. Since the mudstone of Unit 7.1 has a lower velocity and lower density than the overlying diamictite, a negative amplitude peak should result for acoustic reflection from the top of this layer. Indeed, in the seismic line across the CRP-1 drill site a relatively strong negative amplitude is present at a travel time of about 0.14 s which forms the V3/V4 boundary. Therefore, it is suggested that this reflector corresponds to the top of lithostratigraphic Unit 7.1 at 141.5 mbsf. This correlation is supported by the fact, that above the V3/V4 boundary a very strong positive reflection amplitude is seen which can be explained by the impedance contrast in the core at the top of the diamictite at 103 mbsf (0.107 s two-way travel time, respectively). However see Correlation of Seismic Reflectors below.

STRATIGRAPHIC SUMMARY

The stratigraphy of CRP-1 has been presented at three levels: 1:5, 1:20 and 1:500. In this section of the report, the core is described according to logs at a scale of 1:500 (Pig. 18). Logging of the core revealed two main depositional intervals, for which provisional ages of Quaternary and early Miocene have been obtained, largely on the basis of diatom taxa. The two intervals are described in separate articles in this volume.

The Quaternary section (15.00-43.55 mbsf) is distinguished from that of the Miocene in being largely unconsolidated. The boundary is unclear because the core is heavily fractured at this position and the critical boundary was not recovered during drilling. However, diamicton lies above the boundary and sandstone below. Although the drilling operation was not designed to sample unconsolidated sediments, as much as 68% recovery was achieved. Four lithostratigraphic units (1, at the top, to 4) have been identified, with lithostratigraphic Unit 2 being further subdivided into three subunits.

The Miocene section (43.55 mbsf - base of hole at 147.69 mbsf) comprises largely lithified strata. The boundary is taken at the top of a fractured sandstone interval. Recovery of the upper part of the core (around 70%) was little better than that for the Quaternary on account of brittle fractures that pervaded much of the core, and also occasional loose sand layers. Three major lithostratigraphic units (5-7) have been identified, two of which are further subdivided into subunits. The lithostratigraphic units and their principal lithologies for the whole core are as follows:

Quaternary

Unit 1.1, 0.00-19.13 mbsf, diamicton (little recovery)
Unit 2.1, 19.13-22.00 mbsf, diamicton
Unit 2.2, 22.00-29.49 mbsf, sand
Unit 2.3, 29.49-31.89 mbsf, diamicton
Unit 3.1, 31.89-33.82 mbsf, muddy packstone
Unit 4.1, 33.82-43.55 mbsf, diamicton

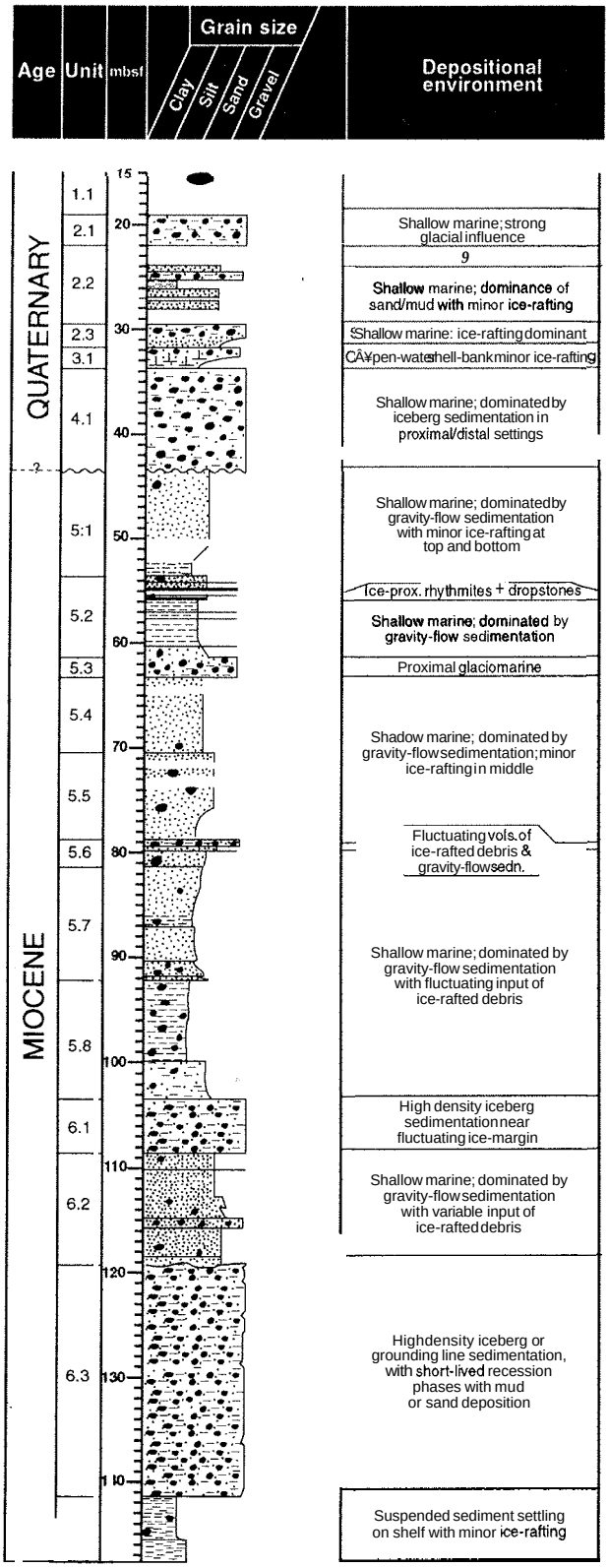

***Fig.** 18* - Graphic log summarising the lithology and lithostratigraphic subdivision of CRP-1.

Miocene

Unit 5.1, 43.55-53.70 mbsf, sandstone
Unit 5.2, 53.70-61.51 mbsf, interbedded siltstone, diamictite and breccia
Unit 5.3, 61.51-63.20 mbsf, diamictite
Unit 5.4, 63.20-70.28 mbsf, sandstone
Unit 5.5, 70.28-78.85 mbsf, sandstone and claystone

Unit 5.6, 78.85-81.16 mbsf, sandstone and siltstone
Unit 5.7, 81.16-92.19 mbsf, siltstone and sandstone
Unit 5.8, 92.19-103.41 mbsf, mudstone
Unit 6.1, 103.41-108.76 mbsf, diamictite
Unit 6.2, 108.76-119.28 mbsf, sandstone
Unit 6.3, 119.28-141.60 mbsf, diamictite
Unit 7.1, 141.60-147.69 mbsf, mudstone

CORRELATION OF SEISMIC REFLECTORS WITH CRP-1

The CRP-1 drillhole sampled only strata above the V3/V4 boundary (Fig. 5). Seismic data indicate that the drillhole finished about 15 m above the boundary, although a major lithological change (diamictite to mudstone) was sampled about 6 m above the base of the hole. This change was taken as the V3/V4 boundary in the Core Properties section above, but on the basis of the limited thickness of the lowest mudstone unit and the discrepancy in depth between the lithological change and the interpreted V3/V4 boundary, we consider that the boundary was not reached.

Strong reflections are associated with the shallower major diamictite units sampled by the drillhole. In some cases the reflections become stronger down dip of thin diamictite units in the drillcore, suggesting that these may thicken to the east. Near the sea floor, the seismic data indicate scour channels. A weak seismic reflection, inferred to correspond to the base of a channel in the region of the drillhole, corresponds closely in depth with the unconformity marking the base of the Quaternary sediments cored.

CRP-1 lies on seismic line NBP9601-89 (Fig. 5, shot point 2032), a W-E line across Roberts Ridge. Reprocessing of line NBP9601-89 has improved the resolution of the data across CRP-1. CRP-1 reached a depth of 148 mbsf, equivalent to 145 ms twt below sea floor (see Core Properties section). Several seismic events can be identified at this depth or above and can be related to the cored section (Fig. 19). The discussion here will be limited to an analysis of the major units as a detailed linkage is uncertain due to the wavelength of the seismic signal. Further analysis using synthetic seismograms will be carried out for the Research Report.

The drillhole cored almost to the boundary between the seismic Units V3 and V4. A double positive peak (compressive, shown black on the seismic records) corresponding to an acoustic impedance increase, has been interpreted for this boundary (Figs. 5 & 19). This boundary crops out at the base of a step in the sea floor. The drillhole terminates at about 15 ms (15 m) above the V3/V4 boundary (Fig. 19).

Lithostratigraphic Unit 7.1 is the lowest unit in the core. Only 6 m of the unit was sampled before drilling ceased, so it could extend significantly below the base of the drillhole. If Unit 7.1 is thicker than *c.* 10 m, its upper boundary, which corresponds to a high negative acoustic impedence contrast surface (from high velocity in Unit 6.3 (diamictite) to low velocity in Unit 7.1 (mudstone)), should appear as distinct reflector with negative amplitude peak, as seen on seismic data (Fig. 5) just above the interpreted V3/V4 boundary. The age of the sediments from the base of the drillhole is estimated as about 23 Ma (Miocene Strata, this volume - section on Diatoms). This is significantly younger than the age inferred for the V3/V4 boundary (late Oligocene, 30 - 34 Ma). This could imply a very condensed section between the base of drill hole and V3/V4 (15 m in 10 my), and preliminary analysis of paleomagnetic data suggests very low sedimentation rates (Miocene Strata, this volume - section on Palaeomagnetism and Mineral Magnetic Properties), but other explanations seem more likely. There is no indication of any significant wedging out (downlap) of the oldest sediments of V3 on the V3/V4 boundary, which support the concept of a missing lower part of V3 in the Cape Roberts region. If the lowest part of V3 had pinched out, it would have been seen on the seismic data by Cooper et al. (1987), who noted that units V3 and V4 are conformable over most of the VLB. A re-evaluation of the correlation of geology and age of the sediments between CIROS-1 and the Cape Roberts region, on the basis of the seismic data, is plainly needed. Furthermore, if the V3/V4 boundary is about 23 Ma in age, then this has implications for the inferred glacial and tectonic history of the region based on seismic data (*e.g.*, Brancolini et al., 1995). A major unconformity in the Ross Sea at about 23 Ma corresponds in time to major plate readjustments in the Southwest Pacific.

The next shallower seismic unit corresponds to the lithostratigraphic Units 6.1, 6.2 and 6.3 from 103 to 142 mbsf. Units 6.1 and 6.3 are composed of diamictite (Unit 6.2 is sandstone) but only Unit 6.1 has a significantly higher velocity than the adjacent units. The top of the Unit 6.1 appears as a high amplitude positive reflector. The physical properties of Unit 6 are fairly homogeneous. This lack of a major change in properties of unit 6 causes the semitransparent character of its corresponding seismic unit with only discontinuous weak reflectors (one may correspond to the upper boundary of the lower diamictite Unit 6.3).

The overlying seismic unit (60 ms thick) is characterised by continuous, high amplitude reflectors, that dip gently eastwards at an angle of about 2.5°. This seismic unit is correlated with lithostratigraphic Unit 5 (from 43 to 103 mbsf), which is mainly composed of alternations of sandstone with generally low velocity, and thin diamictites with higher velocity. These alternations cannot be detected on the seismic line because their thickness is below the resolution of the seismic data. However, towards the east where the seismic unit thickens, some of the thin diamictites extrapolated along dip correspond to continuous high amplitude reflectors that may represent more expanded sections of the thin diamictites units recognised in the CRP-1 core. The continuity in character of the reflectors of this seismic unit to the east of the drill site CRP-1 suggests that the lithology of the shallow part of this unit is similar to that recognized in the core, although the geometry of the reflectors shows a lower dip.

The upper seismic unit corresponds to the lithostratigraphic Units 1.1 - 4.1 (from 0 to 44 mbsf). It is mostly hidden by the ringing effect of the sea floor, but a weak reflection at 45 ms below sea floor corresponds

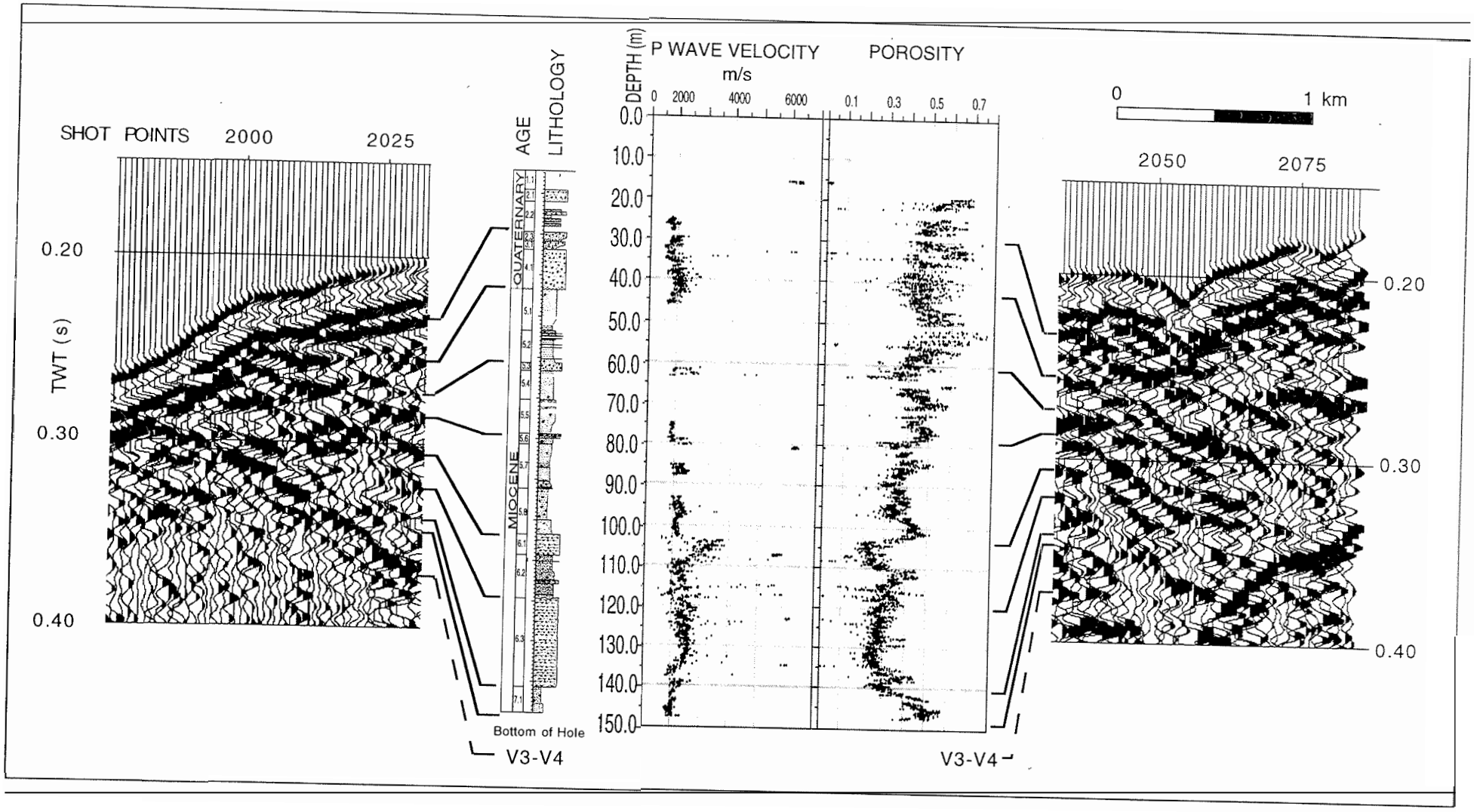

Fig. 19 - Correlation of the CRP-1 results with seismic section NBP9601-89 across the drill site. Core lithology and sequence stratigraphy after section on Stratigraphic Summary, velocity and porosity data after section on Core Properties. Two-way-travel times are converted to depth (velocities after section on Core properties). Seismic section presentation shows positive polarity phases shaded black. Changes in the core properties are linked to the major reflectors (see text).

closely to the the base of Unit 4.1. This discontinuous reflection appears to define a local "cut and fill" or channel geometry, possibly glacial in origin, along most of the seismic lines. A stronger reflection, just discernable through the coda of the strong sea-floor reflection, at about 30 ms below sea floor, may correspond to the top of the diamictite/carbonate Units (2.3 and 3.1) at 30 mbsf.

TECHNIQUES

PALYNOLOGICAL PROCESSING

Introduction

Processing procedures commonly used in palynological research *(e.g.,* Barss & Williams, 1973; Gray, 1965) include: 1) acid digestion of mineral clasts and cements in HCL (to remove carbonates) and HF (to remove silicates) acids, 2) controlled oxidation (to remove organic debris), and the concentration of palynomorphs by heavy liquid separation and /or sieving (Fig. 20). It is evident that sample processing for stratigraphic palynology is relatively complex, compared to that of other microfossil groups, and requires considerable care and skill on the part of the processing technician. It is no overstatement to say that the potential success of any palynological study is determined in the processing laboratory, long before the palynologist scans the first slide (Wrenn, in press).

Consequently, it was important for successful palynological support of the drilling program to establish a palynological processing facility manned by an experienced processor in the Crary Science and Engineering Laboratory. Equally important, special consideration was required for handling harmful vapours generated by HF and HCL acid digestion of samples because of the sensitive environment of Antarctica.

Traditional palynological processing is by cold-acid digestion in open beakers under a fume hood. There are a number of drawbacks to this approach. Rock digestion commonly takes one to two days because cold acid reactions progress slowly and it is often necessary to add fresh acid during digestion to expedite this process. Consequently, the open-beaker method consumes considerable quantities of reagents. In addition, significant harmful vapours are released to the atmosphere, even though the acids are cold. Safety is a major concern because frequent handling of reagents and the presence of acid filled, open beakers are a continual threat to processors. Finally, acid digestion fumes are vented outside the laboratory to the atmosphere.

Venting of acid vapours, particularly those of HF, would not be permitted in Antarctica. Rather than employ traditional open beaker, cold-acid sample digestion, samples were dissolved in hot acids within the closed sample vessel of a Prolabo Model 401 focused microwave acid digestion unit (Fig. 21). The unit focuses microwaves on the acid and sample contained in a closed, microwave-transparent digestion vessel at atmospheric pressure. This maximizes sample heating and increases the reaction rate of rock digestion. (It is important not to heat the sample high enough to increase the natural thermal maturity of the palynomorphs.)

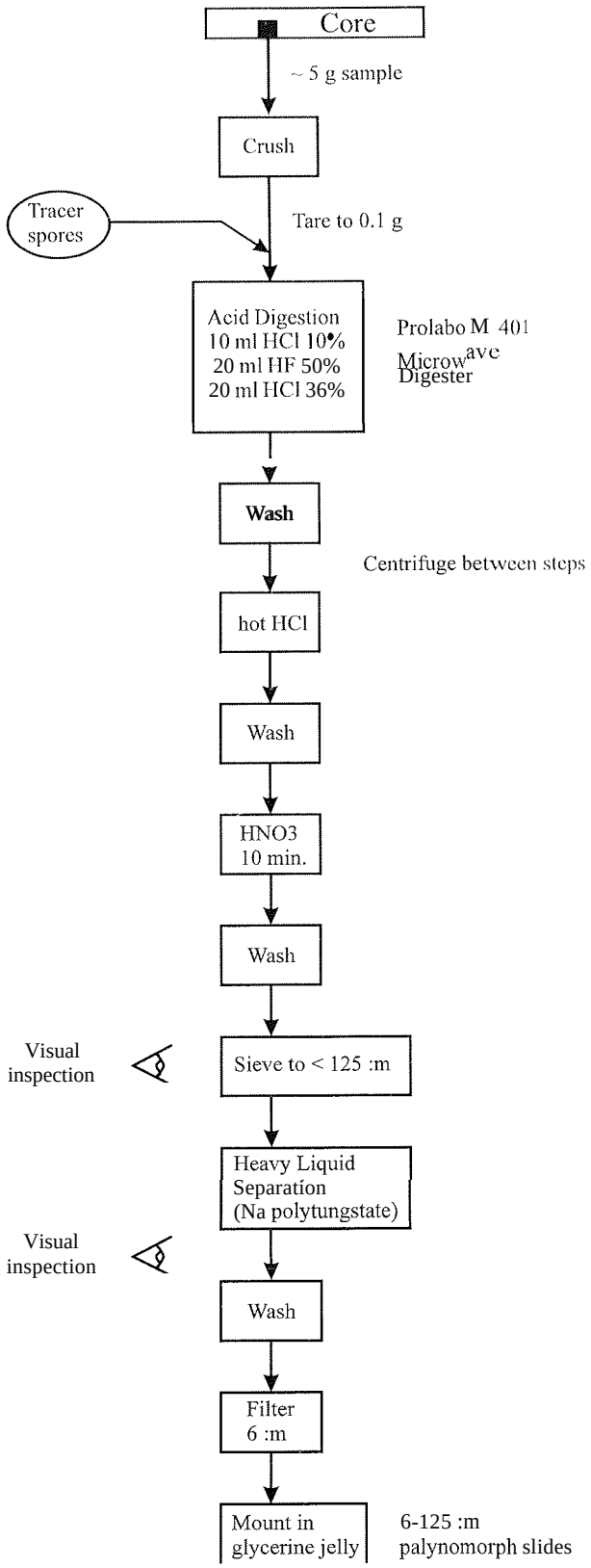

Fig. 20 - Flowchart of palynological-processing procedures used on samples from CRP-1.

Acids are pumped directly from reagent bottles into the digestion vessel, and the duration and degree of sample heating are controlled by a computer. Computer control of

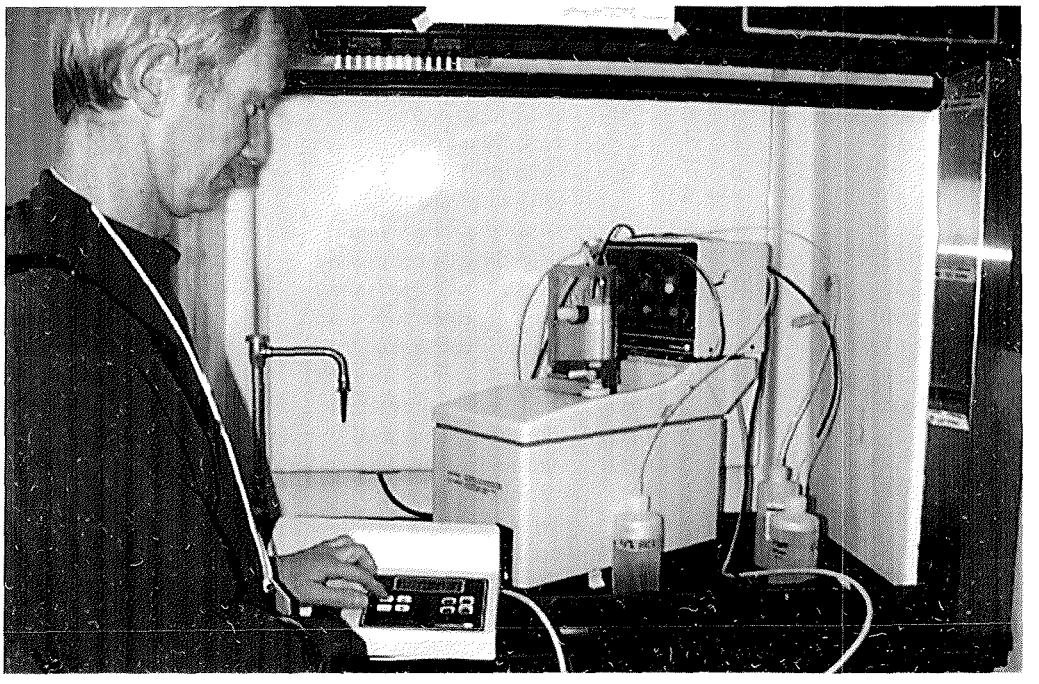

Fig. 21 - Prolabo M401 microwave digestion unit, pump and computer control unit.

reagent pumping minimises the amount of reagent handling by the processor. Vapours generated during hot-acid digestion are evacuated from the vessel and neutralized in a boric acid/sodium hydroxide scrubber (Fig. 22) before being vented to the atmosphere. See Ellin & McClean (1994), Jones (1994), Jones et al. (1995) and Jones & Ellin (in press) for discussions on the use of microwave digestion in palynological sample preparation.

CRP-1 Sample Processing

Ten "fast-track" samples (Tab. 7) were received and processed for palynological analysis during core drilling. An additional 45 samples were selected, where possible, from fine sand and silt units at roughly a 4 m interval; 31 of these were studied for this initial report. Approximately five grams of each sample was processed, except for sample P-6. Ten grams of this fine sandstone were digested in the hope of increasing recovery.

In addition to these general processing steps noted above, one Lycopodium tablet[1] was added to each sample at the start of acid digestion to facilitate the estimation of the palynomorph concentration/gram of sediment (Fig. 20).

Some samples required a second hot HCL treatment after microwave acid digestion to remove precipitates of

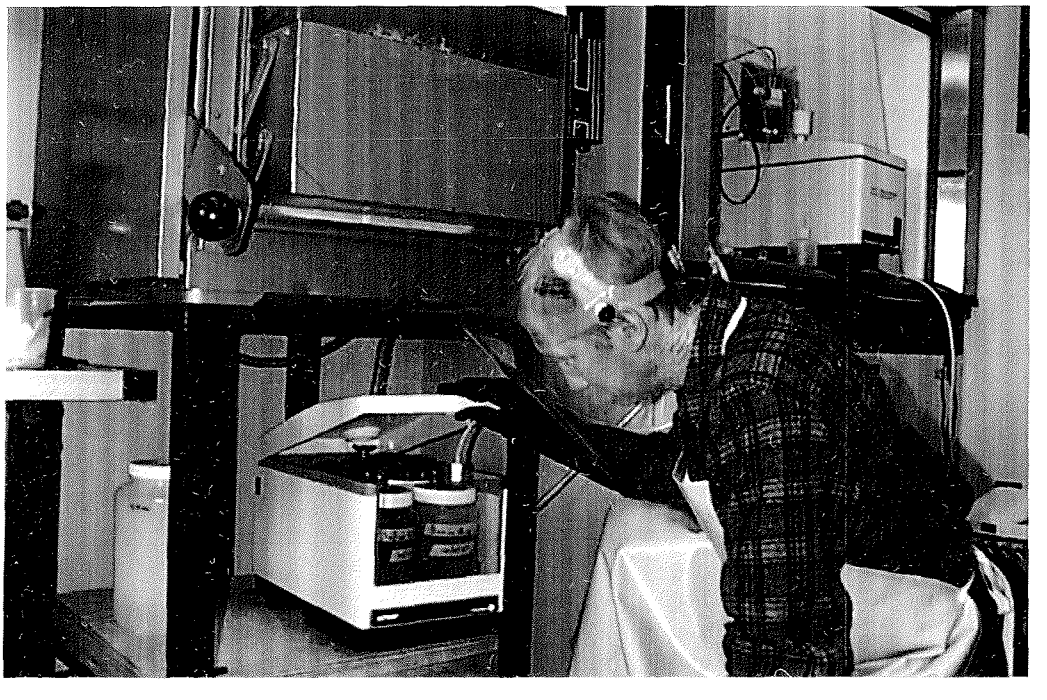

Fig. 22 - Processing technician John Simes (New Zealand) inspecting fume scrubbing unit. Note the microwave unit in the fume hood behind John.

[1] *Lycopodium* tablets were produced by Department of Quaternary Geology, Lund University, Lund, Sweden. Batch#124961; 12 542 +/-414 spores/ tablet.

Tab. 7 - CRP-1 palynology samples proccessed during drilling operations.

Top	Base	Lab. #	Wt (g)	Type	Lithology	Unit
0.00	8.50	P3	c.5	F	muddy diamicton	1.1
20.60	20.61	P51	6.1	R	muddy diamicton	2.1
21.04	21.14	P4	c.5	F	muddy diamicton	2.1
25.10	25.11	P50	6.3	R	sandy mud	2.2
31.50	31.51	P49	5.9	R	soft sandy mud	3.1
32.05	32.15	P5	c.5	F	calcarcous muddy sand	3.1
31.90	31.93			Q	biogcnic calcareous sand	3.1
32.34	32.37			Q	biogenic calcareous sand	3.1
32.37	32.40			Q	biogcnic calcareous sand	3.1
32.58	32.61			Q	biogenic calcareous sand	3.1
32.77	32.80			Q	biogenic calcareous sand	3.1
32.98	33.01			Q	sandy muddy gravel	3.1
33.31	33.34			Q	calcareous sandy mud	3.1
33.50	33.53			Q	calcareous sandy mud	3.1
33.72	33.75			Q	calcareous sandy mud	3.1
34.00	34.01	P38	5.5	R	sandy mudstone	4.1
36.62	36.63	P48	6.9	R	muddy diamicton	4.1
39.06	39.07	P47	6.4	R	sandy muddy gravel	4.1
42.41	42.43	P46	5.9	R	muddy diamicton	4.1
45.04	45.14	P6	10.4	F	fine sandstone	5.1
48.35	48.36	P13	5.4	R	sandy mudstone	5.1
53.50	53.60	P10	5.4	F	siltstone	5.1
54.45	54.46	P17	5.1	R	clayey mudstone	5.2
58.43	58.44	P18	5.4	R	coarse siltstone	5.2
59.58	59.68	P8	5.6	F	coarse siltstone	5.2
62.90	62.91	P19	5.4	R	muddy sandstone	5.3
67.54	67.55	P20	5.6	R	silty sandstone	5.4
70.02	70.03	P21	5.4	R	siltstone	5.4
74.87	74.88	P22	5.6	R	silty sandstone	5.5
78.15	78.25	P11	5.4	F	silty claystone	5.5
78.15	78.25	P16	3.8	F*	silty claystone	5.5
78.75	78.76	P23	5.3	R	silty claystone	5.5
82.18	82.19	P24	5.6	R	massive siltstone	5.7
85.36	85.37	P25	5.6	R	clayey siltstone	5.7
87.42	87.43	P27	5.6	R	siltstone	5.7
92.34	92.35	P28	5.3	R	mudstone	5.8
96.37	96.38	P29	5.3	R	pebbly mudstone	5.8
99.02	99.12	P12	5.1	F	mudstone	5.8
100.47	100.48	P30	5.6	R	mudstone	5.8
104.75	104.76	P31	5.7	R	sandy diamictite	6.1
108.75	108.76	P32	6.0	R	sandy diamictite	6.1
112.44	112.45	P33	5.9	R	silty claystone	6.2
116.45	116.46	P34	5.2	R	sandy siltstone	6.2
120.27	120.28	P35	5.6	R	muddy diamictite	6.3
120.40	120.50	P14	5.2	F	muddy diamictite	6.3
124.08	124.09	P36	5.4	R	siltstone	6.3
128.12	128.13	P37	5.1	R	mudstone	6.3
132.07	132.08	P39	5.6	R	muddy diamictite	6.3
136.20	136.21	P40	5.7	R	muddy diamictite	6.3
139.14	139.15	P41	6.4	R	muddy diamictite	6.3
141.80	141.92	P15	5.3	F	clayey siltstone	7.1
142.34	142.35	P42	5.6	R	clayey siltstone	7.1
144.31	144.32	P44	5.3	R	silty claystone	
145.65	145.66	P43	5.4	R	claystone	
147.68	147.69	P45	6.4	R	silty claystone	

Key to sample type: F=rush, R=regular, Q=foraminiferal processing residue (see text); * reprocessed.

an unknown nature. These precipitates may have been generated from the digestion products of the volcanic clasts that are present in most samples. Due to the limited processing time available during the drilling season, it was not possible to determine the optimum programming of the unit for this rock type to remove these precipitates. Rather, HCL was added to the residue and heated in a hot-water bath on a hot plate, while another sample was being run through the microwave unit. This removed most of the precipitates.

Undigested mineral grains were removed from residues by heavy liquid treatment (Fig. 20) with non-toxic, water-

soluble sodium polytungstate (Sp. Gr. 2.4). This high specific gravity fluid was used because many palynomorphs sank in heavy liquid separations run at a lower specific gravity (Sp. Gr. 2.0). It was discovered that this was due in part to a very thin pyrite coating on the palynomorphs. This imparted a dark gray to black color to the dinocysts and acritarchs, but the coating was so fine grained that the specimens were transparent. Pyritespheres were not noted within the palynomorphs. Treatment of the samples with nitric acid removed the pyrite coating and changed palynomorph color to light brown.

Fine-grained mineral and organic debris was removed by sieving the residue on a 6 p. nylon cloth using a sieving device described by Raine & Tremain (1992). Residues were mounted in glycerin jelly and sealed with fingernail polish.

In many of the Quaternary and Miocene samples small numbers of contaminant pollen and spores were identified, despite care in laboratory cleanliness and the McMurdo laboratory location remote from living plant sources. Modern contaminant specimens could be recognised by a combination of features, including generally colorless or pale yellow exine, remnant protoplasm, and bright (white or greenish) autofluorescence in blue-violet epi-illumination. Contaminant taxa identified reflect the regions of origin of the equipment and personnel involved in the project, and presumably originate from dust adherent to packaging, equipment, and clothing: *Artemisia* and *Betula* from North America, and *Nothofagus* cf. *fusca* and *Dicksonia* from New Zealand. Pollen of *Pinus*, Poaceae, and cosmopolitan weeds (*Rumex*, Haloragaceae) was also identified. A single *Pinus* pollen grain was identified from a glycerine petri dish exposed in the laboratory for a week during processing. The drilling mud (a synthetic polymer) was also checked for contaminants and only rare modern Haloragaceae pollen (possibly of laboratory origin) were found. The *Lycopodium* tablets used for estimation of palynomorph concentration were also examined for purity: no contaminant miospores were encountered during a scan of approximately 17 000 grains of Lycopodium *clavatum* type in a control slide prepared from several dissolved tablets.

Palynological processing in the Crary Laboratory was a success, due in large to the use of the environmentally friendly and efficient focused microwave digestion unit. The speed of acid digestion and the safe handling of acid vapors by the digestion unit made it possible for palynostratigraphic support to be provided onsite in the unique Antarctic environment for the first time. For the Cape Roberts Project, rapid microwave processing meant that palynologic analyses can provide critical input as drilling is in progress. This technology opens the door to safe and fast palynological processing in remote regions of the world, as well as on offshore oil rigs and on board ships.

PALAEOMAGNETIC LABORATORY

The CRP palaeomagnetic laboratory in the Crary Science and Engineering Center (CSEC), McMurdo Station, was the first palaeomagnetic laboratory to be established on the Antarctic continent. It may also be the highest latitude palaeomagnetic laboratory ever established. A number of challenges were encountered during establishment of the laboratory, and we docunient these here to assist future endeavours of this type.

Due to the expense and logistical difficulties involved in using a cryogenic magnetometer in the Antarctic, the laboratory was equipped with two spinner magnetorneters. The AGICO Brno JR-5A magnetometer is the most sensitive spinner magnetometer currently available. The high sensitivity is obtained by rotating the sample at high speed (89.2 revolutions/second), which can produce mechanical instabilities if there is any external vibration of the instrument. In addition, the high rate of rotation can cause poorly consolidated samples to disaggregate. Because of these factors, the laboratory was also equipped with a Molspin spinner magnetometer, which is more robust, but less sensitive, than the AGICO magnetometer. The Molspin magnetometer is well-suited for measuring relatively strongly magnetised and/or poorly consolidated samples, as well as for determining the mineral magnetic properties of selected samples.

Demagnetisation capabilities were provided by a Molspin alternating field (AF) demagnetiser and a Magnetic Measurements MMTD60 Thermal Demagnetiser. An ASC Scientific IM10-30 impulse magnetiser was used for studies of the acquisition of isothermal remanent magnetisation (IRM) and for back-field demagnetisation experiments. A Bartington Instruments MS-2 magnetic susceptibility meter was used for susceptibility measurements. The equipment for the project was contributed jointly by the Istituto Nazionale di Geofisica (Rome, Italy) and the University of California, Davis.

Prior to establishment of the laboratory, a number of rooms in CSEC and in surrounding buildings were assessed for their suitability to house a palaeomagnetic laboratory. In the absence of a magnetically-shielded room, the primary consideration was to find low field gradients in a magnetically "quiet" environment. Of the sites surveyed, CSEC room 242 was found to have the most uniform ambient magnetic field. Vibration measurements, performed with an accelerometer, also indicated that this room was least affected by building vibrations. In order to maintain low ambient field gradients, wooden furniture was built for the room. The components of the furniture were assembled using non-magnetic fastenings. A vibration-dampening table was constructed for the AGICO magnetometer by placing a granite slab on top of a layer of shock-absorbent rubber balls which were set in a rectangular recess in the table. This design proved to be highly effective, even when significant vibrations were caused by movement of large objects on the loading dock adjacent to CSEC 242.

The build-up of electrical static, due to the aridity of the Antarctic atmosphere, is a hazard that can cause problems in the laboratory. In some cases, static discharge from operators to equipment has been known to cause resetting of equipment, which required shutting down, restarting and recalibration. All palaeomagnetic equipment was therefore placed on anti-static mats, and fine-gauge grounding cables attached to wristbands were placed

around the laboratory to enable operators to be grounded at all times while handling equipment and samples.

Cylindrical palaeomagnetic samples (25 mm diameter x 22 mm height) were collected using a modified drill press. In planning for the Cape Roberts project, experience was acquired by sampling similar material from the CIROS-1 core, which is stored at Florida State University, Tallahassee *(cf.* Wilson et al., 1998; Sagnotti et al., submitted). The CIROS-1 core has been stored at 4°C since 1986 and is now almost completely dry. During sampling of the CIROS-1 core, compressed air was used to cool the drill bit. While the CRP cores were expected to be water-saturated at the time of recovery, there was no way of knowing how consolidated the sediments would be. In order to cover all possibilities, the drill press used for sampling the CRP cores was configured so that either water or air could be used as the coolant. Because drilling is not a clean procedure and contamination could occur if sampling is conducted in proximity to other parts of the core, a specially-designed drilling hut was constructed for the palaeomagnetic sampling. The dust produced, when air was used as a coolant, was extracted with an industrial vacuum cleaner. For CRP-1, water was far more satisfactory as a coolant than compressed air.

Our success in establishing the first palaeomagnetic laboratory in Antarctica has demonstrated that, with careful planning and cooperation, it is possible for a group of researchers from two different continents to assemble a comprehensive palaeomagnetic laboratory on a third continent and to have it fully operational within one week of arrival. This laboratory has enabled fulfillment of the primary objective of the palaeomagnetic goals for the Cape Roberts Project *(i.e.*, the initial characterization of the palaeomagnetic and mineral magnetic properties of the CRP-1 core).

CORE MANAGEMENT AND SAMPLING

Drill Site and Cape Roberts Camp

Initial core curation began at the drill site. The drillhole was designated as CRP-1. Downhole depths are expressed as metres and measured to the nearest centimetre, and represent the depth in metres below the sea floor (mbsf). The length of core is defined by depth from the sea floor to the top and bottom; a feature in the core is specified by the depth to its uppermost part. All work was carried out from top to bottom of each core length. The core was boxed as three rows per box, with top to upper left and bottom to lower right.

The core was first cut into one metre lengths and then longitudinally into an Archive and a Working half using a diamond saw. The Archive and Working halves were placed into separate core boxes, each box marked on one end with Archive or Working and the interval of core it contained. Additional yellow plastic separators bearing the interval were placed at the appropriate places in the core box itself. Foam blocking was used to stabilize the core. Any voids in the core were to be filled with foam to mitigate any potential movement of the core during transport.

Sampling of the core began at the drill site, a ten centimetre section of the whole core was taken every 20 m for strength tests, and a ten centimetre section of the Working half was taken also every 20 m as a "fast-track" sample for rapid age determination.

Transportation

Core Boxes to McMurdo Helicopter Pad - Insulated, vinyl-covered carrying cases, with a capacity of three core boxes each, were used to transport the core via helicopter between the Cape Roberts Drill Site, the Cape Roberts Camp, and McMurdo Station. The carrying cases were placed inside the helicopter to protect the core from freezing. An average of four boxes were transported per day, although poor weather created a back log of core at the drill site and a shipment of ten cases on one occasion. The Working half and Archive half of the core were transported on alternate days as a safety measure.

Core Boxes to Core Storage Facility (CSEC-CSF) - The cases containing the core arrived at McMurdo between 10 p.m. and midnight each day. Cases were transported, by truck, from the helicopter pad to the Crary Science and Engineering Center-Core Storage Facility (CSEC-CSF), building number 3. The core boxes were removed from the carrying cases, logged in and placed on shelving. The Archive and Working halves were placed in sepal ate areas of the Facility. The CSEC-CSF was maintained at a temperature of 4°C and humidity of 30%.

"Fast-Track" Samples from the Drill Site - The decision was made to remove at the Drill Site Lab a ten centimetre section of the Working half of the core about every 20 m down hole for rapid dating and to include this with each core shipment. These samples are denoted as "PALAEOGROUP" in the data base.

Paperwork from *the Drill Site* - Related core logs and other coring paper work were placed in the carrying cases along with the core boxes.

Crary Laboratory, McMurdo - A core laboratory was set up in room 201 of the Crary Science and Engineering Center (CSEC). The walls, the floor, the benches, and all equipment in the room were thoroughly cleaned prior to the core arrival at the lab and at the end of each sampling session to minimize the potential for contamination of the core. The temperature of the room was lowered to 18 °C. The humidity of the room was a low 33% despite the addition of a humidifier. The laboratory contained 34 metres of bench space covered with an easily cleaned surface. Fluorescent lighting was augmented by the addition of high intensity halogen lighting to enhance the viewing of the core.

Sequence of Events in the CSEC Core Laboratory

The morning following the arrival of the core at McMurdo Base, the core was repackaged into the carrying cases and transported by truck to the core lab in the CSEC. The core boxes were removed from the carrying cases and placed on the lab benches in sequence, from the top of the core to the lowest interval that had been received at that time.

Initial Core Appearance - In general, the core arrived from the Cape Roberts Camp in good condition. The core was moist with a sheen of water on the cut surface of the sediment. The softer sediment did exhibit longitudinal separation towards the middle of the core. This was most likely due to the relaxation of the sediment and the lack of support. Occasional minor longitudinal shifting within the individual metre-long sections was evident, but was easily rectified.

Core Logs Reclzecked, Photography and Viewing of the Core - After each shipment of the Working half of the core was received, Mike Hambrey and Chris Fielding rechecked the core logs received from the Cape Roberts drill site for discrepancies against the actual core. During this time they also photographed sedi~nentological features of interest. They presented their interpietation of the core to the Cape Roberts science group at the CSEC.

X-radiography - The science plan called for the entire core to be subjected to x-radiography analysis. The x-radiography unit purchased for use by the Cape Roberts Project required that the core be removed from the core boxes and placed on a special designed tray that could be manually positioned in the unit. However the soft and fractured nature of the core above 100 mbsf made this difficult to achieve.

In an effort to complete the science objectives in an expedient manner, a trial box of core was hand transported to the McMurdo Medical Facility, where a standard hospital x-ray unit was used. The results were poor. The decision was made to revert to the original plan and carefully remove selected coherent sections of the core by hand for placement in the x-radiograph tray.

Of the approximately 45.38 metres of Quaternary age sediment only 13.81 metres or 30.5% was X-rayed. Of the 102.30 metres of the older sediment only 53.6 metres or 36.02% was X-rayed. This small percentage was due to the unexpected volume of soft Quaternary age sediment and the fractured nature of the older sediment. Only select sections of the core deemed safe to be removed were subjected to x-radiography analysis. The curator was responsible for the determination and removal of these sections.

Flexible plastic strips of a size that closely approximated the core section to be removed were carefully worked between the core section and the core box. The section was then placed on the specially made carrier for positioning in the x-radiography unit. The correct orientation of the core was maintained during the entire operation.

The plastic sheets and the x-radiograph carrier were washed to prevent contamination prior to the X-radiography of the next core section.

Sample Requests - Prior to the actual sampling, those scientists authorized to receive samples from the core were given a three letter "investigator code" which consisted of the first three letters of their last name, a supply of labels and tooth picks. Each person marked their code on both ends of a 25 mm by 75 mm self-adhesive label using waterproof ink. The label was wrapped around a common wooden toothpick, thus forming a "flag" to mark the interval to be sampled.

Each scientist was also provided with a sample request form on which he/she listed the following information: the date, their investigator code, their name, the core number, the box number, the top and bottom of the interval requested, the volume requested, and any comments on sampling. These forms were returned to the curator to be utilized during data entry and during the actual sampling.

Selecting Sample *Intervals* - Due to the relaxation of time constraints, an average of six boxes or eighteen metres of core was available for sampling at each sampling session. The investigators were reminded at the beginning of each sampling session that sampling "was for core characterization, not detailed analysis" and of the total number of samples, the intervals and volumes of each sample as set forth in the Cape Roberts Science Plan for the older sections of the core. The unexpected recovery of a volume of Quaternary age material necessitated a revised sampling plan. While a plan was formulated, the decision was made to sample the Quaternary age material at the end of the sampling period.

The investigators were given on average one and one half hours to select their intervals by placing their sample flag alongside the core and to fill-in the sample request form. The palaeomagnetic investigators marked their samples by placing 4 mm by 7 mm slips of stiff paper over their requested interval. Copies of the core logs were provided to facilitate their selection of sample intervals. They were also reminded to write legibly and not to contaminate the core by removing and replacing their sample flag in a different location

Disputed Sample Intervals - Disputes between multiple disciplines requesting the same interval were resolved through discussions with the on-ice parties involved, the Project Science Coordinator and the curator.

Data Entry and Sample Labels - The curator entered the data from the completed sample request forms into a relational data base. These data included: the investigator, the core number, the depth interval, the volume of the sample, the date, and comments.

These data were used to provide each investigator with a paper copy of his/her sample request at the end each day's sampling. In addition, a record of the total number of samples removed from the core by each investigator was provided at the end of the sampling programme. The comment section recorded the type of sample taken, *e.g.* sediment, fossil, or clast, and the discipline and type of analysis to be performed with each sample, *e.g.* petrology-thin section or paleontology-diatoms. The information was also used to generate labels using a Seiko Thermal Label Printer. The self-adhesive labels contained the same information as the sample request form for each of the sample bags. The database also contains the address of each science participant of the Cape Roberts Project.

This sample information and other coring information will be included on mirror databases and World Wide Web sites. These will be established by the curatorial facilities at the Antarctic Marine Geology Research Facility, at the Florida State University in Tallahassee, Florida and the Alfred-Wegener-Institute for Polar and Marine Research in Bremerhaven, Germany.

Sampling

Sampling Parties - Due to the volume of core expected, the curator alone could not possibly fulfill all of the sample requests in a timely manner. Therefore, the Cape Roberts science group at the CSEC was formed into sampling parties consisting of four people. These four people divided into two groups each contained a person who removed the sediment from the core and another who held the bag into which the sediment was placed, sealed and placed it in the appropriate requesting investigator's box. The curator supervised these groups.

The sampling parties were arranged so that the palaeontology, sedimentology and petrology disciplines were represented. The majority of persons in the group had previous sampling experience. However, all persons were instructed on the following procedures: the correct orientation of the core in the core boxes, the use of the sample "flags" and the sample request form to locate the correct sample interval, and most importantly, the necessity to use the sampling tool only once per sample and to avoid touching the core with their hands to avoid contamination of the core. The participants were also shown representative styrafoam models of the volumes requested on the sample request forms.

Sampling Priority - Palaeontological samples were taken first, followed by the palaeomagnetic and then the general sampling. Priority was given to on-ice studies of the material.

Palaeomagnetic Sampling - Palaeomagnetists performed their own samplingdue to the special techniques required. To avoid contamination of the core, orientated, coherent sections were removed from the core box, placed on a carrying tray and taken to thepalaeomagneticsampling lab, a separate building located on the loading dock of CSEC room 201. A diamond drill was used to remove the sample. The core section was replaced in the core box in the proper orientation. Hidden faults in some sections necessitated the reconstruction of the core. If the section was badly fragmented it was placed in a bag labeled with the interval and replaced in the core box.

Sampling Equipment - Sampling equipment included measuring tapes, various size plastic bags and vials, separate wash and rinse bottles, common laboratory spatulas, small scoops and forceps for the softer material, and hammers and chisels for the more lithified material. A diamond saw was used to cut large clasts for samples. All of these tools were cleaned prior to the beginning of the sampling session and between the sampling of different intervals. At no time was any tool used more then once before it was cleaned. The cleaning consisted of washing with hot water and a laboratory detergent, rinsing with clean water, and a final wash with filtered water. The tools were allowed to air dry to minimize the potential for contamination of the tools by paper or cloth fibre from a drying medium.

Curatorial Duties after Sampling - The voids left in the core following sampling were filled with carefully cut foam blocks to stabilize the core. The core was misted with filtered water and then returned to the Crary Science and Engineering Center-Core Storage Facility.

In the coie lab the benches, the floor, and all sampling equipment were washed in preparation for the in-xt shipment of core.

Core Shipment

The core was re-examined in the CSEC-CSF prior to packaging for shipment to the facilities in Florida and Germany. The core was checked for the stability of the sediment. Additional foam blocking was added where needed and the core was misted with filtered water a final time before the core-box lids were taped in place.

The core boxes were placed into heavy, reinforced tri wall cardboard containers, sixteen core boxes per container, placed four boxes side by side and four boxes high to minimize crushing. Metal bands were used to strap the container to a wooden pallet. The containers were marked with arrows pointing to the upright position. Fragile, Do Not Freeze, Place Nothing On Top signs were placed on the container.

The pallets were placed into a storage container refrigerated to 4°C. The core containers were to be seemed within the storage unit with no other material placed on top for shipment via the cargo ship *Greenwave* to Lyttleton, New Zealand. The Working half of the core will be off-loaded for air transport to Germany. The Archive half will continue aboard the *Greenwave* to be off-loaded in California and transported overland via refrigerated truck to Florida.

Summary of Curatorial Duties

The curator was responsible for the transportation of the core boxes from the helicopter pad at McMurdo to the Crary Science and Engineering Center-Core Storage Facility (CSEC-CSF), from the CSEC-CSF to the core lab in CSEC room 201, the return of the core to the CSEC-CSF, and the crating and dispatch to the facilities in Florida and Germany.

Because of the higher temperature and lower humidity of the core laboratory (CSEC room 201) core dehydration was a concern. This was counteracted by misting the core with filtered water on a half hourly schedule or as needed as some lithologies dried more rapidly then others.

The curator maintained the stratigraphic integrity of the core during removal of sections for X-radiography, paleomagnetic and general sampling.

The curator reduced the possibility of contamination and minimize disturbance of the core through instruction of proper sampling techniques and maintaining a clean laboratory environment.

All original paperwork, including the core description logs, core recovery logs, physical property and sample request forms, was maintained by the curator.

The curator entered and maintained all data in the data base concerning sampling and generated total lists of all samples taken by each investigator.

All requests by news media and investigators to view the core after the initial sampling and requests for additional samples were coordinated by the curator.

ACKNOWLEDGEMENTS

Fracture Arrays - The fracture study and core scanning were funded by NSF grant OPP-9527394 to T.J. Wilson. Timothy Paulsen was partially supported for the fracture study by NSF/OPP-9527394 and by the Byrd Postdoctoral Fellowship, Byrd Polar Research Center, Ohio State University. Dr. G. Rafat generously volunteered his time and expertise for set up and training on the CoreScan®. Fee waivers and software access providedby DMT-Geotec, Essen, Germany facilitated this research.

Correlation of Seismic Reflectors with CRP-1 - We would like to thank Dr. L. Bartek and Dr. B. Luyendyk for permission to use NB9601 data in this report. Foundation for Research Science and Technology Contract C05XXX supported the work.

REFERENCES

Barren P.J. (ed.), 1986. Antarctic Cenozoic history from MSSTS-1 drillhole, McMurdo Sound. *DSIR Bulletin 237*, Science Information Publishing Centre, Wellington, 174 p.

Barrett P.J. (ed.), 1989. Antarctic Cenozoic history from CIROS-1 drillhole, McMurdo Sound. *DSIR Bulletin 245*, Science Information Publishing Centre, Wellington, 254 p.

Barrett P.J., 1997. *Cape Roberts Project Science Plan.* Antarctic Data Series, no. 20, Victoria University of Wellington, 59 p.

Barrett P.J., Henrys S.A., Bartek L.R., Brancolini G., Busetti M., Davey F.J., Hannah M.J. & Pyne A.R., 1995. Geology of the margin of the Victoria Land basin off Cape Roberts, southwest Ross Sea. In: A.K. Cooper, P.F. Barker & G. Brancolini (eds.), *Geology and Seismic Stratigraphy of the Antarctic Margin, Antarctic Research Series,* 68, AGU, Washington, 183-208.

Barss S. & Williams G.L., 1973. Palynology and nannofossil processing techniques. *Geological Survey of Canada Paper,* **73**(26), 25 p.

Bartek L.R., Henrys S.A., Anderson J.B. & Barrett P.J., 1996. Seismic stratigraphy in McMurdo Sound: implications forglacially influenced early Cenozoic eustatic change. *Marine Geology,* 130, 79-98.

Behrendt J.C., Cooper A.K. & Yuan A., 1987. Interpretation of Marine Magnetic Gradiometer and multichannel seismic-reflection observations over the Western Ross Sea Shelf, Antarctica. In: A.K. Cooper & F.J. Davey (eds.), *The Antarctic Continental Margin: Geology & Geophysics of the Western Ross Sea, Earth Sci.Ser.* Circum-Pacific Council for Energy & Mineral Resources. Earth Sciences Series, 5B, Houston, Tex., 155-177.

Bozzo E., Damaske D., Caneva G., Chiappini M., Ferraccioli F., Gambetta M. & Meloni A., 1997. A High Resolution Aeromagnetic Survey over Proposed Drill Sites Off Shore of Cape Roberts in the Southwestern Ross Sea (Antarctica). In: Ricci C.A. (ed.), *The Antarctic Region: Geological Evolution and Processes,* Terra Antartica Publication, Siena, 1129-1134.

Brancolini G., Cooper A.K. & Coren F., 1995. Seismic facies and glacial history in the western Ross Sea (Antarctica). In: A.K. Cooper, P.F. Barker & G. Brancolini (eds.), *Geology and Seismic Stratigraphy of the Antarctic Margin, Antarctic Research Series,* 68, AGU, Washington, 209.

Brancolini G., De Santis L. & Busetti M., 1994. Structural Evolution across a section south of the Drygalski Ice Tongue (Victoria Land Basin). In: F.M. Van der Wateren, A.L.L.M. Verbers, F. Tessensohn (eds.), *Landscape evolution in the Ross Sea Area, Antarctica,* Rijks Geologische Dienst RGD, 69-75.

Cooper A.K., Brancolini G., Behrendt J.C., Davey F.J., Barrett P.J. & ANTOSTRAT Ross Sea regional working group, 1994. A record of Cenozoic tectonism throughout the Ross Sea and possible controls on the glacial record. In: Cooper A.K., Barker P.F., Webb P.N., Brancolini G. (eds.), The Antarctic Continental Margin: Geophysical and Geological Stratigraphic Records of Cenozoic Glaciation, Paleoenvironments, and Sea-Level Change, *Terra Antartica,* **1**(2), 353-355.

Cooper A.K. & Davey F.J. (eds.), 1987. *The Antarctic Continental Margin: Geology & Geophysics of the Western Ross Sea, Earth Sci.Ser.* Circum-Pacific Council for Energy & Mineral Resources. Earth Sciences Series, 5B, Houston, Tex.

Cooper A.K., Davey F.J. & Behrendt J.C., 1987. Seismic stratigraphy and structure of the Victoria Land basin, western Ross Sea, Antarctica. In: A.K. Cooper & F.J. Davcy (eds.), *The Antarctic Continental Margin: Geology & Geophysics of the Western Ross Sea, Earth Sci.Ser.* Circum-Pacific Council for Energy & Mineral Resources. Earth Sciences Series, 5B, Houston, Tex., 27-65.

Cooper A.K., Davcy F.J. & Hinz K., 1991. Crustal extension and the origin of sedimentary basins beneath the Ross Sea and Ross Ice Shelf, Antarctica. In: M.R.A. Thomson, J.A. Crame & J.W. Thomson (eds.), *Geological Evolution of Antarctica.,* 285-291, Cambridge University Press, Cambridge.

Davey F.J., 1981. Geophysical studies in the Ross Sea region. *J. Roy. Soc. N. Z.,* **11**(4), 465-479.

Davey F.J., 1983. Sedimentary basins of the Ross Sea, Antarctica. *New Zealand Antarctic Record,* **5**(1), 25-29.

Ellin S.J. & McClean D., 1994. The use of microwave heating in hydrofluoric acid digestions for palynological preparations. *Palynology,* 18, 23-31.

Gray J., 1965. Extraction techniques. In: Kummel B. & Raup D. (eds.), *Handbook of Paleontological Techniques, W.* H. Freeman & Co., San Francisco, 530-587.

Hamilton R.J., Sorlien C.C., Luyendyk B.P. & Bartek L.R., 1997. The stratigraphy and tectonic regimes off Cape Roberts, Antarctica. *Contribution #0276-72 TC, Institute for Crustal Studies,* University of Santa Barbara, Santa Barbara, Calif., 17p.

Hannah M.J., Cita M.B., Coccioni R. & Moncchi S., in press. The Eocene/Oligocene boundary at 70 degrees South, McMurdo Sound, Antarctica. *Terra Antartica.*

Henrys S.A., Bartek L.R., Anderson J.B. & Barrett P.J., 1994. Seismic stratigraphy in McMurdo Sound: correlation of high resolution data sets. *Terra Antartica,* 1, 373-374.

Hinz K. & Block M., 1984. Results of geophysical investigations in the Weddell Sea and in the Ross Sea, Antarctica, *Proceedings 11th World Petrol. Congress, London 1983,* Wiley, New York, 279-291.

Houtz R.E. & Davey F.J., 1973. Seismic profiler and sonobuoy measurements in the Ross Sea, Antarctica. J. *Geophys. Res.,* 78, 3448-3468.

Jones R.A., 1994. The application of microwave technology to the oxidation of kerogen for use in palynology. *Review of Paleobotany and Palynology,* **80**, 333-338.

Jones R.A., Dorning K.J., Ellin S.J. & Brooks I.P., 1995. Microwave preparation techniques for the palynological analysis of flint and chert. *Abstract, 7th International Flint Symposium,* Institute of Archaeology and Ethnology, Polish Academy of Science, Al Solidarnosd 105, 0-140, Warsaw, Poland.

Jones R.A. & Ellin S.J., in press. Improved palynological sample preparation using an automated focused microwave digestion system. In: Bryant V.M. Jr. & Wrenn J.H. (eds.), *New Developments* in *Palynomorph Sampling, Extraction, and Analysis,* American Association of Stratigraphic Palynologists, Inc. Contributions Series AASP, Dallas, Texas.

Kulander B.R., Barton C.C. & Dean S.L., 1979. The application of fractography to core and outcrop investigations, *Technical report for the U.S. Department of Energy,* Contract EY-77-Y-21-1321, METC/SP-79/3, 174 p.

Kulander B.R., Dean S.L. & Ward B.J. Jr., 1990. Fractured Core Analysis: Interpretation, Logging, and Use of Natural and Induced Fractures in Core, *American Association of Petroleum Geologists Methods in Exploration Series,* 8, 88 p.

Lorenz J.C., Finley S.J. & Warpinski N.R., 1990. Significance of coring-induced fractures in Mesaverde core, northwestern Colorado. *American Association of Petroleum Geologists Bulletin,* 74, 1017-1029.

Melhuish A., Henrys S.A., Bannister S. & Davey F.J., 1995. Seismic profiling adjacent to Ross Island: Constraints on late Cenozoic stratigraphy and tectonics. *Terra Antartica,* 2, 127-136.

Nelson R.A., Lenox L.C. & Ward B.J. Jr., 1987. Oriented core: Its use, error, and uncertainty. *American Association of Petroleum Geologists Bulletin,* 71, 357-367.

Plumb R.A. & Cox J.W., 1987. Stress directions in eastern North America determined to 4.5 km from borehole elongation measurements. *Journal of Geophysical Research,* 92,4805-4816.

Pyne A.R., 1986. Sea-ice operations: McMurdo Sound-Granite Harbour. *NZ Antarctic Record,* **7**, 5-13.

Raine J.I. & Tremain R., 1992. Apparatus for rapidsievingofpalynological residues. *New Zealand Geological Survey Report PAL* 151, 14 p.

Roberts A.P., Stoner J.S. & Richter C., 1996. Coring-induced magnetic overprints and limitations of the long-core paleomagnetic

measurement technique: Some observations from ODP Leg 160, Eastern Mediterranean Sea. *Proc. ODP, Init. Repts*, 160, College Station, TX, 497-505.

Sagnotti L;, Florindo F., Verosub K.L., Wilson G.S. & Roberts A.P., submitted. Environmentalmagnetic record of Antarctic paleoclimate from Eocene/Oligocene glaciomarine sediments, Victoria Land Basin. *Geophysical Journal International.*

Schmitz D., Hirschmann G., Kessels W., Kohl J., Rohr C. & Dietrich H.G., 1989. Core orientation in the KTB pilot well. *Scientific Drilling*, 1, 150-155.

Weber H., 1994. Analyse geologischer Strukturcn mit einem Bohrkernscanner [Analysis of geological structures using the DMT Corescan® machine]. *Felsbau*, **12**(6), 401-403.

Weber M.E., Niessen F., Kuhn G. & Wiedicke M., 1997. Calibration and application of marinesedimentary physical properties using a mult sensor core logger. *Marine Geology*, 136, 151-172.

Wilson G.S., Roberts A.P., Verosub K.L., Florindo F. & Sagnotti L., 1997. Magnetobiostratigraphic chronology of the Eocene - Oligocene transition in the CIROS-1 core, Victoria Land margin, Antarctica: Implications for Antarctic glacial history. *Geol. Soc. Am. Hull,,* **109**(12), 2-14.

Wrenn J.H., in press. The importance of palynologic sample processing to the oil industry. In: Bryant, Jr. V.M. & Wrenn J.H. (eds.), New *Developments in Palynomorph Sampling, Extraction, and Analysis*, American Association of Stratigraphic Palynologists, Contributions Series AASP, Inc. Dallas, Texas.

Terra Antartica
1998, 5(1), 11-61

Quaternary Strata in CRP-1, Cape Roberts Project, Antarctica

CAPE ROBERTS SCIENCE TEAM*

Abstract - The uppermost part of the core in Cape Roberts Project - 1 (CRP-l), to 43.55 mbsf, is interpreted to be Quaternary in age. The interval comprises poorly consolidated clays, silts, sands, gravels, diamictons, and an association of mixed skeletal carbonate-terrigenous clastic sediments. The interval has been divided into four principal lithostratigraphic units based on major changes in lithology. Some of these units have been further subdivided. Notable within the Quaternary interval is a short section (*c*. 32-34 mbsf) of mixed skeletal carbonate - terrigenous clastic sediment which contains a rich and diverse assemblage of benthic macroinvertebrate fossils. Petrological investigations of large clasts and sands suggests that Quaternary sediments in CRP-lwere derived from a variety of basement sources including Precambrian to Early Palaeozoic metamorphic and granitic rocks, Jurassic dolerites, and the Devonian - Triassic Beacon Supergroup, with a variable though significant contribution from coeval volcanic activity associated with the McMurdo Volcanic Group. The Quaternary section of CRP-l is dated by diatom biostratigraphy at 1.25 - 1.8 Ma, and has also yielded a wide variety of macrofossils and microfossils. Diatoms are the most prevalent fossil group, foraminifers are also ubiquitous, palynomorphs more restricted in occurrence and nannofossils scarce. The assemblage contains the first report of the calcareous dinoflagellate *Thoracosphaera* from the Quaternary of the East Antarctic margin. The invertebrate assemblage, which is virtually in ***situ,*** is dominated by molluscs, with appreciable numbers of bryozoans and lesser numbers of echinoids, serpulid worms, octocorals, barnacles and brachiopods. The section is interpreted to represent shallow-marine depositional environments that experienced considerable variations in climate and proximity to ice, ranging from 1) possible terrestrial exposure during sea-level lowstand, 2) glaciomarine deposition under the influence of nearby glacial ice, 3) deposition under seasonal sea-ice, similar to today, to 4) times of warmer-marine temperatures when carbonate sediments accumulated beneath seas that lacked sea-ice. At least two cycles of relative sea-level rise and fall are recognised from a sequence stratigraphic analysis.

LITHOSTRATIGRAPHY

INTRODUCTION

The Quaternary part of the core is unconsolidated and clearly distinguishable from underlying rocks, which are Miocene, although precise dating of the boundary and of the immediately overlying and underlying rocks has not yet been achieved. Of the four lithostratigraphic units (1, at the top, to 4), defined on the basis of lithology, Unit 2 is further subdivided into three subunits. In the following discussion, the principal Quaternary lithofacies are described. The key characteristics of each unit are then summarised, largely on the basis of the 1:20 scale logs, which are given in Appendix 2; a brief preliminary interpretation is also given. It should be noted that, whereas the diamictons suggest glacial conditions, the sandstones and mudstones may be interpreted both within and outside of a glacial context.

FACIES ANALYSIS

Although many lithologies grade into one another, a number of characteristic facies may be identified. They are defined on the basis of lithology or associations of lithologies, bedding contacts, bed thickness, texture, fabric, sedimentary structures, colour and fossil content. Two distinct facies associations can be identified within the "Quaternary" section (Tab. 1). Association A comprises four facies of a predominantly terrigenous nature, and embraces lithostratigraphic Units 1, 2 and 4. Association B, from Unit 3, also has four facies, but these are rich in a diverse fauna and are thus highly calcareous. Examples of these facies are illustrated in figure 1. The carbonate interval is unique, and is thus described separately in a separate section (Carbonate-Rich Unit section). Several of the other facies are represented in the Miocene section, although in a lithified state, and these are more fully described in Miocene Strata, section on Facies Analysis (this volume).

DESCRIPTION OF SEQUENCE

Lithostratigraphic Unit 1.1 (0.00-19.13 mbsf), Diamicton?

Description. Only one dolerite boulder, at least 40 cm long, some loose gravel, and a few centimetres of diamicton in the "fast-track" samples, were recovered from lithostratigraphic Unit 1.1. The texture of the diamicton was not available for analysis, but clasts were predominantly subrounded and subangular. The lower contact was not recovered.

* J. Anderson, P. Armienti, C. Atkins, P. Barrett, S. Bohaty, S. Bryce, M. Claps, M. Curran, F.J. Davey, L. De Santis, W. Ehrmann, F. Florindo, C. Fielding, M. Hambrey, M. Hannah, D.M. Harwood, S. Henrys, F. Hoelscher, J.A. Howe, R. Jarrard, R. Kettler, S. Kooyman, C. Kopsch, L. Krissek, M. Lavelle, E. Levac, F. Niessen, S. Passchier, T. Paulsen, R. Powell, A. Pyne, G. Rafat, I.J. Raine, A.P. Roberts, L. Sagnotti, S. Sandroni, E. Scholz, J. Simes, J. Smellie, P. Strong, M. Tabecki, F.M. Talarico, M. Taviani, K.L. Verosub, G. Villa, P.N. Webb, G.S. Wilson, T. Wilson, S.W. Wise, T. Wonik, K. Woolfe, J.H. Wrenn.

Tab. I - Summary of facies, facies associations and their process of formation in the Quaternary section

Association A - Quaternary section (Units 1, 2 and 4)

Fades	*Litliology*	*Geometry, Contacts, Structures*	*Fossils*	*Interpretatio n*
A1	Diamicton to muddy/sandy gravel (conglomerate), varying texture and fabric but mainly very poorly sorted, matrix muddy to sandy, variable clast content, clasts <boulder grade, subangular - subrounded.	Composite intervals <8 m+, contacts gradational or sharp, some irregular unit bases, apparently unstratified.	Scattered shell d e b r i s and Miliolid forams in some units.	Glacimarine, fine fraction deposited from aqueous currents and suspension fallout, coarse clasts introduced mainly from floating ice.
A2	Gravel, moderately to well sorted, clast-supported, occurs at unit boundaries.	Single clast thickness layer (3 cm), contacts sharp.	None observed.	Lag deposit, winnowed by current and/or wave activity.
A3	Sand, fine- to medium-grained, variable but generally low mud content.	Simple beds <1.5 m thick, sharp-bounded, normal or reverse grading in some beds	Scattered shell debris and Miliolidforams in some units.	Rapid deposition from submarine currents, possibly density currents.
A4	Mud and sand/mud mixtures, rare granule/pebble clasts.	Intervals <1.3 m thick, associatedwith Facies 3 above.	None observed	Mainly fallout from suspension, distal equivalent of 3 above.

Association B - Quaternary section (Unit 3)

Fades	*Lithology*	*Geometry, Contacts, Structures*	*Fossils*	*Interpretation*
B1 (As 3 above)	Sand, fine- to medium-grained, variable but generally low mud content.	Simple bed <0.2 m thick, sharp-bounded.	Scatteredshell debris and Miliolid forams.	Rapid deposition from submarine currents, possibly density currents.
B2 (As 4 above)	Mud and sand/mud mixtures.	Intervals <1.8 m thick, sharp-bounded, normal and reverse grading, associated with Facies 1 above.	None observed.	Mainly fallout from suspension; distal equivalent of 1 above.
B3	Calcareous muddy diamicton to calcareous silt with dispersedpebbles (Bryomol).	Composite intervals <1.0 m thick, sharp-bounded, crude flat stratification defined by changes in fossil and/or clay content.	Abundant calcareous macrofossils (bryozoans, bivalves, gastropods, echinoid spines, octocorals, ostracods, serpulids, brachiopods), and forams.	Outer, open shelf (no permanent ice cover), little if any agitation, particulate surface, mainly epifauna, minimal transportation, minor ice-rafted debris.
B4	Shell hash (coquina).	Single, 2 cm thick unit, sharp-bounded, some alignment of fossils.	Abundant intact valves of bivalves.	Accumulation of shells in biostrome, in *situ,* during time of minimal sediment supply.

Interpretation. Glacially influenced deposition, but context unknown.

Lithostratigraphic Unit 2.1 (19.13-22.00 mbsf), Diamicton

Description. The principal lithology of lithological Unit 2.1 is a clast-rich to clast-poor muddy diamicton. The massive olive-black (5Y 2/1) diamicton has no visible structure, but there are subtle gradations between muddy diamicton (dominant) and sandy diamicton. Particle sizes range from clay to cobble (possibly boulder) size, with a median in the silt to very fine sand range. Clasts make up <1 to 45% of the sediment, pebbles dominant. Shapes are predominantly subrounded and subangular, with granite and dolerite being the most common. The sand fraction contains slightly more quartz than feldspar, with lesser amounts of volcanic glass. A quartz-rich volcaniclastic sand occurs from 19.13 to 19.57 mbsf. The lower contact of Unit 2.1 was not recovered.

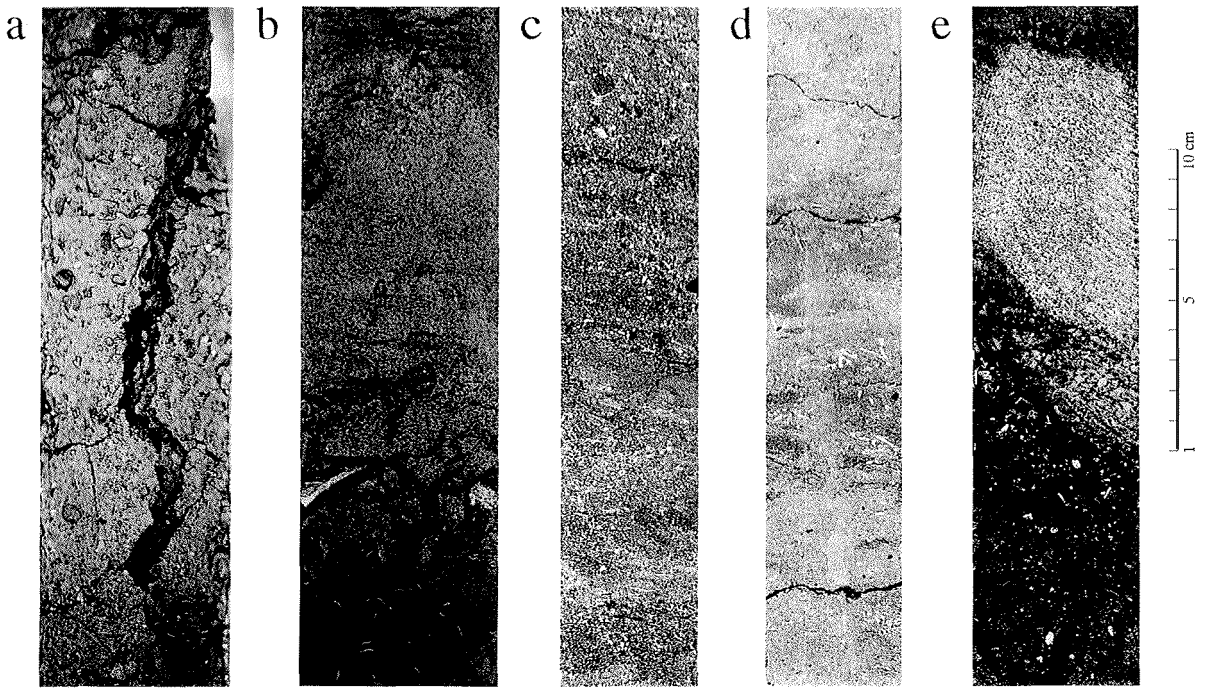

Fig. **1** - Principal facies of the "Quaternary" part of core CRP-1. a) Sand and angular dolerite pebble layer at top of a clast-poor muddy diamicton lithostratigraphic Unit 2.2, 24.38-24.61 mbsf. b) Massive clast-rich muddy diamicton, lithostratigraphic Unit 2.2, 24.70-24.90 mbsf. c) Dolerite lonestone resting on bed of intact and broken shells, belonging to muddy packstone facies, lithostratigraphic Unit 3.1, 32.82-33.04 mbsf. *d)* Shelly clast-rich sandy diamicton, lithostratigraphic Unit 3.1, 33.47-33.71 mbsf. e) Muddy packstone with prominent fragments of bryozoa, lithostratigraphic Unit 3.1, 32.47-32.71 mbsf

Interpretation. The massive diamicton probably represents either sedimentation close to the grounding-line of an ice shelf or glacier tongue, or proximal glacimarine sedimentation in an iceberg-dominated environment where continuous rain-out of basal debris is occurring without significant winnowing by bottom currents or effective biogenic activity. More distal glacimarine conditions are indicated by the intervals with lesser proportions of clasts in a sandy/muddy matrix. The fine-grained component may also be derived from suspended sediment emanating from subglacial streams at a grounding line, or from a variety of other sources.

Lithological Unit 2.2 (22.00-29.49 mbsf), Sand, Sandy Mud and Minor Diamicton

Description. The dominant lithology in lithological Unit 2.2 is an olive-black (5Y 211) moderately to poorly sorted, muddy, fine to medium sand. It is compact but uncemented. The sand component comprises mostly quartz and feldspar, and also more than 10% (locally 30%) volcanic glass. One interval, at 26.50-27.15 mbsf, is fossiliferous, with foraminifera and fragments of bivalves among the fossils identified. Minor facies include (i) sandy mud as a gradational variant of muddy sand; however, the core is disturbed by drilling, and (ii) clast-poor to clast-rich muddy diamicton in which clasts of granite and dolerite up to 3 cm in largest occur. The lower contact was not recovered.

Interpretation. Deposition in a shallow-marine setting is suggested for the sand and mud fractions, but the absence of sedimentary structures precludes identification of the processes involved. The gravel, as well as some other fractions, was probably contributed by icebergs, and, where diamicton is present, a proximal glacimarine setting is envisaged. The glacial component appears to be of basal-ice derivation on the basis of clast shape.

Lithological Unit 2.3 (29.49-31.70 mbsf), Diamicton

Description. Lithological Unit 2.3 is made up mainly of olive-black (5Y 2/1) clast-poor to clast-rich muddy to sandy diamicton. The sediment is compact but uncemented, and is thickly-bedded. It grades especially between pebbly sand and sandy mud, and silty sand and muddy granule gravel. Clasts are up to pebble size (6 mm maximum), in concentrations ranging from 1 to 55%. They are mainly of granite or dolerite, but some consist of weakly indurated sandstone. The lower contact is gradational over 1-2 cm.

Interpretation. Shallow-marine deposition is suggested, with icebergs close to the source glacier dominating the supply of debris. Alternatively, the diamicton may have been deposited just seaward of the grounding-line of the glacier. Recessional phases are indicated by the sandy muds and muddy sands.

Lithological Unit 3.1 (31.70-33.82 mbsf), Muddy Sand and Packstone

Description. Highly fossiliferous, very poorly sorted, muddy gravelly sand makes up lithological Unit 3.1. The colour ranges from greenish grey (5GY 6/1) to olive grey (5Y 4/1). The sediment is compact but uncemented. The unit is characterised by both weak and strong, thin to medium bedding, as well as grain-size variations. Locally bedding is defined by micro-shell beds. Bedding inclined

at a few degrees is typical. Contacts between beds vary from sharp to gradational. Stratification is defined by variations in fossil content and orientation, including bryozoans (dominant), gastropods, foraminifers, bivalves, sponge spicules, echinoderm spines and worm tubes. The clasts range from granules to cobbles, with angular to subrounded shapes. Concentrations of clasts average 1-5%, but locally reach 75%. Lithologies include dolerite (dominant), granite and finer grained volcanics. The terrigenous sand component is mostly quartz and feldspar. Minor lithologies include fossiliferous clast-rich sandy diamicton and fossiliferous calcareous sandy mud. The lower contact is sharp.

Interpretation. Open-water shell-bank, with fossils indicating a 100-150 m water depth, with sedimentation controlled by weak currents. Entire shells are mainly *in situ,* but most of the sediment comprises broken fragments, although these have been transported only a short distance. Slow calcareous sedimentation rates and reworking of bioclastic layers are indicated, superimposed on which is iceberg-rafting of terrigenous sediment. Deposition is probably in a distal position to the glacier grounding-line.

Lithological Unit 4.1 (33.82-43.55 mbsf), Diamicton

Description. Lithological Unit 4.1 comprises weakly stratified, clast-poor to clast-rich muddy to sandy diamicton. Colours range from olive grey (5Y 4/1) to olive black (5Y 211). The sediment is compact and uncemented. Bedding is defined by gradational contacts and gravel concentrations. Clast abundance covers the full range of diamicton types (1-30%), but averages about 3-5%. Clasts are mainly subrounded to subangular in shape. Lithologically, the clasts include volcaniclastic sandstone, granite, mudstone and dolerite. Minor clast lithologies include breccio-conglomerate (up to 80% clasts), sandy mudstone, pebbly fine-grained sandstone and fine-grained volcanic sandstone. A few fossil fragments occur at 4 levels. The core is brecciated below 40 mbsf. The sedimentary contact with Miocene sandstone is missing, and the rock is heavily fractured above and below the boundary.

Interpretation. Shallow-marine sedimentation, with a high input of iceberg-derived debris, is envisaged in a proximal glacimarine setting. Alternatively, deposition near the grounding-line is possible. Background sedimentation of sand and suspended mud is evident in phases with less intense iceberg-rafting, indicating slightly advanced glacier conditions compared with adjacent beds.

SEQUENCE STRATIGRAPHIC INTERPRETATION

A preliminary sequence stratigraphic model has been developed for the entire section cored in CRP-1 (see Miocene Strata, this volume - section on Sequence Stratigraphic Interpretation). The model attempts to account for cyclical vertical arrangements of lithofacies within the core by invoking cycles of relative sea-level change associated with advance and retreat of glaciers across the area of the drillsite.

For the most part, the lithofacies recognised within the Quaternary part of the core are comparable with those from the Miocene section. The principal difference lies in the occurrence of a bioclastic carbonate interval (31-34 mbsf: Facies B3, B4), which has been interpreted as the deposits of a relatively offshore, quiet, intermittently current-washed marine environment. As such, it is broadly similar to the fine-grained clastic facies (B2), perhaps with sonic differences in water temperature and clarity, etc. Using the Facies Scheme detailed above, and the premises outlined in Miocene Strata, section on Sequence Stratigraphic Interpretation (this volume), two complete cycles can be recognised within the cored Quaternary section. These are comparable in vertical facies succession and thickness to those in the Miocene section, and are therefore interpreted in the same way (see Miocene Strata, this volume - Fig. 3, section on Sequence Stratigraphic Interpretation). One significant implication of this is that the controls on sediment accumulation (and perhaps environmental conditions) that were active in the Miocene were also active in the Quaternary.

SEDIMENTOLOGY

INTRODUCTION

In addition to the characterisation of the cored sediment by describing its visual appearance as exposed on the cut surface of the working half, several more specific sedimentological techniques were used. These additional data are used to help characterise the sediment more fully in order to facilitate environmental interpretations and also to help in facies designations. The techniques employed were half core X-radiography of particular intervals, clast shape analyses in diamictons and diamictites, variation of clast proportions down the core, and a comprehensive description of the carbonate-rich interval between 31.89 and 33.82 mbsf. Results from these studies are summarised below.

X-RADIOGRAPHY AND SEDIMENTOLOGICAL FEATURES

X-radiographic images of the half-cores were obtained using a Torrex 120-D x-radiographic machine that produces real-time video imagery as each 1-m-long section of core is passed through the machine. The imagery of the split working half of the core was recorded on S-VHS (NTSC system) video tapes before any sampling had taken place. Settings of x-ray intensity used for exposing the Quaternary section were mostly at 4 mA and 85 kV.

The Quaternary section is very weakly lithified and consequently, most of the core could not be X-radiographed because it was not in a core liner. The total thickness of Quaternary age sediment X-rayed was only 1.91 m (c. 4% of the total Quaternary section). A further problem with X-radiographing this section is its brecciated character, at least in approximately the

Tab. 2 - List of the x-radiographed intervals.

Box	Interval	Lithology
1	20.58-21.04	Diamicton
1	25.72-26.35	Sandy diamicton
2	27.10-27.43	Sandy diamicton
4	32.55-32.82	Laminated shelly sands
6	40.66-40.90	Diamicton with pebbles
7	41.95-42.06	Diamicton with pebbles
7	42.35-42.42	Diamicton
7	44.28-44.44	Diamicton

lower 10 m. A list of the x-radiographed intervals is presented in table 2 and significant features that were noted in these intervals include:

1. Diamictons are internally structureless and do not appear to have a preferred orientation of their clasts as seen in the vertical face. They appear to be more clast-rich and sandy (e.g., 20.58 to 21.04 mbsf; Fig. 2a) than the diamictites in the older intervals of the core below about 45 mbsf.
2. Confirmation that the carbonate-rich interval is stratified is based on the relative proportions of carbonate sand and siliciclastic sediment (e.g., 32.60 to 32.80 mbsf; Fig. 2b). Contacts between the very thin beds defined by this variation are gradational on 0.5 - 1.0 cm scale.

CLAST VARIABILITY

The proportion of area covered by clasts on the cut face of the working half of the core, as expressed as clast percentage, is presented in figure 3 plotted against the stratigraphic depth. These percentages are strongly influenced by the size of individual clasts, and that problem is partly addressed by presenting simple number counts of clasts in the 4-m-log (Appendix 2). Variations in clast percentages are often used as an indicator of proximity to a glacier, and in CRP-1, there is a strong correlation between high clast percentages and the occurrence of diamict. However, individual diamict units contain different clast proportions. For example, the diamictite of Unit 6.3 has a mean clast concentration of about 10% whereas the diamicton of Unit 4.1 has a mean clast concentration of greater than 20%. Furthermore, the proportions of clasts vary greatly within individual diamict units, often between 1% and 100%; the latter number indicates clasts larger than the core diameter.

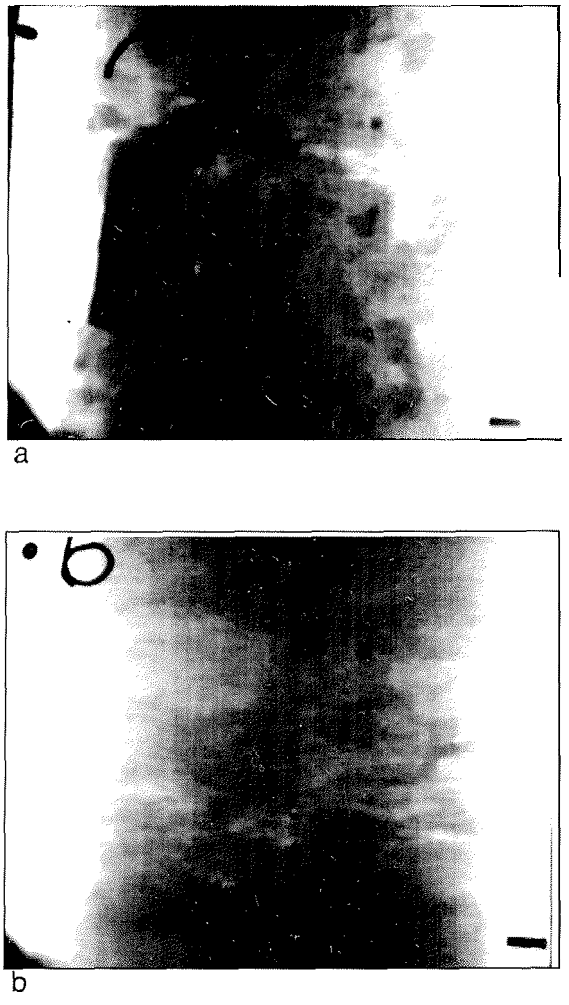

Fig. 2 - Two X-radiographs from the Quaternary interval where scale is shown as 5 cm of depth between the tick marks on the left and right side of the image. The first image (a) is of the diamicton at 20.70 mbsf showing its structureless, coarse texture. The other image (*b*) at 32.60 mbsf is in the carbonate interval and shows the higher siliciclastic content of layers at the top and bottom of the image versus the shelly-rich debris of the thin bed in the middle.

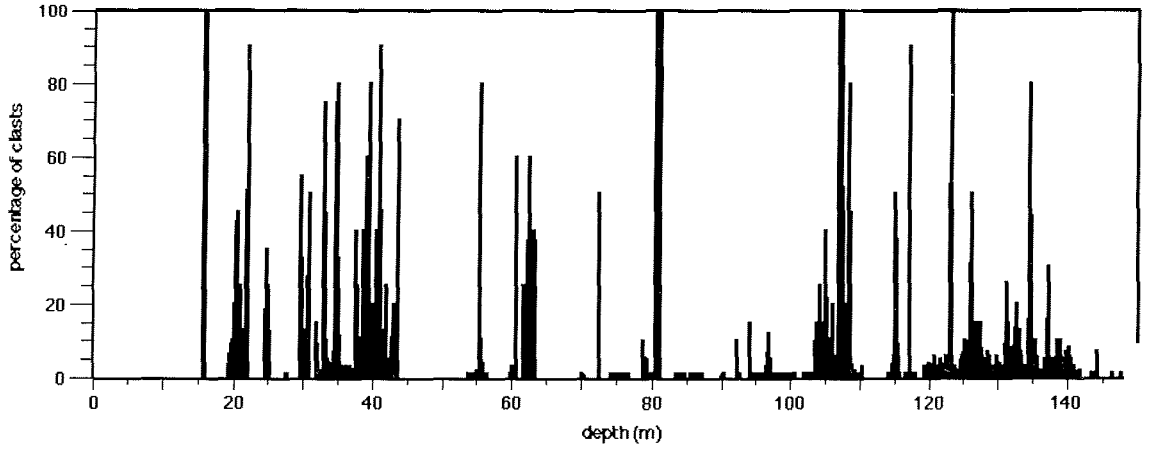

Fig. 3 - Clast percentage, counted on the cut surface of the core working half, plotted against the stratigraphic depth of the CRP-1.

CLAST SHAPE

Introduction

Clasts occur in much of the Quaternary interval of the CRP-1 core down to a depth of 43.55 mbsf. They are more abundant in the diamicton units, making these suitable for clast shape analysis. The three diamicton units sampled were lithostratigraphic Units 4.1 (33.82-43.55 mbsf), 2.3 (22.00-29.49 mbsfj and 2.1 (19.13-22.00 mbsf). A total of 86 clasts were removed from the core and examined. Of these, 34 (39%) were whole clasts, the remainder having been coredor sawn. Lithology of each clast was determined and the roundness assessed using the Krumbein-Powers visual roundness chart. Clasts were then examined for the presence of facets and surface features such as striae. These data are summarised in figure 4.

Roundness

Roundness of clasts in each unit is shown graphically in the histograms in figure 4, and these distributions have been compared with histograms of clast roundness from sediments in a modern glacially influenced Arctic environment (Bennett & Glasser, 1996). Unit 4.1 at the base of the Quaternary section shows a broad distribution with a mean roundness of 0.35 (subangular) typical of subglacially transported debris. The occurrence of rounded clasts may indicate the reworking of older fluvial material into the glacial source.

Only 14 clasts were collectable from Unit 2.3, which is less than desirable for reliable characterisation of the unit. However, the limited data show a similar broad distribution but with a marked peak in the subrounded category, indicating the clasts are also from subglacial debris with reworked fluvial component. In contrast to the two lower diamicton units, a more reliable data set of 40 clasts from Unit 2.1 provides a more complex distribution with peaks in the angular and subrounded categories and a mean roundness of 0.32 (subangular). This is still consistent with a subglacial debris assemblage but suggests also that supraglacial sourced debris is included in the deposit.

Striae, Facets and Lithology

Striae and facets occur on clasts in the diamicton units and are distinguishing characteristics that provide evidence of basal transport in a glacier. Development of these features depends largely on clast lithology. The dominant lithologies in these units are granite and dolerite (over 60% in all three units) with the rest being volcanic and

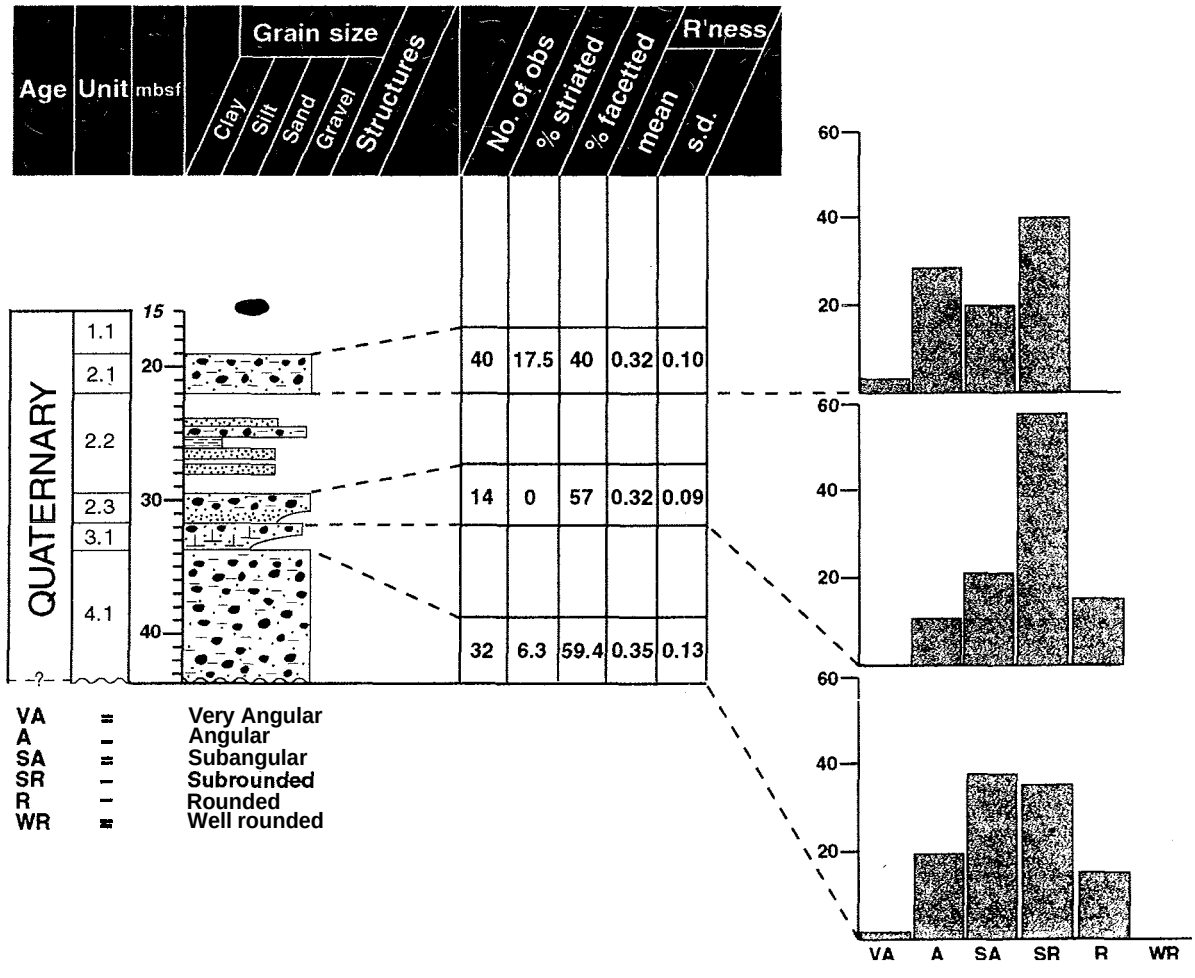

Fig. 4 - Core log for the Quaternary section of CRP-1, showing summary shape characteristics and roundness histograms.

sedimentary in origin. While facets are present on ovei 40% of clasts from all three units and on all lithologics, striae are loss common and found only on the fine grained volcanic, sedimentary, and some dolerite clasts. Unit 4.1 displays 6% striated clasts. Unit 2.3 has none and Unit 2.1 has 17% striated clasts. Several of these clasts showed two and possibly three sets of striae indicating basal transport in a glacier.

Summary

The shape characteristics of clasts in the diamicton units of the Quaternary interval of the CRP-1 core suggest the clasts have undergone subglacial transpoit with the incoiporation of reworked, rounded clasts and, in the case of Unit 2.1, a possible supraglacial component. This indicates ice grounded near the site oi actively calving icebergs introducing ice-iafted debris to the deposit.

DESCRIPTION AND INTERPRETATION OF THE CARBONATE-RICH UNIT

Introduction

A carbonate-rich unit in the Quaternary section between 31.89 and 33.82 mbsf lies in sharp contact with underlying and overlying, predominantly terrigenous sediments (Fig. 5). Here a detailed description of this peculiar unit is provided in order to describe the sedimentary facies, characterize their vertical organization, and interpret their depositional setting.

Ten undisturbed bulk samples were inspected in detail under a binocular microscope for describing microfacies, fabric and major components. Samples were then washed on standard sieves of different mesh-size and the residues were analyzed to better evaluate the components in the various fractions (Tab. 3).

Carbonates of this unit are entirely skeletal, consisting of whole to fragmented hard parts of benthic organisms (Fig. 6). This is hardly surprisingly since biogenic production is the only known Quaternary source for Antarctic carbonate sediments (Domack, 1988; Taviani et al., 1993). Coarse to minute bryozoan skeletal debris predominates over other bioclastic components (mostly foraminifers, molluscs, echinoids and octocorals). As such, these carbonates basically represent a *bryomol* type of sediment, typical of cool-water shelves (Nelson et al., 1988; Schafer et al., 1996).

Description

A detailed sedimentological analysis of the carbonate-rich unit allows us to distinguish four main intervals (Fig. 7).

The core interval between 33.82-33.30 mbsf is a mixed siliciclastic-carbonate sediment with a 10-40% biogenic component. The contact with the underlying diamicton unit is sharp. The colour is greenish grey, gradually becoming darker in the upper part. The terrigenous fraction includes silt and fine-to-very fine polymictic sand; some

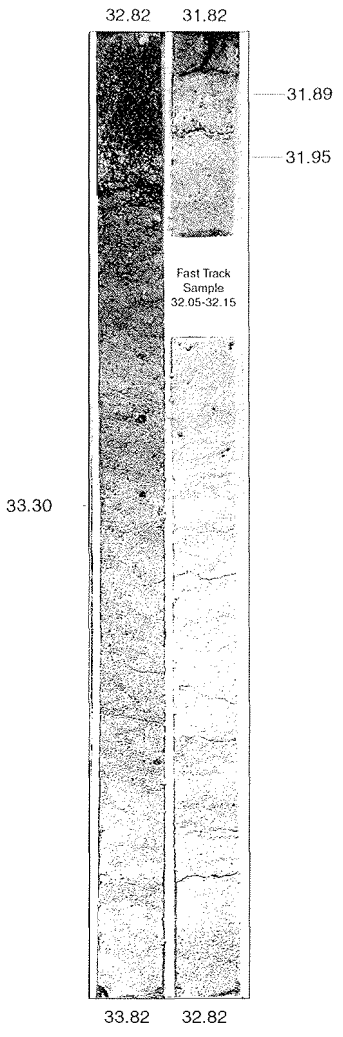

Fig. 5 - Photographic log of the carbonate-rich unit (from 31.89 to 33.82 rnbsf).

granules and small pebbles are present throughout this interval, but their frequency increases upwards. The biogenic sandy-fraction includes bioclasts/biosomes derived from bryozoans, foraminifers, octocorals, gastropods, bivalves, sponge (spicules), barnacles and echinoids.

The base of the interval is thin bedded due to the alternation of coarse bioclast-rich and fine bioclast-poor layers (Fig. 8). This vertical arrangement becomes less evident in the upper part, where layering is poorly defined. Often, elongated fragments of bryozoans and octocorals show imbrication and preferred orientation within the coarse layers.

The interval between 33.30-32.82 mbsf records a decrease in the carbonate component (to 10-15%). The colour darkens rapidly to become olive black at the very top.

This interval shows an increase in ice-rafted debris (IRD) culminating at 32.90 mbsf in the deposition of a predominantly polymictic, poorly sorted layer with cobbles up to 20 cm (Fig. 9). A pocket of coarse, mixed terrigenous-carbonate sediment is evident at the base of a large doleritic cobble (32.95 mbsf). The bioclastic component is mostly echinoid spines and large flat bivalve fragments. Overall, the carbonate biogenic fraction is similar in

Tab. 3 - Description and compositional characteristics of representative intervals of the carbonate-rich unit.

Interval (mbsf)	Sediment type	Main biogenic components > 1 mm	> 500 µm	> 63 µm	Comments
31.93 31.90	mixed siliciclastic-carbonate sand	bryozoans (dominant), benthic foraminifers, bivalves, gastropods, octocorals, echinoids (spines), serpulids, brachiopods	bryozoans (dominant), benthic foraminifers, octocorals, serpulids, sponges (spicules), bivalves, gastropods, echinoids (spines), brachiopods	bryozoans, foraminifers, echinoids (spines)	predominance of lithics (including significant volcanic glass)
32.40 32.37	bioclastic fine-medium sand (carbonate component up to 60-70%)	bryozoans, gastropods, benthic foraminifers, bivalves, octocorals, echinoids (spines), ostracods, serpulids	bryozoans, gastropods	foraminifers, bryozoans, echinoids (spines)	multiple grain thin layers (up to 1 cm), preferred orientation of elongated particles (bryozoans), clay chips
32.37 32.34	bioclastic fine-medium sand (carbonate component up to 60-70%, or higher in the fine fraction)	bryozoans, gastropods, bivalves, serpulids, echinoids	bryozoans, gastropods, bivalves, echinoids (spines), serpulids	bryozoans, foraminifers, echinoids (spines), octocorals, sponges (spicules), gastropods, bivalves	
32.61 32.58	bioclastic fine-medium sand (carbonate component up to 70-80%)	bryozoans, gastropods, bivalves, octocorals, serpulids, echinoids (spines), bivalves	foraminifers, bryozoans, sponges (spicules), ostracods, gastropods, bivalves, octocorals, serpulids	foraminifers, bryozoans, echinoids (spines)	well defined couplets, imbrication and preferred orientation of elongated particles (octocorals and bryozoans), clay chips
32.80 32.77	silty fine sand with bioclasts (with scattered volcanic granules and small gravels)	octocorals, bivalves, echinoids (spines), bryozoans, barnacles, gastropods	octocorals, foraminifers, echinoids (spines), ostracods, serpulids	foraminifers, octocorals, bryozoans, echinoids (spines), sponges (spicules)	some biogenic particles are yellow-stained, fragmented and worn (relatively prolonged exposure on the sea-bottom)
32.98 32.95	sandy silt with bioclasts (carbonate component c. 15%)	bryozoans, gastropods, echinoids (spines), octocorals, barnacles	bivalves, gastropods, echinoids (spines), octocorals	foraminifers, echinoids (spines), bivalves, sponges (spicules)	largest bioclasts concentrated below a dolerite cobble, terrigenous fraction predominantly volcanic
33.01 32.98	silty sand with bioclasts (carbonate component c. 10%)	bryozoans, gastropods, benthic foraminifers, bivalves, echinoids (spines), octocorals, barnacles	bivalves, gastropods, serpulids, echinoids (spines), octocorals	foraminifers, echinoids (spines), bivalves, sponges (spicules)	terrigenous fraction predominantly volcanic

Tab 3 - Continued.

Interval (mbsf)	Sediment type	Main biogenic components > 1 mm	> 500 µm	> 63 µm	Comments
13.34 33.31	mixed siliciclastic-carbonate sand	bryozoans, bivalves, serpulids, echinoids (spines), gastropods, octocorals, benthic foraminifers	bryozoans, bivalves, serpulids, octocorals, gastropods, formas, echinoids (spines)	bryozoans, foraminifers, sponges (spicules), echinoids (spines), serpulids, ostracods	well defined couplets, imbrication and preferred orientation of elongated particles (octocorals and bryozoans)
33.53 33.50	mixed siliciclastic-carbonate sand	bryozoans, echinoids (spines), benthic foraminifers, octocorals, barnacles, bivalves	foraminifers, gastropods, bryozoans, echinoids (spines), ostracods	foraminifers, bryozoans, sponges (spicules), echinoids (spines)	
33.75 33.72	mixed siliciclastic-carbonate sand	bryozoans, echinoids (spines), benthic foraminifers, octocorals, bivalves, gastropods, serpulids, barnacles	foraminifers, bivalves, gastropods, bryozoans, echinoids (spines), ostracods	foraminifers, echinoids (spines), ostracods, bryozoans, sponges (spicules), bivalves	

composition to the interval below. The majority of the coarse bioclastic fraction is concentrated just below the dolerite clast. This interval appears to be massive with no evidence of layering.

Above the IRD layer, the interval between 32.82-31.95 mbsf represents a peak in carbonate accumulation making up to 70% or more of the sediment. The main biogenic components are foraminifers, bryozoans, bivalves, gastropods, octocorals, echinoids, sponges spicules, ostracods and serpulid worm tubes. In a few cases, bryozoans appear to be preserved in growth position (32.50 mbsf: Fig. 10). The terrigenous matrix is represented by silt and fine-to-very-fine sand with minor amounts of coarser dolerite and volcanic granules.

This interval displays a well-developed, thin alternation of bioclast-concentrated (up to several cm thick) and bioclast-depleted levels (normally only few mm thick). The coarse bioclastic layers normally show preferred orientation of elongated bioclasts (generally bryozoans and octocorals) or an imbricated fabric, and in places contain small clay chips. The contact between coarse and fine-grained layers is always discrete, but no evidence of abrupt or scoured surfaces is recognizable.

The interval between 31.95-31.89 mbsf shows a decrease in the carbonate fraction and a greater admixture with ice-rafted detritus. The biogenic component is represented by foraminifers, bryozoans, echinoids, octocorals, and bivalves. The terrigenous component is dominantly poorly sorted silt and fine sand with small dolerite pebbles and granules.

Facies definition

The entire carbonate-rich unit can be conveniently subdivided into two main facies, based on overall composition, proportion between terrigenous and biogenic components, type of sedimentary structures and fabric.

Facies A is basically represented by alternating mm-to-cm-thick, medium to coarse bioclastic layers (packstones) and finer, mm-to-cm-thick muddy layers. Bioclastic layers often display imbricated fabric, total or partial absence of matrix, preferred orientation and packing of its skeletal components (mostly bryozoans). Muddy layers often retain delicate aragonitic biosomes. In certain intervals, there is alternation of coarse and fine-grained layers, forming distinct couplets (Fig. 8). Admixture with terrigenous components varies considerably.

The ratio between terrigenous and bioclastic components may serve to subdivide *Facies A* into two main subfacies.

Subfacies A1 is predominantly terrigenous, although carbonate components are obvious, but often below *c.* 15%. *Subfacies A1* typifies the lower part of the carbonate-rich unit, between 33.82 and 33.30 mbsf. Couplets are well developed (Fig. 8).

Subfacies A2 is predominantly carbonate ($CaCO_3$ content up to *c.* 70-80%), although variable admixture of lithics may be present. When preserved (Fig. 10), couplets are thinner than their equivalents in *Subfacies A1*. A distinct series of couplets predominates in the interval between 32.82 and 32.25 mbsf, grading upward into more homogeneous, coarser, bioclastic sands. This subfacies

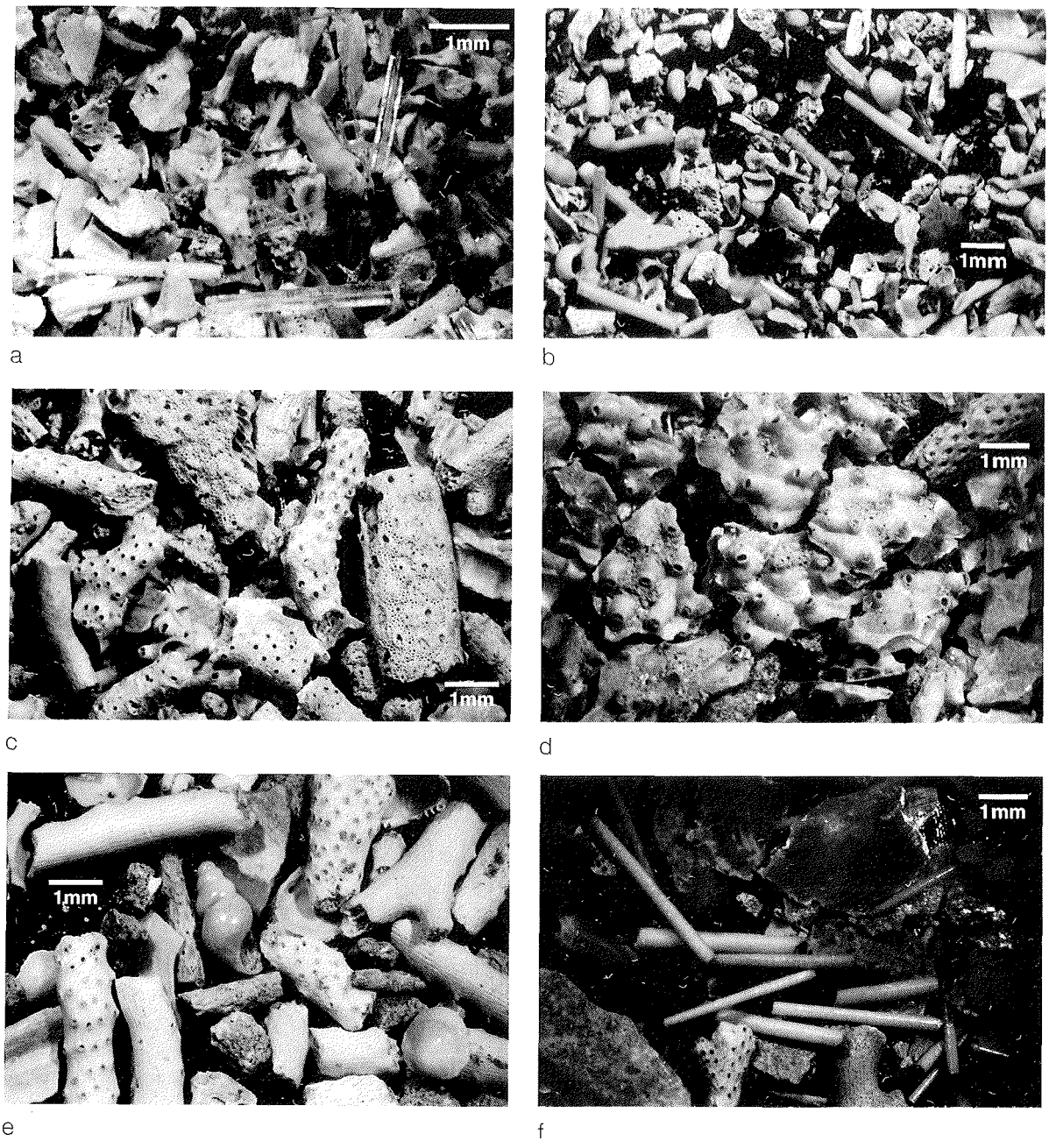

Fig. *6* -Examples of grain assemblages from the carbonate-rich unit. *a)* Carbonate-dominated particle assemblage (fraction > 500 mm): sediment is prevalently fragmented bryozoans, echinoid spines and sponge spicules (32.34 mbsf). b) Carbonate-dominated particle assemblage (fraction > 500 mm): skeletal particles are very diverse and include fragmented bryozoans and molluscs, benthic foraminifers, echinoid spines and sponge spicules (32.77 mbsf). *c)* Bryozoan-dominated skeletal assemblage (fraction > 1 mm); note absolute predominance of elongated-bryozoan skeletal parts (32.58 mbsf). d) Bryozoan-dominated skeletal assemblage (fraction > 1 mm); note absolute predominance of foliaceous-bryozoan skeletal parts (32.37 *mbsf*). ***e)*** Typical *bryomol*-type carbonate sediment (fraction > 1 mm) showing overwhelming importance of bryozoan and molluscs skeletal parts (32.31 mbsf). *f)* Peculiar echinoid-rich gravelly-sand from the base of a large dolerite cobble (32.95 mbsf: fraction > 1 mm).

characterizes the interval between 32.82 and 31.89 mbsf, laying immediately above an IRD rich layer.

Facies B is a predominantly terrigenous sediment with little admixure of a bioclastic component. It may incorporate almost bioclastic-free, pebbly-gravelly sands representing IRD (32.98 mbsf: Fig. 9). The contacts (*c.* 33.30 and 31.95 mbsf) with underlying Facies A are gradational.

Discussion

A persistent depositional theme seems to characterize the entire carbonate-rich unit. The most prominent feature is the repetition of current-influenced bottom conditions resulting in the formation of shell lags alternating with muddy layers. Times of little current activity are marked by the deposition of fine-grained sediment veneers, but these are seldom preserved intact. Currents had enough energy to rework carbonate grains, causing total or partial winnowing of the fine matrix, imbrication of clasts and preferred orientation of elongated particles.

A palaeodepth in excess of 100 m (possibly in the range of 100-150 m or more) has been inferred from the fossil assemblage. Considering the estimated water palaeodepth, it is hypothesized that currents may have

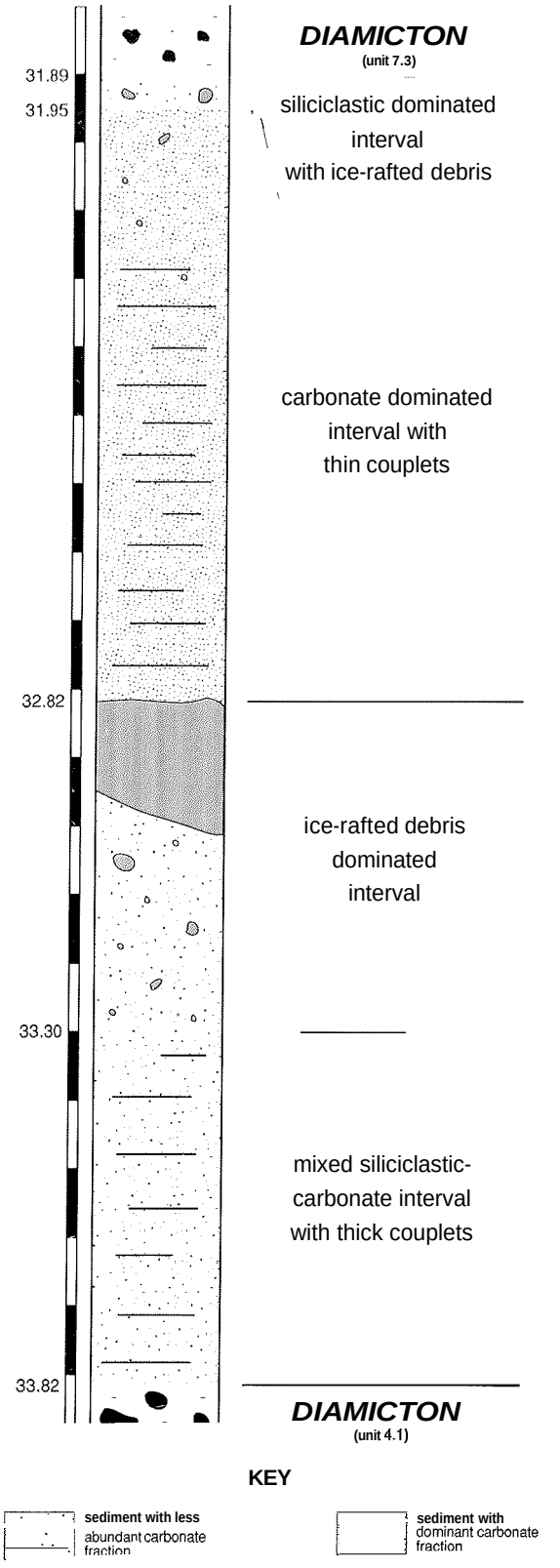

Fig. 7 - Schematic log showing the principal intervals recognized in the carbonate-rich unit.

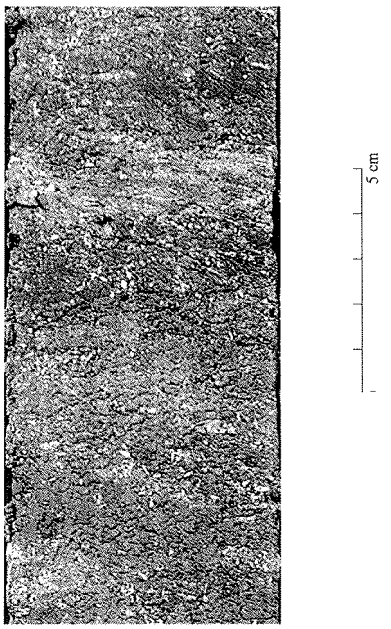

Fig. 8 - Example of the couplets in the Facies A1 (33.80-33.66 mbsf).

Fig. 9 - Detail of the upper part of the Facies B, dominated by ice-rafted detritus. Note relative coarsening of sediment at the base of the large dolerite cobble, possibly eddy-generated (32.85-33.09 mbsf).

been generated during particularly strong storms, not by the direct action of waves, but possibly by return flow currents. The resulting energy was moderate as evidenced by the: (1) preservation of delicate skeletal biosomes within packstones (including thin-walled aragonitic shells), (2) lack of substantial wear in many bioclasts, (3) recurrent preservation of previously-deposited thin layers,

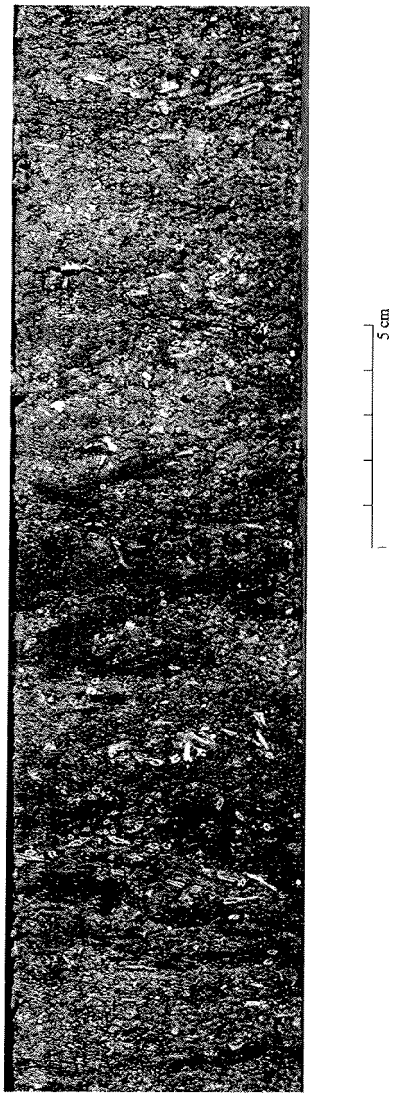

Fig. 10- Detail of the lower part of Facies A2, showing high concentration of bioclastic sediments. The couplets are thinner than in Facies **A1.** In the lower part bryozoans appear to preserved in growth position; in the upper part fragments of bryozoans and octocorals display imbricated fabric (32.44-32.67 mbsf).

(4) complete absence of biota typically thriving under strong bottom currents. It is likely that most bioclasts were sourced only a short distance away from their depositional setting, as suggested by substantially in *situ* branched bryozoans in close association with bryozoan-rich packstones.

Skeletal carbonate muddy sands with similar biota are known to occur in the upper Pleistocene and Recent of Antarctic banks and deep-shelves *(e.g.,* Taviani et al., 1993). There, carbonate sediment may be formed because of the combination of healthy benthic biologic productivity, open-marine conditions, the absence of an ice-shelf, relatively shallow-water depths, and little dilution by terrigenous sediment. It is reasonable to infer that the topographic high on which the site has been drilled had temporarily acted as a sediment-starved bank under open-marine conditions where carbonate biota could thrive at times during the Pleistocene.

This depositional theme shows temporary interruptions, notably by fluxes of poorly sorted terrigenous sediment, most probably ice-rafted detritus. The most conspicuous of these events is marked by the cobble-bearing layer. The external surface of the cobble is devoid of attached epifauna (foraminifers, bryozoans, barnacles or corals) or their biological scars, suggesting short-lived sea-bottom exposure. The sandy fraction of this IRD layer shows evidence of reworking by bottom currents.

In summary, the carbonate-rich unit is interpreted as bank-type sedimentation occurring under open-marine conditions. The presence or absence of seasonal sea-ice cannot be established based on the carbonate sedimentary record alone. Fair-weather conditions are marked by the deposition of muddy layers. Storm-triggered currents may have been episodical, but they generate deposits that are possibly better recorded in the unit because thin, fair-weather layers were more easily winnowed away or reworked. The supply of terrigenous sediment to the carbonate bank was initially high, diminishing with time. The time of prolific carbonate production over the bank marks a period of glacial retreat and optimal climatic conditions. The complete shut-off of the carbonate factory seems to have been quite an abrupt phenomenon, likely linked to a glacial readvance.

PETROLOGY

INTRODUCTION

The clastic (rock and mineral) content of the Quaternary sequence is characterized here. A variety of different methods of analysis was used, based on a primary subdivision according to grain size. The distribution and type of coarse clasts (>2 mm) was examined visually in the core and on selected samples using thin sections; sand-size grains were examined in samples selected from all lithologies encountered, but with special emphasis on sand layers, mainly using smear slides; and XRD measurements using an automated diffractometer system were used to identify and quantify clay minerals in the silt-grade fraction of bulk samples. Together, these methods enabled the provenance and down-hole provenance variations to be documented qualitatively, details of which are given below.

BASEMENT CLASTS

Introduction

This section presents the primary results of a preliminary petrographical investigation of basement clasts in Quaternary strata of the CRP-1 borehole. The supply of clasts from the Precambrian-lower Paleozoic basement into Quaternary marine sediments in the McMurdo Sound area has previously been documented only in a short sequence (<10 m) recovered in the MSSTS-1 borehole, where granitoid and metamorphic rocks have been reported (Barrett et al., 1987). Because of the potentially longer time interval recorded in the CRP-1 core, the distribution and lithological nature of CRP-1 basement clasts may provide a larger dataset recording denudation of the

crystalline basement during the Quaternary. This section describes the pebble- and granule-size classes and deduces the most likely sources.

Methods

Sampling, macroscopic observations and preliminary petrographical analysis (polarized light microscopy) were carried out following a preliminary subdivision of clasts into two main grain-size groups:

1. pebbles with diameters larger than 8 mm, which were extensively sampled and will be included in future laboratory investigations;
2. granules and small pebbles with diameters less than 8 mm, which were examined in the core using a hand lens; selected samples were also examined under the stereo-microscope.

The 8 mm size limit is conventionally chosen as the minimum clast size needed to obtain a detailed and exhaustive petrographical characterization of medium- to coarse-grained rock clasts.

A sampling strategy was adopted to ensure that a collection of samples representing all rock types in the core was obtained. Only small specimens (<1x2x0.5 cm) were completely sampled, whereas most of the coarse pebbles were cut parallel and orthogonal to the core axis in order to avoid complete removal of a whole core segment. Particular care was taken during clast sampling to ensure minimal removal of adhering fine matrix.

Results

The content of crystalline-basement clasts is generally high and ranges up to 40% of the core volume. Fourteen samples were collected and listed in table 4. This table records their clast shape and dimensions, lithology and stratigraphical position. The table also includes the main petrographical features, as well as the most probable source-rock units from the crystalline basement of Victoria Land.

Figure 11 shows the range of lithologies, distribution of the different rock types with depth, and their stratigraphical position within the Quaternary strata. Smaller pebbles and granules are mainly represented by fragments of grey biotite granite in the interval between 16.06 mbsf and 21.90 mbsf, whereas pink biotite granite is the dominant rock facies in the lower part of the sequence. Coarser pebbles are also mainly composed of grey biotite granite, whereas other rock types are distinctly subordinate and include three occurrences of fine-grained foliated granitoid (at 38.04, 42.35 and 43.44 mbsf), two of biotite haplogranite (20.90 and 30.94 mbsf) and one of pink felsic volcanic rock (at 16.06 mbsf).

The grey biotite granite clasts have isotropic fabrics and medium-grained equigranular hypidiomorphic textures. Feldspar phenocrysts are typically 3 to 8 mm in length. Mafic minerals comprise biotite and rare hornblende and constitute 8 to 10% of the rock. Preliminary petrographical analysis of one sample suggests a monzogranitic composition and incipient greenschist facies alteration (sericite after K-feldspar; saussurite after plagioclase; FeMg-chlorite and titanite after red-brown biotite).

The grey biotite haplogranites are very fine- to fine-grained and equigranular hypidiornorphic with a low modal content of red-brown biotite (3-7%).

The foliated granitoids are fine-grained and mainly consist of pale grey plagioclase crystals, up to 1-2 mm in length, set in a chlorite and /or green biotite-rich matrix. The foliation, defined by the preferential orientation of phyllosilicate lamellae, wraps around the plagioclase crystals, providing evidence of sub-solidus (post- or late-magmatic) deformation.

The pink felsic volcanic rock contains phenocrysts of feldspar, quartz (rare) and biotite (rare), set in a very fine-grained orange-pink groundmass (recrystallized glass?). The phenocryst mineralogy suggests a rhyolitic composition.

Provenance

Two main sources can be inferred on the basis of the dominant lithologies and both are part of the Granite Harbour Igneous Complex (calc-alkaline granitoids of Cambro-Ordovician age), which crops out extensively in the Transantarctic Mountains over a distance of c. 2 000 km. The two sources are: 1) post-tectonic granitoids, including either discordant plutons (for grey biotite monzogranites) or dyke swarms (for haplogranites); 2) syntectonic granitoids, including either elongated plutons or sills (foliated granitoids) (Gunn & Warren, 1962; Allibone et al., 1993a, 1993b). Available on-shore geological data indicate that both intrusive suites crop out extensively

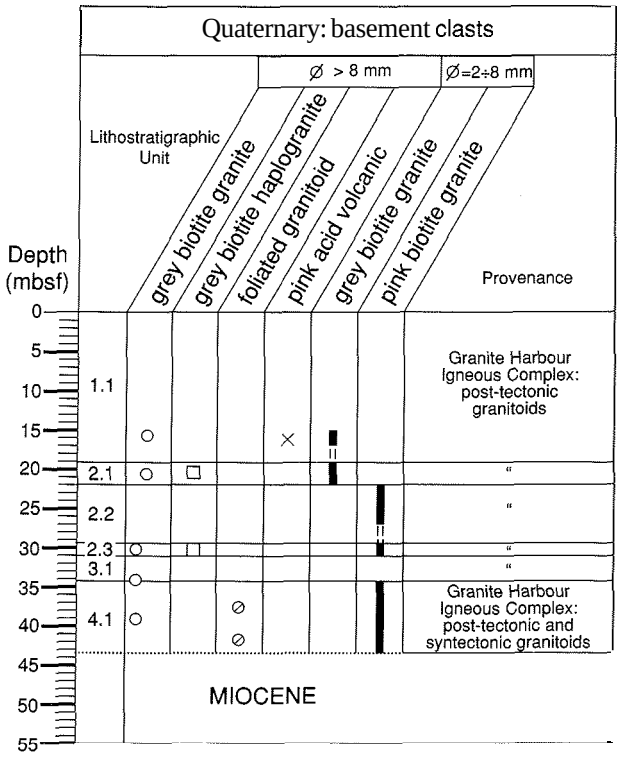

Fig. 11 - Lithology, distribution and provenance of basement clasts in Quaternary strata.

Tab. 4 - Basement clasts in Quaternary strata: list of sampled clasts and preliminary petrographical data.

Sample code	Hole	Box	Top (mbsf)	Bottom (mbsf)	Clast shape	Approximate size (cm)	Lithology	Main petrographical features	Inferred provenance	Lithostratigraphic Unit
TAL60	CRP-1	1	16 06	16 08	sub-angular	4x5x3	pink felsic volcanic nick	ryolitic composition (?), phenocrysts of feldspar, rare quartz and biotite set in a very fine-grained orange-pink groundmass, similar to TAL19	Late Paleozoic Gallipoli Volcanic Suite (?) or G.H.I.C.*	1.1
TAL61	CRP-1	1	16.07	16.08	rounded	3x2x2	grey biotite granite	fine to medium-grained, isotropic fabric, M = 10%	G.H.I.C.	1.1
TAL62	CRP-1	1	20.36	20.39	sub-angular	4x3x3	grey biotite granite	isotropic fabric, equigranular (medium-grained). M = 8%, feldspars: 3 to 8 mm in lenght	G.H.I.C.	1.1
TAL63	CRP-1	1	20.52	20.55	sub-angular	3x2x2	grey biotite granite	isotropic fabric, equigranular (medium-grained). M = 8%, feldspars: 3 to 8 mm in lenght	G.H.I.C.	1.1
TAL64	CRP-1	1	21.90	21.93	angular	0.5x1x1	grey biotite-bearing haplogranite	isotropic fabric, equigranular (fincgrained), M = 3%	G.H.I.C.	1.1
TAL65	CRP-1	3	30.34	30.35	angular	2x1x0.5	grey biotite haplogranite	isotropic fabric, equigranular (very fine-grained), M = 7%	G.H.I.C.	3.1
TAL66	CRP-1	3	30.62	30.65	angular	4x2x2	grey biotite granite	isotropic fabric, equigranular (medium-grained), M = 10%, similar to TAL 25, 27, 30	G.H.I.C.	3.1
TAL67	CRP-1	4	34.20	34.22	angular	2x1x1	grey biotite granite	isotropic fabric, equigranular (fine-grained), alkali feldspars: 2-5 mm in lenght, M = 8%	G.H.I.C.	4.1
TAL68	CRP-1	5	38.04	38.05	sub-rounded	1x1x1	very fine-grained foliated granitoid	very fine-grained, plagioclase crystals, up to 1 mm in size, set in a green micaeous matrix (chlorite or green biotite), similar to TAL 40	G.H.I.C.	4.1
TAL69	CRP-1	6	39.45	39.50	sub-rounded	5x6x5	grey biotite granite	isotropic fabric, equigranular (medium-grained), feldspars: 1-4 mm in lenght, M = 10%	G.H.I.C.	4.1
TAL70	CRP-1	6	39.74	39.77	angular	2x3x2	alteied granitoid	isotropic fabric, dark grey, medium-grained equigranular	G.H.I.C.	4.1
TAL71	CRP-1	6	40.90	40.95	sub-rounded	5x6x4	grey biotite granite	isotropic fabric, heterogranular (medium- to coarse-grained), M = 10%	G.H.I.C.	4.1
TAL72	CRP-1	6	41.92	41.95	sub-rounded	2x3x2	altered granitoid	isotropic fabric, dark colour	G.H.I.C.	4.1
TAL73	CRP-1	7	42.35	42.36	rounded	1x0.5x0.5	fine-grained foliated granitoid	fine-grained, plagioclase crystals, up to 1 mm in size, set in a green micaeous matrix (chlorite or green biotite), similar to TAL 40	G.H.I.C.	4.1
TAL74	CRP-1	7			sub-rounded	1x1x0.5	grey foliated biotite granitoid	fine-grained, foliated fabric, foliation defined by biotite, M = 10%	G.H.I.C.	4.1

Note: Lithostratigraphic unit designation follows figure 18 of Background to CRP-1 (this volume); M = colour index (percentage of mafic minerals); * Granite Harbour Igneous Complex. Samples referred to in the column on petrographical features are from the Miocene strata (see Tab.3, Miocene Strata, this volume).

along the coast between Cape Roberts and Cape Ross, and in the mountain ranges north and south of MacKay Glacier.

A local provenance is uncertain for the pink rhyolite pebble. This rock type is closely similar petrographically to theporphyriticrhyolites of the Late Palaeozoic Gallipoli Volcanics (Dow & Neall, 1974) in northern Victoria Land. Alternatively it might represent a volcanic product of the calc-alkaline Granite Harbour igneous activity. The occurrence of Cambro-Ordovician volcanic rocks has previously not been reported from the area between the Ferrar and MacKay Glaciers. Minor rhyolites also occur in the Cenozoic McMurdo Volcanic Group (Erebus and Melbourne volcanic provinces; Kyle, 1990; Armienti et al., 1991), but they consist of aphyric obsidians and are peralkaline in composition.

CLAY MINERALOGY

Clay mineral analyses were performed on 3 Quaternary samples. After sieving the samples through a 63 μm mesh, the clay fraction was isolated from the silt fraction by settling in glass beakers. The clay fraction was concentrated by centrifuge and then dispersed in about 10 ml water. The clays were mounted as texturally oriented aggregates by dropping about 1 ml of clay suspension onto aluminium tiles and evaporating the water. The mounted clays were solvated with ethylene-glycol vapour for about 12 hrs immediately before the x-ray analyses.

The XRD measurements were conducted on an automated diffractometer system Rigaku Miniflex with CuKa radiation (30 kV, 15 mA). The samples were X-rayed in the range 2-40 °2θ in steps of 0.01 °2θ with a measuring time of two seconds per step. The x-ray diffractograms were evaluated on an Apple Macintosh Personal Computer using the "MacDiff" software (Petschick, unpublished freeware).

The study concentrated on the abundance of the main clay mineral groups smectite, illite, chlorite and kaolinite based on the integrated areas of their basal reflections at *c.* 17 Å (smectite), 10 Å (illite), 7 and 3.54 Å (chlorite), and 7 and 3.57 Å (kaolinite). Only rough estimates rather than percentages can be given (Tab. 5), because of an incomplete separation of the clay from the silt fraction, and because the textural orientation of the clay aggregates on the mounts was incomplete. Especially in coarse-grained sediments, the clay content was too small or the clays were not sufficiently crystalline to yield a clear diffraction

Tab 5 Estimates of the abundance of the main clay mineral groups smectite, illite, chlorite and kaolinite in Quaternary sediments from the drillcore CRP-1. The number of crosses is proportional to the abundance of the clay minerals

Sample	Smectite	Illite	Chlorite	Kaolinite
26.89 mbsf	xxxxx	xx	xx	
30.11 mbsf	dominant			
37.50 mbsf	xxxx	xx	xxxx	

pattern. Thus the x-ray diffraction patterns obtained from many of the samples were very poor.

In the Quaternary sequence of the CRP-1 drillhole, smectite is the dominant clay mineral. Illite and chlorite occur in smaller amounts. Quartz, plagioclase and K-feldspar are also present in all samples. High smectite contents are generally indicative of either chemical weathering under a relatively warm and humid climate with intense hydrolysis or a source area dominated by basalts. Because the host sediments show evidence for ice being present on the nearby Antarctic continent throughout the time represented by the core, chemical weathering on land seems to be an unlikely source for the smectite.

Weathering the Ferrar Dolerite or any other volcanic rock possibly present in the Transantarctic Mountains or in East Antarctica is also an unlikely explanation for the high smectite concentrations, because basement-derived or Beacon-derived illite would probably strongly dilute the smectite. The smectite rather indicates a source local to McMurdo Sound, which is characterized by basaltic volcanic rocks that occur over a wide area between Ross Island and Mt. Morning (McMurdo Volcanic Group). The oldest surface samples of this region are 19 Ma (Kyle, 1990). According to magnetic surveys, many more volcanic centres of similar size but unknown age exist on the present Ross Sea continental shelf, beneath the Ross Ice Shelf and the West Antarctic ice sheet (Behrendt et al., 1994, 1995).

A source area in the McMurdo Volcanic Group is also suggested by the correlation of high smectite contents with high concentrations of volcanic glass observed in smear slides (see Tab. 6). However, glacial transport of sediment to the drill site was not restricted to the McMurdo volcanic outcrops. Thus, the relatively high concentrations of illite and chlorite accompanying smectite at all levels in the core indicate the pervasive influence of basement or sedimentary rocks, as is also indicated by the composition of the clasts distributed through the core.

All smectites in the CRP-1 core seem poorly crystalline. Poor smectite crystallinities have been observed also in the Oligocene and lower Miocene sediments of the nearby drillcores CIROS-1 and MSSTS-1 as well as in the Pliocene to Quaternary sediments of CIROS-2 (Ehrmann, 1997, in press). Although crystallinities are difficult to interpret, the poor smectite crystallinity seems to be characteristic of Oligocene to Recent sediments in McMurdo Sound.

Poor crystallinity is often connected with chemical weathering and intense degradation processes, whereas physical weathering under a glacial climate tends to produce better crystallinities. Because the Miocene sediments of the CRP-1 core show evidence for a glacial climate with physical weathering throughout, the poor crystallinity cannot be due to chemical weathering on land. Possibly the intense alteration processes and smectite formation enhanced in hydrovolcanic rocks erupted subaerially and beneath the ice or in the sea could be a reasonable explanation (Jacobsson, 1978; Wohletz & Sheridan, 1983). Another cause for the poor crystallinities could be the grain size distribution. Generally, larger smectites result in a better crystallinity than smaller smectites. With intense glacial scour on the Antarctic continent resulting in diamicts with abundant silt and clay, smaller and poorer crystalline smectites could possibly be expected.

SAND GRAINS AND PROVENANCE

Introduction

This section describes a preliminary investigation of sand grains in Quaternary sediments in the CRP-1 borehole. The study was undertaken to determine the major sand-size mineral and lithic grains present, their relative abundances and any temporal provenance variations. Although two boreholes (MSSTS-1, CIROS-1) were drilled in McMurdo Sound about 80 km south of the CRP-1 drillsite (Background to CRP-1, this volume - Fig. 1, section on Introduction), one (CIROS-1) failed to recover any Quaternary strata and only a short sequence (<10 m) was obtained in the other (Barrett et al., 1986; George, 1989). Moreover, the results of the MSSTS-1 study relied on only two thin sections of Quaternary samples. Thus, the recovery of 25 m of Quaternary sediments in CRP-1 has yielded a valuable opportunity to determine the detrital sand content of Quaternary debris in a greater number of samples and within a potentially longer time frame. The MSSTS-1 study demonstrated detrital contributions from Precambrian and lower Palaeozoic granitic and metamorphic "basement", quartzose strata of the Devonian-Triassic Beacon Supergroup, intrusive Jurassic Ferrar Dolerites, and alkaline volcanic rocks of the Cenozoic McMurdo Volcanic Group. Detritus derived from the latter was particularly abundant compared with older sections of the drillcore.

Methods

The lack of automated production of thin sections due to unanticipated mechanical problems made the study rely on smear slides for clast identifications. "Fast-track" samples were disaggregated in water and washed to eliminate the fine fraction. This also resulted in unsystematic loss of biotite and this mineral may have been eliminated from a few samples. However, most smear slides were prepared without washing and any biotite loss is unlikely to be generally important. The disaggregated samples were then gently crushed in a mortar to improve the separation of the component grains. Grains were mounted in resin with a refractive index of 1.56. Although no thin sections were made for the Quaternary samples, examination of thin sections of Miocene rocks enabled clast identifications to be verified visually.

Modal proportions of all sand grains were estimated visually using a petrological microscope. The grains were divided into petrographically similar groups (e.g., colourless grains (quartz, feldspar), ferromagnesian minerals, etc). They are described in table 6 and illustrated in figure 12. The modal results are reported in table 7 using dimensionless characters. Although numerical abundances arc used in the text, the values are qualitative only and the data do not correspond to true detrital modes, which should be restricted to counts of scdiments with a selected restricted grain size (usually medium sand). Most of the Quaternary samples are dominated by silt and clay-grade material and only five are composed largely of sand grains. The discussion will focus on the latter although the results for all samples are reported in table 7. Grain-size effects on the "modes" are thus unavoidable and they should be treated with caution.

Previous workers grouped their detrital modes to represent the proportions of sediment derived from the several main local sources described above (Barrett et al., 1986; George, 1989). Whilst it is possible to assign a likely provenance to most of the clasts observed (e.g., Tab. 6), the limitations of using smear slides (and a few unstained thin sections of Miocene samples; Miocene strata, this volume - section on Sand Grains and Provenance) prevented the reliable determination of the relative proportions of different grain types within each group (e.g., distinction between K-feldspar and plagioclase). Moreover, many lithic grains are opaque or sub-opaque in smear slides and often cannot be identified with certainty. By contrast, the volcanic-derived grains (i.e. mainly fine-grained lavas, tuffs and glass) arc often petrographically distinctive and it was relatively simple to estimate their proportion. Any inaccuracies introduced by omitting from the total volcanic counts mineral grains such as "volcanic" clinopyroxenes and feldspars are unimportant if the method of estimating is used consistently and only relative variations in volcanic detritus between samples are considered.

Results

The most abundant sand-size grains are quartz and feldspar (oligoclase, andesine, labradorite, bytownite and slightly kaolinized K-feldspar). Samples with low abundances of quartz and feldspar are invariably from diamictons in which sand-size grains are minor. The

Tab. 6 - Petrographical characteristics and inferred provenance of siliciclastic sand in the CRP-1 drillcore.

Clast type	Description	Provenance
Quartz	Mainly angular to subroundedgrains; minor but ubiquitous rounded-well roundedgrains; sharp to rarely wavy extinction; ubiquitous bubble-trail inclusions and/or rare ?rutile.	Crystalline basement, Beacon Supergroup.
K-feldspar	Distinctive dusty appearance due to partial ?kaolinite alteration; grains often abraded; mainly untwinned, rare tartan twinning (microcline); very rare sanidine.	Mainly crystalline basement.
Plagioclase	Twinned anduntwinned crystals; oligoclase and andesine often abraded and show minor sericite and/or rare epidote. Usually fresh andangular labradorite-bytownite.	Crystalline basement, Ferrar Dolerite, ?Kirkpatrick Basalt. McMurdo Volcanic Group.
Pyroxene	Mainly pale green pyroxene, in two distinctive forms: 1. abraded translucent grains with conspicuous close-spaced cleavage sometimes marked by ?exsolved opaque oxide, and rarer exsolution lamellae; includes low-Ca augite, pigeonite and hypersthene; 2. transparent angular calcic augite, very fresh-looking, lacking other distinctive petrographical features. Wide range of colouredclinopyroxenes (?titanaugite, aegirine).	Two dominant sources: 1. Ferrar Dolerite. 2. McMurdo Volcanic Group. (McMurdo Volcanic Group)
Amphibole	Mainly angular crystals of green to brownish-green hornblende. Minor kaersutite, ?arfvedsonite.	Mostly crystalline basement; ?minor input from altered Ferrar Dol. McMurdo Volcanic Group.
Biotite	Mainly brown flakes, rarely green	Mostly granitic andmetamorphic basement; possible Ferrar Dolerite.
Minor mineral grains	Apatite, zircon, garnet. celadonite, glauconite. Olivine, aenigmatite, magnetite. Celadonite, glauconite.	Crystalline basement. McMurdo Volcanic Group. Alteration of glass.
Lithic clasts	Thinly foliatedfine quartz-sericite phyllite; coarser equigranular quartz-biotiterock; fine polycrystalline quartz. Graphic- andvermicular-textured intergrown quartz and K-feldspar; platy and bladedplagioclase crystals with interstitial quartz, the feldspar lightly altered (sericite/epidote). Fine-grainedpilotaxiticfresh lavas; mainly feldspar laths and/or intergranular ?titanaugite or aegirine. Fine tuffs containing glassy pyroclasts in very fine tuff matrix. Angular to rarely slightly abradedglass coloured brown, pale brown, pale green or colourless; variable vesicularity (colourless glass may be pumiceous) and feldspar or pyroxene crystals (including aegirine).	Metamorphic basement. Ferrar Dolerite. McMurdo Volcanic Group. McMurdo Volcanic Group. McMurdo Volcanic Group (basaltic or basanitic, intermediate and evolved (incl. trachytic) comvositions.

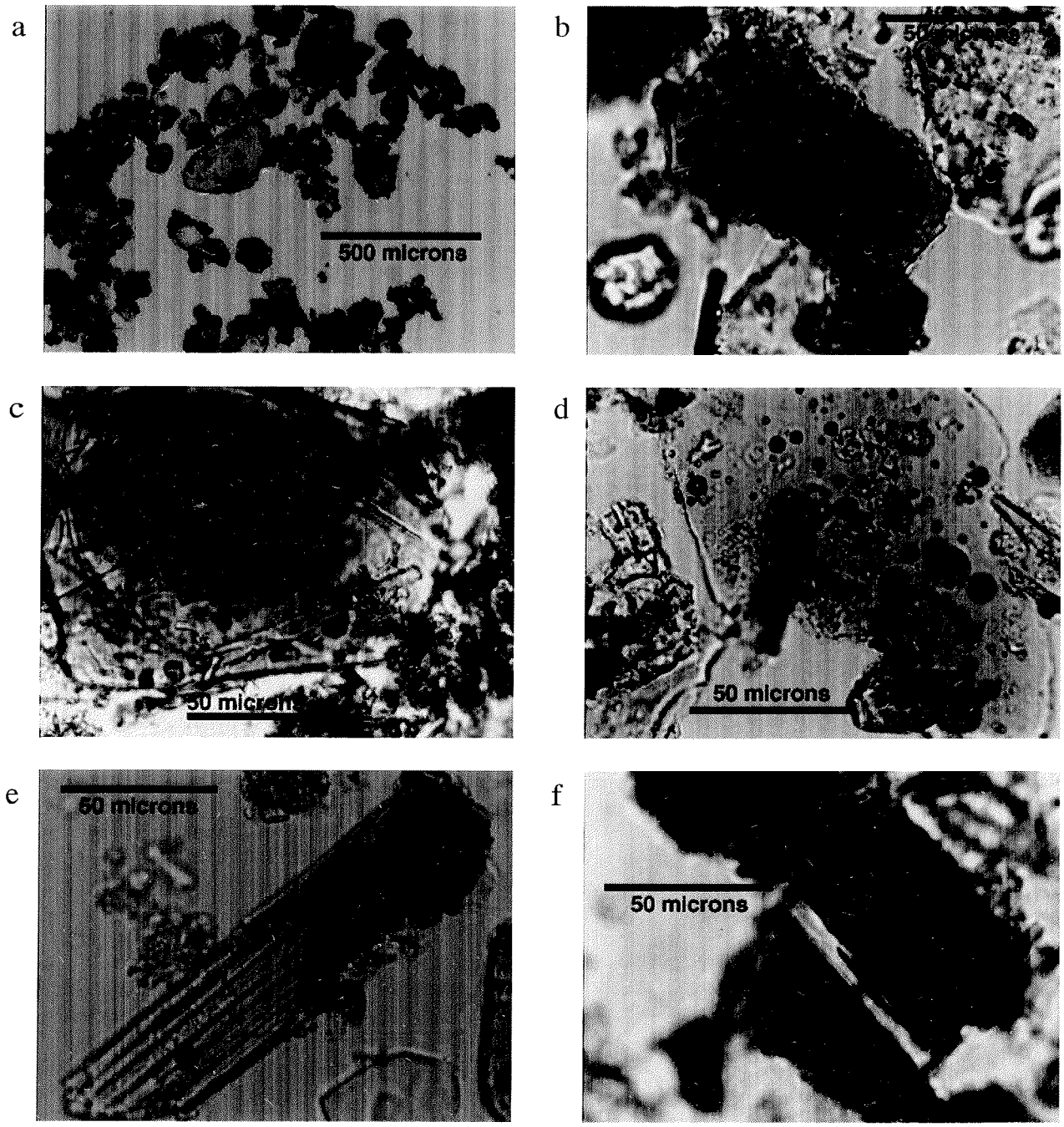

Fig. 12 - Photomicrographs illustrating the petrographical appearance of key sand grains in the CRP-1 drillhole. a) Abraded grains of quartz (light grey; centre) and pyroxene (dark grey; top); b) dark brown vesiculated glass with ovoid vesicles; vesicles in other samples may be elongate; *c)* pale brown glass of intermediate composition, poorly vesiculated and including oligoclase and clinopyroxene crystallites; d) colourless evolved glass with rounded vesicles; this glass type is commonly pumiceous and usually crystal free, always occurring in samples containing aegirine crystals; ***e)*** zoned clinopyroxene crystal compositionally zoned progressively from a very pale green augite core to darker green aegirine rims; *f)* volcanic lithic grain (lava); it is largely opaque because of oxidation of brown glass but a single prominent feldspar lath is evident; pilotaxitic textures are generally common in the lava grains.

quartz, oligoclase-andesine and K-feldspar grains are often well rounded (Fig. 12a), whereas grains of labradorite-bytownite are mostly angular.

Ferromagnesian minerals are mainly translucent, pale green calcium-poor augite, commonly abraded and showing prominent dark cleavage or rarer exsolution lamellae (Fig. 12a). Transparent pale green angular crystals of calcic augite are also common in many samples. Other ferromagnesian minerals are present in minor to trace amounts (often <<1%) and include pink (?)titanaugite, aegirine, (?)aenigmatite, (?)kaersutite, and hornblende (Fig. 12e); olivine was observed in one sample.

Volcanic glass is very common and occurs in three distinctive forms: brown, light brown to green, and colourless (Fig. 12b, c & d). Vesiculation and crystallinity vary and the glasses are essentially unaltered and lack any rounding. The colourless glass is often pumiceous.

Volcanic lithic grains are also common. They comprise fragments of oxidised fine-grained pilotaxitic lavas, which have a wide range of shapes varying from angular to well rounded (Fig. 12f).

Other mineral grains present in trace amounts include green and brown biotite, zircon, tourmaline, garnet and apatite. Bioclastic debris usually comprises traces of

Tab. 7 - Summary of qualitative "detrital modes" for grains of all sizes in Quaternary strata. Data for samples formed predominantly of sand are indicated in bold.

Sample depth (mbsf)	Section type	Lithology (as logged)	Q+F/tot	Volc/tot	Volc. lith/tot	Basic/Evolved glass	Biotite/tot	Comments
19.26	Smear	Diamicton	XXXXXXX	XXXXXXX	XXXX	B	XXXX	Tr. pyroxene, incl. aeeirine: glauconite
20.66	Smear	Diamicton	XXXXXXX	**XXXX**	XXXX	B	XXXX	Common hornblende
21.47	**Smear**	**Diamicton**	**XXXXXXX**	**XXXX**	**XXXX**		**XXXX**	
24.49	Smear	Diamicton	XXXXXXX	XXXX	XXXX	B	**XXXX**	
25.30	Smear	Diamicton	XXXXXXX	XXXXXXX	XXXX	B	**XXXX**	
26.16	Smear	Sandy mud	XXXXXXX	**XXXX**	XXXX	B	XXXX	
26.90	**Smear**	**Medium sand**	**XXXXXXX**	**XXXXXXX**	**XX**	**B**		**Tr. bioclastic, aegirine, hornblende, ?aenigmatite, zircon**
27.76	Smear	Diamicton	XXXXXXX	XXXXXXX	XXXX	BBBE	XXXX	
30.05	Smear	Sand	XXXXXXX	XX	XX	B	XX	Some devitrified basaltic glass; tourmaline, zircon
30.68	Smear	Diamicton	XXXX	XXXX	**XX**	BBE	XXXX	
31.50	**Smear**	**Clayey sand**	**XXXXXXX**	**XXXXXXX**	**XX**	**BBBE**	**X**	**Tr. Bioclastic, aegirine, hornblende, glauconite, tourmaline**
32.05	**Smear**	**bioclastic sst**	**XXXX**	**XX**	**XX**	**BBBE**		**50-60% bioclastic; tr. hornblende, ?kaersutite**
32.45	Smear	Damicton	**X**	**XXXX**		BE		Some basaltic glass with smectite
33.10	Smear	Bioclastic sedt	XXXXXXX	XXXX	**X**	BBE	XX	Tr. Aegirine, hornblende, glauconite
33.45	Smear	Diamicton	XX	**X**		BE	X	Glauconite
33.96	Smear	Silt	XXXXXXX	X		B	X	
35.25	**Smear**	**Diamicton**	**XXXXXXX**	**XX**	**XX**	E		**Tr. bioclastic, aegirine, hornblende, celadonite**
37.70	Smear	Diamicton	XXXX	**X**		B	X	Scarce oxidized basaltic glass
38.37	Smear	Diamicton	XXXXXXX				X	
38.50	Smear	Diamicton	XXXXXXX	XXXXXXX	X	BBBE	X	
38.84	Smear	Diamicton	XXXX	XX	XX	EEB	X	
39.84	Smear	Diamicton	XXXXXXX	XXXX	XX	EEB	X	Tr. Aegirine, hornblende, glauconite
40.80	Smear	Diamicton	XXXXXXX	XX		BE	X	Tr. olivine, apatite; sanidine-bearing glass
41.50	Smear	Diamicton	XXXXXXX	XX	X	BBBE		Tr. hornblende, glauconite
42.80	Smear	Diamicton	XXXXXXX	XX		BBBE	X	Tr. Glauconite

Tr. - trace; B- brown glass; E - colourless glass

B -brown glass; E - evolved (colourless) glass; [number of letters of each denotes approximate relative abundance; e.g., BBBE -brown glass >>> evolved glass]

X - Trace (<1%) XXXX - Common (>5-20%)

XX - Present (>1-5%) XXXXXXX -Abundant (>20%)

siliceous microfossils (spicules, radiolaria/diatoms) but is abundant (50-60%) in one sample (at 32.05 mbsf), in which it consists of fragments of microcrystalline skeletal carbonate.

Although this section is focused solely on sand grain petrology, significant differences with the finer-grained samples examined are worth noting. In the latter, silt is most abundant and is characteristically represented by clay mineral or dark fine-grained bioclastic aggregates. Small glauconite clots or celadonite are widespread. The few fine sand and silt grains present are angular quartz and feldspar fragments, and pyroxene is either scarce or absent.

Provenance

The volumetrically dominant, abraded grains of quartz, K-feldspar and oligoclase-andesine were probably derived mainly from the crystalline basement and Beacon Supergroup (see also Tab. 6). By contrast, abraded grains of pale green calcium-poor augite with prominent dark-coloured cleavage were probably sourced in the Ferrar Dolerite. Volcanic-derived clasts are a distinctive component of all samples and mainly include lithic grains (fine-grained lavas) and conspicuous glass. The glass is compositionally variable. Brown glass is basaltic (basanitic?), pale brown and green glass is intermediate, and colourless glass is evolved. Other volcanic-derived fragments probably include the angular crystals of labradorite-bytownite, pale green augite, aegirine and other, mainly strongly-coloured ferromagnesian minerals ((?)titanaugite, (?)aenigmatite, (?)kaersutite, and hornblende; olivine)). The presence of the coloured ferromagnesian minerals strongly suggests an alkaline volcanic provenance similar to the McMurdo Volcanic Group.

Volcanic glass, particularly vesicular basaltic glass, is almost uniformly abundant in the Quaternary sediments, reaching up to 45% in a sample at 31.5 mbsf (Tab. 7), and it is generally more common than in the Miocene strata (see Miocene Strata, this volume - section on Sand Grains and Provenance). Volcanic lithic grains are also generally more common than in the Miocene strata (up to 10% in a sample at 21.4 mbsf), and they may be the only volcanic component present in some samples. The colourless evolved glasses are often strongly vesiculated and may be present to the exclusion of basaltic glass (e.g., sample at 32.25 mbsf), although basaltic glass is generally overwhelmingly dominant. The presence of ubiquitous aegirine in these rocks suggests that the colourless glass is peralkaline in composition. Peralkaline rocks are common in the McMurdo Volcanic Group *(cf.* Kyle, 1990).

It is notable that, despite the abundance of volcanic detritus in the sand-size population in these samples, it is virtually absent as larger clasts. This observation is at variance with previous studies, which showed numerous volcanic pebbles in both the Oligocene and younger strata, some with intermediate glass compositions (Gamble et al., 1986; Roser & Pyne, 1989). Moreover, the glass fragments in the CRP-1 samples are more commonly associated with grains of (?)volcanic-derived calcic plagioclase than with abundant ferromagnesian minerals. Although minor, pale green calcic augite is persistently present, olivine (which should be common in volcanic detritus derived predominantly from basaltic and/or basanitic compositions) is extremely rare. These observations suggest that much of the glass (and possibly some of the lithic clasts) may be relatively distal airfall tephra, and that the heavier pyroclasts *(e.g.,* ferromagnesian minerals) were largely elutriated from the volcanic plume closer to source. This is consistent with the absence of any known volcanic sources in the area drained by the Mackay Glacier (Gunn & Warren, 1962; Warren, 1962).

Thus, erosion and transport by glaciers were not the sole methods by which clasts were supplied to the Quaternary (and Miocene) strata. The variable ratio of brown to colourless volcanic glasses may closely mirror the proportion of eruptions of basic to evolved compositions in the McMurdo Volcanic Group, and it may prove to be a useful proxy record by which other Quaternary drillcores can be correlated.

PALAEONTOLOGY

INTRODUCTION

The 43-m interval of Quaternary siliciclastic and carbonate sediments, the lower half of which was cored, yielded a wide variety of macrofossils and microfossils, encompassing essentially all fossil groups studied on site. Their occurrences, however, are largely sporadic or discontinuous, and reworked taxa from older units are frequently noted, particularly in the diamictites. Nevertheless, these fossils provide age control, a basis for establishing regional correlations, and important palaeoenvironmental information on what appears to have been a glaciomarine setting that underwent some significant fluctuations.

Of particular palaeontological interest is the unique bioclastic carbonate sediment (lithostratigraphic Unit 3.1; 31.70-33.82 mbsf) in which all fossil groups investigated are present. A brief introduction is given here for each of these groups, which are then further described under separate headings below.

Diatoms are ubiquitous and include marine (planktonic and benthic), fresh- and brackish-water taxa. Their occurrences are discontinuous and, along with their abundances, reflect varying conditions of sea-ice cover, sea-water temperature, sea level, and cover by a glacier tongue or shelf ice. Postulated palaeoenvironments at the site range from possibly terrestrial (top lithostratigraphic Unit 2.2) to open marine in the absence of sea ice (lower Unit 2.2 and Unit 3.1). The tentative diatom age for the better-dated units place them within the lower Quaternary Fragilariopsis kerguelensis Zone (1.25 to 1.6 Ma), perhaps extending up into the lower portion of the Actinocyclus *ingens* Zone.

Pleistocene foraminifers are also ubiquitous, occurring in 8 of 9 samples examined. Most samples contain moderate to rich assemblages. Preservation ranges from well preserved to pristine with highest abundances and diversities in carbonate lithostratigraphic Unit 3.1 and lowest abundances in the diamicton of Unit 4.1. Reworked Pliocene specimens were noted at some levels.

The only Quaternary calcareous nannofossils are few, but well-preserved fragments of *Thoracosphaera*, a calcareous dinoflagellate. Thoracosphaerids have not been reported previously from Pleistocene sediments of the East Antarctic margin, and occur only in the carbonate lithostratigraphic Unit 3.1, mostly in the finest sediments, *i. e.*, unwinnowed muds. Their occurrence could indicate relatively warmer waters for this unit.

Of 10 samples processed for palynomorphs (from all lithostratigraphic subunits except 2.3), 8 yielded spores and pollen (miospores) or organic-walled microplankton (dinoflagellates, acritarchs, and prasinophycean green algae phycoma [cysts]). Acritarchs and prasinophycean algae dominate the palynomorph assemblages, and a number of new taxa of each have been noted. Foraminiferal linings, possibly left behind after calcareous cement or tests were dissolved during diagenesis, were the dominant, and almost the only palynomorph in the carbonate lithostratigraphic Unit 3.1. The terrestrial palynoflora is limited as are conclusions that can be drawn from them, particularly regarding whether they are in situ or reworked. The high relative abundance of *Nothofagidites lachlaniae* in Sample 21.04 mbsf is similar to that reported from the Meyer Desert Fm. of the Sirius Group (Transantarctic Mountains), and parallels the report of this taxon from the mid Pliocene of DSDP Site 274.

The macroinvertebrate assemblage that constitutes most of the carbonate lithostratigraphic Unit 3.1 is largely in situ or nearly so, and is dominated by mollusks (over 35 taxa identified at least to genus) along with appreciable numbers of bryozoans and lesser numbers of echinoids, barnacles, octocorals, serpulid worms, and brachiopods. Aragonitic forms are best preserved in muddy interbeds between winnowed, largely calciticintervals. The generally eurybathal fauna is dominated by vagile and sessile epifauna that are not substantially different from those now living in modern Antarctic shelf/bank environments at near-zero temperatures under seasonal sea-ice.

DIATOMS

Methods

The following presentation and discussion of diatom occurrence in Quaternary sediments of CRP-1 will follow the division of lithostratigraphic units. Sample spacing is variable, but less than 2 m in most intervals (Tab. 8). When only one depth is indicated it represents the upper range of a 1 cm sample interval. All samples were checked initially by examination of a strewn slide of raw sediment. This was prepared by separation and disaggregation in 50 ml water and settling for 1 minute to remove coarse material. A strewn slide was made from the suspended material for a quick check of diatom presence and abundance (Fig. 13; Tab. 8). If warranted, additional concentration was done by sieving through a 25 μ sieve.

Diatom Assemblages

Diatom occurrence and abundance determination is presented in figure 13. Marine diatom occurrence is discontinuous. Absence reflects conditions of ice cover or extremely rapid sedimentation, which would dilute the diatoms. Freshwater and brackish-water diatom assemblages occur near the top of lithostratigraphic Units 2.1, 2.2, and 3.1. Freshwater diatoms at the top of

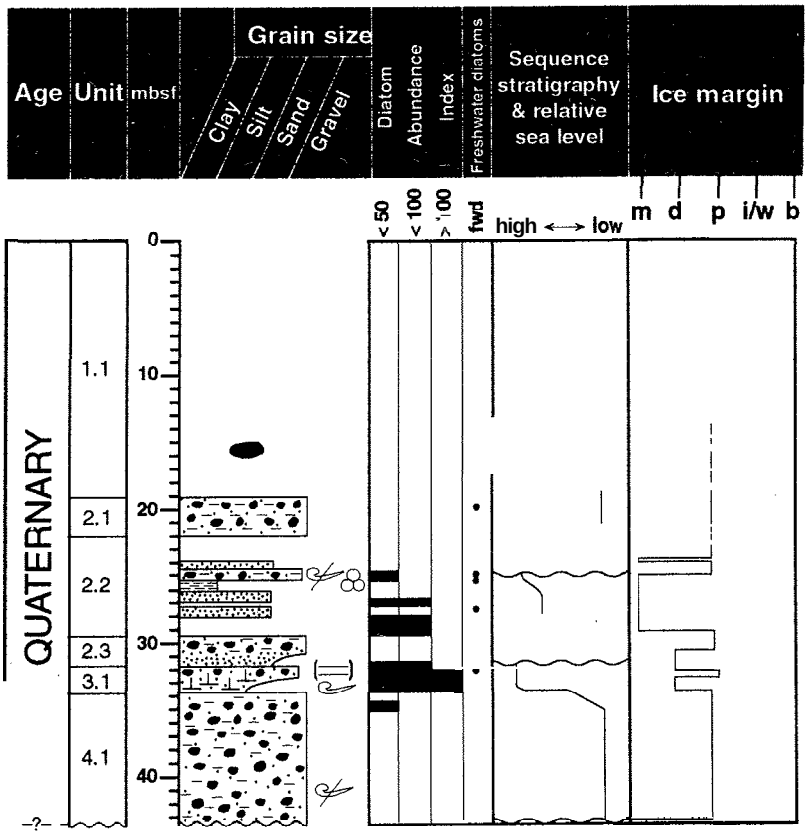

Fig. 13 - CRP-1 Quaternary diatom abundance. Relative diatom abundance is plotted with lithological descriptions, lithostratigraphic unit designations, and depositional interpretations. Black bars represent diatom occurrence with increasing abundance to the right. Five fields-of-view were observed (at 250x) in a raw strewn slide of each sample. Data were collected in six categories: barren (X), <10, <30, <50, <100, or >100 diatom fragments per five fields-of-view. Only samples equal to or exceeding classification of <50 fragments are depicted; lower abundance categories most likely represent intervals of diatom recycling but not production. The presence of freshwater diatoms is indicated in a separate column.

Tab. 8 Sample intervals for initial Quaternary diatom study. Samples intervals are listed with notes on abundance, ecology, and processing techniques

Units	*Sample Interval*	*Abundance*	*Ecology*	*Comments*	*Reworking*			*Processing Notes*
					Freshwater	Marine	Ages	
1.1	8.50-8.51	X	N/A		X	X	M/P	FT; sieve
	16.06-16.07	X	N/A			X		strewn
	19.27-19.28	<10	F	small freshwater pennates only				strewn
	20.04-20.14	<10	N/A			X		FT; sieve
	20.18-20.19	X	N/A	very rare marine fragments		X		strewn
	20.65-20.66	X	N/A					strewn
2.1	20.99-21.00	X	N/A	very rare marine fragments		X		strewn
	21.04-21.14	X	N/A					FT; sieve
	21.51-21.52	X	N/A	very rare marine fragments		X		strewn
	21.54-21.57	X	N/A					strewn
	21.99-22.00	X	N/A	very rare marine fragments		X		strewn
	24.53-24.54	<30	F	benthic freshwater; v. rare marine fragments				strewn
	25.12-25.13	<50	F	benthic freshwater; v. rare marine fragments				strewn
	26.08-26.09	<10	N/A			X		strewn
2.2	26.95-26.96	<100	P	*F. curta present but not common*	X	X	', mM-lM, lO	strewn; float
	27.47-27.48	X	N/A					strewn
	27.81-27.82	<100	P+F	*F. curta common, marine planktics, freshwater*	X			strewn; float
	28.10-28.11	<100	P	*F. curta present but not common*				strewn; float
	30.08-30.09	X	N/A					strewn
?.3	30.70-30.71	X	N/A					strewn
	31.10-31.11	X	N/A					strewn
	31.70-31.71	<100	P+F	freshwater and frags. of marine planktics		X		strewn
	32.05-32.15	>100	P+B	*F. curta absent*				FT; sieve
	32,30	>100	P+B	*F. curta absent*				smear
3.1	31.82-33.62	>100	P+B	40 smear slides in this interval				smear
	32.80	>100	P+B	*F. curta absent*				smear
	33.30 .	>100	P+B	*F. curta absent*				smear
	33.72-33.75	>100	P	*F. curta absent*				strewn; sieve
	34.17-34.18	<10	N/A			X		strewn
	34.56-34.57	<10	N/A			X		strewn
	34.80-34.81	<50	P	Quaternary diatom fragments				strewn; sieve
	35.46-35.47	<30	P+T			X		strewn
	35.88-35.89	<10	N/A			X		strewn
	37.45-37.46	<10	N/A			X		strewn
	37.92-37.93	X	N/A					strewn
	38.44-38.45	X	N/A					strewn
4.1	38.93-38.94	<10	N/A			X		strewn
	39.32-39.33	X	N/A					strewn
	39.96-39.97	X	N/A					strewn
	40.32-40.33	<10	N/A			X		strewn
	40.89-40.90	<10	N/A			X		strewn
	41.27-41.28	X	N/A					strewn
	41.77-41.78	<10	N/A			X		strewn
	42.44-42.45	<10	N/A			X		strewn
	43.04-43.05	X	N/A					strewn

Note: abundance represents the number of diatom fragments observed in five fields-of-view. Diatom assemblages are classified into general ecological groups, where 'P' =planktonic; 'T' = tychoplanktonic; 'B' = benthic, and 'F' = freshwater.

lithostratigraphic Unit *2.2* may indicate terrestrial conditions during a Pleistocene lowstand of sea-level.

Diatom biostratigraphy suggests the interval from *26.95* to *34.80* mbsf belongs to the lower Quaternary *Fragilariopsis kerguelensis* Zone *(1.25* to 1.8 Ma) of Harwood & Maruyama *(1992).* This zone represents the stratigraphic interval between the highest occurrence of *Fragilariopsis barronii (1.25* Ma) down to the highest occurrence of *Thalassiosira kolbei (l.8* Ma). Severalother diatom biostratigraphic events support this age. The

recovery of Thalassiosira elliptipora and *Actinocyclus ingens* up to interval 26.08 to 26.95 mbsf, suggests an age older than 0.65 Ma at this level. The presence of *T.* torokina up to interval 26.08 to 26.95 may suggest an age older than ~4 Ma, although the upper range of this diatom is not well established. The lowest occurrence of Thalassiosira elliptipora indicates an age younger than 2.4 Ma between 34.81 to 35.47 mbsf (Winter & Harwood, 1997). The absence of Thalassiosira fasciculata and T. *inura* from the diatom bearing interval between 26.95 to 34.80 mbsf provides further support for an age younger than 1.8 Ma above 35.46 mbsf.

The Quaternary section of CRP-1 includes three distinct assemblages of marine diatoms: the lower half of lithostratigraphic Unit 2.2 contains a sea-ice flora; the upper interval of lithostratigraphic Unit 3.1 contains an Antarctic diatom assemblage without sea-ice flora; and the lower interval of lithostratigraphic Unit 3.1 contains a warm-water, open-marine assemblage.

Lithostratigraphic Unit 1.1 (0.00-19.13 mbsf), Diamicton

Two samples were examined in this lithostratigraphic unit. Diatoms recovered at 8.50-8.51 mbsf include a mixture of freshwater and marine forms, occurring as isolated specimens and within small sedimentary clasts. Some of these clasts bear rare freshwater diatoms and others bear abundant marine diatoms. The freshwater assemblage includes several species of Navicula, known from Antarctic lakes and streams today. Marine diatoms present in this interval include Thalassiosira torokina (age range 8.2 to ~1.4 Ma) and Stellarima *microtrias* (not age diagnostic), which are often filled with marine diatomaceous sediment. The robust valves of these two diatoms apparently protected the diatom-rich matrix from abrasion. Neither of the assemblages of diatoms is believed to represent the age of the sediment; both are likely reworked, as indicated by the rich marine diatom assemblage in the interior of some diatom valves, and the sparse diatom occurrence in the matrix. This assemblage resembles mixed freshwater and marine diatoms in the upper part of the CIROS-2 and DVDP 10 & 11 drillholes.

Reworking is noted by the presence of the ebridian Pseudoammodochium cf. dictyoides (Miocene to Oligocene) and heavily silicified casts of diatom interiors (Liostephania), which are likely reworked from Eocene to lower Oligocene intervals, correlative with the lower 200 m of CIROS-1. Traces of marine diatom fragments were encountered at 16.06 mbsf.

Lithostratigraphic Unit 2.1 (19.13-22.00 mbsf), Diamicton

This lithostratigraphic unit is largely barren of diatoms, with the exception of isolated freshwater and brackish-water diatoms encountered at 19.27 mbsf, along with rare fragments of marine diatoms. Present are Navicula spp., and other freshwater pennate diatoms, which are not identified here. Melosira charcotii is known from "tidally-influenced ice shelf conditions and other marine proximal, brackish water environments" (Scherer, 1987). Also present are rare fragments of marine diatoms and *Liostephania* silicified casts probably recycled from the Paleogene. The general absence of diatoms from lithostratigraphic Unit 2.1 implies cover by an ice shelf or glacier tongue that did not allow light penetration.

Lithostratigraphic Unit 2.2 (22.00-29.49 mbsf), Sand, Sandy Mud and Minor Diamicton

Two distinct assemblages occur within lithostratigraphic Unit 2.2; freshwater and brackish-water assemblages within the upper three metres, and marine below. A rich assemblage of freshwater and brackish water diatoms occurs at 25.53 and 25.12 mbsf. This assemblage is similar to that reported for lithostratigraphic Unit 2.1, with the presence of Achnanthes, *Hantzschia,* Nitzschia, Navicula, M. charcotii and others. The absence of marine diatoms in both samples may indicate glacial transport of terrestrial sediment with little modification, or terrestrial exposure during a Quaternary lowstand of sea-level (N. hemisphere driven).

Below this interval, a rich assemblage of marine diatoms is present between 26.95 and 28.10 mbsf, with two samples that bear few to no diatoms (Tab. 8). The richest samples contain a lower Pleistocene assemblage of sea-ice diatoms and other marine forms, dominated by *Actinocyclus* actinochilus, Corethron criophilum, *Fragilariopsis curta,* F. matuyamae, F. kerguelensis, F. ritscherii, Thalassiosira elliptopora, T. *lentiginosa* and common *Thalassiothrix* at 27.81 mbsf. The absence of a marine-benthic flora indicates water depth below euphotic zone depth (>~50 m). The abundant presence of F. *curta* suggests sea-ice was a feature of this environment.

The presence of F. *kerguelensis* is interesting as this diatom is more common today in the Polar Frontal Zone, indicating open-oceanic conditions. Rare reworked freshwater taxa are present in low numbers, as well as diatoms reworked from the middle to upper Miocene (*Denticulopsis simonsenii*) and Oligocene (*Kisseleviella carina*).

Lithostratigraphic Unit 2.3 (29.49-31.89 mbsf), Diamicton

Diatoms are barren in this interval except for a sample at 31.70 mbsf, which contains freshwater diatoms. This sample spans the boundary interval between lithostratigraphic Units 2.3 and 3.1. The sparse marine diatom fragments in this sample, which are likely recycled, makes this distinct from the assemblage of lithostratigraphic Unit 3.1. The relationship between lithostratigraphic unit boundaries and the occurrence of freshwater diatoms requires detailed examination. The absence of marine diatoms indicates deposition beneath a floating ice mass, or within turbid water, which inhibited photosynthesis.

Lithostratigraphic Unit 3.1 (31.89-33.82 mbsf), Muddy Sand and Packstone

Lithostratigraphic Unit 3.1 is comprised of three biostratigraphic subunits, designated here as

biostratigraphic Subunit 3.1.1 (upper; 31.89 to 32.82 mbsf), 3.1.2 (middle; 32.82 to 33.15 mbsf), and 3.1.3 (lower; 33.15 to 33.82 mbsf). These biostratigraphic subunits are separated by changes in diatom assemblages and lithology, where Subunit 3.1.1 is very carbonate-rich, Subunit 3.1.2 is carbonate poor, and Subunit 3.1.3 is moderatcly carbonate-rich to clastic.

Forty smear-slide samples were examined in biostratigraphic Subunit 3.1.1. This subunit contains abundant and well-preserved diatoms of similar composition to those recovered from lithostratigraphic Unit 2.2, except for the conspicuous absence of *Fragilariopsis curta* and other diatoms associated with sea-ice and ice-edge communities (Leventer & Dunbar, 1987, 1996). The diatom zonal assignment for Subunit 3.1.1 is within the lower Quaternary *Fragilariopsis kerguelensis* Zone (Harwood & Maruyama, 1992). The assemblage is dominated by *Actinocyclus actinochilus, A. ingens, E. antarctica, Thalassiosira elliptopora,* but with enrichment of *Thalassiothrix* sp. and *Chaetoceros* spp in some samples. Benthic-marine diatoms of the genera *Diploneis, Cocconeis, Nitzschia, Amphora, Pinnularia* and others are also present in low numbers in this interval.

The absence of *F. curta* and other sea-ice diatoms that dominate pelagic Antarctic shelf sediments today, as evident in lithostratigraphic Unit 2.2, indicates waters warmer than -1°C to prevent the formation of sea-ice. However, the waters were still cold, as indicated by the presence of *Actinocyclus actinochilus* and *Eucampia antarctica*. However, 'cold' is a relative term; waters <-1°C are considerably warmer than winter atmospheric temperatures in Antarctica. The presence of this heat source from the open ocean and Ross Embayment through the year impacted mean-annual atmospheric temperatures and precipitation on Antarctica at this time.

An interval barren of diatoms is noted in three samples at 33.01, 33.10, and 33.15 mbsf within Subunit 3.1.2. These samples occur directly below a large ice-rafted dolerite clast in sediment rich in clastic material. This subunit may represent a winnowed horizon or lag deposit, indicating an hiatus of unknown duration.

Biostratigraphic Subunit 3.1.3 (33.30 to 33.62 mbsf) contains an assemblage of rich and moderately well-preserved diatoms including common *Actinocyclus ingens, A. karstenii* (highest appearance at 33.20 mbsf), *Thalassiosira oestrupii, T. torokina,* and large *T. elliptopora*. F. *curta* and other sea-ice diatoms are extremely rare, as in the above subunits. Some elements of the assemblage from Subunit 3.1.1 are present, although A. *actinochilus,* E. *antarctica* and *T. elliptipora* occur in considerably lower numbers in this lower interval. Benthic-marine diatoms are frequent elements of this assemblage. This change in assemblage composition is either due to a brief hiatus and/or due to a significant environmental change. The presence of *T. oestrupii* may reflect warmer conditions than in Subunit 3.1.1, based on the modem distribution of T. *oestrupii*. Rare specimens of the silicoflagellate genus *Dictyocha* are also noted at 33.72-33.75 and at 33.59 mbsf, which may further indicate significant warming in this interval (Bohaty & Harwood, in press).

Lithostratigraphic Unit 4.1 (33.82-43.55 mbsf), Diamicton

Diatoms throughout lithostratigraphic Unit 4.1 are rare and poorly preserved. Most occur as isolated fragments, which are thought to be recycled. One sample at 34.80 mbsf, however, contained *Actinocyclus actinochilus, A. ingens, Thalassiosira elliptipora, T. oestrupii,* and *T. torokina,* suggesting a link to the overlying diatom-rich unit of the F. *kerguelensis* Zone. The absence of diatoms throughout most of this unit indicates a position beneath an ice mass, which prevented diatom productivity.

FORAMINIFERA

Introduction

The unexpectedly thick Pleistocene sequence encountered from 0.00-43.15 mbsf in the Cape Roberts-1 drillhole constitutes an important addition to the very sketchy Pleistocene stratigraphic record in Antarctica. This report presents preliminary foraminiferal results for 9 samples (3 "fast-track", 6 routinecore samples) recovered from that interval. These results are referred to units of the standard lithostratigraphic classification adopted for the drillhole (see Background to CRP-1, Stratigraphic Summary, this volume - Fig. 18). Results for a detailed suite of 10 samples collected from the carbonate lithostratigraphic Unit 3.1 are unavailable at this time.

Most samples contain moderate to rich foraminiferal assemblages (Tab. 9); reworked Pliocene specimens were also encountered at some levels, as noted below. Only one sample, from near the base of the sequence, was non-fossiliferous for foraminifers.

Samples from this interval were collected over a nominal 3 cm of section, unless otherwise noted, and processed using standard techniques. All fossil material was recorded, and a representative selection mounted on slides with the foraminiferal specimens.

Results

Unit 1 (diamicton; 0.00-19.13 mbsf) -Although there was poor recovery from this interval, a bit sample from 8.50 mbsf yielded a sparse assemblage (Tab. 9).

Unit 2 - Two samples (20.04-20.14 and 21.54 mbsf) from lithostratigraphic Unit 2.1 (diamicton; 19.13-22.00 mbsf) contain moderately abundant foraminifers (Tab. 9). Most specimens are pristine, and lack sedimentary infilling, suggesting that they are not reworked.

Lithostratigraphic Unit 2.2 (sand, sandy mud, minor diamicton; 22.00-29.49 mbsf) contains both *in situ* Pleistocene foraminifers, and reworked Pliocene specimens in the single sample of the unit from 26.89 mbsf (Tab. 9). Some Pleistocene specimens appear also to have undergone minor reworking and redeposition. The Pliocene forms, which show affinities with faunas from the Pliocene of Cockburn Island (Gazdzicki & Webb, 1996), are recognised by their darker colour, generally larger size and infilled chambers, and also by the presence of the extinct taxon, *Ammoelphidiella* sp.

Tab. 9 - Quaternary occurrence of foraminfers in selected samples of CRP-1

Unit 4.1	Unit 3.1	Unit 2.2	Unit 2.1	Unit 1.1	Lithostratigraphic Unit
33.90-37.53	32.05-32.15	26.89	20.04-21.54	8.50	Sample Interval (mbsf)
		r			*Ammoelphidiella sp.*
		X	X'		*Angulogerina angulosa*
	X				*Biloculina sp.*
	X		X		*Cassidulinoides parkerianus*
X	X	X	X		*Cassidulinoides porrectus*
	X	r	X		*Cibicides lobatulus*
			X		*Cibicides refulgens*
		X			*Cibicides sp.*
	X				*Cribroelphidium sp.*
	X				*Cyclogyra involvens*
X	X	X	X		*Ehrenbergina glabra*
		X			*Ehrenbergina sp.*
	X		X		*Fissurina spp.*
	X				*Fursenkoina earlandi*
	X				*Glandulina antarctica*
	X				*Globigerina megastoma*
	X	X	X		*Globocassidulina subglobosa*
		X			*Hanzawaia sp.*
	X				*Lagena sp.*
	X		X	X	*Lenticulina* sp.
	X	X			*Neogloboquadrina pachyderma*
				X	*Notorotalia off. taranakia*
r	X				*Oolina spp.*
	X				*Patellina corrugata*
	X				*Pseudobulimina chapmani*
			X		*?Pseudobulimina chapmani*
	X				*Pullenia subcarinata*
	X				*Pyrgo depressa*
	X				*Quinqueloculina sp.*
	X				*Rosalina globularis*
r					*Saracenaria? sp.*
	X				*Sigmoilina umbonata*
	X	X	X		*Trifarina earlandi*
		X	X		Miliolidae
	X				Primitive agglutinated foraminifers
X					Bryozoans
	X				Diatoms
	X	X	X		Echinoderm spines
	X	X			Micromolluscs and mollusc fragments
X			X		Mollusc fragments
	X	X			Ostracods
	X				Radiolarians
X	X	X	X	X	Sponge spicules

The one sample from lithostratigraphic Unit 2.3 (diamicton; 20.49-31.89 mbsf) at 30.11 mbsf contains a mixture of reworked and in situ forms similar to that from Unit 2.2 above, but with lower overall abundance.

Unit 3 (muddy packstone; 31.89-33.82 mbsf) Foraminifera are diverse, abundant and well preserved in a "fast-track" sample at 32.05-32.15 mbsf (Tab. 0). The presence of numerous large (to 3 mm) miliolids is the most striking feature of the assemblage. Ten additional samples from lithostratigraphic Unit 3 have been taken for further study, with results to be available in the future.

The recorded assemblage is common in most Pleistocene sediments from the Ross Sea (Heron-Alien & Earland, 1922), Dry Valley Drilling Project drillholes in Taylor Valley (Webb & Wrenn, 1982), and the Cape Royds-Cape Barne area (Ward & Webb, 1986). Although there is some evidence of current transport, the fauna is considered to be essentially *in* situ, as evidenced by preservation of delicate, spieular agglutinated tests. The fauna occurs under normal marine conditions over a depth range from just below sea level to 500 m. Planktonic foraminifera make up an estimated 3% of the assemblage, suggesting that the site was free from sea ice during summer months.

Unit *4* (diamicton; *33.82-43.55* mbsf) - Samples from 33.90-33.93 mbsf and 37.50-37.53 mbsf yielded sparse assemblages of relatively pristine specimens without infilled chambers, consistent with a Pleistocene age (Tab. 9). The lower sample also contains reworked specimens, recognisable by their yellowish-brown colour and nearly opaque tests.

Discussion

Apart from the excellent fauna present in lithostratigraphic Unit 3, probably the most notable feature of the Pleistocene sequence is the persistent, but sporadic, occurrence of reworked Pliocene foraminifers, and also possibly of contemporaneously reworked Pleistocene taxa. The Pliocene specimens represent a shallower, more shoreward facies than the in situ fauna, with their most likely source lying to the west, along the valley of the Mackay Glacier.

Presence of significant numbers of reworked foraminifers in many parts of the sequence argues for special care in selecting material for radiometric dating.

MACROFOSSILS

Introduction

Macrofossils mostly occur within the carbonate-rich unit between 33.82 and 31.89 mbsf. They contribute significantly to the composition of such biogenic skeletal sediment (bryomol-type) as a mixture of both fresh biosomes and more or less worn bioclasts.

All micropaleontological residues from above and below the carbonate-rich unit were inspected for remains of macrofossils. Only a few intervals provided some material, listed below:

1 - 21.54 mbsf: rare bryozoan fragments;

2 - 26.89 mbsf: abundant echinoid spines, abundant bryozoan fragments, octocorals, bivalves (Mysella sp.),

unidentified bivalve fragment, gastropods (Margaritinae sp.), serpulid polychaete (*Serpula narconensis*);
3 - 26.05 mbsf: echinoid spines, unidentified bivalve fragments;
4 - 30.11 mbsf: echinoid spines, one compressed serpulid worm tube, unidentified bivalve (?Pectinidae sp.) fragments;
5 - 32.05 mbsf: unidentifiable bivalve fragments;
6 - 33.90 mbsf: rare bryozoan fragments.

Taphonomy

Macrofossils recovered from below and above the carbonate-rich unit, show advanced levels of wear and may represent reworked shallow-marine faunas. Generally, only calcitic fossils were present in these assemblages.

The carbonate-rich unit contains instead a very diverse and abundant macrofossil assemblage (Fig. 14). The large-sized, macrofossil-rich "fast-track" sample (32.15-32.05 mbsf) contained a very diverse skeletal assemblage. Qualitatively, mollusc species (>35, not all determined) dominate over other macroinvertebrates, especially bryozoans (apparently not highly diverse but quantitatively significant), echinoids (spines and theca fragments), barnacles (1 species), serpulid polychaete tubes (1-2 species), brachiopods (1 species), and octocorals (1 species). Calcitic and aragonitic skeletal parts are in places exquisitely preserved. Intervals interpreted as current-generated may show a considerably higher number of calcitic macrofossils, especially bryozoans and octocorals. Aragonitic macrofossils are best preserved in muddy layers. With few exceptions, the many taphocoenoses that together constitute the bulk of the carbonate-rich unit are either substantially in situ or have been moved only a short distance away from their life habitats. Incipient pyritisation of gastropod shells (especially eatoniellids) has been observed at 33.01-32.98 mbsf.

Taxonomy

An accurate list of all the various taxa encountered in the Pleistocene portion of the core cannot be supplied at present and will require the assistance of many specialists.

Fig. 14 - Skeletal assemblage from the carbonate-rich unit (32.58 mbsf) showing exceptionally well preserved and diverse macrofossils; the largest shell is a predatory gastropod (*Prosipho*).

However, mollusc shells have been classified at a certain level of confidence, mainly referring to the recent monograph by Dell (1990). A very tentative, and still highly preliminary list of mollusc taxa identified in the sediment fractions coarser than 500 mm, is reported in table 10. The faunal list from the carbonate-rich unit matches very well with molluscs from the present-day Ross Sea (Dell, 1990).

Palaeoenvironmental Remarks

Macrofaunas represented in the fossil assemblages are strongly dominated by vagile and sessile epifauna (suspension feeders, carnivores, scavengers) and seem typical of modern-shelf/bank environments in the Antarctica. Antarctic benthos is typically eurybathic with most taxa distributed over a wide vertical range. Accordingly, a very precise palaeobathymetric assessment may prove challenging and must be derived through the integration of depth-records of multiple taxa. Depths very probably exceeded 100 m, possibly in the range of 100-200 m. This figure must be probably taken as conservative on the low side because macrofossil assemblages contain more than one taxon whose present depth-range is greater than the proposed figure. In situ macrofossils suggest a predominantly calm environment, an inference further supported by the fact that biologic indicators of strong bottom currents are totally lacking. By analogy with the distribution of similar modern assemblages in this region, no proximal ice shelf was present, rather conditions were completely open-marine. Macrofossils offer no definitive clue as to the presence/absence of seasonal sea-ice, which per se does not seem a factor constraining these communities. It is, however, worth reporting that the macrofossil assemblages pertain to communities now living in near-zero temperatures and under the seasonal sea-ice.

Age

Based on taxonomic comparisons at the species-level of the cored macrofossil assemblages with present-day Ross Sea living communities, the age of the carbonate-rich unit is estimated to be Pleistocene. However, it must be mentioned that the true time-distribution of these taxa is virtually unknown.

CALCAREOUS NANNOFOSSILS

Within the top 43 m of the core, calcareous nannofossils have only been found in lithostratigraphic Unit 3.1, where a few Thoracosphaera *saxea* Stradner, 1961, have been identified. The specimens are well preserved, but occur only as fragments; no complete tests have been found. They have been recorded in the following closely spaced samples, which include small "tooth pick" samples (in mbsf): 31.90, 32.29, 32.59, 32.95, 32.98, 33.31, 33.50, 33.65, 33.69, 33.72, 33.80 (Fig. 15). Different procedures have been applied for slide processing; for "tooth pick" samples, smear slides were made, for the remainder a settling technique, to remove particles sized above 25 mm, was used (see previous section on Diatoms).

Tab. 10 -Preliminary list of Mollusca identified in the carbonate-rich unit (33.82-31.89 mbsf). The very high diversity shown by sample 32.15-32.05 mbsf ("fast-track") is enhanced by the larger size of this sample; the overall higher diversity between 32.80 and 32.05 mbsf is real, and it probably reflects better environmental conditions for biota development and/or the preservation of their calcareous fossils.

SPECIES/SAMPLE	33.75 33.72	33.53 33.50	33.34 33.31	33.01 32.98	32.98 32.95	32.80 32.77	32.61 32.58	32.40 32.37	32.37 32.34	32.15 32.05	31.93 31.90
BIVALVIA											
Limopsis sp.											■
Philobrya sublaevis Pelseneer		■					■			■	
Philobrya wandelensis Lamy			■								
Adacnarca limopsoides (Thiele)	■		■	■							■
Pectinidae sp.					■	■				■	
Mysella sp.									■		
Cyamocardium denticulatum (Smith)		■								■	
Limatula (Limatula) simillima Thiele							■			■	
Limatula (Antarctolima) hodgsoni (Smith)						■				■	
Limatula sp.						■		■	■	■	
Cyclocardia astartoides (Martens)	■	■	■							■	
GASTROPODA											
Anatoma euglypta (Pelseneer)										■	
Trochidae spp.			■		■				■		
?Submargarita sp.						■	■	■		■	■
Falsimargarita sp.										■	
Leptocollonia innocens (Thcele)						■				■	■
Lissotesta cf minutissima (Smith)										■	
Lissotesta sp						■		■	■	■	
Brookula cf. rossiana (Thiele)										■	
Iothia coppingeri (Smith)				■							
Eatoniella glacialis (Smith)	■	■					■	■		■	■
Eatoniella (Ovirissoa) kerguelensis (Smith)		■	■	■		■	■	■	■	■	
Onoba gelida (Smith)									■		
Onoba turqueti (Lamy)						■	■	■	■	■	
Powellisetia deserta (Smith)		■					■			■	
Capulus subcompressus Pelseneer	■		■	■		■	■			■	■
Turritellopsis latior Thiele						■				■	
Eumetula spp.					■	■				■	■
Melanella sp.										■	
Torellia mirabilis (Smith)											
Pareuthria innocens (Smith)									■	■	
Meteuthria cf. rossiana Dell										■	
Prosipho contrarius Thiele							■			■	
Prosipho hunteri Hedley	■						■	■		■	■
Prosipho cf. mundus Smith								■	■	■	

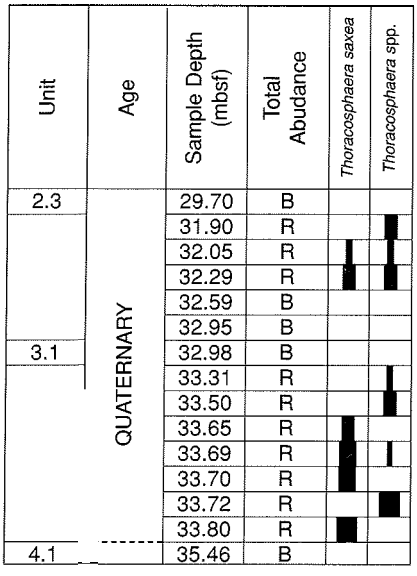

Fig. 15 - Distribution of Thoracosphaerids in the CRP-1 Unit 3.1. B: barren, R: rare.

As stated elsewhere, lithostratigraphic Unit 3.1 is a peculiarcarbonate-rich,fossiliferoussequence, essentially a hash of invertebratemacrofossilshells within an otherwise clastic-rich glacial or glaciomarine sequence. Part of the material has been winnowed and other parts not. The best preservation and more abundant occurrences of these microfossils were recorded in the finest sediment, which is an unwinnowed mud. Two samples from winnowed material (32.95 and 32. mbsf) were barren.

Although the lithostratigraphicunits (1, 2, and 4) at the top of the core were searched for calcareous nannofossils, these all appear to be barren, based on our examination of the following samples (in mbsf):21.04, 29.04, 35.46, 38.93.

Because they fall within the size range of calcareous nannofossils (2 to 30 mm), thoracosphaerids have been included in this group.

From a taxonomic point of view, however, Cenozoic thoracosphaerids have been shown to have a dinoflagellate cyst morphology (Futterer, 1976), thus they belong to the calcareous dinoflagellates.

Thoracosphaerids have not been reported previously from the Quaternary in Antarctica. They have been noted in the upper Eocene-lower Oligocene of the CIROS-1 core in the Ross Sea, 60 km to the south (Monechi & Reale, in press), among a moderately preserved and sparse calcareous nannofossil assemblage. At that time, the climatic conditions in the Antarctic continent were warmer than at present, and cool-water nannoplankton could persist in these marginal enviroments until the earliest Oligocene, when evidence of glaciations are recorded by glaciomarine sediments (Barrett et al , 1989).

A bloom of thoracosphaerids has also been noted to have occurred shortly after the K/T boundary in the lowermost Danian of the Maud Rise (Weddell Sea) (Pospichal & Wise, 1990; Futterer, 1990), as well as in many other areas, where they have been dubbed "disaster forms". In these cases thoracosphaerids were interpreted as opportunistic forms competitive with the other nannofossils, perhaps because of their ability to encyst during difficult times.

Even though thoracosphaerids are not biostratigraphically useful, due to their long range and slow evolutionary rate, they may be able to provide some input to the palaeoenvironmental reconstruction of the late Quaternary, which is known to have been the scenario for environmental changes related to climate.

The presence of thoracosphaerids in the Quaternary, therefore, suggests either a peculiar adaptation to this enviroment, due to their ability to develop cysts, or to warmer conditions at the time of their deposition, or a combination of both.

As the late Neogene/Quaternary were times of rapid climatic change, such conditions may have favoured the presence of thoracosphaerids and opposed to other calcareous nannoplankton. Both calcareous nannofossils and dinoflagellates, however prefer, in general, warmer water (Dale, 1996). Therefore the presence of either would suggest relatively warmer conditions for the deposition of lithostratigraphic Unit 3.1.

PALYNOLOGY

Introduction

The aims of the palynological study of CRP-1 were to assist both in dating the sediments encountered in the drillhole, and in determination of their environment of deposition. Additional possibilities included determination of sediment provenance from redeposited palynomorphs, and characterisation of terrestrial environments from miospores of land plants.

Ten samples from the Quaternary (0.0 to c. 43.0 mbsf) section of the CRP-1 core were processed and examined for palynomorphs during initial core characterization (Background to CRP-1, this volume - Tab. 7, section on Palynology Processing): a drill cuttings sample obtained during seariser installation, two "fast-track" or rush samples forwarded during drilling, and seven additional samples from the regular sampling conducted later.

All samples were processed using the method outlined in Background to CRP-1, section on Palynology Processing (this volume), details of samples taken being listed in table 7 of that section. Taxa recognised from the Quaternary section of CRP-1 are listed in tables 11 and 12. Some terrestrial palynomorphs are illustrated in figure 16.

Marine Microplankton

A low diversity palynomorph assemblage of prasinophycean green algae phycoma (i.e., cysts), and acritarchs, was recovered from several samples (Tab. 11). The acritarchs are a heterogeneous group of palynomorphs of unknown biological origin, though most are probably of algal affinity. No dinoflagellate cysts were observed in this section of the core.

Foraminiferal linings (Miocene Strata, this volume - Fig. 2511, section on Palynology) were the dominant, and almost the only, palynomorph in the 32.05 mbsf sample. This sample was taken from the unique calcareous interval (lithostratigraphic Unit 3.1) between 31.70 mbsf and 33.82 mbsf. This very fossiliferous unit yielded abundant macrofossils, including bivalves, gastropods, and byozoans; a rich foraminiferal assemblage also was present. It seems unreasonable that palynomorphs other than foram

Tab. **11** - Range chart of the all Palynomorphs from the Quaternary section of CRP-1. Shaded samples were not examined for marine microplankton. Marine species are in caps.

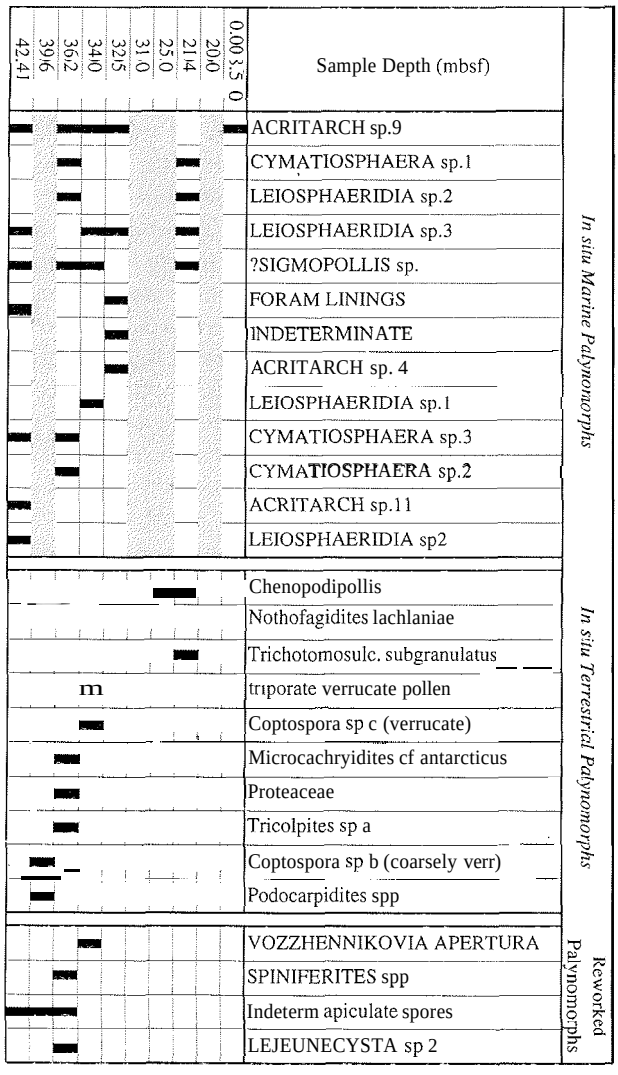

Tub. 12 - Terrestrial Palynomorphs from the Quaternary section of CRP-1

Depth (mbsf)	Cenozoic:	*Chenopodipollis sp.*	*Coptospora sp.b (coarsely verrucate)*	*Coptospora sp.c (verrucate)*	*Dacrydiumites praecupressinoides Couper*	*Microcachryidites cf. antarcticus Cookson*	*Nothofagidites asperus (Cookson)*	*Nothofagidites cf. flemingii (small)*	*Nothofagidites lachlaniae (Couper)*	*Podocarpidites spp.*	*Trichotomosulcites subgranulatus Couper*	Tricolpites sp.a	Reworked Permian-lower Mesozoic:	triporate verrucate pollen	indeterminate apiculate spores
0.00	no miospores observed														
20.60	no miospores observed														
21.04		1							10		1				
25.10									1						
31.50	no miospores observed														
32.05	no miospores observed														
34.00				1										1	
36.62						1				1		1			2
39.06			1							1					1
42.41			1		1			1	1						2

linings are not present in this, the most obviously fossiliferous unit in the core. Additional samples have been selected from the calcareous part of the Quaternary interval and will be studied in the near future.

Well preserved phycoma of Cymatiosphaera-3 dominate the assemblage and occur in low to moderate abundance. Four species of acritarchs were recovered, including *Leiosphaeridia*-2, *Leiosphaeridia*-3, Acritarch-9 and ?*Sigmopollis* (see Miocene Strata, this volume - Tab. 12, section on Palynology, for description notes on selected new taxa). ?*Sigmopollis* sp. has a distinctive s-shaped to undulate cryptosuture that more or less unzips around the circumference of the cell, forming the aperture. The assignment of these specimens to Sigmopollis is tentative because their aperture margin is apparently different from the s-shaped margin characteristic of that genus, and additional study, including SEM analysis, will be needed to determine if the attribution can be confidently made. Leiosphaeridia-3 may be conspecific with ?*Sigmopollis* sp. because specimens are of the same size and colour. However, Leiosphaeridia-3 never exhibits the type of apertural suture typical of ?*Sigmopollis* sp.

All microplankton taxa that appear in Quaternary samples range downhole into or throughout the lower Miocene interval (43.00-147.69 mbsf).

Terrestrial Palynomorphs

Autofluorescence of specimens using a Zeiss epi-illumination system III-RS with blue-violet excitation was used as an aid to discriminate contaminant modern pollen. It also assisted in recognition of Permian-lower Mesozoic miospores reworked from the Beacon Supergroup: these have negligible autofluorescence. Undoubted Cenozoic miospores and marine microplankton from the sequence show a range of autofluorescence colours from yellow to orange, and less stratigraphically well-known taxa with similar autofluorescence weir assigned to this group. Closer examination will be carried out to establish if any consistent patterns occur between different taxa and horizons, which might reflect different thermal alteration and possible reworking.

Very small numbers of Cenozoic pollen and spores, mostly well-preserved, were found in six samples from the Quaternary section. The 21.04 mbsf sample contained the most abundant miospores, an assemblage dominated by pollen of *Nothofagidites lachlaniae* (Fig. 16m) closely comparable to that described from the Sirius Formation of Oliver Bluffs by Hill & Truswell (1993). Single grains of a saccate gymnospenn pollen assigned to *Trichotomosulcites subgranulatus* (Fig. 16j) and a periporate angiosperm pollen, *Chenopodipollis* sp., were also seen.

Other miospores observed in the Quaternary section of CRP-1 include (Tab. 12): Nothofagidites cf. *flemingii* (small); *Tricolpites* sp.a, a distinctive tricolpate pollen seen also in the Miocene section of CRP-1; a triporate angiosperm pollen possibly referable to Proteaceae or Rosaceae (Fig. 16t); and several species of podocarpaceous pollen, *Dacrydiumites praecupressinoides*, *Microcachryidites* sp., and *Podocarpidites* spp. Also present are hilate verrucate spores, Coptospora sp. b (Fig. 16c) and *Coptospora* sp. c (Fig. 16d), comparable to spores of the moss *Conostomum* pentastichum illustrated by Barrow & Lewis Smith (1983) from Holocene peats of South Georgia. Fossil bryophytic spores of this morphological type have also been assigned to the genus Coptospora Dettmann (1963), and this more non-commital classification is used here.

Age and Paleoenvironmental Significance

Species of acritarchs (Leiosphaeridia and ?*Sigmopollis*) and prasinophycean algae (Cymatiosphaera) dominate the palynomorph assemblages recovered from the Quaternary section of the CRP-1 core. These taxa have no age significance in this section. Similar assemblages are reported from Holocene Arctic sediments deposited near sea-ice margins and below open pack ice (Mudie, 1992). The occurrence of these assemblages is used as an indicator of such conditions in Quaternary Arctic deposits for palaeoenvironmental determinations (Mudie & Harland, 1996). Elaboration of the environmental significance of these taxa is presented following discussion of the Miocene palynomorphs.

The limited terrestrial palynoflora permits only tentative conclusions. The relatively high frequency of Nothofagidites in the 21.04 mbsf sample appears to reflect a real difference in source from the other productive samples. This may be due to difference in age and palaeoenvironment, to redeposition from a different source, or a combination of these factors.

The relative abundance of Nothofagidites lachlaniae in the 21.04 mbsf assemblage is similar to that reported

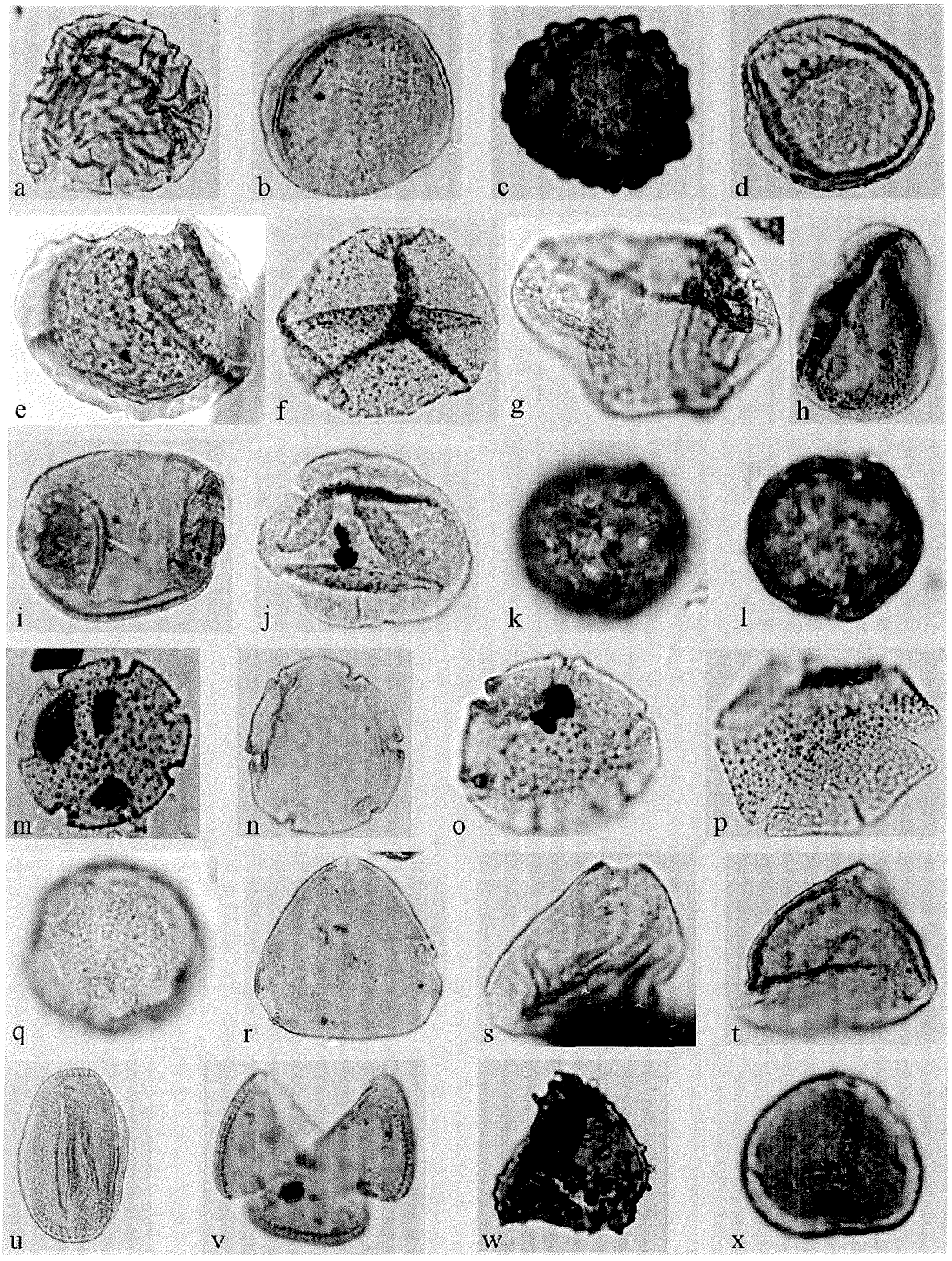

Fig. 16 -Selected miospores from the Quaternary and Miocene sections of CRP-1. Sample depths indicated are the top of the sample interval. Figures are at varied magnifications. "Cenozoic" taxa: *a)* Marchantiaceae (size 88 pm, depth 99.02 mbsf, slide P12/2, England Finder coordinates C43/2); *b) Coptospora* sp.a (59 µm, 70.02 mbsf, P21/1, X43/0); *c) Coptospora* sp.b (40 µm, 39.05 mbsf, P47/1, L46/1); *d) Coptospora* sp.c (33 µm, 34.00 mbsf, P38/1, E28/1); *e) Aequitriradites* sp. (61 *pm,* 147.68 mbsf, P45/1, J32/1); *f) Baculatisporites disconformis* Stover *(44* pm, 96.37 mbsf, P29/1, C39/3); *g) Podocarpidites* sp. (61 µm, 116.45 mbsf, P34/1, X43/0); *h) Dilwynites granulatus* Harris (46 *pm,* 67.54 mbsf, P20/1, T42/1); *i) Phyllocladidites mawsonii* Cookson (41 µm, 67.54 mbsf, P20/1, S40/0); j) *Trichotomosulcites subgranulatus* Couper (33 µm, 21.04 mbsf, P4/1, M32/0); *k, I) Chenopodipollis* sp., two foci of same specimen (21 pm, 99.02 mbsf, P12/1, T47/4); *m) Nothofagidites lachlaniae* (Couper) (33 pm, 21.04 mbsf, P4/1, A52/3); *n) Nothofagidites flemingii* (Couper) (34 µm, 67.54 mbsf, P20/4, V45/0); o) *Nothofagidites* sp. (25 pm, 116.45 mbsf, P34/1, Y42/0); *p) Nothofagidites asperus* (Cookson) (45 *pm,* 116.45 mbsf, P34/1, X44/0); q) Caryophyllaceae (27 pm, 82.18 mbsf, P24/2, T49/0); *r) Proteacidites* cf. *parvus* Cookson (47 µm, 70.02 mbsf, P21/1, C49/0); *s) Triporopollenites ambiguus* Stover (33 µm, 116.45 mbsf, P34/1, D37/0); *t)* triporate pollen cf. Proteaceae (33 µm, 34.00 mbsf, P38/1, M28/0); *u,* v) *Tricolpites* sp.a, equatorially and polarly oriented specimens (47x30 pm, 82.18 mbsf, P24/1, Y32/1; 40 µm, 85.36 mbsf, P25/2, F30/0). Redeposited Permian-lower Mesozoic taxa: *w) Horriditrilates ramosus* (Balme & Hennelly) (31 µm, 99.02 mbsf, P12/2, W46/0); *x) Punctatisporites* sp. (38 *pm,* 108.75 mbsf, P32/2, P48/0).

from the Meyer Desert Formation, Sirius Group (Askin & Markgraf, 1986; Hill & Truswell, 1993). This species also has been reported from middle Pliocene (approximately 3.0 my) sediments in DSDP Site 274 (Fleming & Barron, 1996). These occurences may imply broad correlation with this unit but does not allow precise dating on palynological grounds. The two other taxa recorded from this sample have not so far been reported from the Sirius Group. *Trichotomosulcites subgranulatus* was reported from the upper Eocene section of CIROS-1 drillhole (Mildenhall, 1989), and is also frequent in Ross Sea marine sediments (Truswell, 1983). Known range of the species in New Zealand and Australia is Lower Cretaceous to Palaeogene. *Chenopodipollis chenopodiaceoides* (Martin) was recorded from the Oligocene section of CIROS-1, and referred to the Chenopodiaceae family by Mildenhall (1989). The species has an Oligocene to present known range. The pollen is also similar to that of one of the two extant Antarctic vascular plants, *Colobanthus quitensis*, a cushion plant member of the Caryophyllaceae inhabiting the Antarctic herb tundra formation (Longton, 1985). Whether contemporaneous or reworked, the miospore assemblage reflects a limited diversity vegetation dominated by *Nothofagus*.

No age or paleoenvironmental significance can be attached to the other miospore assemblages, except that if contemporaneous with the time of deposition, their low abundance implies either distance from extensive vegetation, or considerable dilution by barren sediment.

REFERENCES

Allibone A.H., Cox S.C., Grahani I.J., Smillie R.W., Johnstone R.D., Ellery S.G. & Palmer K., 1993a. Granitoids of the Dry Valleys area, southern Victoria Land, Antarctica: field relationships, and isotopic dating. *New Zealand Journal of Geology and Geophysics*, 36, 281-291.

Allibone A.H., Cox S.C. & Smillie R.W., 1993b. Granitoids of the Dry Valleys area, southern Victoria Land: geochemistry and evolution along the early Paleozoic Antarctic Craton margin. *New Zealand Journal of Geology and Geophysics*, **36**, 299-316.

Arniienti P., Civetta L., Innocenti F., Tripodo A., Villari L.& Vita G., 1991. New petrological and geochemical data on Mt. Melbourne volcanic field. Northern Victoria Land, Antarctica. *Memorie della Società Geologica Italiana*, **46,** 397-424.

Askin R.A. & Markgraf V., 1986. Palynomorphs from the Sirius Formation, Dominion Range, Antarctica. *Antarctic Journal of the United States*, **21**, 34-35.

Barrett P.J., Elston D.P., Harwood D.M., McKelvey B.C. & Webb P.N., 1987. Mid-Cenozoic record of glaciation and sea level change on the margin of the Victoria Land basin, Antarctica. *Geology*, 15, 634-637.

Barrett P.J., Hambrey M.J., Harwood D., Pyne A.R. & Webb P.N., 1989. Synthesis. In: Barrett P.J. (ed.), Antarctic Cenozoic history from the CIROS-1 drillhole, McMurdo Sound, *DSIR Bulletin*, **245**, 241-251.

Barrett P.J., McKelvey B.C. & Walker B.C., 1986. Sand provenance. *DSIR Bulletin*, 237, 137-144.

Barrow C.J. & Lewis Smith R.I., 1983. Palynological studies in South Georgia: II. Two profiles in Sphagnum Valley, Cumberland West Bay. *British Antarctic Survey Bulletin*, 58, 15-42.

Behrendt J.C., Blankenship D.D., Finn C.A., Bell R.E., Sweeney R.E., Hodge S.R. & Brozena J.M., 1994. Evidence for Late Cenozoic flood basalts (?)in the West Antarctic Rift System revealed by the CASERTZ aeromagnetic survey. *Geology*, 22, 527-530.

Behrendt J.C., Blankenship D.D., Damaske D. & Cooper A.K., 1995. Glacial removal of Late Cenozoic subglacially emplaced volcanic edifices by the West Antarctic Ice Sheet. *Geology*, 23,1111-1114.

Bennett M.R & Glasser N.F., 1996. *Glacial Geology-Ice Sheets and Landforms*. Chichester: John Wiley.

Bohaty S.M. & Harwood D.M., in press. Southern Ocean Pliocene paleotemperature variation from silicoflagellate biostratigraphy. *Marine Micropaleontology*.

Dale B., 1996. Dinoglagellatc cyst ecology: modeling and geological applications. In: Jansonius J. & McGregor D.C. (ed.), *Palynology: priciplesandapplications*, American Ass. of Stratigr. Palynologysts Foundation, 3, 1249-1275.

Dell R.K., 1990. Antarctic Mollusca. *The Royal Society of New Zealand Bulletin*, 27.

Dettmann M.E., 1963. Upper Mesozoic microfloras from south-eastern Australia. *Proceedings of the Royal Society of Victoria*, 77, 1-148.

Domack E.W., 1988. Biogenic facies in the Antarctic glacimarine environment: basis for a polar glacimarine summary. *Palaeogeography, Palaeoclimatology, Palaeoecology*, **63,** 357 372.

Dow J.A.S. & Neall V.E., 1974. Geology of the lower Rennick Glacier, north Victoria Land, Antarctica. *New Zealand Journal of Geology and Geophysics*, 17, 659-714.

Ehrmann W.U., 1997. Smectite concentrations and crystallinities: indications for Eocene age of glaciomarine sediments in the CIROS-1 drillhole, McMurdo Sound, Antarctica. In: Ricci C.A. (ed.), *The Antarctic Region: Geological Evolution and Processes*, Terra Antartica Publication, Siena, 771-780.

Ehrmann W., in press. Implications of late Eocene to early Miocene clay mineral assemblages in McMurdo Sound (Ross Sea, Antarctica) on paleoclimate and ice dynamics. *Palaeogeogr., Palaeoclimatol., Palaeoecol.*

Fleming R.F. & Barron J.A., 1996 Evidence of Pliocene *Nothofagidites* in Antarctica from Pliocene marine sedimentary deposits (DSDP Site 274). *Marine Micropaleontology*, **27**, 227-236.

Futterer D.D.K., 1976. Kalkige Dinoflagellaten ("Calcodinelloideae") und die systematische Stellung der Thoracosphaeroideae. *N Jahrb. Geol.Palaontol. Abh*, 151, 119-141.

Futterer D.D.K., 1990. Distribution of calcareous dinoflagelatcs at the Cretaceous-Tertiary boundary of the Queen Maud Rise, Eastern Weddell Sea, Antarctica (ODP Leg 113). *Proc. ODP, Sc. Results*, **113**, 533-548.

Gamble J.A., Barrett P.J. & Adams C.J., 1986. Basaltic clasts from Unit 8. *DSIR Bulletin*, 237, 145-152.

Gazdzicki A. & Webb P.N., 1996. Foraminifera from the *Pecten* Conglomerate (Pliocene) of Cockburn Island, Antarctic Peninsula. *Palaeontologica Polonica*, 55, 147-174.

George A., 1989. Sand provenance. *DSIR Bulletin*, **245**, 159-167.

Gunn B. & Warren G., 1962. Geology of Victoria Land between the Mawson and Mulock glaciers. *New Zealand Geological Survey Bulletin*, 71, 157 p.

Hanvood D.M. & Maniyama T., 1992. Middle Eocene to Pleistoccne diatom biostratigraphy of ODP Leg 120, Kerguelen Plateau. *Proc. ODP, Sc. Results*, 120. College Station, TX., 683-733.

Heron-Alien E. & Earland A., 1922. Protozoa, Part II — Foraminifcra: British Antarctic *(Terra Nova)* Expedition, **6**, 25-268.

Hill R.S. & Truswell E.M., 1993. *Nothofagus* fossils in the Sirius Group, Transantarctic Mountains: leaves and pollen and their climatic implications. In: Kennett J.P. & Warnke D.A. (eds.), *The Antarctic paleoenvironment: aperspective onglobalchange. Part II, Antarctic Research Series*, 60, 67-73.

Jakobsson S.P., 1978. Environmental factors controlling the palagonitization of the Surtsey tephra, Iceland. *Bulletin of the Geological Society of Denmark (Special Issue)*, **27**, 91-105.

Kyle P.R., 1990. McMurdo Volcanic Group, Western Ross Embayment. In: LeMasurier W.E. & Thomson J.W. (eds.), *Volcanoes of the Antarctic Plate and Southern Oceans, American Geophysical Union, Antarctic Research Series*, 48, 19-25.

Kyle P.R., 1990. Erebus Volcanic Province. In: LeMasurier W.E. & Thomson J.W. (eds.), *Volcanoes of the Antarctic Plate and Southern Ocean, Antarctic Research Series*, 48, 81-145.

Leventer A. & Dunbar R.B., 1987. Diatom flux in McMurdo Sound, Antarctica. *Marine Micropaleontology*, **12**, 49-64.

Leventer A & Dunbar R.B., 1996. Factors influencing the distribution of diatoms and other algae in the Ross Sea. *Journal of Geophysical Research*, 101, No. C8, 18489-18500.

Longton R.E., 1985. Terrestrial habitats - vegetation. In: Bonner W.N & Walton D.W.H. (eds.), *Key environments—Antarctica*, Pergamon Press, Oxford, 73-105.

Mildenhall D.C., 1989. Terrestrial palynology. In: Barrett P.J. (ed.), Antarctic Cenozoic history from the CIROS-1 drillhole, McMurdo Sound. *DSIR Bulletin,* 245, 119-127.

Monechi S. & Reale V., in press. Calcareous nannofossil assemblage of the CIROS-1 Core (Ross Sea): further assessments on age. *Terra Antartica.*

Mudie P.J., 1992. Circum-Arctic Quaternary and Neogene marine palynofloras: paleoecology and statistical analysis. In: Head M.J. & Wrenn J.H. (eds.), *Neogene and Quaternary dinoflagellate cysts and acritarchs,* American Association of Stratigraphic Palynologists Foundation, Dallas, Texas, 347-390.

Mudie P.J. & Harland R., 1996. Aquatic Quaternary. In: Jansonius J. & McGregor D.C. (eds.), *Palynologic Principles and Applications,* American Association of Stratigraphic Palynologists Foundation, Dallas, Texas, 2, 883-877.

Nelson C.S., Keane S.L. & Head P.S., 1988. Non-tropical carbonate deposits on the modern New Zealand shelf. *Sedimentary Geology,* 60, 71-94.

Pospichal J. & Wise S.W., Jr., 1990. Paleocene to middle Eocene calcareous nannofossils of ODP Sites 689 and 690, Maud Rise, Weddell Sea. *Proc. ODP, Sc. Results,* **113**, 613-638.

Roser B.P. & Pyne A.R., 1989. Wholerock chemistry. *DSIR Bulletin,* 245, 175-184.

Schäfer P., Heinrich R., Zankl H. & Bader B., 1996. Carbonateproduction and depositional patterns of BRYOMOL-carbonates on deep shelf Bank in mid and high northern latitudes. In: Reitner J., Neuweiler F. & Gunkel F. (eds.), *Global and Regional Control on Biogenic Sedimentation. I. Reef Evolution, Research Report,* Gottinger Arb. Geol. Paläont., Gottingen, 101-110.

Scherer R.P., 1987. Paleoenvironmental studies of non-marine diatoms in Quaternary Antarctic sediments. *Antarctic Journal of the United Stairs,* **22**(5), 35-37.

Taviani M., Reid D.E. & Anderson J.A., 1993. Skeletal and isotopic composition and paleoclimatic significance of Late Pleistocene carbonates, Ross Sea, Antarctica. *Journal of Sedimentary Petrology,* ***63,*** 84-00.

Truswell E.M., 1983. Recycled Crctaccous and Tertiary pollen and spores in Antarctic marine sediments: a catalogue. *Palaeontographica* B, 186, 121-174.

Ward B.L. & Webb P.N., 1986. Late Quaternary foraminifera from raised deposits of the Cape Royds-Cape Barne area, Ross Island, Antarctica. *Journal of foraminiferal research,* 16, 176-200.

Warren G., 1962. Geology of Terra Nova Bay-McMurdo Sound area, Victoria Land. *Antarctic* Map *Folio Series,* Plate 13, Folio 12. Geology, American Geographical Society, New York.

Webb P.N. & Wrenn J.H., 1982. Late Cenozoic micropaleontology and biostratigraphy of eastern Taylor Valley, Antarctica. In: Craddock C. (ed.), *SCAR Symposium on Geology and Solid-Earth Geophysics, 1977:* Madison (University of Wisconsin Press), 1117-1122.

Winter D.M. & Hanvood D.M., 1997. Integrated diatom biostratigraphy of Late Neogene drillholes in southern Victoria Land and connection to Southern Ocean records. In: Ricci C.A. (ed.), *The Antarctic Region: Geological Evolution and Processes,* Terra Antartica Publication, Siena, 985-992.

Wohletz K.H. & Sheridan M.F., 1983. Hydrovolcanic explosions II. Evolution of basaltic tuff rings and tuff cones. *Amer. J. of Science,* **283**, 384-413.

Terra Antartica
1998, 5(1), 63-124

TERRA ANTARTICA

Miocene Strata in CRP-1, Cape Roberts Project, Antarctica

CAPE ROBERTS SCIENCE TEAM*

Abstract - Based on the alternation of diamicts with other clastic sedimentary facies, the predominantly lithified Miocene section of CRP-1 has been divided into lithostratigraphic Units 5 to 7, with Unit 5 further divided into 8 subunits and Unit 6 into 3. Petrological investigations of extraformational clasts indicate provenance from probable Cambro-Ordovician granites, metamorphic rocks (Koettlitz Group?), Ferrar dolerite and rhyolites of uncertain affinity. The sand fraction is dominated by grains derived from crystalline basement and the Beacon Supergroup, but volcanic glass, abundant above 62 mbsf, is correlated with the McMurdo Volcanic Group. X-ray diffraction analysis of mud samples shows a similar change in mineralogy over the interval 60-65 mbsf from smectite-dominated above to illite and chlorite-dominated below.

The Miocene section is dated by diatom biostratigraphy at 17.5 -22.4 Ma (early Miocene), which suggests an average sediment accumulation rate of about 21 m/my. The most prevalent fossil groups are diatoms, foraminifers and palynomorphs. The well-preserved marine palynomorph assemblage contains many new acritarchs, and apparently represents the first known palynomorph record from in *situ* lower-Miocene Antarctic sediments. Calcareous nannofossils (Thoracosphaera) are rare to few, as are macrofossils (serpulid worm tubes, echinoid spines, bryozoans, and scallop shells). Palaeoenvironmental interpretations suggest a glacimarine setting warmer than present that underwent some significant fluctuations in water depth and proximity to the ice margin.

A magnetic-polarity stratigraphy has been measured for the lower *c.* 90 m. Four magnetozones defined below 89 mbsf are correlated within the range of Chrons C5Dr to C6 of the Magnetic Polarity Time Scale.

The Miocene section has also been divided into six recurrent lithofacies: diamictite, rhythmically interlaminated fine-grained sandstone and siltstone, well-stratified sandstone, poorly-stratified muddy sandstone, coarse-grained siltstone and fine-grained siltstone. No major changes in facies assemblage have been identified, implying similar variations in environmental conditions throughout.

Last, the succession has been divided by sequence stratigraphic analysis into 10 units, wherein each sequence passes upward from a basal diamict into progressively finer-grained facies, interpreted as a flooding event. Each sequence is thought to record the cyclical advance and retreat of grounded ice across the site, although there is little or no record of glacial advance. The only positive evidence for sediment accumulation under grounded ice has been found in a directional clast fabric in a diamictite at 62.64 mbsf.

LITHOSTRATIGRAPHY

INTRODUCTION

The Miocene part of the core is mainly lithified but appears to be uncemented; some horizons of sand, however, are unconsolidated. The core is heavily brecciated, especially towards the top of the Miocene section, and this is described in Background to CRP-1, section on Core Properties (this volume). It should be noted that a detailed age for the upper boundary of the Miocene section has not yet been determined. The Miocene section has been divided into three main lithostratigraphic units (nos. 5-7), with lithostratigraphic Unit 5 divided into 8 subunits and lithostratigraphic Unit 6 subdivided into a further three. These are defined solely on the basis of lithology. In the following discussion, the principal Miocene lithofacies are described and interpreted. The key characteristics of each lithostratigraphic unit are then summarised, largely on the basis of the 1:20 scale logs, which are given in Appendix 2. A brief preliminary interpretation of the depositional environment of each lithostratigraphic subunit is also given. Although data are only available from a single core and inferences concerning the depositional process are limited, the clear indications of the presence of glacier ice are not in doubt. However, whereas the diamictites suggest glacial conditions nearby, the sandstones and mudstones may be interpreted both within and outside a glacial context.

FACIES ANALYSIS

Six lithofacies recognised within the Miocene section are defined on the basis of lithology or associations of lithologies, bedding contacts and bed thicknesses, texture, fabric, sedimentary structures and colour (Tab. 1). It is recognised that there is scope for further subdivision of these facies, once the details of texture, fabric and sedimentary structure have been investigated more thoroughly.

* J. Anderson, P. Armienti, C. Atkins, P. Barrett, S. Bohaty, S. Bryce, M. Claps, M. Curran, F.J. Davey, L. De Santis, W. Ehrmann, F. Florindo, C. Fielding, M. Hambrey, M. Hannah, D.M. Harwood, S. Henrys, F. Hoelscher, J.A. Howe, R. Jarrard, R. Kettler, S. Kooyman, C. Kopsch, L. Krissek, M. Lavelle, E. Levac, F. Niessen, S. Passchier, T. Paulsen, R. Powell, A. Pyne, G. Rafat, I.J. Raine, A.P. Roberts, L. Sagnotti, S. Sandroni, E. Scholz, J. Simes, J. Smellie, P. Strong, M. Tabecki, F.M. Talarico, M. Taviani, K.L. Verosub, G. Villa, P.N. Webb, G.S. Wilson, T. Wilson, S.W. Wise, T. Wonik, K. Woolfe, J.H. Wrenn.

Tab. 1 - Characteristics of lithofacies recognised in CRP-1.

Facies	Lithology	Geometry, Contacts, Structures	Fossils	Interpretation
1	Diamictite to muddy/ sandy conglomerate, variable texture and fabric but mainly very poorly sorted, variable clast content of pebbles to boulders, shape varies from very angular to well-rounded (most subangular - subrounded).	Sharp-bounded units <22 m thick, some with fining-upward tops, mainly unstratified, but with local wispy lamination, soft-sediment deformation and siltstone partings, local inclined clasts (?imbrication), some coated clasts, one sedimentary dyke.	Scattered shells of ribbed scallops (*Chlamys sp.*).	Glacimarine, sand and mud deposited from aqueous currents and suspension fallout, gravel from floating ice.
2	Rhythmically interlaminated and thinly interbedded fine-grained sandstone and siltstone, scattered clasts up to cobble grade.	?Sharp-bounded unit 0.66 m thick, planar lamination, deformed lamination beneath some clasts.	None observed.	Subaqueous current deposits, possibly proximal glacimarine with ice-rafted dropstones.
3	Sandstone, generally fine- to medium-grained, clean and relatively well-sorted, minor granules and pebbles, rare siltstone partings.	Amalgamated, mainly sharp-bounded beds and units, intervals <4 m thick, some normal grading, also alternating medium-fine laminae, well-stratified with abundant planar/flat stratification, local low-angle cross-bedding and ripple cross-lamination, and rare high-angle cross-bedding.	None observed.	Deposition from dilute, subaqueous submarine currents.
4	Sandstone, generally fine- to medium-grained, variable mud content, rare granules and pebbles, minor siltstone laminae and partings.	Amalgamated, mainly sharp-bounded beds <2 m+ thick, intervals <8 m thick, normal and reverse grading or no upward grain-size trend, floating mud clasts, local silt clast layers mainly at bed bases, vague flat stratification (ripple cross-lamination in X-ray images), load casts.	Minor bioturbation, calcareous serpulid tubes.	Rapid deposition from submarine currents, probably density currents, including traction carpet deposits at base of some beds.
5	Siltstone, coarse-grained to sandy in places, rare granules and pebbles.	Intervals <5 m thick, some coarsening-upward, flat lamination, load casts, siltstone clasts, soft-sediment deformation.	Bioturbation, calcareous serpulid tubes.	Submarine deposition from ?density currents and from suspension.
6	Siltstone, fine-grained, rare granules and pebbles.	Intervals <6 m thick, generally at base of coarsening-upward sequences, primary lamination, disturbed in places by bioturbation.	Bioturbation, calcareous serpulid tubes.	Submarine deposition from suspension.

Facies 1 - Diamictite, Sandy Muddy Conglomerate

Facies 1 consists of very poorly sorted mixtures of gravel, sand, silt and clay, which are generally poorly stratified to unstratified and display little internal organisation into beds (Fig. 1a & b). The lithology comprises a coarse-clast population (granule to boulder grade), generally suspended in and supported by a matrix of mixed sand, silt and clay. The clast and matrix proportions (and the grain size of both components) vary considerably, typically over short vertical intervals. Some diamictite units are punctuated by discrete, fine-grained partings, which are typically up to 10 cm thick and show evidence of soft-sediment deformation (Fig. 1c). A small number of calcareous macrofossils was noted within Facies 1, principally the ribbed scallop *Chlamys* sp., and marine microfossils have been recovered from samples of this and other facies.

Coarse clasts are of both intra- and extraformational rocks. Intraformational debris includes clasts of siltstone clast breccia, fine sandstone, siltstone and dark grey, ?silicified claystone, lithologies characteristic of Facies 4-6 (see below). Extraformational clasts include basic volcanic and intrusive rocks, granites of varying texture and composition, felsic porphyry, and sandstone. The largest clasts penetrated by the core are either dolerite or granite. Coarse clasts are typically very poorly sorted, and range in shape from very angular to well-rounded. Some show elaborate, angular outlines, while some dolerite clasts are almost perfectly rounded (Fig. 1a). One broken clast of dolerite was noted at *c.* 103.83 mbsf, within a cluster of clasts coated by light-coloured ?silt (Fig. 1a). Striae were noted on some smaller clasts. Little evidence of stratification was noted, although some elongate clasts are inclined, suggestive of imbrication. Two intervals (133.57-133.81, 139.05-139.31 mbsf) preserve mud-lined, sand-filled sedimentary dykes, *c.* 1.5 cm wide, the upper of which appears to emanate from a mixed, fine-grained horizon immediately below that interval (Fig. 1b).

Macrofossils within Facies 1 indicate a marine environment less than 100 m deep, and this is consistent with microfossil assemblages found in the diamictites. The poorly sorted and in many cases angular nature of the coarse debris suggests that a variety of glacial processes may have played a role in delivering this sediment. Much of the gravel noted, however, probably arrived at the depositional site by falling through the water column from floating ice. Such a process can be established more confidently in a few cases where poorly defined lamination is deformed beneath coarse clasts. A broadly glacimarine origin is inferred for Facies 1, whereby sand-, silt- and clay-grade sediment was delivered from a glacier terminus some (unknown) distance from the drillsite, and mixed by

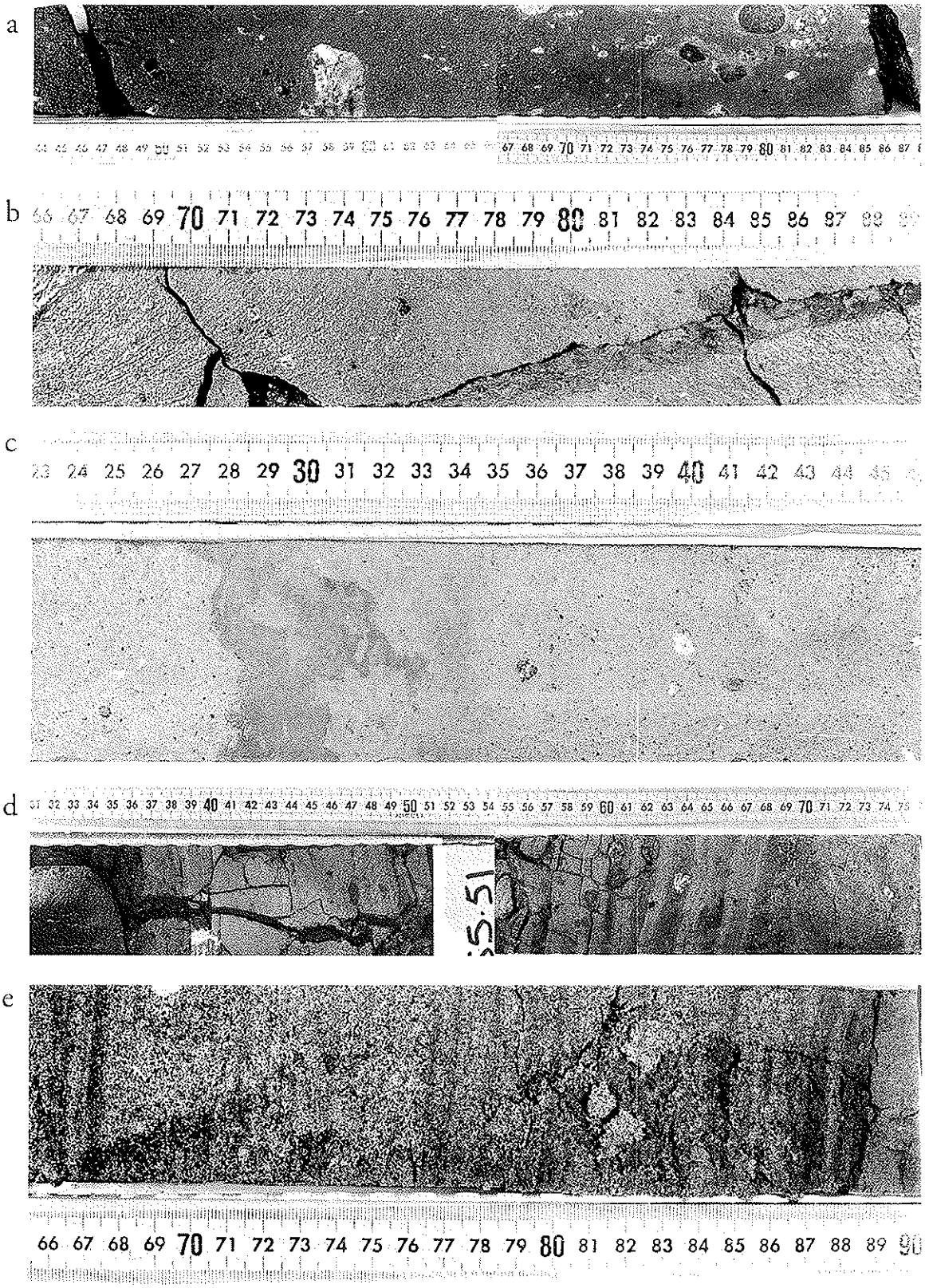

Fig. 1 - Photographs of representative lithofacies from CRP-1. *a)* Facies 1 - unstratified, clast-poor, sandy diamictite at 103.44-103.66 mbsf and turbated, clast-rich, sandy diamictite at 103.66-103.88 mbsf, with coarse-extraformational clasts (principally dolerite and granite) distributed irregularly through the lithology. Note the highly irregular shape of the large granite clast at 103.57-103.60 mbsf, the smaller split/coated dolerite clast at 103.50 mbsf, the cluster of clasts at 103.76-103.85 mbsf (some well rounded) and the occurrence of a light-coloured coating around these clasts. *b)* Facies 1 - clast-poor, muddy diamictite at 133.66-133.89 mbsf, showing mud-lined/sand-filled clastic dyke cutting the lithology. The dyke may be sourced from the dark-coloured (muddy) horizon at 133.85-133.89 mbsf. *c)* Facies 1 - clast-poor, muddy diamictite at 134.23-134.45 mbsf, showing a soft-sediment-deformed siltstone parting (134.28-134.33 mbsf). *d)* Facies 2 - interlaminated and thinly interbedded sandstones and siltstones, with scattered coarse clasts, at 55.31-55.75 mbsf. Note the occurrence of flat lamination and local ripple cross-lamination, the local deformation of lamination beneath some clasts (*e.g.*, at 55.54-55.55 mbsf), and the brittle microfault cutting the lithology at 55.36-55.42 mbsf). *e)* Facies 3 - relatively well-sorted and quartzofeldspathic, fine- to medium-grained sandstones at 90.64-90.90 mbsf, showing extensive development of flat stratification and local low-angle cross-bedding.

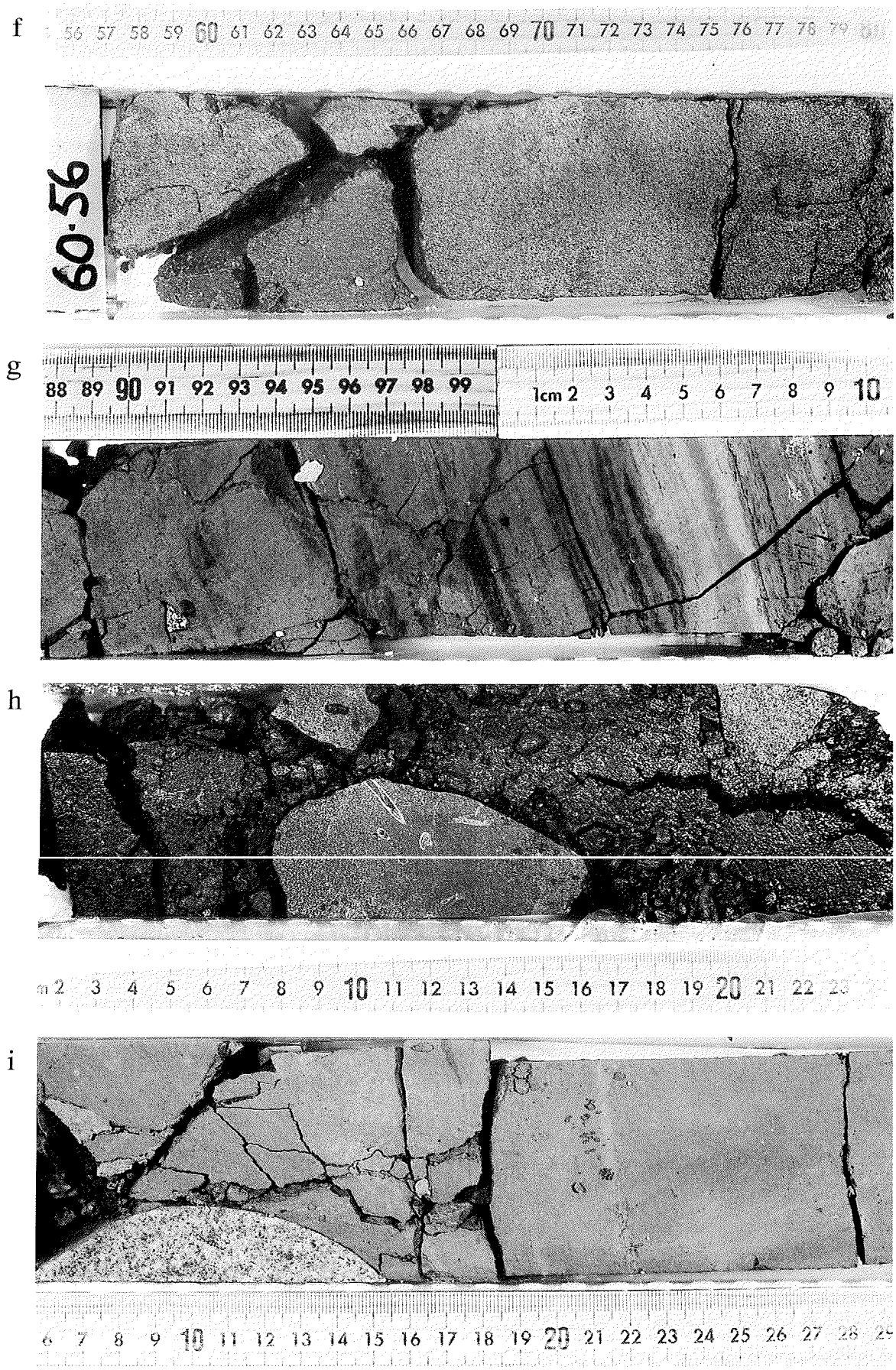

Fig. 1 - Continued. *f)* Facies 4 -very fine- to medium-grained, muddy sandstones at 60.56-60.80 mbsf, showing siltstone clast conglomerate horizon at the base of a bed at 60.72-60.80 mbsf, and overlying normally graded sandstone, *g)* Facies 4/5 - sharp-bounded, muddy sandstones, and interlaminated sandstones/siltstones at 69.88-70.12 mbsf. h) Facies 4/5 - brecciated, muddy fine-grained sandstones at 46.00-46.24 mbsf, showing preservation of calcareous serpulid tubes within a well-cemented concretion at 46.08-46.16 mbsf. *i)* Facies 6 - fine-grained siltstones with rare coarse clasts at 94.05-94.30 mbsf, showing local development of stratification *(e.g.,* 94.22 mbsf).

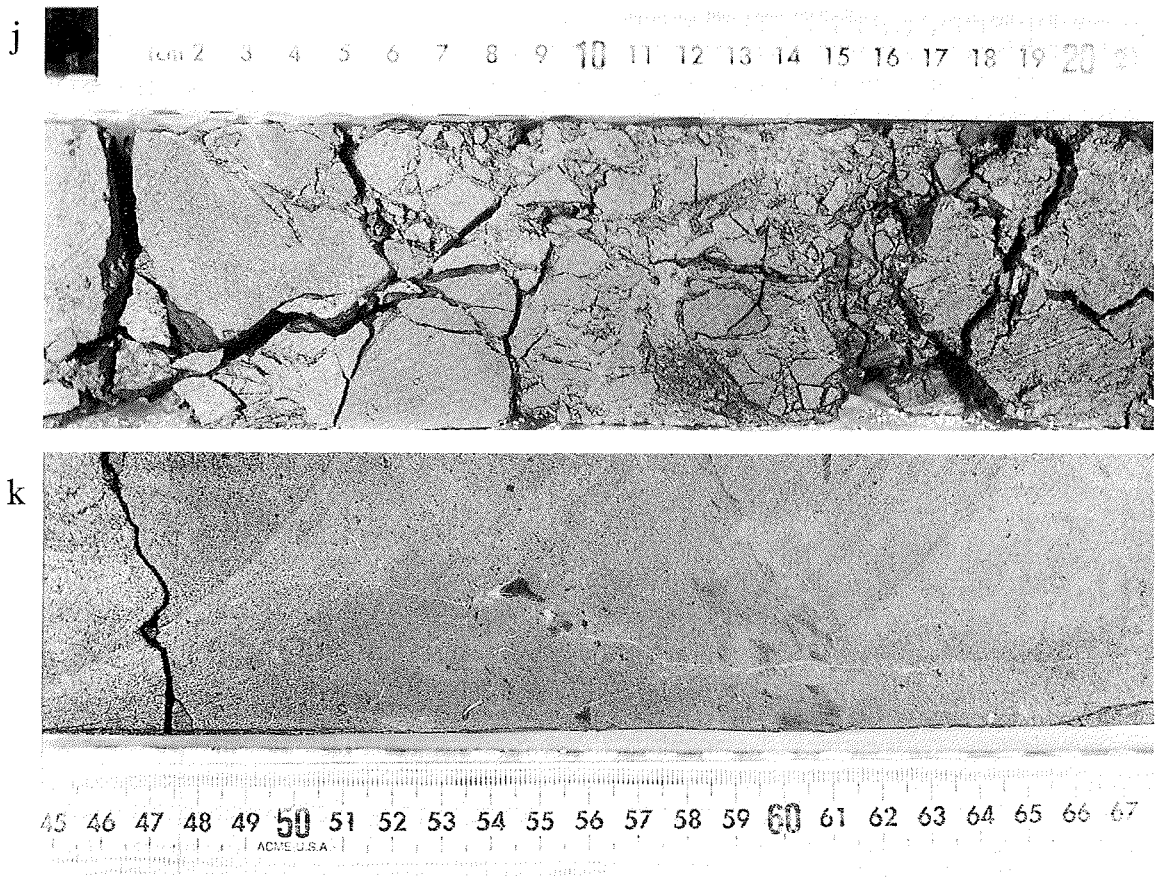

Fig. **1** - Continued. j) Sandstones of Facies 4 at 49.99-50.23 mbsf, showing intense, post-depositional fracturing and brecciation of core. Note how the boxwork of fractures has segmented the rock into enclaves that could be interpreted as clasts. Most of the fractures illustrated are open, but some are filled with a fine-grained, in part possibly crystalline material. k) Siltstones of Facies 6 at 95.45-95.68 mbsf, showing an extensive, near vertical fracture that has been refracted around sparse coarse clasts, and is filled by a finely crystalline material.

physical processes in the marine environment. Coarse debris were dropped from floating ice, and changes in the abundance of such gravel are used elsewhere to give a first approximation as to the proximity of a glacier terminus (Summary of Results from CRP-1, this volume - Fig. 4). No unequivocal evidence of subglacial deposition was noted within the diamictites, although the sedimentary dykes noted above could have formed during a period of loading by ice and/or diamict over the region. Fine-grained partings may indicate hiatuses in the accumulation of glacimarine sediment, perhaps due to fluctuations in the position of a glacier terminus.

Facies 2 - Rhythmically Interlaminated Sandstone and Siltstone with Lonestones

Facies 2 comprises thinly, rhythmically interbedded and interlaminated fine-grained sandstone and siltstone, in roughly equal proportions, with dispersed gravel of varying grade and clast shape (Fig. 1d). Individual beds are 2 - 20 mm thick, and tabular across the width of the core. Beds are characterised by a planar stratification, which is deformed beneath some lonestones. Individual sandstone beds and laminae are moderately to well-sorted.

The alternation of coarse and fine laminae is suggestive of a subaqueous environment affected regularly by alternating high- and low-energy conditions. The presence of lonestones with deformation of lamination beneath them suggests the introduction of coarse debris from floating ice. This distinctive, rhythmically bedded facies is similar to deposits termed "cyclopsams" by Mackiewicz et al. (1984), and interpreted by those authors as the deposits of ice-proximal glacimarine environments affected by tidal flux. The role of tidal processes cannot be established in the present case, but a setting relatively close to a source of glacier ice is suggested by the abundance of apparently ice-rafted debris.

Facies 3 - Stratified, Moderately- to Well-Sorted Sandstones

This facies consists of generally fine- to medium-grained, moderately- to well-sorted sandstones of quartzofeldspathic composition, which are organised into grain-size-differentiated laminae and beds (Fig. 1e). Sandstones are arranged in stacked, amalgamated units up to 5 m thick, such that individual beds are difficult to define. Internal stratification is well-developed in this facies, most commonly flat stratification and low-angle cross-stratification, with less abundant ripple cross-lamination and rare high-angle cross-bedding.

Facies 3 contains no macrofossils, but from its intimate association with other fossiliferous lithologies it may be interpreted as the product of sediment deposition in a marine setting. The abundance of physical sedimentary

structures and the persistent grain-size sorting in this facies points towards deposition from dilute, tractional currents, of varying strength. In the absence of any unequivocal wave-generated or combined-flow structures, the low-angle cross-bedding noted may be interpreted as truncated cross-bedding, suggesting in turn that sands were mostly laid down under physical conditions close to or within the plane bed stability field. Accordingly, Facies 3 is interpreted as reflecting a shallow-submarine environment into which coarse sediments were introduced by dilute currents.

Facies 4 - Poorly Stratified, Poorly Sorted Sandstones

Facies 4 comprises relatively muddy, poorly sorted and poorly stratified sandstones with rare, thin silt laminae, which form sharp-based and in many cases fining-upward beds up to 2 m thick (Fig. 1f, g & h). Amalgamated intervals of Facies 4 sandstones vary up to 8 m thick. These sandstones are typically dark olive grey in colour in contrast to the lighter grey colour of Facies 3. Many beds are normally graded, some with a siltstone clast breccial conglomerate horizon at or near the base (Fig. 1f), while a few beds (e.g., 141.24-141.82 mbsf) display inverse grading with a coarse fraction "floating" near the top of the bed. Other beds contain floating siltstone clasts suspended within apparently massive or poorly stratified sandstone.

Sedimentary structures are sparsely developed within Facies 4. Some beds show load-casted bases, and vague flat stratification is widespread, but few other structures were noted on the surface of the core. X-radiography of selected sections, however, revealed flat stratification and ripple cross-lamination in several beds (see section on X-Radiography and Sedimentological Features). Biogenic structures are rare within this facies: serpulid tubes were recorded in a few places (Fig. 1h), and indeterminate bioturbation noted at a number of horizons.

Amarine environment of deposition is indicated by the fossil evidence. The sharp-based, often graded and poorly stratified nature of Facies 4 is suggestive of deposition from at least partly or temporarily turbulent sediment gravity flows (density-modified grain flows or turbidity flows). Clast-rich horizons near the base of some beds are interpreted as traction carpet deposits, while floating intraformational clasts may reflect the role of buoyancy in some flows. Inverse grading is also considered an indicator of higher flow viscosity among the spectrum of sediment gravity flows (Nemec & Steel, 1984; Nemec, 1990). Accordingly, Facies 4 is interpreted as the product of periodic sediment gravity flows across the submarine surface. No direct evidence of formative water depth is evident from the sediments themselves, but the fossil assemblage in this and associated facies is suggestive of depths no greater than 100 m.

Fades 5 - Coarse-Grained Siltstones

Facies 5 comprises coarse-grained or sandy siltstones that are intimately associated with Facies 4, in many cases forming the upward-fining, upper part of Facies 4 beds (Fig. 1g & h). Other occurrences arc associated with coarsening-upward sequences up to a few metres thick (e.g., 76-79 mbsf). Flat stiatification is evident in a few cases, as is load casting and indeterminate soft-sediment deformation, and floating siltstone clasts were noted at a few horizons (e.g., 59-60 mbsf). Both serpulids and bioturbation were noted as in Facies 4.

The intimate association and similarity of Facies 4 and 5 indicates a genetic link between the two. Accordingly, Facies 5 is intepreted as reflecting the waning-flow and/or distal portions of the density currents responsible Sot Facies 4.

Facies 6 - Fine-Grained Siltstones

Facies 6 consists of intervals of fine-grained siltstone up to 6 m thick (Fig. 1i), which are in places laminated and in others either apparently massive or bioturbated. Serpulid tubes were noted at a few horizons.

The fine-grained siltstones of Facies 6 are interpreted to have formed by fallout of fine sediment from suspension in the (marine) water column.

Secondary Brecciation of Core

A large proportion of the core from CRP-1 is affected to a varying extent by fracturing and brecciation (Fig. Ij & k). Although the origin of this fracturing is open to more than one plausible interpretation, it is clear that the deformation was brittle, and therefore that it occurred after the section had been at least partly lithified. This is evident from the geometry and non-facies-specific nature of fracturing, and the filling of some fractures by a finely crystalline material. From a sedimentological perspective, the importance of this phenomenon is that it has formed breccias with fabrics that could be misinterpreted as primary depositional frameworks. True (intraformational) sedimentary breccias do occur within the cored succession, but are considerably more localised than secondary breccias, and can be identified confidently only when a clear distinction between the grain-size of clasts and matrix can be made.

Discussion

The facies assemblage indicates that the Miocene section in CRP-1 accumulated in mainly shallow-marine environments of deposition, at times under the influence of floating ice and perhaps offshore from glacier termini. The balance of evidence suggests, however, that there is no depositional record of grounded ice in CRP-1, except possibly in lithostratigraphic Unit 5.3 (see section on Clast Fabric). The most clearly ice-proximal sediments are the diamictites of Facies 1, and attempts are made elsewhere in this report to assess the proximity of glacier ice based on the density of clasts per unit length of core. Facies 2 may also record proximal glaciomarine environments. Given its better sorting, generally coarser grain-size and more stratified nature, Facies 3 is interpreted to have formed in shallower water than Facies 4, and by somewhat different physical processes. Given the above-mentioned attributes,

the dilute water currents held responsible for Facies 3 may have been associated with outflows from fluvioglacial deltas. Facies 4 and 5, which are closely associated with Facies 3, shows evidence of deposition from more sediment-charged, sediment gravity flows, and may reflect either or both of a change in water character (salinity, density, temperature, etc.) and a change in water depth. Facies 6 is interpreted to represent the most distal and/or deepest-water environment recorded in the core.

Based on the present-day subsea topography of the western Ross Sea and inspection of seismic reflection data, it is considered likely that the submarine surface was irregular with significant slopes in places (a ramp, rather than shelf geometry) during most of the time represented by the cored section. Some periods of progradation are evident from clinofosms in the seismic records, and some channelling has also been noted. A flat shelf with a distinct shelf break, such as occurs on most continental margins, is not apparent from seismic data in the study area (see Background to CRP-1, this volume - section on Regional Setting). Accordingly, schematic illustrations of the interpreted depositional environment of Facies 1 - 6 during times of 1) relative ice advance and 2) relative ice retreat shown in figure 2 depict a ramp setting.

DESCRIPTION OF SEQUENCE

Lithostratigraphic Unit 5.1 (43.15-53.70 mbsf), Sandstone and Mudstone

Description. Lithostratigraphic Unit 5.1 is a sparsely fossiliferous, moderately to well sorted, fine-grained sandstone, with colour ranging from black (N1) to olive black (5Y 2/1). The sediment is lithified but appears to be uncemented. The rock is fractured and has a fitted fabric, with brecciation affecting 50-100% of the core. The breccia is composed of fragments of granule to small pebble size. Some fractures are filled with fine-grained sand (colour: SYR 2/1). Typical principal components of the sandstone are quartz, feldspar and volcanic rock fragments, with *c.* 10-15% each of volcanic glass and clay. Traces of diatoms, sponge spicules and foraminifers are also present. Bedding is poorly preserved, although wispy and weak parallel lamination is visible in places. A low degree of burrowing and bioturbation is evident throughout much of this interval. Molluscs occur at several levels, while a single granite clast is present at 45.54 mbsf. Poorly sorted sandy mudstone is present below 48.14 mbsf. It has the same colour as the sandstone, and its patterns of brecciation and burrowing are similar to those seen in the sandstone, with which it has a gradational relationship. Individual beds of clayey siltstones, with slight to moderate bioturbation, and moderately sorted siltstone also occur here. Gravel concentrations, washed during drilling, occur at two intervals, and include granite and possibly volcaniclastic sandstone. A sharp contact with the underlying unit is evident.

Interpretation. Shallow-marine conditions are suggested from the preservation of marine flora and fauna, and by indications of bioturbation. Although the precise mode of emplacement of the sand and sandy mud is unclear, gravity flows are a likely explanation. The volcanic material, which may have originated as airfall, was probably reworked by currents. Although direct indications of glacial supply are absent in this interval (except for a few isolated clasts near the top and bottom of the unit), sedimentation rates appear to have been high.

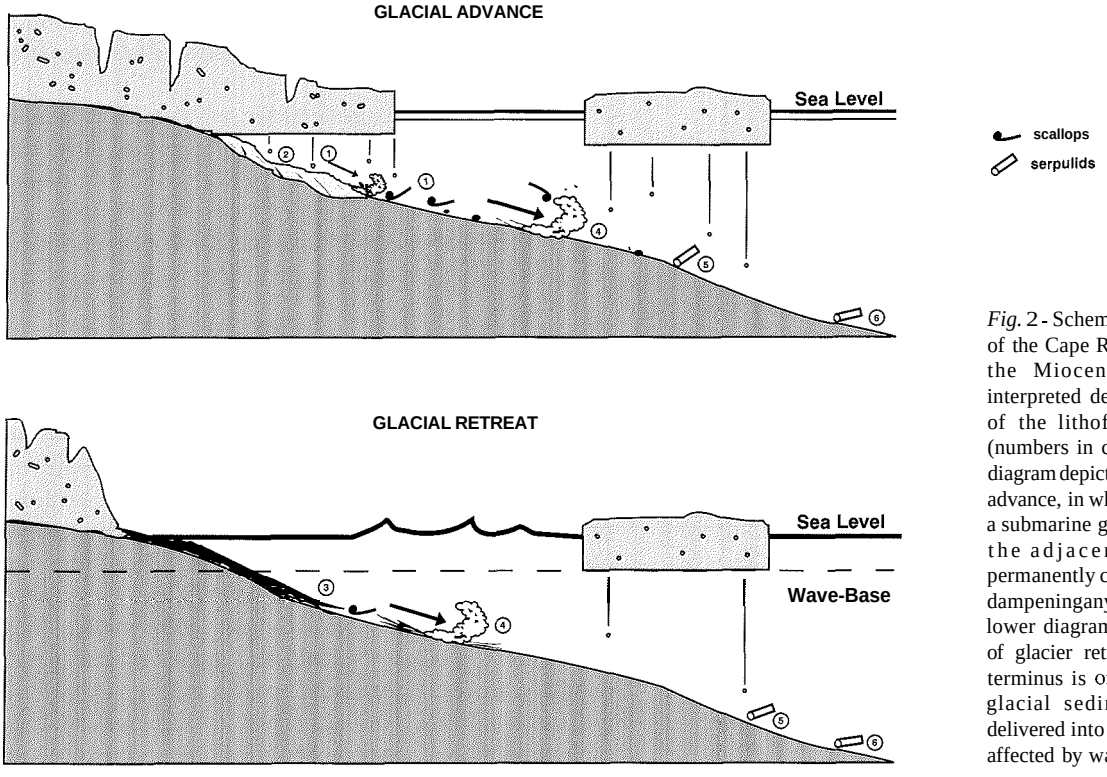

Fig. 2 - Schematic cross-sections of the Cape Roberts area during the Miocene, showing the interpreted depositional context of the lithofacies recognised (numbers in circles). The upper diagram depicts a period of glacier advance, in which the glacier has a submarine grounding line, and the adjacent sea is semi-permanently covered by ice, thus dampening any wave activity. The lower diagram depicts a period, of glacier retreat, such that its terminus is onland, and fluvio-glacial sediments are being delivered into a shallow sea more affected by wave activity.

Lithostratigraphic Unit 5.2 (53.70-61.46 mbsf), Interbedded Siltstone, Diamictite and Breccia

Description. Lithostratigraphic Unit 5.2 has poorly sorted siltstone as its dominant lithology, but the siltstone is interbedded with thin beds of diamictite and sandstone, all of which are lithified but appear to be uncemented. The siltstone is olive black (5Y 2/1) and medium bedded. A few unidentified macrofossils and diatoms are present, and bioturbation occurs at various levels. Grain composition includes quartz (dominant), feldspar and minor rock fragments. Massive muddy sandstone, fine-grained and medium-grained sandstone, sandy clast-rich diamictite, and silty claystone intraformational breccia form sharply defined beds within this unit. A unit of laminated sandstone with outsize clasts is present at 55.21-55.51 mbsf. Excluding the breccias, gravel-sized clasts vary in abundance throughout the unit, from less than 1% to as much as 20% in the diamictites. The largest clast is boulder size (dolerite), measuring 30 cm along the core; it appears to have disrupted the laminae beneath. Other clasts are composed of very fine-grained sandstones. The lower boundary was not recovered.

Interpretation. The diamictites were probably deposited from a neighbouring ice margin. The laminites resemble those formed in modern tidewater glacier settings, and it is tentatively suggested that they are analogous to tidal rhythmites (or "cyclopels", *cf.* Mackiewicz et al., 1984). If so, they would have formed close to a glacial cliff. The unit as a whole probably represents sedimentation in a proximal glaciomarine setting, probably via gravity-flow processes, with a variable input of ice-rafted debris. Alternatively, the facies represented in lithostratigraphic Unit 5.2 may have been deposited by a variety of subaqueous currents, ranging from dilute currents to density currents, with additional material contributed by settling of ice-rafted dropstones and suspended load.

Lithostratigraphic Unit 5.3 (61.46-63.30 mbsf), Diamictite

Description. Lithostratigraphic Unit 5.3 is an olive black (5Y 2/1), clast-rich to clast-poor sandy diamictite. This interval is lithified but appears not to be cemented. The diamictite is thickly bedded and fossil-bearing (including bivalve shell fragments). Clast percentages range from 1 to 60% (hence the sediment is locally a muddy sandy breccio-conglomerate), although mostly they are less than 5%, and include granules to medium pebbles of subrounded and subangular shape. Clast lithologies are varied and include: dolerite, granite, mudstone, and possibly other volcanic rocks and organic fragments. On average, the matrix comprises *c.* 35% quartz, *c.* 15% feldspar, *c.* 15% volcanic rock fragments, *c.* 10% volcanic glass and *c.* 20% clay. Shell fragments occur at two levels. The lower contact is sharp.

Interpretation. Shallow-marine conditions are indicated by the biogenic material, but the dominant processes were probably iceberg-rafting and deposition from suspension close to the ice margin.

Lithostratigraphic Unit 5.4 (63.20-70.28 mbsf), Sandstone

Description. Lithostratigraphic Unit 5.4 is a poorly sorted silty sandstone, ranging from olive black (5Y 2/1) to olive grey (5Y 4/1). This interval is lithified but appears not to be cemented. The rock varies from structureless to stratified and parallel-laminated. Other sedimentary structures include cross-lamination and soft-sediment deformation features; also, the stratification is inclined, in places at up to 20°. Fining-upward intervals are evident between 66.30 and 66.90 mbsf. A few clasts are present towards the base of the unit. Other lithologies include silty claystone with diatoms (67.40-67.71 mbsf), and intraformational sandstone breccias at 69.20-69.35 mbsf and 69.35-69.57 mbsf.

Interpretation. A shallow-marine environment dominated by gravity-flow sedimentation is suggested, but with current-induced sedimentation for the laminated and cross-laminated intervals. Few direct indications of glaciers are present, except for lonestones (ice-rafted) near the base of this unit. However, in view of the high sedimentation rates evident, it is conceivable that gravity-flow sediments were supplied by glacial streams, perhaps *via* a delta.

Lithostratigraphic Unit 5.5 (70.28-78.85 mbsf), Sandstone and Claystone

Description. Lithostratigraphic Unit 5.5 is an olive-black (5Y 2/1), poorly sorted fine-grained sandstone. The sediment is lithified to soft, and appears not to be cemented. This unit varies from laminated to massive, and shows a few signs of soft-sediment deformation and bioturbation. Below 75 mbsf, the sandstone grades into silty claystone. Clasts are dispersed through the middle part of this unit, but do not exceed small pebble size. Their shapes range from very angular to subrounded, and clast lithologies include dolerite, basalt and volcanic glass. The base of the unit is sharp.

Interpretation. Shallow-marine sedimentation, similar to lithostratigraphic Unit 5.4, but with a greater influence of iceberg sedimentation, except towards the base where lonestones are absent and silty claystone is the dominant facies. This finer-grained facies may have been formed by deposition of suspended sediment, derived from a glacier.

Lithostratigraphic Unit 5.6 (78.85-81.16 mbsf), Diamictite, Sandstone and Siltstone

Description. Clast-rich sandy diamictite and fine- to very fine-grained sandstone are the main lithologies in lithostratigraphic Unit 5.6, with an intraformational fine-grained sandstone breccia at 79.54-79.75 mbsf. Olive-black (5Y 2/1) is the dominant colour. The rocks are lithified, but appear to be uncemented. There is evidence of bioturbation and soft-sediment deformation. The diamictite is medium bedded, and grades up into small pebble/granule conglomerate beds near the top of the unit. Diffuse sandstone laminae occur at two levels. Clasts include cobbles of granite, pebbles of fine-grained dolerite

and granules of quartz. The fine-grained sandstone below 79.24 mbsf has wispy lamination in part, but is mostly massive. The base of the unit is sharp.

Interpretation. Shallow-marine sedimentation, influenced by fluctuating balance between gravity flow input and iceberg-rafting, is envisaged. The conglomerate bed may represent a lag deposit, resulting from reworking by bottom currents.

Lithostratigraphic Unit **5.7 (81.16-92.19** mbsf), Siltstone and Sandstone

Description. Poorly sorted siltstone and silty very fine/fine-grained sandstone, ranging from olive-black (5Y 411) to grey-green (5Y 2/1), are the dominant lithologies in lithostratigraphic Unit 5.7. The sediment is lithified, but appears to be uncemented. Although parts of the core are massive, the bulk of the unit is medium-bedded. Repeated fining-upward beds are present, especially below 90.89 mbsf. Minor lithologies include intraformational breccia and moderately sorted medium- and coarse-grained sandstone. The breccia comprises clasts and matrix of the same material as the host rock. The clasts range from rounded to angular. Post-depositional brecciation is superimposed upon the intraformational brecciation, and distinguishing the two types is problematic in places. Scattered through the unit are exotic clasts of pebble and granule size, including dolerite and granite. Rare bivalve shells also occur. The base of the unit is sharp.

Interpretation. The dominant processes identified in this unit are gravity flows which produced the fining-upward sandy/muddy and brecciated intervals, probably associated with unstable slopes in shallow-marine waters. Sedimentation was sporadic, but rapid when it occurred. Alternating periods of iceberg-rafting and ice-free conditions are indicated by the distribution of exotic clasts.

Lithostratigraphic Unit **5.8 (92.19-103.41** mbsf), **Mudstone**

Description. Unit 5.8 comprises poorly sorted siltstone and mudstone with scattered pebbles. The core is lithified, but appears to be uncemented. Bedding is mainly overprinted, the sediment being mottled and obviously bioturbated in places. Sandstone laminae and thin beds a few centimetres thick, some of which are black, occur sporadically throughout the unit. Some sandstone intervals have sharp contacts with the bounding mudstone intervals, although commonly these contacts have been affected by soft-sediment deformation. Other sandstone beds have gradational boundaries. A few fining-upward sandstone beds are present. Bivalve fragments occur at several levels. Clasts are angular to subrounded, and are mostly of granule and pebble size, although the largest has a downcore dimension of 5 cm. Lithologies represented are granite, dolerite, black fine-grained volcanic rock and quartz. The lower contact of the unit is sharp.

Interpretation. This unit appears to be dominated by gravity flow deposits comprising fining-upward sandy/muddy intervals, which probably were generated on unstable slopes in a shallow-nunine setting. Bioturbation of the sediment, however, may have destroyed evidence of other processes. Ice-rafting, indicated by the distribution of exotic clasts, was an ongoing process throughout the deposition of this unit, probably in a proximal/distal glacimarine setting. The increasing number of clasts up the unit may indicate that a glacier became increasingly proximal to the depositional site through time.

Lithostratigraphic Unit **6.1 (103.41-108.76** mbsf), **Diamictite**

Description. Lithostratigraphic Unit 6.1 is an olive-black (5Y 2/1), clast-poor sandy diamictite. The rock is lithified, but appears to be uncemented. This unit is mainly massive, although laminae and thin, sharply defined beds of silty fine to coarse sandstone occur at some levels. Exotic-clast percentages range from 2 to 10%. Clasts are angular to rounded and include granite, dolerite, basalt, and black volcanic rocks; there are also mudstone intraclasts. A single diamictite clast is also present. The largest clast, of granite, measures 7 cm. Some clasts are coated with silt. The unit has a sharp base.

Interpretation. Iceberg sedimentation, with near-continuous rain-out, is thought to have been the dominant process responsible for forming this unit, probably in a shallow-marine setting. The shape of the clasts indicates both supraglacial transport (angular clasts) and transport at the bed of a glacier before being deposited in the sea. Alternatively, the supply of diamictite could be linked to a nearby grounding-line position of the ice-mass. The sandstone intervals without clasts indicate short periods without significant iceberg activity.

Lithostratigraphic Unit **6.2 (108.76-119.28** mbsf), Sandstone

Description. Poorly to moderately sorted, olive-black (5Y 2/1), fine- to medium-grained sandstone is the dominant lithology in lithostratigraphic Unit 6.2. The sediment is lithified, but appears to be uncemented. The sandstone varies from medium-bedded to laminated (both mainly inclined), and shows signs of soft-sediment deformation and bioturbation, especially below 115 mbsf. Several fining-upward beds occur, but the majority of beds appear uniform, sharply bounded and inclined. Minor lithologies include thin beds of clayey siltstone, silty claystone, coarse-grained sandstone, intraformational breccia, diamictite and weakly developed laminites; the latter occur as laminated fine sandstone intervals between 109 and 110 mbsf. The diamictite (115.12-115.82 mbsf) ranges from clast-poor to clast-rich (<1 to 50% clasts) and includes thin beds of sandstone with dispersed clasts. Clasts are distributed discontinuously through the unit, but they become more common downwards. Their shape ranges from angular to subrounded. Clast lithologies include granite, dolerite, basalt and volcanic glass. The base of the unit is sharp, but irregular.

Interpretation. Slope-related shallow-marine sedimentation, with sporadic gravity flows indicated by

fining-upward cycles, are envisaged, but with an influence of iceberg sedimentation, especially towards the base. The diamictite suggests ice-proximal conditions, with some winnowing by bottom currents, as indicated by concentrations of pebble clasts. The laminated sandstones may be cyclopels. The facies association in this unit is consistent with the development of a grounding-line fan, the better-sorted sedirnents being suggestive of subaquatic subglacial discharge of meltwater.

Lithostratigraphic Unit 6.3 (119.28-141.60mbsf), Diamictite

Description. Lithostratigraphic Unit 6.3 is a sequence of clast-poor to clast-rich, olive-black (5Y 211) muddy diamictite. The rock is lithified, but appears to be uncemented. This unit is uniformly massive for thicknesses of several metres, although laminae, thin deformed beds, lenses and wispy partings of claystone, siltstone and sandstone occur at some levels. At 133.57-133.77 mbsf a prominent clastic dyke extends from a siltstone horizon below. Clast percentages range from <1 to *c.* 26%. Clasts are angular to well-rounded and include granite, dolerite, other volcanic rocks and lesser proportions of soft sediment (diamictite, fossiliferous siltstone, sandstone, siltstone and mudstone) clasts. Fossil fragments occur rarely. The unit has a sharp base.

Interpretation. Iceberg sedimentation, with continuous rain-out close to the ice margin, is believed to dominate the unit, although minor reworking events, associated with occasional cessation of ice-rafted debris input, are indicated by the finer-grained clastic sediment layers. Disturbance of the sediment, including redeposition, is indicated by the presence of soft-sediment deformation features. Alternatively, the supply of diamictite could be linked to a nearby grounding-line position of an ice-mass. There are few sedimentary indicators of water depth.

Lithostratigraphic Unit 7.1 (141.60-147.69 mbsf), Claystone

Description. Lithostratigraphic Unit 7.1 comprises poorly sorted, olive-grey (5Y 4/1) silty claystone and clayey siltstone. The sediment is lithified, but appears to be uncemented. The claystone is finely laminated in part but, visually, lamination appears to have been weakened by bioturbation. More extensive lamination does remain visible in x-ray images. A thin bed of clast-poor muddy diamictite occurs at the top of the unit, while layers and lenses of fine-grained sandstone, including bioturbated fine-grained sandstone, and intraformational breccia occur towards the base. Clasts are sparsely scattered through the unit, and are dominated by small pebbles and granules of dolerite and granite. Mineral-filled vertical fractures occur at 142.20 mbsf.

Interpretation. Deposition in quiet water is suggested by the laminated horizons, which probably formed by fine-fraction settling from suspension with little reworking by ambient currents or gravity flows (*i.*e., distal turbidites). Exotic clasts indicate episodic glacial influence.

SEQUENCE STRATIGRAPHIC INTERPRETATION

A preliminary sequence stratigraphic model is proposed here to account for the cyclical arrangement of lithofacies noted above (Fig. 3). It is based on the premise that changes in grain-size reflect changes in depositional enemy, and hence relative water depth in a general sense.

The presence of several cycles or "sequences" within the cored Miocene section suggests a condensed succession representing several discrete intervals, each bounded by hiatuses, consistent with the location of the CRP-1 borehole close to the western margin of the West Antarctic Rift. Given the total thickness of the cored Miocene section and palaeontological data, an estimate of 23 m/my sedimentation rate has been made, which is slow within the context of extensional sedimentary basins. Since short-term sedimentation rates in glacially-influenced depositional systems can be very high (metres per year), it is likely that substantial amounts of time are recorded by hiatal surfaces within the core.

A number of abrupt upward increases in sediment calibre occur through the cored Miocene section, most hut not all are at the base of diamictite intervals (Fig. 3). If the interpretation of diamictites as glacimarine deposits is accepted, then this together with the abrupt grain-size increase suggests a significant facies dislocation at the base of diamictite bodies. It is suggested that these abrupt contacts are sequence boundaries (Regressive Surfaces of Erosion), recording a drop in relative sea-level associated with a cycle of glacier advance and retreat across the area. Furthermore, the core records clear fining-upward trends at the top of almost all diamictite units, which can be interpreted in terms of a progressive rise in relative sea-level following a glacial advance cycle. The core can thus be divided into sequences, the basal boundary of each of which lies at the base of a diamictite (or another coarse-grained facies in two cases), which then fines upward into sandstones and siltstones. The upper parts of some sequences show a degree of coarsening-upward, and the topmost parts of a few sequences show accumulations of discrete, sharp-bounded Facies 3-5 beds, reflecting progradation on a minor scale. Significantly, however, no evidence of substantial progradation (large-scale coarsening-upward sequences) is recorded within the core.

If the diamictite units or their positional equivalents are interpreted as recording a cycle of glacial advance and retreat, then the question arises as to whether the diamictites and equivalents record only the glacial retreat or both advance and retreat. The observation that sequence boundaries are preceded by very little if any evidence of progradation argues against the latter, suggesting rather that much of the record of glacial advance has been removed by erosion. Since there is no evidence in the core for wave activity or other high-energy physical processes, nor evidence for subaerial exposure of surfaces, it is suggested that in each cycle the advance of grounded ice across the area of the drillsite was responsible for the removal of progradational deposits. This idea is supported by the presence of common intraformational clasts within the core.

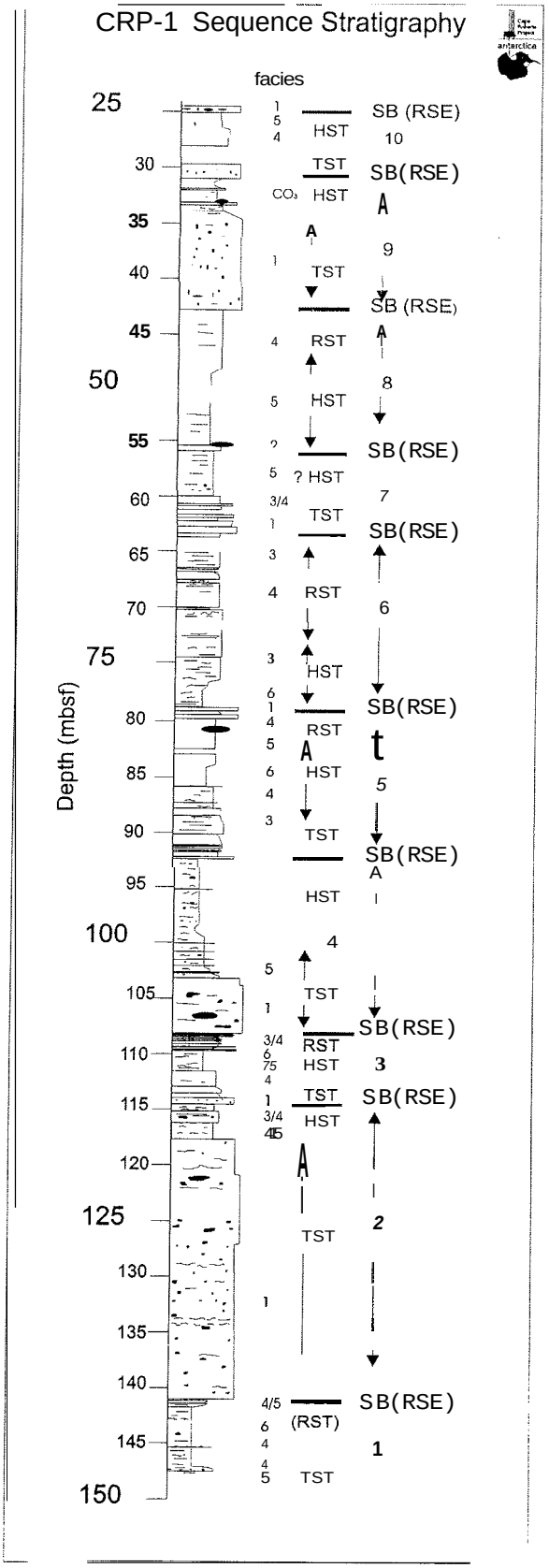

Fig. 3 - Graphic sedimentological log of the CRP-1 core, showing the distribution of Facies 1-6, and the division of the succession into sequences based on the recognition of sequences boundaries at abrupt facies dislocations. SB - Sequence Boundary, RSE - Regressive Surface of Erosion, TST - Transgressive Systems Tract, HST - Highstand Systems Tract, RST - Regressive Systems tract.

Figure 3 illustrates the proposed division of the cored succession into sequences. Even though successive sequences may preserve slightly different combinations of facies, there is nonetheless a consistency in the facies composition **of** sequences as described above. Thus, diamictite units (Facies 1) or their positional equivalents (Facies 2/3) arc interpreted as late lowstand to early transgressive systems tract deposits, sandstones of Facies 3 and 4 as recording transgressive systems tracts, and the fine-grained facies (5 and 6) the highstand systems tract. Some minor regressive systems tract deposits may be preserved below sequence boundaries. A significant implication of this interpretation is that few if any lowstand systems tract deposits are recorded at this locality, but that such facies might logically be expected to be preserved elsewhere (perhaps in areas where clinoforms have been recorded on seismic surveys). Channel features of the order of 10's of m deep and up to 1 km wide also noted on seismic reflection lines may record the passage of grounded glaciers across the sea floor at certain times.

The sequences recorded in the CRP-1 core show characteristics that are different from sequences developed on non-glaciated continental margins. In the latter, the progradational record (highstand systems tract) is well represented, and often accounts for a substantial proportion of the sequence thickness, whereas in CRP-1 this section is evidently truncated by erosion. Furthermore, sequences in non-glaciated shallow-marine environments typically show a transgressive record that is truncated by shoreface erosion, whereas CRP-1 shows transgressive deposits that are uninterrupted by significant erosion. This is interpreted to reflect the inability of waves and associated currents to effectively mobilise sediment on the sea floor in the presence of floating ice.

If correct, this analysis suggests that in settings proximal to the continental edge such as the Cape Roberts drilling sites, deposits recording progradation and advance of glaciers are likely to be removed by erosion, and that significant periods of time may therefore be recorded in the sequence boundaries recognised at the base of diamictite and other lithofacies.

SEDIMENTOLOGY

INTRODUCTION

Further to the visual description of the working half of the core, the Miocene section, below approximately 45 mbsf, was described in detail using a number of specific techniques. The use of a variety of different analyses assists in furthering our understanding of the facies and therefore depositional environment during the Miocene. After visual description, and core logging, the working half of the core was X-rayed. This enabled the observations on any internal structure, sediment fabrics and lonestones to be taken. Details of the X-radiography on specific intervals are given below. Analysis of clast fabric and shape was conducted on certain, individual sections, thereby giving a more detailed account of the depositional environment.

X-RADIOGRAPHY AND SEDIMENTOLOGICAL FEATURES

X-radiographic images of the half-cores were obtained using a Torrex 120-D x-radiographic machine that can produce real-time video imagery as each 1-m-long section of core is passed through the machine. The imagery of the split working half of the core was recorded on S-VHS (NTSC system) video tapes before any sampling had taken place. Settings of x-ray intensity used for exposing the Miocene section were mostly at 3 mA and 85 kV for upper internal sands and 3 or 4 mA and 90 to 95 kV for diamictites and the sections in the lower 50 m of core, which were more lithified. We found that the sharpness of the image increased at higher mA settings and the higher voltage was needed for penetrating diamictites and more lithified internals. Another aspect to note was that granitic clasts had an attenuation similar in character to that of the matrix of the diamictites. Commonly, those clasts could be distinguished based mainly on the increased attenuation of the X-rays by their mafic minerals.

The Miocene section is more lithified than the Quaternary section, and consequently longer internals could be X-radiographed. However, because most of the cored sediment remains uncemented, some long sections were still too soft to X-radiograph without the core being in a core liner. Furthermore, approximately the upper 10 m (down to below 60 mbsf,) of this internal of the core is brecciated and consequently is also very difficult to X-ray without being in a core liner. The total thickness of sediment of Miocene age X-rayed was 44.74 mbsf (c. 45 % of the total Miocene section). A list of the x-radiographed internals is presented in table 2. Significant features that were noted in these internals include:

1. In general, most of the internals of the mudstone, siltstone and claystone are internally structureless in visual appearance as well as in X-radiography (there are numerous internals but, *e.g.* 58.80 to 58.93 mbsf; Fig. 4a). This characteristic can be used to indicate several points about the nature of sedimentation and post-depositional processes:
   either
   a) the sediment has been heavily bioturbated. The X-radiography, however, shows very little evidence of bioturbation in the sediment. Some sections of the cores do exhibit bioturbation (e.g., 145.70 mbsf; Fig. 4b), but those sections appear to be rare. The apparent lack of bioturbation may be due either to (i) a very uniform original lithology in which there is no density contrast to selectively impede the X-rays even if it is bioturbated, or (ii) to the fact that the sediment has not been bioturbated. The latter interpretation is preferred because the sediments do not show visual evidence of heavy bioturbation;

   or

   b) the sediment was deposited very rapidly from suspension without significant sorting and reworking processes. Furthermore, consistent particle-size distributions appear to have been introduced in suspension into the environment over the period when these internals were deposited.

   Given (a) and (b), very rapid sedimentation appears to have produced the many structureless units.
2. Some intervals of the fine-grained units do show stratification on X-radiographs that cannot be seen visually (*e.g.*, 119.30 mbsf; Fig. 4c). The stratification occurs as a range from thin laminae to thin beds, and locally shows evidence of soft-sediment deformation. The observation of this stratification shows that it is possible to detect stratification in the fine-grained units using this x-radiographic technique in these cores and thus the apparent structureless appearance in X-radiographs of many other internals in the core is probably real. It also indicates either that sedimentation rates were high enough to inhibit infaunal burrowing, or that other physical/chemical environmental factors were not conducive to benthic life.
3. Diamictites in the Miocene part of the section appear to have fewer clasts than those in the Quaternary part of the section. Most of the diamictites are structureless (many occurrences with a good example between 62.58 to 62.82 mbsf; Fig. 4d). Most commonly the clasts (granule and coarser sizes) do not appear to show any preferred orientation in the vertical section. Clast proportions often vary down the cores over 10s of centimetres so that their name changes from clast-poor to clast-rich, by definition (e.g., interval 104.81 to 105.25 mbsf,). This appearance indicates that if the diamictites are glacial, they were mostly likely formed either by rainout from under a floating glacier-tongue or short ice shelf (waterlain till) or by deposition in a zone of intense iceberg rafting where there was relatively lower input from glacifluvial discharges. An alternative origin may be non-glacial or indirectly glacial, where the diamictites originate from subaqueous debris flows.
4. Where structures occur in the diamictites they are of discrete laminae of very fine sandstone, siltstone or claystone, commonly exhibiting sharp contacts and soft sediment deformation (e.g., interval 128.00 to 130.00 mbsf; Fig. 4e). Preferred clast orientation in the vertical plane occasionally occurs in these intervals (107.50 mbsf; Fig. 4f), and these are the only places in the core where clast orientation is seen. The apparent long axes of the clasts lie parallel in planes that commonly dip steeply or appear to delineate limbs of folds. These features, soft-sediment deformation, presence of clast orientation and the geometry of the clast orientation, combine to indicate that these types of diamictites probably were deposited originally on a slope by debris flows. This deposition was probably very rapid because the sediments still had a high water content when they experienced soft-sediment deformation. They are likely to have been stacked in pulses and interstratified with minor sorted sediment pulses, following which the pile experienced minor creep down slope sediment to further deform the mass. Apparent amalgamated contacts (122.20 mbsf; Fig. 4g), and other contacts that are sharp but show soft sediment deformation between a diamictite and another unit (124.10 mbsf; Fig. 4h), further support this interpretation.

Tab. 2 Miocene age x-radiography intervals, with sedimentological features.

Box	Interval	Lithology	Box	Interval	Lithology	Box	Interval	Lithology
11	55.57-55.69	Thinly bedded muddy fine sdst.	11	58.23-58.32	siltstone laminae	12	58.80-58.95	coarse siltstone and mud clasts
12	59.18-59.37	Laminated siltstone, bioturbated x2 clasts	12	60.66-60.75	Medium sdst, intraformational clast	12	61.65-61.78*	Medium sdst with clast
13	62.58-62.82	Muddy sdst diamict	13	62.82-63.15	Diamictite	14	67.00-67.27	Silty fine sdst
14	67.44-67.57	Silty fine siltstone	14	67.60-67.68	Silty claystone with diatoms	15	70.03-70.10	Thinly bedded olive grey siltstone
15	70.24-70.35	Thinly bedded siltstone/sdst contact	16	74.13-74.60	Silty fine sdst	16	74.99-75.59	Silty bioturbated sdst
17	77.59-77.72	Silty claystone	17	78.92-79.18	Clast rich sandy diamictites	17	79.53-79.72*	Silty fine sdst with clasts and laminae
18	81.51-82.15	Massive siltstone	19	85.36-85.65	Massive clayey siltstone	19	85.80-86.68*	Silty fine sdst
20	86.93-87.26*	Poorly sorted siltstones	20	90.19-90.27	Coarse sdst	21	90.64-90.80	Graded sdst
21	92.00-92.43	Graded sdst	21	93.16-93.47	Clayey siltstone	22	94.19-94.34	Mudstone
22	94.50-94.66	Mudstone	22	95.30-95.72	Massive siltstone	22	95.83-95.99	Massive siltstone with silt laminae
22	96.32-97.02*	Diamictite	23	97.47-98.02	Fine sdst	23	98.07-98.65	Fine sdst
23	99.37-99.91	Fine sdst	24	100.02-100.50	Bioturbated clayey siltstone	24	100.60-100.90	Bioturbated clayey siltstone
24	101.69-102.10	Bioturbated clayey siltstone	24	102.18-102.58	Bioturbatedclayey siltstone	24	102.69-102.88	Bioturbated clayey siltstone - with clastic layers
25	103.34-104.37*	Diamictite	25	104.81-105.29	Diamictite	25	105.42-106.13	Diamictite
26	106.28-106.44	Diamictitewith scattered sand layers	26	106.59-	Diamictite	26	107.43-107.72	Diamictite
26	107.80-108.47	Diamictite	26	108.56-108.89	Diamictite	26	109.02-109.13	sdst with microfaults
27	109.13-109.59	sdst with microfaults	27	109.71-110.26*	sdst	27	110.31-110.51*	sdst
27	109.94-111.75	Sdst	28	112.16-113.16	sdst	28	113.16-114.16	Diamictite
28	114.74-114.91	Diamictite	29	115.22-116.22	sdst	29	116.42-116.53	Sandy silt
29	116.96-117.04	Sandy silts	29	117.72-118.13	Silty sdst	30	118.45-118.56	Diamictite
30	119.08-119.15	Diamictite	30	199.22-119.43	Diamictite	30	119.69-119.86	Diamictite
30	120.07-120.28	Diamictite	31	121.30-122.30	Diamictite	31	122.30-123.30	Diamictite
31	123.30-124.17*	Diamictite	32	124.17-124.41	Muddy diamictite	32	124.52-124.78	Muddy diamictite
32	124.85-125.17	Muddy diamictite	32	125.17-126.04	Muddy diamictite	32	126.17-127.09	Muddy diamictite
33	127.09-127.62	Poorly sorted diamictite	33	127.62-128.09	Poorly sorted diamictite	33	128.09-128.18	Poorly sorted diamictite
33	128.25-129.09	Poorly sorted diamictite	33	129.09-129.30	Poorly sorted diamictite	33	129.44-130.09	Poorly sorted diamicitite
34	130.09-131.09	Clast poor muddy diamictite	34	131.09-132.09	Clast poor muddy diamictite	34	132.09-133.09	Clast poor muddy diamictite
35	133.09-134.09	Clast poor muddy diamictite	35	134.09-134.86	Clast poor muddy diamictite	35	135.09-135.33	Clast poor muddy diamictite
35	135.60-136.07	Clast poor muddy diamictite	35	138.73-139.22	Clast poor muddy diamictite	36	139.22-140.22	Diamictite
36	141.28-141.82	Silt sand laminae	36	142.02-142.35	Diamictite	38	142.52-142.65	Laminated claystone
38	143.25-143.65	Claystone	38	143.65-144.65	Silty claystone	38	144.65-144.87	Silty claystone
38	145.02-145.59	Silty claystone	39	145.59-146.59	Silty claystone	39	146.59-147.69	Silty claystone

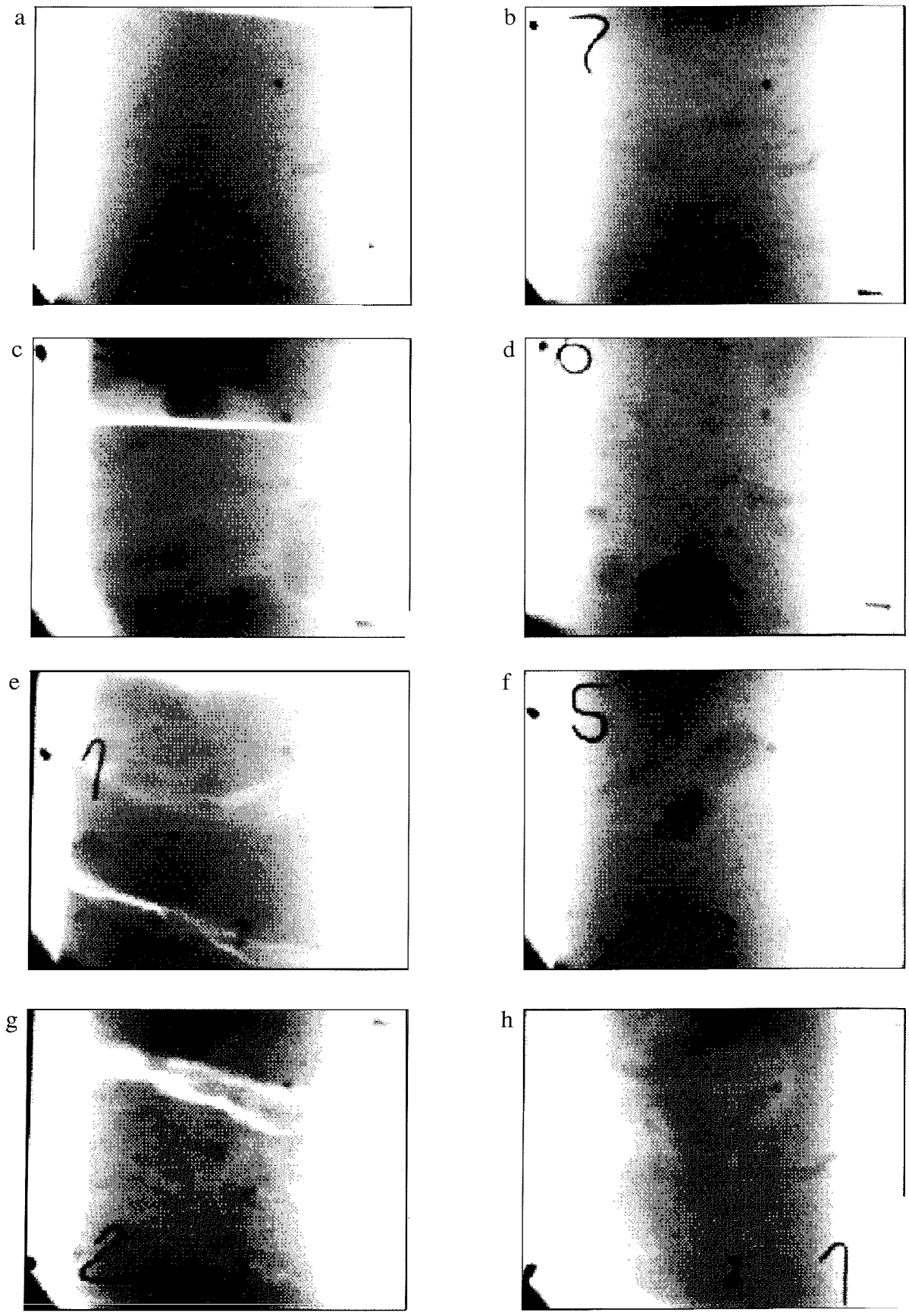

Fig. 4 - Eight X-radiographs from the Miocene interval where scale is shown as 5 cm of depth between the tick marks on the left and right side of the image. The first image (a) is of the siltstone at 20.70 mbsf showing it is internally structureless. A claystone with faint bioturbation (b) is from 145.70 mbsf; a sandy mudstone with dispersed clasts (c; from 119.30 mbsf) shows internal stratification on the X-radiograph that is not visible on the split core surface; a structureless diamictite (*d*) from 62.60 mbsf; a deformed sandstone layer (*e*; just by the "1" in the image) with sharp contacts within a diamictite interval from 128.10 mbsf; local preferred clast orientation in a diamictite (*f*) from 107.50 mbsf; an amalgamated contact between two diamictite beds (g) from 122.20 mbsf; and a highly deformed contact (*h*) between siltstone above and diamictite below at 124.10 mbsf (in this image it is difficult to see but the contact winds between the bottom left and the top right).

CLAST VARIABILITY

The proportion of area covered by clasts on the cut face of the working half of the core, as expressed as clast percentage, is presented in Quaternary Strata, figure 3, section on Clast Variability (this volume) plotted against the lithostratigraphic log. These percentages are strongly influenced by the size of individual clasts, and that problem is partly addressed by presenting simple number counts of clasts in the 4-m-log (Appendix 2). Variations in clast percentages are often used as an indicator of proximity to a glacier, and in CRP-l, there is a strong correlation between high-clast percentages and the occurrence of diamict. However, individual diamict units contain different clast proportions. For example, the diamictite of Unit 6.3 has a mean-clast concentration of about 10% whereas the diamicton of Unit 4.1 has a mean-clast concentration of greater than 20%. Furthermore, the proportions of clasts vary greatly within individual diamict units, often between 1% and 100%; the latter number indicates clasts larger than the core diameter.

CLAST FABRIC

Two-dimensional clast-fabric analyses were made on horizontal surfaces of core taken from four levels within diamictites in the Miocene section, namely in lithostratigraphic Units 5.3, 6.1 and 6.3 (Fig. 5). Relatively clast-rich intact samples were taken, and the orientation of the long-axes of 50 coarse sand grains and gravel (where the a/b axial ratio was greater than 2) were recorded in relation to the cut surface down the middle of the core, using a binocular microscope. Data were plotted on rose diagrams grouped into 30° sectors. Although a less powerful technique than three-dimensional analysis, two-dimensional fabrics have proved useful, along with other evidence, in discriminating basal till(ite)s from waterlain till(ite)s and gravity-flow deposits, especially when the Chi^2 test was used, for example in the CIROS-l core (Hambrey, 1989) and at ODP Sites 739 and 742 in Prydz Bay (Hambrey et al., 1991).

The highest level analysed was 62.64 mbsf (lithostratigraphic Unit 5.3). Here, a strong preferred orientation fabric was determined that is statistically significant at the 95% level. This type of fabric is typical of basal tills. The other samples, at 105.64 mbsf (lithostratigraphic Unit 6.1), 122.94 mbsf and 139.31 mbsf (both lithostratigraphic Unit 6.3), show fabric patterns that show no significant preferred orientation. These fabrics show no statistically significant preferred orientations, and are typical of waterlain tills, proximal glaciomarine sediments or gravity flows.

CLAST SHAPE

Introduction

The Miocene interval of the CRP-l core from the bottom (147.69 mbsf) up to a depth of 43.55 mbsf contains several diamictite units. Clasts are present in much of the interval, but the higher abundance in the diamictites makes these units suitable for clast-shape analysis. A total of 129 clasts were collected from three diamictite units. These were lithostratigraphic Units 6.3 (141.60-147.69 mbsf), 6.1 (103.41-108.76 mbsf) and 5.3 (61.51-63.20 mbsf). Many of these were damaged by coring or saw splitting, and only 8 (6.2%) whole clasts could be extracted. Lithology of each clast was determined. Roundness, one of the basic components of shape, was determined using the Krumbein - Powers visual roundness chart, which provided mean roundness and percentages of clasts in each of six roundness categories. Clasts were also examined for other features such as facets and for surface features such as striae. These data are summarised in figure 6.

Roundness

Roundness of clasts in each unit is presented as histograms in figure 6. These have been compared with histograms of clast roundness from sediments in a modern glacially influenced Arctic environment (Bennett & Glasser, 1996).

The lowermost diamictite, lithostratigraphic Unit 6.3, is over 22 m thick, and clasts have been divided into two populations (upper and lower) to detect any significant change in shape characteristics within the unit. The lower part of the unit (below 130.00 mbsf) shows a broad distribution consistent with that of a typical subglacially transported debris signature. The presence of a significant number (18.6%) of clasts in the rounded category suggests there is a component of reworked fluvial sediment in the deposit. This contrasts with data from the upper part of

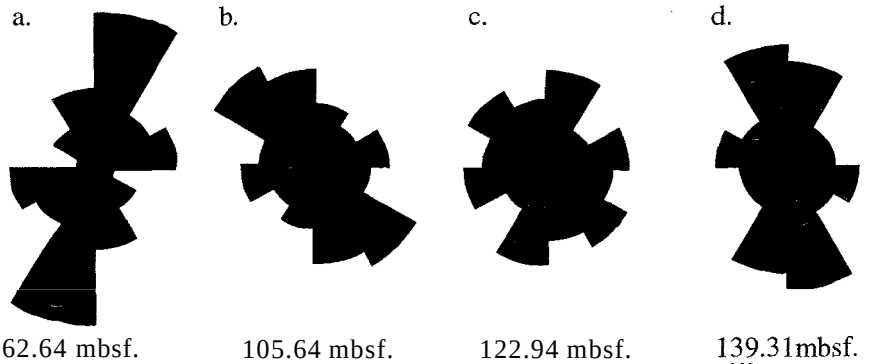

Fig. 5 - Rose diagrams illustrating two-dimensional clast fabric in the horizontal plane in diamictites from four levels, Fifty grains were measured in all cases, Chi-squared values are given to indicate the statistical validity of any preferred orientation.

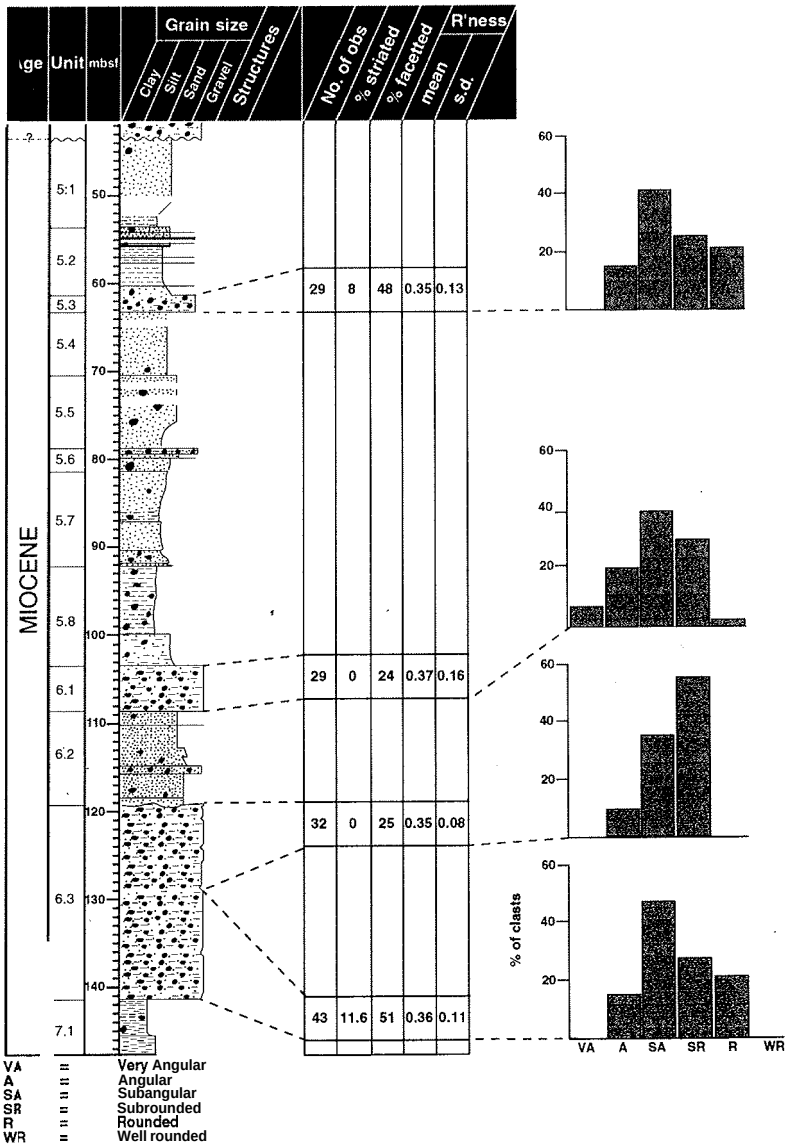

Fig. *6* - Core log of the Miocene section of the CRP-1, showing summary shape characteristics and roundness histograms.

Unit 6.3 (above 130.00 mbsf), which displays a distinct lack of rounded clasts and a peak in the sub-rounded category. While this distribution is still considered characteristic of subglacially transported sediment, the lack of rounded clasts suggests that there is no reworked, fluvial sediment component.

Likewise, the clast population from Unit 6.1 has a broad roundness distribution with a mean roundness in the subangular category and is typical of subglacially transported clasts. The presence of 24.1% of clasts in the angular and very angular categories indicates the possibility of supraglacial source debris in the deposit. Clasts in Unit 5.3 are comparable with subglacially transported clasts, again with a significant (20%) of clasts in the rounded category suggestive of reworking.

Striae, Facets and Lithology

Facetted surfaces occur on clasts in all Miocene diamictites examined, and striae were present in Units 6.3 (lower) and 5.3. As in the Quaternary section, the development of these features depends largely on clast lithology. If present, however, they provide good evidence of basal transport in a glacier. Granite and dolerite clasts are dominant (at least 72%) in all the units, with volcanic and sedimentary clasts making up the remainder. Facets were present on all lithologies, but striae are more common on sedimentary and fine-grained dolerite clasts. The basal part of Unit 6.3 has 5 (11.6%) striated clasts, with only one set visible in most cases but with one clast showing at least two sets of striae on a facet. This is in clear contrast to the upper part of Unit 6.3, which has no striated clasts. Unit 6.1 also has no striated clasts, whereas Unit 5.3 has 2 (8%) of clasts displaying striae, one of which appears to have two or three sets of striae preserved.

Summary

The shape characteristics of clasts in the Miocene section of CRP-1 suggest the clasts have experienced subglacial transport and that all units contain rounded, possibly reworked, fluvial sediment except Unit 6.3 (upper). Clasts from Unit 6.1 suggest the incorporation of some supraglacial material also. The presence of facets in all

units and striae in two units also indicates a strong glacial influence indicating that ice was either grounded or actively calving near the site, thereby introducing ice-raftcd sediment to the deposit.

PETROLOGY

INTRODUCTION

Examination of the detrital components of the Miocene strata was based mainly on selection of samples according to grain size, following procedures similar to those described in Quaternary Strata, section on Petrology (this volume), but with additional x-ray diffraction investigations to quantify a wider range of minerals present (not just clay species). Organic geochemistry of bulk samples was also used to provide information on total carbon, organic carbon, sulphur and nitrogen contents. The use of these multi-disciplinary methods was designed to provide as broad a characterization as possible of the bulk mineralogy and rock detritus contributing to the sequence, the results of which are described below.

BASEMENT CLASTS

Introduction

This section focuses on the preliminary petrographical examination of basement clasts within the Miocene strata of the CRP-1 borehole. It includes the description of all basement clasts belonging to the "pebble" and "cobble" grain-size classes (4 to 64 mm, and 64 to 256 mm, respectively), data on granules, and some inferences concerning the most likely source-rock units.

Previous drillholes (CIROS-1, MSSTS-1) on the western edge of the Victoria Land Basin provided evidence of significant and persistent influxes of basement-derived pebbles throughout most of the recovered strata. In particular, basement pebbles, including granites, granitic gneisses and biotite schists (George, 1989), were reported as forming a large proportion (35 to 80%) of the clasts in the lower Miocene strata recovered by CIROS-1 (Hambrey et al., 1989). Similar contributions were recognized in the Miocene record of the MSSTS-1 core (Barrett et al., 1986).

Methods

Sampling, macroscopic observations and preliminary petrographical analyses (polarized-light microscopy) were performed following the same procedure and sample management adopted for the Quaternary strata (see Quaternary Strata, this volume - section on Basement Clasts).

Due to the large number of pebbles suitable for preparation as thin sections, 8 clasts, representative of the principal lithological varieties, were selected. The sections were mounted in epoxy resin, uncovered and unstained.

Results

Visual estimation of the Miocene strata indicates that the basement-clast content is very variable. In particular the finer pebbles (dimensions around 1x0.5x0.5 cm), and sometimes even granules, are practically absent or in minor proportions in lithostratigraphic Units 5.1, 5.4, 5.5, 5.7, 6.2 and 7.1. In contrast, granules to coarse pebbles are abundant in lithostratigraphic Units 5.3, 5.8, and particularly in Units 6.1 and 6.3, where the basement clasts range up to to 55-60% volume (*i.e.* at 124.31-126.05 mbsf in Unit 6.3 and 104.55-108.49 mbsf in Unit 6.1).

Figure 7 shows the lithological range, distribution and position of the different rock types within the 12 lithostratigraphic units distinguished in the Miocene strata. As in the Quaternary strata, finer pebbles and granules mainly consist of two main lithologies: grey biotite granite, sharply dominant in Units 5.2, 5.3, 5.8 (lower part), 6.1, 6.2. and 6.3; pink biotite granite, prevailing in Units 5.5 and 5.8 (upper part), and mixed together with the grey variety in Unit 6.1.

For the coarser pebbles (average diameter >8 mm), a wider range of lithologies distinguish the Miocene basement clasts from those occurring in the Quaternary section. Fifty-five samples were collected and are listed in table 3. The table provides information on the stratigraphical position, clast shape and dimensions, and lithology, and

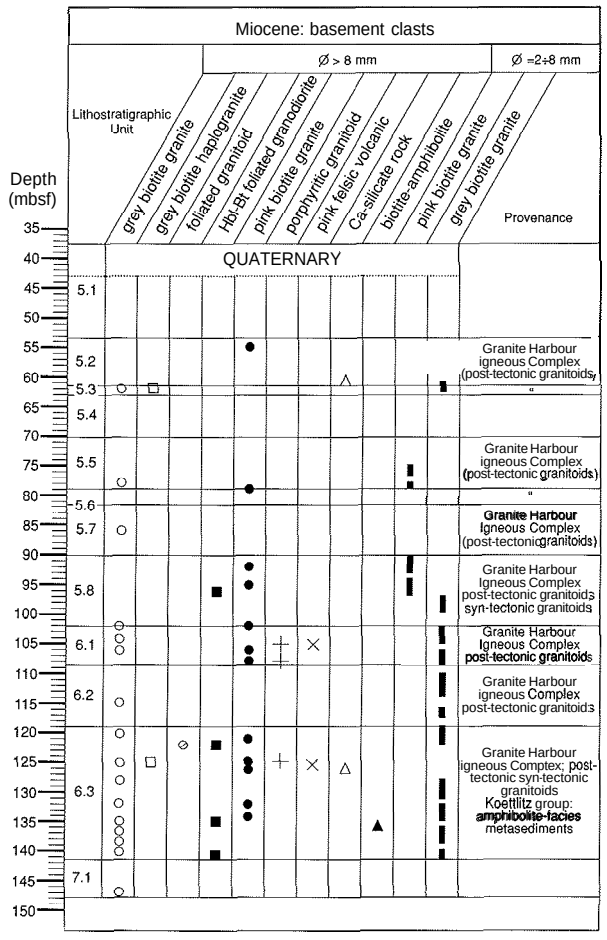

Fig. 7 - Lithology, distribution and provenance of basement clasts in the Miocene strata.

Tab. 3 - Basement clasts in the Miocene strata: list of sampled clasts and preliminary petrographical data.

Sample code	Hole	Box	Top (mbsf)	Bottom (mbsf)	Clast shape	Approximate size (cm)	Lithology	Main petrographical features	Inferred provenance	Lithostratigraphic Unit
TAL1	CRP-1	8	47.19	47.20	rounded	2x1.5x1	dolerite	very fine grained, isotropic fabric, dark greenish grey, no alteration crust	Ferrar Group	5.1
TAL2	CW-1	9	52.42	52.43	rounded	2x1x1	dolerite	very fine grained, isotropic fabric, dark greenish grey, no alteration crust	Ferrar Group	5.1
TAL3	CRP-1	11	55.54	55.55	sub-angular	1x1x1	pink biotite sycnogranitc	isotropic fabric, equigranular (medium-grained), M = 8%, feldspars: 3 to 8 mm in length,	G.H.I.C.*	5.2
TAL4	CRP-1	12	61.52	61.53	sub-angular	1x1x1	Ca-silicate rock	brick-red alkali feldspar phenocrysts dark green, isotropic fabric, fine-grained, thinly layered with a mm-thick layer rich in dark grey quartz	Kocttlitz Group	5.3
TAL5	CW-1	13	62.05	62.06	angular	0.5x1x1	pink-grey biotite monzogranite	isotropic fabric, equigranular (medium-grained),pale pink alkali feldspars: 0.5 to 4 mm in length, M = 11%	G.H.I.C.	5.3
TAL6	CRP-1	13	62.18	62.19	angular	1x1x1	grey biotite-bearing haplogranite	isotropic fabric, equigranular (fine-grained), M = 3%	G.H.I.C.	5.3
TAL7	CRP-1	13	62.38	62.39	angular	0.5x1x1	poorly sorted calcareous litharenite	angular quartz grains, and lithic fragments of quartzite, sericitized plagioclase, biotite, calcite and chlorite (diagenetic)	Unknown Tertiary (?) sedimentary sequence	5.3
TAL8	CRP-1	13	62.58	62.59	angular	1x1x1	grey biotite granite	isotropic fabric, equigranular (medium-grained), alkali feldspars: 2-5 mm in length, M = 8%. similar to TAL 27	G.H.I.C.	5.3
TAL9	CRP-1	17	78.91	78.92	angular	0.5x1x1	grey biotite-bearing granite	isotropic fabric, equigranular (medium-grained), M = 8%, altered biotite (as in TAL 18), similar to TAL 27, 18	G.H.I.C.	5.5/5.6
TAL10	CRP-1	17	79.11	79.12	angular	1x1x1	pink biotite syenogranite	isotronic fabric, equigranular (medium-grained), reddish pink alkali feldspars: 2-8 mm in length, M = 11%, similar to TAL 16	G.H.I.C.	5.6
TAL11	CRP-1	18	80.51	80.56	boulder	5x6x4	gabbroid	isotropic fabric, dark greenish grey, medium-grained equigranular, sub-ophitic intergranular structure	Ferrar Group(?) or G.H.I.C.	5.6
TAL12	CRP-1	19	86.54	86.55	angular	0.3x0.7x1	grey biotite granite	isotropic fabric, equigranular (medium-grained). M = 10%, similar to TAL 25, 27, 30	G.H.I.C.	5.7
TAL13	CRP-1	22	94.05	94.15	rounded	10x4x3	grey biotite granite	isotopic fabric, equigranular (fine-grained), M = 12%	G.H.I.C.	5.8
TAL14	CRP-1	22	96.34	96.35	angular	1.5x1x1	biotite-hornblende granodiorite	heterogranular (fine to coarse-grained), oriented fabric (weak foliation defined by hornblende and biotite), plagioclase phenocrysts: up to 8 mm in length, usually 2-3 mm (recrystallized aggregates), M = 12%, similar to TAL 36	G.H.I.C.	5.8
TAL15	CRP-1	25	103.59	103.62	angular	3x4x2	altered coarse-grained granitoid	abundant saussurrite aggregates after plagioclase (green patches), rare biotite flakes	G.H.I.C.	5.8/6.1
TAL16	CRP-1	25	103.69	103.71	sub-angular	2x1x0.5	pink-reddish biotite granite	isotropic fabric, equigranular (medium-grained), M = 12%, brick-red alkali feldspars: 2 to 8 mm in length, similar to TAL 3	G.H.I.C.	6.1
TAL17	CRP-1	25	103.91	103.93	sub-rounded	2x0.5x0.5	grey biotite granite	isotropic fabric, equigranular (medium-grained), feldspars: 1-4 mm in length, M = 10%, similar to TAL 27, 18, 25, 30	G.H.I.C.	6.1
TAL18	W - 1	25	104.06	104.08	angular	1x1x0.5	grey biotite-bearing granite	isotropic fabric, equigranular (medium-grained), feldspars: 2-4 mm in length, M = 8%, biotite transformed to chlorite, similar to TAL 27, 25, 30	G.H.I.C.	6.1
TAL19	CRF-1	25	104.13	104.17	angular	5x4x3	pink felsic volcanic rock	ryolitic composition (?), phenocrysts of feldspar, rare quartz and biotite set in a very fine-grained orange-pink groundmass	Late Paleozoic Gallipoli Volcanic Suite (?)	6.1
TAL20	CRP-1	25	104.54	104.55	angular	1x1x0.5	pink felsic volcanic rock	ryolitic composition (?), phenocrysts of feldspar, rare quartz and biotite set in a very fine-grained orange-pink groundmass, similar to TAL19	Late Paleozoic Gallipoli Volcanic Suite (?)	6.1
TAL21	CRP-1	25	104.60	104.61	sub-rounded	0.7x0.5x1	altered granite(?)	quartz-rich, isotropic fabric, green saussurrite aggregates after plagioclase	G.H.I.C.	6.1
TAL22	CRP-1	25	104.76	104.78	sub-rounded	1x3x2	dark porphyritic granitoid	sub-euhedral phenocrysts of feldspar, 3-4 mm in length, lying in an very fine grained grey groundmass, monzonitic or monzogranitic (?) in composition, similar to TAL 29 but with a higher content in biotite	G.H.I.C.	6.1
TAL23	W - 1	25	104.99	105.05	angular	6x4x3	grey biotite-bearing granite	equigranular (medium-grained), isotropic fabric, feldspars: 2 to 6 mm in length, M = 7%, similar to TAL 27	G.H.I.C.	6.1
TAL24	CRP-1	25	105.88	105.92	angular	4x3x3	pale pink biotite granite	medium/coarse-grained, isotropic fabric, feldspars: 3 to 10 mm in length, M = 12%, probable syenogranite composition, similar to TAL 10, 34	G.H.I.C.	6.1
TAL25	CRP-1	26	106.30	106.32	angular	1x0.5x0.5	grey biotite-bearing granite	isotropic fabric, equigranular (medium-grained), feldspars: 2 to 4 mm in length, M = 10%, similar to TAL 27, 30	G.H.I.C.	6.1

Note: Lithostratigraphic Unit designation follows figure 18 of Background to CRP-1 (this volume); M = colour index (percentage of mafic minerals); * Granite Harbour Igneous Complex. The list also includes a few dolerites (Jurassic Ferrar Group) and one poorly sorted litharenite of unknown age and provenance.

Tab. 3 - Continued.

Sample code	Hole	Box	Top (mbsf)	Bottom (mbsf)	Clast shape	Approximate size (cm)	Lithology	Main petrographical features	Inferred provenance	Lithostratigraphic Unit
TAL26	CRP-1	26	107.13	107.23	angular	10x6x6	yellow-grey biotitc granite	isotropic fabric, equigranular (medium/coarse-grained), yellowisch alkali feldspars: 3 to 10 mm in length, M = 11%, compositionally similar to TAL 24	G.H.I.C.	6.1
TAL27	CRP-1	26	108.10	108.13	angular	3x2x2	grey biotite granite	equigranular (medium-grained), feldspars: 2 to 5 mm in length, M = 8%	G.H.I.C.	6.1
TAL28	CRP-1	26	108.19	108.23	angular	4x2x2	pink-red biotitc-bearing syenogranite	heterogranular, isotropic fabric, pink-red alkali feldspars: 2 to 7 mm in length, M = 7%, similar to TAL 10	G.H.I.C.	6.1
TAL29	CRP-1	26	108.49	108.52	angular	3x2x3	porphyritic biotite-bearing monzogranite	feldspar phenocrysts, 2 to 5 mm in lcngth, set in a very fine-grained grey groundmass, similar to TAL 22	G.H.I.C.	6.1
TAL30	CRP-1	28	115.06	115.11	angular	5x6x4	grey biotite monzogranite	fine to medium-grained, layering due to grain-size variations, occurrence of rare small crystals of garnet, pale brown alkali feldspar, M = 10%, with mm-thick layers, compositionally similar to TAL 25, 27	G.H.I.C.	6.2
TAL31	CRP-1	29	117.04	117.07	angular	3x6x4	dolerite	fine/medium-grained, slightly foliated, rich in plagioclase and biotite	G.H.I.C.	6.2
TAL32	CRP-1	30	120.62	120.64	angular	2x1x1	grey biotite granite	isotropic fabric, equigranular (fine-grained), feldspars: 1-2 mm in lcngth, M = 8%	G.H.I.C.	6.3
TAL33	CRP-1	30	121.16	121.18	sub-rounded	2x1x0.5	grey biotite granite	equigranular (fine-grained), feldspars: up too 2 mm in length, M = 8%, similar to TAL 13, 32	G.H.I.C.	6.3
TAL34	CRP-1	31	121.65	121.67	sub-rounded	2x1x1	pink biotite granite	isotropic fabric, equigranular (medium-grained), pink alkali feldspars: 2 to 6 mm in length, M = 8%, similar to TAL 10, 24	G.H.I.C.	6.3
TAL35	CRP-1	31	121.84	121.85	sub-rounded	2x1x2	pink biotite granite	equigranular (fine-grained), isotropic fabric, feldspars: less than 1 mm in length, M = 7%, similar to TAL 13, except the alkali feldspar colour	G.H.I.C.	6.3
TAL36	CRP-1	31	122.33	122.34	angular	2x1x0.5	biotite-hornblende granodiorite	equigranular (medium/coarse-grained), mafic minerals and palgioclase: 3 to 8 mm in length, M = 10%	G.H.I.C.	6.3
TAL37	CRP-1	31	122.56	122.57	angular	1x1.5x0.5	fine-grained foliated granitoid	fine-grained, plagioclase crystals, up to 1 mm in size, set in a green micaeous matrix (chlorite or green biotite), similar to TAL 40	G.H.I.C.	6.3
TAL38	CRP-1	32	124.30	124.31	sub-angular	0.3x0.3x0.3	grey biotite monzogranite	finelmedium-grained, isotropic fabric, M = 9%, similar to TAL 55	G.H.I.C.	6.3
TAL39	CRP-1	32	124.55	124.56	angular	0.3x1x0.5	leucocratic granite	equigranular (medium-grained), isotropic fabric, M = 3%	G.H.I.C.	6.3
TAL40	CRP-1	32	124.67	124.68	sub-rounded	1x0.5x0.5	dark grey foliated granitoid	fine-grained, foliated fabric. foliation defined by biotite (partly transformed to chlorite) and wrapping feldspar crystals, 1-2 mm in size	G.H.I.C.	6.3
TAL41	CRP-1	32	124.76	124.8	rounded	6x3x4	yellowish-grey biotite haplogranite	isotropic fabric, equigranular (fine-grained), M = 5%	G.H.I.C.	6.3
TAU2	CRP-1	32	124.92	124.93	sub-rounded	1x2x1	grey biotite haplogranite	isotropic fabric, equigranular (fine-grained), M = 3%	G.H.I.C.	6.3
TAL43	CRP-1	32	125.14	125.15	sub-angular	1x0.5x1	reddish-pink biotite syenogranite	isotropic fabric, equigranular (medium/coarse-grained), brick-red alakali-feldspars: 3 to 8 mm in lenght, altered biotite, M = 8%, similar to TAL 3, 28	G.H.I.C.	6.3
TAL44	CRP-1	32	125.40	125.45	rounded	5x0.5x3	garnet-bearing biotite granite	heterogranular and layered, fine-grained cm-thick layers carrying garnet alternate with coarser-grained layers where alkali feldspar phenocrysts are up to 12 mm in lenght	G.H.I.C.	6.3
TAL45	CRP-1	32	125.87	125.88	angular	2x1x1	pink felsic volcanic rock	ryolitic composition (?), phenocrysts of feldspar, rare quartz and biotite set in a very fine-grained orange-pink groundmass, similar to TAL19	Late Paleozoic Gallipoli Volcanic Suite (?)	6.3
TAL46	CRP-1	32	126.05	126.09	sub-rounded	6x6x4	pink biotite syenogranite	slightly heterogranular (medium to coarse-grained), isotropic fabric, alkali feldspars: 2 to 10 mm in lenght, M = 10%, similar to TAL 10, 24	G.H.I.C.	6.3
TAL47	CRP-1	32	126.76	126.77	angular ?	1x1x0.5	pale green Ca-silicate rock	fine-grained, mainly composed of a granoblastic aggregate of plagioclase-hornblende+/-diopside with mm-thick patches enriched in hornblendepale green Ca-silicate rock ?	Koettlitz Group	6.3
TAL48	CRP-1	33	128.59	128.61	sub-rounded	3x1x1	pink-grey biotite monzogranite	isotroipc fabric, fine-medium grained, M = 9%	G.H.I.C.	6.3
TAL49	CRP-1	34	131.98	132.01	sub-rounded	3x2x4	pink biotite syenogranite	equigranular (medium-grained), alkali feldspars: 2 to 6 mm in length, M = 7%	G.H.I.C.	6.3
TAL50	CRP-1	34	132.71	132.74	sub-rounded	3x1x1.5	grey biotite monzogranite	fine to medium-grained, layering due to grain-size variations, pale brown alkali feldspar, M = 10%, with mm-thick layers, compositionally similar to TAL 25, 27, 30	G.H.I.C.	6.3
TAL51	CRP-1	35	134.51	134.54	sub-rounded	4x3x1.5	pink biotite monzogranite	isotropic fabric, heterogranular (medium to coarse-grained), alkali feldspars: 3 to 10 mm in length, M = 10%	G.H.I.C.	6.3
TAL52	CRP-1	35	134.71	134.74	sub-angular	4x3x2	biotite-hornblende granodiorite	slightly foliated fabric, foliation defined by hornblende and biotite, plagioclase porphyroclasts, up to 6 mm in length, wrapped by the foliation, M = 18%, comparable to TAL59	G.H.I.C.	6.3

Tub. 3 - Continued.

Sample code	Hole	Box	Top (mbsf)	Bottom (mbsf)	Clast shape	Approximate size (cm)	Lithology	Main petrographical features	Inferred provenance	Lithostratigraphic Unit
TAL53	CRP-1	35	134.96	135.00	sub-angular	5x3x3	grey biotitc granite	equigranular (medium-grained), feldspars: 2 to 5 mm in length, M = 8%	G.H.I.C.	0.3
TAL54	CRP-1	35	135.33	135.36	sub-rounded	3x4x3	Ca-silicate rock and margin of a granitic vein (or a plagioclase-quartz metamorphic layer)	very fine grained, compositional layering defined by a 1.5 cm-thick layer rich in diopside and plagioclase, and bv hornblende-rich layers	G.H.I.C.	0.3
TAL55	CRP-1	36	136.40	136.42	sub-angular	2x3x1	grey biotite granite	fine grained, equigranular, isotropic fabric, M = 8%. similar to TAL 58	G.H.I.C.	6.3
TAL56	CRP-1	36	137.62	137.65	angular	3x2x1	grey biotite-bearing granite	equigranular (medium-grained), isotropic fabric, feldspars: 2 to 6 mm in length, M = 7%, similar to TAL 23	G.H.I.C.	*0.3*
TAL57	CRP-1	36	138.45	138.47	angular	3x2x1	biotite-bearing amphibolite	fine-grained, foliation defined by hornblende and biotite	Koettlitz Group	0.3
TAL58	CRP-1	37	139.33	139.34	sub-angular	1x0.5x0.5	grey biotite granite	fine grained, equigranular, isotropic fabric, M = 8%, similar to TAL 55	G.H.I.C.	0.3
TAL59	CRP-1	37	140.31	140.33	sub-angular	3x2x2	biotite-hornblende granodiorite	slightly foliated fabric, foliation defined by hornblende and biotite, plagioclase porphyroclasts, up to 6 mm in length, wrapped by the foliation, M = 18%, comparable to TAL52	G.H.I.C.	6.3

also includes their main petrographical features, as well as the most probable source-rock units in the crystalline basement of Victoria Land.

Nine lithologies were recognized. They comprise dominant grey and pink biotite granites, subordinate hornblende-biotite foliated granodiorite and foliated granitoid, four metamorphic rock types including one amphibolite and three Ca-silicate rocks, two grey biotite haplogranites, three porphyritic granitoids and two pink felsic volcanic rocks.

Both grey granite and pink granite clasts are persistent throughout most of the lithostratigraphic units. In particular, lithostratigraphic Units 6.1 and 6.3 show the highest content of these two lithological facies, with the grey granite generally present in slighltly higher proportions.

The main petrographical features of grey biotite granites are similar to those described from the Quaternary strata (Quaternary Strata, this volume - section on Basement Clasts). Fabrics are typically isotropic without any evidence of significant syn- or post-magmatic deformation. Grain-sizes range from fine to medium/coarse, the average length of feldspar phenocrysts being between 2 and 8 mm. Textures are equigranular, sometimes heterogranular, and hypidiomorphic (Fig. 8). Mafic minerals (red-brown biotite

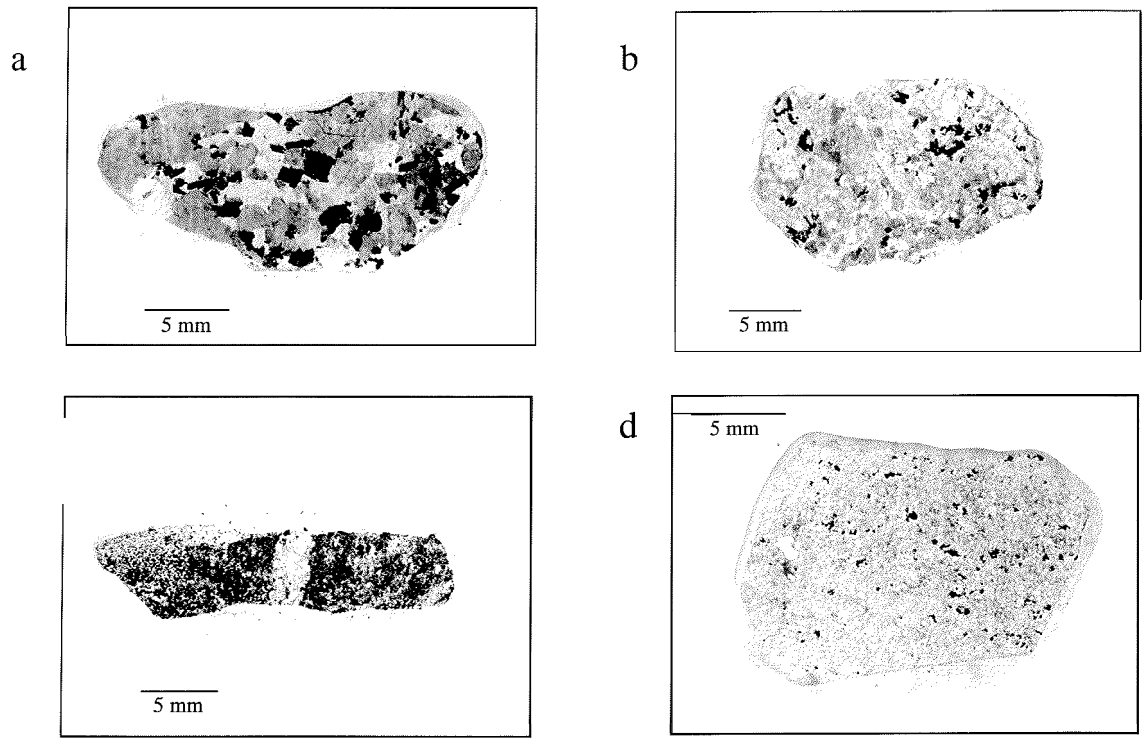

Fig. 8 - Photomicrographs of the principal basement-rock types in the Miocene strata, a) Pink biotite syenogranite (55.54-55.55 mbsf), ipidiomorphic texture with altered alkali feldspar phenocrysts, up to 10 mm in length, saussuritized plagioclase, chloritized biotite flakes and interstitial quartz. b) Grey medium- to coarse-grained biotite monzogranite (62.05-62.06 mbsf); hypidiomorphic texture with scattered biotite, partly sericitized alkali feldpar and plagioclase. *c)* Ca-silicate rock (61.52-61.53 mbsf): this rock consists of a fine-grained granoblastic aggregate of diopside and plagioclase, amphibole and a layer enriched in quartz and plagioclase. d) Grey biotite haplogranite (62.18-62.19 mbsf). Fine grained sub-polygonal granular aggregate of feldspars, quartz and minor biotite.

+/- olive-green hornblende) generally range from 7 to 12%. Mineral assemblages consist of alkali feldspar (perthitic orthoclase, sometimes transformed into a felty micro-aggregate of kaolinite), plagioclase (oligoclase-andesine displaying a marked normal compositional zoning and partly transformed into sericite or saussurite), quartz, red-brown or dark olive-green biotite (in places replaced by FeMg-chlorite+/-prehnite+/-epidote), green hornblende, opaque minerals, monazite/zircon and allanite. Modal proportions of alkali feldspar, plagioclase and quartz indicate that monzogranitic compositions predominate.

Rare garnet was found in two samples of grey biotite granite from the lower part of the core, one in lithostratigraphic Unit 6.2 (at 115.06 mbsfj and one in Unit 6.3 (at 125.40 mbsf). Both samples are heterogranular and characterized by a compositional and grain-size layering defined by cm-thick fine-grained layers, which contain 1-2 mm crystals of garnet, alternating with coarser-grained layers where alkali feldspar phenocrysts are up to 12 mm in length. Although muscovite was not observed during the macroscopic examination, the occurrence of garnet indicates a peraluminous composition.

The pink biotite granites are commonly equigranular medium-grained and typically contain pink or orange to brick-red subhedral alkali feldspars, 2 to 8 mm in length (Fig. 8). Fabrics are always isotropic, textures hypidiomorphic and the content of maficminerals (biotite, hornblende) ranges between 7 to 12%. Some of the samples have quartz/K-feldspar/plagioclase modal proportions indicating monzogranitic compositions but most are syenogranitic.

Pebbles consisting of hornblende-biotite foliated granodiorite (four clasts) and of foliated granitoid (one clast) occur only in the lower part of the core. Foliated granodiorite clasts first appear at 96.34 mbsf within lithostratigraphic Unit 5.8, and between 122 and 140 mbsf (Unit 6.3). The foliated granitoid (probably a deformed haplogranite and similar to those in the Quaternary strata) also occurs in Unit 6.3.

The foliated granodiorites are equigranular and medium/coarse-grained, and their mafic contents (red-brown biotite and green hornblende) range from 10 to 18%. The foliation is defined by the preferential dimensional orientation of both biotite and hornblende and by the alignment of plagioclase laths. Petrographical examination of one sample at 122.33 mbsf shows that plagioclase crystals are compositionally zoned with andesine cores and calcic oligoclase rims. Alkali feldspar (perthitic ortoclase) occurs as coarser-grained poikilitic crystals carrying inclusions of biotite and plagioclase; accessory minerals include zircon, monazite, apatite and opaque minerals.

The occurrence of grey biotite haplogranites is documented by only two clasts: at 62.18 mbsf and at 124.92 mbsf (litostratigraphical Units 5.3 and 6.3). Both are fine-grained and with a low modal content of biotite (around 3%) (Fig. 8). Microscopic examination of the first one reveals an interlobate to sub-polygonal granular structure, poikilitic grains of microcline containing rounded inclusions of quartz, oligoclase and green-brown biotite partly replaced by Fe-Mg chlorite +/- prehnite,

Pebbles of porphyritic granitoids are restricted to the lower part of the core, within lithostratigraphic Units 6.1 and 6.2. They are characterized by idiomorphic phenocrysts of orthoclase, oligoclase and quartz set within a fine to very-fine grained felsic groundmass with scattered aggregates of red-brown biotite. In thin section, quartz phenocrysts show undulose extinction, and plagioclase and orthoclase are partly replacecl by sericite. The feldspars are often fragmented and contain microfractures filled by the felsic groundmass, suggesting that the rock suffered brittle deformation before the groundmass had fully crystallized.

Amphibolite-facies metamorphic rocks are mainly concentrated in Unit 6.3, elsewhere only occurring in litostratigraphic Unit 5.2 (Fig. 7). The three pebbles of Ca-silicate rocks have fine-grained granoblastic textures and are formed of diopside, calcic plagioclase, quartz, amphibole and biotite (Fig. 8). A mm-scale compositional layering is rarely present. The layering comprises alternating bands of coarser labradorite, minor quartz and diopside, and finer plagioclase, diopside, microcline and green amphibole (poikiloblasts). Accessory minerals include abundant titanite (2%) and rare opaque minerals. A fine-grained amphibolite pebble at 138.45 mbsf has a marked foliation defined by hornblende and minor biotite; the high modal content in plagioclase, together with quartz and biotite, suggest a sedimentary derivation.

The two pebbles of pink felsic volcanic rocks (at 104.17 and at 125.87 mbsf) contain phenocrysts of plagioclase, K-feldspar (both deeply replaced by a brownish felty micro-aggregate) and quartz, and an orange-pink groundmass of recrystallized glass with scattered fine-grained grains of secondary epidote and chlorite. The phenocryst mineralogy suggests a rhyolitic composition.

Provenance

Macroscopic and petrographical observations indicate that several basement lithologies were involved as sources of basement clasts in Miocene sedimentary strata recovered in the CRP-l drillhole. As in the Quaternary sequence (Quaternary Strata, this volume - section on Basement Clasts), most of the basement pebbles were supplied by source rock-units belonging to the Cambro-Ordovician Granite Harbour Igneous Complex, which is the dominant component in the local basement (Gunn & Warren, 1962; Allibone et al., 1993a, 1993b). The Miocene strata also contain metamorphic rocks such as Ca-silicate rocks, which are known to be a common metasedimentary lithology in the amphibolite facies Koettlitz Group south of Mackay Glacier (Grindley & Warren, 1962; Findlay et al., 1984; Allibone, 1992).

The regional geology of granitoids in the area between Ferrar and MacKay Glaciers (Gunn & Warren, 1962; Allibone et al., 1993a, 1993b) further constrains the provenance of the granitoid clasts. Syn-tectonic granitoids are the likeliest source for the pebbles of foliated granitoids and hornblende-biotite foliated granodiorites in the lower part of the core. Similarly, post-tectonic granitoids, including dyke swarms, may be the source of the pebbles of grey biotite monzogranites, pink biotite granites and of haplogranites- porphyritic granitoids.

The provenance of the pinkryolitepebbles is uncertain. In Victoria Land, comparable porphyritic rhyolites occur in the upper Palaeozoic Gallipoli Volcanics (Dow & Neall, 1974). However, a closer provenance from presently unknown outcrops of Granite Harbour volcanic units in the Mackay Glacier region cannot be excluded.

CLAY MINERALOGY

Clay-mineral analyses were performed on 16 Miocene samples. The methods have been described in the chapter on the Quaternary (see Quaternary Strata, this volume - section on Clay Mineralogy). The results are presented in table 4.

Smectite, illite and chlorite have been observed in all samples and are the most common clay minerals throughout the Miocene part of the core. Kaolinite may occur as trace amounts in a few samples. Quartz, plagioclase and K-feldspar are present in high amounts in all samples.

In the upper part of the Miocene sequence, down to 60-65 mbsf, the composition of the clay fraction of the sediments resembles that of the Quaternary sequence (see Quaternary Strata, this volume - Tab. S, section on Clay Mineralogy). Poorly crystalline smectite is the dominant clay mineral; illite and chlorite occur in smaller amounts. This assemblage indicates a source area in the McMurdo Volcanic Group with some influence of basement and/or sedimentary rocks. For a detailed discussion, see Quaternary Strata, section on Clay Mineralogy (this volume).

The clay-mineral assemblages of the lower part of the CRP-1 core, in contrast, are dominated by illite, with chlorite being common and smectite occurring in lesser amounts. This assemblage, which also dominates the Oligocene to lower Miocene sediments of the drillcores CIROS-1 and MSSTS-1 (Ehrmann, 1997, in press), is typical of the physical weathering of a source area consisting of granitic or metamorphic basement and sedimentary rocks, as occurs in the Transantarctic Mountains and on the East Antarctic craton. From the clay-mineral record alone, however, it is hard to tell where the ice came from during the deposition of the lower part of the core. It is possible that the ice still came from the south with a smaller volcanic area available and therefore lower smectite contents. However, theoretically it would also be possible to explain the clay-mineral assemblages by ice coming from the west.

X-RAY MINERALOGY

In order to provide a general characterization of the bulk mineralogy of the Miocene sediments from CRP-1, seven samples were analyzed using a Rigaku Miniflex+ x-ray diffraction (XRD) system at the Crary Science and Engineering Laboratory. The materials analyzed were sub-sampled from the seven Miocene "fast-track" samples, dried in an oven at 60°C, and powdered in a ball mill. The powders were then prepared as random (unoriented) pressed powder mounts on aluminum sample holders and glycolated for 12 hours prior to XRD analysis. Each sample was scanned over the range of 3-45° 2θ, with a step size of 0.02° and a scan time of 2 seconds/step. The data were recorded digitally and processed with JADE 3+ software. Data processing included: 1) removing background from the XRD pattern, 2) calibrating the analyzed pattern against the known peak positions for quartz, and 3) identifying mineral phases with a search/match routine that employs the International Center for Diffraction Data (ICDD) Powder Diffraction File (PDF) on CD-ROM.

Sample locations and the minerals identified in each sample are listed in table 5. Quartz and plagioclase feldspars are the dominant phases in each sample, with lesser amounts of K-feldspars present in some samples. Other minerals show low intensity peaks on the XRD patterns, suggesting low abundances, and occur discontinuously in the Miocene section; these include a variety of phyllosilicates (chlorite, illite/muscovite, possible interstratified illite/chlorite), amphiboles, and pyroxenes.

Tab. 4 - Estimates of the abundance of the main clay mineral groups smectite, illite, chlorite and kaolinite in sediments from the drillcore CRP-1. The number of crosses is proportional to the abundance of the clay minerals.

Sample	Smectite	Illite	Chlorite	Kaolinite
45.18 mbsf	x x x x x	x	x x x	traces
53.50 mbsf	x x x x	x x x x	x x	
54.70 mbsf	x x x x x	x	x	
59.58 mbsf	x x x x x	x	x	
65.90 mbsf	x x	x x x x	x x x x	traces
67.60 mbsf	x x	x x x x x	x x x	traces
72.60 mbsf	x x	x x x x	x x x	traces
77.45 mbsf	x x x	x x x x	x x x	traces
78.15 mbsf	no diffraction pattern			
85.78 mbsf	x x x	x x x x x	x x	
99.02 mbsf	x x	x x x x x	x x x	
109.15 mbsf	x x x	x x x x	x x x	traces
120.40 mbsf	x x	x x x x	x x x	
131.80 mbsf	x	x x x x	x x x x	
141.80 mbsf	x x	x x x x x	x x x	
147.33 mbsf	x x x	x x x x	x x x	

Tab 5 Minerals identified by x-ray diffraction analysis in bulk samples from CRP-1

Depth (mbsf)	Mineral Present
45.20	Quartz
	Variety of feldspars (albite, anorthite)
	Chlorite?
	Interstratified illite/chlorite?
53.50	Illite
	Quartz
	Variety of feldspars (albite, anorthite, anorthoclase?, microcline?)
	Amphibole?
59.60	Illite
	Quartz
	Variety of feldspars (albite, anorthite, orthoclase, sanidine)
	Amphibole?
78.20	Illite
	Quartz
	Variety of feldspars (albite, anorthite, sanidine?)
	Amphibole?
99.10	Illite/muscovite
	Quartz
	Variety of feldspars (albite, anorthite, orthoclase)
	Amphibole?
120.40	Illite/muscovite
	Quartz
	Variety of feldspars (albite, anorthite)
	Augite
	Amphibole?
	Diopside?
141.80	Illite/muscovite
	Quartz
	Variety of feldspars (albite, anorthite, microcline)
	Amphibole?

The data generated by these analyses cannot be used quantitatively to determine the abundances of the various minerals present. However, comparing the intensities of two XRD peaks (one chosen for each mineral of interest) can provide a useful qualitative indicator of the variations in relative abundances of those two phases through a stratigraphic section (*e.g.*, Scheidegger & Krissek, 1982; Jones & Blatt, 1984). In this case, a variety of peak area ratios have been calculated to determine the relative abundances of: 1) total feldspar (especially plagioclase feldspar) and quartz, and 2) K-feldspar and quartz. The relative abundances of total feldspar and quartz are presented as the average of three peak intensity ratios: 4.04 Å (plagioclase)/4.25 Å (quartz), 3.76 Å (feldspar)/4.25 Å (quartz), and 2.85 Å (plagioclase)/4.25 Å (quartz). The average of three peak intensity ratios is used, rather than the individual peak intensity ratios, in order to reduce the amount of scatter in the resulting profile. The stratigraphic profile of average feldspar/quartz peak intensity ratios is shown in figure 9.

The relative abundances of K-feldspar and quartz are presented as the average of four peak intensity ratios: 3.82 Å (K-feldspar)/4.25 Å (quartz), 2.77 Å (K-feldspar)/4.25 Å (quartz), 2.16 Å (K-feldspar)/4.25 Å (quartz), and 2.11 Å (K-feldspar)/4.25 Å (quartz). As with the total feldsparlquartz parameter, the average of multiple peak intensity ratios is used to reduce scatter in the profile of K-feldspar/quartz relative abundances. The stratigraphic profile of average K-feldspar/quartz peak intensity ratios is shown in figure 10.

The general structures of the average feldsparlquartz ratio profile (Fig. 9) and the average K-feldsparlquartz ratio profile (Fig. 10) are similar, with a maximum in each case located in the region between 60 and 120 mbsf. One potential reason for these compositional variations is a

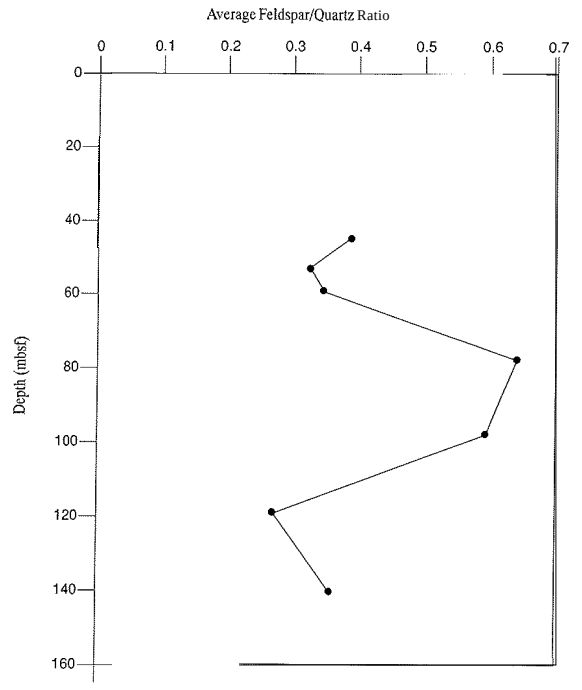

Fig. *9* - Stratigraphicprofile of feldspar/quartz XRD peak intensity ratios for bulk sediments from CRP-1. Each ratio plotted is the average of three separate peak intensity ratios. The feldspar considered in these ratios is predominantly plagioclase.

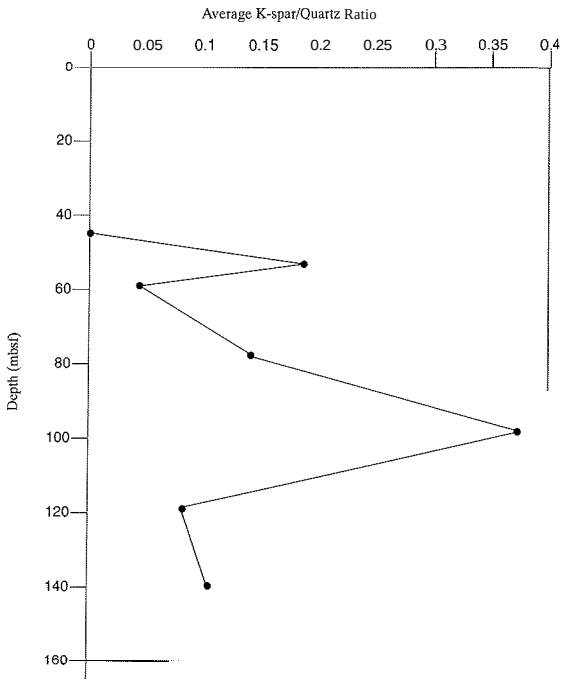

Fig. *10* - Stratigraphic profile of K-feldspar/quartz XRD peak intensity ratios for bulk samples from CRP-1. Each ratio plotted is the average of four separate peak intensity ratios.

change in sediment grain size, since feldsparlquartz ratios tend to decrease as grain size decreases (Blatt, 1992). With the exception of the fine sand sampled at 45.2 mbsf, however, these samples were all taken from levels classified as silty claystones, clayey siltstones, siltstones, or clast-poor diamictites with a muddy matrix. As a result, the grain size of the bulk sediment analyzed does not appear to vary significantly between samples, thereby minimizing the possibility that the patterns observed in figures 9 and 10 are primarily a result of grain-size changes downcore.

A second possible explanation for the patterns seen in figures 9 and 10 is a change in sediment provenance during the period of deposition. The possible role of changing source contributions can be evaluated by comparing the variations in bulk mineralogy, sand fraction composition (see section on Sand Grains and Provenance), and coarse-clast composition (see section on Basement Clasts) through the Miocene section; this comparison suggests a three-fold compositional subdivision of the Miocene section. Above 60 mbsf, both the feldspar/quartz and the K-feldsparlquartz ratios are low, the sand fraction contains abundant volcanic glass and volcanic rock fragments, and the sand-sized feldspars are dominated by plagioclase. In the internal 60-120 mbsf, the feldspar1 quartz and K-feldspar/quartz ratios increase, the volcanic component in the sand fraction is significantly reduced, the sand-sized feldspars are dominated by K-feldspars, and the larger clasts indicate a greater contribution of K-feldspar-rich basement lithologies. Below 120 mbsf, the characteristics of the sand fraction and the larger clasts are similar to those in the interval 60-120 mbsf, but the feldsparlquartz and K-feldspar/quartz ratios decrease.

Below 60 mbsf, the coarser grain sizes are consistently enriched in K-feldspar-bearing phases, and a similar enrichment in the bulk sediment is indicated by the K-feldsparlquartz ratio for the internal 60-120 mbsf. This consistent pattern of enrichment suggests that basement rocks were more important than contemporaneous volcanic centers as contributors of sediment at that time. The feldsparlquartz ratio is also high for the internal 60-120 mbsf, however, indicating that relatively plagioclase-rich sub-sand-sized material was also supplied at this time. This feldspar-rich fine component may have been supplied either: 1) by weathering that preferentially removed plagioclase from the sand-sized fraction of basement-derived material and concentrated the plagioclase in the corresponding fine fraction (suggesting a predominance of physical weathering processes), or 2) from another source lithology, such as the Palaeozoic/Mesozoic sedimentary sequence. Below 120 mbsf, the bulk sediment feldsparlquartz ratios and K-feldspar1 quartz ratios are low, suggesting that a relatively quartz-rich supply of sub-sand-sized material diluted the basement input during deposition of the oldest part of CRP-1. This quartz-rich source, which may have been the Palaeozoicl Mesozoic sedimentary sequence, apparently did not provide significant amounts of coarse-grained material, because its effect is not recognized in the compositions of the sand or gravel fractions.

Above 60 mbsf, the feldsparlquartz ratios and the K-feldspar/quartz ratios are low, the sand fraction contains abundant volcanic glass and volcanic rock fragments, and the sand-sized feldspars are dominated by plagioclase. The sand-fraction characteristics clearly demonstrate the importance of a contemporaneous volcanic source, tentatively identified as the McMurdo Volcanic Group. The contrast between relatively plagioclase-rich sands and relatively plagioclase-poor bulk sediment, however, indicates that the volcanic supply was diluted by quartz-rich input of sub-sand-sized material at this time. The origin of this quartz-rich component is unknown at present, but possibilities include: 1) material recycled from the Palaeozoic/Mesozoic sedimentary sequence, or 2) material originating from basement lithologies, but weathered to remove the K-feldspar-bearing phases observed below 60 mbsf (which suggests extensive chemical weathering).

Further studies of sediment provenance, based particularly on sandstone petrography and sediment geochemistry, will be pursued in the future.

ORGANIC GEOCHEMISTRY

Methods

Samples were collected at c. 5 m internals and were intended to be representative of the major lithologies penetrated by the CRP-1 hole. All lithological units were sampled except for lithostratigraphic Units 1.1 and 2.3 (diamicton units) and lithostratigraphic Units 5.3 and 5.6 (diamictite units). Only the matrix of diamictitic units was analyzed: clasts larger than granules were returned to the curator.

All samples were freeze-dried, ground and homogenized with a mortar and pestle, and stored in 15 ml glass vials. All glassware and equipment used in sample preparation were cleaned using Micro solution and water followed by a purified water rinse. The cleaning was followed by sequential rinses with 1% aqueous hydrochloric acid, methanol, and dichloromethane. Analyses were performed using a Carlo-Erba NA 1500 NCS analyzer and sulphanilamide as a standard. Two sets of analyses were performed. 1) Total carbon (TC), total sulphur (TS), and total nitrogen (TN) measurements were made on all samples. 2) A second portion of the powdered samples was loaded into silver capsules, weighed, and stored in a desiccator overnight with concentrated hydrochloric acid as outlined by Hedges & Stern (1984). The total organic carbon (TOC) contents of these latter samples were then measured. In principle, inorganic carbon content could be determined by difference. In practice, the extremely low amount of inorganic carbon in all but one sample and the poor precision of the carbon measurements made calculation of meaningful values for inorganic carbon impossible.

Results and **Discussion**

Although the precision obtained for measurements of total nitrogen and total sulphur was within expected limits for the technique used (±14% of the measured value for N and ±20% of the measured value for S), the precision

obtained for the carbon determinations was considerably poorer than expected (±50% of the measured value). A series of carbon determinations was performed after adding vanadium pentoxide to the sample capsules in an effort to determine whether the lack of precision resulted from incomplete combustion of refractory organic matter. No improvement in precision was noted. The poor precision for the carbon data is apparently caused by sample heterogeneity. The heterogeneity must be caused by very fine grains that have very high carbon contents. These grains must not have significant sulphur or nitrogen contents as those analyses were unaffected. The TC and TOC contents (Tab. 6) of these samples are low: TOC values are all below 1% and average 0.4%. Inorganic carbon contents must also be extremely low. The sole exception is sample 33.68-33.69 mbsf for which a meaningful inorganic carbon content of 4.4% can be calculated.

The small amounts of organic carbon preserved in these samples are apparently derived from terrigenous sources rather than directly from aquatic organisms. The TOC/TN values are high (Fig. 11): these values exceed 10 for all samples and exceed 100 in the lowermost diamictite encountered by the CRP-1 core (Unit 6.3). Organic matter derived largely from aquatic organisms has TOCKN values that are significantly less than 10, whereas the TOC/TN values of organic matter derived from land plants is significantly greater than 10 (Bordovskiy, 1965). Coal also has TOC/TN values significantly greater than 10. The organic matter in the CRP-1 core probably comprises coal detritus or perhaps fragments of higher land plants. The presence of coal detritus would explain the imprecision of the carbon measurements: a single fine particle of coal would change the carbon measurement significantly but would not affect the nitrogen measurement and would probably not affect the sulphur measurement.

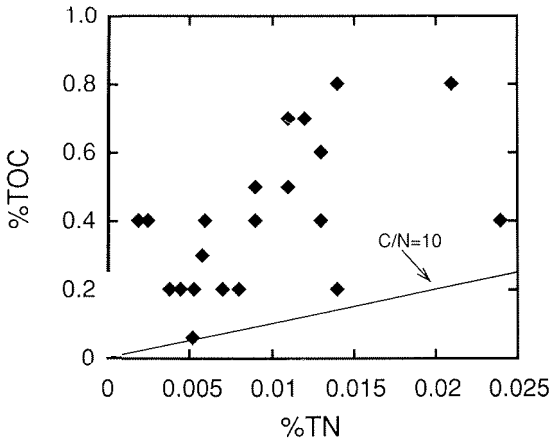

***Fig.** 11* - Plot of TOC *versus* TN for CRP-1 samples. The locus of points where TOC/TN = 10 is designated by the line.

Some of the organic matter produced in the water column did reach the sediment-water interface but was mineralized during sedimentary diagenesis: small but reproducible amounts of sulphur were detected in all samples. This sulphur was presumably fixed as ferrous sulphide as a byproduct of bacterial reduction of sulphate. The samples from the CRP-1 core are quite variable when plotted in TS versus TOC space (Fig. 12). The variability reflects the sources of organic matter deposited with these sediments and the oxygenated environment in which the organic matter was deposited. Those samples in which the TS/TOC values are high, were deposited during periods of

Tab. *6* - Values of total carbon (TC), total organic carbon (TOC), total nitrogen (TN) and total sulphur (TS) obtained from samples of the CRP-1 core.

Sample Depth (mbsf)	**%TC**	**%TOC**	**%TN**	**%TS**
19.31-19.32	0.2±0.1	0.2±0.1	0.007±0.001	0.024±0.00
26.35-26.36	0.09±0.0	0.2±0.1	0.0053±0.0007	0.024±0.00
33.68-33.69	4.8±0.7	0.4±0.2	0.024±0.003	0.05±0.01
38.83-38.84	0.4±0.2	0.2±0.1	0.008±0.001	0.28±0.06
44.40-44.41	0.8±0.4	0.2±0.1	0.008±0.001	0.43±0.09
54.22-54.23	0.4±0.2	0.7±0.4	0.012±0.002	0.32±0.06
58.00-58.01	0.5±0.3	0.6±0.3	0.013±0.002	0.14±0.03
65.65-65.66	0.2±0.1	0.2±0.1	0.0045±0.0006	0.11±0.02
69.94-69.95	0.6±0.3	0.8±0.4	0.021±0.003	0.5±0.1
77.00-77.01	0.2±0.1	0.7±0.3	0.011±0.002	0.14±0.03
83.20-83.21	0.6±0.3	0.7±0.3	0.011±0.002	0.14±0.03
86.50-86.51	0.4±0.2	0.4±0.2	0.009±0.001	0.14±0.03
91.17-91.18	0.05±0.0	0.06±0.0	0.0052±0.0007	0.24±0.05
94.89-94.90	0.4±0.2	0.3±0.2	0.0058±0.0008	0.42±0.08
97.45-97.46	0.4±0.2	0.5±0.3	0.011±0.001	0.13±0.02
101.44-101.45	0.5±0.2	0.2±0.1	0.014±0.002	0.18±0.04
106.60-106.61	0.3±0.2	0.2±0.1	0.0038±0.0005	0.11±0.02
112.86-112.87	0.4±0.2	0.4±0.2	0.009±0.001	0.15±0.03
118.44-118.45	0.3±0.1	0.4±0.2	0.009±0.001	0.30±0.06
123.60-123.61	0.10±0.0	0.4±0.2	0.0019±0.0003	0.08±0.02
126.93-126.94	0.3±0.2	0.4±0.2	0.0025±0.0004	0.06±0.01
130.46-130.47	0.2±0.1	0.4±0.2	0.0060±0.0008	0.12±0.02
137.40-137.41	0.2±0.1	0.5±0.2	0.009±0.001	0.13±0.03
142.16-142.17	0.4±0.2	0.8±0.4	0.014±0.002	0.16±0.03
		0.4±0.2	0.013±0.002	0.21±0.04

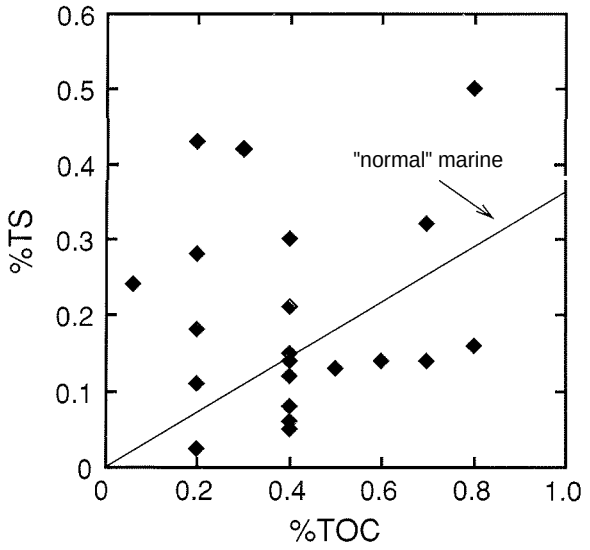

Fig. 12 - Plot of TS *versus* TOC for CRP-1 samples. The line labelled "normal marine" is taken from Berner (1984).

higher organic productivity. The intervals from which samples with TS/TOC values exceed 0.5 correspond well to intervals with high Diatom Abundance Index values (*e.g.*, see Fig. 15, section on Diatoms). On the other hand, a number of samples have very low TS/TOC values. These low ratios suggest that much of the organic matter deposited with sediment was refractory and not a suitable substrate for biogenic sulphate reduction. The samples containing the more refractory organic matter also have high TOC/TN values (Tab. 6).

The imprecision of the carbon determinations, the overall high TOC/TN values, and the variable nature of the TS/TOC values are evidence that the organic matter deposited with these sediments comprised refractory organic matter (either detrital coal or terrigenous plant detritus) with variable amounts of organic matter derived from aquatic organisms. The more labile fraction of this organic material was mineralized during early diagenesis whereas the refractory detritus was preserved.

SAND GRAINS AND PROVENANCE

Introduction

This section describes the sand fraction of samples obtained from Miocene strata in the CRP-1 drillhole. It is a preliminary investigation, undertaken to determine the range of sand-size mineral and lithic grains present, to estimate visually their relative proportions, and to provide initial information on provenance and any temporal variations. Although the results are described as detrital modes, it was not possible to use systematic quantitative determinations (*cf.* the Gazzi-Dickinson method), and the data are only qualitative. The observations are based largely on smear slides of sand-grade sediments obtained by sampling every 4-5 m, although samples of all grain sizes were examined every 1-2 m (Tab. 7). The slides were prepared in the same manner as described in Quaternary Strata, section on Sand Grains and Provenance (this volume), but they were also supplemented by a small number of unstained grain mounts and normal (uncovered) thin sections, which were used to verify identifications. About 40 rock samples, mainly from sandstone strata, were obtained for thin section determination of the detrital modes, but unanticipated problems with the automated production of thin sections prevented the examination of these samples; they will form the basis of future laboratory studies.

Previous studies described sand grains and provenance of samples from the MSSTS-1 and CIROS-1 drillholes, situated c. 80 km south of CRP-1 (Barrett et al., 1986; George, 1989; Background to CRP-1, this volume - Fig. 1). These studies reported a varied provenance reflecting the local geology of the Transantarctic Mountains in southern Victoria Land, including granitoid and predominantly high-grade metasedimentary rocks of an Upper Precambrian-lower Palaeozoic "basement"; quartzose sedimentary rocks of the Devonian-Triassic Beacon Supergroup; sills, dykes and lavas of the Jurassic Ferrar Dolerite and Kirkpatrick Basalt; and alkaline volcanic rocks of the Cenozoic McMurdo Volcanic Group. Temporal variations in provenance were noted by the previous workers, who divided their samples into several petrofacies based on the dominant grains present (mainly quartz, feldspar and volcanic types).

Criteria used to identify the grains encountered are summarized in Quaternary Strata, table 6 (this volume), and a summary table of estimated detrital modes is presented in table 7. In view of significant problems in identifying some minerals (George, 1989), the grain types were divided into obvious natural groupings based on petrographical appearance (e.g. colourless grains (quartz and feldspar), ferromagnesian minerals, etc.)) and the relative abundances were estimated visually using a petrological microscope. Although numerical values for modal abundances are given in the following descriptions, results in figures 13 and 14 and table 7 are presented in analogue form using symbols in order to highlight their qualitative nature. This is to avoid the data assuming an unrealistic precision if quoted indiscriminately.

Detrital modes are normally focused on a single sand-size category (usually medium sand). The CRP-1 smear slide samples are dominated by fine sand and finer-grained material, from lithofacies consisting mainly of marine diamictite, siltstone and sandstone. Undesired grain size effects on the detrital modes are likely to be introduced working with such fine material and including samples with a wide range of grain sizes. Thus, only data for predominantly sandy layers are used here to describe the modal variations, although many finer-grained samples were also examined routinely (Tab. 7). Despite perceived inaccuracies in the method of visual estimation adopted, observed major modal variations are likely to be geologically significant.

Results

Throughout the Miocene section, the samples examined are dominated by colourless grains of abraded quartz and lesser K-feldspar (likely orthoclase, minor microcline, rare sanidine), and predominantly angular fresh plagioclase

Tab. 7 - Summary of qualitative "detrital modes" for grains of all sizes in Miocene strata.

Sample depth (mbsf)	Section type	Lithology (as logged)	Q+F/tot	Volc/tot	Volc. lith/tot	Basic/Evolved glass	Biotite/tot	Comments
43.90	Smear	Fine sandstone	XXXX	XXXXXXX	X	BBE	X	Abundant glass and organic matter
44.60	Smear	Fine sandstone	XXXXXXX	XXXX	XX	BBBE		Abundant glass and organic matter
45.18	**Smear**	**Fine sandstone**	**XXXXXXX**	**XXXXXXX**	**XXXXXXX**	**BE**	**X**	**Tr. bioclastic, biotite, aegirine, garnet (pink), phyllite, polyquartz**
45.83	Smear	Fine sandstone	XX	XX		BE	X	No sand
46.95	Smcar	Fine sandstone	XX	XXXX	X	B	X	Larger grains are basaltic glass
47.74	Smear	Fine sandstone	XXXX	XX	X	BBBE	XX	Very small quartz grains
48.90	Smear	Sandy mst	XXXX	XX	-	BBBE	XX	Very small quartz grains
50.00	Smcar	Sandy mst	XXXX	X	X	BE	XX	Very small quartz grains
53.00	Smear	Sandstone	XXXXXXX		-		XX	Very small quartz grains
53.5	**Smear**	**Clayey sst [silt]**	**XXXXXXX**	**X**	**-**	**?**	**-**	**Tr. hornblende, garnet**
54.00	Smear	Siltstone	XXXX	X		B	XX	Very small quartz grains
54.75	Smear	Clayey siltstonc						
56.29	Smear	Clayey siltstone	XXXXXXX	XXXXXXX		B	X	Largest grains are basaltic glass
56.82	Smear	Claycy siltstonc	XX	X	-	E		Rare colorless glass
58.13	Smear	Clayey siltstonc	XXXX	X	X	E	X	Rare colorless glass
58.93	Smear	Clayey siltstone	XXXXXXX	XXXXXXX	X	BBE	XX	Largest grains arc basaltic glass; tr. aegirine
59.58	**Smear**	**Silty f sst [silt]**	**XXXXXXX**	**XXXX**	**X**	**BBBE**		**Tr. bioclastic, garnet, hornblende, ?kaers, epid, phyllite, polyqtz**
60.05	**Smear**	**Sity f sst**	**XXXXXXX**	**XXXX**	**X**	**BBE**	**XXXX**	**Tr. aegirine**
60.92	Smear	Fine sandstone	XXXXXXX	XXXX	X	BBE		
60.99	**Section**	**Fine sandstone**	**XXXXXXX**	**XXXX**	**XX**	**B**	**X**	**Tr. aenigm, hbl., epid, gt (pink); magnetite, phyll, polyqtz**
61.88	**Section**	**F-m sandstone**	**XXXXXXX**	**XXXX**	**XX**	**BBBE**	**X**	**Tr. bioclastic, aegirine, hornblende, garnet, polyqtz**
61.94	**Smear**	**Fine sst [diamict]**	**XXXXXXX**	**XX**	**X**	**BBBE**	**X**	**Tr.aegirine**
62.12	Smear	Muddy sst	XXXX	-	-		XXXX	No sand
65.27	**Section**	**Silty sandstone**	**XXXXXXX**	**X**	**X**	B	**X**	**Tr. ?aenigmatite, zircon, ?celadonite**
65.75	Smear	Diamictite	XXXXXXX	XX		BE		Tr. aegirine, glauconite
66.57	Smear	Diamictite	XXXXXXX	XX		BBE	X	Tr. glauconite
67.10	Smear	Sandstone	XXXXXXX	XX	-	BBBE	XXXX	Tr. glauconite. hornblende
67.60	Smear	Fine sandstone	XXXX					No ferromagnesian minerals
69.75	Smear	Silty fine sst	XXXX				X	No ferromagnesian minerals
70.04	Smear	Silty fine sst	XXXX				X	No ferromagnesian minerals
70.08	Smear	Silty fine sst	X		-			No ferromagnesian minerals
72.51	**Section**	**Fine sandstone**	**XXXXXXX**	**X**	**X**	**B**		**Tr. ?aenigmatite/kaersutite, hornblende, epidote, fine fsp-biot metam**
73.55	**Smear**	**Sandstone**	**XXXXXXX**	**XX**		**BBE**	**X**	**Tr. bioclastic, aegirine, hypersthene, ?aenigmatite**
74.61	Smear	Sandstone	XXXXXXX	XXXX		B	XXXX	Tr. glauconite
76.50	Smear	Green mudstone	XXXX	X		?	XX	Rare clinopyroxene
77.44	Smear	Diamictite	XXXX					No clinopyroxene
78.94	Smear	Silty fine sst	XX	X	-	?	X	Rare clinopyroxene
79.48	**Smear**	**Sity sst [diamict]**	**XXXXXXX**	**X**	**-**	**BE**	**-**	**Tr. hornblende.**
82.20	Smear	Siltstone	XXXXXXX	X	X	B	XX	No clinopyroxene
82.43	Smear	Sandstone	XXXXXXX	X	-	B	X	No clinopyroxene
85.37	**Smear**	**Siltstone**	**XXXXXXX**	**XX**	**XX**	?		**Tr. hornblende**
85.39	Smear	Siltstone	XXXXXXX	X	-	B	XX	Largest grains arc glass
86.94	Smcar	Siltstone	XXXX	X	-	BBBE	X	
87.44	Smear	Siltstone	XX	X	-	B	X	Rare clinopyroxene
89.50	**Smear**	**Fine sandstone**	**XXXXXXX**	**X**	**X**	?	**X**	**Tr. ?aenigmatite, aegirine**
91.17	Smear	Fine sandstone	XXXXXXX	XX	-	BBE	X	Tr. aegirine
92.45	Smear	Mudstone	XXXX	X	X	E	XX	
	Smear	Mudstone	XX	X			XXXX	No clinopyroxene

Tr. - trace; Q+F - quartz + feldspar

B - brown glass; E - evolved (colourless) glass; [number of letters of each denotes approximate relative abundance; ***e.g.***, BBBE - brown glass >>> evolved glass]

X - Trace (<1%) XXXX - Common (>5-20%)

XX - Present (>1-5%) XXXXXXX - Abundant (>20%)

Tab. 7 - Continued.

Sample depth (mbsf)	Section type	Lithology (as logged)	Q+F/tot	Volc/tot	Volc. lith/tot	Basic/Evolved glass	Biotite/tot	Comments
95.48	Smear	Mudstone	XXXX	X		B	XX	
96.62	Smear	Sandstone	XXXXXXX	X	-	B	X	
98.35	Smear	Very fine sst	XX	-	-		XXXX	No sand
99.02	Smear	siltstone-mdst	**XXXXXXX**	**X**	**X**	**BBE**		Tr. **bioclastic, ??arfvedsonite,** hornblende
99.97	Smear	Fine sandstone	XX	X	-	B	XXXX	Rare pale brown glass
100.85	Smear	Clayey siltstone	XX	X	X	E	X	
102.45	Smear	Clayey sst	XX	X	X	E	XX	Tr. aegirine, hornblende
102.52	Smear	Clayey sst [silt]	**XXXXXXX**	**X**	**X**	BE	**XXXX**	Tr. **?aegirine,** garnet, hornblende
104.44	Smear	Diamictite	XXXXXXX	X	?	B	X	
105.52	Smear	Diamictite	XXXXXXX	XX	-	B	X	
106.69	Smear	Sandstone	XXXXXXX	XX	X	B	X	Tr. hornblende; some biotite altered
108.69	Smear	Silty sand	XX	X	-	B	XXXX	Tr. orthopyroxene; some biotite altered
112.32	Smear	Silly sand	XX	X	-	BBE		Tr. glauconite, no clinopyroxene sand grains
114.39	Smear	**Silty** sandstone	**XXXXXXX**	**XX**	**X**	**BBE**	**XXXX**	Tr. aegirine, kaersutite
115.65	Smear	Sandstone	XX	X	-	BBB	XXXX	Tr. kaersutite
117.60	Smear	Sandstone	**XXXXXXX**	**-**	**-**		**X**	Tr. ?hornblende, aegirine, garnet
118.50	Smear	Sandy siltstone	XXXXXXX	XX	X	BBE	XX	Some altered basaltic glass, hornblende
120.40	Smear	Diamictite		**X**	**-**	**BBE**		Tr. **?aenigmatite**
122.49	Smear	Diamictite	XX	X	-	B	XX	Tr. hornblende
125.00	Smear	Diamictite	XXXX	X	-	B	XXXX	Tr. hornblende
126.43	Smear	Diamictite	XXXXXXX	X	-	B	XX	Tr. Hornblende
128.83	Smear	Diamictite	XXXXXXX	X	X	BBBE	X	Tr. hornblende
130.45	Smear	Clay	XXXXXXX	X	-	B		
132.73	Smear	Diamictite	XXXXXXX	X	-	B	X	Tr. hornblende
133.32	Smear	Black siltstone	XXXXXXX	X	-	B	X	
135.63	Smear	Clayey siltstone	XXXXXXX	X	-	B	XXXX	
136.92	Smear	Diamictite	**XXXXXXX**	**X**	**-**	B	**XXXX**	Tr. bioclastic, hornblende
138.83	Smear	Diamictite	**XXXXXXX**	**XX**	**X**	B	**XXXX**	Tr. bioclastic, **?biotite** (green), hornblende
141.80	Smear	Clayey siltstone	**XXXXXXX**	**XX**	**XX**	BBBE	**X**	Tr. bioclastic, biotite (green), hornblende
142.20	Smear	Clayey siltstone	XX				XXXX	

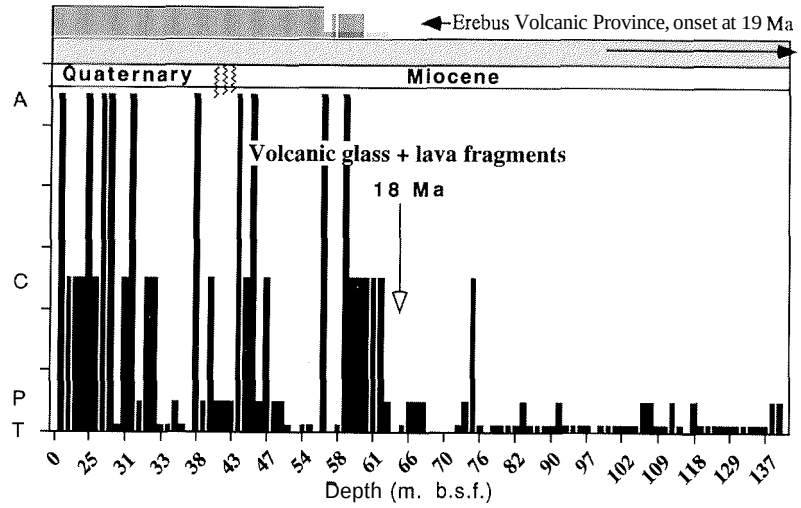

Fig. *13* - Diagram summarising the distribution and relative abundance of volcanic glass and lava fragments in Quaternary and Miocene strata of the CRP-1 drillcore (based on Tab. 7, Quaternary Strata, this volume). The age of subaerial volcanism in the McMurdo Volcanic Group and of Tertiary alkaline plutons (Meander Intrusive Group) are also shown (Kyle, 1990; Tonarini et al., in press), for comparison. The age of the section at which there is a prominent change in abundance of volcanic detritus (at 62 mbsf; c. 18 Ma) is inferred from depth-age correlations described in section on Palaeontology.

(oligoclase, andesine and labradorite, generally fresh but not uncommonly with minor sericite or rare epidote alteration). These typically form 60-80% of the mode. Although most of the quartz grains are angular to subrounded, distinctive sparse (<1%) rounded to well-rounded quartz grains are also present.

Pale green pyroxene is the most common of the *ferromagnesian minerals.* It occurs in two distinctive forms: i) predominantly angular transparent calcic augite crystals lacking other distinctive features and which are most common above c. 62 mbsf; and ii) translucent green, strongly abraded pyroxenes; these are mainly calcium-poor augite, less commonly pigeonite or rare hypersthene. The translucent pyroxenes characteristically have conspicuous dark-coloured, close-set cleavage planes and, less commonly, exsolution lamellae; the dark coloration of the cleavage planes is due to (?)exsolved opaque oxide, which is sometimes developed so extensively that much of the grain is opaque, making it hard to distinguish unambiguously from some lithic clasts. Minor amounts of green-brownish green amphibole (likely hornblende), pink (?titaniferous) clinopyroxene and aegirine are ubiquitous and there are sporadic grains of kaersutite, aenigmatite and possible arfvedsonite. The ferromagnesian minerals form a significant component of most samples, typically 5-10%, which does not vary systematically with depth in the Miocene section.

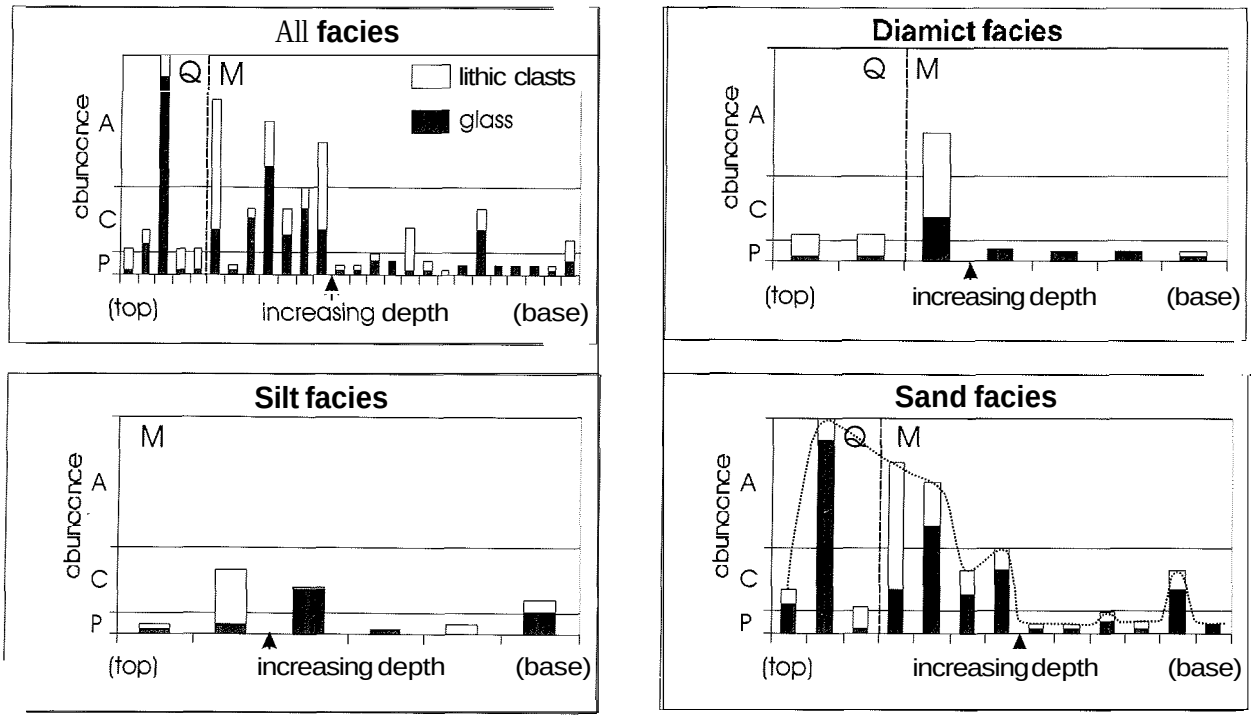

Fig. 14 - Diagrams summarising modal abundances of volcanic lithic and glass grains in Quaternary and Miocene sand-grade samples only, from the CRP-1 drillcore. The data are shown in a summary plot for all sand-grade samples and divided into samples obtained from the three principal facies present in the sequence, in order to illustrate the marked variations in abundance of volcanic detritus between samples from the different facies. Numerical modes are plotted but are expressed in the diagram using the analogue size categories of table 7. Arrow denotes position in drillcore at which there is a prominent change in volcanic-clast abundances (c. 62 mbsf). Abbreviations: Q – Quaternary; M – Miocene. P, C, A – see table 7.

Fragments of *volcanic glass* are a major component of samples above 62 mbsf, diminishing markedly below but present to the base of the section. They are angular, essentially unaltered and vary in colour from brown to pale brown and colourless; some brown glass is oxidised and largely opaque. The fragments often contain feldspar and/or pyroxene crystallites and generally a few tiny ovoid vesicles. With an increasing proportion of crystals, the vitric clasts grade into intersertal-textured volcanic lithic grains (below). Brown glass is overwhelmingly dominant in most samples and is frequently the sole glass type present, but colourless glass may rarely predominate (Tab. 7). There is a striking association between glass content and the lithofacies from which the sand fraction was derived (Fig. 13). Although the data set is small, sandy samples from diamict and siltstone lithofacies show no correlation with depth in the drillhole and the proportion of glass fragments is either uniformly low, or low but variable (diamict and siltstone lithofacies, respectively). By contrast, glass shows a clear association with samples from sandstone lithofacies, with well marked down-hole variations.

There is a wide variety of *lithic grains* present, but they are generally only conspicuous above *c.* 62 mbsf. Grain shapesvary widely but aremainly subangular-subrounded. The most common lithic grains are volcanic, composed of fine-grained pilotaxitic and intersertal lavas containing fresh feldspar laths or pyroxene (augite, titaniferous augite or aegirine) and unaltered brown or colourless glass; they are rarely associated with grains of glassy fine tuff. The volcanic lithic grains are generally a comparatively small but persistent detrital population. Above *c.* 62 mbsf they typically form ≤5%, rising rarely to c. 30%, but below that depth the proportion diminishes to ≤1-2%, and they are apparently absent in several samples. Other lithic types are modally uncommon (typically <<1% individually). They comprise vermicular- and graphic-textured intergrown quartz and K-feldspar; grains with coarse platy plagioclase crystals, or bladed plagioclase with interstitial quartz and/or rare clinopyroxene, the plagioclase showing variable alteration (minor chlorite, epidote); a variety of metamorphic clasts, including fine quartz-feldspar-mica phyllite, coarse and fine polycrystalline quartz and equigranular quartz-plagioclase aggregates.

Other mineral grains include biotite, epidote, magnetite, glauconite, celadonite, zircon and garnet, all of which occur in trace amounts (<<1%) in the sand-grade fraction. *Bioclastic detritus* is ubiquitous, typically trace amounts of fragmented siliceous sponge spicules and radiolaria or diatoms.

Provenance and Temporal Variations

The dominant source for the Miocene strata is the Precambrian and lower Palaeozoic basement (granitoid and metamorphic units) and Beacon Supergroup sedimentary strata, which mainly contributed the abundant colourless grain population, together with biotite, garnet and zircon (Quaternary Strata, this volume - Tab. 6). Although they account for 60-80% of most samples, their respective proportions are unknown. The presence of low-grade phyllite is unusual and noteworthy because the known outcrops of these rocks are small and restricted to areas near the Skelton and Koettlitz glaciers, about 200 km to the south of the CRP-1 drillsite (Grindley & Warren, 1964). Detritus derived from a likely Ferrar Dolerite source are common and persistent. Few fragments of Ferrar Dolerite itself are present, but Ferrar-like pyroxenes dominate the ferromagnesian mineral population. Ferrar-derived grains become less important above 62 mbsf. No clasts of Kirkpatrick Basalt were identified.

Volcanic-derived detritus consist mainly of grains of essentially fresh lava andpyroclasticrocks and brown and colourless glass. The freshness and presence of alkaline volcanic minerals (sanidine, ?titanaugite, aegirine, kaersutite, aenigmatite and ?arfvedsonite), both within the lithic grains and as minerals, are distinctive characteristics indicating likely basaltic (or basanitic) and evolved, peralkaline compositions. The volcanic population is believed to be derived exclusively from an alkalinevolcanic province similar to parts of the McMurdo Volcanic Group (MVG), although subaerial outcrops of the MVG range in age only down to 19 Ma (Kyle, 1990). However, similar volcanic clasts also persist to the bases of the MSSTS-1 and CIROS-1 drillholes, in strata of Pliocene to Eocene age (<36 Ma), indicating a more prolongued history of alkaline volcanism in the region than is suggested by the subaerial outcrops (Barrett et al. 1986; George 1989; Hannah et al., in press).

Whereas the glassy fragments generally show little evidence for abrasion, the lithicvolcanicgrains are variably subangular to subrounded, suggesting different sources and a more prolongued transport history for the latter. Many lithic grains may have been eroded from volcanic outcrops, whereas the glass may represent airfall tephra. The absence of olivine from the heavy mineral fraction (normally present as phenocrysts in basalt-trachyte rocks) is enigmatic, but it may be an indication of the preferential elutriation of denser tephra from eruption columns (see Quaternary Strata, this volume - section on Sand Grains and Provenance). The proportion of total volcanic fragments (lithic and vitric) is dominated by fluctuations in the amount of glassy material present, whereas the proportion of lithic volcanic grains is comparatively constant. This suggests that the volume of glass is linked directly to the airfall distribution of tephra from broadly coeval explosive eruptions. These tephra, from at least two compositionally contrasting sources, would have been widely distributed areally. The abundance of brown glass suggests that basaltic or basanitic centres were more active throughout the Miocene (and Quaternary; see Quaternary Strata, this volume - section on Sand Grains and Provenance), but there were periods when evolved activity may have been dominant. A prominent increase in volcanic detritus takes place above 62 mbsf, and it is also reflected in a marked "step" in the data for downhole sediment porosity and magnetic susceptibility (Background to CRP-1, this volume - section on Core Properties). Unless an unconformity is present (and is otherwise unrecognised), the shift to abundant volcanic detritus in the younger strata suggests either that subaerial eruptive activity may have become widespread at about

that time, or that there was a significant shift in provenance. Miocene volcanic centres were widely distributed in Victoria Land after c. 19 Ma, at least (Kyle, 1990). Prior to that, the only Tertiary alkaline volcanic centres known were probably situated in northern Victoria Land (Tonarini et al., 1997). Similar marked reductions in volcanic input were also described in lower Miocene strata in the MSSTS-1 and CIROS-1 boreholes (Barrett et al., 1986; George, 1989).

PALAEONTOLOGY

INTRODUCTION

The 103-m lower-Miocene, siliciclastic section yielded a variety of microfossils and some macrofossils, encompassing essentially all fossil groups studied on site. Most consistently present are the diatoms, palynomorphs, and foraminifers. Abundances and diversities vary according to group. These fossils provide: 1) age control, 2) a basis for calculating sedimentation rates and establishing regional correlations, and 3) important palaeoenvironmental information on what appears to have been a glaciomarine setting that underwent some significant fluctuations in water depth and proximity to the ice margin. Reworked taxa from older units are noted, though generally in lesser numbers relative to the Quaternary.

Of particular palaeontological interest is the plethora of new marine palynomorph taxa discovered in CRP-1. These are especially noteworthy because this is believed to be the first report from the Antarctic region of any in situ palynomorphs in lower Miocene sediments.

A brief introduction is given here for all microfossil and macrofossil groups. These are then further described in sections below.

Diatoms are among the most prevalent fossils present and include marine (planktonic and benthic) but no fresh- or brackish-water taxa. Their occurrences are discontinuous and, along with their abundances, reflect varying sedimentation rates, cover by glacier tongues or shelf ice, or productivity in an open-marine environment. Recurrence of intervals rich in benthic diatoms suggest fluctuations in water depth to less than 50 m in many intervals. Rare diatom fragments throughout the core denote glacial recycling of marine sediment, but no lower Oligocene or older specimens were noted. Silicoflagellates and ebridians are consistently present in the diatom-bearing intervals. Diatoms provide an age of 17.5 to 22.4 Ma for the lower Miocene section, and an average sedimentation rate estimated to be ~21 m/my.

Foraminiferal assemblages were found in 15 of 45 samples examined. Those between 43.15 to ~120.00 mbsf were mostly barren or contained sparse assemblages with 1-2 species. They occur more consistently in Units 6.3 and 7.1, with an apparent downhole trend toward higher abundances and diversities. Planktonic forms are very rare, which suggests deposition in relatively shallow-water, inshore environments.

The only Miocene calcareous nannofossils were rare, moderately preserved fragments of *Thoracosphaera*, the same calcareous dinoflagellate observed in the Quaternary section (see Quaternary Strata, this volume - section on Palaeontology). Specimens in Sample 103.40 mbsf may be in situ, whereas others in a sedimentary clast from a diamictite at 123.80 mbsf are considered to be reworked.

Well-preserved marine palynomorphs were present and occasionally common in all 28 Miocene samples processed for palynomorphs; species diversity is low to moderate. The majority are considered to be in situ and represent an Antarctic assemblage not previously known to science. The assemblage is dominated by acritarchs, more than 15 of which are new. Prasinophycean green algae are also among the most abundant and consistently occurring palynomorphs. In the Arctic, acritarchs and prasinophyceanalgae are major components of Quaternary deposits and the Holocene marine flora. These occurrences provide a modern analogue for interpreting the Miocene occurrences in CRP-1. Dinocyst assemblages are of low abundance and diversity but consist of protoperidinoid cysts, a form not seen in the Quaternary deposits of the core. This might indicate milder conditions during the Miocene at the CPR-1 drill site. As in the Quaternary section of CRP-1 (see Quaternary Strata, this volume - section on Palaeontology), foraminiferal linings were common in many samples.

Miospores are present in small numbers in most samples, including reworked Permian-lower Mesozoic taxa, which are most prevalent around 70 mbsf. Also present at that level and between 100-120 mbsf are relatively abundant Nothofagidites spp., Podocarpidites spp., and a range of angiosperm taxa that may or may not be in situ.

Macrofossils are rare to sparse but rather homogenous in assemblage composition throughout the lower Miocene. They consist of serpulid (polychaete) worm tubes, echinoid spines, bryozoans, and *Chlamys* (scallop) shells. They seem indicative of silted shelf environments with estimated depths shallower than 100 m, possibly between 20-80 m. The absence of true polar pectinid bivalves (Adamussium) suggest temperatures warmer than present and perhaps warmer than during the Oligocene.

DIATOMS

Methods

Sample spacing for this study of lower Miocene diatoms of CRP-1 is variable, but less than 2 m for most intervals (Tab. 8). All samples were checked initially by examination of a strewn slide of raw sediment. This was prepared by separation and disaggregation in 50 ml water and settling for 1 minute to remove coarse material. A strewn slide was made from the suspended material for a quick check of diatom presence and abundance (Fig. 15; Tab. 8). If warranted, additional concentration was done by sieving through a 25 mm sieve, and in some samples, density separation was performed using a Sodium Polytungstate solution of 2.2 specific gravity, See Harwood (1986, appendix) for description of sieving and other methods used in diatom preparation.

Tab. 8 - Sample intervals for initial Miocene diatom study. Sample intervals are listed with notes on abundance, ecology, biostratigraphically important taxa, and processing techniques. Abundance represents the number of diatom fragments observed in five fields-of-view.

Units	Sample Interval	Abundance	Ecology	Comments	Code	Published Age			Depth Range	Processing Notes
5.1	top of Unit 5.1			below FAD *Actinocyclus ingens*	D1	>16.3 Ma	C5Cn.1n	H&M	44.08 mbsf	
	top of Unit 5.1			below FAD *Denticulopsis maccollumii*	D2	>16.6 Ma	C5Cn.3n	H&M	44.08	
	43.57-43.58	<10	P+B	***in situ*** early Miocene						strewn
	44.08-44.09	<30	P	***in situ*** early Miocene						strewn; sieve
	44.58-44.59	<10	N/A							strewn
	44.93-44.94	<10	N/A							strewn
	45.04-45.14	<10	N/A							FT; strewn;sieve; float
	45.92-45.93	<10	P							sieve
	47.04-47.05	<10	P							sieve
	48.06-48.07	X	N/A							sieve
	48.90-48.91	<10	P							sieve
	50.00-50.01	<10	N/A							sieve
	51.71-51.72	<10	P							sieve
	53.01-53.02	<10	P							sieve
	53.50-53.60	<10	P							FT; strewn; sieve; float
5.2	55.40-55.41	<30	P							sieve
	57.51-57.52	<30	P							sieve
	58.75-58.76	<100	B							sieve; float
	59.58-59.68	<50	B	LAD *T. praefraga*	D3	18.4-18.1 Ma	C5En to C5Dr	Y&A; H&M; H+	59.58-58.75	FT; sieve; float
	59.98-59.99	<50	B							sieve
5.3	62.11-62.12	<50	N/A							sieve
5.4	63.37-63.38	X	N/A							strewn
	65.80-65.81	<100	P+T							strewn
	66.16-66.17	>100	P							sieve
	67.56-67.57	>100	P							strewn
	69.73-69.74	>100	P							strewn; sieve
5.5	72.58-72.59	>50	P							strewn
	74.91-74.92	>100	P							strewn; sieve
	77.05-77.06	>100	P							strewn
	78.15-78.25	<30	P							FT; strewn, sieve; float
	78.61-78.62	<30	B	shallow benthic assemblage						strewn; sieve
5.6	80.12-80.13	<100	P							strewn
5.7	81.41-81.42	<30	P							strewn
	83.29-83.30	<30	P							strewn
	85.21-85.22	<50	P							strewn
	86.85-86.86	<50	P							strewn
	88.81-88.82	<100	P							strewn; sieve
	91.22-91.23	<100	P	LAD *Asteromphalus symmetricus*	D4	18.5	C5En	H&M	88.81-91.22	strewn; sieve

Note: diatom assemblages are classified into general ecological groups, where 'P' =planktonic; 'T' = tychoplanktonic; and 'B' = benthic. Biostratigraphic datums for each taxon are abbreviated as 'FAD' = First Appearance Datum, 'LAD' = Last Appearance Datum, and 'FCAD' = First Common Appearance Datum. Abbreviations in the 'Published Age' column refer to the following sources: B&B = Baldauf & Barron (1991), G&B = Gersonde & Burckle (1990), H = Harwood (1986), Hc = Harwood (1989), H&M = Harwood & Maruyama (1992), H+ = Harwood et al. (1992). and Y&A = Yanagisawa & Akiba (submitted).

Tab. 8 - Continued.

Units	Sample Interval	Abundance	Ecology	Comments	Code	Published Age	Depth Range	Processing Notes
5.8	94.85-94.86	<50	P					strewn
	96.24-96.25	>100	P					strewn; sieve
	98.77-99.78	>100	P					strewn
	99.02-99.12	>100	P					FT; strewn; seive; float
	100.27-100.28	>100	P					strewn; sieve
	101.31-101.32	<100	P					smear
	102.24-102.25	>100	P	FCAD *Thalassiosira praefraga*	D5	20.3 Ma C6r to C6N Y&A; H&M; H+	103.40-102.24	strewn; sieve
	103.39-103.40	<10	N/A					smear
6.1	104.55-104.56	<10	N/A					strewn
	106.44-106.45	<10	N/A					strewn
6.2	108.78-108.79	<10	N/A					strewn
	110.79-110.80	<30	N/A					strewn
	112.46-112.47	<30	N/A					strewn
	114.76-114.77	<10	N/A					strewn
	115.95-115.96	<50	P					strewn
	116.48-116.49	<10	N/A					strewn; sieve
	118.56-118.57	<50	P+T					strewn; sieve
6.3	120.40-120.50	<30	P					FT; strewn; sieve; float
	120.95-120.96	<30	N/A					strewn
	122.73-122.74	<30	N/A					strewn
	123.80 clast	<30	N/A					smear
	123.80 matrix	<30	N/A					smear
	125.51-125.52	<30	N/A					strewn
	127.79-127.80	<50	N/A					strewn
	129.59-129.60	<50	B					strewn
	131.67-131.68	<50	P					strewn; sieve
	134.30-134.31	<100	P					strewn; sieve
	136.85-136.86	<30	N/A					strewn
	138.75-138.76	<50	N/A					strewn
	139.77-139.78	<10	N/A					strewn
	141.48-141.49	<10	N/A					strewn
7.1	141.80-141.92	<100	P+B	LAD *Stephanopyxis spinosissima*	D6	21.9 to 22.6 Ma C6A(?) to C6AAr.3r and at 58 m in MSSTS H; H+	141.80-141.48	FT; strewn; sieve; float
	142.60-142.61	c50	N/A					strewn
	143.73-143.77	<30	N/A					strewn
	145.46-145.50	<10	N/A					strewn
	145.50-145.51	<30	N/A					strewn
	145.72-145.76	<30	N/A					strewn
	146.51-146.52	<50	B					strewn; sieve; float
	146.79-146.83	<100	P+B					strewn; sieve
	147.68-147.69	c100	P					strewn; sieve
	147.69			above LAD *Kisseleviella carina*	D7	<25 Ma (at 145m in CIROS-1) Hc		

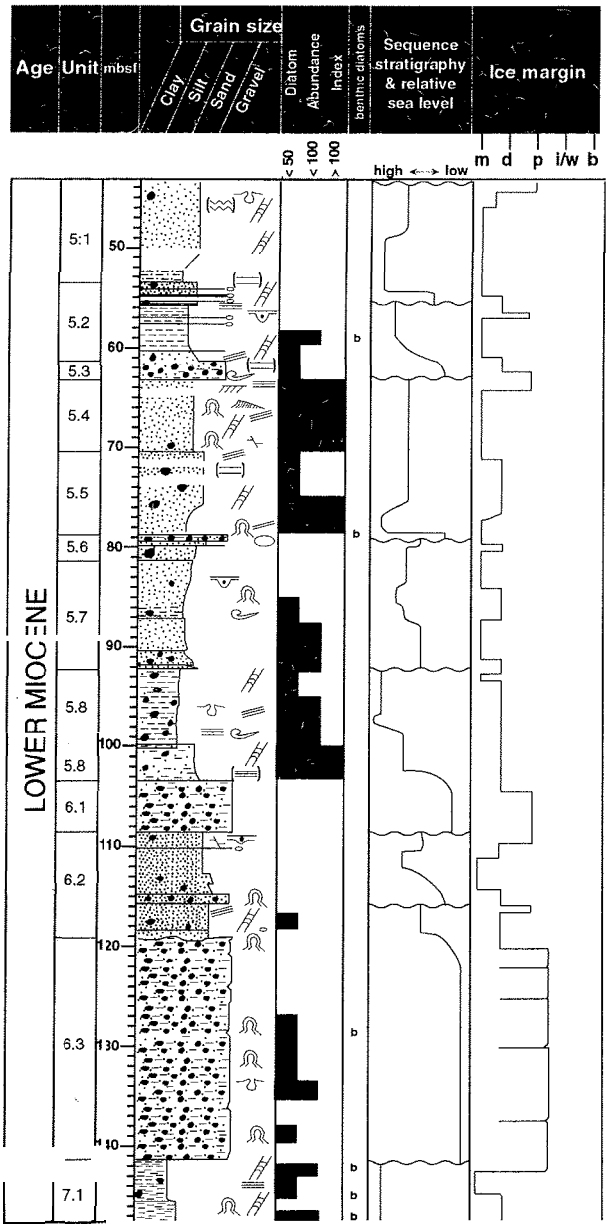

Fig. 15 - Miocene diatom abundance. Relative diatom abundance is plotted with lithological descriptions, lithostratigraphic unit designations, and depositional interpretations. Black bars represent diatom occurrence with increasing abundance to the right. Five fields-of-view were observed (at 250x) in a raw strewn slide of each sample. Data were collected in six categories: barren (X), <10, <30, <50, <100, or >100 diatom fragments per five fields-of-view. Only samples equal to or exceeding <50 fragments are depicted; lower abundance categories most likely represent intervals of diatom recycling, but not production. Most intervals are dominated by open marine plankton, but a few intervals contain rich assemblages of benthic diatoms. These intervals are noted with a lower case "b." There is agreement between high diatom abundance and intervals interpreted to represent high relative sea level, as seen in the lower part of Lithostratigraphic Unit 5.5, within lithostratigraphic Unit 5.8, in the lower part of lithostratigraphic Unit 6.2.

Description of Diatom Assemblages

Diatom occurrence and abundance for the lower Miocene section of CRP-1 is presented in figure 15 and table 8. Marine diatom occurrence is discontinuous throughout this section of CRP-1, with several intervals of high diatom abundance. Diatom absence or low abundance reflects either conditions of ice-cover or extremely rapid sedimentation, where high sedimentation rate and water column turbidity would dilute diatom abundance and limit productivity. Diatom occurrence with more than 50 fragments in 5 fields-of-view at (250x) is interpreted to represent open-water productivity and *in situ* diatom sedimentation (Fig. 15; Tab. 8). Rare diatom fragments are present throughout the core as a result of glacial recycling of marine sediments. In diatom-poor intervals, the diatom assemblages appear to be nearly contemporaneous, eroded locally from lateral correlatives of underlying lithostratigraphic units, or reworked from the upper Oligocene sections reported in the MSSTS-1 and CIROS-1 drillholes (Harwood, 1986,1989). There is no evidence for reworking of lower Oligocene or older Paleogene diatoms into the Miocene sequence of CRP-1. Silicoflagellates and ebridians are common members of the siliceous fossil phytoplankton and occur in most of the diatomaceous intervals.

The Miocene section of CRP-1 includes several ecological associations of marine diatoms. These reflect environmental conditions of variable water depth. A preliminary assessment of diatom assemblage ecology from CRP-1 is presented in table 8. The following characteristic assemblages are noted in order of decreasing water depth: (1) assemblages dominated by pelagic marine planktonic *Coscinodiscus* and *Stephanopyxis* spp., designated *'P'* on table 8; (2) assemblages with high abundance of *Paralia*, a filamentous tychoplanktonic ('T') diatom from the benthic environment, which often occurs in high numbers in the plankton; (3) assemblages with high numbers of a large, unknown triangular-shaped diatom and the benthic genus *Isthmia*, are designated as 'B'; (4) assemblages with increased numbers of benthic adnate *Cocconeis* spp., *Rhabdonema* spp. and *Grammatophora* spp., are designated as 'B'; and (5) benthic assemblages of *Isthmia* and *Arachnoidiscus*, are also assigned 'B'. The association of 'B+P' reflects that benthic diatoms are often transported into deepwater and mixed with open-marine planktonic diatoms. Future research will focus on documenting assemblage changes through the lower Miocene succession as a proxy for relative sea-level, in support of sequence stratigraphic interpretations for CRP-1 (see section on Sequence Stratigraphic Interpretation).

Biogeographic Considerations

As with diatom assemblages and distributions from CIROS-1 and MSSTS, there is considerable difficulty in correlation to Antarctic shelf sequences using established Southern Ocean diatom biostratigraphic schemes (Harwood & Maruyama, 1992). We expect that this results from local environmental effects of temperature, salinity, turbidity, proximity to ice and ice cover, as well as regional paleobiogeographic controls on diatom bioprovinces in the southern high latitudes. Biogeographic barriers appear to have been strong at this time, preventing the southward migration of Southern Ocean zonal taxa such as *Lisitzinia ornata, Rocella gelida, Azpeitia gombosi, Coscinodiscus rhombicus, Rossiella symmetrica,*

Bogorovia spp., *Thalassiosira spumellaroides*, *Hemiaulus taurus* and Nitzschia *maleinterpretaria* (Harwood, 1991). Recoveiy of these pelagic taxa in the CRP-1 interval is interpreted to represent open-rnarine conditions and will enable a correlation between the Ross Sea diatom stratigraphy and that of the Southern Ocean. Also, docunientation of the biostratigraphic ranges of lower Miocene diatoms from CRP-1 will further enable the construction of a zonation for the Antarctic continental shelf.

Diatom Biostratigraphy

Several key diatom biostratigraphic events enable the construction of an age vs. depth model for CRP-1 (Fig. 16). The biostratigraphic data fall in general agreement on a straight line, which is the simplest interpretation. Although this line indicates that no major gaps in time are identified between 43.55 and 147.69 mbsf, small time breaks arc likely to be present. Variations in sedimentation rate are expected but cannot be resolved biostratigraphically at this time. Diatom events, however, enable a relatively precise determination for the lower Miocene section between 17.5 to 22.4 Ma (Tab. 8; Fig. 16). Average sediment accumulation rate during the early Miocene is interpreted to be –21 m/my. This is similar to sediment accumulation rates for the upper Oligocene to lower Miocene sections of CIROS-1 (Harwood et al., 1989a) and MSSTS-1 (Harwood, 1986). Published ages used in figure 16 were converted to the timescale of Berggren et al. (1995).

The absence of *Actinocyclus ingens* (event D1) suggests an age older than 16.3 Ma within anomaly correlative C5Cn.1n (Barron & Baldauf, 1995) at 43.55 mbsf. Both of

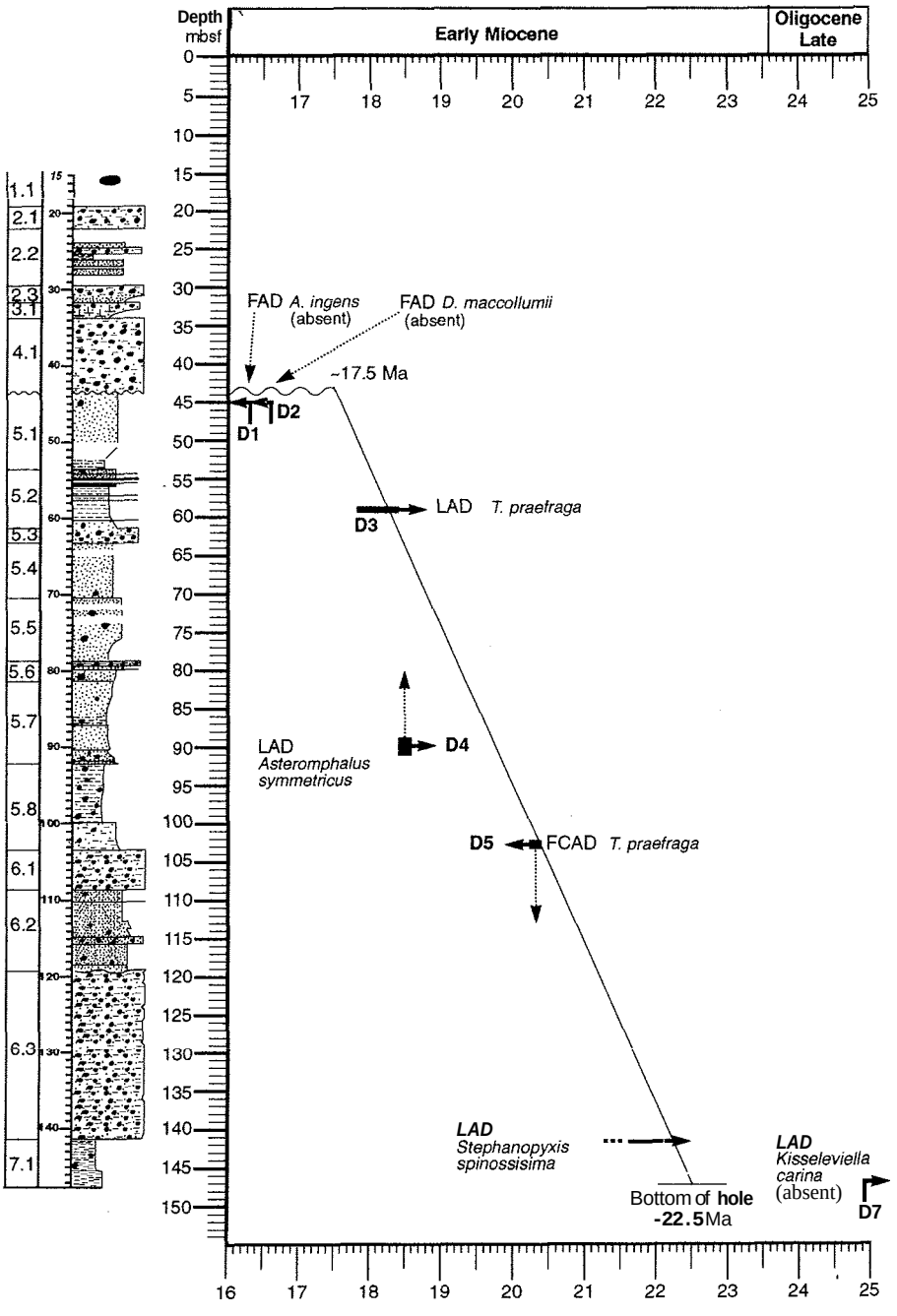

Fig. *16* - Miocene age-depth model for CRP-1. Diatom biostratigraphic datums are plotted at appropriate depths and ages for the Miocene section of CRP-1. Arrows indicate direction of uncertainty due to possible facies or environmental controls on diatom distributions.

these datums approximate the boundary between the lower and middle Miocene. Similarly, the top of the lower Miocene section (at 43.55 mbsf) is older than 16.6 Ma based on the absence of *Denticulopsis maccollumii* (Fig. 16; event D2). This datum occurs within anomaly correlative C5Cn.3n in ODP Site 748 (Harwood et al., 1992), at an age of 16.6 Ma according to Berggren et al. (1995).

The range of *Thalassiosira praefraga* (synonyms: *Coscinodiscus* sp. 1 of McCollum, 1975; *Thalassiosira fraga* of Gersonde & Burckle, 1990, of Baldauf & Barron, 1991, of Harwood et al., 1989a, and of Harwood & Mamyama, 1992) provides two key biostratigraphic datums for CRP-1 - diatom events D3 and D5 (Fig. 16). An age of 18.4 Ma to 17.8 Ma is suggested for depth 58.75 to 59.68 mbsf based on the Last Appearance Datum (LAD) of *Thalassiosira praefraga* (event D3 on Fig. 16). The older age for this datum is derived from Yanagisawa & Akiba (submitted) from the North Pacific. Harwood & Maruyama (1992) record this datum in the Southern Ocean at ODP Hole 751A within the lower part of anomaly correlative C5Dr (Harwood et al., 1992) with an age of 17.8 Ma according to Berggren et al. (1995). Other reports place this datum slightly older within the upper part of C5En (Gersonde & Burckle, 1990; Barron & Baldauf, 1995). This datum defines the boundary between *T. fraga* subzones "b" and "c" of Harwood & Mamyama (1992).

The First Common Appearance Datum (FCAD) of *T. praefraga* (102.24 to 103.39 mbsf) is reported at 20.3 Ma (Yanagisawa & Akiba, submitted) from the North Pacific region. This agrees with a first occurrence in the lower part of anomaly correlative C6n or the upper part of C6r from Antarctic drillholes (Gersonde & Burckle, 1991; Baldauf & Barron, 1991; Harwood & Mamyama, 1992; Harwood et al., 1992). We reinterpret the magnetostratigraphic interpretations of Harwood et al. (1992) for ODP Sites 747 and 748 guided by the above ages for *T. praefraga (T. fraga).* We use the published age of 20.3 Ma for the first common appearance datum of *T. praefraga.* In CRP-1, it first appears as a common element of the diatom assemblages at a level just above lithostratigraphic Unit 6, a diamictite, which is barren of diatoms (Fig. 15; Tab. 8). The presence of this diamictite probably causes a truncation of the lower range of *T. praefraga.* This implies that the age for the FCAD of *T. praefraga* is slightly younger than 20.3 Ma at this depth (see arrow at event D5 on Fig. 16, showing the direction this datum would move if suitable facies continued downcore).

Asteromphalus symmetricus is rare and discontinuous in CRP-1. For this reason, the highest occurrence of this diatom will likely be noted at a level higher than 88.81 to 91.23 mbsf (see arrow on event D4 in Fig. 16) as further examination extends the range of event D4 into higher stratigraphic levels. This datum occurs within the upper part of anomaly correlative C5En in ODP Site 748 (Harwood et al., 1992), at an age of 18.5 Ma according to Berggren et al. (1995).

The LAD of *Stephanopyxis spinossisima* in MSSTS-1 at 58 mbsf (Harwood, 1986) was interpreted by Harwood et al. (1989a) to be within reversed polarity of anomaly correlative C6AA, or possibly C6A. This indicates an age between 21.9 to 22.6 Ma according to Berggren et al. (1995) for the interval from 141.48 to 141.80 mbsf in CRP-1 (diatom event D6; Fig. 16).

The maximum age at the bottom of the hole must be younger than the LAD of *Kisseleviella carina*, which has a highest appearance in CIROS-1 at 145 mbsf (~25 Ma). The absence of this taxon in CRP suggests a maximum age for the bottom of CRP-1 (diatom event D7).

Correlation to Other Lower Miocene Antarctic Sections

The diatom assemblages from CRP-1 resemble diatom floras recovered from diatomaceous sediment clasts within the RISP Site J-9 (82° 22'S; 68° 38'W) cores beneath the Ross Ice Shelf (Harwood et al., 1989b). Lower Miocene sediment clasts contain between 72 to 92% diatoms and little terrigenous debris, reflecting the widespread distribution of diatoms during the early Miocene in the Ross Sea. Diatoms were clearly abundant at this time around the Antarctic margin, yet we know little of them as existing lower Miocene reference sections are limited.

Deep Sea Drilling Project (DSDP) cores in the Ross Sea span the upper Oligocene to lower Miocene in Site 270 and the lower Miocene to middle Miocene in Site 272 (Hayes, et al., 1975). Although these sites were chosen to provide overlap in the recovered sections, a gap of 3 my is interpreted to exist between these sites within the lower Miocene (Steinhauff et al., 1987). Only one sample from DSDP Site 270, Core Interval 13-3, 110-112, contained diatoms (Steinhauff et al., 1987) due to diagenetic alteration of other diatomaceous sediments to opal C-T and opal Q (chert). The intervals in DSDP Site 272 that are correlative to the lower Miocene of CRP-1 are similarly altered to opal C-T in Unit 2B and to opal **Q** in Unit 2C (Hayes et al., 1975).

The distribution of *Kisseleviella carina* in Core Section 13-3 of DSDP Site 270 and its absence in both DSDP Site 272 and CRP-1 (Fig. 16) indicate the gap between the DSDP drillholes may be represented, in part, within CRP-1. The range of *Thalassiosira praefraga* enables a good correlation between DSDP Hole 272 (Cores 20 to 29) (Savage & Ciesielski, 1983) and CRP-1 (102 to 59 mbsf) (Tab. 8).

The lower Miocene succession from CRP-1 probably overlaps slightly with the upper intervals of both CIROS-1 and MSSTS drillholes. Combination of these three sections will provide a composite stratigraphy for the western Ross Sea representing nearly 20 my, from 36.0 Ma to 17.5 Ma. Useful references for taxonomy and biostratigraphy of the lower Miocene include: McCollum (1975), Schrader (1976), Schrader & Fenner (1976), Gombos (1977), Weaver & Gombos (1981), Gombos & Cielsielski (1983), Harwood (1986), Harwood (1989), Harwood et al. (1989a), Gersonde & Burckle (1990), Baldauf & Barron (1991), and Harwood & Maruyama (1992).

Diatom Assemblages

The following presentation and discussion of diatom occurrence in lower Miocene sediments of CRP-1 will

proceed through the division of lithostratigraphic units. Details of abundance and sample depth are presented in table 8. The assemblages of diatoms vary as a result of fluctuating water depth, but in general the samples contain many common taxa. Table 9 lists the diatoms recovered from the lower Miocene succession from CRP-1. Some assemblages contain more than 50 taxa, as indicated in table 9. The composite flora for the lower Miocene of CRP-1 will likely exceed 90 taxa of diatoms, silicoflagellates, and ebridians. The names of many diatoms are still in an informal state. The terms MSSTS, CIROS and RISP refer to informal nomenclature used in the papers by Harwood (1986), Harwood (1989), and Harwood et al. (1989), respectively. These will require formal designation in the future.

Lithostratigraphic Unit 5.1 (43.55-53.70 mbsf), sandstone and mudstone - The diatom fragments present in lithostratigraphic Unit 5.1 are thought to be recycled due to low abundance and poor preservation (fragmentation), except for one sample at 44.08-44.09 mbsf. This sample contains a sparse planktonic diatom flora that is related to lower Miocene assemblages in this drillhole.

Lithostratigraphic Unit 5.2 (53.70-61.51 mbsf), interbedded siltstone, diamictite and breccia - The diatoms in lithostratigraphic Unit 5.2 shift from a benthic assemblage at the base to one reflecting a deeper, open-water environment at 59.58-59.99 mbsf (Fig. 15). Water depth for the lower interval is estimated as less than 50 m or less in this environment, the approximate depth where the euphotic zone would illuminate the sea floor. Diatoms are sparse in the upper two samples in this lithostratigraphic unit.

Lithostratigraphic Unit 5.3 (61.51-63.20 mbsf), diamictite - One sample was examined from this lithostratigraphic unit. The diatoms are highly fragmented and poorly preserved. *Paralia, Stephanopyxis* and *Pseudammodochium* sp. cf. *dictyoides* are present. Pieces of diatomaceous sediment occur as small clasts in the sieved fractions, suggesting a source from existing sediment of a contemporaneous age.

Lithostratigraphic Unit 5.4 (63.20-70.28 mbsf), sandstone - This lithostratigraphic unit contains a rich flora of planktonic diatoms recognized in four of five samples examined. The uppermost sample at 63.37 to 63.38 mbsf is barren of diatoms, except for rare diatom fragments and rare clasts of diatomaceous sediment. Authigenic minerals of dolomite, calcite or siderite are present along with fine grains of mudstone.

Lithostratigraphic Unit 5.5 (70.28-78.85 mbsf), sandstone - This lithostratigraphic unit contains a rich flora of planktonic diatoms, which continues into the overlying lithostratigraphic unit. The base at 78.61-78.62 mbsf was deposited under very shallow water, as indicated by the presence of benthic diatoms and rare planktonic diatoms. The assemblages are highly fragmented.

Lithostratigraphic Unit 5.6 (78.85-81.16 mbsf), diamictite, sandstone and siltstone - One sample was examined from this lithostratigraphic unit. Planktonic marine diatoms are present in relatively high abundance, but are fragmented.

Lithostratigraphic Unit 5.7 (81.16-92.19 rnbsf), siltstone and mudstone - This lithostratigraphic unit contains an assemblage of planktonic diatoms that decrease in abundance upwards.

Lithostratigraphic Unit 5.8 (92.19-103.41 mbsf), mudstone - This lithostratigraphic unit contains a rich assemblage of planktonic diatoms, although the lowest sample at 103.39 to 103.40 mbsf is nearly barren. An assemblage of well-preserved diatoms, with the notable occurrence of *Chaetoceros* frustules, occurs at 91.22-91.23 mbsf.

Tab. 9 - Miocene diatom taxa. List of taxa recorded in the lower Miocene section of CRP-1 in preliminary observations. Assemblages of representative samples are annotated with the following symbols: '#' = Sample 59.58-59.68, '*' = Sample 99.02-99.12, and '+' = Sample 146.51-146.52.

Actinoptychus senarius
Arachnoidiscus sp. A MSSTS #+
Arachnoidiscus spp. *+
Asteromphalus symmetricus *
Auliscus sp. *
Biddulphia sp. +
Chaetoceros setae *+
Chaetoceros spp. #*+
Chrysophycean cysts #*+
Cocconeis antiqua var. tenuistriata #*+
Cocconeis costata #*+
Cocconeis sp. A MSSTS +
Cocconeis sp. D MSSTS #+
Corbisema triacantha +
Corethron spine *
Coscinodiscus oculoides *+
Coscinodiscus oculusiridus #*+
Coscinodiscus radiatus
Coscinodiscus sp. A. MSSTS #*
Dactyliozolen antarcticus
Diploneis sp. +
Distephanus speculum *+
Endictya robusta *
Endictya hungarica #
Entopyla australis var. gigantea #+
Entoplya sp. *
Eunotia grovei +
Gen. et sp. indet. DCIROS-1 #+
Grammatophora charcotii #*+
Grarnmatophora spp. +
Hyalodiscus radiatus var. maximus *+
Hyalodiscus sp. +
Isthmia sp. #*+
Lyradiscus ovalis +
Melosira sp. +
Nitzschia sp. A RISP *
Odontella aurita +
Paralia clavigera #+
Paralia sol var. marginalis #
Paralia sulcata #
Pleurosigma sp. #*
Porosira sp. A +
Pseudammodochium cf. dictyoides #*+
Pseudammodochium sphaericum #
Rhabdonema japonicum +
Rhabdonema sp. cf. R. elegans #*+
Rhabdonema spp. +
Rhaphoneis sp. MSSTS #+
Rhizosolenia hebetatagroup *+
Rhizosoleniapraebarboi +
Rhizosolenia sp. A CIROS +
Septamesocena pappii #*+
Stellarima microtrim #*+
Stephanopyxis grunowii #*
Stephanopyxis sp. C MSSTS #*+
Stephanopyxis spinossisima +
Stephanopyxis spp. +
Stephanopyxis turn's #*+
Stictodiscus hardmanianus #+
Synedra / Fragilaria sp. A CIROS #*+
Synedra jouseana *+
Thalassiosira praefraga #*
Thalassiosira nanseni #*+
Thalassiothrix sp.
Triangle' sp. *A* #*+
Trigonium arcticum #+
Trinacria excavata #*+
Trinacria racovitzae #*+
Trinacria spp. +
Xanthopyxis sp. A RISP +

Lithostratigraphic Unit 6.1 (103.41-108.76 mbsf), diamictite - Two samples from this lithostratigraphic unit contain only rare fragments of diatoms.

Lithostratigraphic Unit 6.2 (108.76-119.28 mbsf), sandstone - This lithostratigraphic unit contains a poor assemblage of diatoms and fragments of diatoms, except for the sample at 118.56-119.57 mbsf, where planktonic and tychoplanktonic diatoms increase in number.

Lithostratigraphic Unit 6.3 (119.28-141.60 mbsf), diamictite - The diatom assemblages within this lithostratigraphicunit arevariable in the different samples, ranging between benthic, planktonic and barren of diatoms (Tab. 8).

Lithostratigraphic Unit 7.1 (141.60-147.69 mbsf), mudstone - A rich assemblage of mixed benthic and planktonic diatoms is present near the top and base of this lithostratigraphicunit. The middle of this lithostratigraphic unit from 145.76 to 143.73 mbsf contains a few diatoms of indeterminate ecology.

FORAMINIFERA

Introduction

A total of 45 samples (7 "fast-track" and 38 routine), covering the interval from 45.04 mbsf to 147.38 mbsf, were examined from the Miocene section of the CRP-1 drillhole, and 15 contained faunas. These samples are listed in table 10. Based on sedimentological and palaeontological studies, the top of the Miocene sequence was provisionally placed at 43.55 mbsf, and the well was considered to be still in Miocene strata when the total depth of 147.69 mbsf was attained.

'Fast-track" samples typically span a 10-cm interval of core, while the routine core samples are smaller, being collected over a nominal 5-cm interval. Routine core samples average about 75 grammes of undried material. Samples were processed using standard techniques, and wet-sieved into >1 mm, >500 p, >63 μ and <63 μ size fractions. After drying, the first 3 fractions were searched for foraminifers and the last reserved for making smear slides or for other studies.

All fossil material, including diatoms, sponge spicules, macrofossil fragments, etc., was recorded during picking, and is listed in table 10, but samples lacking foraminifers are here considered to be non-fossiliferous. In cases where there was a large amount of >63 p residue, the sample was subdivided using a microsplitter to yield at least 2 well covered picking trays of residue for examination; this defines the minimum criterion for determining a sample as non-fossiliferous.

Results

In the discussion below, samples are referred to units defined in the standard lithostratigraphic classification adopted for the drillhole (see Background to CRP-1, this volume - Fig. 18). Unless otherwise noted, samples are cited by only their top depths, and represent a 5-cm interval.

Unit 5 (43.55-103.41 mbsf) - Twenty routine and 5 "fast -track" samples were examined from this interval, with 6 yielding faunas. Foraminiferal abundance was low to very low in all productive samples.

A single sample from Unit 5.1 (sandstone and mudstone; 43.55-53.70 mbsf) contains a few specimens of *Cribroelphidium* sp.

Two of five samples from Unit 5.2 (interbedded siltstone, diamictite and breccia; 53.70-61.51 mbsf) proved fossiliferous, with the following species recorded: *Cribroelphidium* sp. (dominant), *Cibicides* spp., *Pyrulinoides?* sp., *Oolina* sp., *Nodosaria* sp., *Rosalina* sp., and indeterminate agglutinated taxa.

In Unit 5.4 (sandstone; 63.20-70.28 mbsf), a single specimen of *Cribroelphidium* sp. was recovered from 67.60 mbsf. Two other samples from the interval proved non-fossiliferous.

Four of 5 samples from Unit 5.5 (sandstone; 70.28-78.85 mbsf) were unfossiliferous. A sample from 78.15-78.25 mbsf yielded a solitary, well preserved specimen of *Ammoelphidiella* sp. Morphological1y diverse forms composed of equigranuiar particles, observed at 77.45 mbsf, 78.15 mbsf and 78.49 mbsf, are tentatively interpreted as trace fossils, possibly burrow fillings.

Two of three samples from Unit 5.7 (siltstone and sandstone; 81.16-92.19 mbsf) contained sparse assemblages with *Cribroelphidium* sp. and *Ammoelphidiella* sp.

Seven samples, collected throughout Unit 5.8 (mudstone 92.19-103.41 mbsf), all proved to be barren of foraminifers.

Unit 6 (103.41-141.60 mbsf) -Fourteen samples were examined from the unit; foraminifers were recovered from 6 of these.

Only one of six samples collected in Unit 6.2 (sandstone; 108.76-119.28 mbsf) contained foraminifers, with a single, poorly preserved specimen of *Cribroelphidium* sp. recorded from 113.26 mbsf.

Although specimen numbers tend to be very low in Unit 6.3 (diamictite; 119.28-141.60 mbsf), foraminfers occur much more consistently than in overlying units, being present in 5 of 8 samples. This marks the beginning of a trend toward better faunas. Taxa recorded from the unit are: *Cribroelphidium* sp., *Nononiella bradyi, Melonis* sp., *Pyrgo* cf. *fornasinii*, and *Pyrunlinoides?* sp.

Unit 7 (141.60-147.69 mbsf TD) - Foraminifers occur in low-medium abundance, with good to very good preservation, in four of the six samples from this thin unit. The following taxa have been recorded: *Cribroelphidium* sp., *Nonioinella bradyi, Nodosaria* sp., *Pyrulinoides?* sp., and *Pseudonodosaria* sp.

Discussion

The upper part of the sequence (43.15-c. 120.00 mbsf), which includes all of Unit 5, and also Units 6.1 and 6.2, is characterised by samples which are either non-fossiliferous or, less frequently, which contain sparse foraminiferal assemblages with 1-2 species, normally *Cribroelphidium* sp. or *Nonionella* sp. Foraminifers occur more consistently in Units 6.3 and 7.1, with an apparent trend downhole toward both higher abundance and higher diversity. This provides some optimism that more extensive faunas will be

Tab. 10 - Foraminiferal samples from CRP-1 drillhole.

Base	Unit	Forams?	Other fossil material
45.14	5.1	No	spicules
53.6	5.1	Yes	spicules, echinoderm fragments
54.75	5.2	No	
56.83	5.2	No	wood fragments
58.38	5.2	No	
58.61	5.2	No	
59.68	5.2	No	diatoms, spicules, echinoderm & mollusc fragments
65.95	5.4	No	insect? fragments
67.65	5.4	Yes	sponge spicules
69.95	5.4	No	diatoms, spicules
72.65	5.5	No	diatoms
75.99	5.5	No	diatoms, spicules
77.5	5.5	No	trace fossils?
78.25	5.5	Yes	trace fossils?
78.49	5.5	No	trace fossils?
81.87	5.7	No	
85.83	5.7	Yes	diatoms, spicules
87.47	5.7	Yes	diatoms
93.53	5.8	No	diatoms, mollusc fragments
49.49	5.8	No	
96.3	5.8	No	spicules, wood fragments
97.23	5.8	No	spicules, wood fragments
99.12	5.8	No	diatoms, spicules
99.95	5.8	No	diatoms
102.1	5.8	No	diatoms
108.9	6.2	No	spicules
109.2	6.2	No	spicules
111.69	6.2	No	spicules
113.31	6.2	Yes	spicules
116.48	6.2	No	spicules
119.2	6.2	No	spicules
120.5	6.3	No	spicules
123.89	6.3	No	
128.25	6.3	Yes	
129.2	6.3	Yes	echinoderm fragments
131.85	6.3	No	spicules, woodfragments
133.99	6.3	Yes	echinoderm fragments
136.97	6.3	Yes	
141.24	6.3	Yes	
141.92	7.1	No	spicules
142.25	7.1	Yes	diatoms, spicules
142.64	7.1	Yes	diatoms, spicules
144.65	7.1	Yes	echinoderm fragments
145.97	7.1	Yes	echinoderm fragments
147.38	7.1	No	spicules

recovered in subsequent drillholes slightly deeper than the maximum level penetrated in CRP-1.

Two factors may account for the absence of foraminifers in many samples: high sedimentation rate/unfavourable bottom environment and dissolution during diagenesis. It is probable that both have played a part. In some cases, few specimens are recovered, but are well preserved, suggesting dilution by rapid sedimentation. In other instances, specimens are etched, suggesting partial dissolution. Furthermore, many palynological preparations from apparently non-fossiliferous intervals contain common foraminiferal test linings, again pointing to post-depositional removal.

Planktonic foraminifers are very rare in the Miocene section. The only known specimen is a juvenile *Globigerina* sp. indet. (CPS id.), first observed by S. Wise in a nannofossil preparation from 101.31-101.32 mbsf. The specimen is tiny, c. 50 p, and other similar specimens would be unlikely to be retained in foraminiferal residues, which normally cut off at 63 p. The near absence of planktonic types, together with the common occurrence of *Cribroelphidium* and *Nonionella*, suggests deposition in a relatively shallow-water, inshore environment. Increase in abundance and faunal diversity below *c.* 120 mbsf may indicate a trend towards somewhat deeper and more offshore conditions in the older part of the sequence.

Miocene foraminiferal faunas from CRP-1, although less diverse, bear a general resemblance to upper Oligocene-lower Miocene assemblages described by Leckie & Webb (1985) from lithostratigraphic Unit 2 (especially 21 to 2B) at DSDP Site 270. The latter faunas, however, have a much greater offshore aspect. *Ammoelphidiella*, which ranges no higher than upper Pliocene, is common to both sites.

The faunas also are similar to those recovered from lithostratigraphic Units 5, 7, 8, 9 and 15, in the Oligocene to lower Miocene sequence at CIROS-1 (Webb, 1989), and contain an identical form of *Cribrorotalia* sp., as well as having other taxa in common.

MACROFOSSILS

Introduction

Macrofossils plainly visible in the half of the core available for sampling were identified, and potential macrofossil-bearing core-intervals were searched quickly for less obvious body fossils and moulds through the inspection of fractured surfaces. A few macrofossils were also identified within micropalaeontological residues. Macrofossils occur in both unlithified and semilithified sediment, and within concretions at specific intervals throughout the Miocene section.

Macrofossils are rare and sparse within the Miocene section of the core. They were noted in the following intervals:

1 - 46.10 mbsf: serpulid polychaete tubes (concretion: Fig. 17);
2 - 53.50 mbsf: echinoid spines;
3 - 59.58 mbsf: echinoid spines, bryozoan and unidentifiable (bivalve?) fragments;
5 - 62.19 mbsf: *Chlamys* sp., echinoid spines;
6 - 62.34 mbsf: serpulid polychaete tube, ?*Chlamys* sp. and dissolution vugs left after leaching of undetermined macroinvertebrates;
7 - 86.64 mbsf: serpulid polychaete tubes (semi-consolidated concretion);
8 - 95.08 mbsf: serpulid polychaete tube;
9 - 137.66 mbsf: *Chlamys* sp. (imprint only);
10 - 138.82 mbsf: serpulid polychaete tubes, undetermined macrofossils (clast: Fig. 18);
11 - 144.60 mbsf: echinoid spines;
12 - 145.92 mbsf: echinoid spines.

Fig. 17 - Largest serpulid-bearing carbonate concretion (46.10 mbsf).

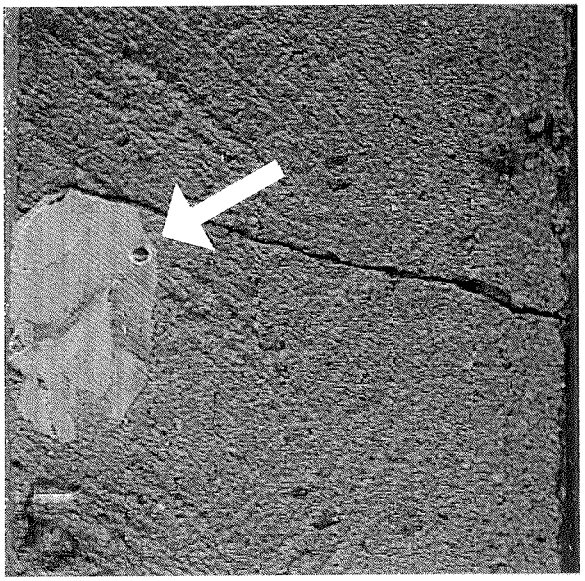

Fig. 18 - Clast of serpulid-bearing (arrow) carbonate concretion (138.82 mbsf).

Taxonomy

Phylum: Mollusca
Class: Bivalvia
Family: Pectinidae

Chlamys (s.l.) sp.

The material consists of two reasonably fresh but broken (by coring) fragments of a rather large and ribbed pectinid shell from 62.19 mbsf, estimated to have been in excess of 6 cm in height (Fig. 19). The incompleteness of this shell (auricles and hinge, as well as a large part of the shell are missing) prevents a more accurate taxonomic assessment. The original shell material is apparently still preserved and may prove valuable for Ss-dating and stable oxygen and carbon isotope analysis for palaeoenvironmental reconstructions, including palaeotemperature. A small shell fragment at 62.34 mbsf and the external imprint left on a muddy sandstone matrix at 137.66 mbsf are believed to belong to this same, probably undescribed, taxon.

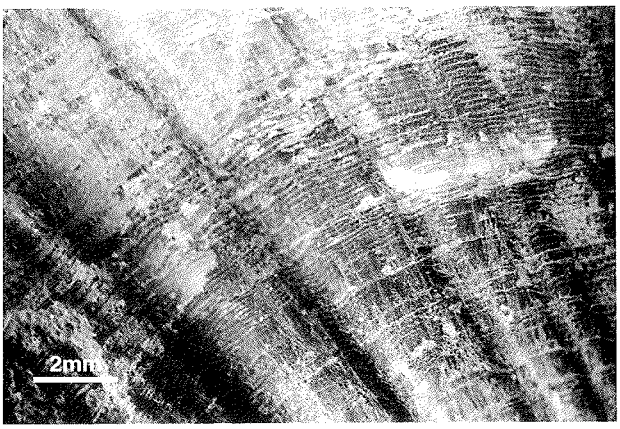

Fig. 19 - Detail of the external ornamentation of the best preserved ribbed pectinid shell (*Chlamys* sp.: 62.19 mbsf).

Phylum: Annelida
Class: Polychaeta
Family: Serpulidae

Serpulid worms, undifferentiated

The material consists of a number of straight or slightly curved, thin walled, conical calcareous tubes (Figs. 20, 21 & 22). A distinct annular ornamentation is obvious in the few, well-preserved specimens (Fig. 23). These tubes are circular in section, although some of them show a variable degree of compression and fragmentation. The largest tube is 17 mm in length, 2.5 mm in width and 0.1 mm in thickness (46.10 mbsf: Fig. 21). Most tubes are filled with sediment that is in places finer than the surrounding matrix. Hollow tubes within concretions are almost invariably recrystallized by late carbonate cement. Pristine tubes, possibly retaining the original shell material, are quite rare (62.34, 95.08 mbsf). These worm tubes belong to an undetermined serpulid polychaete and represent the most common macrofossil remains in the Miocene section of the core. In many cases they occur in concretions. Judging from the recurrence of clutches of individuals, this species appears to have been gregarious in life.

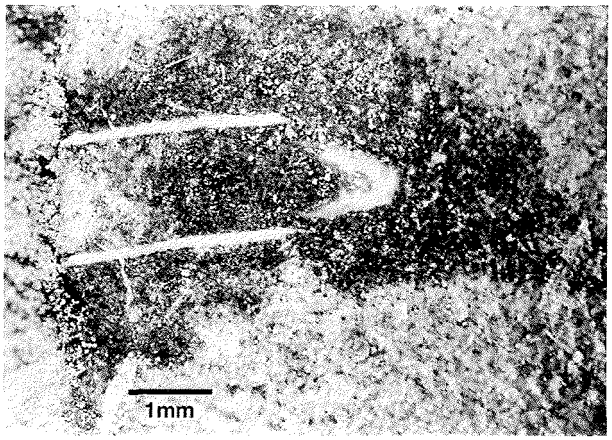

Fig. 20 - Serpulid polychaete tubes from the concretion at 46.10 mbsf; note the circular shape of one uncompressed serpulid tube and the axial section of another one, showing a significant degree of fragmentation.

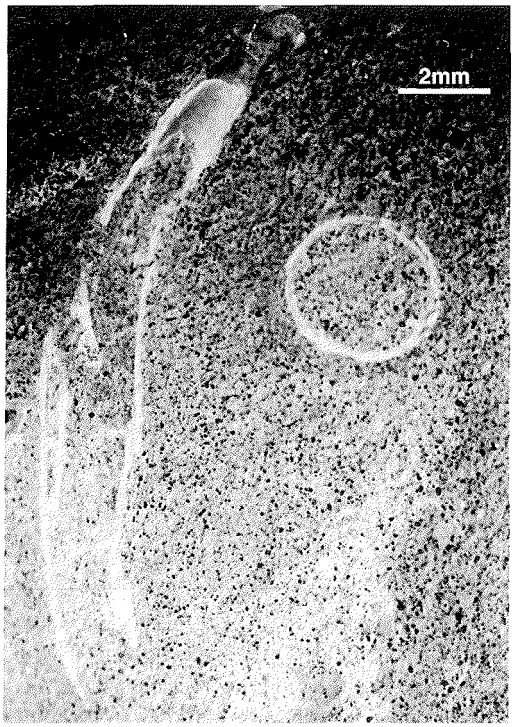

Fig. 21 - The largest serpulid tube (17 cm) recovered in CRPl (46.10 mbsf), showing filling by fine-grained sediment and recrystallization accompanied by precipitation of carbonate cement.

Stratigraphic Distribution

Chlamys sp. from the CRP-1 core bears some analogy with the Miocene *Chlamys* n.sp. (aff. *natans*) from DSDP Site 272 in the Ross Sea described by Dell & Fleming (1975). Serpulids appear to be a fossil marker in the

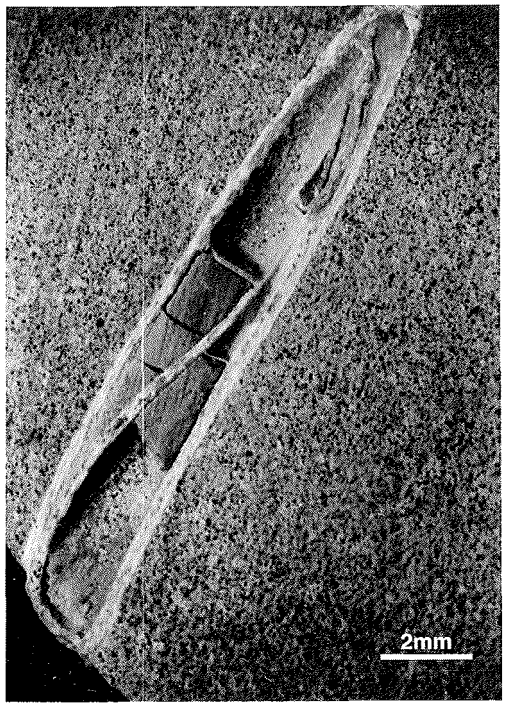

Fig. 22 - Fragmented terminal part of a serpulid tube from a semiconsolidated concretion (86.64 mbsf); note association with dark fine-grained matrix.

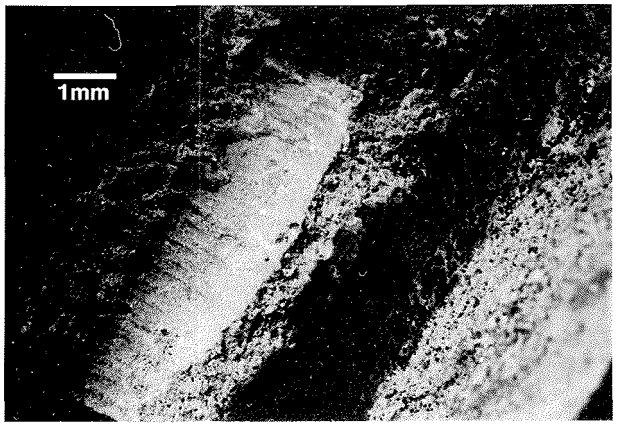

Fig. 23 - Well-preserved serpulid tube showing annular ornamentation (62.34 mbsf).

Miocene section of the core, but their complete biostratigraphic range is unknown. It must be observed that the Miocene taxon does not appear to have analogy with any present-day worm tubes of the Antarctic region but shows instead some affinity with the Miocene worm tubes reported by Dell & Fleming from DSDP Site 270. In conclusion, the macrofossils from the CRP-1 core suggest, although do not prove, a Miocene age for the core interval between c. 46-140 m.

Taphonomy

Most macrofossils appear to have been influenced by *post-mortem* processes. Pectinids are disarticulated and most serpulids are isoriented and parallel to bedding, not in life position.

The Miocene section has been affected by diagenetic processes, principally significant carbonate dissolution. In fact, the most frequent macrofossils, i.e. pectinids and serpulids, are probably diageneticrelics since their calcitic skeletons are quite durable with respect to other calcareous taxa. At places (137.66 mbsf) even pectinid shells are completely dissolved, calling for extreme care in deriving environmental conditions based on absence of calcareous fossils. The presence of non-calcareous fossils, or apparent dominance of monospecific fossil assemblages, may be the result of severe leaching.

It is worth mentioning the rare occurrence of serpulid-bearing calcareous concretions at different stages of lithification. This process seems to have created pseudoclasts (46.10 mbsf: Fig. 17), at times cannibalized within other layers (138.82 mbsf: Fig. 18). Fossils from these concretions were exposed to significant recrystallization, accompanied by the formation of carbonate cements in vugs and fissures.

Palaeoenvironmental Remarks

All recognizable macrofossils are marine invertebrates belonging to extinct taxa, so palaeoenvironmental deductions are necessarily highly speculative. Nevertheless, macrofaunas seem to be indicative of silted shelf environments with estimated depths shallower than 100 m, possibly in the range of 20-80 m. Input of siliciclastic particles may have been very high at times, as suggested by the dominance of gregarious serpulid worms, by analogy with some Recent environments characterized by similar worm-tube assemblages.

The macrofauna seems to be homogeneous throughout the core, a possible indication that the entire lower Miocene section may represent a relatively short time span characterized by the recurrence of rather similar shallow-marine, highly silted environments. During these intervals no ice shelf was likely present in the vicinity, and conditions may have been completely open-marine.

The macrofossils point to warmer-than-present and (possibly) warmer-than-Oligocene seawater temperatures at the time of deposition. This argument seems better supported by the absence of true polar pectinid bivalves (Adamussium spp.), which characterize the Quaternary (Adamussium colbecki Smith) and Oligocene (Adarnussium ? n.sp.) of Antarctica (e.g., Dell, 1990; Beu & Dell, 1989). These were possibly replaced during the Miocene by ribbed *Chlamys* of cold-temperate affinity (Dell & Fleming, 1975).

CALCAREOUS NANNOFOSSILS

Calcareous nannofossils were found in very few of the Miocene samples examined, and these consisted only of rare, moderately to poorly preserved fragments of Thoracosphaera, the same group observed in the Quaternary lithostratigraphic Unit 3.1 (see Quaternary Strata, this volume - section on Calcareous Nannofossils, for a discussion on this occurrence, the specimen preparation, and the nature of Thoracosphaera). As with the Quaternary, no other nannofossil taxa were observed in the Miocene samples.

The most consistent and presumably in situ occurrence of Thoracosphaera was in Miocene sample 103.40 mbsf, where two fragments up to 30x40 mm were noted. Scattered throughout the slide were a few sets of 1-4 thoracosphaerid plates and other calcite debris. These specimens are classified as Thoracosphaera sp. cf. *saxea* in that they have solid plates with few if any pores. They lack, however, well-developed digitations along the plate boundaries as is characteristic of that species. This may be a function of preservation; high-order interference colours up to yellow suggest some secondary calcite overgrowth on the specimens. Two subjacent samples, 104.55 and 106.44 mbsf, had trace amounts of small fragments that may possibly be Thoracosphaera, but these are suspect; there was also no appreciable amount of carbonate in the matrix of those samples.

Thoracosphearid fragments are more numerous, however, in Miocene sample 123.80 mbsf, which is a large sedimentary mudstone clast from lithostratigraphic Unit 6.1, a diamictite. The fragments are few in number, but over a half dozen were noted, ranging in size from 20x24 to 26-40 mm. The matrix is replete with micritic and/or detrital carbonate. The clast has obviously been reworked into the diamictite. ***As*** such, it may represent an older unit and a warmer paleoenvironment if our inferences concerning Thoracosphaera as discussed in Quaternary Strata (this volume) are correct.

The presumably in situ occurrence of Thoracosphaera in Sample 103.40 mbsf is also of interest. It lies directly above the lithostratigraphic Unit 6.1 diamictite and at the base of Unit 5.8, a mudstone. ***As*** such it occurs within a major transgression (see section on Sequence Stratigraphic Interpretation) and in a unit with a diatom abundance index of >100 (see section on Diatoms), which can be interpreted as a maximum flooding surface of the high stand system tract. Overlying Samples 101.31 and 100.27 in Unit 5.8, however, were barren of Thoracosphaera and had no appreciable carbonate in the matrix, thus occurrence is not a consistent characteristic of this unit.

One factor that might govern whether Thoracosphaera will be preserved in sample is the amount of carbonate in the matrix. Wherever this taxon was positively identified in the CRP-1 core, there was a noticeable amount of carbonate, either detrital and/or biogenic, in the sample

matrix. The presence of other carbonate may serve to buffer the pore water fluids sufficiently to prevent dissolution of these microfossils, which otherwise may be destroyed through diagenesis where such fluids are strongly undersaturated with respect to $CaCO_3$.

Other Miocene samples examined for calcareous nannofossils that were barren are (in mbsf): 45.04, 45.92, 47.04, 48.06, 48.90, 50.00, 51.71, 53.50, 54.22, 55.40, 56.29, 57.52, 58.75, 59.58, 62.11, 63.37, 66.38, 69.73, 72.58, 74.91, 77.05, 78.15, 81.41, 85.21, 88.81, 91.22, 913.14, 96.24, 98.77, 99.02, 108.78, 110.79, 112.46, 114.76, 116.48, 119.42, 120.40, 123.80, 125.52, 130.85, 131.67, 138.75, 139.77, 141.48, 141.80, 146.51 and 146.93.

PALYNOLOGY

Marine Microplankton

Twenty-eight samples from between 45.04 and 147.68 mbsf were processed for palynological analysis and their assemblages documented. Of these, seven were "fast-track" samples; the remainder were taken as part of the normal sampling process. Well preserved marine palynomorphs are present, occasionally common in all samples (Tab. 11). Species diversity is low to moderate throughout the drillhole. We consider that the majority of the marine palynomorphs recovered from the Miocene section are in situ and represent an Antarctic assemblage which has not previously been reported,

Most of the taxa included in this assemblage appear to be new and are referred to using open nomenclature. The criteria used in distinguishing selected taxa are given in table 12. A detailed taxonomic study is planned for the second Cape Roberts Project volume. Selected species are illustrated in figures 24, 25 and 26.

As far as we are aware, there have been no previous reports from the Antarctic region of any in situ palynomorphs from sediments younger than early Oligocene in age except for Holocene material. Paleogene palynomorph assemblages are well documented from around the Antarctic (e.g., Wilson, 1967, 1989; Kemp, 1975; Wrenn & Hart 1988; Hannah, 1994, in press). Many are components of an endemic Southern Ocean assemblage referred to as the Transantarctic Flora (Wrenn & Hart, 1988). Reworked members of this assemblage commonly occur in late Oligocene sediments (Truswell, 1986; Wilson, 1989; Hannah, 1994, in press) and were observed in the lower Miocene section of the CRP-1 drillhole.

The Miocene assemblage in CRP-1 is dominated by acritarchs; more than fifteen informal species are listed in table 11. Acritarch species, ?*Sigmopollis* sp, Acritarch sp. 9, Leiosphaeridia sp. 1 and Leiosphaeridia sp. 3 range throughout the Quaternary and Miocene sections of the drillhole. Most other acritarch species appear in a stepwise fashion between 48.35 and 58.43 mbsf. The greatest abundance and diversity of these forms occurs above 99.02 mbsf.

The various species assigned to Leiosphaeridia are the most persistent palynomorph group in the drillhole, being recognised in almost every sample examined. Below 99.02 mbsf, where the other acritarchs disappear, *Leiosphaeridia* often becomes the major component of the palynomorph assemblage. Truswell (1986) also reported the presence of leiospheres in almost every sample examined from the slightly older sediments of the MSSTS-1 drillhole.

Prasinophaycean green algae are present in the core samples (Tab. 11). Cymatiosphaeridium sp. 3 makes its first appearance in the Quaternary section and is consistently present down-section to the base of the drillhole. The large Prasiniophyte *Pterospermella* sp. is sporadically present in the upper part of the Miocene section between 45.04 and 78.75 mbsf.

A low diversity, in situ dinocyst assemblage dominated by species of *Lejeunecysta* was recovered from the Miocene section. In the upper part of the section, Lejeunecysta fallax is present. The last in place appearance of this species marks the topmost Miocene sample examined in CRP-1. The presence of a poorly preserved species of Lejeunecysta at 36.62 mbsf is considered to be result of reworking. Lower in the drillhole two other dinocyst species are prominant. Lejeunecysta sp. 1 differs from Lejeunecysta fallax in being larger in size with a very broad cingulum and a large archaeopyle. *Phelodinium* sp. is also larger than *Lejeunecysta* fallax. It differs from both species of Lejeunecysta by being cavate and possessing more prominent apical and antapical horns.

As in the Quaternary section foraminiferal linings were common in many Miocene samples. Fragments of arthropods and ?scolecodonts were also a minor but persistent component of the in situ palynomorph assemblage.

Reworked, fragmented and hyaline dinocysts are found in several samples scattered throughout the drillhole, but increase in abundance towards its base. Vozzennikovia apertura, the most commonly identified reworked dinocyst, was first encountered at 35.00 mbsf within the Quaternary section. Its highest Miocene appearance is at 58.43 mbsf, and occurs in samples down to 120.27 mbsf. Other forms recognised include Spinidinium *macmurdoense*, Deflandrea antarctica, Alterbidinium sp. cf. *asymmetricum,* Hystrichosphaeridium sp. cf. *latirictum,* and *Operculodinium bergmannii.* The latter species is restricted to the Eocene (Wrenn & Hart, 1988), whereas the remaining species range into the lower Oligocene (Raine et al., 1997). Rare specimens of *Paralecaniella* indentata at 48.35 and 70.02 mbsf are considered to be a result of reworking. Elsewhere this species can range throughout the Tertiary (Wrenn & Hart, 1988), however, in CRP-1 its preservational state is similar to the other reworked material.

Terrestrial Palynology

Miospores are present in small numbers in most samples from the Miocene section (Tab. 13). Neglecting modern contaminants, which can usually be easily recognised (see Background to CRP-1, this volume - section on Palynology Processing), two components can be distinguished, Cenozoic and Permian to lower Mesozoic.

Permian-lower Mesozoic miospores are present in several samples, notably around 70 mbsf. They include

Tab. 11 - Range chart of all Palynomorphs from the Quaternary and Miocene sections of CRP-1. *a) In situ* marine palynomorphs. Shaded samples were not examined for marine microplankton.

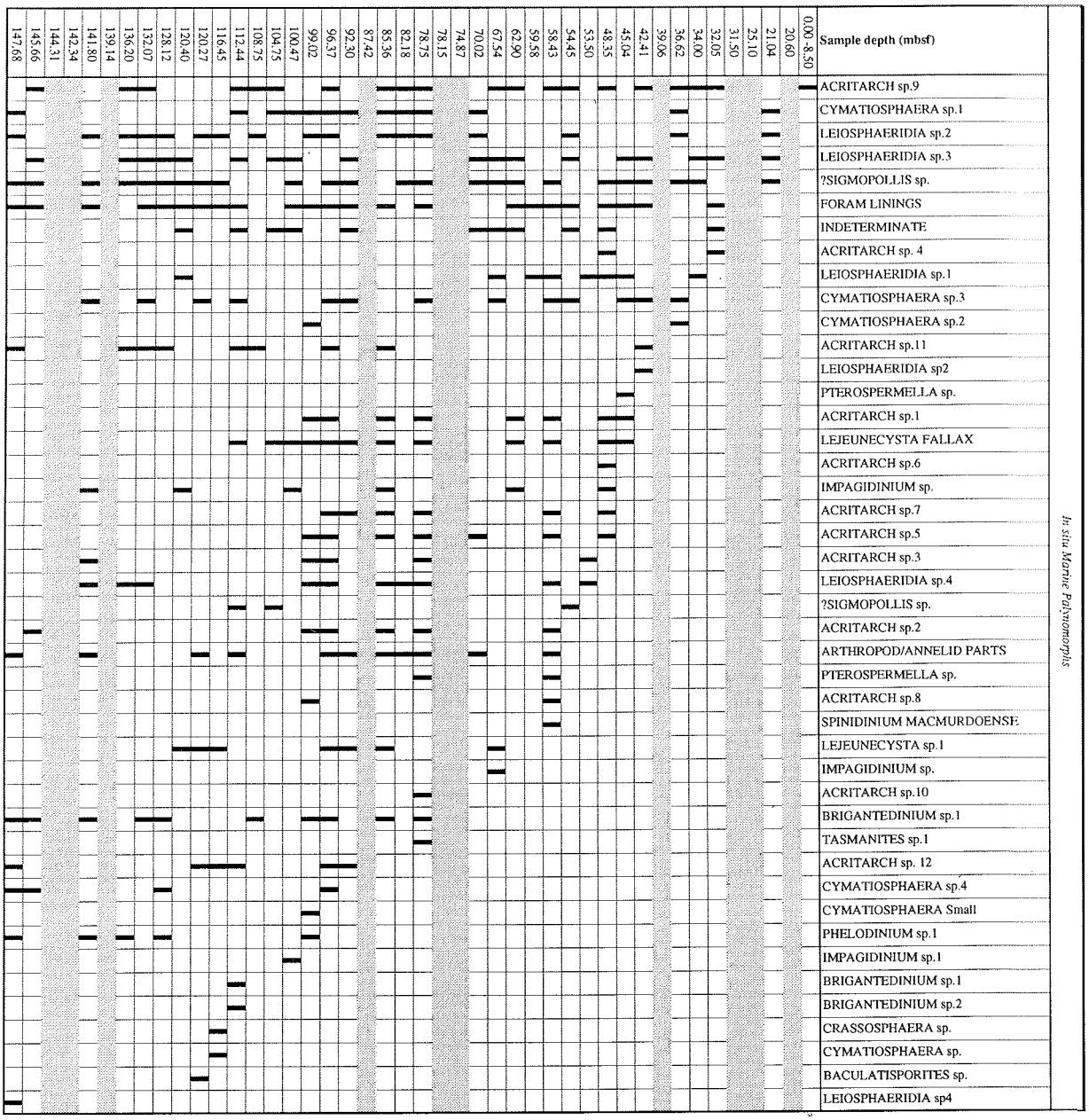

taeniate and non-taeniate bisaccate pollen and a variety of spores. These are noticeably deeper in colour than recognisably Cenozoic specimens, yellow-brown to brown in transmitted light, and display little or no autofluorescence. Commonly, they have adherent deep brown organic material, perhaps kerogen from parent carbonaceous sediments or coals.

The Cenozoic component is generally yellow to light yellow-brown in transmitted light, and has yellow to orange autofluorescence. Specimens are generally moderately well-preserved. In contrast to the apparently monospecific Quaternary sample from 21.04 mbsf, Miocene samples contain a number of Nothofagidites species. With the exception of single specimens of N. *asperus* (menziesii-pollen type) at 116.45 and 120.27 mbsf, all are of the *fusca*-pollen type, and include N. flemingii and *N.* lachlaniae as well as undifferentiated other species.

A distinctive and relatively constant element, prominent in some samples, is Tricolpites sp. a. This tricolpate angiosperm pollen has a tectate wall structure with prominent, commonly grouped columellae. It may be conspecific with Tricolpites sp. 2 of Truswell (1983) and pollen from the Sirius Formation of Oliver Bluffs illustrated by Askin & Markgraf (1986) and compared by these authors with that of Polygonaceae or Labiatae. Mildenhall (1989) referred apparently similar pollen from the lower part of CIROS-1 drillhole to *Perfotricolporites* digitatus Guzman, but the CRP-1 pollen does not have digitate columellae.

Other angiosperm taxa include Chenopodipollis sp. similar to that seen in the Quaternary section, and another periporate pollen with fewer apertures distinguished as Caryophyllaceae. Pollen of Proteaceae is represented by an aggregate of pollen at 99.02 mbsf, and single grains of Proteacidites cf. *parvus* and Triporopollenites ambiguus

Tab. 11 Continued. b) In *situ* terrestrial palynomorphs / marine & terrestrial reworked palynomorphs. Marine species are in caps.

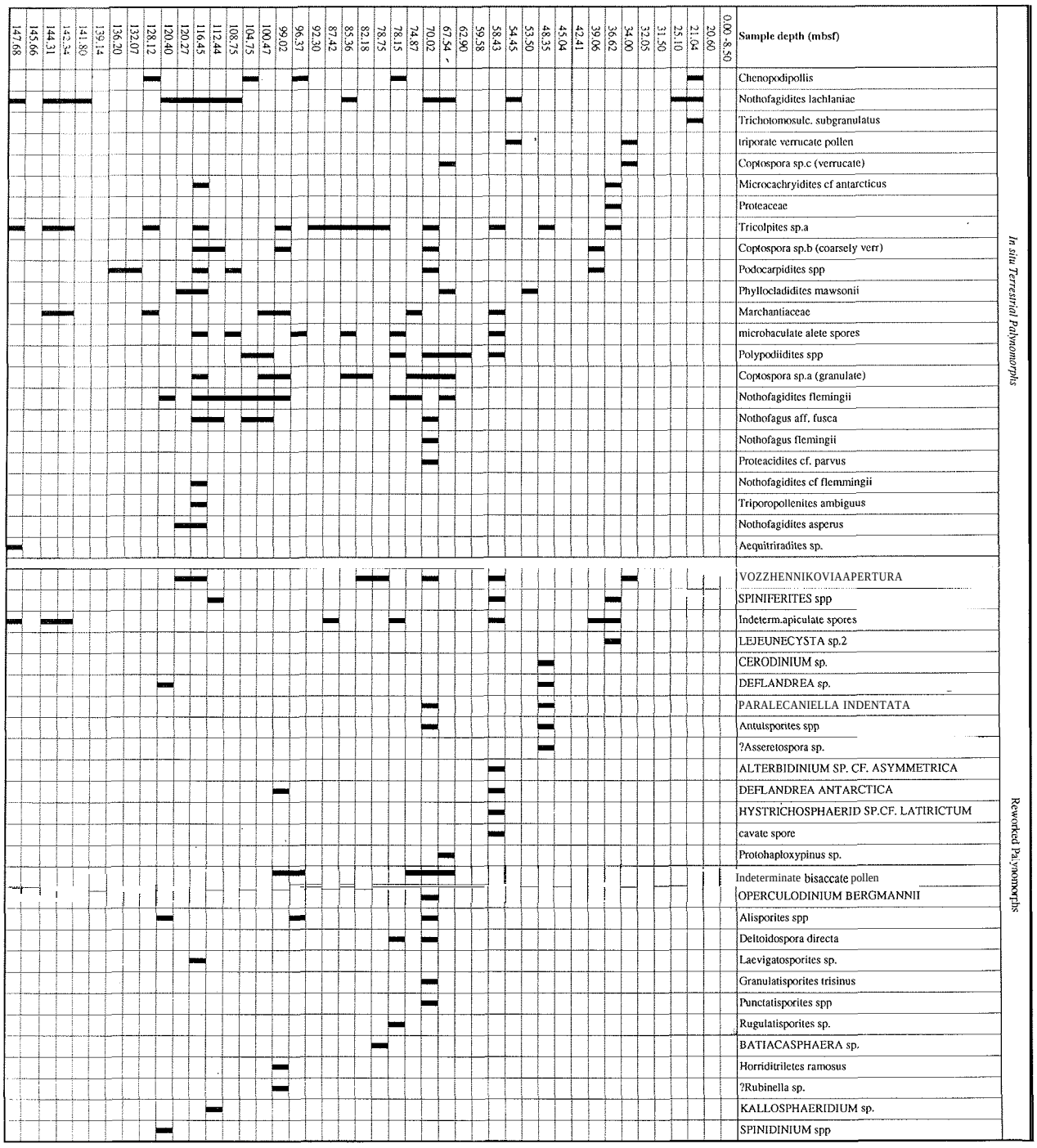

at 116.45 mbsf. The named species are closely comparable to *Triporopollenites* sp. and *T.* cf. T. *ambiguus* illustrated by Mildenhall (1989) from the lower part of the CIROS-1 sequence.

Coniferous pollen is less abundant, and is represented by *Podocarpidites* spp., *Phyllocladidites mawsonii* and *Microcachryidites* sp., all of Podocarpaceous affinity, and *Dilwynites granulatus* (Araucariaceae). Fern spores are represented only by *Baculatisporites disconformis* and *Polypodiidites* sp.

Bryophytic spores comprise a distinctive element of the Cenozoic palynoflora. Marchantiaceae (Hepaticae) are represented at several horizons by an apparently alete (possibly hilate) spore with folded exoexine, similar to spores of *Clevea robusta* illustrated by Erdtman (1957). Hilate spores with single layered wall structure have been referred to *Coptospora* Dettmann. Two species with, respectively, granulate and coarsely verrucate sculpture have been distinguished in the Miocene section, but the diversity may easily be greater. They may represent Hepaticae, as suggested by Dettmann (1963), but as noted in the Quaternary (see Quaternary Strata, this volume - section on Palynology), there is also a close resemblance to spores of the moss *Conostomum*. Folded specimens of the more coarsely verrucate species might be mistaken for spores of *Polypodiidites* Couper. *Aequitriradites* sp.,

Tab. 12 -Characteristic features of selected taxa in open nomenclature. Most of the taxa noted in the core are undescribed, or as yet unattributable by us to known taxa due to the lack of palynological literature on hand for the unexpectedly young section recovered by the con;. The distinguishing characteristics of some of the taxa reported in open nomenclature are given in the informal descriptions below.

Taxa	Characteristics	Figure
Acritarch 1	Subsphcrical-spherical, hollow, thin-walled (< 1µm) ccntral body bearing >100 evenly distributed processes; each process tapers distally to a capitatc termination. Diameter: ~20-25µm. Processes: ~6-8µm long. (Process shape and terminations are distinctive).	25b
Acritarch 2	Medium sized with short noncapitate processes fairly densely distributed over the central body.	25c
Acritarch 3	Similar distribution of spines to Acritarch 2 but with very short conical spines.	25e,f
Acritarch 5	Very short, slightly conical spines widely scattered over the medium sized central body.	25h
Acritarch 6	Numerous fine hair like processes densely covering the central body.	
Acritarch 7	Large very solid blade like spines cover the central body. A very distinctive form.	25i,j
Acritarch 8	Very small central body with 3-4 very long processes radiating away from it. Process terminations are dendritic.	
Acritarch 9	Subspherical. Indistinct amorphous to fibrous outer wall, black, generally thick (~2-6µm) and apparently including many fine fragments within the wall (?composite wall structure); inner wall smooth and thin (<1µm thick). Diameter: ~20-30µm. (The outer wall structure is distinctive).	25k,l
Acritarch 11	Moderate in size, very thin roughly textured wall which is often broken.	
Brigantedinium sp.1	Amber brown cyst; low (<1µm) and narrow (<1µm) surface sculpturing of ridges forming inerlocking lacuna up to 10µm across. Body may fracture into angular sections. Broad hexa 2a archeopyle, asymmetric. Operculum free. Diameter 60-90µm. (Distinctive archeopyle when observable,colour and surface sculpturing).	26a,b,c,f
Cymatiosphaera sp.1	About 12pm in diameter, light yellow central body, wall about 1µm thick. Hyaline membranes about lpm high delimiting at least 11 fields.	25d
Cymatiosphaera sp.3	Smooth brown central body; occasional anastomosing network of lines running over the surface. Hyaline, outer wall forms low (2-9µm) membranes that delimit at least 14 polygonal areas on the surface of the central body. Diameter, overall: 39-55µm; central body: 33-37µm.	
Lewsphaeridiu sp.1	Smooth, thin walled (1µm), spherical, and hyaline leiosphere. A simple lateral rupture or cryptosuture is evident on some specimens. Rarely folded. Diameter approximately 10µm. (Size and hyaline wall is distinctive).	
Lewsphaeridiu sp 2	Smooth, thin-walled (~1µm), hyaline, subspherical to spherical leiosphere. A simple lateral rupture or cryptosuture may be present.Often folded. Diameter ~25µm. (Size and thin hyaline wall are distinctive).	
Leiosphaeridia sp. 3	Smooth, thin-walled (+1µm), subspherical to spherical light yellow leiosphere. No excystment structure evident. Rarely folded. Diameter ~25µm. (Lack of excystment structure, size and color are distinctive).	25j
Phelodinium sp.1	Large, smooth double walled peridinoid. Margins straight to concave between horns. Apical horn long blunt distally; antapical horns also long, distally tapered and rounded, may have solid tips. Antapical horns widely separated. 2a intercalary archeopyle. Cyst 80-110µm long; 62-84µm wide.	26d,g
?*Sigmopollis* sp 1	Medium sized, light yellow, discoidal to subspherical, smooth cyst. Sigmoidal-to-undulate excystment structure in thin wall (<1-1.5µm). A tongue projects from one side of the excystment margin, a matching groove occurs on the other side. Diameter: 32-38µm. (Excystment feature is distinctive).	

recorded only from 147.68 mbsf, is another taxon with bryophytic affinity; Dettmann (1963) has noted similarity to the extant family Sphaerocarpaceae (Hepaticae). Although the taxon is more typical of the Jurassic and Cretaceous, fluorescence colour of the CRP-1 specimen could not be distinguished from that of undoubted Cenozoic taxa.

Palaeoenvironmental Significance - Terrestrial Palynomorphs

As noted above, reworked miospores of Permian or lower Mesozoic age occur throughout the section. Opaque carbonaceous fragments, probably in part derived from Beacon Supergroup coal measures, are abundant. The limited oxidation applied to the CRP-1 samples (10 minutes nitric acid digestion) probably reduced the number of miospores extracted from these fragments, compared to the CIROS-1 and MSSTS-1 drillholes in which an apparently greater diversity of reworked miospores were observed (Mildenhall, 1989; Truswell, 1986). Granulatisporites *trisinus* has been widely recorded from the Permian, but not the Triassic, of southern continents, and it is likely that most of the other taxa are also derived from Permian strata.

Discrimination of younger redeposited miospores is critical to the interpretation of the CRP-1 Miocene miospore sequence. In CIROS-1 Mildenhall (1989) recorded redeposited Jurassic or Cretaceous pollen, e.g., Classopollis classoides (Pflug). Although some of the taxa here classed as "Cenozoic" first appear in the Mesozoic, none are definitely restricted to pre-Miocene strata elsewhere. Neither can precise age assessment can be made from lower range limits of the Cenozoic miospore assemblage. Chenopodipollis spp. are not known from pre-Oligocene strata in Australia or New Zealand (Mildenhall, 1989), but other taxa, where known, first appear in Eocene or older strata.

Mildenhall (1989) considered that much of the CIROS-1 miospore assemblage was contemporaneous with sedimentation, although some could be redeposited from Eocene or Paleocene strata. Contemporaneity was supported by the occurrence of Chenopodipollis, by the presence of pollen aggregates suggesting deposition of anthers and therefore a nearby vegetation source, and by the occurrence of a *Nothofagus* leaf in the upper part of the Oligocene section at 215 m (Hill, 1989). The CRP-1 assemblage, although more restricted, has many taxa in common with that of CIROS-1. An aggregate of Proteaceae pollen occurs in CRP-1 at 99.02 mbsf. Unfortunately the stratigraphic distribution of taxa in CIROS-1 has not so far been tabulated, limiting detailed biostratigraphic comparison.

The occurrence of specimens of Eocene-early Oligocene dinoflagellates of the "Transantarctic Flora" in

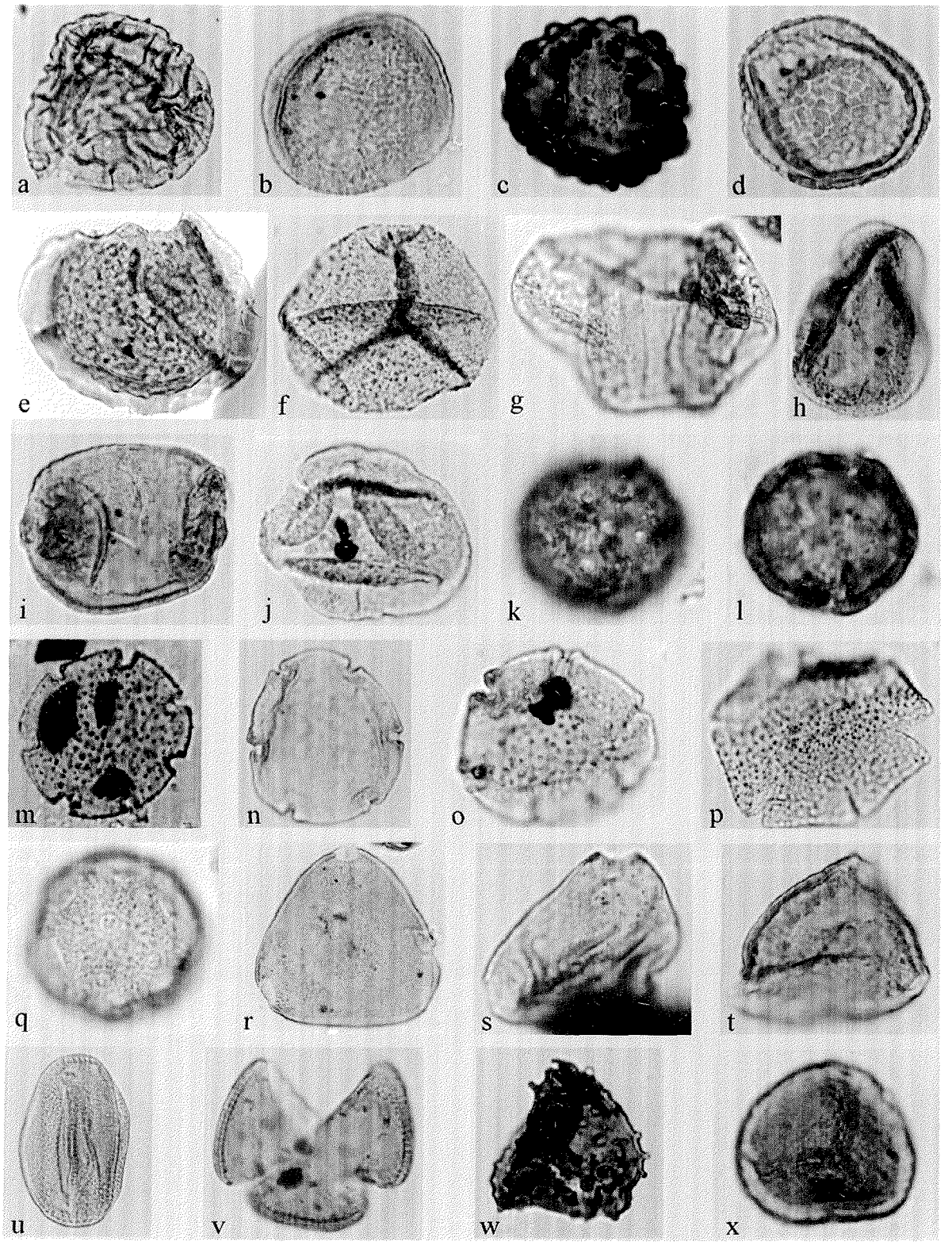

Fig. 24 - Selected miospores from the Quaternary and Miocene sections of CRP-1. Sample depths indicated are the top of the sample interval. Figures are at varied magnifications. "Cenozoic" taxa: *a)* Marchantiaceae (size 88 **p**, depth 99.02 mbsf, slide P12/2, England Finder coordinates C43/2); *b) Coptospora* sp.a (59 pm, 70.02 mbsf, P21/1, X43/0); *c) Coptospora* sp.b (40 µm, 39.05 mbsf, P47/1, L46/1); *d) Coptospora* sp.c (33 pm, 34.00 mbsf, P38/1, E28/1); *e) Aequitriradites* sp. (61 µm, 147.68 mbsf, P45/1, J32/1); *f) Baculatisporites disconformis* Stover (44 pm, 96.37 mbsf, P29/1, C39/3); *g) Podocarpidites* sp. (61 pm, 116.45 mbsf, P34/1, X43/0); *h) Dilwynites granulatus* Harris (46 **p**, 67.54 mbsf, P20/1, T42/1); *i) Phyllocladidites mawsonii* Cookson (41 pm, 67.54 mbsf, P20/1, S40/0); *j) Trichotomosulcites subgranulatus* Couper (33 µm, 21.04 mbsf, P4/1, M32/0); *k, l) Chenopodipollis* sp., two foci of same specimen (21 pm, 99.02 mbsf, P12/1, T47/4); *in) Nothofagidites lachlaniae* (Couper) (33 µm, 21.04 mbsf, P4/1, A52/3); *n) Nothofagidites flemingii* (Couper) (34 µm, 67.54 mbsf, P20/4, V45/0); *o) Nothofagidites* sp. (25 pm, 116.45 mbsf, P34/1, Y42/0); *p) Nothofagidites asperus* (Cookson) (45 pm, 116.45 mbsf, P34/1, X44/0); q) Caryophyllaceae (27 pm, 82.18 mbsf, P24/2, T49/0); *r) Proteacidites* cf. *parvus* Cookson (47 pm, 70.02 mbsf, P21/1, C49/0); *s) Triporopollenites ambiguus* Stover (33 pm, 116.45 mbsf, P34/1, D37/0); *t)* triporate pollen cf. Proteaceae (33 pm, 34.00 mbsf, P38/1, M28/0); *u, v) Tricolpites* sp.a, equatorially and polarly oriented specimens (47x30 pm, 82.18 mbsf, P24/1, Y32/1; 40 µm, 85.36 mbsf, P25/2, F30/0). Redeposited Permian-lower Mesozoic taxa: *w) Horriditrilates ramosus* (Balme & Hennelly) (31 pm, 99.02 mbsf, P12/2, W46/0); *x) Punctatisporites* sp. (38 pm, 108.75 mbsf, P32/2, P48/0).

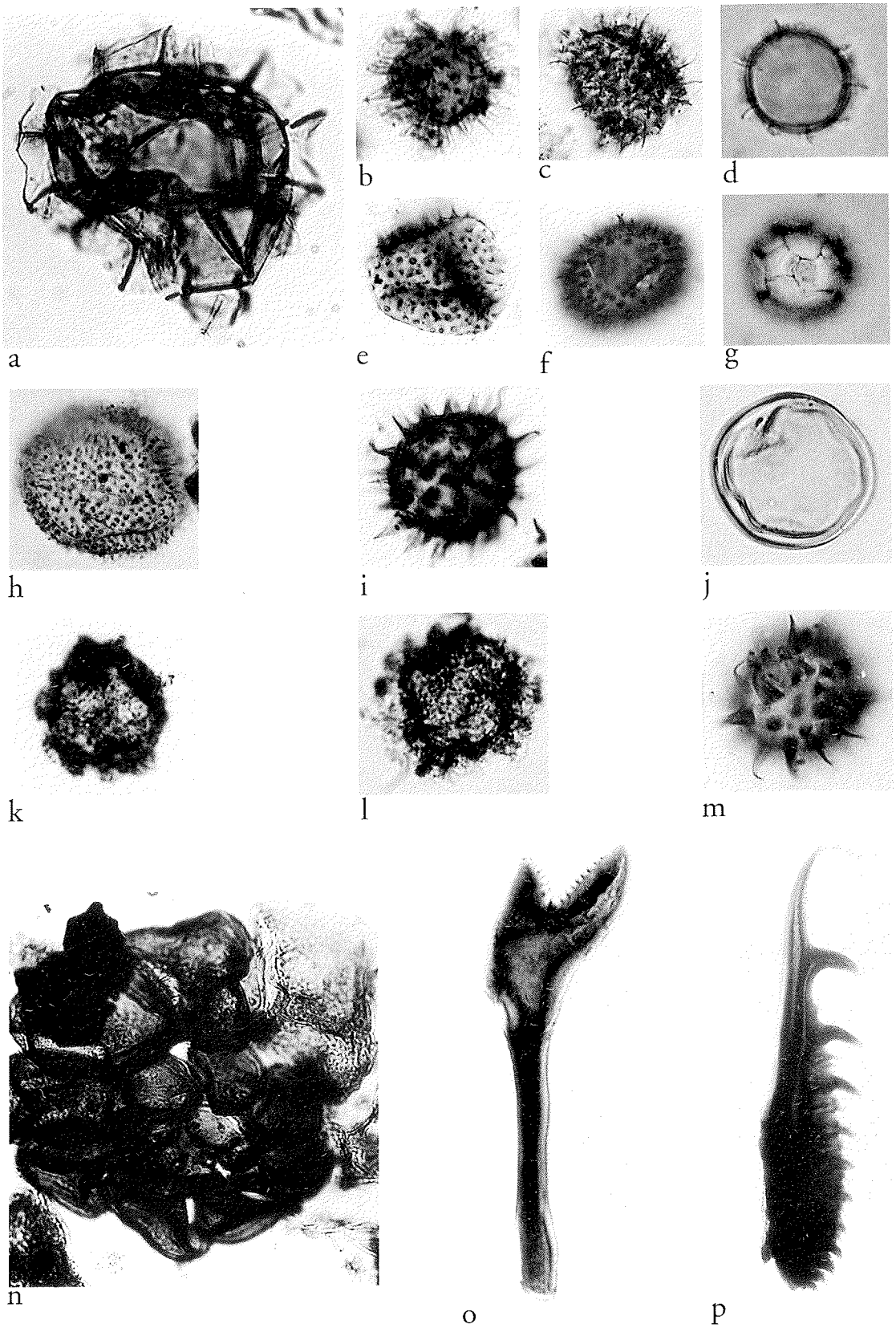

Fig. 25 - Selected palynomorphs from CRP-1. Sample depths indicated are for the top of the sample interval. Figures are a different magnification. a) *Cymatiosphaera* sp. 4 (size 45 mm, depth 96.37 mbsf, slide P29/1, England finder coordinates Y43/3); b) Acritarch sp. 1 (central body diameter: 22 mm, 48.35 mbsf, P13/1, E40/3); c) Acritarch sp. 2 (28 mm, 99.02 mbsf. P12/5, Q53/3); d andg) Cymatiosphaera sp. 1 (11.8 mm. 85.36 mbsf, P24/1, G42); ***e)*** Acritarch sp. 3 (29.5 mm, 99.02 mbsf, P12/5, R51/3); *f)* Acritarchsp. 3 (26.5 mm, 94.02 mbsf, P12/5, N47/4); *h)* Acritarchsp.5 (30 mm, 78.15 mbsf, P16/1, N40/1); i) Acritarch sp. 7 (central body diameter: 17.6 mm, 48.35 mbsf, P13/1, G53/0); *j) Leiosphaeridia* sp. 2 (35.2 mm, 145.65 mbsf, P43/1, S45/1); k) Acritarch sp. 9 (14.3 mm, 48.35 mbsf, P13/1, J47/2); *l)* Acritarch sp. 9 (37.4 mm, 112.44 mbsf, P33/1, U30/3); m) Acritarch sp. 7 (17.5 mm, 85.36 mbsf, P25/1, T51/4); *n)* Foraminiferal lining (154 mm, 48.35 mbsf, P13/1, D46/2); o) Arthropod part (length: 123 mm, 100.47 mbsf, P30/1, P43-3); p) Arthropod part (length:206.5 mm, 78.15 mbsf, P16/2, Y48/2).

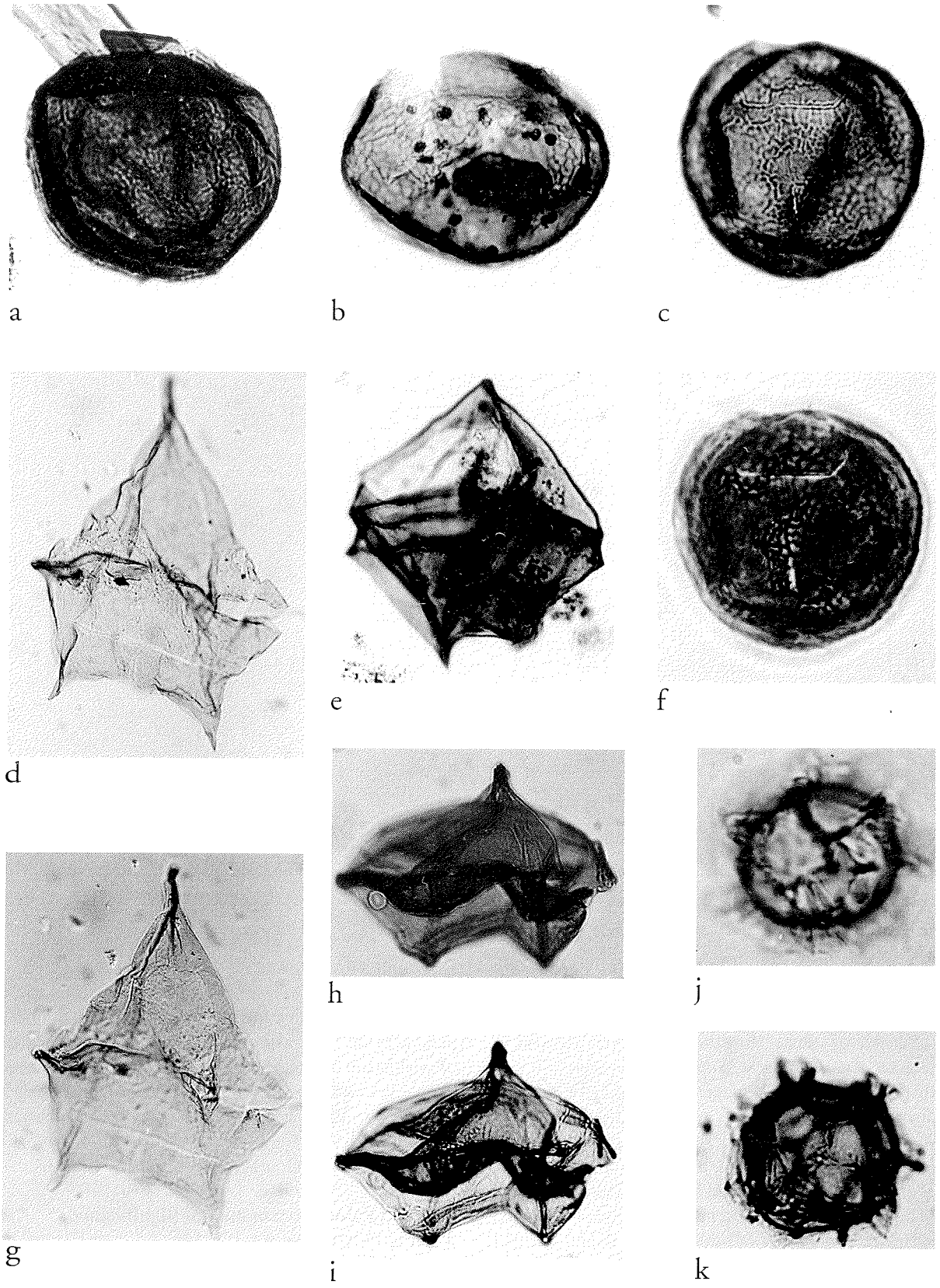

Fig. 26 - Selected palynomorphs from CRP-1. Sample depths indicated are for the top of the sample interval. Figures are a different magnification. *a)Brigantedinium* sp. **1** (size 68 mm, depth 145.65 mbsf, slide P43/1, England finder coordinates D32/2); b) *Brigantedinium* sp. **1** (72.6 mm, 145.65 mbsf, P43/1, E36/0); *c* and *f) Brigantedinium* sp. 1 (68.2 mm, 145.65 mbsf, P43/1, E36/0); *d* and *g) Phelodinium* sp. *1* (112x74.8 mm, 141.80 mbsf, P15/2, V45/4); *e) Lejeunecysta fallax* (70.4x63.8 mm, 48.35 mbsf, P13/1, H33/4); *h* and *i) Lejeunecysta* sp. **1** (94.6x70.4 mm, 120.4 mbsf, P14/1, G36/4); *j) Cymatiosphaera* sp. 2 (39.6 mm, 100.47 mbsf, P43/1, G36); k) *Cymatiosphaera* sp. 3 (44 mm, 100.47 mbsf, P43/1, G36).

Tab. *13* - Terrestrial Palynomorphs from the Miocene section of CRP-1.

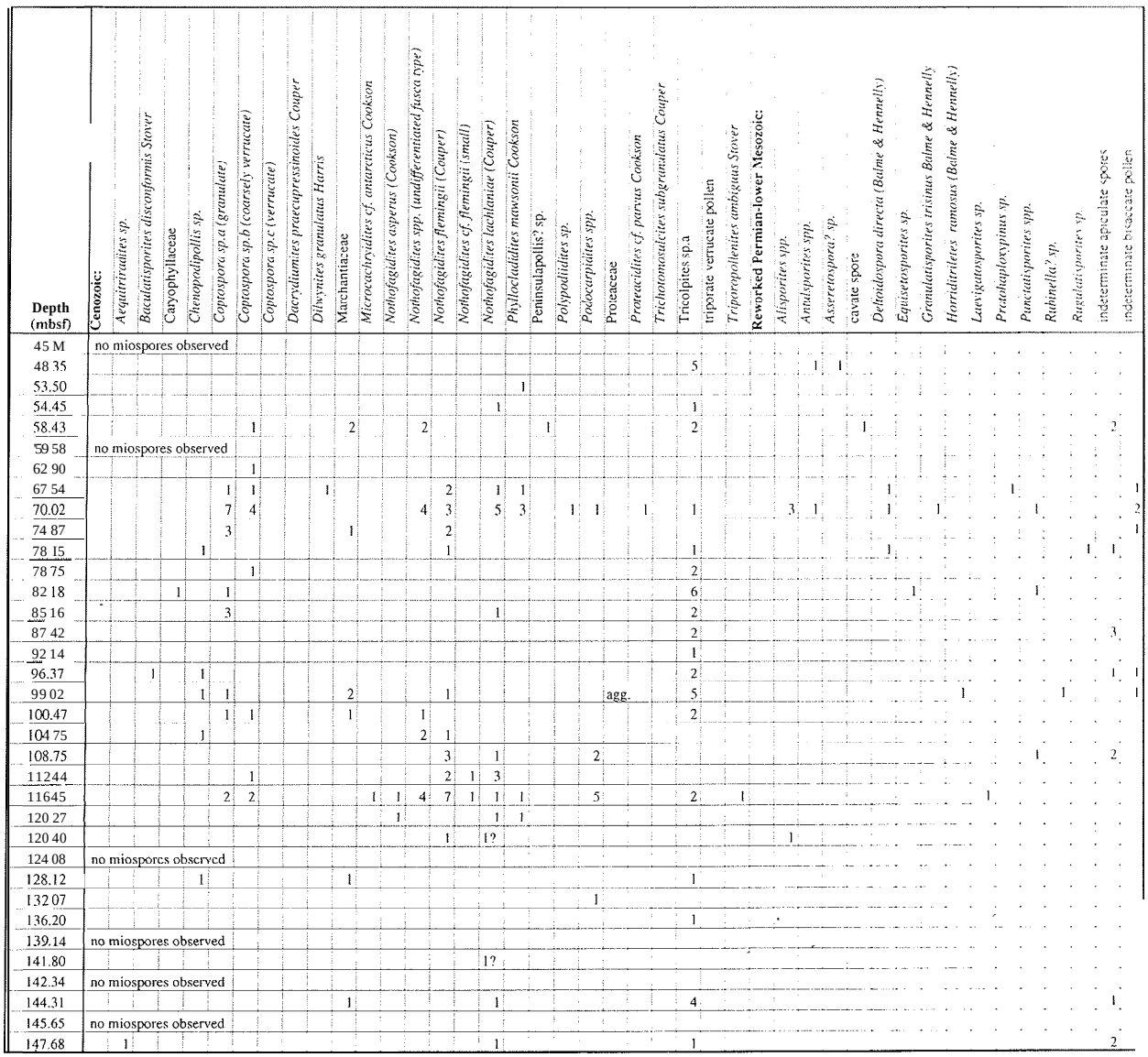

Depth (mbsf)	Cenozoic:	*Aequitriradites sp.*	*Baculatisporites disconformis Stover*	Caryophyllaceae	*Chenopodipollis sp.*	*Coptospora sp.a (granulate)*	*Coptospora sp.b (coarsely verrucate)*	*Coptospora sp.c (verrucate)*	*Dacrydiumites praecupressinoides Couper*	*Dilwynites granulatus Harris*	Marchantiaceae	*Microcachryidites cf. antarcticus Cookson*	*Nothofagidites asperus (Cookson)*	*Nothofagidites spp. (undifferentiated fusca type)*	*Nothofagidites flemingii (Couper)*	*Nothofagidites cf. flemingii (small)*	*Nothofagidites lachlaniae (Couper)*	*Phyllocladidites mawsonii Cookson*	Peninsulapollis? sp.	*Polypodiidites sp.*	*Podocarpidites spp.*	Proteaceae	*Proteacidites cf. parvus Cookson*	*Trichotomosulcites subgranulatus Couper*	Tricolpites sp.a	triporate verrucate pollen	*Triporopollenites ambiguus Stover*	**Reworked Permian-lower Mesozoic:**	*Alisporites spp.*	*Arildsporites spp.*	*Asseretospora? sp.*	cavate spore	*Deltoidospora directa (Balme & Hennelly)*	*Equisetosporites sp.*	*Granulatisporites trisinus Balme & Hennelly*	*Horriditriletes ramosus (Balme & Hennelly)*	*Laevigatosporites sp.*	*Pratahaploxypinus sp.*	*Punctatisporites spp.*	*Rubinella? sp.*	*Rugulatisporites sp.*	indeterminate apiculate spores	indeterminate bisaccate pollen
45 M	no miospores observed																																										
48 35																									5					1	1												
53.50																		1																										
54.45																	1							1																				
58.43							1				2			2					1					2								1										2	
59 58	no miospores observed																																										
62 90							1																																			
67 54						1	1			1					2		1	1														1				1						1
70.02						7	4							4	3		5	3		1	1		1					3	1			1		1			1					2
74 87						3					1				2																											1
78 15					1										1										1							1								1	1	
78 75							1																		2																	
82 18				1		1																			6							1										
85 16						3											1								2																	
87 42																									2																3	
92 14																									1																	
96.37			1		1																				2																1	1
99 02					1	1					2				1								agg.		5													1		1		1
100.47						1	1				1			1											2																	
104 75					1									2	1																											
108.75															3		1					2																			1		2	
112 44							1								2	1	3																										
116 45						2	2					1	1	4	7	1	1	1				5			2		1													1			
120 27													1				1	1																								
120 40															1		1?													1													
124 08	no miospores observed																																										
128.12					1						1														1																	
132 07																						1																				
136.20																									1																	
139.14	no miospores observed																																										
141.80																	1?																									
142.34	no miospores observed																																										
144.31											1						1								4																	1	
145.65	no miospores observed																																										
147.68		1															1								1																2	

CRP-1 Miocene section indicates that concurrent redeposition of miospores of similar age is possible. There is, however no obvious correspondence between occurrences of these dinoflagellates and diversity/ abundance of, for example, Nothofagidites spp.

Inspection of table 12 suggests that it may be possible to distinguish two sources of Cenozoic miospores. Nothofagidites spp., Podocarpidites spp., and a range of angiosperm species occur relatively abundantly at 70.02 mbsf and between 100 and 120 mbsf. This assemblage could be interpreted to represent a Nothofagus-dominated woodland with a variety of other woody plants. Another component, comprising Tricolpites sp. a, Coptospora spp., and Marchantiaceae is more consistently present through the sequence. Both this consistency and the relatively high frequency of Tricolpites sp. a in some samples suggest that it may be derived from a local vegetation of low diversity. Although Gramineae, characteristic of vegetation of the modern Subantarctic zone, are absent, this local vegetation may have been similar in form to that of the present day herb tundra formation of the Cool to Cold Antarctic zones distinguished by Greene (1964). This formation, rich in bryophytes but with a low diversity of vascular plants, is present in the coastal Antarctic Peninsula, and islands near or within the boundary of the Antarctic Convergence. If this vegetation represents a climatic climax, then the Nothofagus-dominated vegetation may represent warmer climatic intervals, long distance transport, or reworking from Oligocene and/or Eocene strata.

Age and Palaeoenvironmental Significance - Marine Palynomorphs

Because most of the marine palynomorph assemblage is either new or reworked, little can be added to the age determination of CRP-1 provided by the diatoms (see Quaternary Strata & Miocene Strata, this volume - section on Diatoms). However, the consistent presence of the dinocyst Lejeunecysta fallax indicates an age of no younger than middle Miocene

for the section below 45.04 mbsf, which is consistent with the ages provided by the diatoms.

The most abundant and consistently occurring palynomorphs in the Quaternary and Miocene sections of the core are acritarchs and phycoma of prasinophycean green algae. Also present are low diversity, low abundance dinoflagellate cyst assemblages but these are restricted to the Miocene interval. Many of these taxa are undescribed and contributed little to dating the core. However, they are of paleoenvironmental significance because they parallel northern high latitude Quaternary-Holocene assemblages.

Acritarchs, particularly leiospheres, are a major component of some modern sea-ice alga assemblages and of Arctic Quaternary-Holocene deposits. Studies of sea-ice margins on the Beaufort and Barents shelves showed that *Leiosphaeridia* were most abundant at the contact margin between the pack ice and the seasonal ice. Here, they constituted 20-70% of the plankton assemblages that also included dinocysts, archaeomonads and prasinophytes. Other acritarchs, such as Cyclopsiella, *Halodinium*, Beringiella and *Sigmopollis*, are commonly reported from these settings, as well as from Arctic estuaries (Mudie, 1992).

Prasinophycean algae, particularly Cymatiosphaera, are abundant in the normal to low salinity, nutrient-rich waters that upwell off northeastern Greenland and in North Baffin Bay (Mudie, 1992). *Pterosperma* occur in low salinity, stratified water layers in Arctic fjords, though they are more commonly found in oceanic water masses (Mudie, 1992). Prauss & Reigel (1989) suggested that fossil prasinophycean algae preferred very low salinity and low temperature conditions. This was based on the paleogeographic distribution, the inferred paleoclimates, and the very low delta ^{13}C values of the prasinophycean phycoma of these deposits.

Comparable trends have been reported for protoperidinioid marine dinocysts which dominate Neogene-Holocene cold water Arctic assemblages. Protoperidinioids are heterotrophic, non-photosynthetic dinoflagellates (Fensome et al., 1993) that generally produce brown to dark brown cysts.

Quaternary-Holocene glacial sediments in ODP 646, in the Labrador Sea, were dominated by cysts of *Brigantedinium* (De Vernal & Mudie, 1989b), a typical protoperidinoid cyst of the region, as were Holocene glaciomarine sedirnents in Norway, Arctic Canada and Svalbard (Dale, 1996). Protoperidinioid assemblages recovered from Miocene deposits of ODP 647 cores from Baffin Bay were well developed in settings interpreted to have been influenced by: 1) high river discharge, 2) falling sea level, 3) cold currents, or 4) ice cover (Head et al., 1989b).

Dale (1996) observed that protoperidiniacean heterotrophs are typical of cold Arctic waters and are dominant in upwelling areas due to high nutrient input that supports a rich phytoplankton community, the prey of the heterotrophs. Others also have noted the dominance of heterotrophic protoperidinioids in polar regions (based primarily on studies in the Arctic) and that they are limited by light and salinity (Taylor, 1987; Mudie, 1992), rather than by a shortage of nutrients as is often the case with photosynthetic dinoflagellates in other areas.

Recent studies have shown that the Antarctic annual sea ice, including that in the Ross Sea, provides shelter and a growth substratum for a complex microbial community, including microalgae (see Knox, 1992, for a review of this research). Much of this microalgae occurs within the lower layers of the sea ice, often in brine pockets. When the sea ice breaks up and melts, the niicroalgae are released into the water column, becoming a rich source of nutrients for heterotrophs, including protoperidinoid dinoflagellates. This enrichment of surface waters with nutrients from above, rather than below as is the case with upwelling, might be called "downwelling". Vast plankton blooms are initiated by "downwelling" along the annual ice margin and within the dispersing pack ice during the Austral summer.

Overall, these reports indicate that acritarchs, prasinophytes and protoperidinioid dinocysts are abundant today in sediments deposited under nutrient-rich, cold waters of normal to slightly low salinity, often in association with pack and seasonal sea ice. This has been documented in widely separated areas of the Arctic and is inferred for the Antarctic seas considering the algae blooms noted above. These associations provide an initial model for understanding comparable palynomorph assemblages from the CRP-1.

The in situ dinocyst assemblages in CRP-1 are low in diversity and dominated by species of *Lejeunecysta* spp., *Phelodinium*-1, and *Brigantedinium* spp.; all of these are protoperidinoid cysts. Additional study of the core samples, particularly with regard to the acritarchs, is required before a detailed paleoenvironmental interpretation can be proposed. However, initial interpretations are possible.

In situ dinocyst assemblages are well developed in samples at 48.35 mbsf, within the interval between 85.36-100.47 mbsf, and especially in the lowermost sampled interval (141.80-147.68 mbsf). The marine environment was favorable for the development of the heterotrophic dinocyst assemblages during the time that sediments in these samples were deposited. Conditions may have included:

- relatively warmer, though still cold, water temperatures;
- seasonal melting of sea ice and open-pack ice;
- lower salinity surface water conditions, and
- high phytoplankton productivity, perhaps initiated by "downwelling" of the sea-ice microbial community during sea-ice break up.

The absence of these, or comparable younger protoperidinioid taxa, from Quaternary samples may indicate that sharply harsher conditions prevailed than during the Miocene.

PALAEOMAGNETISM AND MINERAL MAGNETIC PROPERTIES

INTRODUCTION

The goal of this work was to provide an initial characterization of the palaeomagnetic and mineral magnetic properties of CRP-1 and to develop a preliminary magnetic polarity zonation for the core. The laboratory

facilities and equipment used in this study are described in Background to CRP-1, section on Palaeomagnetic Laboratory (this volume). In the Quaternary interval (c. 19-43 mbsf), the lithofacies are dominated by coarse-grained sediments (including diamictons) that are poorly consolidated and extremely fractured. Because of difficulties in obtaining coherent samples, this part of the core was deemed unsuitable for palaeomagnetic sampling. Preliminary biostratigraphic analyses indicate that the remainder of the core (c. 43-148 mbsf) is likely to be early Miocene (c. 17.5-22.3 Ma) in age (see section on Diatoms). This interval is more consolidated and less fractured than the Quaternary interval and is dominated by generally finer-grained lithofacies. All of the palaeomagnetic samples discussed in this report come from the lower interval.

SAMPLING

Standard palaeomagnetic samples (25 mm diameter x 22 mm height) were drilled using a modified drill press (see Background to CRP-1, this volume - section on Palaeomagnetic Laboratory). Sampling was achieved by selecting the interval of core to be drilled, removing the appropriate core section from the core box, and placing the section on a tray with the flat surface down. Orientation with respect to vertical was maintained by marking the outer surface of the core to indicate the upward direction. The orientation of the sample was preserved by centering the drilling on this mark. Azimuthal orientation of individual core sections was not maintained because there are frequent core breaks; in addition, concentric (circumferential) markings on the upper and lower surfaces of intact pieces of core indicate that many parts of the core underwent substantial rotation within the drill barrel. Lack of azimuthal orientation does not pose a problem for magnetostratigraphic studies because the field has a steep inclination at the high latitude of the CRP-1 site. As a consequence, this parameter is sufficient to uniquely determine polarity (*i.e.*, negative (upward) magnetisations correspond to normal polarity; positive (downward) magnetisations correspond to reversed polarity).

Our preferred strategy was to sample the CRP-1 core at an interval of 0.5 m. This strategy was adopted to preclude missing any short polarity intervals due to inadequate sampling. As noted above, the time interval represented by CRP-1 is estimated to be 17.5 - 22.3 Ma. In this interval, the shortest polarity intervals occur between 21.7 and 24.2 Ma (Fig. 27) and have a duration of 50 - 300 ky (Cande & Kent, 1995). For a uniform sedimentation rate, the above strategy would result in samples which are spaced at 20 - 25 ky intervals. However, the sedimentation rate is not necessarily uniform and, more importantly, this level of sampling was not possible in some parts of CRP-1. The lower sampling resolution in intervals of unsuitable lithology could cause problems if they correspond to portions of the Magnetic Polarity Time Scale (MPTS) that have high reversal frequency and short polarity intervals, such as the interval from 21.7 to 24.2 Ma.

One hundred and fifty five samples were collected from the interval between 58.80 and 147.56 mbsf. Fourteen pairs of samples, each separated stratigraphically by a few cm, were collected at regular intervals from varying lithofacies through-out the core. These samples were used for a pilot study, which was aimed at determining the most suitable demagnetisation technique for routine treatment of the samples.

Diamictites comprise a significant part of the interval between 58.80 and 147.56 mbsf. Whenever possible, samples were selected from fine-grained horizons within this interval; however, there was often no alternative lint to sample diamictites or sandstone-dominated lithofacies. The diamictite matrix is often silt-sized and, therefore, potentially useful for palaeomagnetic study. However, very coarse sand grains, granules and pebbles within samples from diamictites pose a problem because the deposition of such large particles would be controlled by gravitational rather than magnetic forces. Thus, their orientation could not be expected to represent the geomagnetic field at or near the time of deposition. This problem would be most severe for strongly magnetic basic igneous material, which is a common clast constituent in the core. The presence of such grains means that care should be taken in interpreting palaeomagnetic data from coarse-grained intervals.

During sampling, x-ray images of the CRP-1 core were used to identify clast-free intervals. However, this method was not ideal in that acidic-igneous clasts were not detected because they have the same x-ray density as the quartzo-feldspathic matrix. The possible presence of clasts was taken into account by adopting a conservative interpretive approach within coarse-grained lithologies. After magnetic measurements were completed, such samples were examined to determine the presence of clasts. Results from such samples are considered reliable only if no clasts are visible within a sample, if the palaeomagnetic inclinations are consistently steep throughout coarse-grained intervals, and if the results from these intervals are consistent with results from surrounding finer-grained intervals.

Measurements

All measurements of natural remanent magnetisation (NRM), including measurements after each stepwise alternating field (AF) and thermal demagnetisation step, were performed with the AGICO spinner magnetometer (see Background to CRP-1, this volume - section on Palaeomagnetic Laboratory). Approximately 20% of the samples were either too friable or too weakly magnetised to measure with a spinner magnetometer. These samples will be measured at a later date with a cryogenic magnetometer in Rome.

The study of the palaeomagnetism of the CIROS-1 core (Wilson et al., 1998) was undertaken to constrain the chronology of that core as well as to provide experience with handling material that was expected to be analogous to the Cape Roberts cores. The results from the CIROS-1 core clearly indicated how samples should be treated to obtain high-quality data. However, the material in the CRP-1 core is of different age from the CIROS-1 core and may have a different provenance. For these reasons, a new

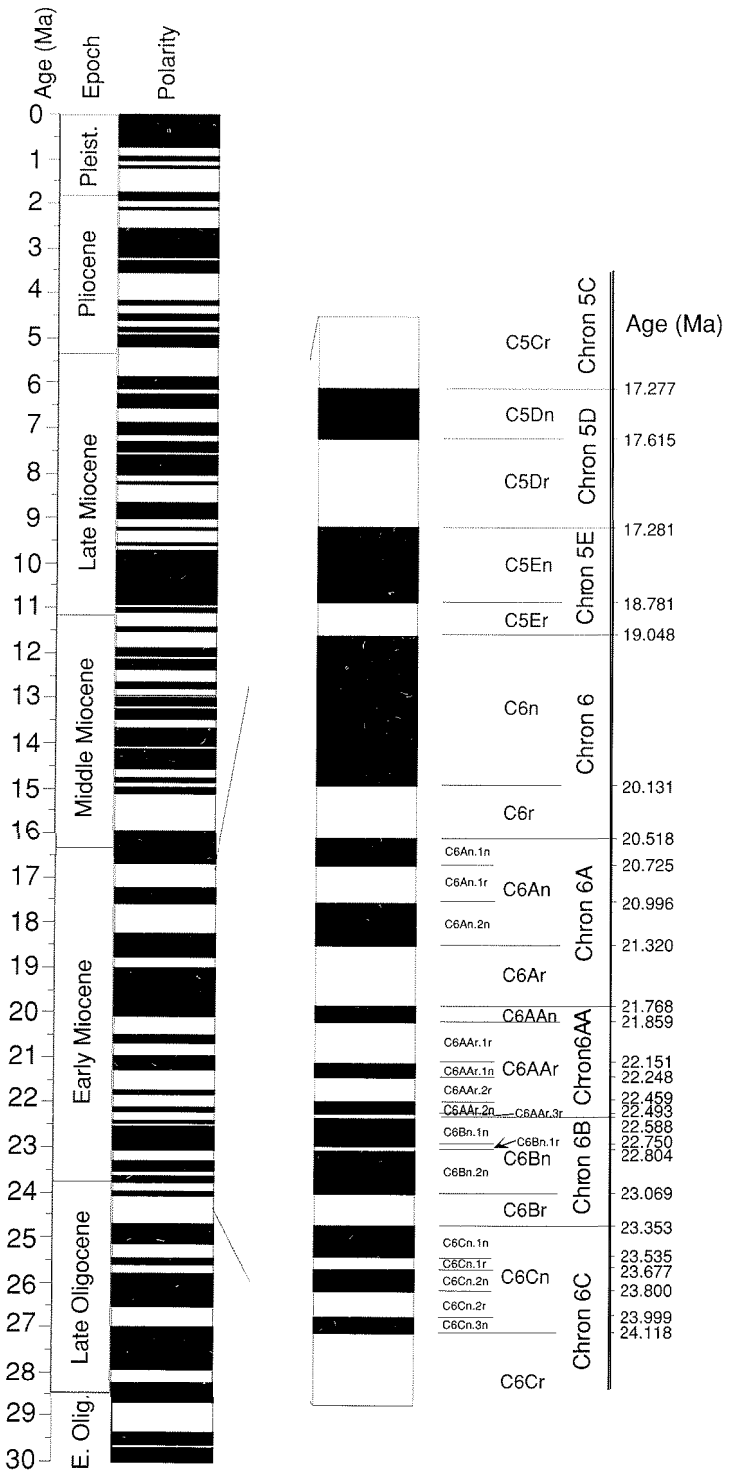

Fig. 2 7 - Magnetic polarity timescale (MPTS) of Cande & Kent (1995) for 0 - 30 Ma. An expanded plot of the MPTS is shown in the inset for the period of relevance to the CRP-l core (c. 17.0 - 24.5 my). The positions of geological epoch boundaries are from Berggren et al. (1995).

pilot study was conducted to understand the palaeomagnetic behaviour and magnetic characteristics of the CRP-1 core.

The pilot study was conducted by subjecting one sample from each set of 14 paired samples to stepwise AF demagnetisation while the corresponding sample was subjected to thermal demagnetisation. All of the samples subjected to AF demagnetisation were measured at steps of 0.5, 10, 15, 20, 25, 30, 40, and 50 mT; for some samples, some of the following steps were added: 35, 45, 60, 70, 80, 90, and 100 mT. Thermal demagnetisation was conducted in 40° increments from 80°C to 600°C. After each thermal demagnetisation step, the magnetic susceptibility was measured to monitor for thermal alteration. Further heating was abandoned if the susceptibility increased by more than about 30%, with concomitant loss of coherence in the palaeomagnetic signal.

Mineral magnetic studies were conducted on 10 of the 14 AF-demagnetised samples from the pilot study, as well as another 8 samples which had been collected for physical properties studies and which were loaned to us for

palaeomagnetic analysis. These samples were given an isothermal remanent magnetisation (IRM) with inducing fields of 0.01, 0.02, 0.05, 0.1, 0.2, 0.3, 0.5, 0.7 and 1 T. The IRM (at 1 T) was then demagnetised by inverting the sample and applying back-fields of 5, 10, 20, 30, 40, 50, 60, 80, 100, and 300 mT. These high-field remanent magnetisations were measured with the Molspin spinner magnetometer (see Background to CRP-1, this volume - section on Palaeomagnetic Laboratory). Isothermal rcmanent magnetisation acquisition and back-field demagnetisation studies were performed to determine the coercivity of remanence (B) and a parameter known as the S-ratio ($-IRM_{-0.3T}/IRM_{1T}$). These parameters provide information about the bulk coercivity of the magnetic assemblage and are therefore useful in understanding the magnetic mineralogy (e.g., King & Channell, 1991; Verosub & Roberts, 1995). The IRM at 1 T (IRM_{1T}) and the magnetic susceptibility (K) are useful indicators of magnetic mineral concentration, and the ratio, IRM_{1T}/κ, provides information about grain-sizevariation, as long as the magnetic assemblage is dominated by a single magnetic mineral (e.g., Verosub & Roberts, 1995). Magnetic susceptibility data were also compared with the whole-core susceptibility log that was obtained at the Cape Roberts drill site.

RESULTS

Pilot Study

Results of the pilot study and preliminary mineral magnetic analyses indicate that themagneticcharacteristics of the recovered sediments vary with depth in the core (Figs. 28 & 29). In general, sediments between 58 and 80 mbsf and between 114.0 and 116.5 mbsf are relatively coarse-grained and less stably magnetised than the other Miocene sediments from CRP-1. Samples from these two intervals have relatively high coercivity (Fig. 28a & b), relatively low concentrations of ferrimagneticgrains (Fig. 28c & e), and a large, sub-vertical, chilling-induced magnetic overprint that is usually removed by AF demagnetisation at 5 mT (Fig. 29a). Such drilling-induced overprints are common in palaeomagnetic studies associatedwith drilling projects and were routinely observed in the CIROS-1 core (Wilson et al., 1998). Overprints that are sufficiently strong to completely remagnetise sediments have compromised palaeomagnetic studies associated with the Ocean Drilling Program for many years (e.g., Roberts et al., 1996; Fuller et al., in press).

In the intervals between 58 and 80 mbsf and between 114 and 116.5 mbsf in the CRP-1 core, the drilling-induced overprint usually comprises 75 - 85% of the NRM. This makes it difficult to isolate a stable characteristic remanence component from the demagnetisation data for these samples, particularlywith AF demagnetisation (*e.g.*, Fig. 29a). Although the drilling-induced overprint also affects thermal demagnetisation data, thermal demagnetisation appears to be more effective in isolating the characteristic remanence direction in samples from these intervals (e.g., Fig. 29b). Thermal demagnetisation was therefore used for all other samples from 58.8 to 80.0 mbsf and from 114.0 to 116.5 mbsf.

The magnetic behaviour of pilot samples from the relatively lower coercivity zones (80 to 114 mbsf and 116.5 to 147.0 mbsf; Fig. 28a &b) indicates that the magnetic carriers are much more stable than in the higher coercivity zones, although the behaviour varies somewhat with lithology (Fig. 29c-f). For many of the paired samples from this interval, there is close agreement between the characteristic remanence directions identified by AF and thermal demagnetisation (e.g., Fig. 29g &h). Moreover, in most cases, AF demagnetisation at 5 or 10 mT was sufficient to remove the drilling-induced overprint. In a few cases, there was a relatively large drilling-induced overprint for samples from the lower coercivity zones (e.g., Fig. 29d). Even though it is difficult to identify a characteristic remanence component in some of the AF-demagnetised data, it is not clear whether thermal

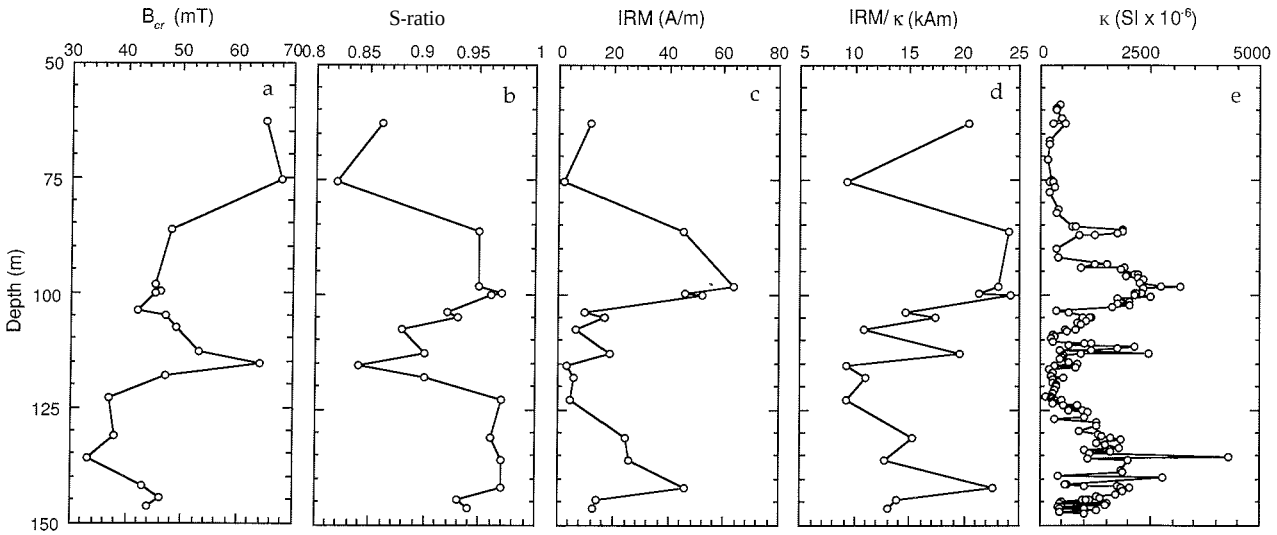

Fig. 28 - Down-core variations in magnetic properties from preliminary rock magnetic analyses from the CRP-1 core: *a)* coercivity of remanence (B); b) S-ratio; c) IRM at 1 T; (IRM_{1T}); d) IRM_{1T}/κ; and ***e)*** magnetic susceptibility (K).

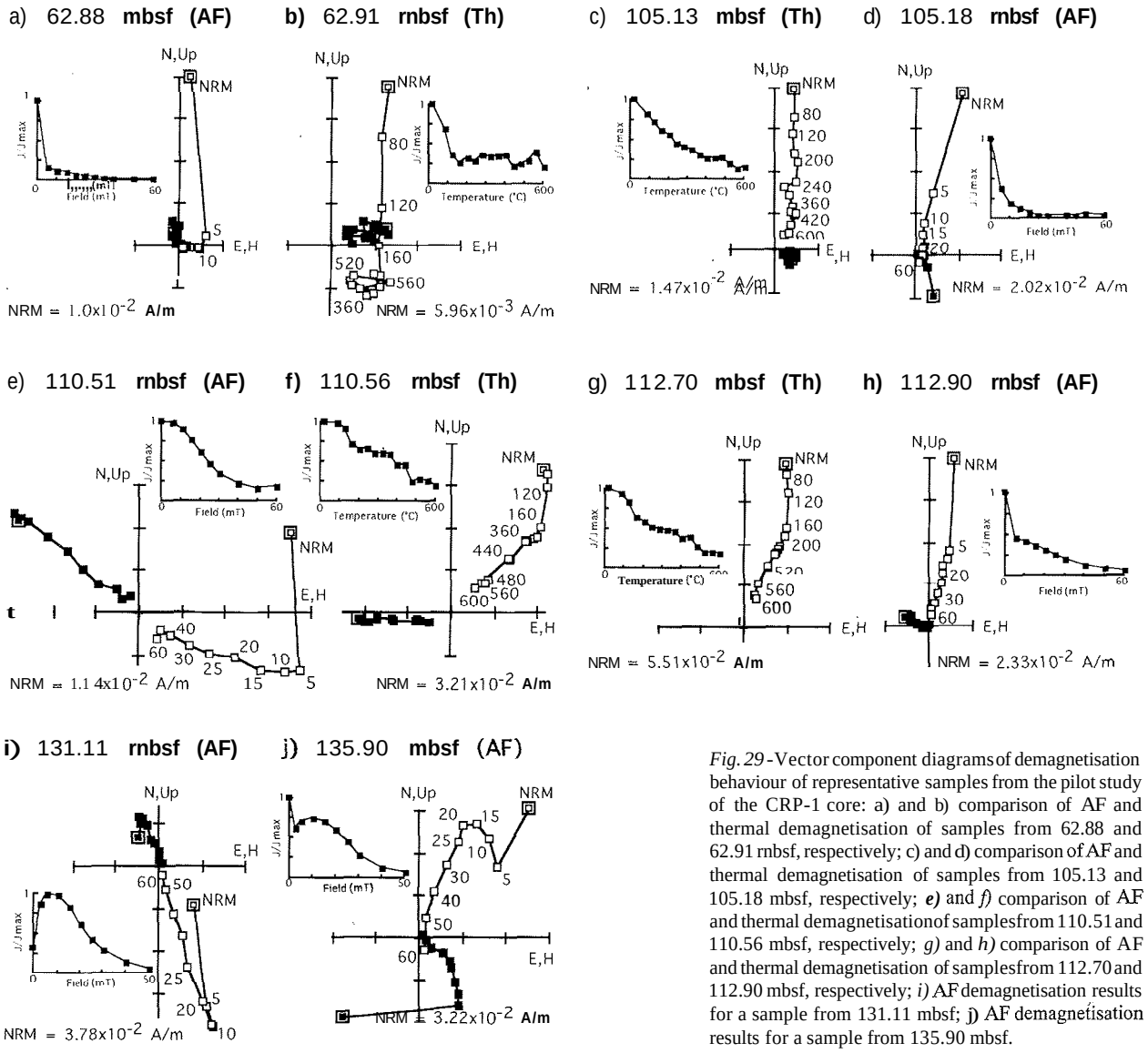

Fig. 29 - Vector component diagrams of demagnetisation behaviour of representative samples from the pilot study of the CRP-1 core: a) and b) comparison of AF and thermal demagnetisation of samples from 62.88 and 62.91 rnbsf, respectively; c) and d) comparison of AF and thermal demagnetisation of samples from 105.13 and 105.18 mbsf, respectively; ***e)*** and *f)* comparison of AF and thermal demagnetisation of samples from 110.51 and 110.56 mbsf, respectively; *g)* and *h)* comparison of AF and thermal demagnetisation of samples from 112.70 and 112.90 mbsf, respectively; *i)* AF demagnetisation results for a sample from 131.11 mbsf; j) AF demagnetisation results for a sample from 135.90 mbsf.

demagnetisation of the sister sample enabled adequate removal of the drilling-induced overprint (Fig. 29c). It was decided that it is preferable to deal with the dominant drilling-induced overprint in AF demagnetisation data than to use the apparently stable, but possibly erroneous, results from thermal demagnetisation. Given the success of AF demagnetisation in isolating characteristic remanence directions for most samples from the low coercivity intervals, all other samples from these intervals were treated with AF demagnetisation.

Clearly, mineral magnetic properties are useful in identifying zones of different magnetic behaviour, and it would have been useful to conduct more detailed analyses of such properties. However, this was not possible because of time restrictions. It should also be noted that the drilling-induced overprint can be beneficial: in cases where it does not completely remagnetise the sample, the consistently steep, upward orientation of the overprint provides unambiguous evidence that neither the core nor the samples have been mistakenly inverted at any stage. For example, with one pair of samples, opposing polarities were identified for the two samples that were treated with different demagnetisation techniques (Fig. 29e &f). Data for both samples display clear evidence of a steep normal polarity drilling-induced overprint, which indicates that both samples were correctly oriented. It therefore appears that the reversed (Fig. 29e) and normal (Fig. 29f) polarity directions recorded by these samples are real and that there is a polarity transition in the vicinity of these samples.

The origin of the drilling-induced overprint is not easily understood. The ease with which the overprint is removed by AF demagnetisation at peak fields of 5 - 10 mT could indicate the presence of coarse (multi-domain) magnetic particles. However, the mineral magnetic data imply that samples from above 80 mbsf and at about 115 mbsf, which are strongly affected by the drilling-induced overprint (*e.g.*, Fig. 29a), have high coercivity, as indicated by B_{cr} and S-ratio values (Fig. 28a & b). Coercivities in these zones are higher than those of many of the samples from other parts of the sequence, which are

not so severely affected by the overprint. It is possible that this problem involves differing responses of the different materials to AF and direct field demagnetisation. Additional mineral magnetic work is needed to resolve this dilemma.

Anomalous palaeomagnetic behaviour was also observed in a sample from a diamictite at 135.90 mbsf (Fig. 29j). The data clearly indicate the presence of a normal polarity drilling-induced overprint (0 - 5 mT), a reversed polarity component (5 - 15 mT) and a stable normal polarity component (20 - 60 mT). We interpret this three-component magnetisation as a composite magnetisation arising from the presence of one or more clasts within the sediment matrix. For example, the reversed polarity component could be due to the presence of a coarse-grained igneous clast that was oriented with a downward magnetisation. This sample, which represents the most anomalous behaviour observed in the pilot study, demonstrates the need to exercise extreme caution in interpreting data from coarse-grained lithofacies where the effects of a single clast could preclude interpreting the data in terms of a magnetisation acquired at, or near, the time of deposition.

Palaeomagnetic Behaviour

One hundred and twenty-two samples were analysed in the Crary Science and Engineering Center (CSEC) laboratory. Due to their brittle and fractured nature, the remaining 33 samples were put aside for later measurement on a cryogenic magnetometer. Almost all of the analysed samples display a low coercivity near-vertical, normal polarity component that is interpreted to represent a drilling-induced overprint. In most cases, this component was removed with peak AFs of 5 - 10 mT (Fig. 30). For reversed-polarity samples (e.g., Fig. 30 h-j), the overprint can be easily identified in vector component diagrams; for normal-polarity samples, it is sometimes easier to identify the overprint on plots of intensity versus demagnetisation level because the steepness of the geomagnetic field at the CRP-1 site can make it difficult to distinguish between the overprint and a true geomagnetic field direction solely on the basis of inclination. Occasionally, the drilling-induced overprint and the original remanence had completely overlapping coercivity spectra. In these situations, it was not possible to isolate the two components (e.g., Fig. 30 d).

For six thermally-demagnetised samples, the drilling-induced component was clearly not removed (e.g., Fig. 30f), and these samples were excluded from subsequent interpretations. Stable palaeomagnetic behaviour was evident from the vector component plots of 95 of the remaining 116 samples. In each case, the characteristic remanence direction was determined using a best-fit line that was constrained through the origin of the vector component diagram (Fig. 30). Steep normal polarity directions were observed for 52 stably magnetised samples (e.g., Fig. 30a-c), and steep reversed polarity directions were observed for 32 samples (e.g., Fig. 30h-j); remanence directions for the remaining 11 samples were neither steep nor clearly of reversed or normal polarity (e.g., Fig. 30e). Samples with abnormally low inclinations (e.g., Fig. 30e) or with 3-component magnetisations (e.g., Figs. 30g & 29j) were found to be from diamictite intervals which contained small clasts of dolerite. The magnetisation of these samples is probably dominated by clasts whose orientation was not controlled by the ambient magnetic field during deposition.

For 21 samples, stable characteristic remanence directions could not be obtained; however, the polarity of 9 of these samples could be inferred from the trend exhibited during demagnetisation (e.g., Fig. 29b). It was not possible to determine the polarity for the remaining 12 samples. In most cases, the drilling-induced overprint was the dominant component, and the majority of the magnetisation was lost during the first few demagnetisation steps (e.g., Fig. 29a).

Magnetic Polarity Stratigraphy

A tentative magnetic polarity zonation for the lower 90 m of the CRP-1 core is shown in figure 31. Generally, for the studied interval, the record appears to have been divided equally between normal and reversed polarity. The polarity zonation shown in figure 31 may change slightly after analysis of further samples. However, we do not expect much change in the interval below 81 mbsf. Between 58 and 81 mbsf, further study is essential to understand the magnetic mineralogy and the behaviour of individual samples. A few samples from this interval have not been measured, and, although the general trend seems to be of reversed polarity, we cannot be certain of the details of the polarity record in this interval.

Normal polarity dominates the interval from c. 82-124 mbsf, with 2 thin reversed polarity intervals at c. 105 mbsf and 118 mbsf, respectively, and a 20-m-thick interval of reversed polarity between 124 and 144.74 mbsf. A single stable but low inclination (30°) sample at 110.5 mbsf may mark another thin reversed polarity interval. However, the interval between 110.0 and 112.5 mbsf also contains several stable intermediate to low angle normal polarity samples. This interval may represent a geomagnetic excursion. Until the nature of the polarity record in this interval is clarified, a "?" indicates the uncertainty in interpretation of this interval on figure 31, Below 144.74 mbsf, the sampling interval was only 30 cm on average, and the data alternate between reversed and normal polarity. Every sample from this interval is stably magnetised and has an unambiguous vector endpoint, which is consistent with alternating polarity in slowly-deposited sediments. This is not unexpected, because preliminary biostratigraphic analysis (see section on Diatoms) indicated that the basal part of the CRP-1 core is of earliest - middle early Miocene age, and this interval of the MPTS has a high frequency of reversals (Fig. 27). Detailed additional sampling will be necessary to determine whether all polarity zones have been identified in this interval of the core.

DISCUSSION

An interpretation of the polarity of the CRP-1 core is plotted in figure 32 against lithology and stratigraphic cycles which are interpreted to be due to relative sea-level

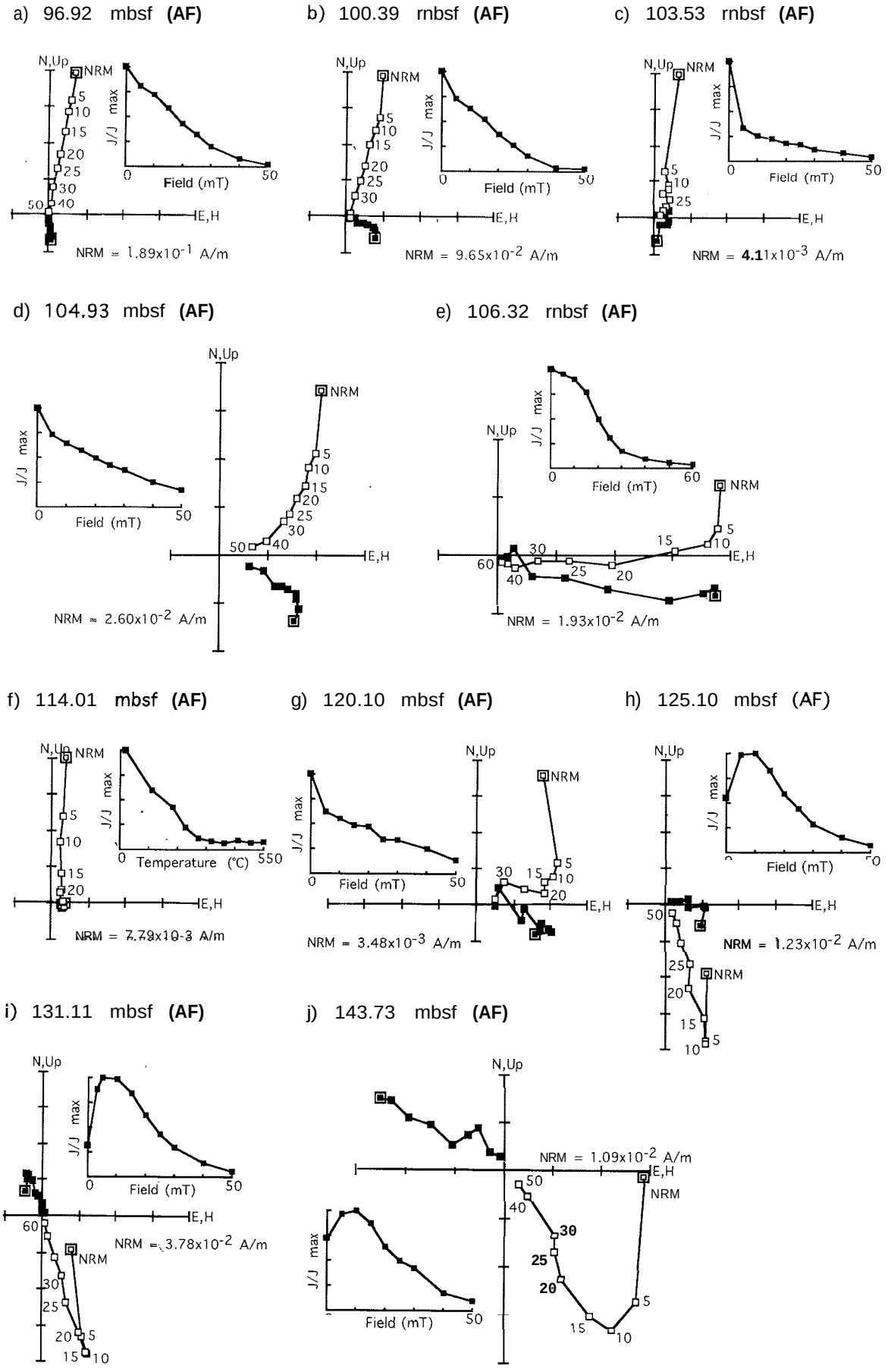

Fig. *30* - Vector component diagrams of demagnetisation behaviour of representative samples for each magnetozone in the CRP-1 core: a) normal polarity sample from 96.92 mbsf; b) normal polarity sample from 100.39 mbsf; c) normal polarity sample from 103.53 mbsf; d) sample with two components of magnetisation with overlapping coercivity spectra from 104.93 mbsf; *e)* low inclination sample from 106.32 mbsf; *f)* sample dominated by drilling-induced overprint from 114.01 mbsf; g) multi-component sample of unknown polarity from 120.10 mbsf; *h)* reversed polarity sample from 125.10 mbsf; i) reversed polarity sample from 131.11 mbsf; j) reversed polarity sample from 143.73 mbsf.

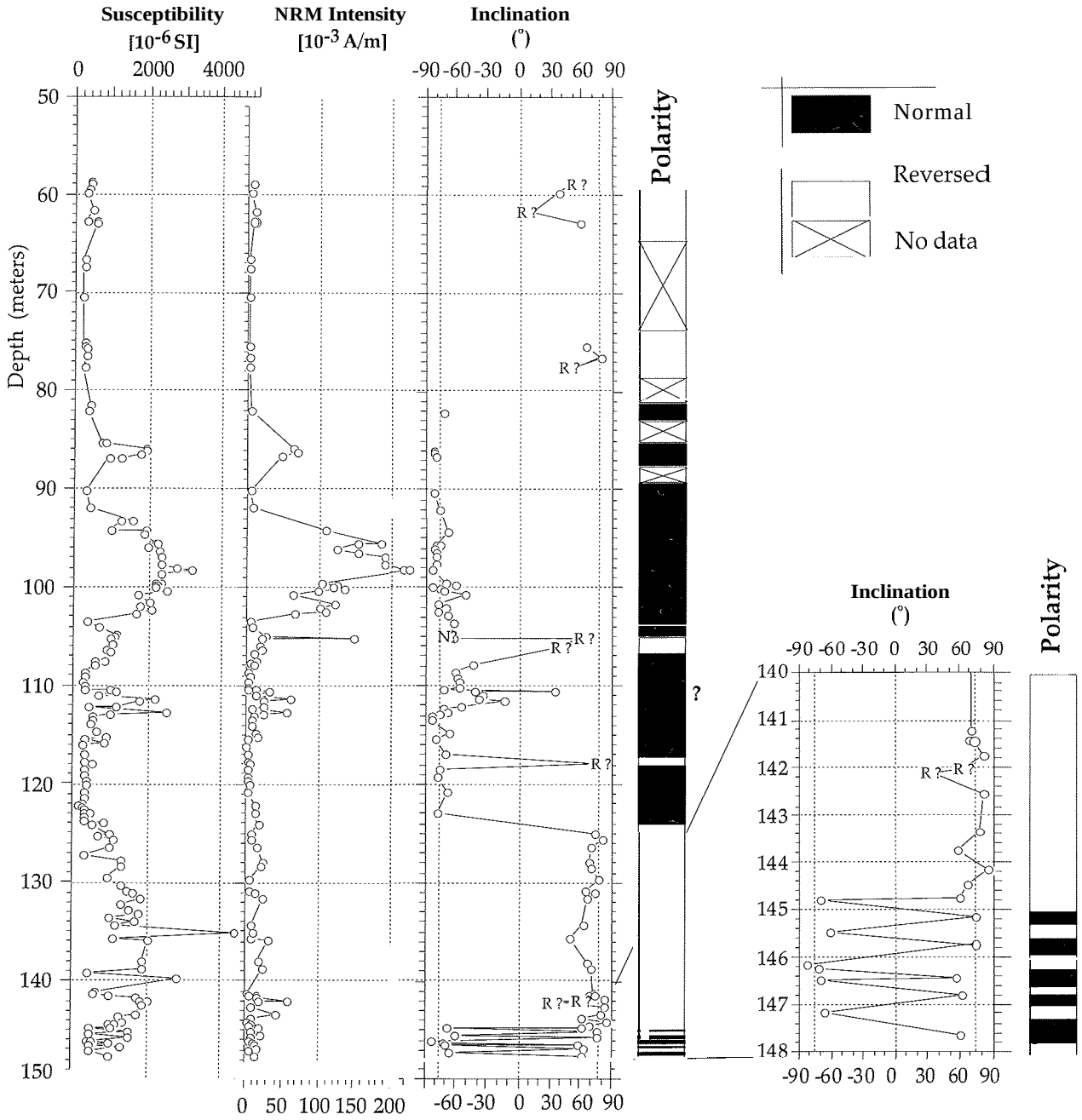

Fig. 31 - Log of magnetic polarity zonation (black = normal polarity, white = reversed polarity), inclination, natural remanent magnetisation (NRM) intensity, and susceptibility for the CRP-1 core. R? (N?) denote samples that displayed a clear trend toward reversed (normal) polarity but for which a stable characteristic component was not isolated before the intensity of remanence became too weak to measure. ***An*** enlargement of the polarity data for the lower 7 m of the CRP-1 core is shown on the right-hand side.

change (see section on Sequence Stratigraphic Interpretation). It should be noted that the polarity intervals are not related to lithologic features; that is, polarity, and the ability to interpret palaeomagnetic data, appear to be independent of lithofacies. Also, the boundaries between polarity zones occur almost exclusively within lithologic units or cycles rather than at lithostratigraphic breaks or cycle boundaries. In the case of CRP-1, these cycle boundaries have been interpreted as regressive erosion surfaces (see section on Sequence Stratigraphic Interpretation). If significant time is missing at any of these unconformities, it is likely that polarity reversal boundaries would be observed at these stratigraphic breaks. The magnetic polarity stratigraphy suggests that there is not a significant amount of missing time distributed throughout the sequence. However, the possibility that significant time is missing at one or two stratigraphic breaks cannot be excluded.

For the purpose of correlation with the MPTS, the polarity record has been divided into four magnetozones: an upper reversed polarity interval (<82 mbsf, R1), which has yet to be analysed in detail; a predominantly normal polarity intewal (82-124 mbsf, N1), which includes two reversed polarity zones in the lower part and a few intervals that have yet to be analysed; a second interval of reversed polarity (124.00-144.74 mbsf, R2); and an intewal at the

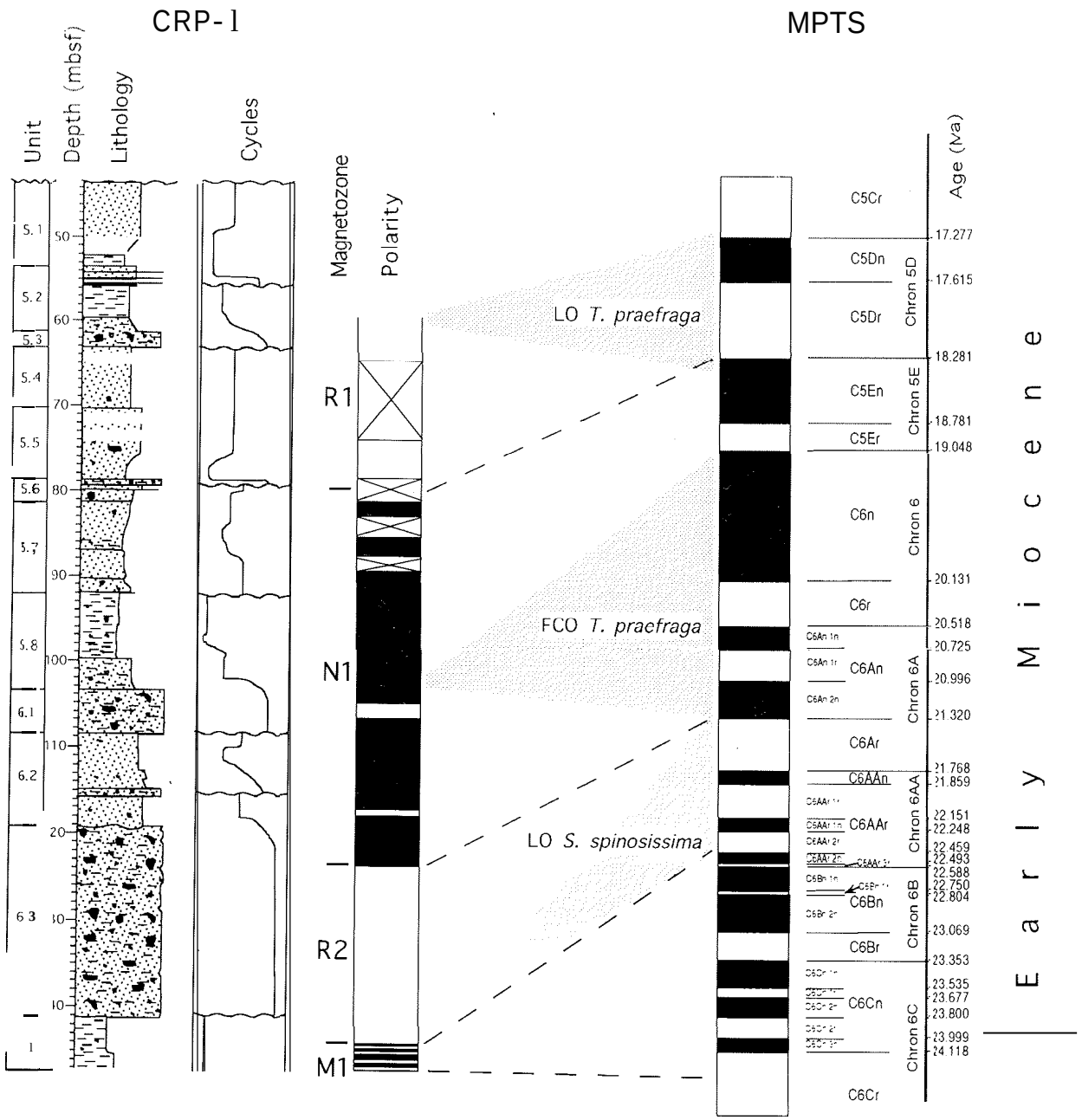

Fig. 32 - Preliminary correlation of the CRP-1 magnetic polarity zonation with the magnetic polarity timescale (MPTS) of Cande & Kent (1995) and Berggren et al. (1995). Magnetic polarity symbols are defined in figure 32. Shaded correlations represent the diatom events discussed in the text. The distributed nature of the shading indicates the maximum published ranges of these datums. The dashed lines indicate an initial correlation of the magnetozones with the MPTS (see text for discussion). Further refinement of the diatom datums and correlation of the magnetic polarity record with the MPTS is discussed in Summary of Results from CRP-1 (this volume).

base of the record (144.74-147.69 mbsf, M1) with alternating normal and reversed polarity.

Due to the variable nature of the lithofacies, it is likely that there are large fluctuations in sedimentation rate. Therefore, the thicknesses of the identified magnetozones cannot be directly compared to the duration of polarity chrons. Furthermore, even though there was a high reversal frequency in the early Miocene (the time interval represented by the lower 100 m of the CRP-1 core; see section on Diatoms), magnetozone M1 probably represents a period of slow, but continuous or subcontinuous, sedimentation, perhaps on the order of 2 m/my. Based on the lithostratigraphy, the lower *c.* 3 m of magnetozone R2 would be expected to represent equally slow, but continuous, sedimentation. The upper part of magnetozone R2 occurs within a diamictite, which may have been rapidly deposited, and which might not represent much time. Magnetozones R1 and N1 encompass a variety of lithofacies, and, at best, it may be possible to specify an average rate of sedimentation for these intervals.

The diatom flora from the CRP-1 core include species from the *Thalassiosira fraga* Zone, which suggests that the lower 104 m of the record is of early Miocene age (see section on Diatoms). Several diatom datums more closely

constrain a possible correlation. These include the last occurrence (LO) of *Stephanopyxis spinosissima* at *c.* 141.5 mbsf, the first common occurrence (FCO) of *T. praefraga* (syn. *T. fraga*) at *c.* 102.2-103.4 mbsf, and the last occurrence (LO) of *T. praefraga* at *c.* 58.8-60.0 mbsf. The LO of *S. spinosissimu* is known from MSSTS-1 (syn *S.* sp. A, Harwood et al., 1989, see section on Diatoms) to occur within Chrons C6AA and C6A. The FCO of T. *praefraga* is reported to occur in Chron C6An at ODP Sites 747 and 748 from the Kerguelen Plateau (Harwood & Maruyama, 1992; Harwood et al., 1992). However, its first occurrence in Sites 747 and 748 has been reinterpreted in this volume (see section on Diatoms) to be in chrons C6n or C6r. The LO of *T. praefrugu* is reported to occur in Chron C5D or possibly latest Chron C5E from ODP sites 747 and 748 (Harwood & Maruyama, 1992; Harwood et al., 1992, see section on Diatoms). The maximum possible ranges of these preliminary diatom correlations are shaded in figure 32. Using these diatom datum ranges and the preliminary polarity stratigraphy of the CRP-1 core, R1 can be tentatively correlated with Chron C5Dr and possibly up into Chron C5Cr. N1 can be correlated with Chrons C6An through C5E, and R2 can be correlated with Chrons C6AAr through C6Ar. The basal part of the record (M1) may correspond to Chrons C6C through C6B. A more refined correlation to the MPTS using further diatom data (see section on Diatoms) is discussed in Summary and Preliminary Interpretation of CRP-1 (this volume). A conclusive correlation with the MPTS will not be possible until more detailed palaeomagnetic studies are conducted.

ADDITIONAL WORK

The above-reported initial characterisation studies have served to identify several areas that warrant additional work. The magnetostratigraphy of the CRP-1 core clearly needs to be refined. Although high quality palaeomagnetic results have been obtained from many of the CRP-1 samples, it is still important to characterize the mineral magnetic properties of different parts of the core. The mineral magnetic measurements will serve as the basis for studies of the environmental magnetic record of the CRP-1 core. Finally, it should be noted that the lower part of the CRP-1 core may correspond to the upper part of both the CIROS-1 core (see Barrett, 1989) and the MSSTS-1 core (see Barrett, 1986). Additional palaeomagnetic and environmental magnetic studies of these two cores may allow development of an integrated correlation between the CRP-1, CIROS-1 and MSSTS-1 cores.

ACKNOWLEDGMENTS

Palaeomagnetism and Mineral Magnetic Properties - The palaeomagnetism group thanks Rich Jarrard for allowing us to use his samples for AF demagnetisation studies. The palaeomagnetic component of the Cape Roberts Project was supported by grants from the National Science Foundation to Kenneth L. Verosub, Andrew P. Roberts, and Gary S. Wilson and from the *Programma Nazionale di Ricerche in Antartide* to Leonardo Sagnotti and Fabio Florindo. We are grateful to Glen Burnside and the science construction staff of Antarctic Support Associates for their patience, efficiency, and cooperation. Without their assistance, this undertaking would not have been possible.

REFERENCES

Allibone A.H., 1992. Low pressure/high temperature metamorphism of Koettlitz Group schists in the Taylor Valley and Ferrar Glacier regions. *New Zealand Journal of Geology and Geophysics*, **35,** 115-127.

Allibone A.H., Cox S.C., Graham I.J., Smillie R.W., Johnstone R.D., Ellery S.G. & Palmer K., 1993a. Granitoids of the Dry Valleys area, southern Victoria Land, Antarctica: field relationships, and isotopic dating. *New Zealand Journal of Geology and Geophysics*, **36**, 281-291.

Allibone A.H., Cox S.C. & Smillie R.W., 1993b. Granitoids of the Dry Valleys area, southern Victoria Land: geochemistry and evolution along the early Paleozoic Antarctic Craton margin. *New Zealand Journal of Geology and Geophysics*, **36**, 299-316.

Askin R.A. & Markgraf V., 1986. Palynomorphs from the Sirius Formation, Dominion Range, Antarctica. *Antarctic Journal of the United States*, 21, 34-35.

Baldauf J.G. & Barron J.A., 1991. Diatom biostratigraphy: Kerguelen Plateau and Prydz Bay regions of the Southern Ocean. *Proc. ODP, Sc. Results*, 119, 547-598.

Barrett P.J. (ed.), 1986. Antarctic Cenozoic history from the MSSTS-1 drillhole, McMurdo Sound. *DSIR Bulletin*, 237, 174 p.

Barrett P.J. (ed.), 1989. Antarctic Cenozoic history from the CIROS-1 drillhole, McMurdo Sound. *DSIR Bulletin*, 245,254 p.

Barrett P.J., McKelvey B.C. & Walker B.C., 1986. Sand provenance. *DSIR Bulletin*, 237, 137-144.

Barron J.A. & Baldauf J.G., 1995. Cenozoic marine diatom biostratigraphy and applications to paleoclimatology and paleoceanography. In: Blome C.D. (ed.), *Siliceous microfossils, Paleontological Society Short Courses in Paleontology*, 8, 107-118.

Bennett M.R & Glasser N.F., 1996. Glacial Geology- Ice Sheets and Landforms. J. Wiley (ed.), Chichester.

Berggren W.A., Kent D.V., Swisher III C.C. & Aubrey M.P., 1995. A revised Cenozoic geochronology and biostratigraphy. In: Berggren W.A., Kent D.V., Aubrey M.P. & Hardenbol J. (eds.), *Geochronology, Time Scales, and Stratigraphic Correlation, Soc. Econ. Paleontol. Mineral., Spec. Publ.*, 54, 129-212.

Bemer R.A., 1984. Sedimentary pyrite formation: An update. *Geochimica et Cosmochimica Acta*, 48, 605-615.

Beu A.G. & Dell R.K., 1989. Mollusca. In: Barrett P.J. (ed.), Antarctic Cenozoic history from the CIROS-1 drillhole, McMurdo Sound, *DSIR Bulletin*, 245, 135-141.

Blatt H., 1992. *Sedimentary Petrology*, 2nd ed. W.H. Freeman (ed.), New York.

Bordovskiy O.K., 1965. Accumulation and transformation of organic substance in marine sediments. *Marine Geology*, 3, 3-114.

Cande S.C. & Kent D.V., 1995. Revised calibration of the geomagnetic polarity time scale for the Late Cretaceous and Cenozoic. *J. Geophys. Res.*, 100, 6093-6095.

Dale B., 1996. Dinoflagellate cyst ecology: modeling and geological applications. In: Jansonius J. & McGregor D.C. (eds.), *Palynology: principles and applications, Chapter 31, American Association of Stratigraphic Palynologists Foundation*, Dallas, 1249-1275.

Dell R.K., 1990. Antarctic Mollusca. *The Royal Society of New Zealand Bullettin*, 27.

Dell R.K. & Fleming C.A., 1975. Oligocene-Miocene bivalve Mollusca and other macrofossils from Sites 270 and 272 (Ross Sea), DSDP, Leg 28. *Initial Reports of the Deep-Sea Drilling Project*, 28, 693-703.

Dettmann M.E., 1963. Upper Mesozoic microfloras from south-eastern Australia. *Proceedings of the Royal Society of Victoria*, 77, 1-148.

De Vernal A. & Mudie P.J., 1989b. Pliocene and Pleistocene palynostratigraphy of ODP sites 646 and 647, eastern and southern Labrador Sea. In: Srivastava S.P., Arthur M.A., Clement B., et al. (eds.), *Proc. ODP, Sc. Results*, 105,401-422.

Dow J.A.S. & Neall V.E., 1974. Geology of the lower Rennick Glacier, north Victoria Land, Antarctica. *New Zealand Journal of Geology and Geophysics*, 17, 659-714.

Ehrmann W.U., 1997. Smectite concentrations and crystallinities: indications for Eocene age of glaciomarine sediments in the CIROS-1 drillhole, McMurdo Sound, Antarctica, In: Ricci C.A. (ed.), *The Antarctic Region: Geological Evolution and Processes*, Terra Antartica Publication, Siena, 771-780.

Ehrmann W., in press. Implications of late Eocene to early Miocene clay mineral assemblages in McMurdo Sound (Ross Sea, Antarctica) on paleoclimate and ice dynamics. *Palaeogeogr., Palaeoclimatol., Palaeoecol.*

Fensome R.A., Taylor F.J.R., Norris G., Sarjeant W.A.S., Wharton D.I. & Williams G.L., 1993. A classification of fossil and living dinoflagellates. *Micropaleontology, Special Publication*, 7, 1-351

Findlay R.H., Skinner D.N.B. & Craw D., 1984. Lithostratigraphy and structure of the Koettlitz Group, McMurdo Sound, Antarctica. *New Zealand Journal of Geology and Geophysics*, 27, 513-536.

Fuller M., Hastedt M. & Herr B., in press. Coring-induced magnetization of recovcrcd ODP sediment. *Proc. ODP, Sci. Res.*, 157.

George A., 1989. Sand provenance, *DSIR bulletin*, 245, 159-167.

Gersonde R. & Burckle L.H., 1990. Neogene biostratigraphy of ODP Leg 113, Wcddell Sea (Antarctic Ocean). *Proc. ODP, Sc. Results*, **113**, 761-789.

Gombos A.M., 1977. Paleogene and Neogene diatoms from the Falkland Plateau and Malvinas outer basin, Leg 36, Deep Sea Drilling Project. *Initial Reports of the Deep Sea Drilling Project*, 36, 575-687.

Gombos A.M. & Ciesielski P.F., 1983. Late Eocene to early Miocene diatoms from the southwest Atlantic. *Initial Reports of the Deep Sea Drillitzg Project*, 71,583-634.

Greene S.W., 1964. Plants of the land. In: Priestley R., Adie R.J. & Robin G. de Q. (eds.), *Antarctic Research*, Butterworths, London, 240-253.

Grindley G.W. & Warren G., 1964. Stratigraphic nomenclature and correlation in the western part of the Ross Sea. In: Adie R.J. (ed.), *Antarctic geology*, Amsterdam, North Holland Publishing Co., 314-333.

Grindley G.W. & Warren G., 1964. Stratigraphic nomenclature and correlation in the western Ross Sea region, Antarctica. In: Adie R.J. (ed.), *Antarctic Geology*, North Holland Publishing Company, Amsterdam, 206-219.

Gunn B.M. & Warren G., 1962. Geology of Victoria Land between the Mawson and Mulock Glaciers, Antarctica. *New Zealand Geological Survey Bulletin*, **71.**

Hambrey M.J., 1989. Grain fabric. In: Barrett P.J. (ed.), Antarctic Cenozoic History from the CIROS-1 Drillhole, McMurdo Sound, Antarctica, *DSIR Bullettin*, **245**, 59-62.

Hambrey M.J., Barrett P.J. & Robinson P.H., 1989. Stratigraphy. In: Barrett P.J. (ed.), Antarctic Cenozoic history from the CIROS-1 drillhole, McMurdo Sound, *DSIR Bulletin*, **245**, 23-48.

Hambrey M.J., Erhmann W.U. & Larsen B., 1991. The Cenozoic glacial record of the Prydz Bay continental shelf, East Antarctica. In: Barron J., Larsen B. & Shipboard Scientific Party (eds.), *Leg 119, Kerguelen Plateau and Prydz Bay, Antarctica*, **119B**, Sc. Results, 77-132.

Hannah M.J., 1994. Eocene dinoflagellates from CIROS-1 drillhole, McMurdo Sound Antarctica. *Terra Antartica*, **1**, 371.

Hannah M.J., in press. Climate controlled dinoflagellate distribution in late Eocene / earliest Oligocene strata from the CIROS-1 drillhole, McMurdo Sound, Antarctica. *Terra Antartica.*

Hannah M.J., Cita M.B., Coccioni R. & Monechi S., in press. The Eocene/Oligocene boundary at 70 degrees South, McMurdo Sound Antarctica. *Terra Anfartica.*

Harwood D.M., 1986. Diatoms. In: Barrett P.J. (ed.), Antarctic Cenozoic history from the MSSTS-1 drillhole, McMurdo Sound, *DSIR Bullettin*, 237, 69-108.

Harwood D.M., 1989. Siliceous Microfossils. In: Barrett P.J. (ed.), Antarctic Cenozoic history from the CIROS-1 drillhole, McMurdo Sound, *DSIR Bullettin*, **245**, 67-97.

Harwood D.M., 1991. Cenozoic diatom biogeography on the southern high-latitudes: inferred biogeographic barriers and progressive endemism. In: Thomson M.R.A., Crame J.A. & Thomson J.W. (eds.), *Geological Evolution of Antarctica*, Cambridge, Cambridge University Press, 667-673.

Harwood D.M., Barrett P.J., Edwards A.R., Rieck H.J. & Webb P.N., 1989a. Biostratigraphy and chronology. In: Barrett P.J. (ed.), Antarctic Cenozoic history from the CIROS-1 drill-hole, McMurdo Sound, *DSIR Bulletin*, **245**, 231-239.

Harwood D.M., Lazarus D., Abelmann A., Aubry M.P., Berggren W.A., Heider F., Inokuchi H., Maruyama T., McCartney K., Wei W. & Wise S.W. Jr., 1992. Neogene integrated ~nagnetobiostratigraphy of the Southern Kerguelen Plateau, ODP Leg 120. *Proc. ODP, Sci. Res.*, 120, 1031-1052.

Harwood D.M. & Maruyama T., 1992. Middle Eocene to Pleistocene diatom biostratigraphy of ODP Leg 120, Kerguelen Plateau. *Proc. ODP, Sci. Res.*, **120**, 683-733.

Harwood D.M., Schcrcr R.P. & Wcbb P.N., 1989b. Multiple Miocene marine productivity events in West Antarctica as recorded in upper Miocene sediments beneath the Ross Ice Shelf (Site J-9). *Marine Micropaleontology*, **15**, 91-115.

Hayes D.E., Frakes L.A., Barrett P.J., Burns D.A., Chen P.H., Ford A.B., Kaneps A.G., Kemp E.M., McCollum D.W,, Piper D.J., Wall R.E. & Webb P.N., 1975. *Initial reports of the Deep Sea Drilling Project*, 28, U.S. Government Printing Office, Washington, D.C.

Head M.J., 1989b. Palynology dinocyst stratigraphy of the Eocene and Oligocene in ODP Leg 105, Hole 647A, Labrador Sea. In: Srivastava S.P., Arthur M.A., Clement B. et al. (eds.), *Proc. ODP, Sc. Results*, **105**, 515-550.

Hedges J.I. & Stern J.H., 1984. Carbon and nitrogen determinations of carbonate containing solids. *Limnology and Oceanography*, 29, 657-663.

Jones R.L. & Blatt, H., 1984. Mineral dispersal patterns in the Pierre Shale. *J. Sedimentary Petrology*, **54**, 17-28.

Kemp E.M., 1975. Palynology of the Leg 28 drillsites, Deep Sea Drilling Project. *Initial reports of the Deep Sea Drilling Project*, 28, 599-621.

King J.W. & Channel1 J.E.T., 1991. Sedimentary magnetism, environmental magnetism, and magnetostratigraphy. *U.S. Natl Rep. Int. Union Geod. Geophys. 1987-1990, Rev. Geophys.*, **29**, 358-370.

Knox G.A., 1992. *The biology of the Southern Ocean. Studies in Polar Research*, Cambridge University Press, Cambridge, 444 p.

Kyle P.R., 1990. McMurdo Volcanic Group, western Ross embayment. In: LeMasurier W.E. & Thomson J.W. (eds.), *Volcanoes of the Antarctic Plate and Southern Oceans, American Geophysical Union, Antarctic Research Series*, 48, 19-25.

Leckie M.A. & Webb P.N., 198.5. Late Paleogene and early Neogene foraminifers of Deep Sea Drilling Project Site 270, Ross Sea, Antarctica. In: Kennett J.P., Von der Broch, C.C. et al. (eds.), *Initial Reports of the Deep Sea Drilling Project* XC, 1093-1142.

Mackiewicz N.E., Powell R.D., Carlson P.R. & Molnia B.F., 1984. Interlaminated ice-proximal glacimarine sediments in Muir Inlet, Alaska. *Marine Geology*, **57**, 113-147.

McCollum D.W., 1975. Diatom stratigraphy of the Southern Ocean. *Initial Reports of the Deep Sea Drilling Project*, **28**, 515-571.

Mildenhall D.C., 1989. Terrestrial palynology. In: Barrett P.J. (ed.), Antarctic Cenozoic history from the CIROS-1 drillhole, McMurdo Sound, *DSIR bulletin*, 245, 119-127.

Mudie P.J., 1992. Circum-Arctic Quaternary and Neogene marine palynofloras: paleoecology and statistical analysis. In: Head M.J. & Wrenn J.H. (eds.), *Neogene and Quaternary dinoflagellate cysts and acritarchs, American Association of Stratigraphic Palynologists Foundation*, Dallas, 347-390.

Nemec W., 1990. Aspects of sediment movement on steep delta slopes. In: Colella A. & Prior D.B. (eds.), *Coarse-Grained Deltas, International Association of Seditnentologists Special Publication*, **10**, 29-73.

Nemec W. & Steel R.J., 1984. Alluvial and coastal conglomerates: their significant features and some comments on gravelly mass-flow deposits. In: Koster E.H. & Steel R.J. (eds.), *Sedimentology of Gravels and Conglomerates, Canadian Society of Petroleum Geologists Memoir*, 10, 1-31.

Prauss M. & Riegel W., 1989. Evidence from phytoplankton associations for causes of black shale formation in epicontinental seas. *Neues Jahrbuch fur Geologie und Palaontologie, Monatshefte*, 11, 671-682.

Raine J.I., Askin R.A., Crouch E.M., Hannah M.J., Levy R.H. & Wrenn J.H., 1997. Palynomorphs. In: Hannah M.J. & Raine J.I. (eds.), *Southern Ocean Late Cretaceous / Early Cenozoic biostratigraphic datums, Institute of Geological and Nuclear Sciences science report*, **97**(4), 25-33.

Roberts A.P., Stoner J.S. & Richter C., 1996. Coring-induced magnetic overprints and limitations of the long-core paleomagnetic measurement technique: Some observations from ODP Leg 160, Eastern Mediterranean Sea. *Proc. ODP, Init. Reports*, **160**, 497-505.

Savage M.L. & Ciesielski P.F., 1983. A revised history of glacial sedimentation in the Ross Sea region. In: Oliver R.L., James P.R. &

Jago J.B. (eds.), *Antarctic Earth Science, Australian Academy of Science*, Canberra, 555-559.

Scheidegger K.F. & Krissek L.A., 1982. Dispersal and deposition of eolian and fluvial sediments off Peru and northern Chile. *Geological Society of America Bulletin*, 93, 150-162.

Schrader H.J., 1976. Cenozoic planktonic diatom biostratigraphy of the southern Pacific Ocean. *Initial Reports of the Deep Sea Drilling Project*, 35, 605-672.

Schrader H.J. & Fenner J., 1976. Norwegian Sea Cenozoic diatom biostratigraphy and taxonomy. *Initial Reports of the Deep Sea Drilling Project*, 38, 921-1 099.

Steinhauff D.M., Renz M.E., Harwood D.M. & Webb P.N., 1987. Miocene diatom biostratigraphy of DSDP Hole 272: stratigraphic relationship to the underlying Miocene of Hole 270, Ross Sea. *Antarctic Journal of the United States*, **22**(5), 123-125.

Taylor F.J.R., 1987. The biology of dinoflagellates. *Botanical monographs*, **21**, 1-785.

Tonarini S., Rocchi S., Armienti P. & Innocenti F., 1997. Constraints on timing of Ross Sea rifting inferred from Cainozoic intrusions from northern Victoria Land, Antarctica. In: Ricci C.A. (ed.), *The Antarctic Region: Geological Evolution and Processes*, Terra Antartica Publication, Siena, 511-522.

Truswell E.M., 1983. Recycled Cretaceous and Tertiary pollen and spores in Antarctic marine sediments: a catalogue. *Palaeontographica B*, 186, 121-174.

Truswell E.M., 1986. Palynology. In: Barrett P.J. (ed.), Antarctic Cenozoic history from the MSSTS-1 drillhole, McMurdo Sound, *DSIR Bullettin*, 237, 131-134.

Verosub K.L. & Roberts A.P., 1995. Environmental magnetism: Past, present, and future. *J. Geophys. Res.*, **100,** 2175-2192.

Weaver F.M. & Gombos A.M., 1981. Southern high-latitude diatom biostratigraphy. In: Warme T.E., Douglas R.G., and Winterer E.L. (eds.), *The Deep Sea Drilling Project: A Decade of Progress*, Special Publication of the Society of Economic Paleontologists and Mineralogists, **32**, 445-470.

Webb P.N., 1989. Benthic foraminifera. In: Barrett P.J. (ed.), Antarctic Cenozoic history from the CIROS-1 drillhole, McMurdo Sound, *DSIR Bulletin*, **245**, 99-118.

Wilson G.J., 1967. Some new species of lower Tertiary dinoflagellates from McMurdo Sound, Antarctica. *New Zealand Journal of Botany*, **5**, 57-83.

Wilson G.J., 1989. Marine palynology. In: Barrett P.J. (ed.), Antarctic Cenozoic history from the CIROS-1 drillhole, McMurdo Sound, *DSIR Bulletin*, **245,** 129-134.

Wilson G.S., Roberts A.P., Verosub K.L., Florindo F. & Sagnotti L., 1997. Magnetobiostratigraphic chronology of the Eocene - Oligocene transition in the CIROS-1 core, Victoria Land margin, Antarctica: Implications for Antarctic glacial history. *Geol. Soc. Am. Bull.*, **109**(12), 2-14.

Wrenn J.H. & Hart G.F., 1988. Paleogene dinoflagellate cyst biostratigraphy of Seymour Island, Antarctica. In: Feldmann R.M. & Woodburne M.O. (eds.), *Geology and Palaeontology of Seymour Island, Antarctic Peninsula, Geological Society of America Memoir*, 169, 321-447.

Yanagisawa Y. & Akiba F., submitted. Refined Neogene diatom biostratigraphy for the northwest Pacific around Japan, with an introduction of code numbers for selected diatom biohorizons. *Journal of Geological Society of Japan.*

Terra Antartica
1998, **5**(1), 125-137

Summary of Results from CRP-1, Cape Roberts Project, Antarctica

CAPE ROBERTS SCIENCE TEAM*

Abstract - Poorly consolidated diamicton, silt, sand, gravel, and a mixed skeletal carbonate-terrigenous facies was cored from 16 m down to 43.55 mbsf and dated as 1.25 to 1.80 Ma (early Quaternary) from diatom biostratigraphy. Depositional environments range among 1) possible terrestrial exposure, 2) glacimarine sedimentation from nearby glacier ice, 3) deposition under sea-ice like today and 4) shallow-marine sea-ice free carbonate sedimentation, representing much warmer temperatures than today. At least two cycles of rise and fall in sea level are recognised. The pre-Quaternary section comprises mainly diamictite, sandstone and siltstone, organised in a cyclic fashion considered to reflect 6-8 variations in relative sea level and/or glacial advance-retreat. Depositional environments were largely shallow-water glacimarine with sedimentation associated with temperate-glacier termini. Diatom biostratigraphy and magnetostratigraphy indicate the strata range from 22.4 to 17.5 Ma in age (average sediment accumulation rate of 21 m/my). These strata record the first extensive Neogene volcanism in the region around 18 my ago, and contain the first post-Eocene marine-dinoflagellate assemblage (at least 15 new species). Another first report is of the calcareous dinoflagellate (Thoracosphaera), found in both Miocene and Quaternary sediment at CRP-1. The pre-Quaternary section of CRP-1 reaches down almost to the base of seismic Unit V3, previously interpreted as representing mid-Oligocene shallowing and glacial advance in the Victoria Land Basin. Results from CRP-1 suggests that the base of V3 could be as much as 8 my younger. This should be resolved by future drilling planned off Cape Roberts.

INTRODUCTION

The Cape Roberts Project is a cooperative drilling project involving personnel from Australia, Germany, Italy, New Zealand, UK and USA. The aim of the project is to recover continuous core through c. 1 300 m of strata, thought to record the period from 30 million years before present (Ma) to possibly 100 Ma, beneath the western side of McMurdo Sound. The project is named after Cape Roberts, the staging point for the offshore drilling and a small promontory 125 km north west of McMurdo Station and Scott Base (Fig. 1).

The project is designed to address two questions:

- did ice sheets grow and decay on Antarctica, with attendant changes in global sea level, prior to the earliest Oligocene 34 Ma ago, when it is widely believed the first extensive ice formed on the continent?
- at what time did this region begin to rift to form the Ross Sea and the Transantarctic Mountains?

Implicit in these objectives is the determination of age, and lithological calibration to be provided by coring for the seismic stratigraphy of the Victoria Land Basin, based on an extensive array (40 000 line km) of seismic surveys in the western Ross Sea.

The strata to be cored form a seaward-dipping succession 10-15 km offshore from Cape Roberts, and seaward of the boundary between the Transantarctic

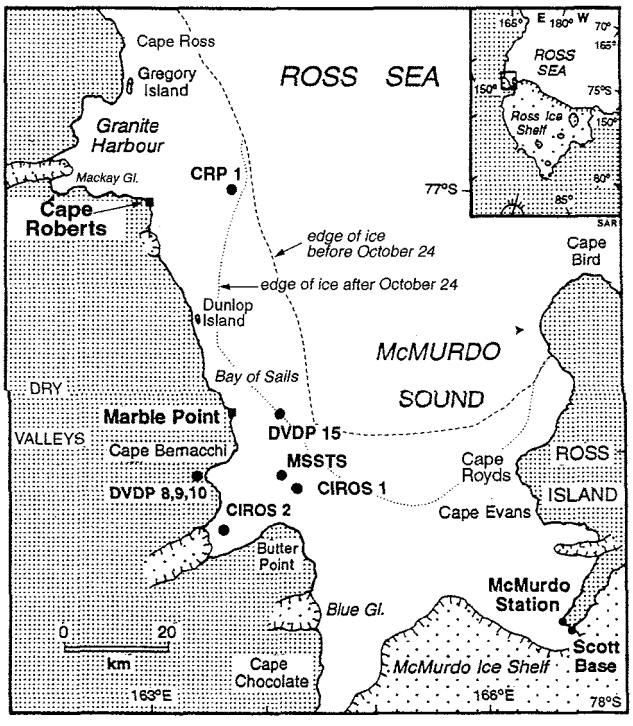

***Fig.** 1* - Map of the south west corner of the Ross Sea, showing the locations of Cape Roberts, CRP-1 and other drill sites in the area, and McMurdo Station/Scott Base, the main staging point for the project. The edge of the fast ice before and after the October 24 break-out is also shown.

* J. Anderson, P. Armienti, C. Atkins, P. Barrett, S. Bohaty, S. Bryce, M. Claps, M. Curran, F.J. Davey, L. De Santis, W. Ehrmann, F. Florindo, C. Fielding, M. Hambrey, M. Hannah, D.M. Harwood, S. Henrys, F. Hoelscher, J.A. Howe, R. Jarrard, R. Kettler, S. Kooyman, C. Kopsch, L. Krissek, M. Lavelle, E. Levac, F. Niessen, S. Passchier, T. Paulsen, R. Powell, A. Pyne, G. Rafat, I.J. Raine, A.P. Roberts, L. Sagnotti, S. Sandroni, E. Scholz, J. Simes, J. Smellie, P. Strong, M. Tabecki, F.M. Talarico, M. Taviani, K.L. Verosub, G. Villa, P.N. Webb, G.S. Wilson, T. Wilson, S.W. Wise, T. Wonik, K. Woolfe, J.H. Wrenn.

Mountains (TAM) block and the Victoria Land Basin (VLB) (Fig. 2). Seismic surveys of the basin have traced three sequences into the 2 000 m+ of sedimentary section off Cape Roberts (V3, V4 and V5, Fig. 3). Correlations with the CIROS-1 hole 70 km to the south indicate that most of the strata are more than 30 Ma old (Bartek et al., 1996). The Cape Roberts Project aims (over two or three years) to core 1 200 m or more of this section by drilling at least three holes ranging in depth from 400 to 700 m and overlapping so as to ensure a continuous stratigraphic record.

Cape Roberts - 1 (CRP-1) was drilled from a rig established on sea-ice some 15 km east of Cape Roberts, western McMurdo Sound, Antarctica (Fig. 1) during October, 1997. The hole was sited in a relatively offshore position on the western flank of a submarine ridge, designed to penetrate the youngest part of the section identified from seismic reflection records (Fig. 2). CRP-1 was drilled to a depth of 147.69 m and was cored continuously, apart from the uppermost 20 m. The drill hole encountered a succession of clastic sediments and sedimentary rocks with one short interval of carbonate sediments. The succession has been interpreted in terms of a lower Quaternary (Pleistocene) section to 43.55 metres below sea floor (mbsf) unconformably overlying a lower Miocene interval (43.55 to 147.69 mbsf). Both sections represent predominantly glacimarine deposition modulated by significant variation in climate, sea-level and ice cover.

This chapter summarises results of research conducted during and immediately following the drilling of the hole, at the Cape Roberts drill site and base camp, and at the Crary Science and Engineering Center (CSEC), McMurdo Station, respectively. An account of the litho-, bio-, seismic- and sequence-stratigraphy of the hole is given, together with an initial appraisal of petrology, palaeontology and physical properties of the cored section.

DRILLING HISTORY

The drilling rig was set up on the sea-ice off Cape Roberts in early October, and after some delay in setting the sea riser, coring of CRP-1 began on October 17, 1997. Coring the upper part of the section proved difficult, due to unconsolidated sediments and the brecciated character of much of the core, but an average core recovery of 68% was nonetheless achieved. Unstable down-hole conditions continued into the more consolidated Miocene section due to the persistence of the fracturing and brecciation mentioned above, and substantial volumes of drilling fluid were lost to the formation. More consolidated strata (mainly diamictite) were encountered at 100 mbsf and core recovery rose to 98%.

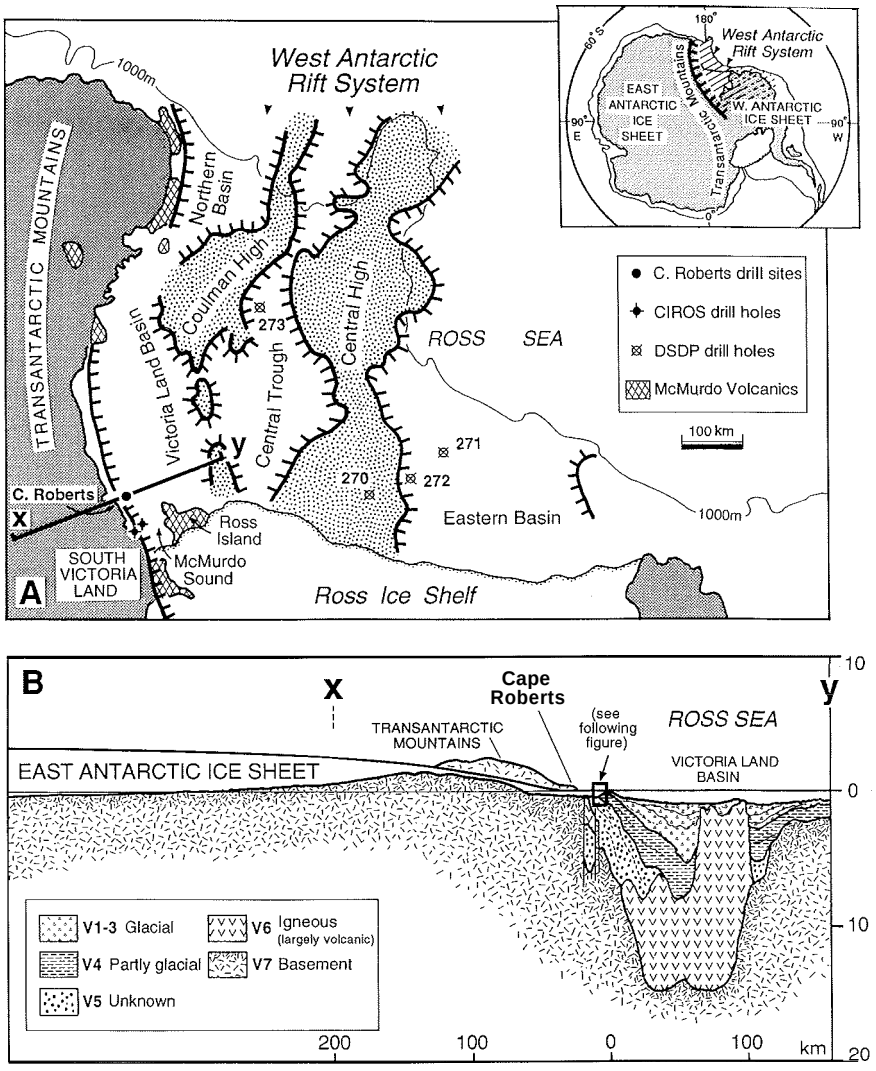

Fig. 2 - Map of Ross continental shelf (A) and cross-section through the edge of the east Antarctic Rift System (B), showing the location of Cape Roberts with respect to the East Antarctic Ice Sheet, the Transantarctic Mountains and the Victoria Land Basin. The location of figure **3,** with the 3 planned drill sites off Cape Roberts, is also shown.

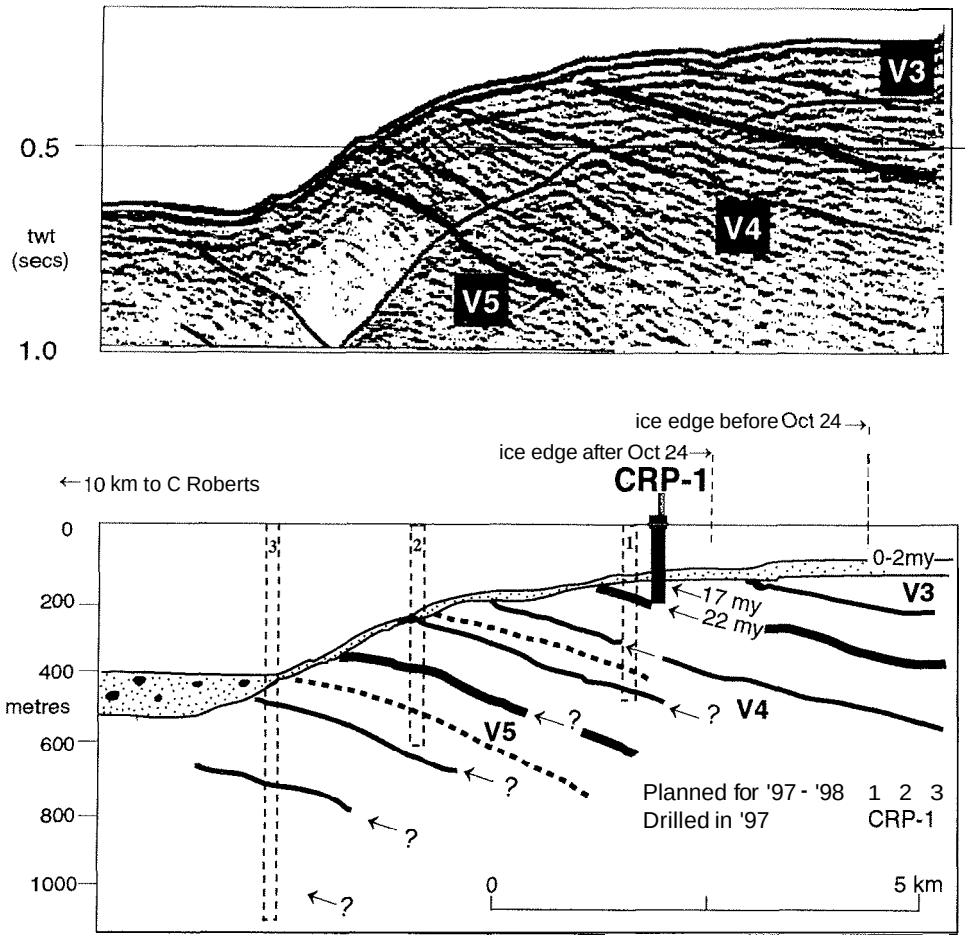

Fig. 3 - Geological section based on seismic data from NBP96-89 (adapted from Fig. 3.5by S.A. Henrys in Barrett, 1997), showing CRP-1 and the ages obtained by the Cape Roberts Science Team (see Quaternary and Miocene Strata, this volume).

Core was split and boxed at the drill site, and transported first to the Cape Roberts base camp and hence to McMurdo Station by helicopter on a daily basis. The decision to case and cement the H rod was made on October 23, but the consequences of a severe storm at that time forced abandonment of the drill site. The retrieval of the drilling rig to safe refuge at Cape Roberts was completed on October 25. Following an appraisal of sea-ice conditions after the storm, the decision was taken to conduct no further drilling in the 1997 season.

LITHOSTRATIGRAPHY

The core comprises a succession of interbedded diamictite, conglomerate, sandstone, siltstone, claystone and in the upper part of the core the unconsolidated equivalents of these lithologies together with a short interval of mixed carbonate-clastic sediment. A graphic log illustrating the lithological succession and lithostratigraphic subdivision of the core is shown as figure 4. The basis for the lithostratigraphic division is the alternation throughout the core between units dominated by diamicts and those composed predominantly of other clastic sedimentary facies. Accordingly, seven principal lithostratigraphic units are recognised, some of which are divided into several sub-units (Fig. 4).

The uppermost part of the core (to 43.55 mbsf, base of lithostratigraphic Unit 4.1) is poorly consolidated and contains microfossils indicating an early Pleistocene age, whereas the underlying section is moderately lithified and contains lower Miocene microfossils throughout. Much of the core is affected by fracturing and brecciation, believed to have largely formed naturally by brittle deformation of the rock, though the origin of this brecciation is at present unclear.

PETROLOGY

Petrological investigations have been conducted on gravel, sand and mud fractions of sediments from CRP-1. Studies of extraformational clasts from diamicts and conglomerates/gravels indicate provenance from the Transantarctic Mountains. Clasts include granites of probable Cambro-Ordovician age, metamorphic rocks perhaps of the Koettlitz Group, Ferrar Dolerite (Jurassic) and rhyolites of uncertain affinity. Metamorphic clasts are present only in the lower Miocene section. The sand fraction is dominated by grains derived from crystalline basement and the Beacon Supergroup (Devonian-Triassic), mainly quartz and feldspar, with rarer biotite, tourmaline, zircon, garnet, and minor but persistent pyroxene from the Ferrar Dolerite. Additionally, grains of volcanic glass (varying in composition from basaltic to intermediate and evolved, including trachytic) and lithic fragments (mainly oxidised, fine-grained lavas) are abundant in the upper part of the hole, decreasing sharply below 62 mbsf. This

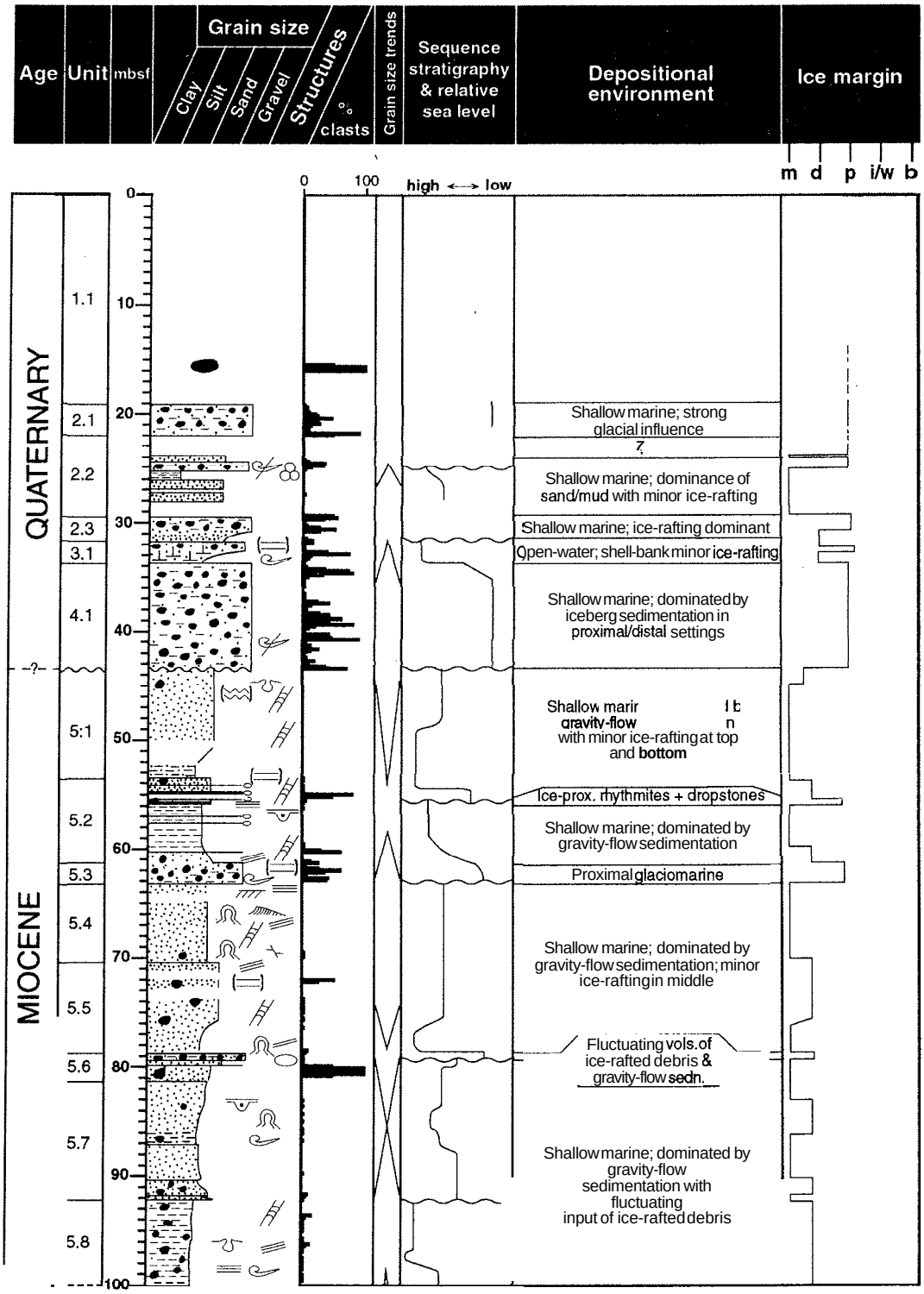

Fig. 4 - For caption see next page.

abrupt influx of volcanic detritus, correlated with the onset of McMurdo Volcanic Group activity, corresponds to the base of lithostratigraphic Unit 5.3, base of sequence stratigraphic Unit 7 (see below), and an abrupt downward decrease in magnetic susceptibility related to a decrease in ferromagnesian-mineral content. X-ray diffraction analysis of mud samples shows a similar change in mineralogy over the interval 60-65 mbsf from smectite-dominated above to illite and chlorite-dominated below. These changes mirror that from volcanic-dominated to volcanic-poor in the sand fraction, and a causal link is considered likely.

PALAEONTOLOGY

QUATERNARY

The Quaternary section of CRP-1 is dated by diatom biostratigraphy at 1.25 - 1.80 Ma, though it has yielded a

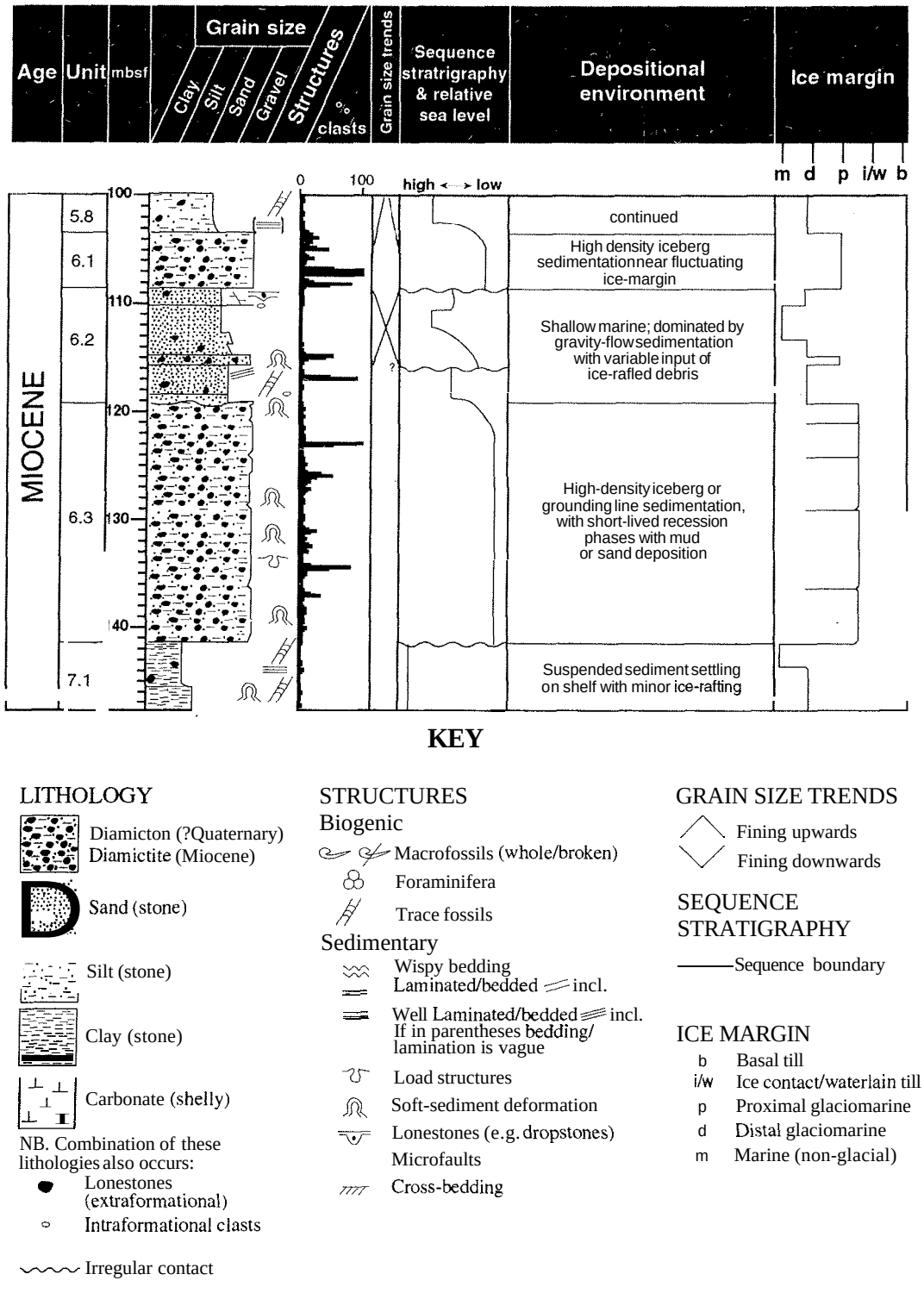

Fig. 4 -Summary log for CRP-1 showing lithologies, lithostratigraphy, extraformational-clast concentration, interpreted depositional settings, relative sea-level curve and interpreted proximity to glaciers.

wide variety of macrofossils and microfossils. Their occurrences, however, are largely sporadic or discontinuous, and reworked taxa from older units were frequently noted, particularly in the diamicts. Nonetheless, these fossils provide age control and important palaeoenvironmental information on what appears to have been a glacimarine setting that underwent significant fluctuations.

Diatoms are the most prevalent fossil group and include marine (planktonic and benthic), fresh and nearshore-brackish water taxa. Their occurrences, along with their abundances, reflect varying conditions of sea-ice cover, sea-water temperature, sea level, and cover by a glacier tongue or ice shelf. Postulated palaeoenvironments at the site range from possibly terrestrial to open marine with an absence of sea ice, to marine sea-ice covered.

Pleistocene foraminifers are also ubiquitous, consisting of over 30 benthic and planktonic taxa, but calcareous nannofossils are few and consist only of well-preserved fragments of *Thoracosphaera*, a calcareous dinoflagellate.

This is the first report of this group from the Quaternary of the East Antarctic margin.

Palynomorphs, present in 8 of 10 samples examined, include spores and pollen (miospores) and organic-walled microplankton (dinoflagellates, acritarchs and prasinophycean green algae cysts). Also noted in organic rcsidues were foraminiferal linings, which were the dominant andalmost the only palynomorph in the carbonate lithostratigraphic Unit 3.1. The terrestrial palynoflora is limited and includes forms such as *Nothofagidites lachlaniae* that may or may not be *in* situ.

Of particular palaeontological interest is the unique bioclastic carbonate (lithostratigraphic Unit 3.1) in which all fossil groups are present. The invertebrate assemblage is largely *in situ* or nearly so, and is dominated by molluscs (over 35 taxa identified at least to genus) along with appreciable numbers of bryozoans and lesser numbers of echinoids, serpulid worms, octocorals, barnacles and brachiopods.

MIOCENE

The section from 43.55 mbsf to the bottom of the hole is dated as 17.5 - 22.4 Ma (lower Miocene) by diatom biostratigraphy. This suggests an average sediment accumulation rate (uncorrected) of *c.* 21 m/my. The most prevalent fossils groups are the diatoms, palynomorphs and foraminifers. Calcareous nannofossils *(Thoracosphaera)* are rare to few, as are macrofossils. Palaeoenvironmental interpretations suggest a glacimarine setting that underwent some significant fluctuations in water depth and proximity to the ice margin.

Diatoms include marine (planktonic and benthic) but no fresh- or nearshore-brackish-water taxa. Their occurrences are discontinuous and, along with their abundances, reflect varying sedimentation rates, cover by glacier tongues or shelf ice, or productivity in an open-marine environment. Recurrence of intervals rich in benthic diatoms suggests fluctuations in water depth to less than 50 m below sea level (bsl) in many intervals.

Benthic foraminiferal assemblages were found in 15 of 45 samples examined. Those between 43.15 and *c.* 120.00 mbsf were mostly rare or barren, but abundances and diversities increased down hole below that point. Planktonic forms are very rare, which suggests sediment depositioninrelativelyshallow-water,inshoreenvironments.

Of particular palaeontological interest is the plethora of new marine palynomorph taxa, an especially noteworthy discovery in that this is believed to be the first report of *in situ* antarctic palynomorphs in lower Miocene strata. The well-preserved assemblage is dominated by acritarchs, more than 15 species of which are new. Prasinophycean green algae are also among the most abundant and consistently occurring palynomorphs. Dinocyst assemblages are of low abundance and diversity but consist of protoperidinoid cysts, a form not seen in the Quaternary deposits of the core. This might indicate milder-climatic conditions during the Miocene at the CRP-1 drill site.

Miospores are present in small numbers in most samples, including reworked Permian - lower Mesozoic taxa, which are most prevalent around 70 mbsf. Also present at that level and between 100 and 120 mbsf are relatively abundant *Nothofagidites* spp., *Podocarpidites* spp., and a range of angiosperm taxa that may or may not be *in situ.*

Macrofossils consist of serpulid (polychactc) worm tubes, echinoid spines, bryozoans, and *Chlatnys* (scallop) shells. These seem indicative of silted shallow-marine environments, with estimated depths shallower than 100 m bsl, possibly between 20 and 80 m bsl, substantially shallower than the present range in depth for the Miocene section, around 190 to 300 m bsl. The absence of true polar pectinid bivalves (*Adamussium*) suggests temperatures warmer than present.

AGE MODEL AND CORRELATION TO THE MAGNETIC POLARITY TIME SCALE (MPTS)

Diatom biostratigraphy suggests the interval from 26.95 to 34.80 mbsf belongs to the lower Quaternary *Fragilariopsis kerguelensis* Zone (1.25 to 1.80 Ma) of Harwood & Maruyama (1992). This zone represents the stratigraphic interval between the highest occurrence of *Fragilariopsis barronii* (event D2q on Fig. 5), down to the highest occurrence of *Thalassiosira kolbei* (event D4q). Other diatom biostratigraphic events that support this age are indicated on figure 5. The recovery of *Thalassiosira elliptipora* and *Actinocyclus ingens* up to interval 26.08 to 26.95 mbsf, suggests an age older than 0.65 Ma at this level (event D1q). The presence of *T. torokina* up to interval 26.08 to 26.95 mbsf may suggest an age older than ~1.4 Ma, although the upper range of this diatom is not well established. The lowest occurrence of *Thalassiosira elliptipora* indicates an age younger than 2.4 Ma between 34.81 to 35.47 mbsf (event D5q) (Winter & Harwood, 1997). The absence of *Thalassiosira fasciculata* and *T. inura* from the diatom bearing interval between 26.95 to 34.80 mbsf provides further support for an age younger than 1.8 Ma above 35.46 mbsf. The diatom-bearing interval (26.95 to 34.80 mbsf) was apparently deposited within a time interval less than 550 000 years during the early Quaternary. The 2m-thick, fossiliferous Unit 3.1 represents only a fraction of this time period, perhaps less than 100 000 years. The Quaternary is separated from the lower Miocene section of CRP-1 by an unconformity at 43.55 mbsf that represents approximately 15 my from 1.8 to 17.5 Ma (Fig. 5).

In situ marine diatoms also provide biostratigraphic age control for the lower Miocene portion of the CRP-1 core (Miocene Strata, this volume - section on Diatoms). Biostratigraphic reference comes from Antarctic data in the nearby MSSTS-1 and CIROS-1 drill holes and from data in nearby Ocean Drilling Program (ODP) drill holes. Magnetic polarity stratigraphy has been measured for the lower *c.* 90 m of the CRP-1 drill hole (Miocene Strata, this volume - section on Palaeomagnetism and Mineral Magnetic Properties). Palaeomagnetic analysis was not possible on the upper *c.* 60 m of the core because it was poorly consolidated and heavily fractured. The fracturing also precluded sample collection and analysis in much of

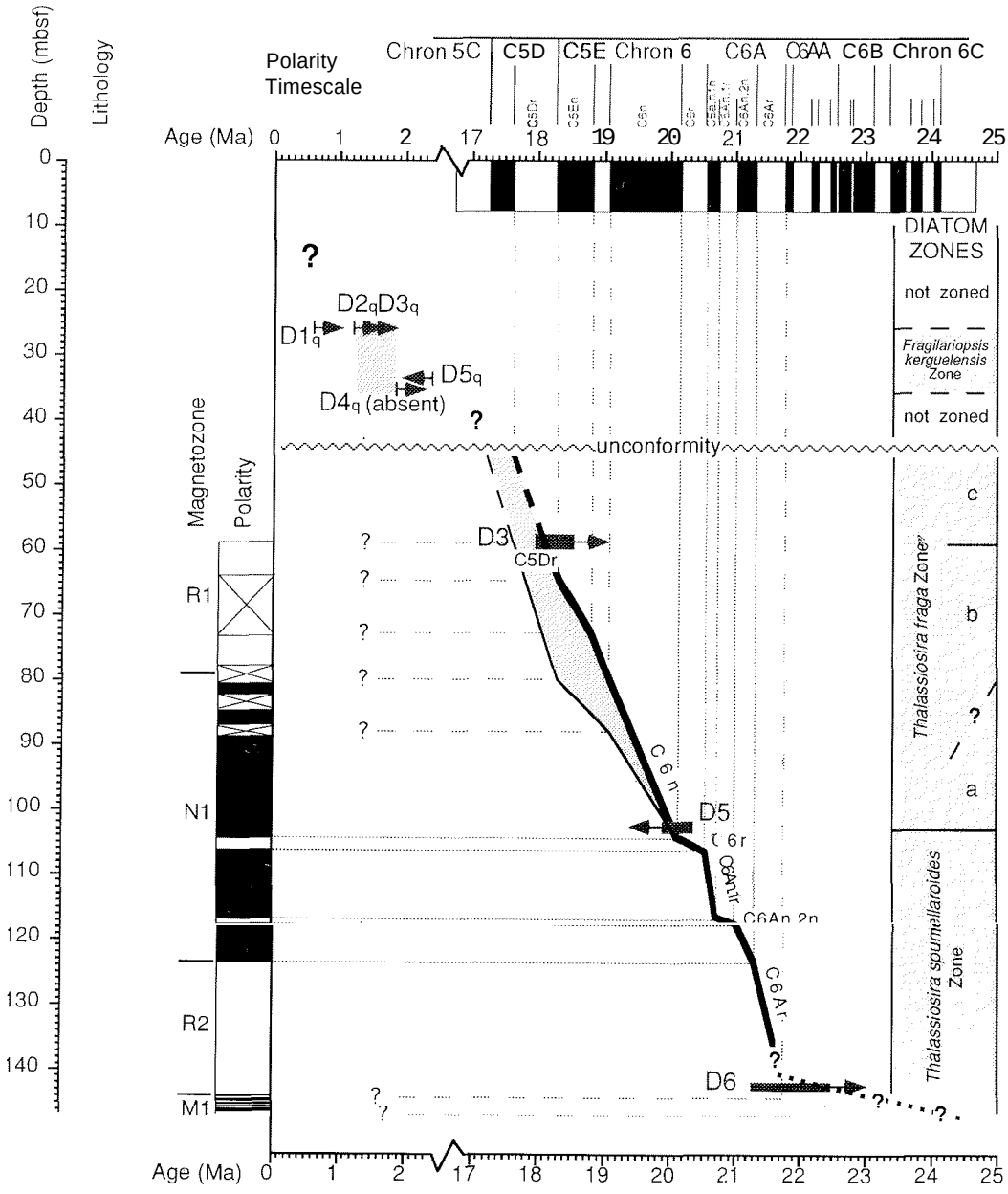

Fig. 5 - Correlation of the CRP-1 borehole with magnetic polarity timescale of Cande & Kent (1995) and Berggren et al. (1995) using the magnetic polarity zonation defined in Miocene Strata, section on Palaeomagnetism and Mineral Magnetic Properties (this volume) and diatom datum events defined in Quaternary and Miocene Strata, section on Diatoms (this volume). Polarity zonation: black is normal, white is reversed, and hashed is where no data are available. Diatom datums for Quaternary events: D1q = Last Appearance Datum (LAD) of *A. ingens* and T. *elliptipora;* D2q = *LAD* of F. *barronii*; D3q = *LAD* of *T. torokina;* D4q = LAD of T. *kolbei,* T. *inura* and *T. fasciculata*; and D5q = First Appearance Datum (FAD) of T. *elliptipora.* Diatom datums for the lower Miocene follow the scheme from Miocene Strata, section on Palaeontology (this volume); D3 = Last Occurrence (LO) of T. *praefraga,* D5 = First Common Appearance (FCO) of T. *praefraga,* D6 = LO of *S. spinossisima.* Line of correlation: solid is correlation of individual polarity events with the MPTS, dashed is where polarity events are ambiguous and correlation is continued using only biostratigraphic datums, dotted line is representative only and is not well-defined. Two interpretations are presented for the interval from 60 to 90 mbsf, with the favoured interpretation marked by the heavier line.

the interval between 58 and 89 mbsf. Below 89 mbsf stable endpoint-polarity solutions were achieved for almost all samples measured, resulting in a reliable polarity record within which 4 magnetozones are defined (Fig. 5): an upper poorly defined reversed polarity interval (<82 mbsf, R1); a predominantly normal polarity interval (82-124 mbsf, N1) which includes two thin intervals in the upper part for which no data is available and two reversed polarity zones in the lower part; a second interval of reversed polarity (124.00-144.47 mbsf, R2); and an interval at the base of the record (144.47-147.69 mbsf, M1) with high frequency alternating normal and reversed polarity.

Three key diatom datum events tightly constrain correlation to the MPTS: the Last Appearance Datum (LAD) of *Stephanopyxis spinossisima* (141.48-141.80 mbsf, D6, Fig. 5), First Common Appearance Datum (FCAD) of *Thalassiosira praefraga* (102.24-103.39 mbsf, D5, Fig. 5), and LAD of *T. praefraga* (58.75-59.68 mbsf, D3, Fig. 5). The LAD of *S. spinossisirna* (D6) in the MSSTS-1 drillhole

(58 mbsf, Harwood, 1986) occurs in reversed polarity which, because of the incomplete recovery and numerous unconformities in the upper part of MSSTS-l, Harwood et al., (1989), were able to restrict to chrons C6AA and C6A only in their integrated correlation with CIROS-1. The FCAD of *T. praefraga* (D5) is well known and reported to range from the upper part of chron C6r through chron C6n in Southern Ocean ODP drill holes (Gersonde & Burckle, 1990; Baldauf & Barron, 1991; Harwood & Maruyama, 1992; Harwood et al., 1992). Harwood & Maruyama (1992) also report the LAD of T. *praefraga* (D3) in the lower part of anomaly C5Dr but other reports place this datum slightly older in the upper part of C5En (Gersonde & Burckle, 1990; Barron & Baldauf, 1995).

In CRP-1, the LAD of *T. praefraga* (D3) occurs in an interval of reversed polarity (58-65 mbsf) in magnetozone R1 (Fig. 5). This interval of reversed polarity must correlate within C5Dr. Because of the underlying interval with no polarity data, it is not known whether the lower reversed polarity interval of magnetozone R1 (74.00-78.50 mbsf) also correlates with C5Dr, or whether it correlates with chron C5Er. Lower in the core, the FCO of T. *praefraga* (D5) occurs within an interval of normal polarity above 105 mbsf in the middle of magnetozone N1 (Fig. 5). This interval of normal polarity must therefore correlate with chron C6n of the MPTS. Because there is no obvious lithologic break at the base of the normal polarity interval it is most likely that the underlying reversed polarity interval (105-107 mbsf) correlates with chron C6r of the MPTS, and the underlying two intervals of normal polarity are likely correlative with C6A.n1n and C6A.n2n. Lower still in the core the LO of S. *spinossisima* occurs within reversed polarity magnetozone R2. This may correlate with any or all of the reversed polarity sub-chrons in chrons C6AA and C6A, but it is most likely that much of R2 correlates with chron C6Ar. This brackets the lower portion of magnetozone N1, as suspected, with the N-R-N-R sequence (105-125 mbsf) correlative with C6An.1n, C6An.1r and C6An.2n. (Fig. 5).

Guided by these correlations, two interpretations are possible for the interval 60 to 88 mbsf. The first and favored interpretation, because it is a better match to datum D3, implies that C6N continues through the intervals with no polarity data up to ~80 mbsf. This interpretation also implies that C5En lies within the broad interval of no polarity data from 65 to 75 mbsf. This interpretation is represented by the heavy line. An alternative interpretation implies that C5En is present between 80-87 mbsf, representing one or both of the normal poarity events in this interval (Fig. 5). In this case, the interval of reversed polarity between 77-60 mbsf correlates to C5Dr.

The lower mudstone (Unit 7.1) of CRP-1 cannot at present be correlated with the MPTS. The lowermost 3 m of CRP-1, magnetozone M1, contains many thin polarity events that may, if they represent polarity sub-chrons, correlate somewhere within the high reversal frequency interval including chrons C6Cn, C6B and C6AA.

On the basis of the above correlations, the average sedimentation rate between c. 140 mbsf and the unconformity at 44 mbsf is about 20 m/my with little or no time loss recognised in unconformities (though sedimentary facies and sequence stratigraphic analysis suggest considerable time could be missing at many levels though the core). Below 140 mbsf the rapid polarity changes suggest a sedimentation rate that is likely to be an order of magnitude lower.

SEISMIC CORRELATIONS TO THE VICTORIA LAND BASIN, AND CORE PHYSICAL PROPERTIES

In the light of drilling results, a re-evaluation of the seismic-reflection interpretation has been carried out. The bottom of CRP-1 is now interpreted to lie within c. 15 m of the seismic sequence boundary V3/V4, which by correlation with the CIROS-1 borehole was thought to he of late Oligocene age (30 Ma). The oldest sediments in CRP-1, however, areestimated from diatom biostratigraphy and magnetostratigraphy to be c. 23 Ma, which demands re-evaluation of previous correlations. Three seismically definable units are recognised (Background to CRP-1, this volume - Fig. 19, section on Correlation of Seismic Reflectors with CRP-l), and correspond to Quaternary lithostratigraphic Units 1-4, and lower Miocene Unit 5, and Units 6/7. An alternative interpretation that the lithostratigraphic Unit 6/Unit 7 boundary represents the V3/V4 boundary is considered less likely. The reflector corresponding to the base of the Quaternary succession shows truncation of underlying strata against steep-sided channel features.

The seismicunits defined above correspond to changes in physical properties (magnetic susceptibility, P-wave velocity and porosity as interpolated from density) measured on the core at the drill site. The core has been divided into six units based on changes in the above-mentioned physical properties (Background to CRP-1, this volume - Fig. 16, section on Physical Properties), which show close correspondence also to the lithostratigraphic units noted above and sequence stratigraphic divisions described below.

PALAEOENVIRONMENTAL INTERPRETATION

In order to address the first of the two questions posed by the project, namely the history of growth and decay of the Antarctic ice sheet and its links with sea-level change, a detailed sedimentological analysis of the core was conducted. Firstly, a facies analysis was carried out on a bed-by-bed basis, followed by a sequence stratigraphic analysis at a broader scale to identify patterns and trends through the vertical succession.

The recovered parts of the Quaternary section comprise diamicton of varying texture and fabric with coarse clasts up to boulder grade principally of granite and dolerite, interbedded with sands, muds, minor gravels and a short interval (31.89-33.82 mbsf) of mixed skeletal carbonate-terrigenous clastic sand/gravel. Two facies associations have been recognised, each containing four lithofacies. Association A,

comprising diamicton, gravel, sand and mud, is interpreted to reflect sediment accumulation in glacimarine environments, whereas Association B, comprising calcareous silt, shell hash deposits, sand and mud, is interpreted to record sediment accumulation in offshore-marine carbonate banks (Quaternary Strata, this volume - Tab. 1, section on Facies Analysis).

The lower Miocene section contains facies that are more lithified but otherwise comparable to the overlying Quaternary section, with the exception of the carbonate facies which is absent. The interval has been divided into six recurrent lithofacies: diamictite, rhythmically interlaminated fine-grained sandstone and siltstone, well-stratified sandstone, poorly-stratified muddy sandstone, coarse-grained siltstone and fine-grained siltstone. These facies arc interpreted in terms of sediment deposition in glacimarine environments by a combination of tractional currents, fallout from suspension and dropping of coarse debris from floating ice (Miocene Strata, this volume - Tab. 1, section on Facies Analysis).

Two different approaches have been taken to the interpretation of the sedimentary sequence cored in CRP-1. One approach is based on a direct comparison between the CRP-1 core and facies found in modern glacial settings, embracing cold, dry, "polar" glaciation as in modern Antarctica at one end of a spectrum, and warm, wet, "temperate" glaciation as in Alaska at the other. In between, modern Arctic and sub-Arctic glaciated areas provide alternative depositional models *(e.g.,* Powell, 1984; Hambrey, 1994; Powell & Domack, 1995). This "comparative facies" approach aims at providing an interpretation of the cored sequence in terms of ice margin variation.

The alternative view is based on recurring lithologic patterns, but notably variations in grain size, where fining trends are related in a general way to rising sea level. It uses the facies scheme presented in Miocene Strata, section on Facies Analysis (this volume) and derives an interpretation of relative sea-level variation that is not predicated on any particular model or analogue. It also embodies the view that only limited inferences can be made of past glacial environments from lithofacies. The two approaches are seen as distinctively different but complementary,

Diamict is the facies most indicative of a glacial setting, although non-glacial processes may also produce diamicts. The apparently unstratified character of much of this facies suggests a proximal glacial setting, perhaps a water-lain till, where continuous rain-out of fine- to coarse-grained sediment is taking place. Massive diamicts may form both subglacially and in the marine environment: one widely-used means of distinguishing the two alternatives is clast-orientation fabric. Random fabrics suggest deposition in water, whereas directional fabrics are indicative of basal till. Of four samples studied, three suggested the former, whereas one (at 62 mbsf) showed a directional fabric suggestive of deposition as a subglacial till.

Otherpoorly-sorted sediments, containing <1% coarse clasts, include muddy sandstone and sandy mudstone. These can form by a variety of processes and in various environments, although a glacialcontext seems reasonable. However, unless the strata contain a direct glacial imprint, such as the presenceof ice-rafted debris, a cautious approach to interpretation has been adopted. Sediment deposition from density currents, as indicated by bed character and internal structure, is consistent with both glacially and non-glacially influenced environments.

Better-sorted siltstones and sandstones could be interpreted as arising from sedimentation close to a glacier grounding-line by efflux from a subglacial stream in the context of the "glacial" model, or as the deposits of dilute aqueous currents in any marine setting. In volumetric terms, rhythmically laminated sediments are rare, but some examples of "cyclopsams" and "cyclopels" (Mackiewicz et al., 1984) have been recognised. These facies form in modern glacial fjord settings such as in Alaska, and have been used as an indicator of an ice-proximal setting, especially where evidence of ice-rafted debris is also preserved. In the case of the bioclastic carbonate facies (lithostratigraphic Unit 3.1), the glacial context is unclear except that ice-rafted debris is present in some parts of that interval. Biological indicators suggest that interglacial conditions prevailed at this time, with shallow-marine deposition in an area free of sea-ice.

The comparative facies approach for the Miocene section suggests that there were at least six significant advance and retreat episodes (Fig. 4), though they are seen possibly as the result of local variation in the ice front and not necessarily resulting from sea-level change. Ice distal deposits are considered to be poorly represented in the section, possibly on account of subglacial erosion by advancing ice.

A sequence stratigraphic analysis has also been conducted using the facies scheme presented in Miocene Strata, section on Facies Analisis (this volume), and based on the premise that changes in grain-size reflect changes in depositional energy, and hence relative water depth in a general sense. The succession has been divided into 10 sequences (Miocene Strata, this volume - Fig. 3, section on Sequence Stratigraphic Interpretation; Fig. 4), each bounded by an abrupt upward increase in grain-size that is interpreted as a sequence boundary (regressive surface of erosion). Each sequence passes upward from a basal diamict into progressively finer-grained facies, interpreted as recording a flooding event. According to this model, sequences are interpreted to record the cyclical advance and retreat of (grounded) ice across the area of the drill site, whereby glacial advances leave little if any sedimentary record, diamicts are deposited during glacial retreat and the other facies are formed in deeper water during interglacial periods. An important ramification of this model is that sequence boundaries may indicate gaps in the stratigraphic record, such that substantial periods of time may be unrecorded. This hypothesis is supported by the fact that short-term sedimentation rates in modern glacimarine environments may be of the order of metres per year, yet the long-term average sediment accumulation rate for the Miocene section in CRP-1 is 21 m/my.

The summary log (Fig. 4) provides an interpretation of inferred depositional environments in a general sense, and stratigraphic patterns, based on analysis of facies and their associations, and taking into account palaeoecological data available at the time of writing. From these analyses, a curve showing the interpreted relative position of the ice margin has been constructed, and an interpretation of relative sea-level fluctuations also given.

QUATERNARY ENVIRONMENTS AND DEPOSITIONAL HISTORY

The Quaternary section in CRP-1 yielded a diversity of depositional environments ranging from conditions 1) of possible terrestrial exposure during sea-level lowstand, 2) of glacimarine deposition under the influence of nearby glacial ice, 3) of deposition under seasonal sea-ice, similar to today, and 4) of warmer marine temperatures when carbonate sediments accumulated beneath seas that lacked sea-ice. At least two cycles of relative sea-level rise and fall are recognised from the sequence stratigraphic analysis (Fig. 4).

The passage of glacial ice across or close to the drill site is recorded by diamicts, which from their fossil content are interpreted to have been deposited in shallow-marine water. The identification of reworked Pliocene foraminifers in some samples indicates the incorporation of older glacimarine sediments into the Quaternary record. The possibility of non-marine conditions is raised by the identification of an exclusively freshwater diatom assemblage at 24.53 and 25.13 mbsf, although the lithofacies from which these samples were taken suggests a marine environment. This, together with the recognition of *Nothofagidites* pollen in a diamicton at 21 mbsf, is suggestive of incorporation of older glacigenic sediments and their contained fossils into the Quaternary record.

Preservation of marine sands and silts with little or no ice-rafted coarse debris, and the preservation of a modern, sea-ice diatom assemblage in Unit 2.2 is suggestive of sediment accumulation under conditions similar to today, when perhaps a seasonal sea-ice cover developed across the shallow-marine environment.

In contrast, the bioclastic carbonate sediments of lithostratigraphic Unit 3.1 were deposited under conditions that were warmer than today, as indicated by the presence of the calcareous nannoplankton *Thoracosphaera* sp. and the silicoflagellate genus *Dictyocha*, and the absence of a diatom assemblage that today inhabits the sea-ice environment. This unit has important implications for the understanding of Quaternary climate and glaciation history.

Modern and presumably Quaternary glaciers in the McMurdo Sound region are well below freezing in the upper few hundred metres, but are locally at pressure melting point where the ice is thick. As a consequence they carry unsorted basal debris (typically sand and gravel with minor mud) in layers metres thick (Barrett et al., 1981). The Quaternary section of the CRP-1 core is provisionally

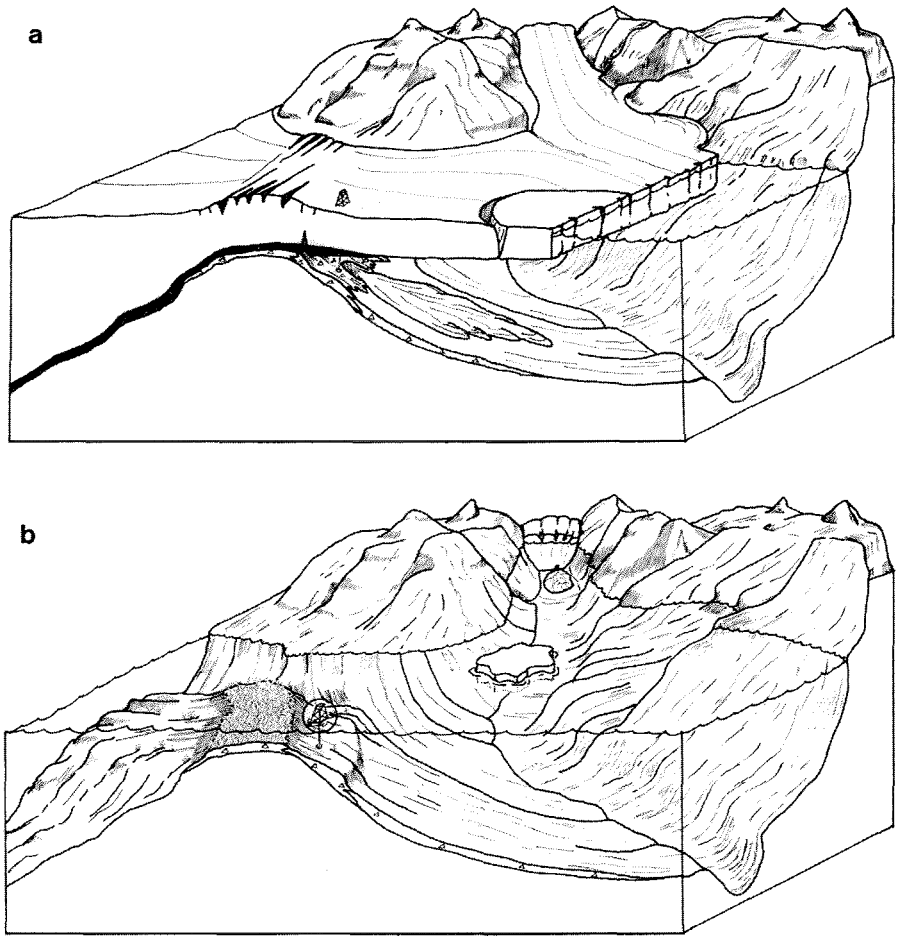

Fig. 6 - Perspective illustrations of the palaeoenvironment of the Cape Roberts area during early Quaternary times viewed from offshore. The illustrations are not to scale to allow marine environments to be emphasised. The drilling rig is circled.
a) Quaternary retreat phase from expanded ice in Ross Sea while its grounding line is pinned on Roberts Ridge and a floating shelf is fed by a glacier from the ice sheet behind the mountains. Subglacial till is deposited on the ridge, with waterlain till deposited just beyond the grounding line and debris flows move diamicts down slope toward Mackay Sea Valley.

b) Quaternary interglacial phase with glaciers almost gone and only rare icebergs crossing the drill site. A carbonate-rich epibenthic community is established on Roberts Ridge.

interpreted on the same basis. An artist's impression of the depositional setting, in which grounded ice enters the area from McMurdo Sound to the south (left) and from the TAM to the west (via the Mackay valley), is shown in figure 6a. The cold-ice front of the resulting glacier complex would be grounded on the south side of the rise and floating on the north side; sediments arising from interaction of ice with the marine environment are illustrated. An impression from the same viewpoint of the interglacial period represented by carbonate Unit 3.1 is shown in figure 6b.

MIOCENE ENVIRONMENTS AND DEPOSITIONAL HISTORY

A similar cyclicity to that noted above is recorded within the Miocene section, with seven complete and one partial cycle(s) of relative sea-level change recognised in the sequence stratigraphic analysis (Fig. 4). The most distal facies recorded occurs in the lowermost 6 m of the core, which from palaeomagnetic analysis is also believed to have accumulated an order of magnitude more slowly than other facies. The abrupt base of a diamictite that overlies this interval (Unit 7.1/6.3 boundary: Fig. 4) may or may not correspond to the "V3/V4" seismic sequence boundary noted in seismic-reflection records.

Macro- and microfossil assemblages indicate entirely marine environments of deposition. The extremes of environmental fluctuation preserved within the Quaternary record (bioclastic carbonates, freshwater diatom-bearing sediments) are not represented in the Miocene section. Nonetheless, significant cyclical fluctuations in environment, perhaps in proximity to an ice front and/or in water depth, are recorded in the lithofacies and associated macro- and microfossil assemblages. The only positive evidence for sediment accumulation under grounded ice has been found in a directional clast fabric in a diamictite at 62.64 mbsf. Nonetheless, the sequence stratigraphic analysis suggests that grounded ice may have passed across the drill site a number of times, leaving a record only of glacial retreat and the subsequent relative sea-level rise. No major changes in facies assemblage have been identified within the Miocene section, implying that similar variations in environmental conditions prevailed throughout.

In contrast to the Quaternary, climates of the Miocene are generally believed to have been milder. From the available evidence, it is difficult to judge whether Miocene glaciers were polythermal (as in southern Greenland, Svalbard and parts of the Canadian Arctic) or temperate (like Alaska and Patagonia), but from the evidence to hand an ice cliff, grounded on the sea floor, is the most likely scenario for glacier termini. The facies associated with such settings have a much larger component of fine melt water-transported sediment (Anderson & Ashley, 1991). An impression of the ice margin as a temperate or polythermal ice margin retreats across the CRP-1 drill site

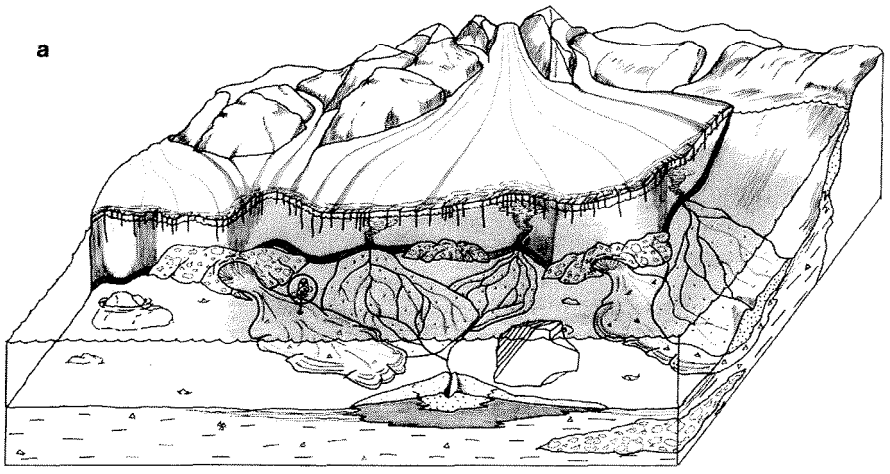

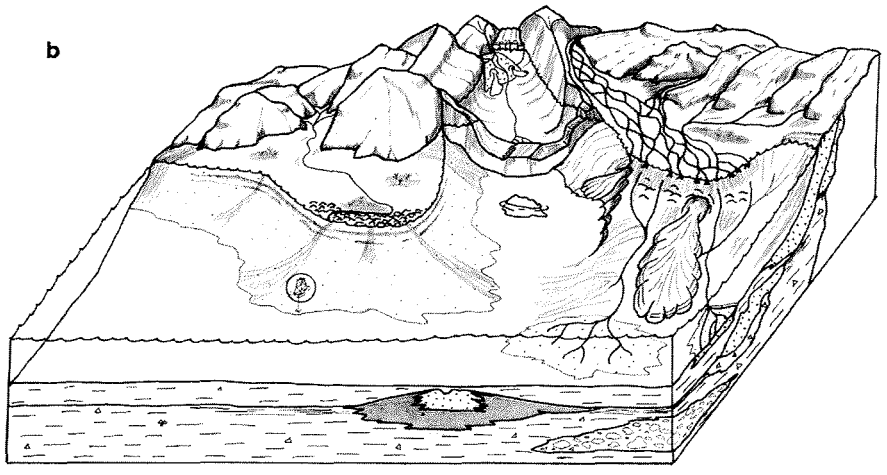

Fig. 7 - Perspective illustrations of the palaeoenvironment of the Cape Roberts area during early Miocene times viewed from offshore. The illustrations are not to scale to allow marine environments to be emphasised. The drilling rig is circled. ***a)*** Miocene glacial advance as temperate or polythermal glaciers expand out from the (lower) Transantarctic Mountains towards the drill site, occasionally extending beyond. Much of the time the site accumulated sediment rapidly close to the grounding line of a glacial tidewater cliff, where sediments include morainal bands, grounding line fans and iceberg zone facies associations.

b) Miocene ice in retreat with most ice gone apart from remnants of valley and tidewater glaciers. Most sediment is delivered to the coast by rivers and distributed by waves and currents. Only a very small proportion of the debris is ice-rafted.

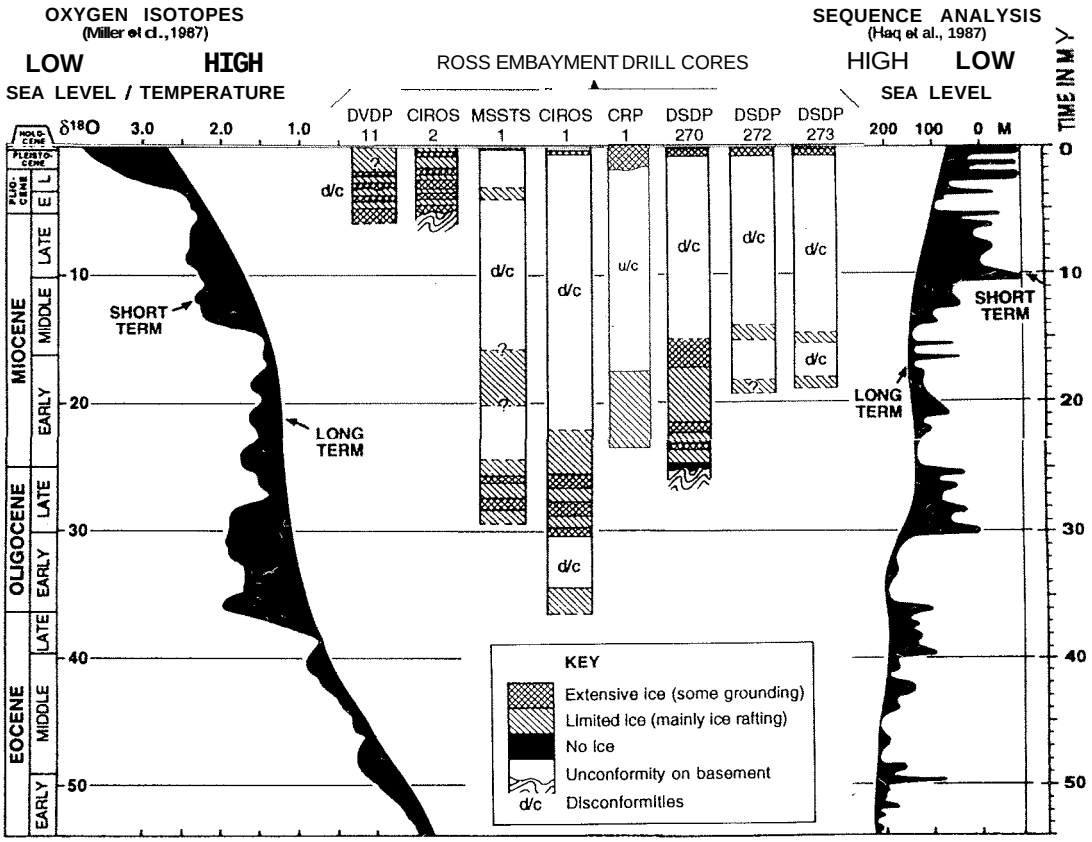

Fig. 8 - Summary log of CRP-1 shown in the context of other drilling in the region, the oxygen isotope curve of Miller et al. (1987) and the sea-level curve of Haq et al. (1987). Modified from Hambrey & Barrett (1993).

is shown in figure 7a. A palaeogeography is illustrated in which glaciers emanated only from the TAM to the west, coalescing to form a broad, north-south elongate front along the TAM front, and contributing to the basin-ward thickening Miocene sequence. The impression shown in figure 7b is of an interglacial period with virtually no ice but for a few small glaciers and floating bergs - suggested by sparse but persistent coarse sand and grit scattered through the Miocene sequence.

CONCLUSIONS

The following points are seen as the major scientific findings from CRP-1:

- need for revision of the seismic stratigraphy of the Victoria Land Basin. The discovery that strata near the base of V3 are around 8 my younger than expected indicates the need for a major review of basin stratigraphy, though this will be best undertaken when

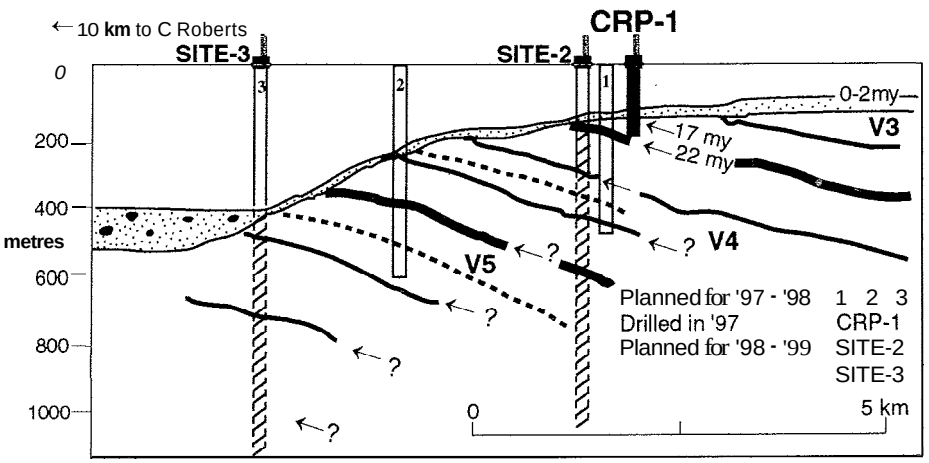

Fig. 9 - Interpreted seismic profile for NBP8901-89 (location shown in Miocene Strata, this volume - Fig. 4, section on Regional Setting), showing CRP-1 and the locations proposed for two further drillholes, each with a target depth of 700 mbsf, to core the entire sequence.

coring has reached into V5;
- characterisation of variations in glacial and glacimarine environments in the early Miocene and Quaternary. Two different approaches separately indicate around 10 major variations in ice extent and relative sea level through the cored interval;
- identification of a significant, relatively warm-climate facies in the early Quaternary with a rich and varied calcareous and siliceous biota;
- documentation of new fossil biotas from the Antarctic region (palynomorphs, *Thoracosphaera*) and development of a biostratigraphic database for future use in correlation within and beyond Antarctica;
- documentation of a period (20-22 Ma) not before recorded from the Victoria Land Basin (Fig. 8).

FUTURE PLANS

With around 10% of the sequence cored the project is well short of its objectives. A further season's drilling has been planned for under the present budget, and this will proceed. A number of difficulties were encountered in both drilling and core retention, most of which relate to unstable hole conditions to a depth of 100 m. The drilling system is currently under review so as to provide increased flexibility for the drill team to improve recovery and hole stability.

The next hole to be drilled will begin just above the oldest strata reached by CRP-1 and have a target depth of 700 m (Fig. 9). The value of the hole in regional terms is seen as the coring of the two oldest sequence boundaries in the Victoria Land Basin. For the goals of the project this hole should extend the history recorded by CIROS-1 70 km to the south further back in time, and possibly into the Palaeocene,

REFERENCES

Anderson J.B. & Ashley G.A., 1991. Glacial marine sedimentation; palaeoclimatic significance; a discussion. In: Anderson J.B. & Ashley G.A. (eds.), *Glacial marine sedimentation; paleoclimatic significance, Geological Society of America Special Paper*, 261, 223-226.

Baldauf J.G. & Barron J.A., 1991. Diatom biostratigraphy: Kerguelen Plateau and Prydz Bay regions of the Southern Ocean, *Proc. ODP, Sc. Results*, **119**, 547-598.

Barrett P.J., Pyne A.R. & Ward B.L., 1981. Modern sedimentation in McMurdo Sound, Antarctica. In: Oliver R.L., James P.R. & Jago J.B. (eds.), *Antarctic Earth Science, Australian Academy of Science*, Canberra, 550-555.

Barron J.A. & Baldauf J.G., 1995. Cenozoic marine diatom biostratigraphy and applications to palaeoclimatology and paleoceanography. In: Blome C.D. (ed.), *Siliceous microfossils, Paleontological Society Short Courses in Paleontology*, **8**, 107-118.

Bartek L.R., Henrys S.A., Anderson J.B. & Barrett P.J., 1996. Seismic stratigraphy in McMurdo Sound: implications for glacially influenced early Cenozoic eustatic change. *Marine Geology*, 130, 79-98.

Berggren W., Kent D.V., Swisher C.C. III & Aubrey M.P., 1995. A revised Cenozoic geochronology and biostratigraphy. In: Berggren W.A., Kent D.V., Aubrey M.P. & Hardenbol J. (eds.), *Geochronology, Time Scales and Stratigraphic Correlation, Society of Economic Paleontologists and Mineralogists Special Publication*, 54, 129-212.

Cande S.C. & Kent D.V., 1995. Revised calibration of the geomagnetic polarity time scale for the Late Cretaceous and Cenozoic. *Journal of Geophysical Research*, **100**, 6093-6095.

Gersonde R, & Burckle L.H., 1990. Neogene biostratigraphy of ODP Leg 113, Weddell Sea (Antarctic Ocean). *Proc. ODP, Sc. Results*, **113**, 761-789.

Gombos A.M., 1977. Paleogene and Neogene diatoms from the Falkland Plateau and Malvinas outer basin, Leg 36, Deep Sea Drilling Project. *Initial Reports of the Deep Sea Drilling Project*, **36**, U.S. Government Printing Office, Washington, D.C., 575-687.

Hambrey M.J., 1994. *Glacial Environments*. UCL Press, London, 294p.

Hambrey M.J. & Barrett P.J., 1993. Cenozoic sedimentary and climatic record, Ross Sea Region, Antarctica. In: Kennett J.P. & Warnke D.E. (eds.), *The Antarctic Palaeoenvironment: a Perspective on Global Change, American Geophysical Union Antarctic Research Series*, 60, 91-124.

Haq B.U., Hardenbol J. & Vail P.R., 1987. Chronology of fluctuating sea levels since the Triassic. *Science*, 235, 1156-1167.

Harwood D.M., 1986. Diatoms. In: Barrett P.J. (ed.), Antarctic Cenozoic history from the MSSTS-1 drillhole, McMurdo Sound, *DSIR Bulletin*, 237, 69-108.

Harwood D.M., Barrett P.J., Edwards A.R., Rieck H.J. & Webb P.N., 1989. Biostratigraphy and chronology. In: Barrett P.J. (ed.), Antarctic Cenozoic history from the CIROS-1 drillhole, McMurdo Sound, *DSIR Bulletin*, **245**, 231-239.

Harwood D.M. & Maruyama T., 1992. Middle Eocene to Pleistocene diatom biostratigraphy of ODP Leg 120, Kerguelen Plateau. *Proc. ODP, Sc. Results*, 120, 683 -733.

Harwood D.M., Lazarus D., Abelmann A., Aubry M.P., Berggren W.A., Heider F., Inokuchi H., Maruyama T., McCartney K., Wei W. & Wise S.W., Jr., 1992. Neogene integrated magnetobiostratigraphy of the Southern Kerguelen Plateau, ODP Leg 120. *Proc. ODP, Sc. Results*, 120, 1031-1052.

Mackiewicz N.E., Powell R.D., Carlson P.R. & Molnia B.F., 1984. Interlaminated ice-proximal glacimarine sediments in Muir Inlet, Alaska. *Marine Geology*, 57, 113-147.

Miller K.G., Fairbanks R.G. & Mountain, G.S., 1987. Tertiary oxygen isotope synthesis, sea level history and continental margin erosion. *Paleoceanography*, 2, 1-19.

Powell R.D., 1984. Glacimarine processes and inductive lithofacies modelling of ice shelf and tidewater glacier sediments based on Quaternary examples. *Marine Geology*, 57, 1-52.

Powell R.D. & Domack E.W., 1995. Glacimarine environments. In: Menzies J. (ed.), *Glacial Environments -Processes, Sediments and Landforms*, Butterworth-Heinemann, Boston, 445-486.

Winter D.M. & Harwood D.M., 1997. Integrated diatom biostratigraphy of Late Neogene drillholes in southern Victoria Land and connection to Southern Ocean records. In: Ricci C.A. (ed.), *The Antarctic Region: Geological Evolution and Processes*, Terra Antartica Publication, Siena, 985-992.

Terra Antartica
1998, 5(1), 139-140

Appendix 1

Core Recovery Data for CRP-l

			CORE RUNS		CORE RECOVERY				ROCK TYPE/AGE
RUN	DAY	TIME	START	END	m	sum	%	cum %	(not for quoting-see main body of report)
1	17	01:30	15.00	15.63	0.00	0.00	0	0	UNIT 1 0.00-19.13 m
2	17	03:10	15.63	16.06	0.43	0.43	100	93	**Run 1** corcdgrout and 2 cored dolerite boulder
3	17	05:20	16.06	19.07	0.10	0.53	3	15	
4	17	06:00	19.07	19.57	0.44	0.97	88	24	UNIT2 19.13-31.70 m
5	17	07:44	19.57	22.00	2.40	3.37	99	53	Pebbly sandy mud (diamicton) with scattered
6	17	12:00	22.00	25.05	0.67	4.04	22	43	boulders andoccasional muddy volcanic sands
7	17	13:00	25.05	28.13	3.05	7.09	99	57	Deposition from glaciers, marine currents, waves
8	17	13:00	28.13	31.18	1.69	8.78	55	56	*Age 0-2 my*
9	17	16:40	31.18	34.30	3.10	11.88	99	64	
10	17	20:00	34.30	36.01	1.48	13.36	87	66	UNIT3 31.70-33.82 m
	DRILL 20.38 m		**REC**	**13.36 m**			66%		Muddy limestone with small clam shells
11	17	23:00	36.01	36.85	0.25	13.61	30	64	Deposition in shallow water andlittle glacial discharge
12	18	00:20	36.85	39.95	2.18	15.79	70	65	*Age 1.0-1.8 my*
13	18	03:20	39.95	40.95	1.40	17.19	140	68	UNIT433.82-43.55 m
14	18	04:55	40.95	42.35	1.21	18.40	86	69	Pebbly sandy mud (diamicton)
15	18	06:50	42.35	43.45	1.04	19.44	95	70	Deposition fromnearby glaciers
16	18	07:40	43.45	45.28	1.84	21.28	101	72	*Age 1-2 my*
18	18	15:30	46.10	46.60	1.32	22.60	264	73	
19	18	17:30	46.60	48.20	1.36	23.96	85	73	UNIT 5.1-5.7 43.55-92.19 m
20	18	20:00	48.20	49.30	1.00	24.96	91	74	Volcanic fine sandstone at top- mixedsiltstone and
	DRILL 13.29 m		**REC**	**11.60 m**			**87%**		sandstone in lower part. Brecciatedin places.
21	18	21:00	49.30	50.70	0.93	25.89	66	74	Deposition in shallow water by marine currents
22	18	23:50	50.70	52.00	0.67	26.56	52	73	Icebergs initially but ice retreating with time.
23	19	05:00	52.00	53.11	0.80	27.36	72	73	*AgeI7.0-18.5 my at 53 m*
24	19	07:00	53.11	54.20	0.30	27.66	28	72	
25	19	12:30	55.00	57.30	2.30	29.96	100	72	
26	19	14:15	57.30	59.40	2.10	32.06	100	73	
27	19	15:30	59.40	61.25	1.85	33.91	100	74	
28	19	17:30	61.25	63.50	2.25	36.16	100	75	
	DRILL 14.20 m		**REC**	**11.20 m**			**79%**		
29	19	20:40	63.50	65.40	0.50	36.66	26	74	
30	19	22:30	65.40	66.45	0.95	37.61	90	74	
31	20	01:15	66.45	68.05	1.60	39.21	100	75	
32	20	02:28	68.05	68.78	0.67	39.88	92	75	
33	20	04:30	68.78	70.90	1.98	41.86	93	76	
34	20	06:17	70.85	72.92	0.78	42.64	38	74	
35	20	10:30	72.92	73.95	0.52	43.16	50	74	
36	20	12:20	73.95	74.65	0.52	43.68	74	74	
37	20	14:30	74.65	76.80	1.97	45.65	92	75	
38	20	16:00	76.80	78.15	1.33	46.98	99	75	*Agel8.5-20.5 my a! 78m*
39	20	17:30	78.15	81.00	2.85	49.83	100	76	
40	20	19:50	81.00	82.80	1.58	51.41	88	77	
	DRILL 19.30 m		**REC**	**15.25 m**			**79%**		
41	20	21:50	82.80	83.75	0.63	52.04	66	76	
42	20	23:30	83.75	84.97	1.22	53.26	100	77	
43	21	02:00	84.97	87.92	2.84	56.10	96	78	
44	21	03:45	87.92	89.82	1.40	57.50	74	77	
45	21	06:17	89.82	91.59	1.40	58.90	79	78	UNIT 5.8 92.19-103.41 m
46	21	13:30	91.59	92.95	1.01	59.91	74	77	Mudstoncwithscatteredpebbles
47	21	13:30	92.95	94.50	1.45	61.36	94	78	Deposition in mod deep water with floating bergs
48	21	17:30	94.50	97.50	2.97	64.33	99	79	*Age 18.5-20.5 my at 99 m*
49	21	19:30	97.50	100.50	3.03	67.36	101	79	
	DRILL 17.70 m		**REC**	**15.95 m**			**90%**		

			CORE RUNS		CORE RECOVERY				ROCK TYPE/AGE
RUN	DAY	TIME	START	END	m	sum	%	cum %	(not for quoting-see main body of report)
50	22	21:00	100.50	102 99	2 44	69.80	98	80	
51	22	00:30	102.99	105.42	2 30	72 10	95	80	UNIT 6 103 41-141.60 m
52	22	03:30	105.42	108.56	3.10	75.20	99	81	Pebbly muddy sand (diamictite) with fine well-sorted
53	22	06:00	108.56	111.48	2.88	78.08	99	81	sandstone beds - real "chasers" - at 115-117 m
54	22	09:15	111.48	114.60	3.06	81.14	98	82	Deposition in shallow water with glaciers nearby
55	22	10:45	114.60	116.40	1.80	82.94	100	82	
56	22	13:00	116.40	119.00	2.47	85.41	95	83	
57	22	18:30	119.00	121.20	2.14	87.55	97	83	
	DRILL	**20.70 m**	**REC**	**20.19 m**			**98%**		
58	22	20:30	121.20	124.15	3.03	90.58	103	83	
59	22	23:15	124.15	127.13	2.92	93.50	98	84	
60	23	01:45	127.13	129.60	2.44	95.94	99	84	
61	23	05:15	129.60	132.56	3.00	98.94	101	85	
62	23	09:30	132.56	135.30	2.84	101.78	104	85	
63	23	12:45	135.30	137.65	2.05	103.83	87	85	
64	23	15:15	137.65	140.45	2.80	106.63	100	85	
	DRILL	**19.25 m**	**REC**	**19.08 m**			**99%**		
65	23	20:27	140.45	143.18	2.29	108.92	84	85	UNIT7.1 141.60-147.69 m
66	23	23:45	143.18	144.98	1.73	110.65	96	86	Mudstone with lonestones
67	24	02:00	144.98	147.69	2.67	113.32	99	86	Deposition in deeperwater with glaciers more distant
	DRILL	**7.24 m**	**REC**	**6.69 m**	**2.67**	**113.32**	**92%**		***Age** 22-24* **my**
	END OF HOLE								

Notes. 1) Coring ran from October 17 to 24. Time is when the inner tube reached the rig floor. 2) Core run limits arc in mbsf (metres below sea floor). 3) The summary of each day's coring is made for 20.00 hours to coincide with the 12 hourly shift change. 4) The description of rock type and age were compiled for immediate reference during the drilling phase.

Terra Antartica
1998, 5(1), 141-175

Appendix *2*

1:20 Core Logs

The following logs were prepared at Cape Roberts Camp a scale of 1:20. The logs are based on the working half of the core. The strip images to the left of the logs were acquired at the Drill Site using a DMT line scan camera. The images are derived from the core box images presented in Appendix 3.

The image collection system was supplied by DMT-Geotec, Essen, Germany, and subsequent image processing was completed using CorelDraw 7.

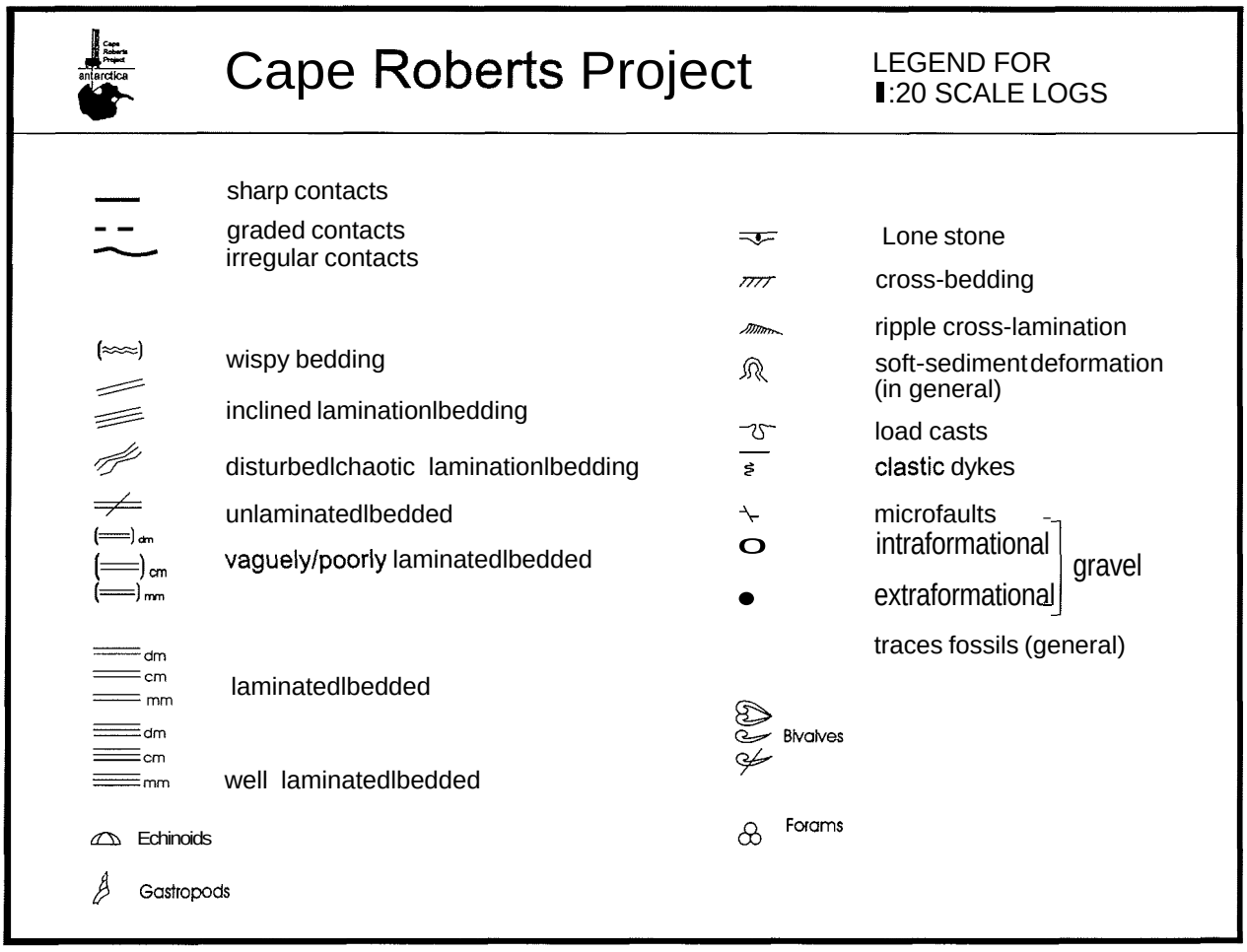

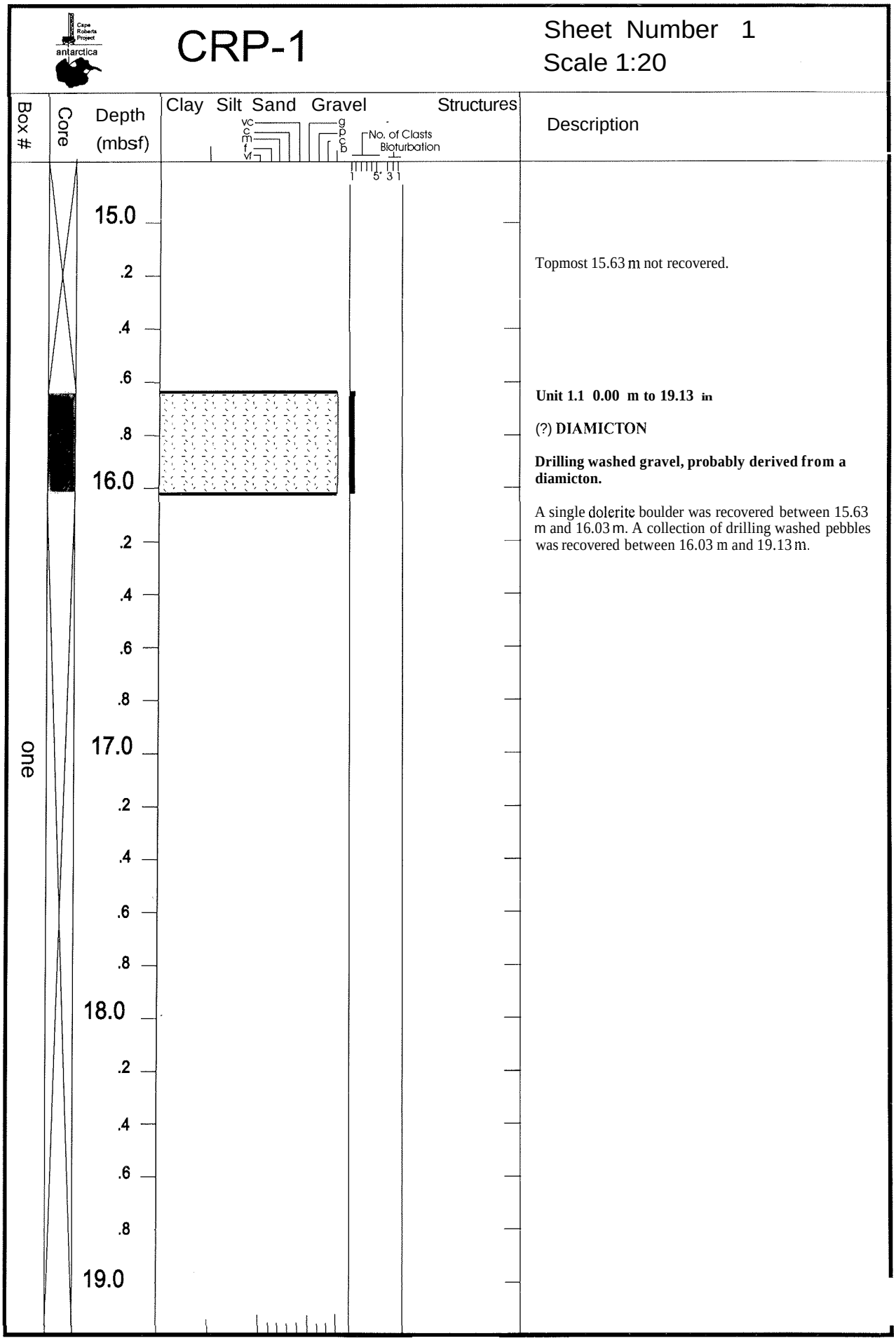
Cape Roberts Project
antarctica
CRP-1
Sheet Number 1
Scale 1:20
Box #
Core
Depth (mbsf)
Clay Silt Sand Gravel
vc c m f vf
g p c b
No. of Clasts
Bioturbation
1 5 3 1
Structures
Description
one
15.0
.2
.4
.6
.8
16.0
.2
.4
.6
.8
17.0
.2
.4
.6
.8
18.0
.2
.4
.6
.8
19.0
Topmost 15.63 m not recovered.
Unit 1.1 0.00 m to 19.13 in
(?) DIAMICTON
Drilling washed gravel, probably derived from a diamicton.
A single dolerite boulder was recovered between 15.63 m and 16.03 m. A collection of drilling washed pebbles was recovered between 16.03 m and 19.13 m.

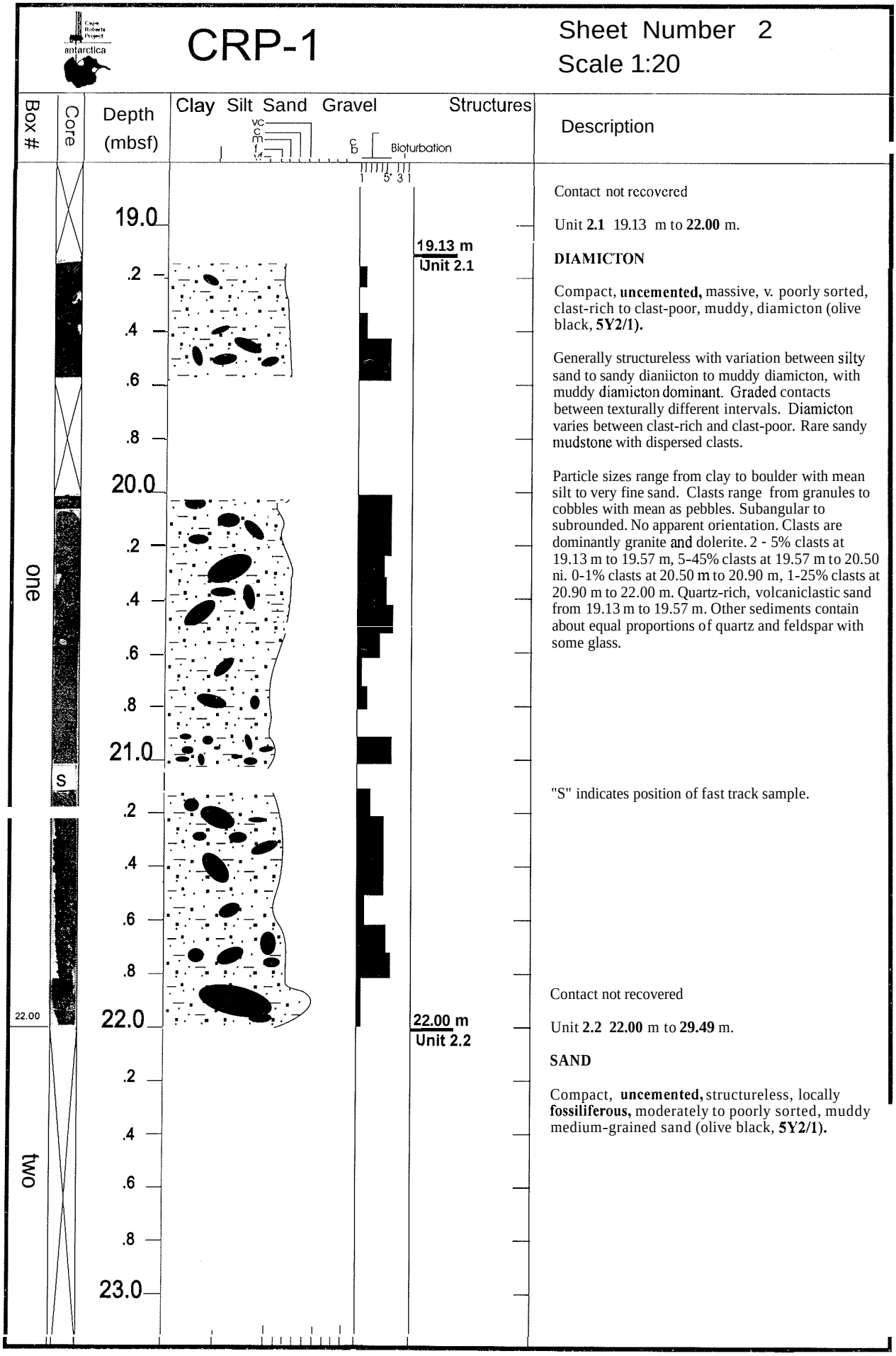
CRP-1
Sheet Number 2
Scale 1:20
Box #
Core
Depth (mbsf)
Clay Silt Sand Gravel
vc c m f vf
Structures
Bioturbation
Description
19.0
.2
.4
.6
.8
20.0
.2
.4
.6
.8
21.0
.2
.4
.6
.8
22.0
.2
.4
.6
.8
23.0
one
S
two
22.00
19.13 m
Unit 2.1
22.00 m
Unit 2.2
Contact not recovered
Unit 2.1 19.13 m to 22.00 m.
DIAMICTON
Compact, uncemented, massive, v. poorly sorted, clast-rich to clast-poor, muddy, diamicton (olive black, 5Y2/1).
Generally structureless with variation between silty sand to sandy dianiicton to muddy diamicton, with muddy diamicton dominant. Graded contacts between texturally different intervals. Diamicton varies between clast-rich and clast-poor. Rare sandy mudstone with dispersed clasts.
Particle sizes range from clay to boulder with mean silt to very fine sand. Clasts range from granules to cobbles with mean as pebbles. Subangular to subrounded. No apparent orientation. Clasts are dominantly granite and dolerite. 2 - 5% clasts at 19.13 m to 19.57 m, 5-45% clasts at 19.57 m to 20.50 ni. 0-1% clasts at 20.50 m to 20.90 m, 1-25% clasts at 20.90 m to 22.00 m. Quartz-rich, volcaniclastic sand from 19.13 m to 19.57 m. Other sediments contain about equal proportions of quartz and feldspar with some glass.
"S" indicates position of fast track sample.
Contact not recovered
Unit 2.2 22.00 m to 29.49 m.
SAND
Compact, uncemented, structureless, locally fossiliferous, moderately to poorly sorted, muddy medium-grained sand (olive black, 5Y2/1).

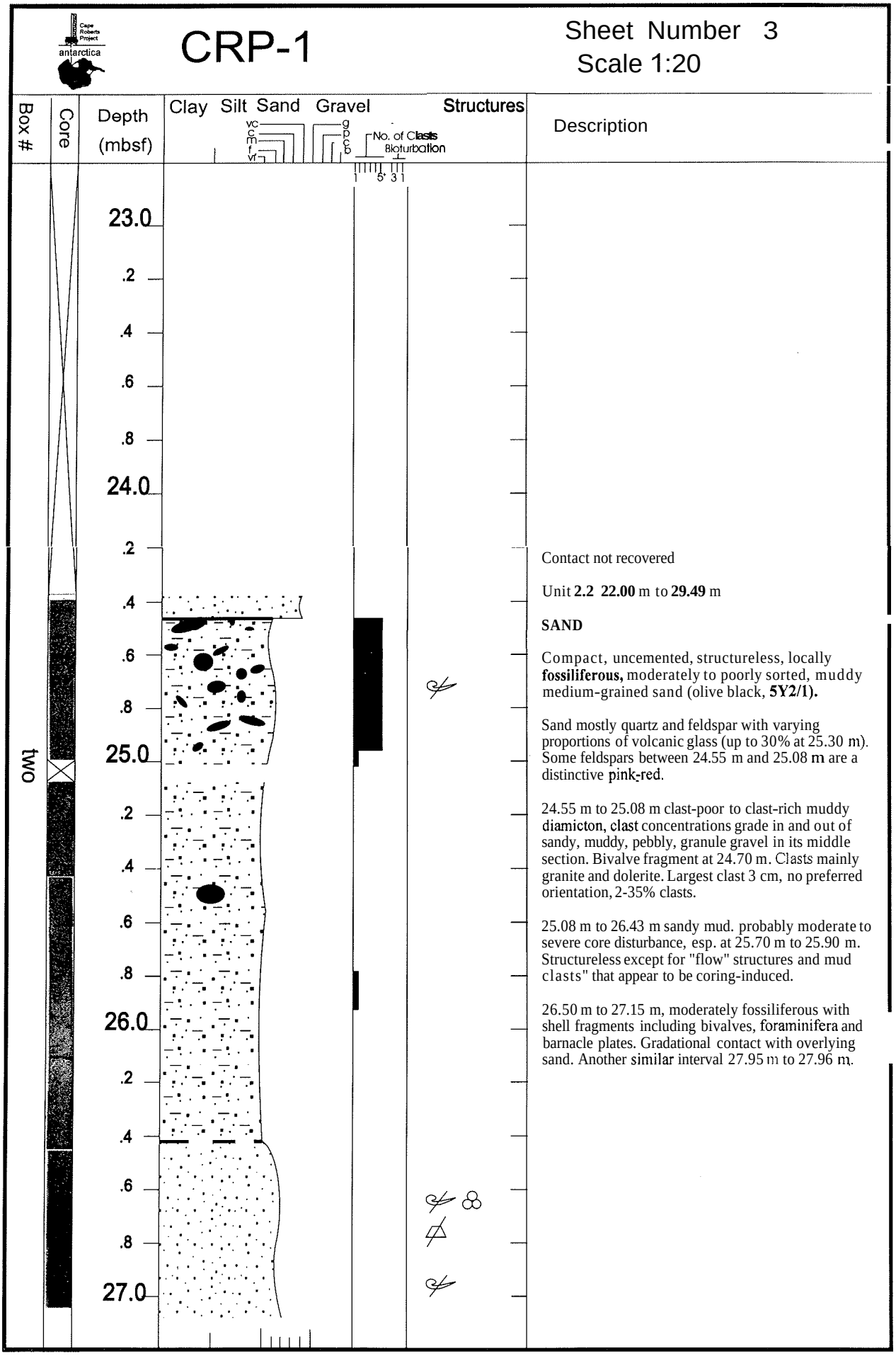
Cape Roberts Project
antarctica
CRP-1
Sheet Number 3
Scale 1:20
Box #
Core
Depth (mbsf)
Clay Silt Sand Gravel
vc c m f vf
g p c
Structures
No. of Clasts
Bioturbation
1 5 3 1
Description
23.0
.2
.4
.6
.8
24.0
.2
.4
.6
.8
25.0
.2
.4
.6
.8
26.0
.2
.4
.6
.8
27.0
two
Contact not recovered
Unit 2.2 22.00 m to 29.49 m
SAND
Compact, uncemented, structureless, locally fossiliferous, moderately to poorly sorted, muddy medium-grained sand (olive black, 5Y2/1).
Sand mostly quartz and feldspar with varying proportions of volcanic glass (up to 30% at 25.30 m). Some feldspars between 24.55 m and 25.08 m are a distinctive pink-red.
24.55 m to 25.08 m clast-poor to clast-rich muddy diamicton, clast concentrations grade in and out of sandy, muddy, pebbly, granule gravel in its middle section. Bivalve fragment at 24.70 m. Clasts mainly granite and dolerite. Largest clast 3 cm, no preferred orientation, 2-35% clasts.
25.08 m to 26.43 m sandy mud. probably moderate to severe core disturbance, esp. at 25.70 m to 25.90 m. Structureless except for "flow" structures and mud clasts" that appear to be coring-induced.
26.50 m to 27.15 m, moderately fossiliferous with shell fragments including bivalves, foraminifera and barnacle plates. Gradational contact with overlying sand. Another similar interval 27.95 m to 27.96 m.

CRP-1

Sheet Number 4
Scale 1:20

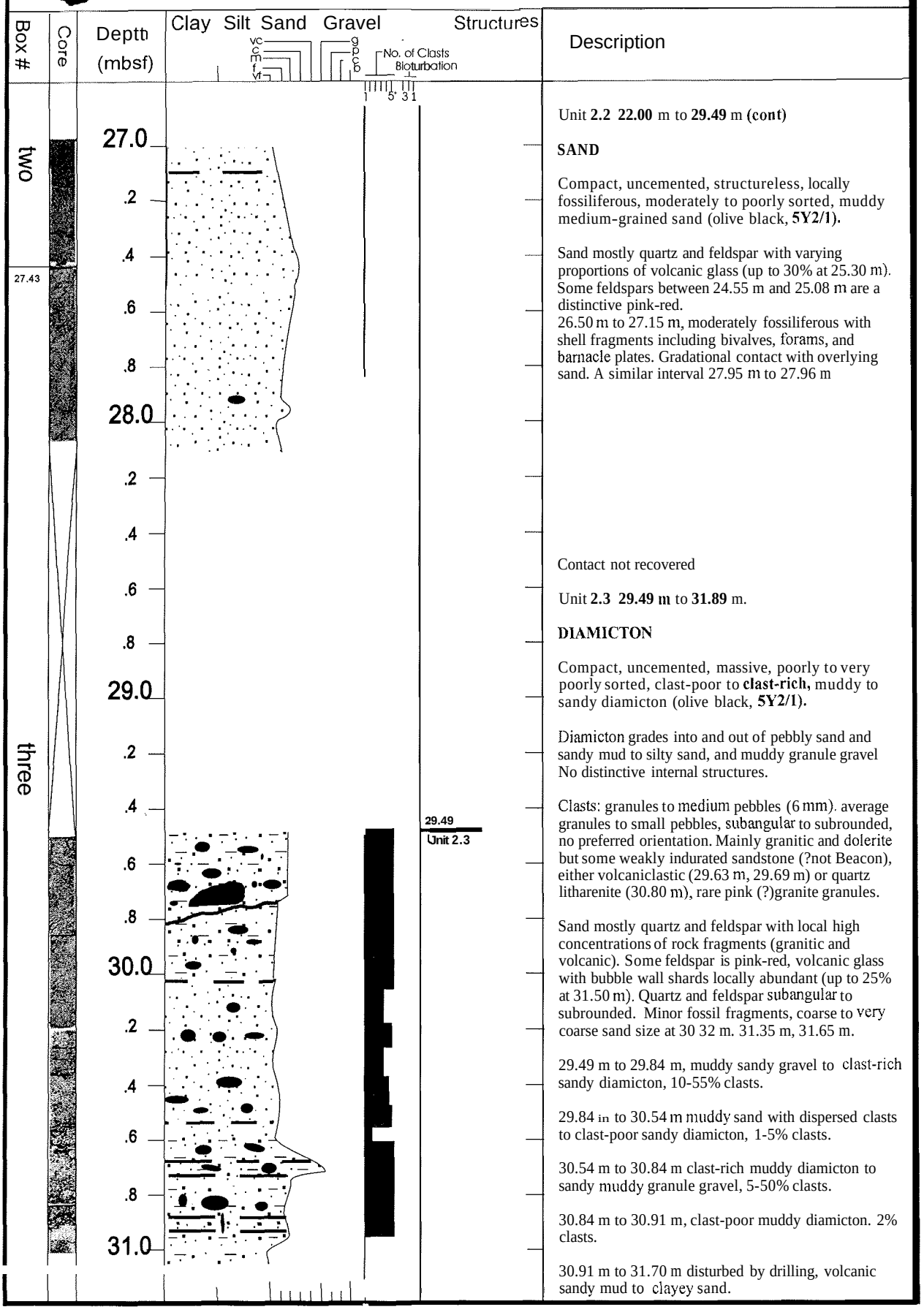

Description

Unit **2.2** **22.00** m to **29.49** m **(cont)**

SAND

Compact, uncemented, structureless, locally fossiliferous, moderately to poorly sorted, muddy medium-grained sand (olive black, **5Y2/1).**

Sand mostly quartz and feldspar with varying proportions of volcanic glass (up to 30% at 25.30 m). Some feldspars between 24.55 m and 25.08 m are a distinctive pink-red.
26.50 m to 27.15 m, moderately fossiliferous with shell fragments including bivalves, forams, and barnacle plates. Gradational contact with overlying sand. A similar interval 27.95 m to 27.96 m

Contact not recovered

Unit **2.3** **29.49 m** to **31.89** m.

DIAMICTON

Compact, uncemented, massive, poorly to very poorly sorted, clast-poor to **clast-rich,** muddy to sandy diamicton (olive black, **5Y2/1).**

Diamicton grades into and out of pebbly sand and sandy mud to silty sand, and muddy granule gravel No distinctive internal structures.

Clasts: granules to medium pebbles (6 mm). average granules to small pebbles, subangular to subrounded, no preferred orientation. Mainly granitic and dolerite but some weakly indurated sandstone (?not Beacon), either volcaniclastic (29.63 m, 29.69 m) or quartz litharenite (30.80 m), rare pink (?)granite granules.

Sand mostly quartz and feldspar with local high concentrations of rock fragments (granitic and volcanic). Some feldspar is pink-red, volcanic glass with bubble wall shards locally abundant (up to 25% at 31.50 m). Quartz and feldspar subangular to subrounded. Minor fossil fragments, coarse to very coarse sand size at 30 32 m. 31.35 m, 31.65 m.

29.49 m to 29.84 m, muddy sandy gravel to clast-rich sandy diamicton, 10-55% clasts.

29.84 in to 30.54 m muddy sand with dispersed clasts to clast-poor sandy diamicton, 1-5% clasts.

30.54 m to 30.84 m clast-rich muddy diamicton to sandy muddy granule gravel, 5-50% clasts.

30.84 m to 30.91 m, clast-poor muddy diamicton. 2% clasts.

30.91 m to 31.70 m disturbed by drilling, volcanic sandy mud to clayey sand.

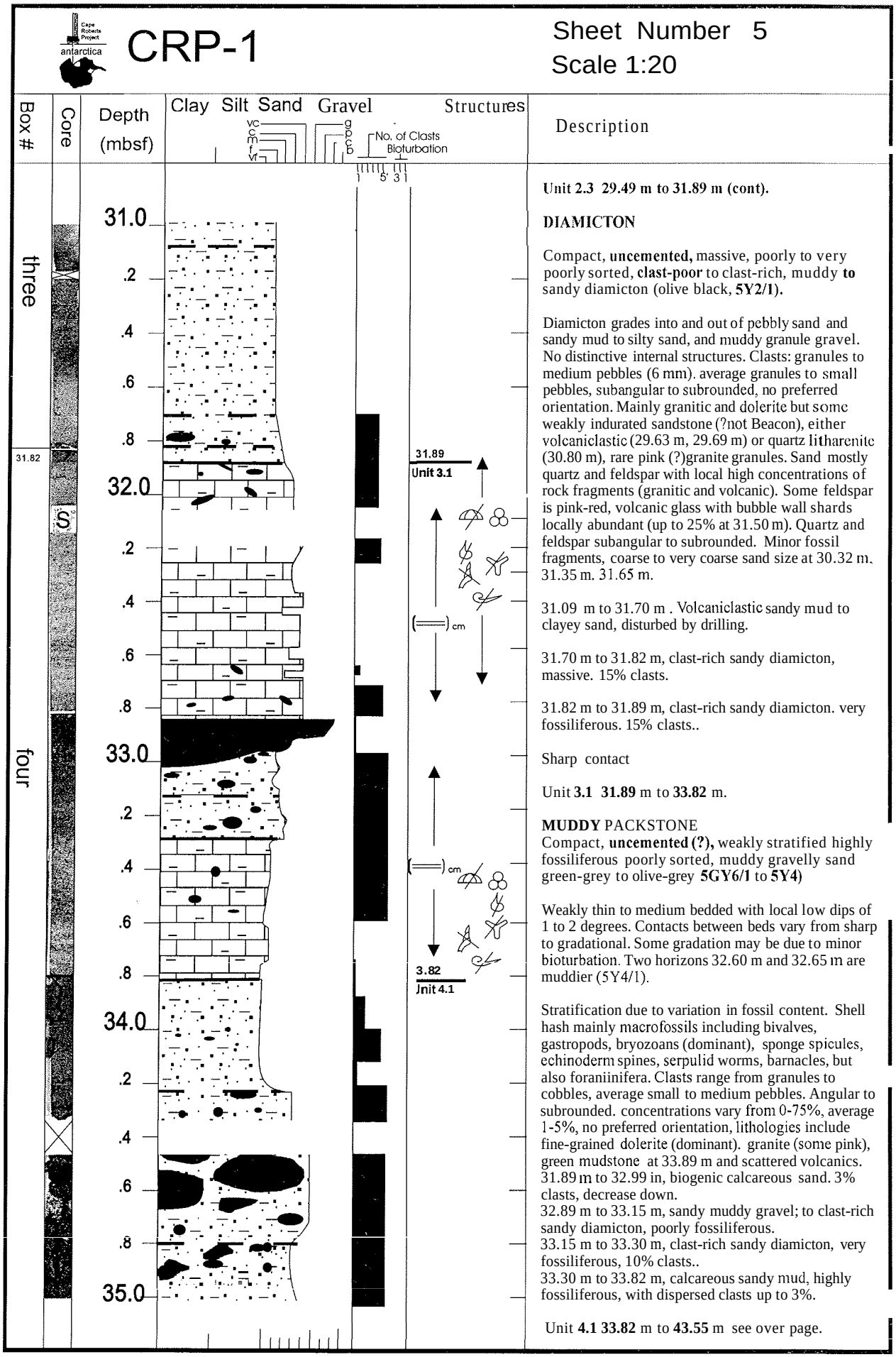

Unit 2.3 29.49 m to 31.89 m (cont).

DIAMICTON

Compact, **uncemented,** massive, poorly to very poorly sorted, **clast-poor** to clast-rich, muddy **to** sandy diamicton (olive black, **5Y2/1).**

Diamicton grades into and out of pebbly sand and sandy mud to silty sand, and muddy granule gravel. No distinctive internal structures. Clasts: granules to medium pebbles (6 mm). average granules to small pebbles, subangular to subrounded, no preferred orientation. Mainly granitic and dolerite but some weakly indurated sandstone (?not Beacon), either volcaniclastic (29.63 m, 29.69 m) or quartz litharenite (30.80 m), rare pink (?)granite granules. Sand mostly quartz and feldspar with local high concentrations of rock fragments (granitic and volcanic). Some feldspar is pink-red, volcanic glass with bubble wall shards locally abundant (up to 25% at 31.50 m). Quartz and feldspar subangular to subrounded. Minor fossil fragments, coarse to very coarse sand size at 30.32 m. 31.35 m. 31.65 m.

31.09 m to 31.70 m . Volcaniclastic sandy mud to clayey sand, disturbed by drilling.

31.70 m to 31.82 m, clast-rich sandy diamicton, massive. 15% clasts.

31.82 m to 31.89 m, clast-rich sandy diamicton. very fossiliferous. 15% clasts..

Sharp contact

Unit **3.1 31.89** m to **33.82** m.

MUDDY PACKSTONE
Compact, **uncemented (?),** weakly stratified highly fossiliferous poorly sorted, muddy gravelly sand green-grey to olive-grey **5GY6/1** to **5Y4)**

Weakly thin to medium bedded with local low dips of 1 to 2 degrees. Contacts between beds vary from sharp to gradational. Some gradation may be due to minor bioturbation. Two horizons 32.60 m and 32.65 m are muddier (5Y4/1).

Stratification due to variation in fossil content. Shell hash mainly macrofossils including bivalves, gastropods, bryozoans (dominant), sponge spicules, echinoderm spines, serpulid worms, barnacles, but also foraniinifera. Clasts range from granules to cobbles, average small to medium pebbles. Angular to subrounded. concentrations vary from 0-75%, average 1-5%, no preferred orientation, lithologies include fine-grained dolerite (dominant). granite (some pink), green mudstone at 33.89 m and scattered volcanics.
31.89 m to 32.99 in, biogenic calcareous sand. 3% clasts, decrease down.
32.89 m to 33.15 m, sandy muddy gravel; to clast-rich sandy diamicton, poorly fossiliferous.
33.15 m to 33.30 m, clast-rich sandy diamicton, very fossiliferous, 10% clasts..
33.30 m to 33.82 m, calcareous sandy mud, highly fossiliferous, with dispersed clasts up to 3%.

Unit **4.1 33.82** m to **43.55** m see over page.

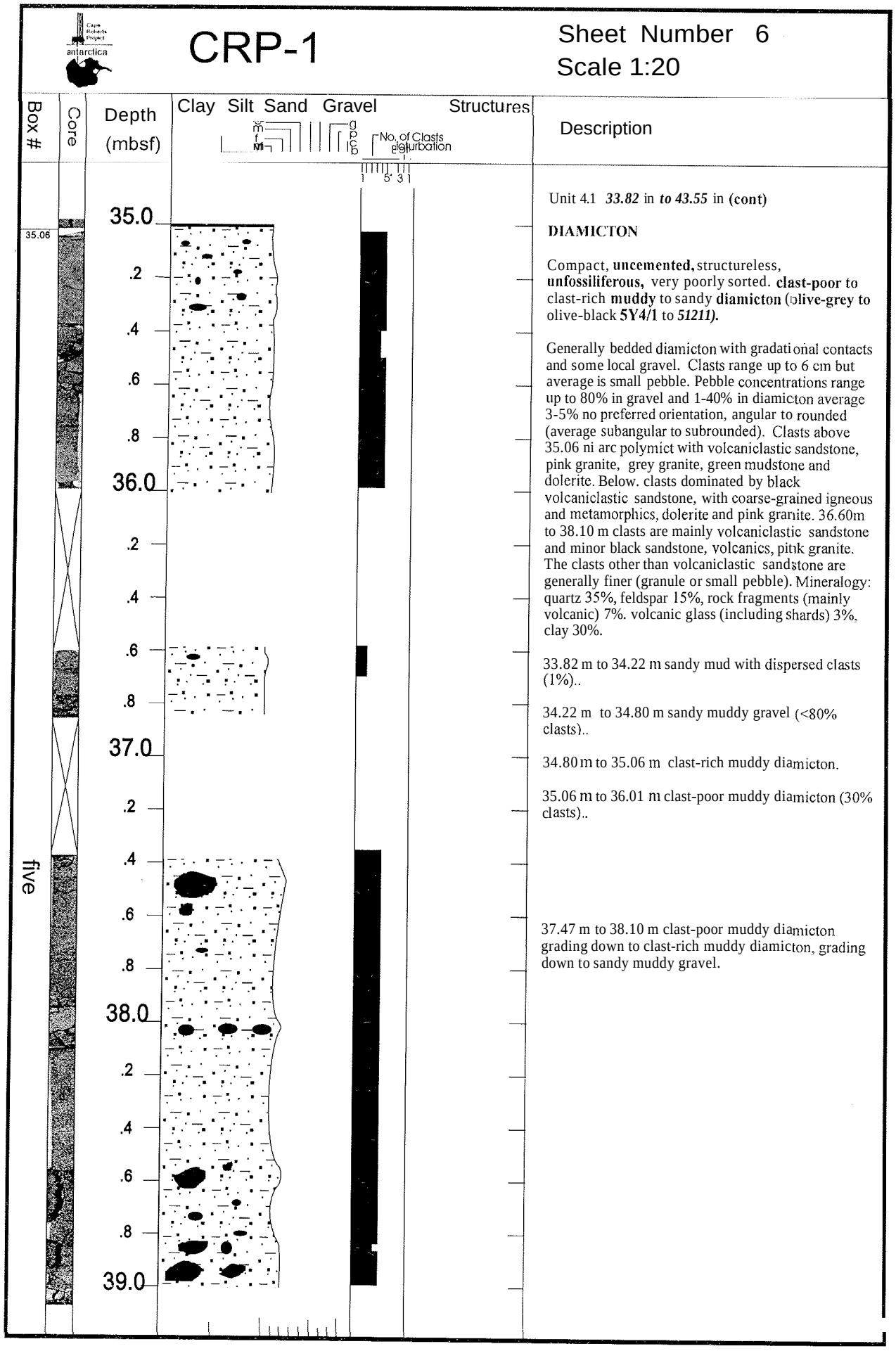

Unit 4.1 ***33.82*** in ***to 43.55*** in **(cont)**

DIAMICTON

Compact, **uncemented,** structureless, **unfossiliferous,** very poorly sorted. **clast-poor to** clast-rich **muddy** to sandy **diamicton** (olive-grey to olive-black **5Y4/1** to ***51211).***

Generally bedded diamicton with gradational contacts and some local gravel. Clasts range up to 6 cm but average is small pebble. Pebble concentrations range up to 80% in gravel and 1-40% in diamicton average 3-5% no preferred orientation, angular to rounded (average subangular to subrounded). Clasts above 35.06 ni arc polymict with volcaniclastic sandstone, pink granite, grey granite, green mudstone and dolerite. Below. clasts dominated by black volcaniclastic sandstone, with coarse-grained igneous and metamorphics, dolerite and pink granite. 36.60m to 38.10 m clasts are mainly volcaniclastic sandstone and minor black sandstone, volcanics, pitnk granite. The clasts other than volcaniclastic sandstone are generally finer (granule or small pebble). Mineralogy: quartz 35%, feldspar 15%, rock fragments (mainly volcanic) 7%. volcanic glass (including shards) 3%, clay 30%.

33.82 m to 34.22 m sandy mud with dispersed clasts (1%)..

34.22 m to 34.80 m sandy muddy gravel (<80% clasts)..

34.80 m to 35.06 m clast-rich muddy diamicton.

35.06 m to 36.01 m clast-poor muddy diamicton (30% clasts)..

37.47 m to 38.10 m clast-poor muddy diamicton grading down to clast-rich muddy diamicton, grading down to sandy muddy gravel.

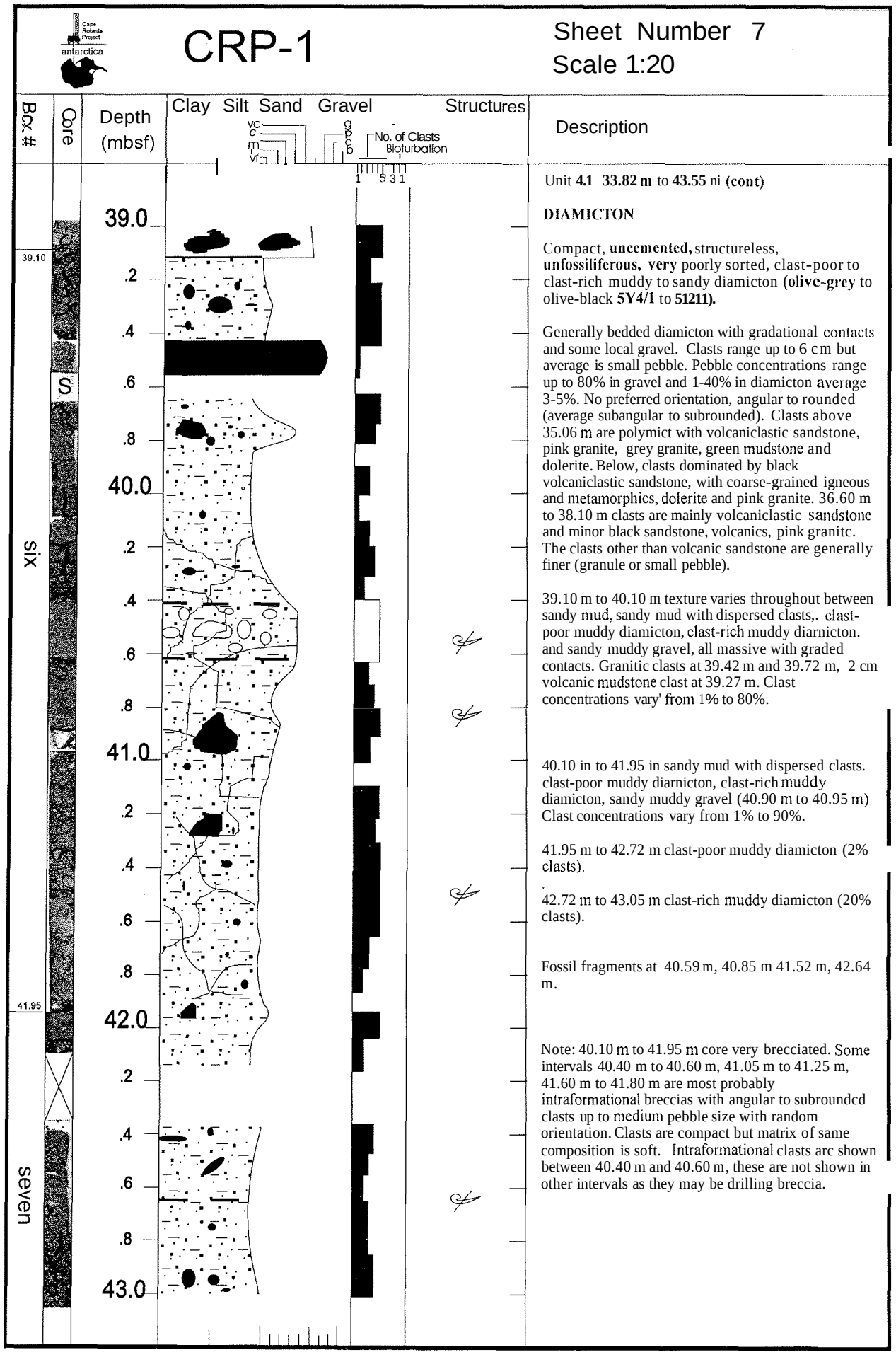

Unit **4.1 33.82 m** to **43.55** ni **(cont)**

DIAMICTON

Compact, **uncemented,** structureless, **unfossiliferous, very** poorly sorted, clast-poor to clast-rich muddy to sandy diamicton **(olive-grey** to olive-black **5Y4/1** to **51211).**

Generally bedded diamicton with gradational contacts and some local gravel. Clasts range up to 6 cm but average is small pebble. Pebble concentrations range up to 80% in gravel and 1-40% in diamicton average 3-5%. No preferred orientation, angular to rounded (average subangular to subrounded). Clasts above 35.06 m are polymict with volcaniclastic sandstone, pink granite, grey granite, green mudstone and dolerite. Below, clasts dominated by black volcaniclastic sandstone, with coarse-grained igneous and metamorphics, dolerite and pink granite. 36.60 m to 38.10 m clasts are mainly volcaniclastic sandstone and minor black sandstone, volcanics, pink granitc. The clasts other than volcanic sandstone are generally finer (granule or small pebble).

39.10 m to 40.10 m texture varies throughout between sandy mud, sandy mud with dispersed clasts,. clast-poor muddy diamicton, clast-rich muddy diarnicton. and sandy muddy gravel, all massive with graded contacts. Granitic clasts at 39.42 m and 39.72 m, 2 cm volcanic mudstone clast at 39.27 m. Clast concentrations vary' from 1% to 80%.

40.10 in to 41.95 in sandy mud with dispersed clasts. clast-poor muddy diarnicton, clast-rich muddy diamicton, sandy muddy gravel (40.90 m to 40.95 m) Clast concentrations vary from 1% to 90%.

41.95 m to 42.72 m clast-poor muddy diamicton (2% clasts).

42.72 m to 43.05 m clast-rich muddy diamicton (20% clasts).

Fossil fragments at 40.59 m, 40.85 m 41.52 m, 42.64 m.

Note: 40.10 m to 41.95 m core very brecciated. Some intervals 40.40 m to 40.60 m, 41.05 m to 41.25 m, 41.60 m to 41.80 m are most probably intraformational breccias with angular to subroundcd clasts up to medium pebble size with random orientation. Clasts are compact but matrix of same composition is soft. Intraformational clasts arc shown between 40.40 m and 40.60 m, these are not shown in other intervals as they may be drilling breccia.

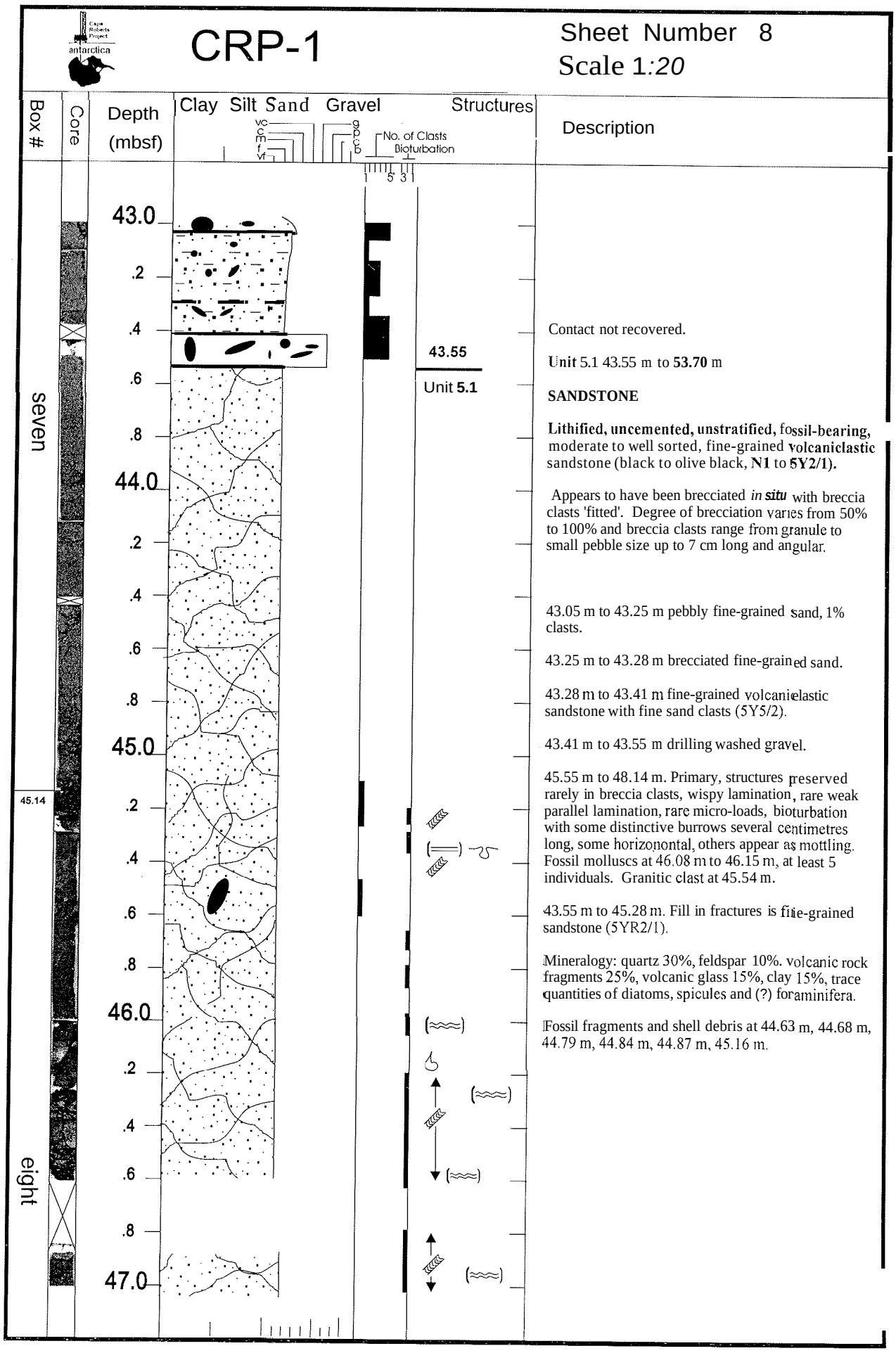
CRP-1
Sheet Number 8
Scale 1:20
Box #
Core
Depth (mbsf)
Clay Silt Sand Gravel
Structures
No. of Clasts
Bioturbation
Description
seven
eight
45.14
43.0
.2
.4
.6
.8
44.0
.2
.4
.6
.8
45.0
.2
.4
.6
.8
46.0
.2
.4
.6
.8
47.0
43.55
Unit 5.1
Contact not recovered.
Unit 5.1 43.55 m to 53.70 m
SANDSTONE
Lithified, uncemented, unstratified, fossil-bearing, moderate to well sorted, fine-grained volcaniclastic sandstone (black to olive black, N1 to 5Y2/1).
Appears to have been brecciated in situ with breccia clasts 'fitted'. Degree of brecciation varies from 50% to 100% and breccia clasts range from granule to small pebble size up to 7 cm long and angular.
43.05 m to 43.25 m pebbly fine-grained sand, 1% clasts.
43.25 m to 43.28 m brecciated fine-grained sand.
43.28 m to 43.41 m fine-grained volcaniclastic sandstone with fine sand clasts (5Y5/2).
43.41 m to 43.55 m drilling washed gravel.
45.55 m to 48.14 m. Primary, structures preserved rarely in breccia clasts, wispy lamination, rare weak parallel lamination, rare micro-loads, bioturbation with some distinctive burrows several centimetres long, some horizonontal, others appear as mottling. Fossil molluscs at 46.08 m to 46.15 m, at least 5 individuals. Granitic clast at 45.54 m.
43.55 m to 45.28 m. Fill in fractures is fine-grained sandstone (5YR2/1).
Mineralogy: quartz 30%, feldspar 10%. volcanic rock fragments 25%, volcanic glass 15%, clay 15%, trace quantities of diatoms, spicules and (?) foraminifera.
Fossil fragments and shell debris at 44.63 m, 44.68 m, 44.79 m, 44.84 m, 44.87 m, 45.16 m.

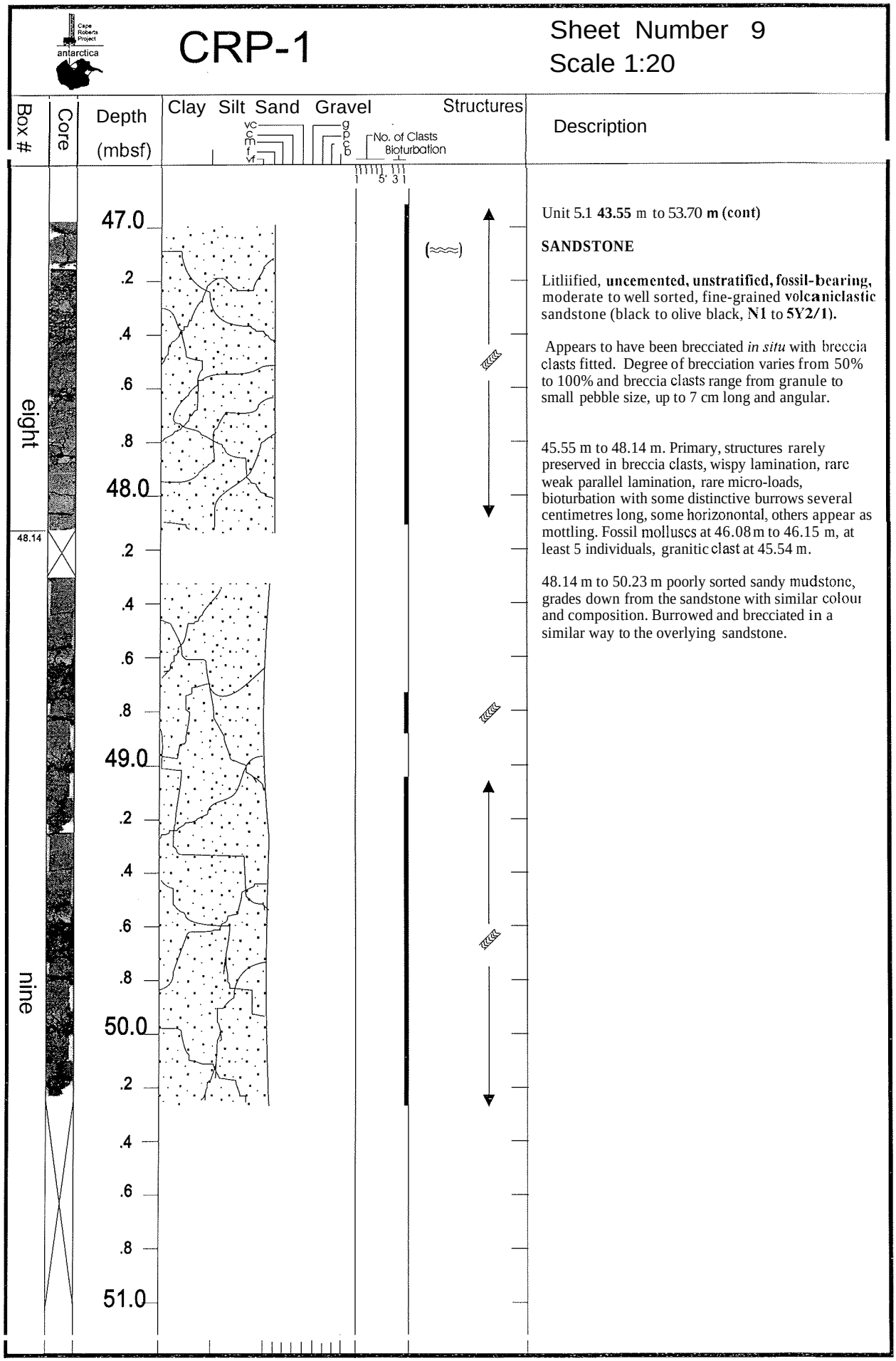
Cape Roberts Project
antarctica
CRP-1
Sheet Number 9
Scale 1:20
Box #
Core
Depth (mbsf)
Clay Silt Sand Gravel
vc c m f vf
g p s b
No. of Clasts
Bioturbation
1 5 3 1
Structures
Description
eight
nine
48.14
47.0
.2
.4
.6
.8
48.0
.2
.4
.6
.8
49.0
.2
.4
.6
.8
50.0
.2
.4
.6
.8
51.0
Unit 5.1 43.55 m to 53.70 m (cont)
SANDSTONE
Litliified, uncemented, unstratified, fossil-bearing, moderate to well sorted, fine-grained volcaniclastic sandstone (black to olive black, N1 to 5Y2/1).
Appears to have been brecciated in situ with breccia clasts fitted. Degree of brecciation varies from 50% to 100% and breccia clasts range from granule to small pebble size, up to 7 cm long and angular.
45.55 m to 48.14 m. Primary, structures rarely preserved in breccia clasts, wispy lamination, rare weak parallel lamination, rare micro-loads, bioturbation with some distinctive burrows several centimetres long, some horizonontal, others appear as mottling. Fossil molluscs at 46.08 m to 46.15 m, at least 5 individuals, granitic clast at 45.54 m.
48.14 m to 50.23 m poorly sorted sandy mudstone, grades down from the sandstone with similar colour and composition. Burrowed and brecciated in a similar way to the overlying sandstone.

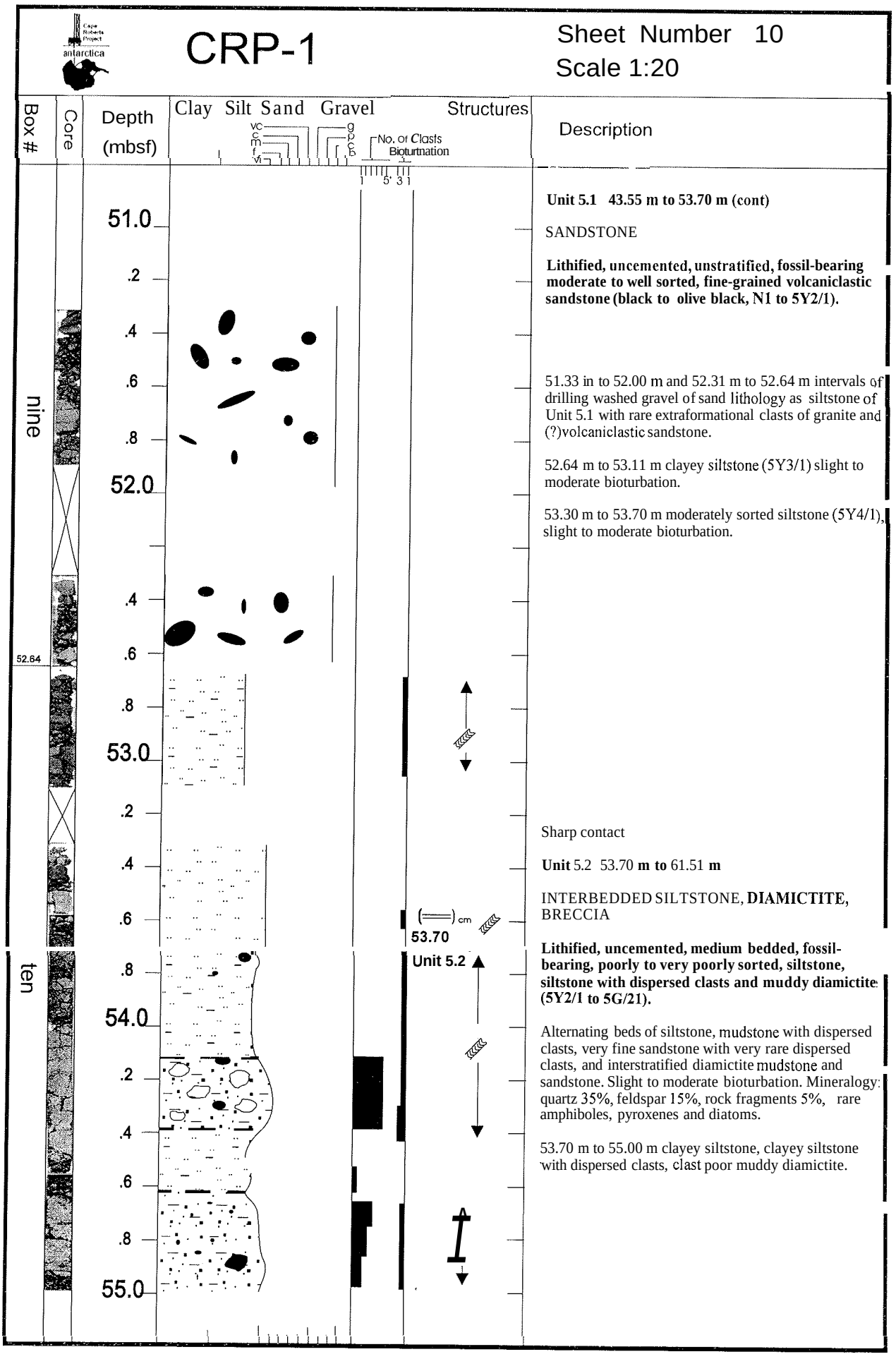
CRP-1
Sheet Number 10
Scale 1:20
antarctica
Box #
Core
Depth (mbsf)
Clay Silt Sand Gravel
Structures
No. of Clasts
Bioturbation
Description
nine
ten
51.0
.2
.4
.6
.8
52.0
.4
.6
52.64
.8
53.0
.2
.4
.6
53.70
Unit 5.2
.8
54.0
.2
.4
.6
.8
55.0
Unit 5.1 43.55 m to 53.70 m (cont)
SANDSTONE
Lithified, uncemented, unstratified, fossil-bearing moderate to well sorted, fine-grained volcaniclastic sandstone (black to olive black, N1 to 5Y2/1).
51.33 in to 52.00 m and 52.31 m to 52.64 m intervals of drilling washed gravel of sand lithology as siltstone of Unit 5.1 with rare extraformational clasts of granite and (?)volcaniclastic sandstone.
52.64 m to 53.11 m clayey siltstone (5Y3/1) slight to moderate bioturbation.
53.30 m to 53.70 m moderately sorted siltstone (5Y4/1), slight to moderate bioturbation.
Sharp contact
Unit 5.2 53.70 m to 61.51 m
INTERBEDDED SILTSTONE, DIAMICTITE, BRECCIA
Lithified, uncemented, medium bedded, fossil-bearing, poorly to very poorly sorted, siltstone, siltstone with dispersed clasts and muddy diamictite (5Y2/1 to 5G/21).
Alternating beds of siltstone, mudstone with dispersed clasts, very fine sandstone with very rare dispersed clasts, and interstratified diamictite mudstone and sandstone. Slight to moderate bioturbation. Mineralogy: quartz 35%, feldspar 15%, rock fragments 5%, rare amphiboles, pyroxenes and diatoms.
53.70 m to 55.00 m clayey siltstone, clayey siltstone with dispersed clasts, clast poor muddy diamictite.

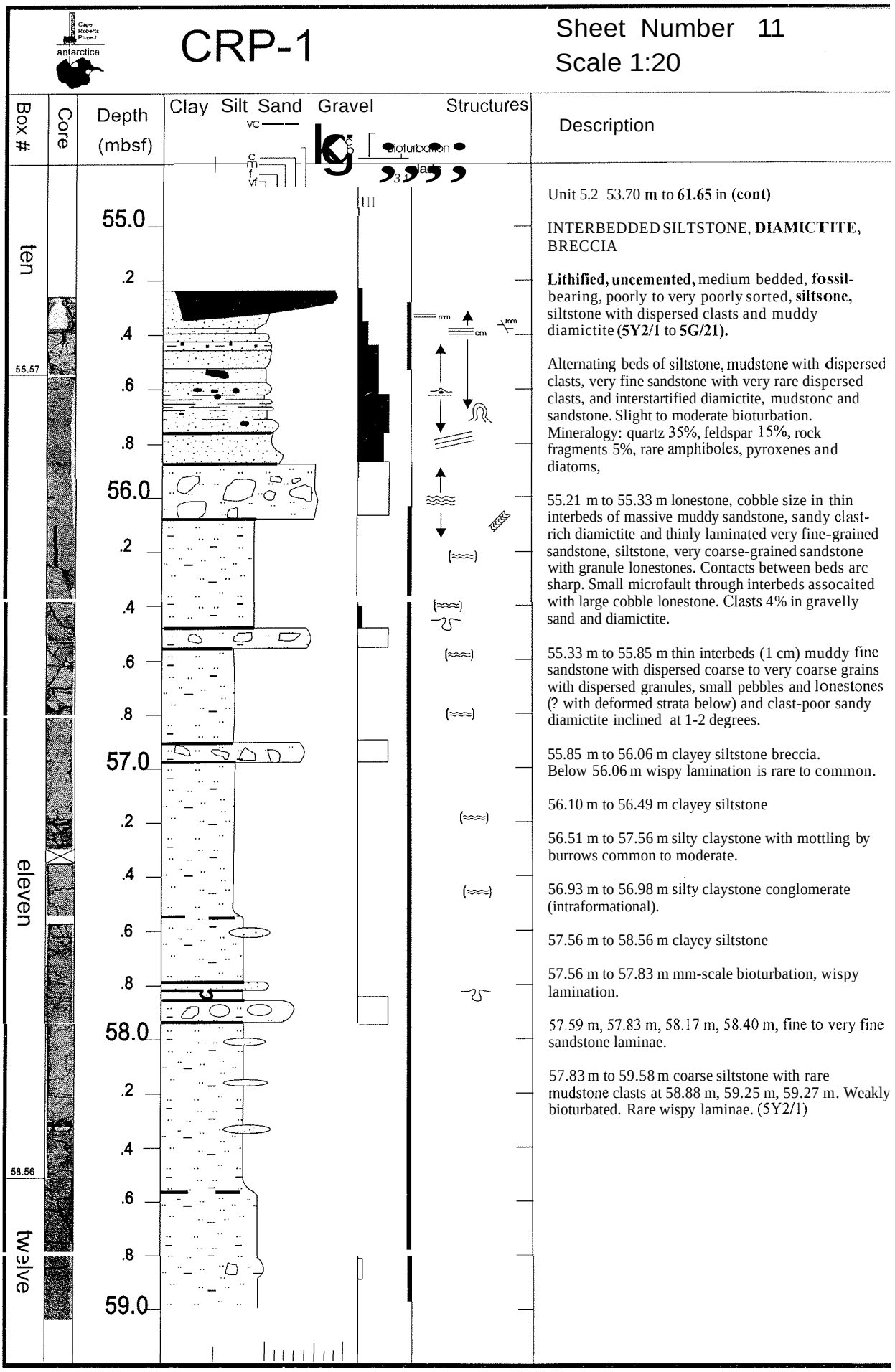

Unit 5.2 53.70 **m** to **61.65** in **(cont)**

INTERBEDDED SILTSTONE, **DIAMICTITE**, BRECCIA

Lithified, uncemented, medium bedded, **fossil**-bearing, poorly to very poorly sorted, **siltsone,** siltstone with dispersed clasts and muddy diamictite **(5Y2/1** to **5G/21).**

Alternating beds of siltstone, mudstone with dispersed clasts, very fine sandstone with very rare dispersed clasts, and interstartified diamictite, mudstonc and sandstone. Slight to moderate bioturbation. Mineralogy: quartz 35%, feldspar 15%, rock fragments 5%, rare amphiboles, pyroxenes and diatoms,

55.21 m to 55.33 m lonestone, cobble size in thin interbeds of massive muddy sandstone, sandy clast-rich diamictite and thinly laminated very fine-grained sandstone, siltstone, very coarse-grained sandstone with granule lonestones. Contacts between beds arc sharp. Small microfault through interbeds assocaited with large cobble lonestone. Clasts 4% in gravelly sand and diamictite.

55.33 m to 55.85 m thin interbeds (1 cm) muddy fine sandstone with dispersed coarse to very coarse grains with dispersed granules, small pebbles and lonestones (? with deformed strata below) and clast-poor sandy diamictite inclined at 1-2 degrees.

55.85 m to 56.06 m clayey siltstone breccia. Below 56.06 m wispy lamination is rare to common.

56.10 m to 56.49 m clayey siltstone

56.51 m to 57.56 m silty claystone with mottling by burrows common to moderate.

56.93 m to 56.98 m silty claystone conglomerate (intraformational).

57.56 m to 58.56 m clayey siltstone

57.56 m to 57.83 m mm-scale bioturbation, wispy lamination.

57.59 m, 57.83 m, 58.17 m, 58.40 m, fine to very fine sandstone laminae.

57.83 m to 59.58 m coarse siltstone with rare mudstone clasts at 58.88 m, 59.25 m, 59.27 m. Weakly bioturbated. Rare wispy laminae. (5Y2/1)

CRP-1

Sheet Number 12
Scale 1:20
Logged by: RDP on 20-10-97

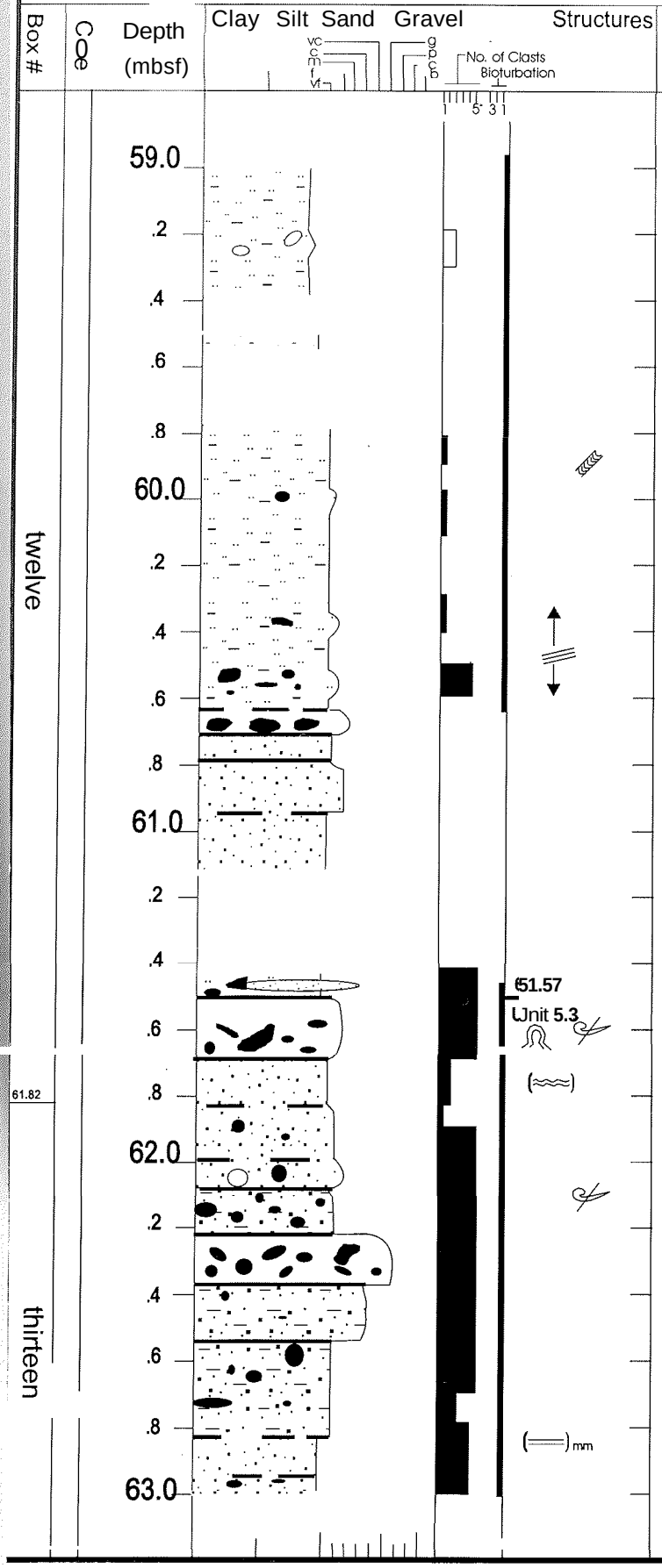

Description

Sub-unit 2.2 53.70 m to 61.46 m

INTERBEDDED SILTSTONE, DIAMICTITE, BRECCIA
Lithified, uncemented, medium bedded, fossil-bearing, poorly to very poorly sorted, siltsone, siltstone with dispersed clasts and muddy diamictite (5Y2/1 to 5G/21).

Alternating beds of siltstone, mudstone with dispersed clasts, very fine sandstone with very rare dispersed clasts, and interstartified diamictite, mudstone and sandstone. Slight to moderate bioturbation. Mineralogy: quartz 35%, feldspar 15%, rock fragments 5% *?*, rare amphiboles, pyroxenes and diatoms.

57.83 m to 59.58 m Coarse siltstone with rare mudstone clasts at 58.88 m, 59.25 m, 59.27 m. Weakly bioturbated. Rare wispy laminae. (5Y2/1)

59.78 m to 60.37 m very poorly sorted silly fine sandstone with medium to coarse sandstone grains (5Y2/1) with parallel laminated very fine sandstone clasts at 60.00 m, 60.34 m, 60.36 m.

60.37 m to 60.47 m Soft sediment deformed, disrupted, brecciated, fine sandstone, with grey fine sandstone as matrix.

60.47 to 60.56 m sandstone breccia of fine sandstone (5Y4/1) clasts with 40% medium sandstone matrix (5Y2/1).

59.94 m disecrete horizontal burrow,
60.56 m to 60.64 m poorly sorted fine sandstone with scattered very coarse sand.
60.64 m to 60.76 m medium sandstone breccia clasts in fine sandstone matrix.
60.76 m to 60.80 m fine sandstone, poorly sorted.
60.80 m to 60.96 m medium sandstone.
60.96 m to 61.14 m fine sandstone, poorly sorted.

Contact not recovered

Sub-Unit 3.1 61.46 m to 63.20 m

DIAMICTITE

Lithified, uncemented, medium thick bedded, fossil-bearing, very poorly sorted, clast-rich to clast-poor sandy diamictite (olive-black, 5Y2/1).

Interbedded siltstone with scattered granules, poorly sorted fine sandstone, muddy sandstone with dispersed clasts and muddy sandy conglomerate.

61.46 m to 61.51 m siltstone with scattered granules to small pebbles (pink granite, doierite), Fine sandstone lens (5Y5/2) with sharp contacts, 0.5 cm thick, intraclast of sandstone just above lens in siltstone.

61.51 m to 61.69 m sandy clast-rich diamictite. Clasts rounded to subangular with random orientation, pink granite, fine grained doierite, ?volcanics, and deformed siltstone clasts,

61.69 m to 61.82 m Poorly sorted fine sandstone with muddy matrix, ToD 2 cm soft sediment mudstone clasts

. . .next page.

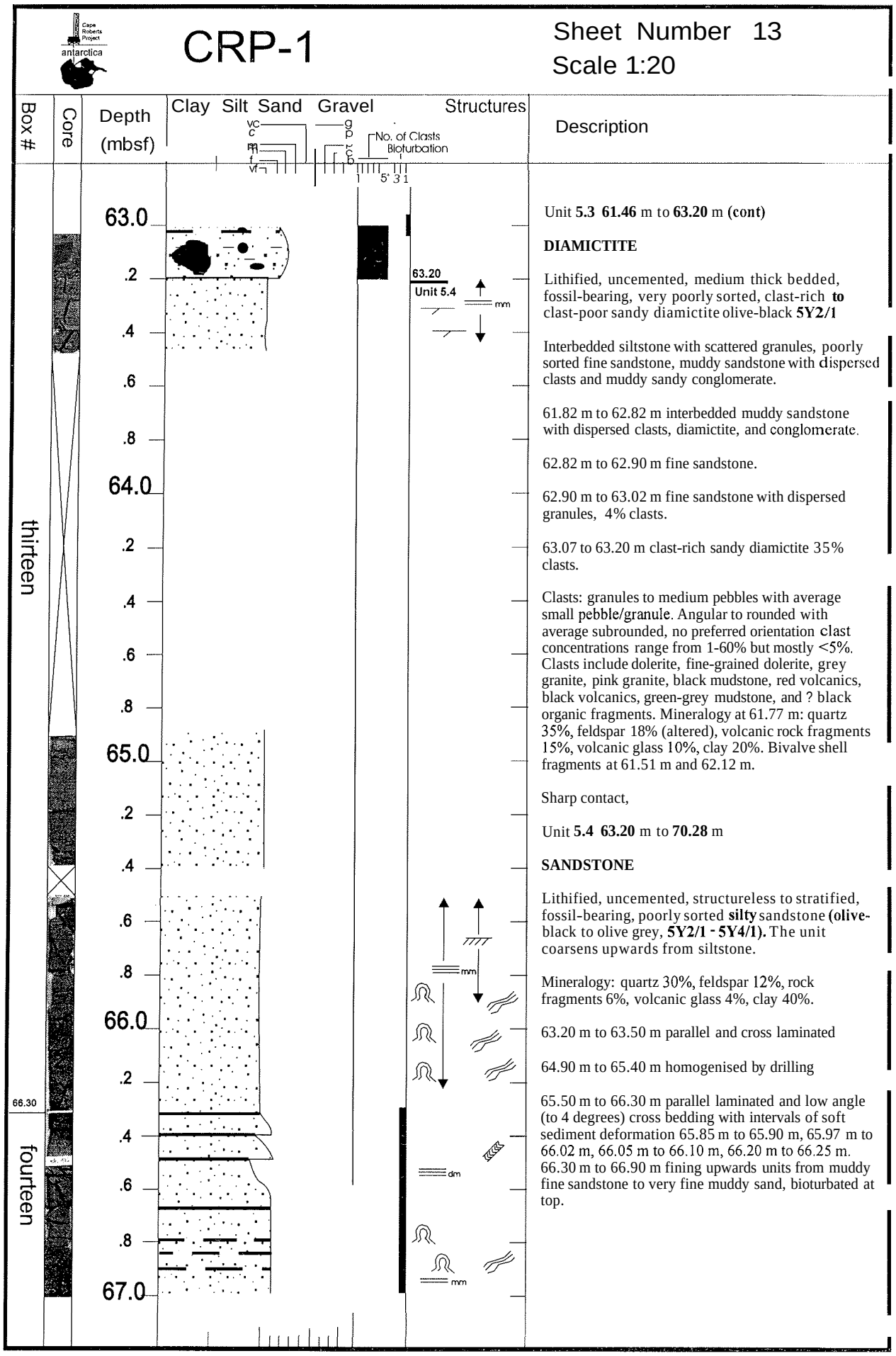

Unit **5.3 61.46** m to **63.20** m **(cont)**

DIAMICTITE

Lithified, uncemented, medium thick bedded, fossil-bearing, very poorly sorted, clast-rich **to** clast-poor sandy diamictite olive-black **5Y2/1**

Interbedded siltstone with scattered granules, poorly sorted fine sandstone, muddy sandstone with dispersed clasts and muddy sandy conglomerate.

61.82 m to 62.82 m interbedded muddy sandstone with dispersed clasts, diamictite, and conglomerate.

62.82 m to 62.90 m fine sandstone.

62.90 m to 63.02 m fine sandstone with dispersed granules, 4% clasts.

63.07 to 63.20 m clast-rich sandy diamictite 35% clasts.

Clasts: granules to medium pebbles with average small pebble/granule. Angular to rounded with average subrounded, no preferred orientation clast concentrations range from 1-60% but mostly <5%. Clasts include dolerite, fine-grained dolerite, grey granite, pink granite, black mudstone, red volcanics, black volcanics, green-grey mudstone, and ? black organic fragments. Mineralogy at 61.77 m: quartz 35%, feldspar 18% (altered), volcanic rock fragments 15%, volcanic glass 10%, clay 20%. Bivalve shell fragments at 61.51 m and 62.12 m.

Sharp contact,

Unit **5.4 63.20** m to **70.28** m

SANDSTONE

Lithified, uncemented, structureless to stratified, fossil-bearing, poorly sorted **silty** sandstone **(olive-**black to olive grey, **5Y2/1 - 5Y4/1).** The unit coarsens upwards from siltstone.

Mineralogy: quartz 30%, feldspar 12%, rock fragments 6%, volcanic glass 4%, clay 40%.

63.20 m to 63.50 m parallel and cross laminated

64.90 m to 65.40 m homogenised by drilling

65.50 m to 66.30 m parallel laminated and low angle (to 4 degrees) cross bedding with intervals of soft sediment deformation 65.85 m to 65.90 m, 65.97 m to 66.02 m, 66.05 m to 66.10 m, 66.20 m to 66.25 m. 66.30 m to 66.90 m fining upwards units from muddy fine sandstone to very fine muddy sand, bioturbated at top.

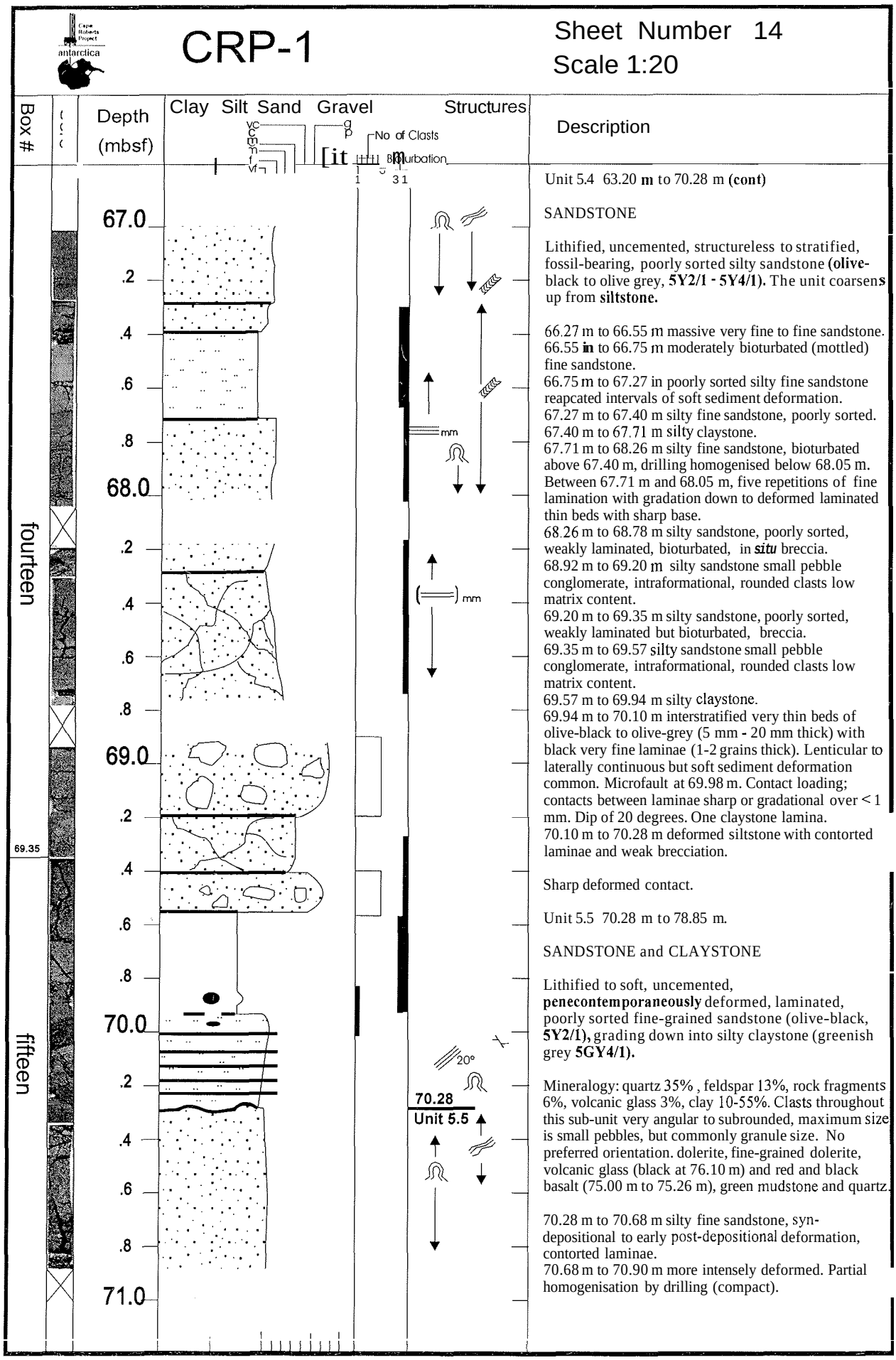

Unit 5.4 63.20 m to 70.28 m (cont)

SANDSTONE

Lithified, uncemented, structureless to stratified, fossil-bearing, poorly sorted silty sandstone (olive-black to olive grey, 5Y2/1 - 5Y4/1). The unit coarsens up from siltstone.

66.27 m to 66.55 m massive very fine to fine sandstone.
66.55 m to 66.75 m moderately bioturbated (mottled) fine sandstone.
66.75 m to 67.27 m poorly sorted silty fine sandstone reapcated intervals of soft sediment deformation.
67.27 m to 67.40 m silty fine sandstone, poorly sorted.
67.40 m to 67.71 m silty claystone.
67.71 m to 68.26 m silty fine sandstone, bioturbated above 67.40 m, drilling homogenised below 68.05 m. Between 67.71 m and 68.05 m, five repetitions of fine lamination with gradation down to deformed laminated thin beds with sharp base.
68.26 m to 68.78 m silty sandstone, poorly sorted, weakly laminated, bioturbated, in *situ* breccia.
68.92 m to 69.20 m silty sandstone small pebble conglomerate, intraformational, rounded clasts low matrix content.
69.20 m to 69.35 m silty sandstone, poorly sorted, weakly laminated but bioturbated, breccia.
69.35 m to 69.57 silty sandstone small pebble conglomerate, intraformational, rounded clasts low matrix content.
69.57 m to 69.94 m silty claystone.
69.94 m to 70.10 m interstratified very thin beds of olive-black to olive-grey (5 mm - 20 mm thick) with black very fine laminae (1-2 grains thick). Lenticular to laterally continuous but soft sediment deformation common. Microfault at 69.98 m. Contact loading; contacts between laminae sharp or gradational over < 1 mm. Dip of 20 degrees. One claystone lamina.
70.10 m to 70.28 m deformed siltstone with contorted laminae and weak brecciation.

Sharp deformed contact.

Unit 5.5 70.28 m to 78.85 m.

SANDSTONE and CLAYSTONE

Lithified to soft, uncemented, **penecontemporaneously** deformed, laminated, poorly sorted fine-grained sandstone (olive-black, **5Y2/1),** grading down into silty claystone (greenish grey **5GY4/1).**

Mineralogy: quartz 35% , feldspar 13%, rock fragments 6%, volcanic glass 3%, clay 10-55%. Clasts throughout this sub-unit very angular to subrounded, maximum size is small pebbles, but commonly granule size. No preferred orientation. dolerite, fine-grained dolerite, volcanic glass (black at 76.10 m) and red and black basalt (75.00 m to 75.26 m), green mudstone and quartz.

70.28 m to 70.68 m silty fine sandstone, syn-depositional to early post-depositional deformation, contorted laminae.
70.68 m to 70.90 m more intensely deformed. Partial homogenisation by drilling (compact).

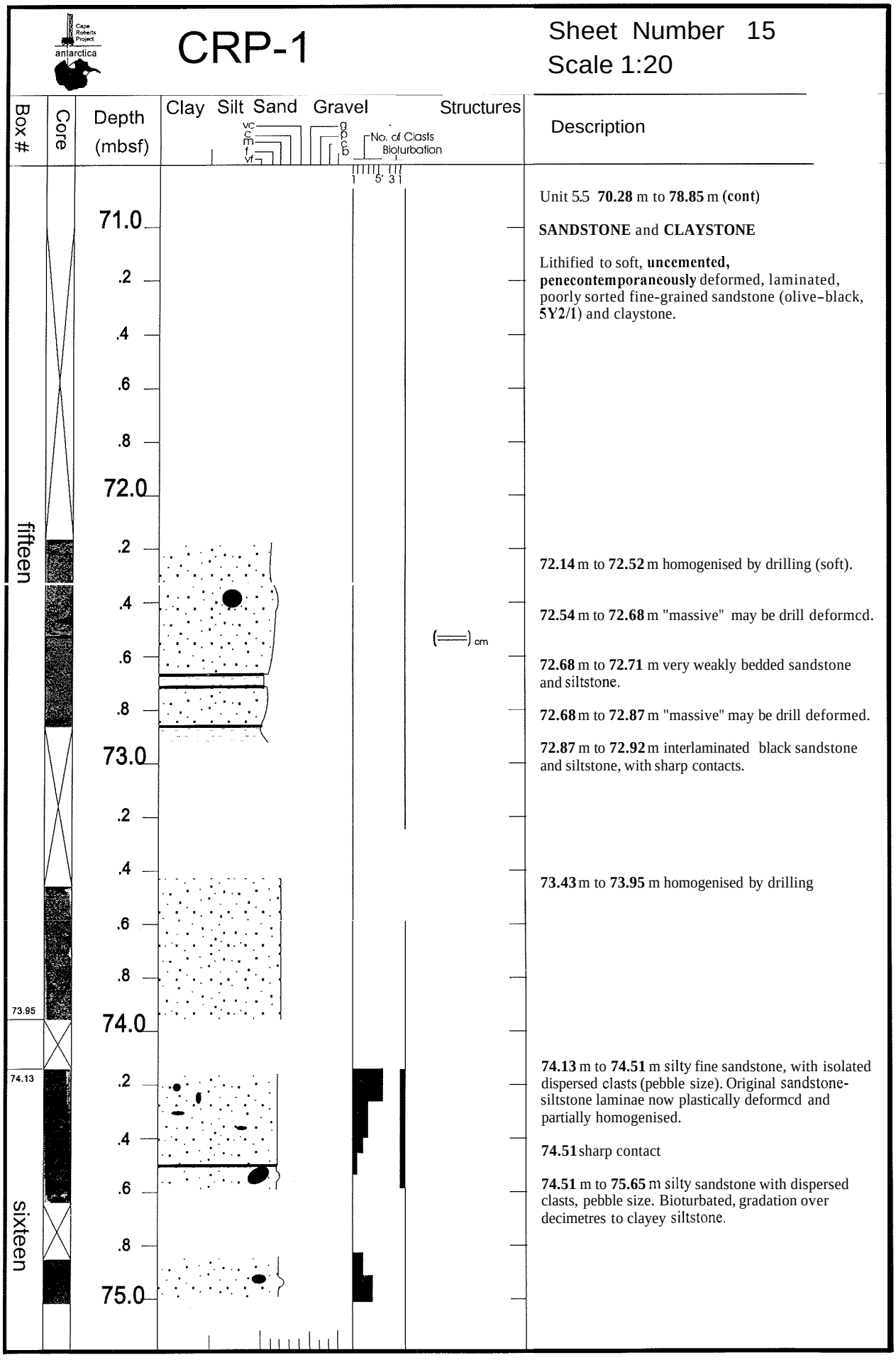
Case Roberts Project
antarctica
CRP-1
Sheet Number 15
Scale 1:20
Box #
Core
Depth (mbsf)
Clay Silt Sand Gravel
vc c m f vf
g p cg
No. of Clasts
Bioturbation
1 5 3 1
Structures
Description
fifteen
sixteen
71.0
.2
.4
.6
.8
72.0
.2
.4
.6
.8
73.0
.2
.4
.6
.8
73.95
74.0
74.13
.2
.4
.6
.8
75.0
cm
Unit 5.5 70.28 m to 78.85 m (cont)
SANDSTONE and CLAYSTONE
Lithified to soft, uncemented, penecontemporaneously deformed, laminated, poorly sorted fine-grained sandstone (olive-black, 5Y2/1) and claystone.
72.14 m to 72.52 m homogenised by drilling (soft).
72.54 m to 72.68 m "massive" may be drill deformcd.
72.68 m to 72.71 m very weakly bedded sandstone and siltstone.
72.68 m to 72.87 m "massive" may be drill deformed.
72.87 m to 72.92 m interlaminated black sandstone and siltstone, with sharp contacts.
73.43 m to 73.95 m homogenised by drilling
74.13 m to 74.51 m silty fine sandstone, with isolated dispersed clasts (pebble size). Original sandstone-siltstone laminae now plastically deformcd and partially homogenised.
74.51 sharp contact
74.51 m to 75.65 m silty sandstone with dispersed clasts, pebble size. Bioturbated, gradation over decimetres to clayey siltstone.

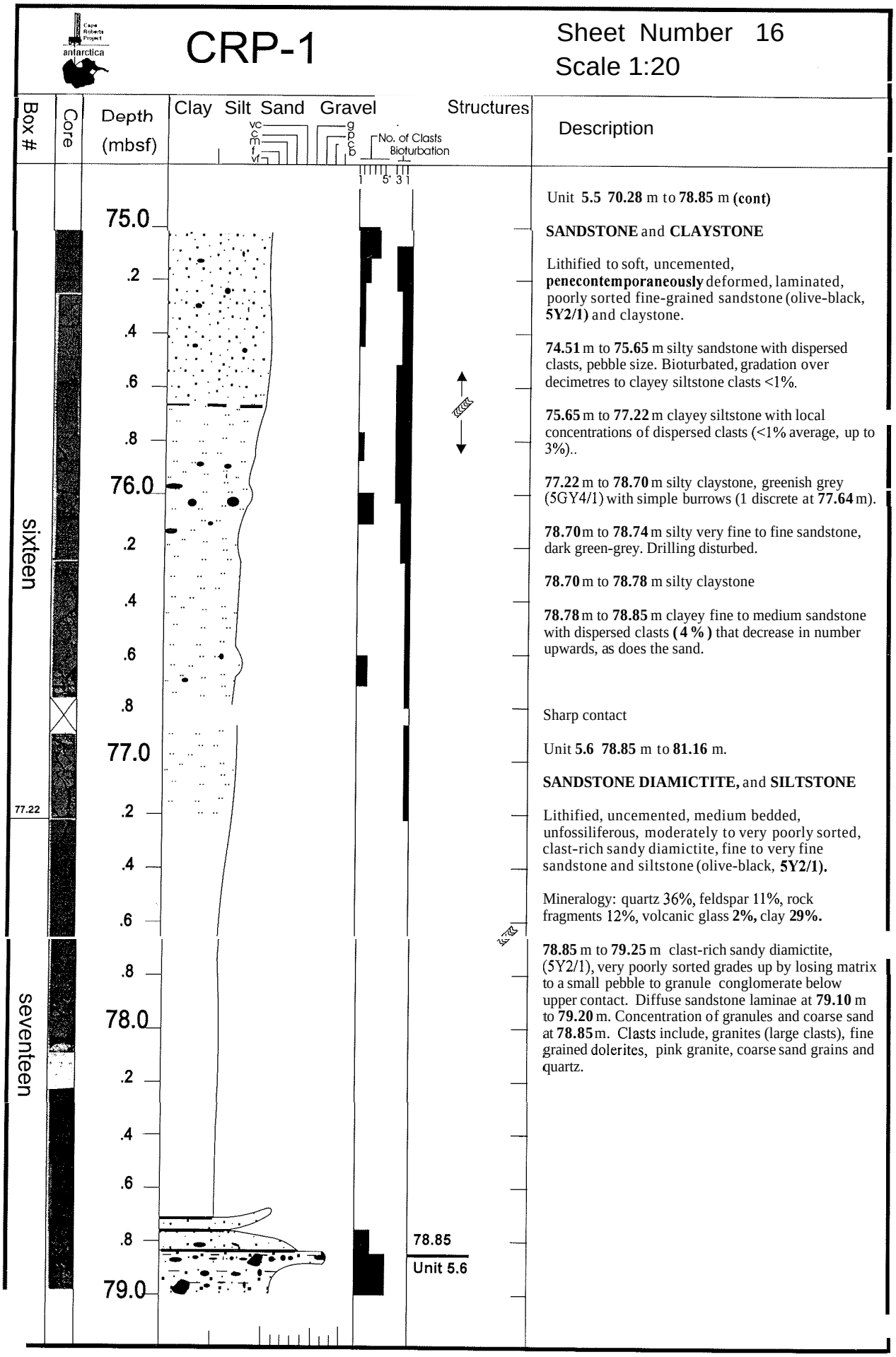
CRP-1
Sheet Number 16
Scale 1:20
Box #
Core
Depth (mbsf)
Clay Silt Sand Gravel
vc c m f vf
g p c b
No. of Clasts
Bioturbation
1 5 3 1
Structures
Description
sixteen
seventeen
75.0
.2
.4
.6
.8
76.0
.2
.4
.6
.8
77.0
77.22
.2
.4
.6
.8
78.0
.2
.4
.6
.8
79.0
78.85
Unit 5.6
Unit 5.5 70.28 m to 78.85 m (cont)
SANDSTONE and CLAYSTONE
Lithified to soft, uncemented, penecontemporaneously deformed, laminated, poorly sorted fine-grained sandstone (olive-black, 5Y2/1) and claystone.
74.51 m to 75.65 m silty sandstone with dispersed clasts, pebble size. Bioturbated, gradation over decimetres to clayey siltstone clasts <1%.
75.65 m to 77.22 m clayey siltstone with local concentrations of dispersed clasts (<1% average, up to 3%)..
77.22 m to 78.70 m silty claystone, greenish grey (5GY4/1) with simple burrows (1 discrete at 77.64 m).
78.70 m to 78.74 m silty very fine to fine sandstone, dark green-grey. Drilling disturbed.
78.70 m to 78.78 m silty claystone
78.78 m to 78.85 m clayey fine to medium sandstone with dispersed clasts (4 %) that decrease in number upwards, as does the sand.
Sharp contact
Unit 5.6 78.85 m to 81.16 m.
SANDSTONE DIAMICTITE, and SILTSTONE
Lithified, uncemented, medium bedded, unfossiliferous, moderately to very poorly sorted, clast-rich sandy diamictite, fine to very fine sandstone and siltstone (olive-black, 5Y2/1).
Mineralogy: quartz 36%, feldspar 11%, rock fragments 12%, volcanic glass 2%, clay 29%.
78.85 m to 79.25 m clast-rich sandy diamictite, (5Y2/1), very poorly sorted grades up by losing matrix to a small pebble to granule conglomerate below upper contact. Diffuse sandstone laminae at 79.10 m to 79.20 m. Concentration of granules and coarse sand at 78.85 m. Clasts include, granites (large clasts), fine grained dolerites, pink granite, coarse sand grains and quartz.

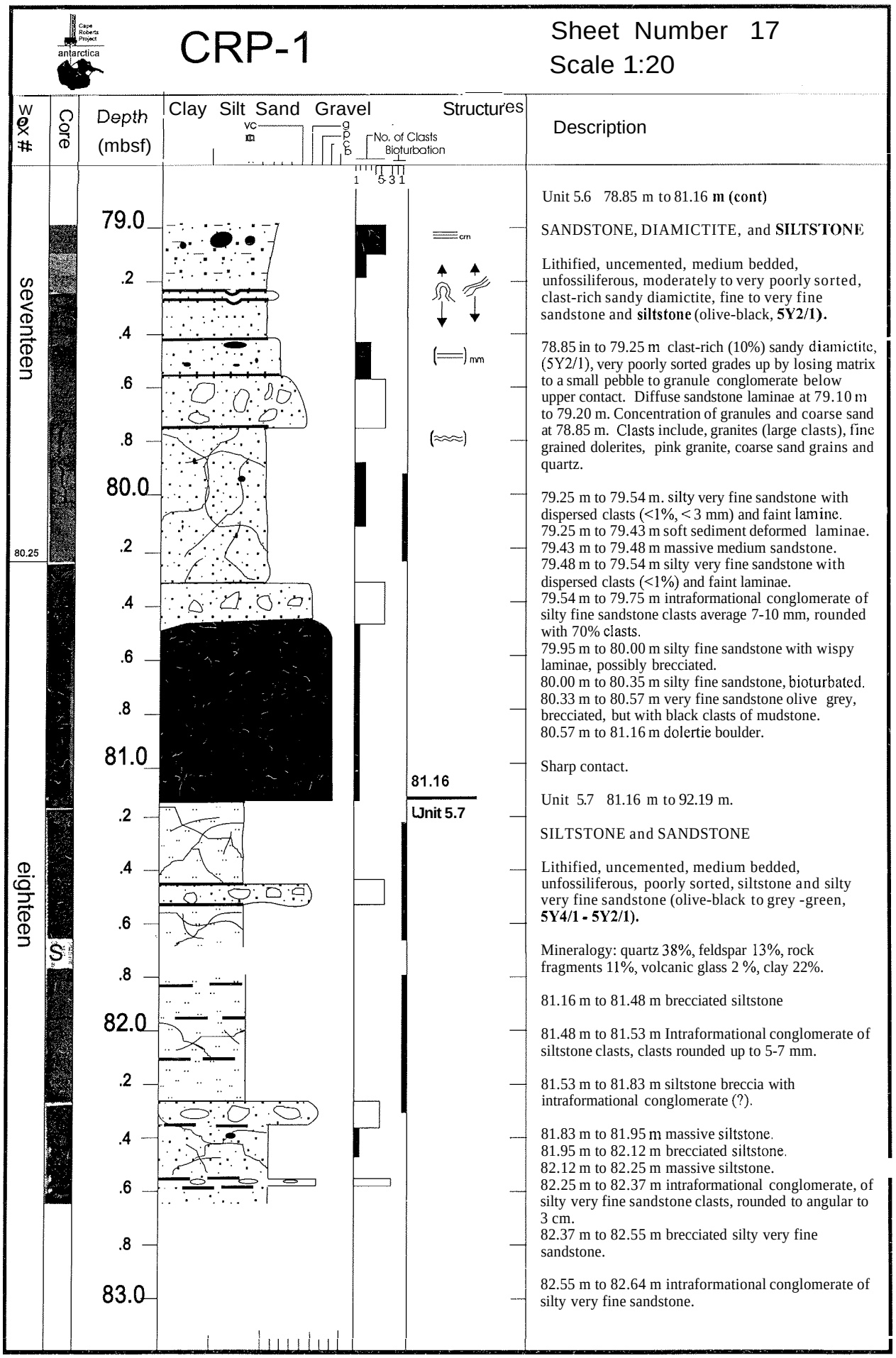

Unit 5.6 78.85 m to 81.16 **m (cont)**

SANDSTONE, DIAMICTITE, and **SILTSTONE**

Lithified, uncemented, medium bedded, unfossiliferous, moderately to very poorly sorted, clast-rich sandy diamictite, fine to very fine sandstone and **siltstone** (olive-black, **5Y2/1).**

78.85 in to 79.25 m clast-rich (10%) sandy diamictite, (5Y2/1), very poorly sorted grades up by losing matrix to a small pebble to granule conglomerate below upper contact. Diffuse sandstone laminae at 79.10 m to 79.20 m. Concentration of granules and coarse sand at 78.85 m. Clasts include, granites (large clasts), fine grained dolerites, pink granite, coarse sand grains and quartz.

79.25 m to 79.54 m. silty very fine sandstone with dispersed clasts (<1%, < 3 mm) and faint lamine.
79.25 m to 79.43 m soft sediment deformed laminae.
79.43 m to 79.48 m massive medium sandstone.
79.48 m to 79.54 m silty very fine sandstone with dispersed clasts (<1%) and faint laminae.
79.54 m to 79.75 m intraformational conglomerate of silty fine sandstone clasts average 7-10 mm, rounded with 70% clasts.
79.95 m to 80.00 m silty fine sandstone with wispy laminae, possibly brecciated.
80.00 m to 80.35 m silty fine sandstone, bioturbated.
80.33 m to 80.57 m very fine sandstone olive grey, brecciated, but with black clasts of mudstone.
80.57 m to 81.16 m dolertie boulder.

Sharp contact.

Unit 5.7 81.16 m to 92.19 m.

SILTSTONE and SANDSTONE

Lithified, uncemented, medium bedded, unfossiliferous, poorly sorted, siltstone and silty very fine sandstone (olive-black to grey -green, **5Y4/1 - 5Y2/1).**

Mineralogy: quartz 38%, feldspar 13%, rock fragments 11%, volcanic glass 2 %, clay 22%.

81.16 m to 81.48 m brecciated siltstone

81.48 m to 81.53 m Intraformational conglomerate of siltstone clasts, clasts rounded up to 5-7 mm.

81.53 m to 81.83 m siltstone breccia with intraformational conglomerate (?).

81.83 m to 81.95 m massive siltstone.
81.95 m to 82.12 m brecciated siltstone.
82.12 m to 82.25 m massive siltstone.
82.25 m to 82.37 m intraformational conglomerate, of silty very fine sandstone clasts, rounded to angular to 3 cm.
82.37 m to 82.55 m brecciated silty very fine sandstone.

82.55 m to 82.64 m intraformational conglomerate of silty very fine sandstone.

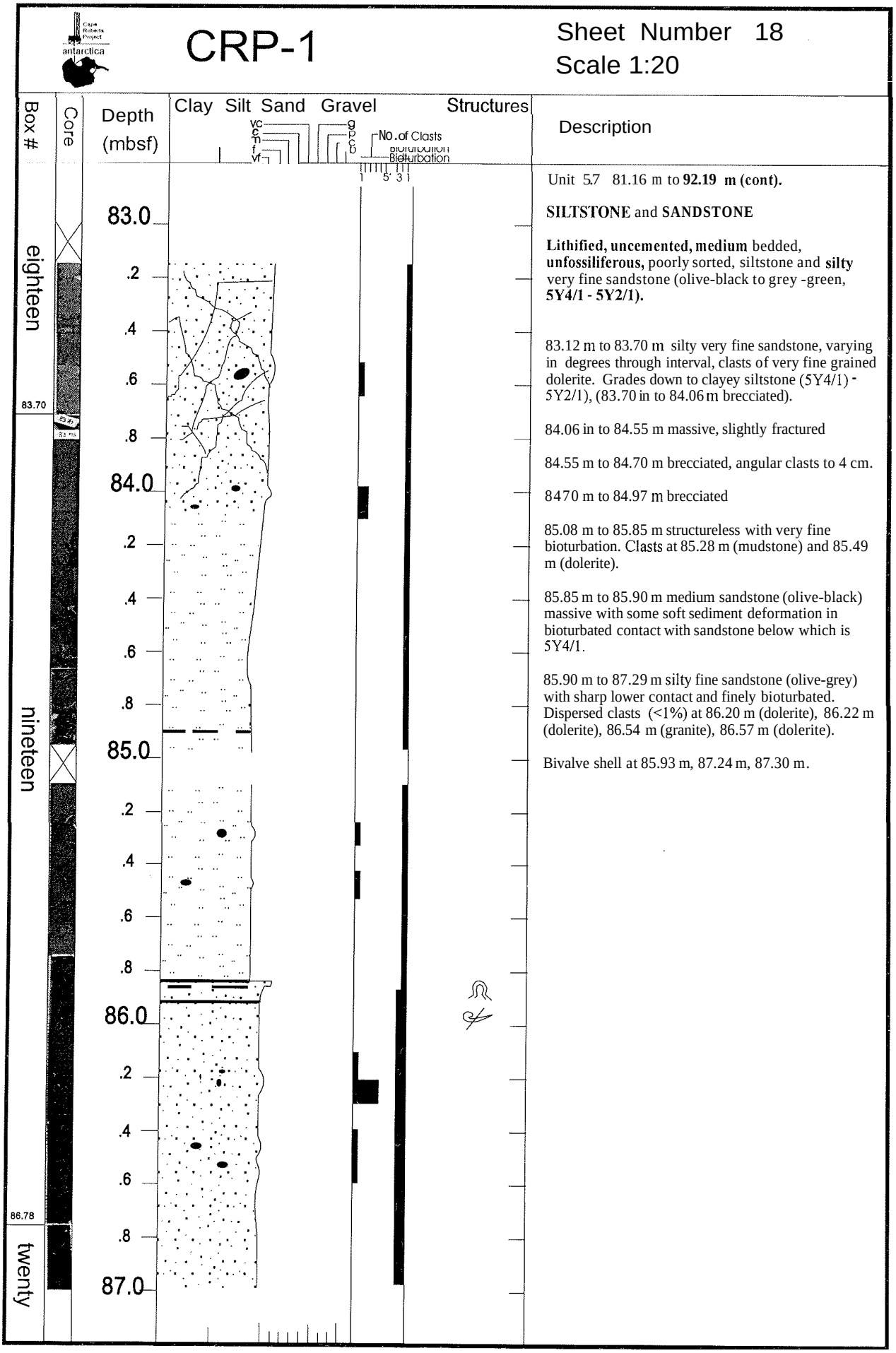

Unit 5.7 81.16 m to **92.19 m (cont).**

SILTSTONE and **SANDSTONE**

Lithified, uncemented, medium bedded, **unfossiliferous,** poorly sorted, siltstone and **silty** very fine sandstone (olive-black to grey -green, **5Y4/1 - 5Y2/1).**

83.12 m to 83.70 m silty very fine sandstone, varying in degrees through interval, clasts of very fine grained dolerite. Grades down to clayey siltstone (5Y4/1) - 5Y2/1), (83.70 in to 84.06 m brecciated).

84.06 in to 84.55 m massive, slightly fractured

84.55 m to 84.70 m brecciated, angular clasts to 4 cm.

8470 m to 84.97 m brecciated

85.08 m to 85.85 m structureless with very fine bioturbation. Clasts at 85.28 m (mudstone) and 85.49 m (dolerite).

85.85 m to 85.90 m medium sandstone (olive-black) massive with some soft sediment deformation in bioturbated contact with sandstone below which is 5Y4/1.

85.90 m to 87.29 m silty fine sandstone (olive-grey) with sharp lower contact and finely bioturbated. Dispersed clasts (<1%) at 86.20 m (dolerite), 86.22 m (dolerite), 86.54 m (granite), 86.57 m (dolerite).

Bivalve shell at 85.93 m, 87.24 m, 87.30 m.

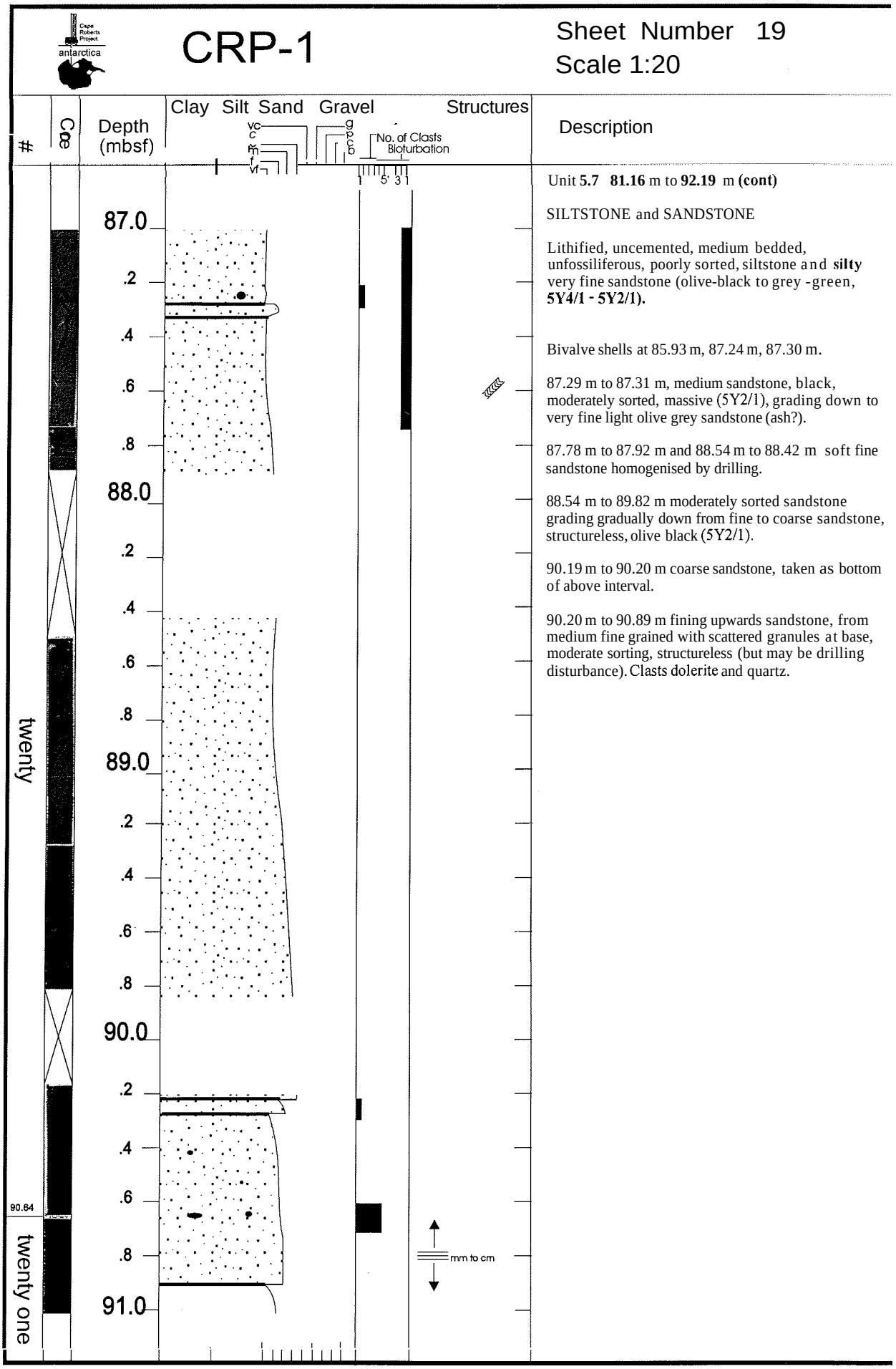

Description

Unit **5.7** **81.16** m to **92.19** m **(cont)**

SILTSTONE and SANDSTONE

Lithified, uncemented, medium bedded, unfossiliferous, poorly sorted, siltstone and **silty** very fine sandstone (olive-black to grey -green, **5Y4/1 - 5Y2/1).**

Bivalve shells at 85.93 m, 87.24 m, 87.30 m.

87.29 m to 87.31 m, medium sandstone, black, moderately sorted, massive (5Y2/1), grading down to very fine light olive grey sandstone (ash?).

87.78 m to 87.92 m and 88.54 m to 88.42 m soft fine sandstone homogenised by drilling.

88.54 m to 89.82 m moderately sorted sandstone grading gradually down from fine to coarse sandstone, structureless, olive black (5Y2/1).

90.19 m to 90.20 m coarse sandstone, taken as bottom of above interval.

90.20 m to 90.89 m fining upwards sandstone, from medium fine grained with scattered granules at base, moderate sorting, structureless (but may be drilling disturbance). Clasts dolerite and quartz.

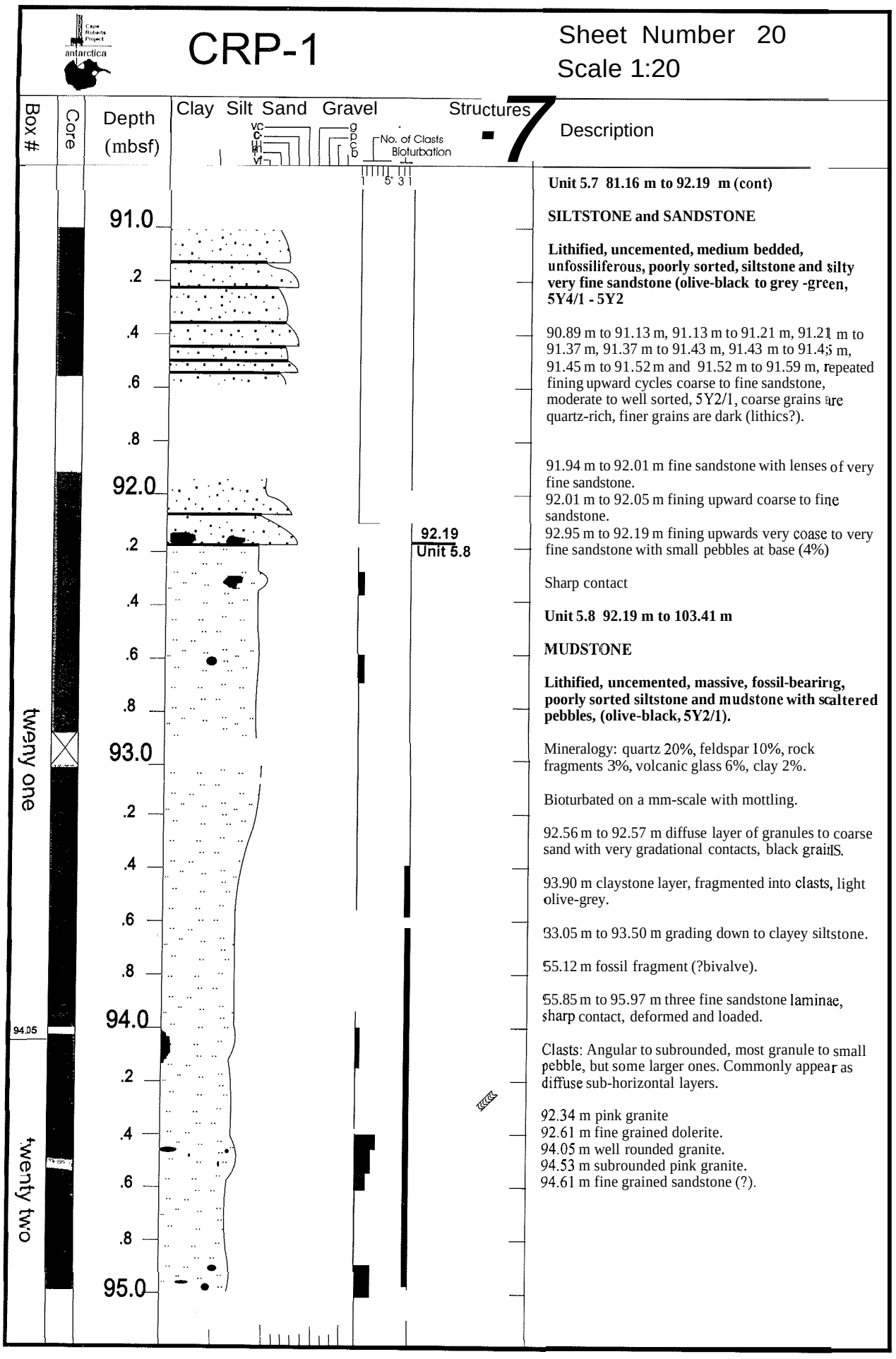

Unit 5.7 81.16 m to 92.19 m (cont)

SILTSTONE and SANDSTONE

Lithified, uncemented, medium bedded, unfossiliferous, poorly sorted, siltstone and silty very fine sandstone (olive-black to grey -green, 5Y4/1 - 5Y2

90.89 m to 91.13 m, 91.13 m to 91.21 m, 91.21 m to 91.37 m, 91.37 m to 91.43 m, 91.43 m to 91.45 m, 91.45 m to 91.52 m and 91.52 m to 91.59 m, repeated fining upward cycles coarse to fine sandstone, moderate to well sorted, 5Y2/1, coarse grains are quartz-rich, finer grains are dark (lithics?).

91.94 m to 92.01 m fine sandstone with lenses of very fine sandstone.
92.01 m to 92.05 m fining upward coarse to fine sandstone.
92.95 m to 92.19 m fining upwards very coase to very fine sandstone with small pebbles at base (4%)

Sharp contact

Unit 5.8 92.19 m to 103.41 m

MUDSTONE

Lithified, uncemented, massive, fossil-bearing, poorly sorted siltstone and mudstone with scaltered pebbles, (olive-black, 5Y2/1).

Mineralogy: quartz 20%, feldspar 10%, rock fragments 3%, volcanic glass 6%, clay 2%.

Bioturbated on a mm-scale with mottling.

92.56 m to 92.57 m diffuse layer of granules to coarse sand with very gradational contacts, black grains.

93.90 m claystone layer, fragmented into clasts, light olive-grey.

93.05 m to 93.50 m grading down to clayey siltstone.

95.12 m fossil fragment (?bivalve).

95.85 m to 95.97 m three fine sandstone laminae, sharp contact, deformed and loaded.

Clasts: Angular to subrounded, most granule to small pebble, but some larger ones. Commonly appear as diffuse sub-horizontal layers.

92.34 m pink granite
92.61 m fine grained dolerite.
94.05 m well rounded granite.
94.53 m subrounded pink granite.
94.61 m fine grained sandstone (?).

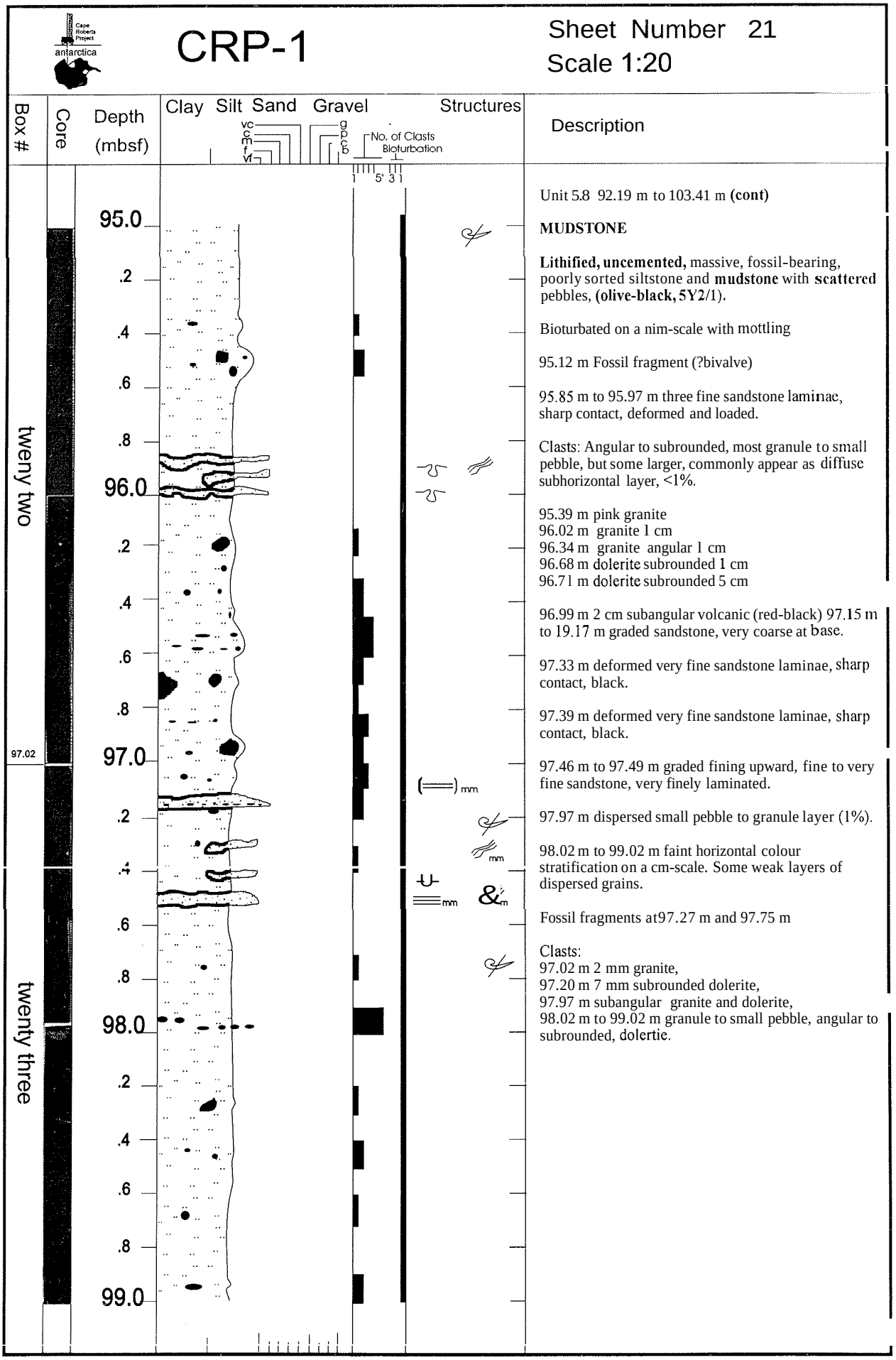

Unit 5.8 92.19 m to 103.41 m **(cont)**

MUDSTONE

Lithified, uncemented, massive, fossil-bearing, poorly sorted siltstone and **mudstone** with **scattered** pebbles, **(olive-black, 5Y2/1).**

Bioturbated on a nim-scale with mottling

95.12 m Fossil fragment (?bivalve)

95.85 m to 95.97 m three fine sandstone laminae, sharp contact, deformed and loaded.

Clasts: Angular to subrounded, most granule to small pebble, but some larger, commonly appear as diffuse subhorizontal layer, <1%.

95.39 m pink granite
96.02 m granite 1 cm
96.34 m granite angular 1 cm
96.68 m dolerite subrounded 1 cm
96.71 m dolerite subrounded 5 cm

96.99 m 2 cm subangular volcanic (red-black) 97.15 m to 19.17 m graded sandstone, very coarse at base.

97.33 m deformed very fine sandstone laminae, sharp contact, black.

97.39 m deformed very fine sandstone laminae, sharp contact, black.

97.46 m to 97.49 m graded fining upward, fine to very fine sandstone, very finely laminated.

97.97 m dispersed small pebble to granule layer (1%).

98.02 m to 99.02 m faint horizontal colour stratification on a cm-scale. Some weak layers of dispersed grains.

Fossil fragments at97.27 m and 97.75 m

Clasts:
97.02 m 2 mm granite,
97.20 m 7 mm subrounded dolerite,
97.97 m subangular granite and dolerite,
98.02 m to 99.02 m granule to small pebble, angular to subrounded, dolertie.

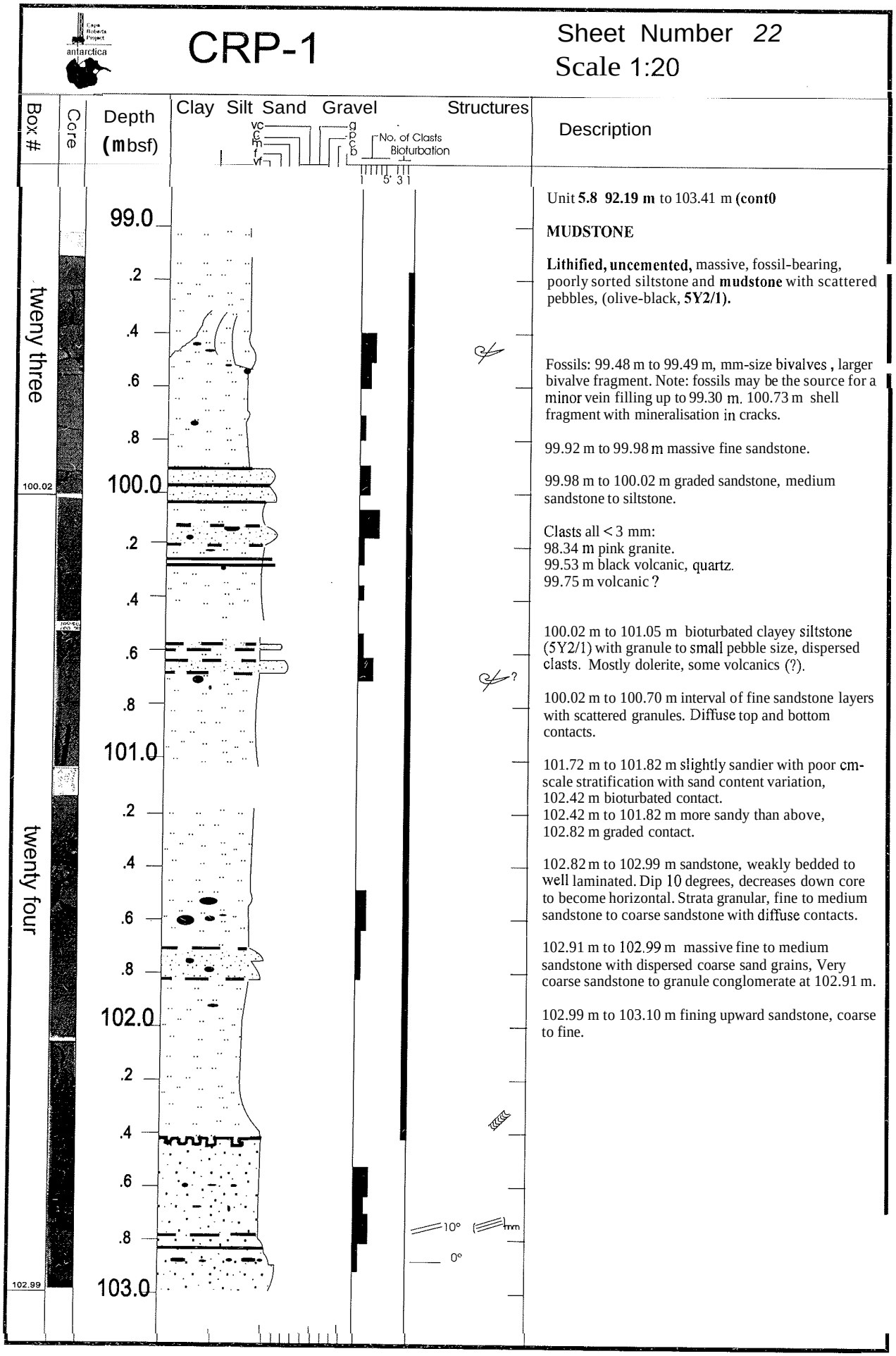

Unit **5.8 92.19 m** to 103.41 m **(cont0**

MUDSTONE

Lithified, uncemented, massive, fossil-bearing, poorly sorted siltstone and **mudstone** with scattered pebbles, (olive-black, **5Y2/1).**

Fossils: 99.48 m to 99.49 m, mm-size bivalves , larger bivalve fragment. Note: fossils may be the source for a minor vein filling up to 99.30 m. 100.73 m shell fragment with mineralisation in cracks.

99.92 m to 99.98 m massive fine sandstone.

99.98 m to 100.02 m graded sandstone, medium sandstone to siltstone.

Clasts all < 3 mm:
98.34 m pink granite.
99.53 m black volcanic, quartz.
99.75 m volcanic ?

100.02 m to 101.05 m bioturbated clayey siltstone (5Y2/1) with granule to small pebble size, dispersed clasts. Mostly dolerite, some volcanics (?).

100.02 m to 100.70 m interval of fine sandstone layers with scattered granules. Diffuse top and bottom contacts.

101.72 m to 101.82 m slightly sandier with poor cm-scale stratification with sand content variation,
102.42 m bioturbated contact.
102.42 m to 101.82 m more sandy than above,
102.82 m graded contact.

102.82 m to 102.99 m sandstone, weakly bedded to well laminated. Dip 10 degrees, decreases down core to become horizontal. Strata granular, fine to medium sandstone to coarse sandstone with diffuse contacts.

102.91 m to 102.99 m massive fine to medium sandstone with dispersed coarse sand grains, Very coarse sandstone to granule conglomerate at 102.91 m.

102.99 m to 103.10 m fining upward sandstone, coarse to fine.

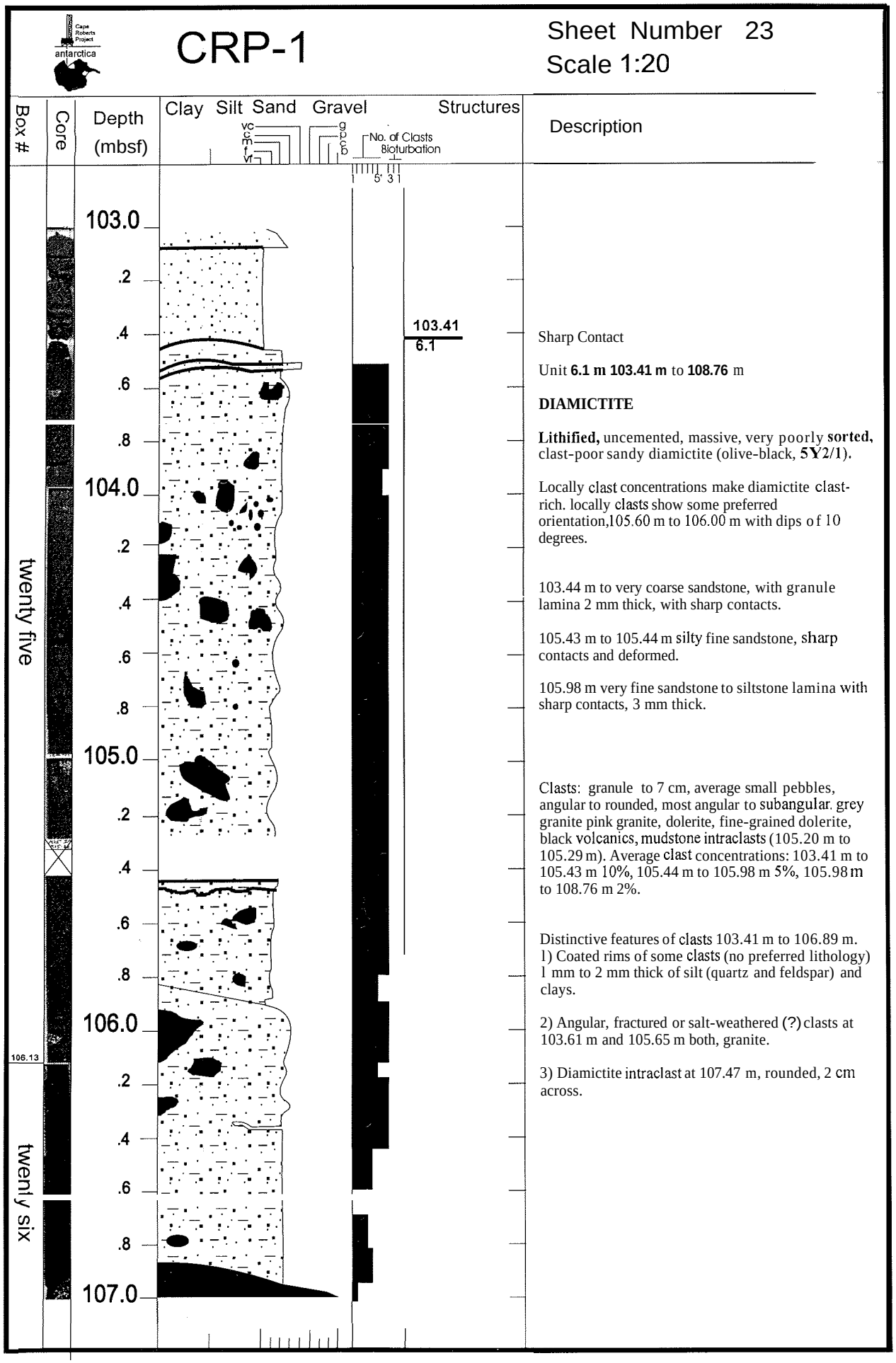

Sharp Contact

Unit **6.1 m 103.41 m** to **108.76** m

DIAMICTITE

Lithified, uncemented, massive, very poorly **sorted,** clast-poor sandy diamictite (olive-black, **5Y2/1**).

Locally clast concentrations make diamictite clast-rich. locally clasts show some preferred orientation,105.60 m to 106.00 m with dips of 10 degrees.

103.44 m to very coarse sandstone, with granule lamina 2 mm thick, with sharp contacts.

105.43 m to 105.44 m silty fine sandstone, sharp contacts and deformed.

105.98 m very fine sandstone to siltstone lamina with sharp contacts, 3 mm thick.

Clasts: granule to 7 cm, average small pebbles, angular to rounded, most angular to subangular. grey granite pink granite, dolerite, fine-grained dolerite, black volcanics, mudstone intraclasts (105.20 m to 105.29 m). Average clast concentrations: 103.41 m to 105.43 m 10%, 105.44 m to 105.98 m 5%, 105.98 m to 108.76 m 2%.

Distinctive features of clasts 103.41 m to 106.89 m. 1) Coated rims of some clasts (no preferred lithology) 1 mm to 2 mm thick of silt (quartz and feldspar) and clays.

2) Angular, fractured or salt-weathered (?) clasts at 103.61 m and 105.65 m both, granite.

3) Diamictite intraclast at 107.47 m, rounded, 2 cm across.

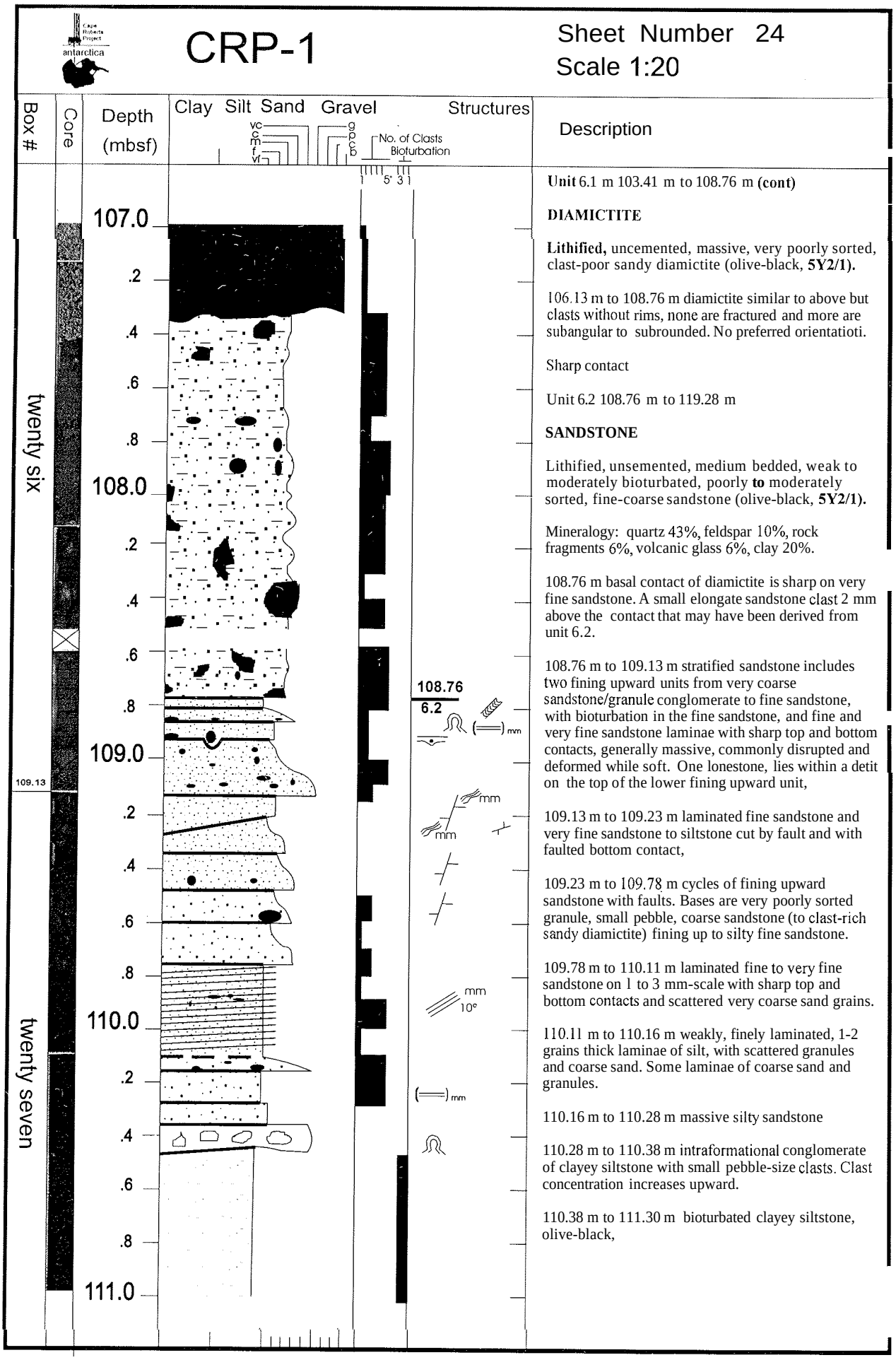

Unit 6.1 m 103.41 m to 108.76 m **(cont)**

DIAMICTITE

Lithified, uncemented, massive, very poorly sorted, clast-poor sandy diamictite (olive-black, **5Y2/1).**

106.13 m to 108.76 m diamictite similar to above but clasts without rims, none are fractured and more are subangular to subrounded. No preferred orientatioti.

Sharp contact

Unit 6.2 108.76 m to 119.28 m

SANDSTONE

Lithified, unsemented, medium bedded, weak to moderately bioturbated, poorly **to** moderately sorted, fine-coarse sandstone (olive-black, **5Y2/1).**

Mineralogy: quartz 43%, feldspar 10%, rock fragments 6%, volcanic glass 6%, clay 20%.

108.76 m basal contact of diamictite is sharp on very fine sandstone. A small elongate sandstone clast 2 mm above the contact that may have been derived from unit 6.2.

108.76 m to 109.13 m stratified sandstone includes two fining upward units from very coarse sandstone/granule conglomerate to fine sandstone, with bioturbation in the fine sandstone, and fine and very fine sandstone laminae with sharp top and bottom contacts, generally massive, commonly disrupted and deformed while soft. One lonestone, lies within a detit on the top of the lower fining upward unit,

109.13 m to 109.23 m laminated fine sandstone and very fine sandstone to siltstone cut by fault and with faulted bottom contact,

109.23 m to 109.78 m cycles of fining upward sandstone with faults. Bases are very poorly sorted granule, small pebble, coarse sandstone (to clast-rich sandy diamictite) fining up to silty fine sandstone.

109.78 m to 110.11 m laminated fine to very fine sandstone on 1 to 3 mm-scale with sharp top and bottom contacts and scattered very coarse sand grains.

110.11 m to 110.16 m weakly, finely laminated, 1-2 grains thick laminae of silt, with scattered granules and coarse sand. Some laminae of coarse sand and granules.

110.16 m to 110.28 m massive silty sandstone

110.28 m to 110.38 m intraformational conglomerate of clayey siltstone with small pebble-size clasts. Clast concentration increases upward.

110.38 m to 111.30 m bioturbated clayey siltstone, olive-black,

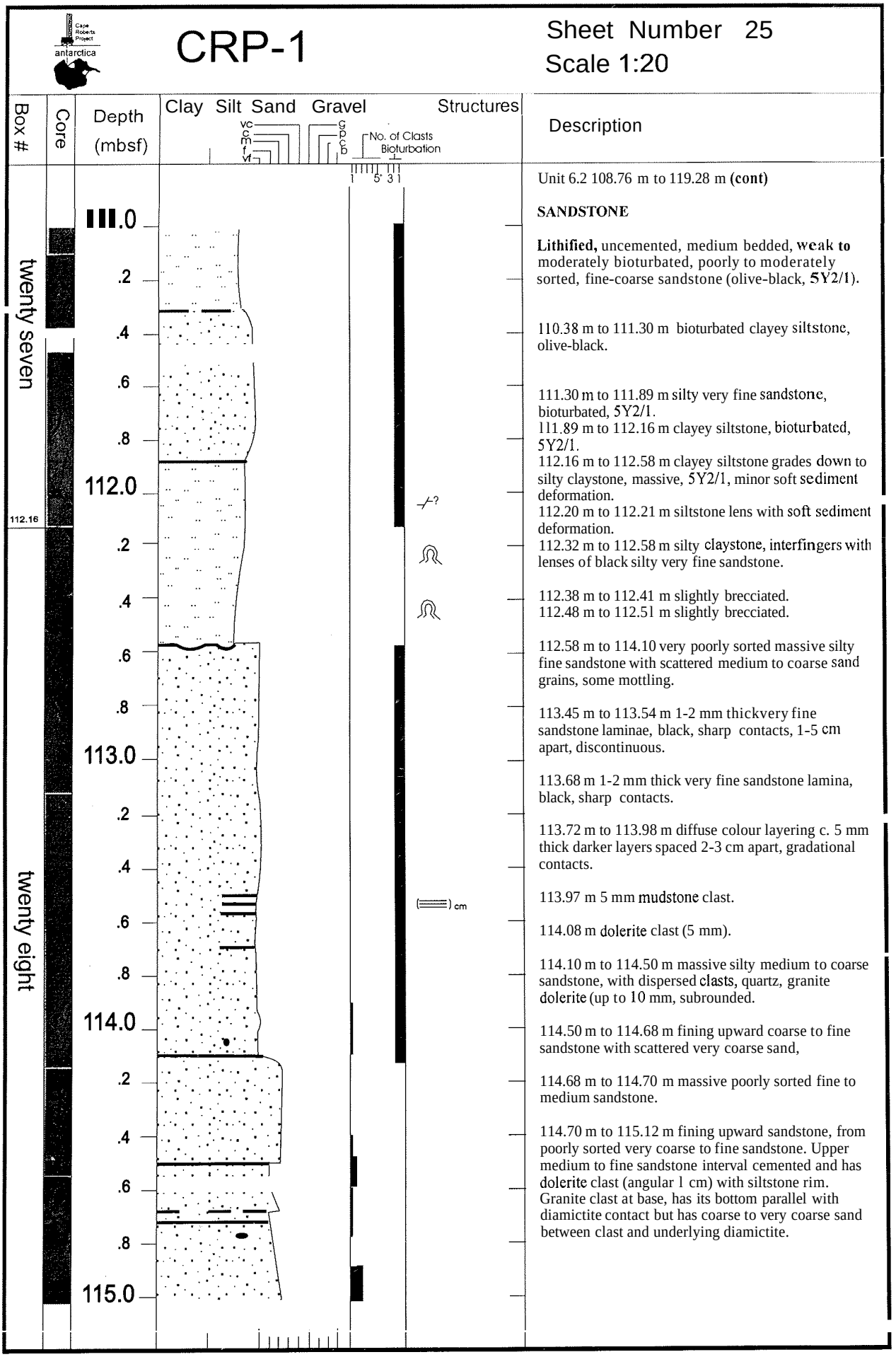

Unit 6.2 108.76 m to 119.28 m **(cont)**

SANDSTONE

Lithified, uncemented, medium bedded, **weak to** moderately bioturbated, poorly to moderately sorted, fine-coarse sandstone (olive-black, 5Y2/1).

110.38 m to 111.30 m bioturbated clayey siltstone, olive-black.

111.30 m to 111.89 m silty very fine sandstone, bioturbated, 5Y2/1.
111.89 m to 112.16 m clayey siltstone, bioturbated, 5Y2/1.
112.16 m to 112.58 m clayey siltstone grades down to silty claystone, massive, 5Y2/1, minor soft sediment deformation.
112.20 m to 112.21 m siltstone lens with soft sediment deformation.
112.32 m to 112.58 m silty claystone, interfingers with lenses of black silty very fine sandstone.

112.38 m to 112.41 m slightly brecciated.
112.48 m to 112.51 m slightly brecciated.

112.58 m to 114.10 very poorly sorted massive silty fine sandstone with scattered medium to coarse sand grains, some mottling.

113.45 m to 113.54 m 1-2 mm thickvery fine sandstone laminae, black, sharp contacts, 1-5 cm apart, discontinuous.

113.68 m 1-2 mm thick very fine sandstone lamina, black, sharp contacts.

113.72 m to 113.98 m diffuse colour layering c. 5 mm thick darker layers spaced 2-3 cm apart, gradational contacts.

113.97 m 5 mm mudstone clast.

114.08 m dolerite clast (5 mm).

114.10 m to 114.50 m massive silty medium to coarse sandstone, with dispersed clasts, quartz, granite dolerite (up to 10 mm, subrounded.

114.50 m to 114.68 m fining upward coarse to fine sandstone with scattered very coarse sand,

114.68 m to 114.70 m massive poorly sorted fine to medium sandstone.

114.70 m to 115.12 m fining upward sandstone, from poorly sorted very coarse to fine sandstone. Upper medium to fine sandstone interval cemented and has dolerite clast (angular 1 cm) with siltstone rim. Granite clast at base, has its bottom parallel with diamictite contact but has coarse to very coarse sand between clast and underlying diamictite.

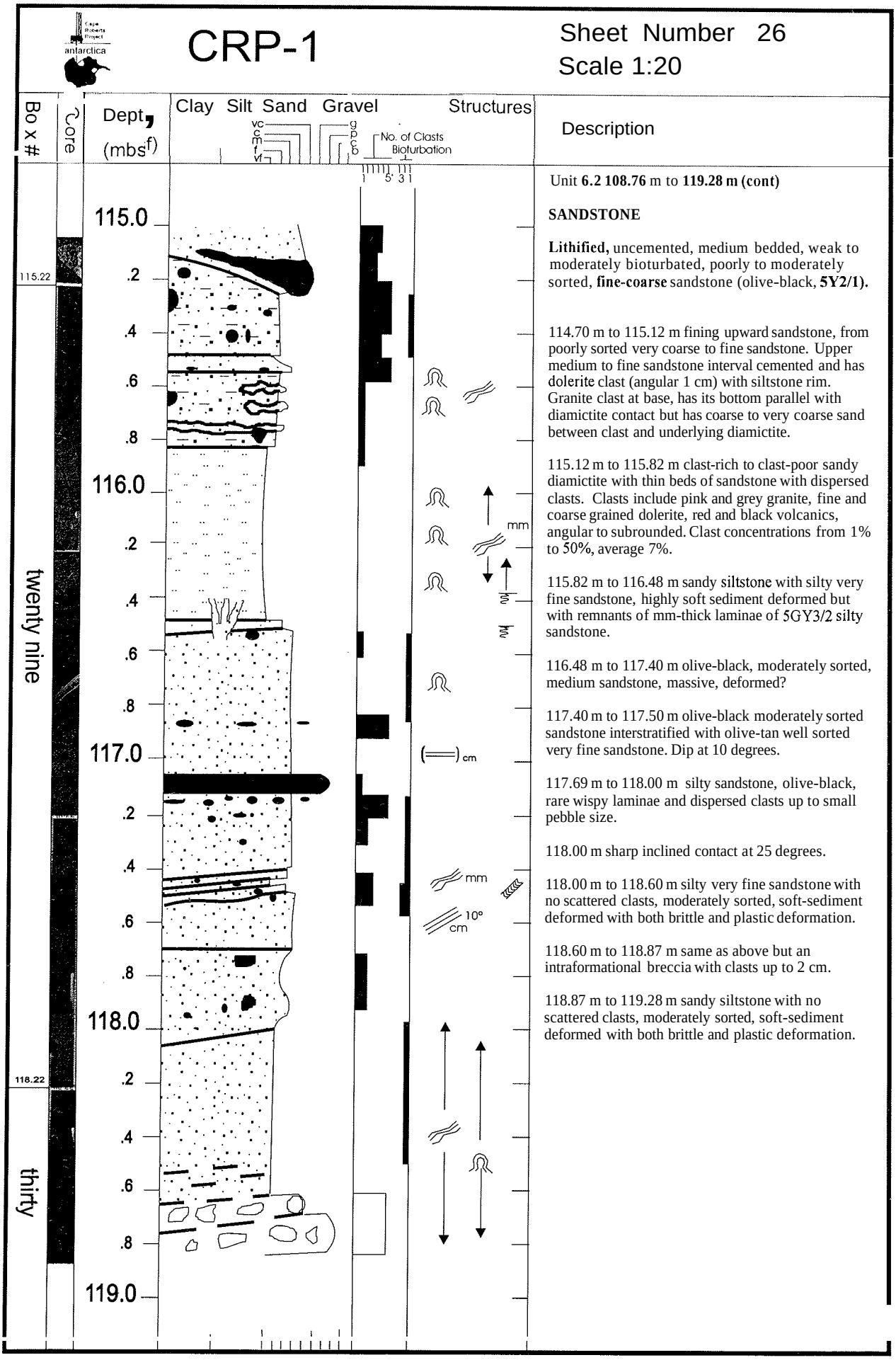

Unit **6.2 108.76** m to **119.28 m (cont)**

SANDSTONE

Lithified, uncemented, medium bedded, weak to moderately bioturbated, poorly to moderately sorted, **fine-coarse** sandstone (olive-black, **5Y2/1).**

114.70 m to 115.12 m fining upward sandstone, from poorly sorted very coarse to fine sandstone. Upper medium to fine sandstone interval cemented and has dolerite clast (angular 1 cm) with siltstone rim. Granite clast at base, has its bottom parallel with diamictite contact but has coarse to very coarse sand between clast and underlying diamictite.

115.12 m to 115.82 m clast-rich to clast-poor sandy diamictite with thin beds of sandstone with dispersed clasts. Clasts include pink and grey granite, fine and coarse grained dolerite, red and black volcanics, angular to subrounded. Clast concentrations from 1% to 50%, average 7%.

115.82 m to 116.48 m sandy siltstone with silty very fine sandstone, highly soft sediment deformed but with remnants of mm-thick laminae of 5GY3/2 silty sandstone.

116.48 m to 117.40 m olive-black, moderately sorted, medium sandstone, massive, deformed?

117.40 m to 117.50 m olive-black moderately sorted sandstone interstratified with olive-tan well sorted very fine sandstone. Dip at 10 degrees.

117.69 m to 118.00 m silty sandstone, olive-black, rare wispy laminae and dispersed clasts up to small pebble size.

118.00 m sharp inclined contact at 25 degrees.

118.00 m to 118.60 m silty very fine sandstone with no scattered clasts, moderately sorted, soft-sediment deformed with both brittle and plastic deformation.

118.60 m to 118.87 m same as above but an intraformational breccia with clasts up to 2 cm.

118.87 m to 119.28 m sandy siltstone with no scattered clasts, moderately sorted, soft-sediment deformed with both brittle and plastic deformation.

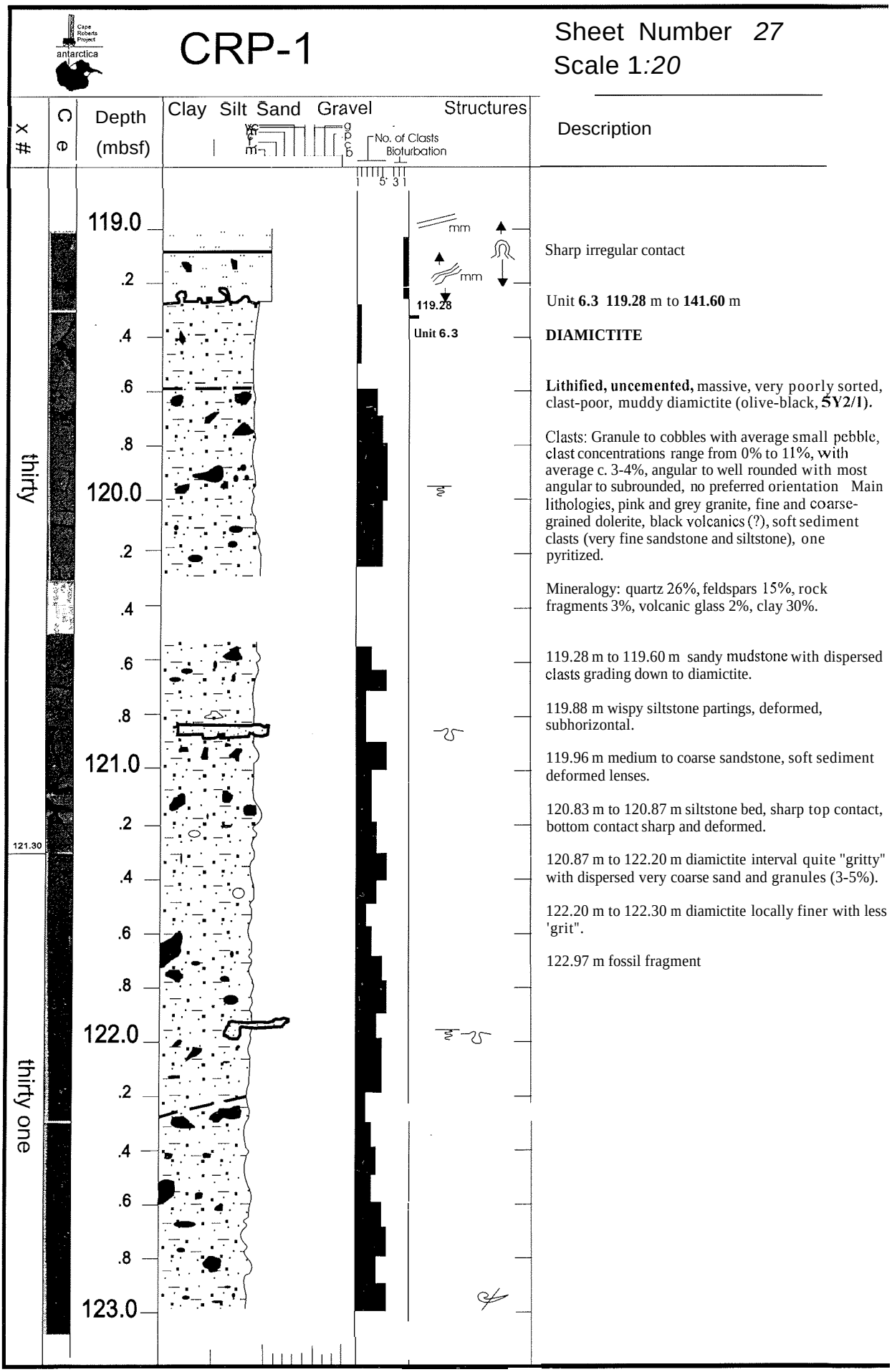
Cape Roberts Project
antarctica
CRP-1
Sheet Number 27
Scale 1:20
x
Core
Depth (mbsf)
Clay Silt Sand Gravel
Structures
No. of Clasts
Bioturbation
Description
thirty
thirty one
121.30
119.0
.2
.4
.6
.8
120.0
.2
.4
.6
.8
121.0
.2
.4
.6
.8
122.0
.2
.4
.6
.8
123.0
mm
mm
119.28
Unit 6.3
Sharp irregular contact
Unit 6.3 119.28 m to 141.60 m
DIAMICTITE
Lithified, uncemented, massive, very poorly sorted, clast-poor, muddy diamictite (olive-black, 5Y2/1).
Clasts: Granule to cobbles with average small pebble, clast concentrations range from 0% to 11%, with average c. 3-4%, angular to well rounded with most angular to subrounded, no preferred orientation Main lithologies, pink and grey granite, fine and coarse-grained dolerite, black volcanics (?), soft sediment clasts (very fine sandstone and siltstone), one pyritized.
Mineralogy: quartz 26%, feldspars 15%, rock fragments 3%, volcanic glass 2%, clay 30%.
119.28 m to 119.60 m sandy mudstone with dispersed clasts grading down to diamictite.
119.88 m wispy siltstone partings, deformed, subhorizontal.
119.96 m medium to coarse sandstone, soft sediment deformed lenses.
120.83 m to 120.87 m siltstone bed, sharp top contact, bottom contact sharp and deformed.
120.87 m to 122.20 m diamictite interval quite "gritty" with dispersed very coarse sand and granules (3-5%).
122.20 m to 122.30 m diamictite locally finer with less 'grit".
122.97 m fossil fragment

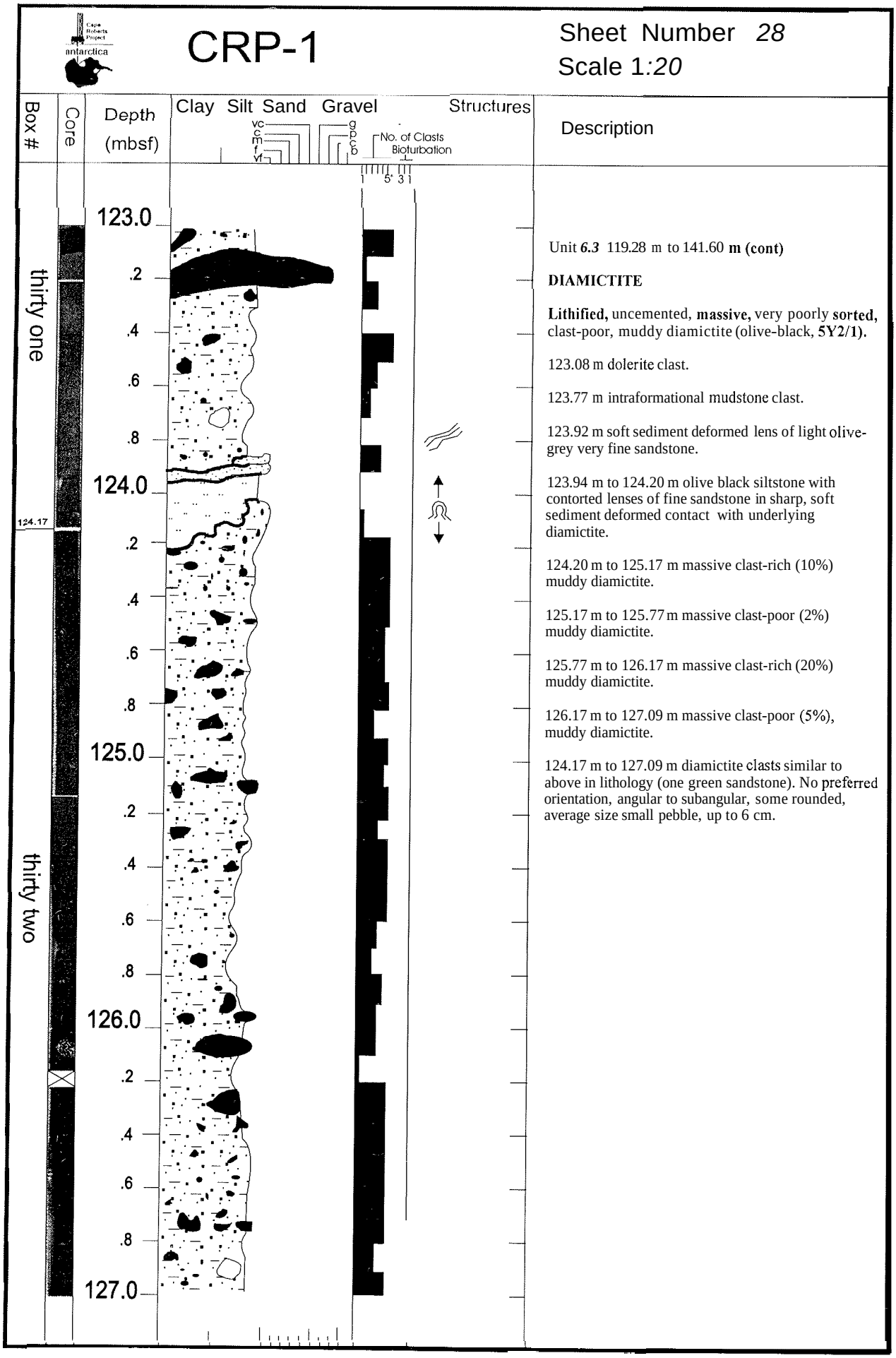

Unit **6.3** 119.28 m to 141.60 **m (cont)**

DIAMICTITE

Lithified, uncemented, **massive,** very poorly **sorted,** clast-poor, muddy diamictite (olive-black, **5Y2/1).**

123.08 m dolerite clast.

123.77 m intraformational mudstone clast.

123.92 m soft sediment deformed lens of light olive-grey very fine sandstone.

123.94 m to 124.20 m olive black siltstone with contorted lenses of fine sandstone in sharp, soft sediment deformed contact with underlying diamictite.

124.20 m to 125.17 m massive clast-rich (10%) muddy diamictite.

125.17 m to 125.77 m massive clast-poor (2%) muddy diamictite.

125.77 m to 126.17 m massive clast-rich (20%) muddy diamictite.

126.17 m to 127.09 m massive clast-poor (5%), muddy diamictite.

124.17 m to 127.09 m diamictite clasts similar to above in lithology (one green sandstone). No preferred orientation, angular to subangular, some rounded, average size small pebble, up to 6 cm.

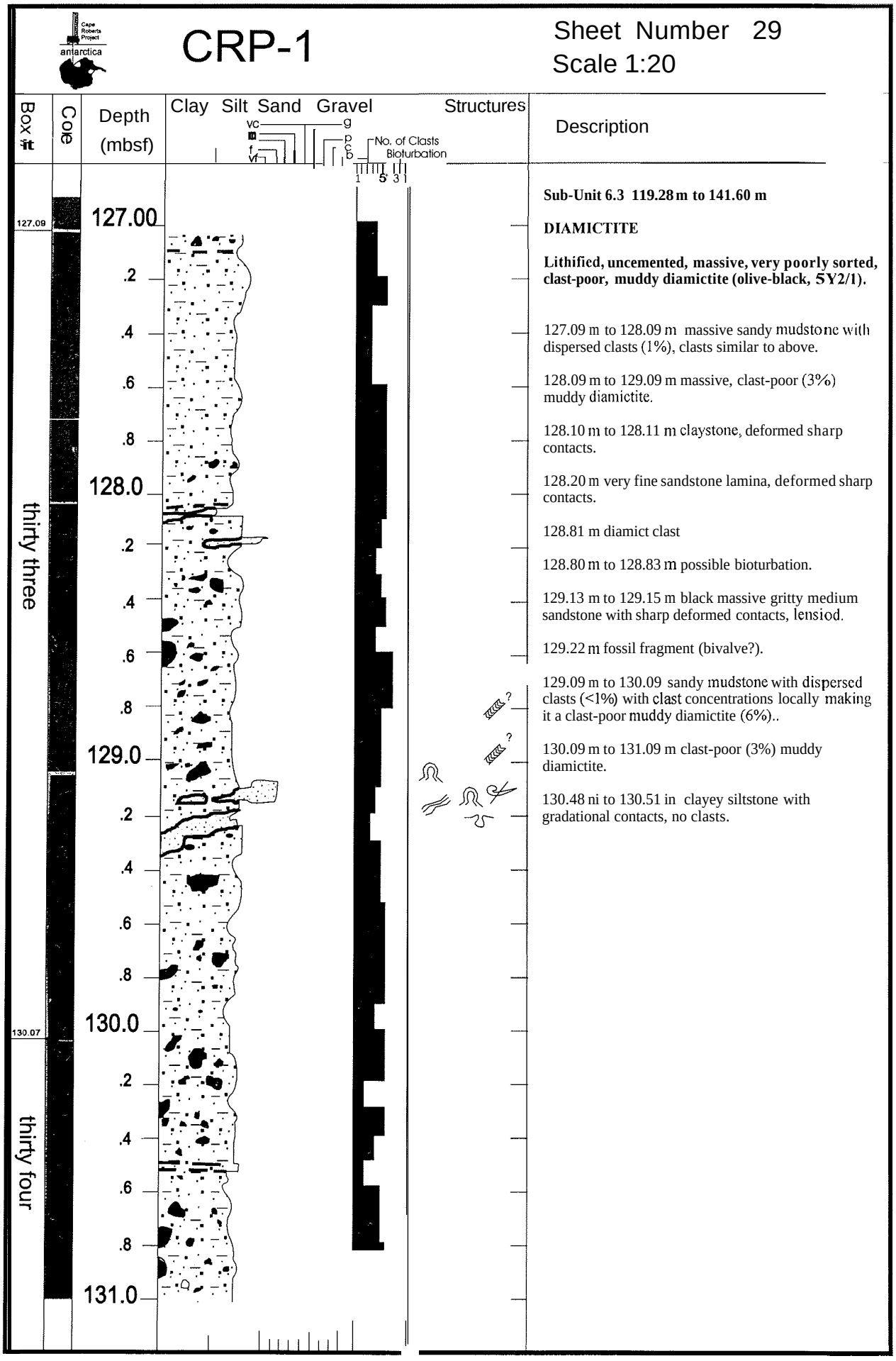
Cape Roberts Project
antarctica
CRP-1
Sheet Number 29
Scale 1:20
Box
Core
Depth (mbsf)
Clay Silt Sand Gravel
vc m f vf g p c
No. of Clasts
Bioturbation
1 5 3 1
Structures
Description
127.09
130.07
thirty three
thirty four
127.00
.2
.4
.6
.8
128.0
.2
.4
.6
.8
129.0
.2
.4
.6
.8
130.0
.2
.4
.6
.8
131.0
Sub-Unit 6.3 119.28 m to 141.60 m
DIAMICTITE
Lithified, uncemented, massive, very poorly sorted, clast-poor, muddy diamictite (olive-black, 5Y2/1).
127.09 m to 128.09 m massive sandy mudstone with dispersed clasts (1%), clasts similar to above.
128.09 m to 129.09 m massive, clast-poor (3%) muddy diamictite.
128.10 m to 128.11 m claystone, deformed sharp contacts.
128.20 m very fine sandstone lamina, deformed sharp contacts.
128.81 m diamict clast
128.80 m to 128.83 m possible bioturbation.
129.13 m to 129.15 m black massive gritty medium sandstone with sharp deformed contacts, lensiod.
129.22 m fossil fragment (bivalve?).
129.09 m to 130.09 sandy mudstone with dispersed clasts (<1%) with clast concentrations locally making it a clast-poor muddy diamictite (6%)..
130.09 m to 131.09 m clast-poor (3%) muddy diamictite.
130.48 ni to 130.51 in clayey siltstone with gradational contacts, no clasts.

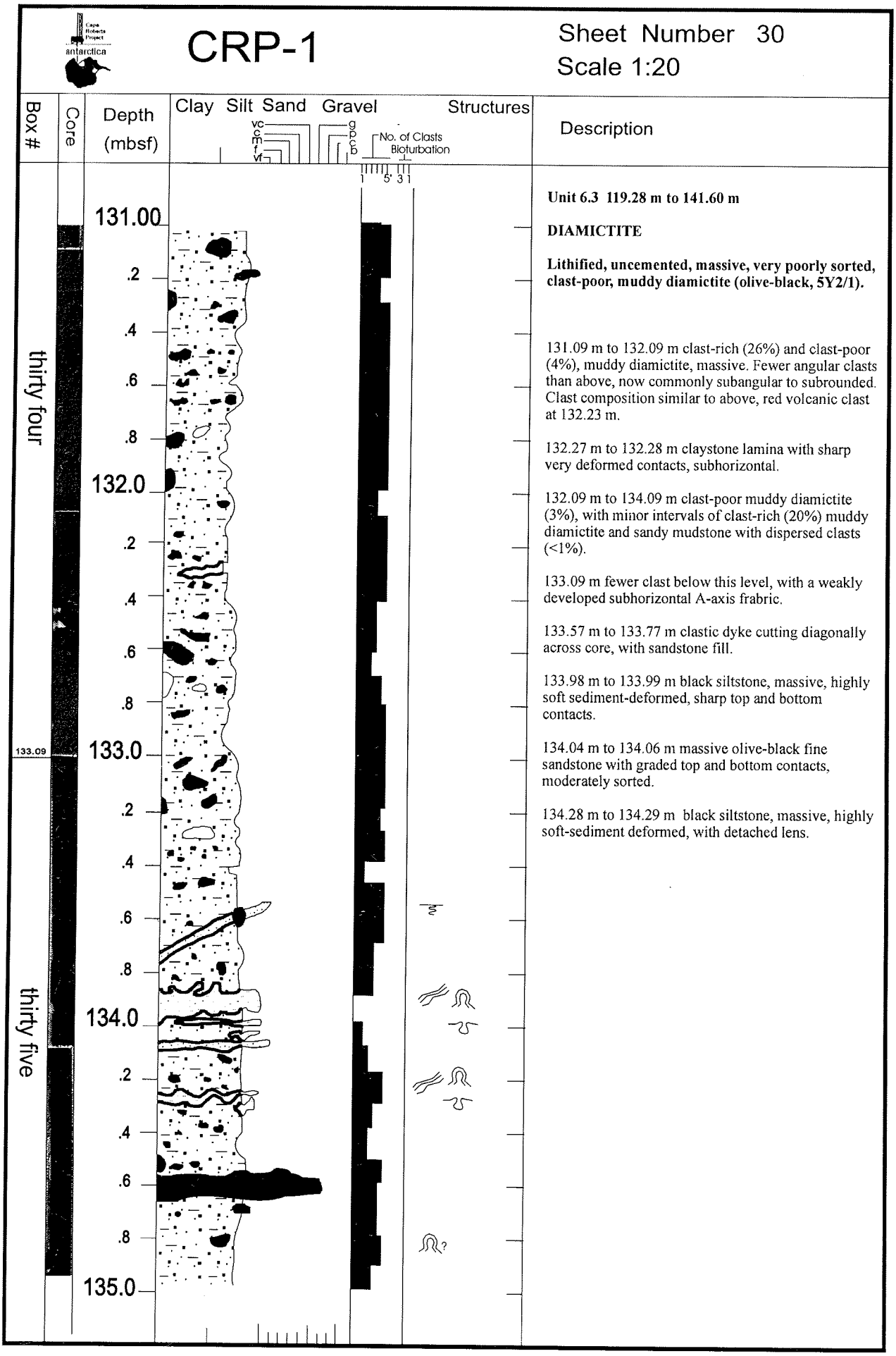
CRP-1
Sheet Number 30
Scale 1:20
Box #
Core
Depth (mbsf)
Clay Silt Sand Gravel
vc c m f vf
g p c b
Structures
No. of Clasts
Bioturbation
1 5 3 1
Description
thirty four
thirty five
133.09
131.00
.2
.4
.6
.8
132.0
.2
.4
.6
.8
133.0
.2
.4
.6
.8
134.0
.2
.4
.6
.8
135.0
Unit 6.3 119.28 m to 141.60 m
DIAMICTITE
Lithified, uncemented, massive, very poorly sorted, clast-poor, muddy diamictite (olive-black, 5Y2/1).
131.09 m to 132.09 m clast-rich (26%) and clast-poor (4%), muddy diamictite, massive. Fewer angular clasts than above, now commonly subangular to subrounded. Clast composition similar to above, red volcanic clast at 132.23 m.
132.27 m to 132.28 m claystone lamina with sharp very deformed contacts, subhorizontal.
132.09 m to 134.09 m clast-poor muddy diamictite (3%), with minor intervals of clast-rich (20%) muddy diamictite and sandy mudstone with dispersed clasts (<1%).
133.09 m fewer clast below this level, with a weakly developed subhorizontal A-axis frabric.
133.57 m to 133.77 m clastic dyke cutting diagonally across core, with sandstone fill.
133.98 m to 133.99 m black siltstone, massive, highly soft sediment-deformed, sharp top and bottom contacts.
134.04 m to 134.06 m massive olive-black fine sandstone with graded top and bottom contacts, moderately sorted.
134.28 m to 134.29 m black siltstone, massive, highly soft-sediment deformed, with detached lens.

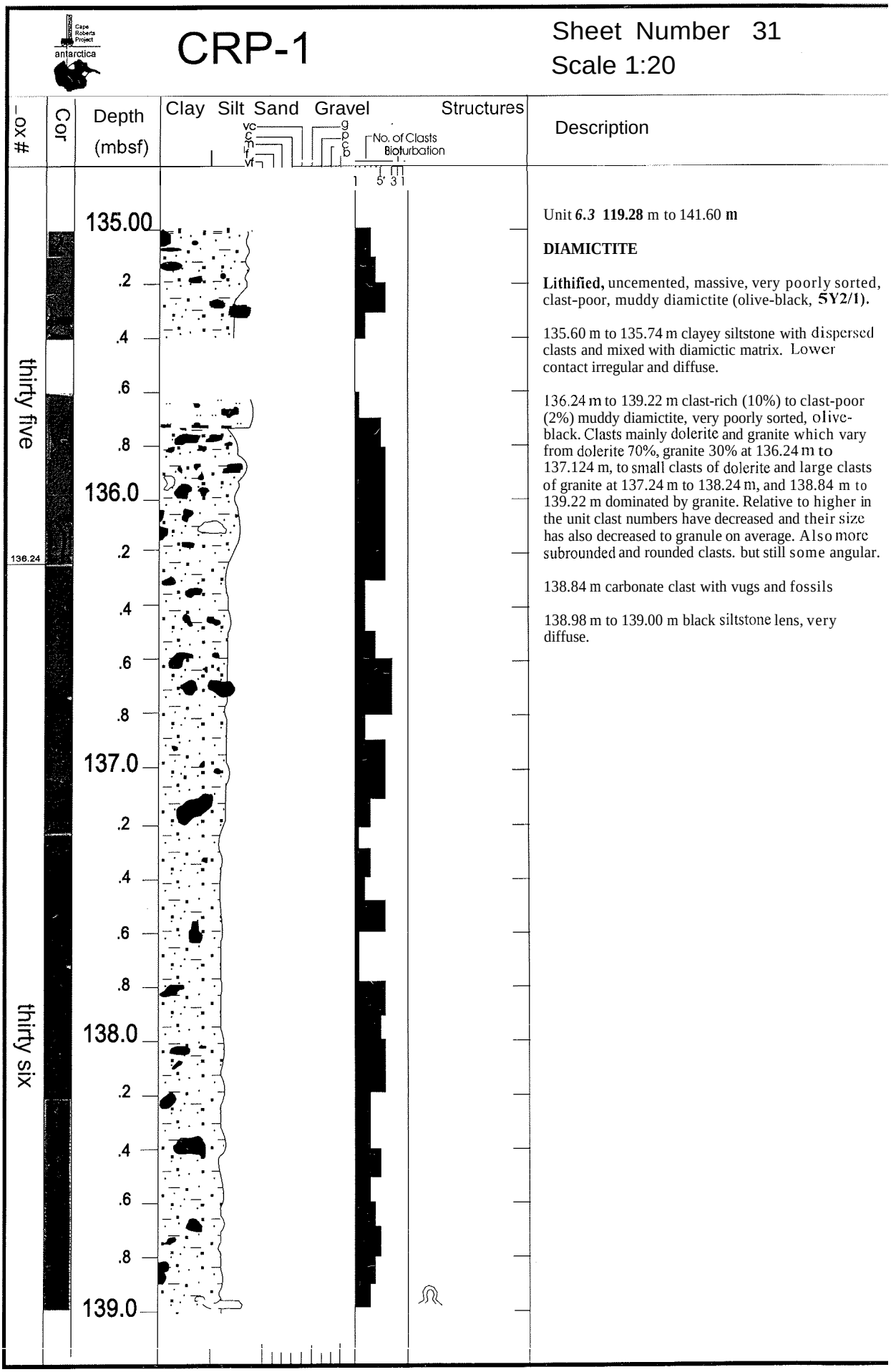

Unit *6.3* **119.28** m to 141.60 **m**

DIAMICTITE

Lithified, uncemented, massive, very poorly sorted, clast-poor, muddy diamictite (olive-black, **5Y2/1).**

135.60 m to 135.74 m clayey siltstone with dispersed clasts and mixed with diamictic matrix. Lower contact irregular and diffuse.

136.24 m to 139.22 m clast-rich (10%) to clast-poor (2%) muddy diamictite, very poorly sorted, olive-black. Clasts mainly dolerite and granite which vary from dolerite 70%, granite 30% at 136.24 m to 137.124 m, to small clasts of dolerite and large clasts of granite at 137.24 m to 138.24 m, and 138.84 m to 139.22 m dominated by granite. Relative to higher in the unit clast numbers have decreased and their size has also decreased to granule on average. Also more subrounded and rounded clasts. but still some angular.

138.84 m carbonate clast with vugs and fossils

138.98 m to 139.00 m black siltstone lens, very diffuse.

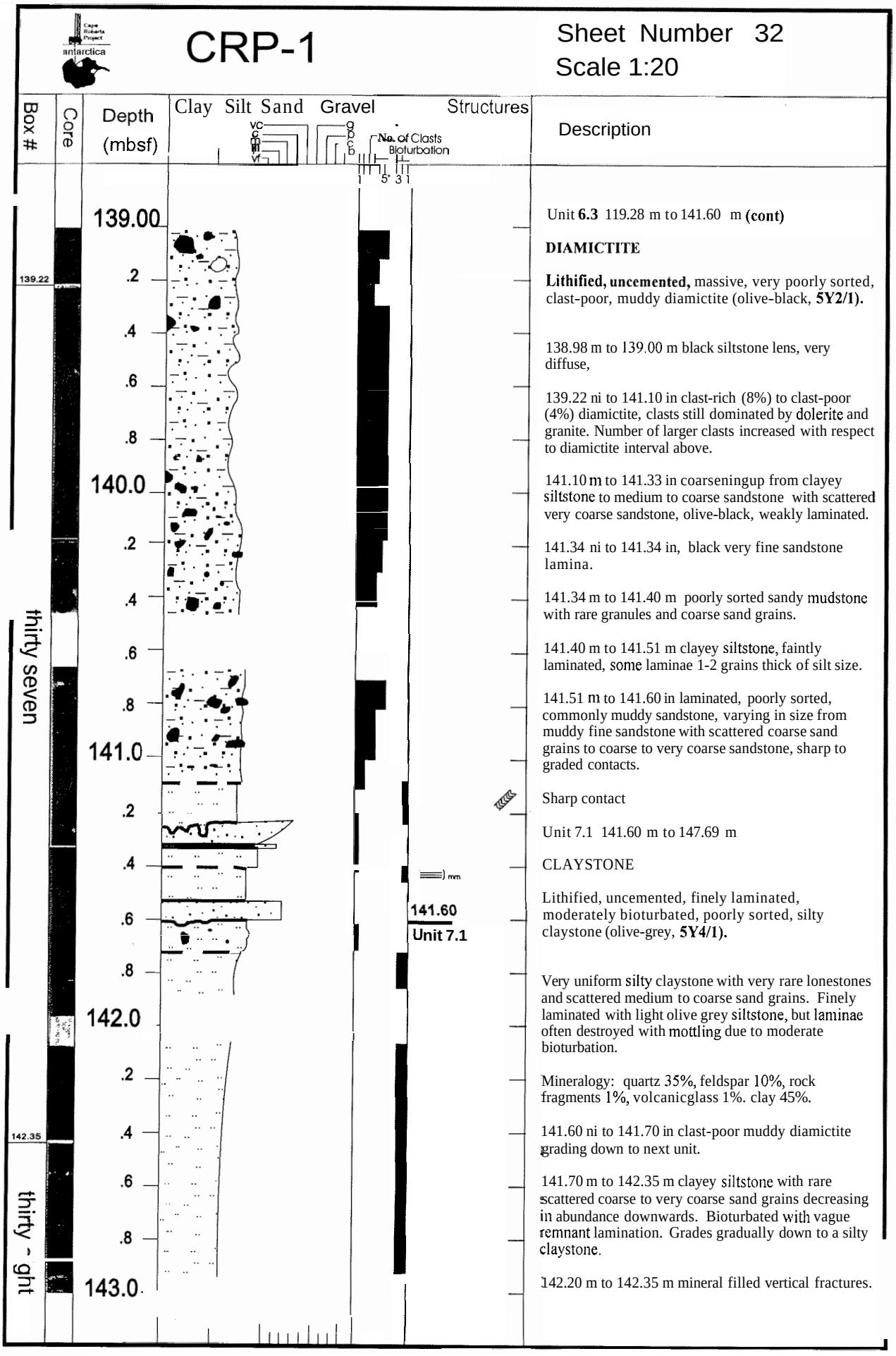
Cape Roberts Project
antarctica
CRP-1
Sheet Number 32
Scale 1:20
Box #
Core
Depth (mbsf)
Clay Silt Sand Gravel
vc c m f vf
g c m f
Structures
No. of Clasts
Bioturbation
1 5 3 1
Description
139.00
.2
.4
.6
.8
140.0
.2
.4
.6
.8
141.0
.2
.4
.6
.8
142.0
.2
.4
.6
.8
143.0
139.22
142.35
thirty seven
thirty - ght
mm
141.60
Unit 7.1
Unit **6.3** 119.28 m to 141.60 m **(cont)**
DIAMICTITE
Lithified, uncemented, massive, very poorly sorted, clast-poor, muddy diamictite (olive-black, **5Y2/1).**
138.98 m to 139.00 m black siltstone lens, very diffuse,
139.22 ni to 141.10 in clast-rich (8%) to clast-poor (4%) diamictite, clasts still dominated by dolerite and granite. Number of larger clasts increased with respect to diamictite interval above.
141.10 m to 141.33 in coarseningup from clayey siltstone to medium to coarse sandstone with scattered very coarse sandstone, olive-black, weakly laminated.
141.34 ni to 141.34 in, black very fine sandstone lamina.
141.34 m to 141.40 m poorly sorted sandy mudstone with rare granules and coarse sand grains.
141.40 m to 141.51 m clayey siltstone, faintly laminated, some laminae 1-2 grains thick of silt size.
141.51 m to 141.60 in laminated, poorly sorted, commonly muddy sandstone, varying in size from muddy fine sandstone with scattered coarse sand grains to coarse to very coarse sandstone, sharp to graded contacts.
Sharp contact
Unit 7.1 141.60 m to 147.69 m
CLAYSTONE
Lithified, uncemented, finely laminated, moderately bioturbated, poorly sorted, silty claystone (olive-grey, **5Y4/1).**
Very uniform silty claystone with very rare lonestones and scattered medium to coarse sand grains. Finely laminated with light olive grey siltstone, but laminae often destroyed with mottling due to moderate bioturbation.
Mineralogy: quartz 35%, feldspar 10%, rock fragments 1%, volcanicglass 1%. clay 45%.
141.60 ni to 141.70 in clast-poor muddy diamictite grading down to next unit.
141.70 m to 142.35 m clayey siltstone with rare scattered coarse to very coarse sand grains decreasing in abundance downwards. Bioturbated with vague remnant lamination. Grades gradually down to a silty claystone.
142.20 m to 142.35 m mineral filled vertical fractures.

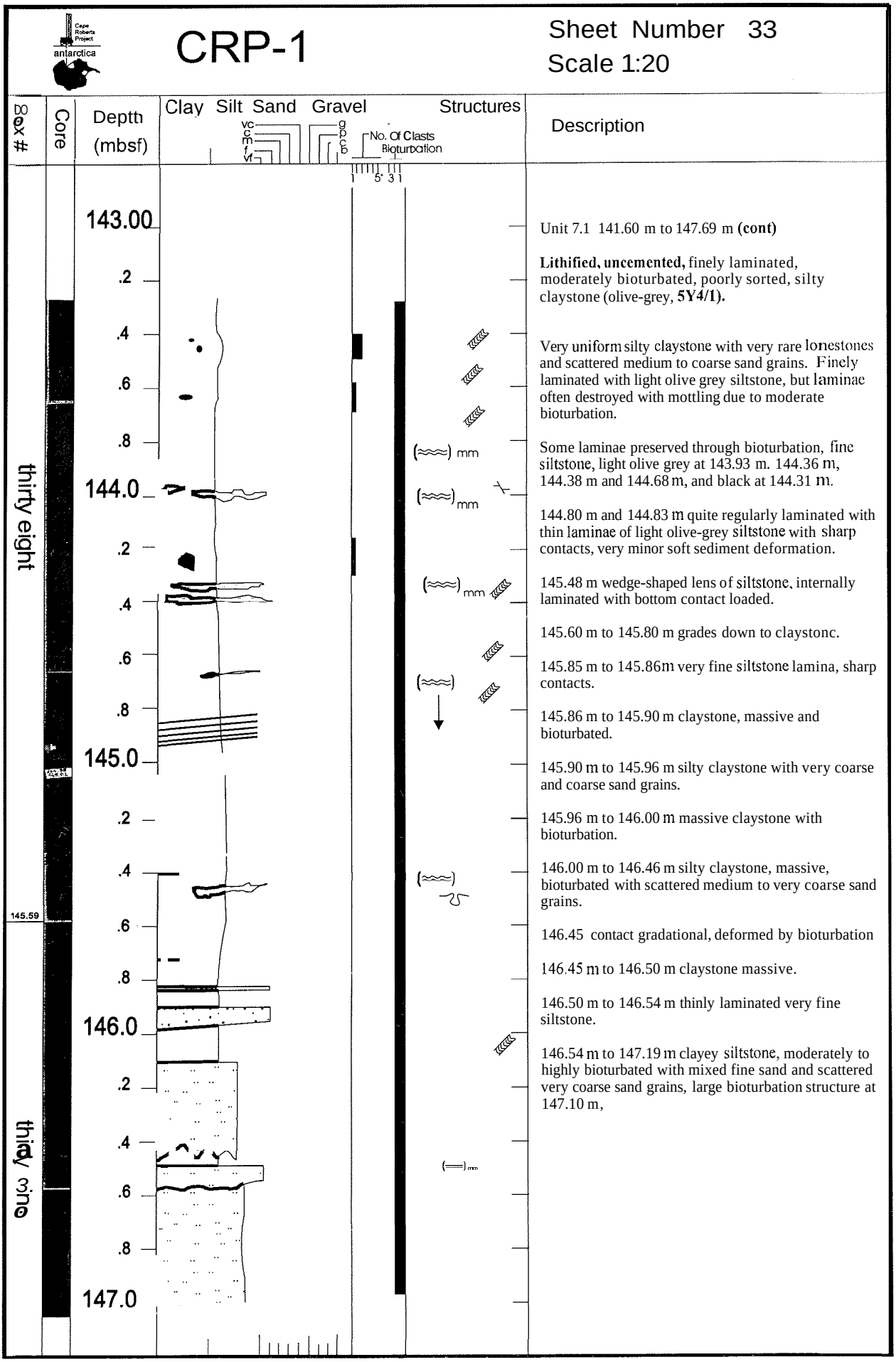

Unit 7.1 141.60 m to 147.69 m **(cont)**

Lithified, uncemented, finely laminated, moderately bioturbated, poorly sorted, silty claystone (olive-grey, **5Y4/1).**

Very uniform silty claystone with very rare lonestones and scattered medium to coarse sand grains. Finely laminated with light olive grey siltstone, but laminae often destroyed with mottling due to moderate bioturbation.

Some laminae preserved through bioturbation, fine siltstone, light olive grey at 143.93 m. 144.36 m, 144.38 m and 144.68 m, and black at 144.31 m.

144.80 m and 144.83 m quite regularly laminated with thin laminae of light olive-grey siltstone with sharp contacts, very minor soft sediment deformation.

145.48 m wedge-shaped lens of siltstone, internally laminated with bottom contact loaded.

145.60 m to 145.80 m grades down to claystonc.

145.85 m to 145.86m very fine siltstone lamina, sharp contacts.

145.86 m to 145.90 m claystone, massive and bioturbated.

145.90 m to 145.96 m silty claystone with very coarse and coarse sand grains.

145.96 m to 146.00 m massive claystone with bioturbation.

146.00 m to 146.46 m silty claystone, massive, bioturbated with scattered medium to very coarse sand grains.

146.45 contact gradational, deformed by bioturbation

146.45 m to 146.50 m claystone massive.

146.50 m to 146.54 m thinly laminated very fine siltstone.

146.54 m to 147.19 m clayey siltstone, moderately to highly bioturbated with mixed fine sand and scattered very coarse sand grains, large bioturbation structure at 147.10 m,

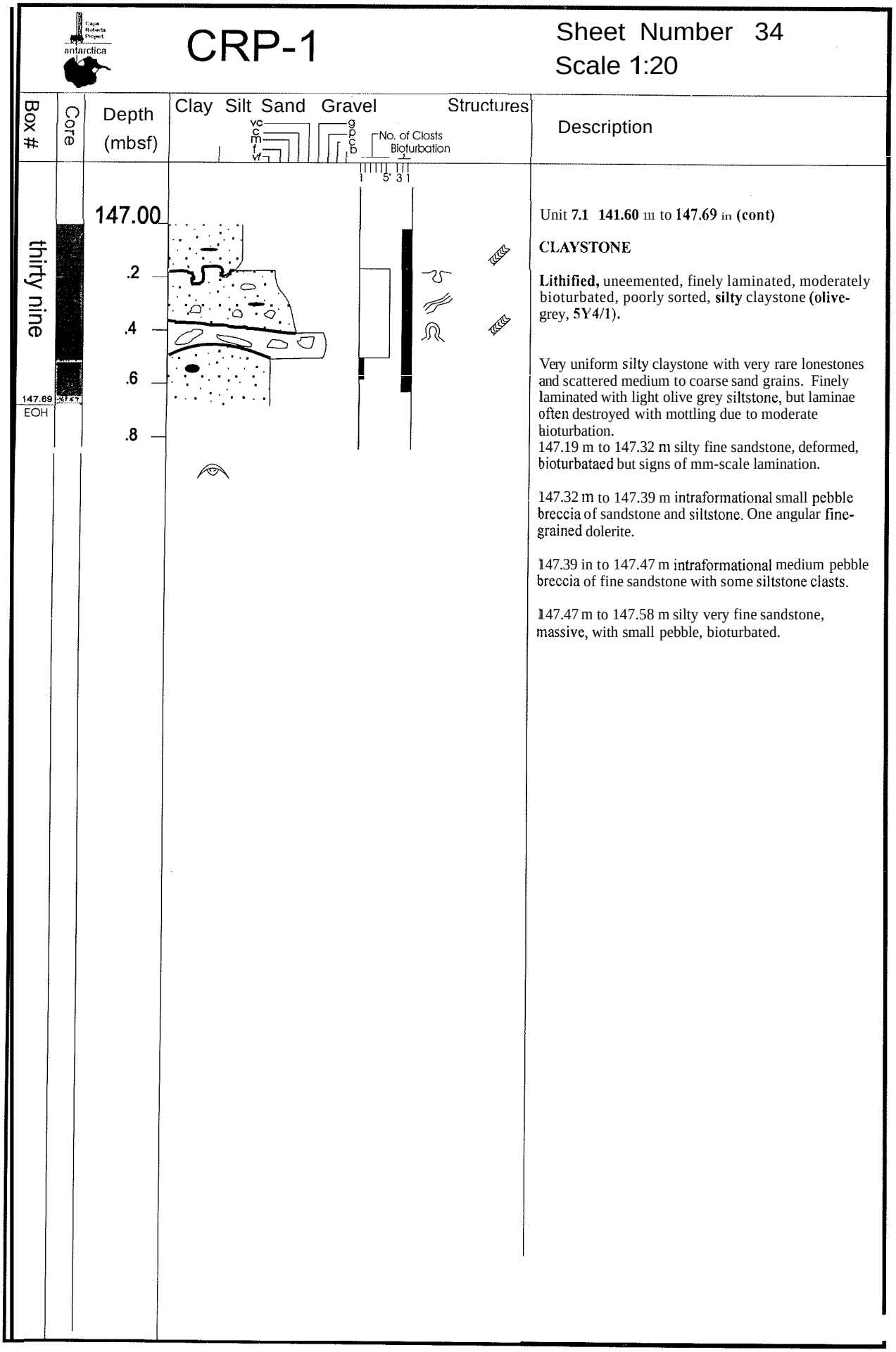
CRP-1
Sheet Number 34
Scale 1:20
Box #
Core
Depth (mbsf)
Clay Silt Sand Gravel
vc c m f vf
g p c b
No. of Clasts
Bioturbation
1 5 3 1
Structures
Description
147.00
.2
.4
.6
.8
thirty nine
147.69
EOH
Unit 7.1 141.60 m to 147.69 m (cont)
CLAYSTONE
Lithified, uneemented, finely laminated, moderately bioturbated, poorly sorted, silty claystone (olive-grey, 5Y4/1).
Very uniform silty claystone with very rare lonestones and scattered medium to coarse sand grains. Finely laminated with light olive grey siltstone, but laminae often destroyed with mottling due to moderate bioturbation.
147.19 m to 147.32 m silty fine sandstone, deformed, bioturbataed but signs of mm-scale lamination.
147.32 m to 147.39 m intraformational small pebble breccia of sandstone and siltstone. One angular fine-grained dolerite.
147.39 in to 147.47 m intraformational medium pebble breccia of fine sandstone with some siltstone clasts.
147.47 m to 147.58 m silty very fine sandstone, massive, with small pebble, bioturbated.

Terra Antartica
1998, **5**(1), 177-187

TERRA ANTARTICA

Appendix *3*

Core Box Images

The following images of the working half of the core, prior to transport and sampling, were acquired at the Drill Site using a DMT line scan camera. Four scans were required to fully image each box. The 24-bit RGB images were converted to greyscale (8-bit) and spliced without resampling to preserve the original image resolution.

Each core box, as reproduced in this appendix, consists of a single 1 200 dpi bitmap image (c. 5 000 x 1 200 pixels). Individual image files occupy approximately 6Mb, and between 6 Mb and 8 Mb when in memory. The images are available on CD. Sliced colour images (24-bit RGB) are also available at the same resolution, these files occupy approximately 20 Mb of disk space and 30 Mb when in memory.

The image collection system was supplied by DMT-Geotec, Essen, Germany, and subsequent image processing was completed using CorelDraw 7.

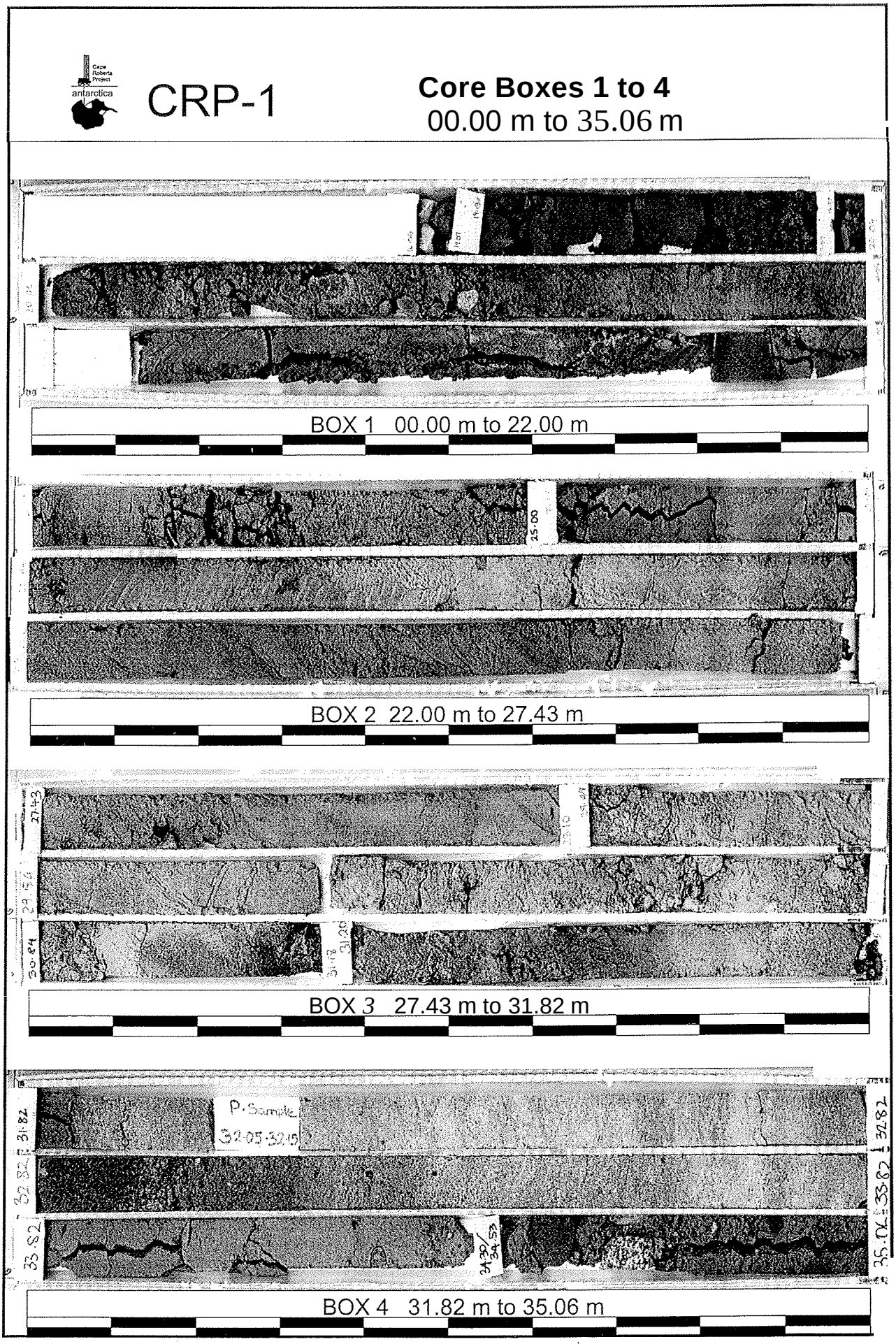
Cape Roberts Project
antarctica
CRP-1
Core Boxes 1 to 4
00.00 m to 35.06 m
BOX 1 00.00 m to 22.00 m
BOX 2 22.00 m to 27.43 m
BOX 3 27.43 m to 31.82 m
BOX 4 31.82 m to 35.06 m

CRP-1

Core Boxes 5 to 8
35.06 m to 48.14 m

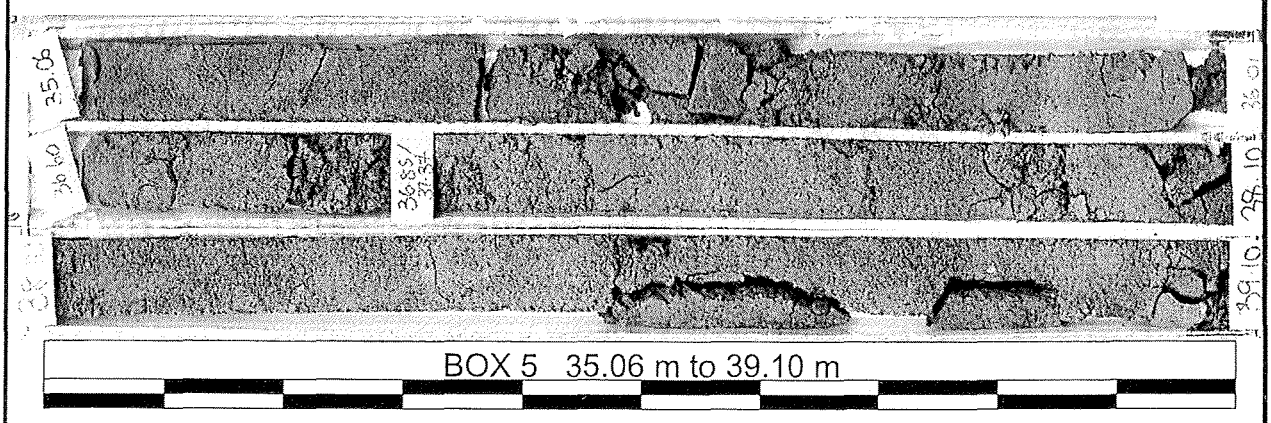

BOX 5 35.06 m to 39.10 m

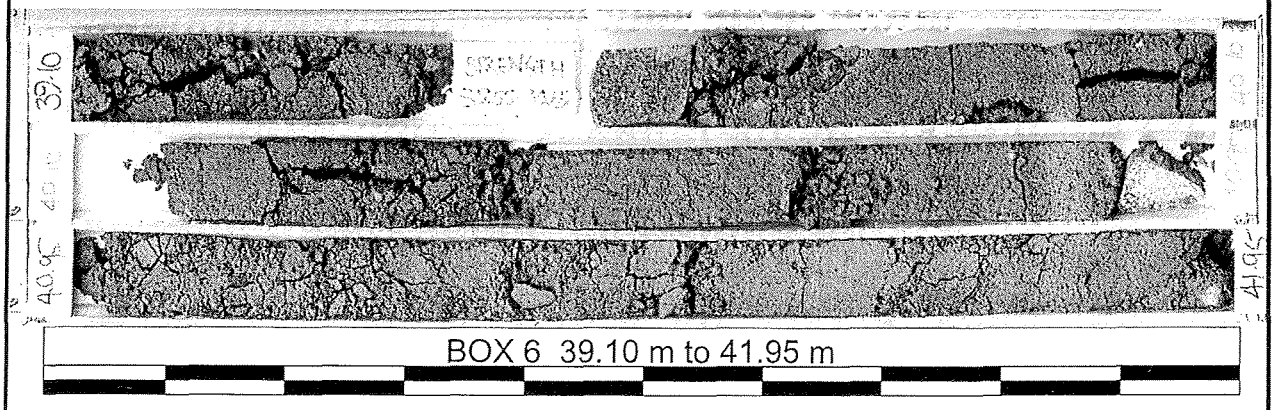

BOX 6 39.10 m to 41.95 m

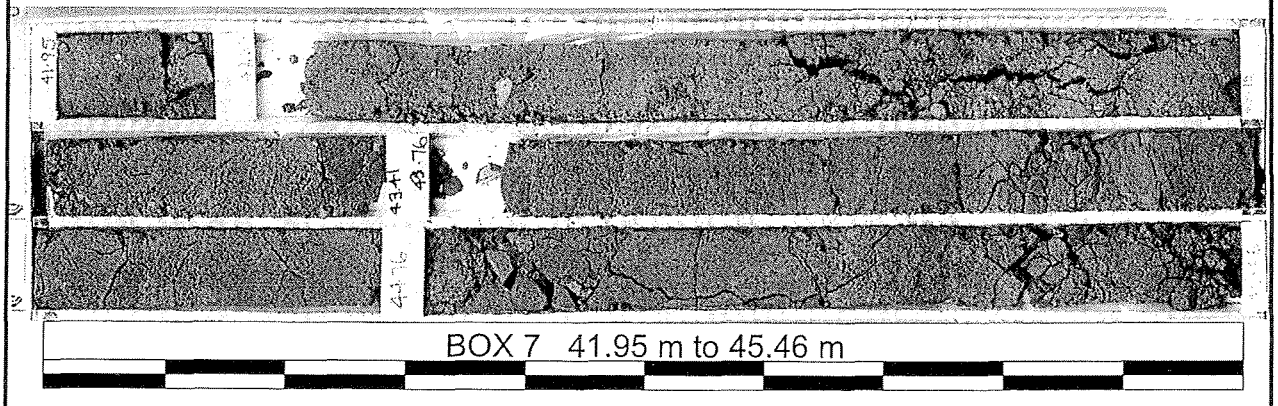

BOX 7 41.95 m to 45.46 m

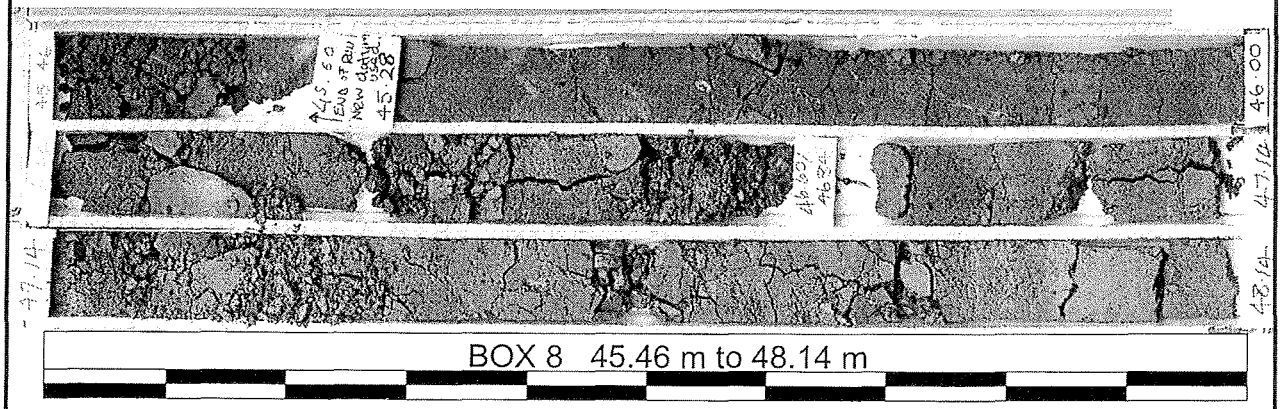

BOX 8 45.46 m to 48.14 m

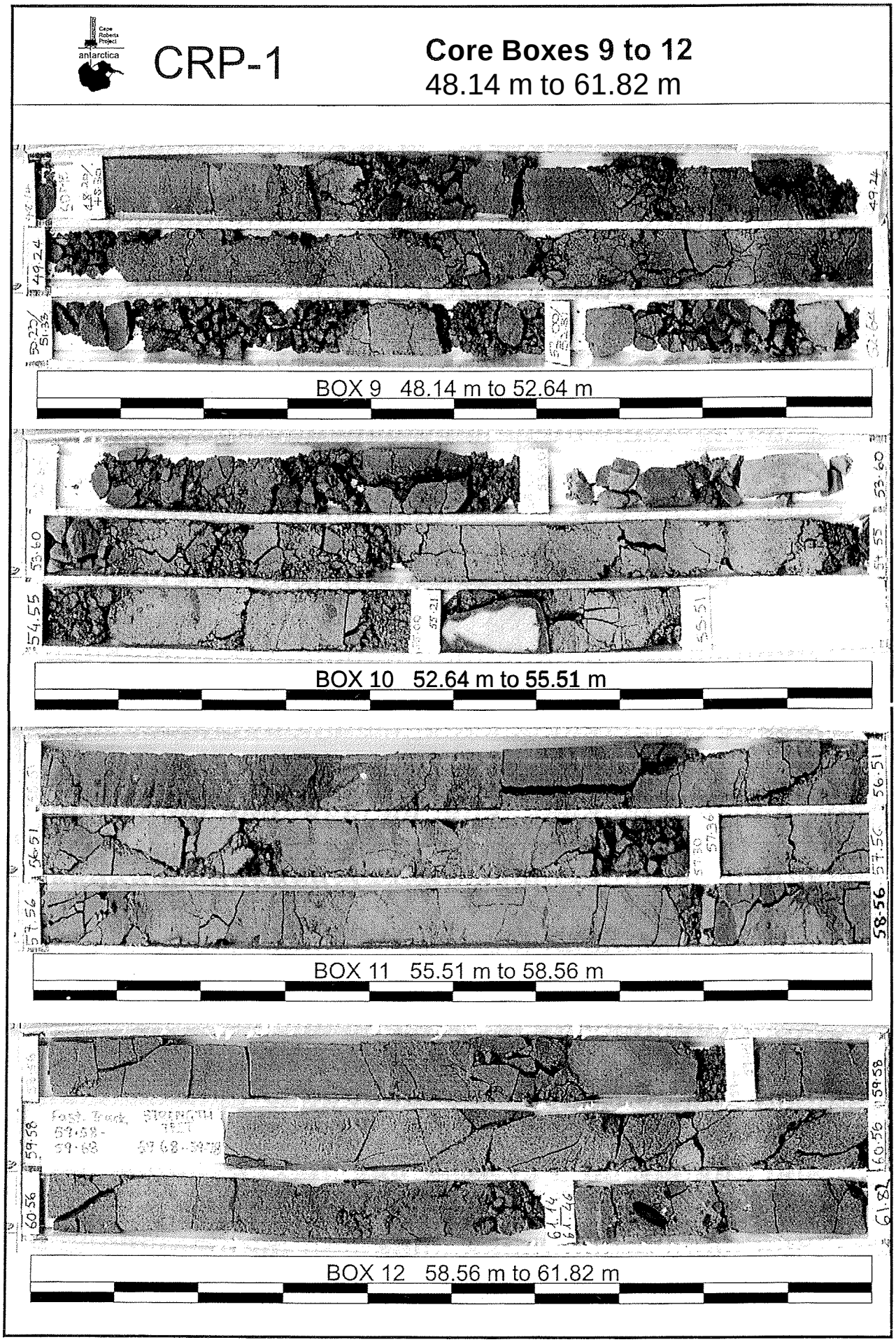
Cape Roberts Project
antarctica
CRP-1
Core Boxes 9 to 12
48.14 m to 61.82 m
BOX 9 48.14 m to 52.64 m
BOX 10 52.64 m to 55.51 m
BOX 11 55.51 m to 58.56 m
BOX 12 58.56 m to 61.82 m

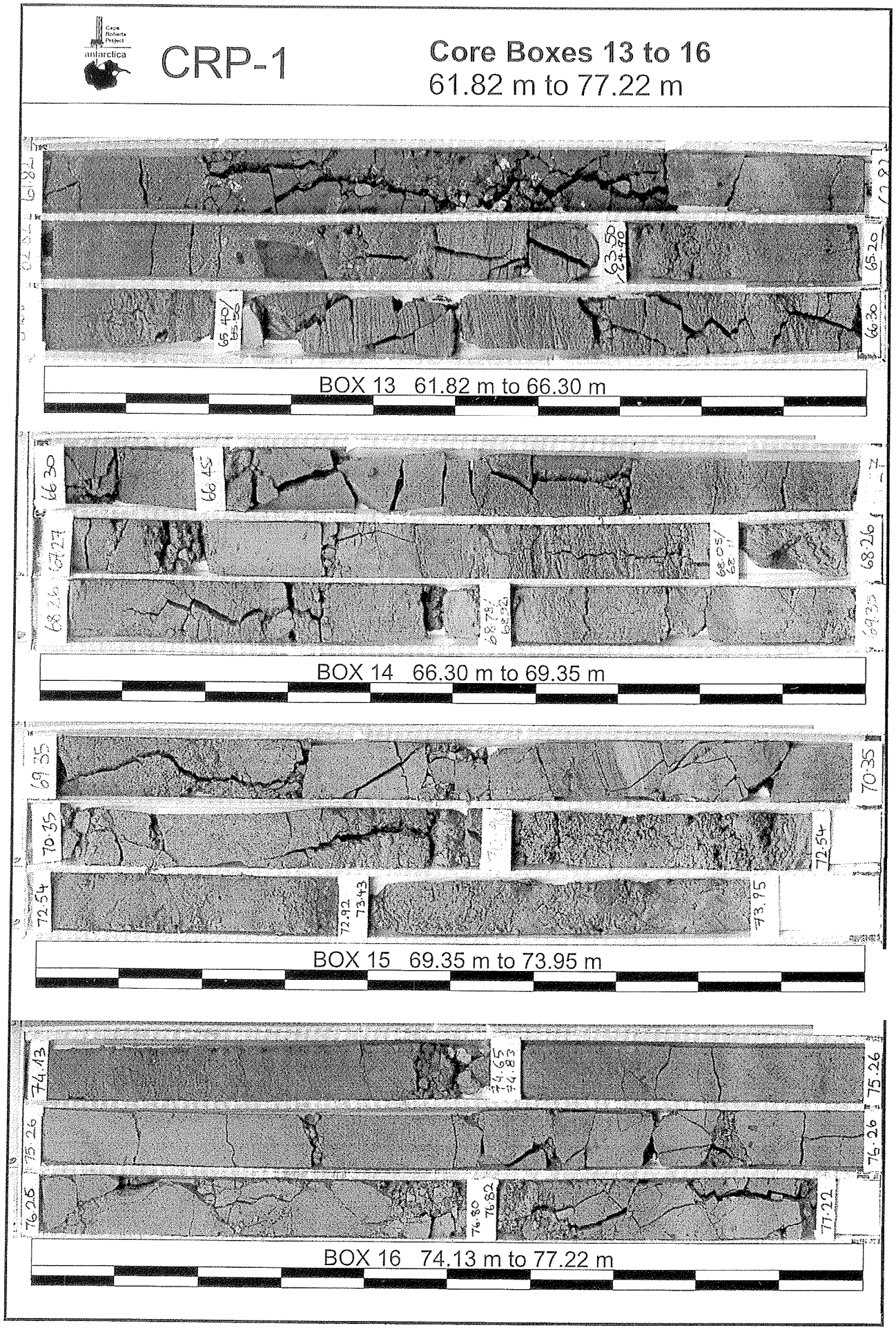
CRP-1
Core Boxes 13 to 16
61.82 m to 77.22 m
BOX 13 61.82 m to 66.30 m
BOX 14 66.30 m to 69.35 m
BOX 15 69.35 m to 73.95 m
BOX 16 74.13 m to 77.22 m

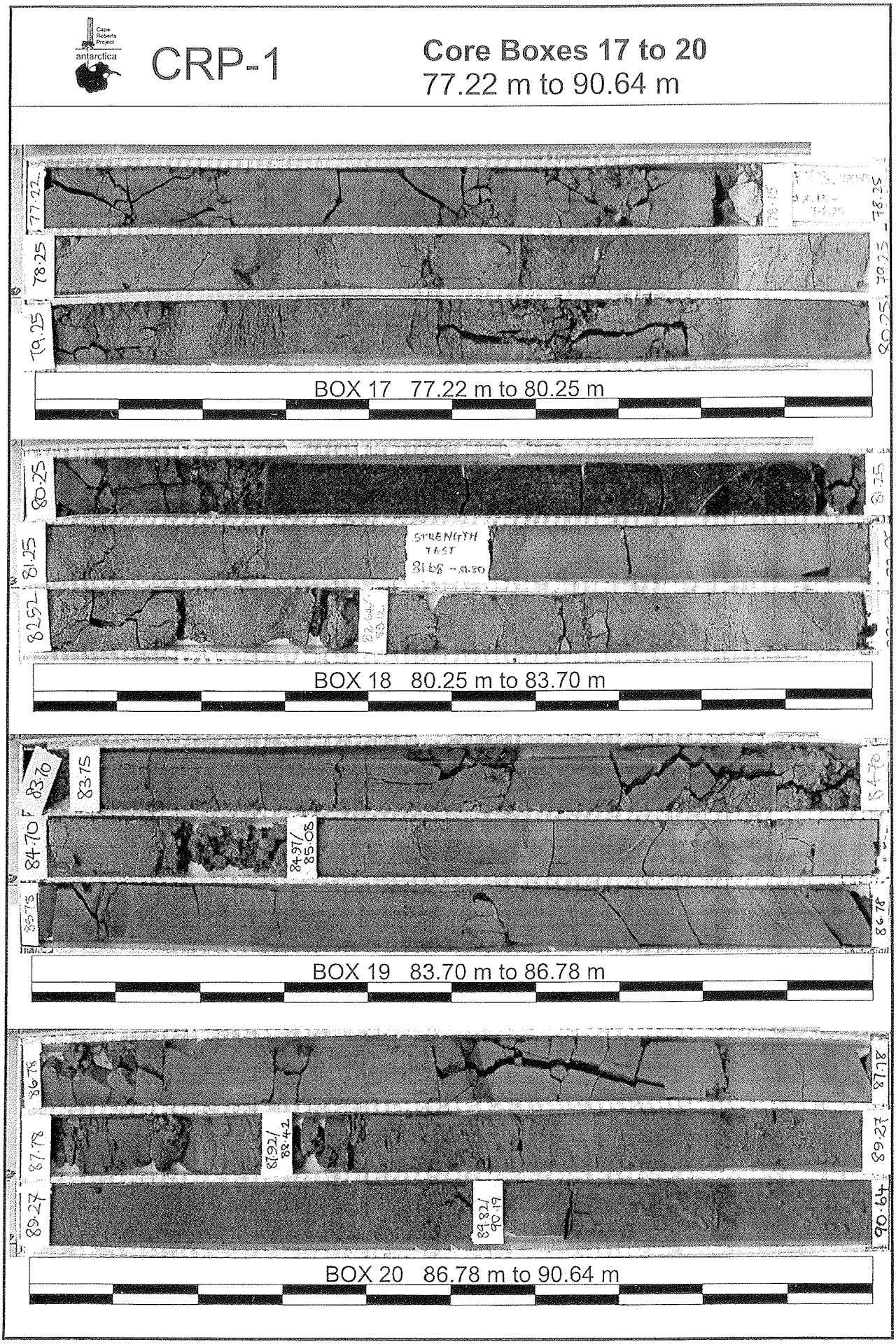
Cape Roberts Project
antarctica
CRP-1
Core Boxes 17 to 20
77.22 m to 90.64 m
77.22
78.25
79.25
80.25
BOX 17 77.22 m to 80.25 m
80.25
81.25
82.92
STRENGTH TEST
BOX 18 80.25 m to 83.70 m
83.70
83.75
84.70
85.78
BOX 19 83.70 m to 86.78 m
86.78
87.78
89.27
BOX 20 86.78 m to 90.64 m

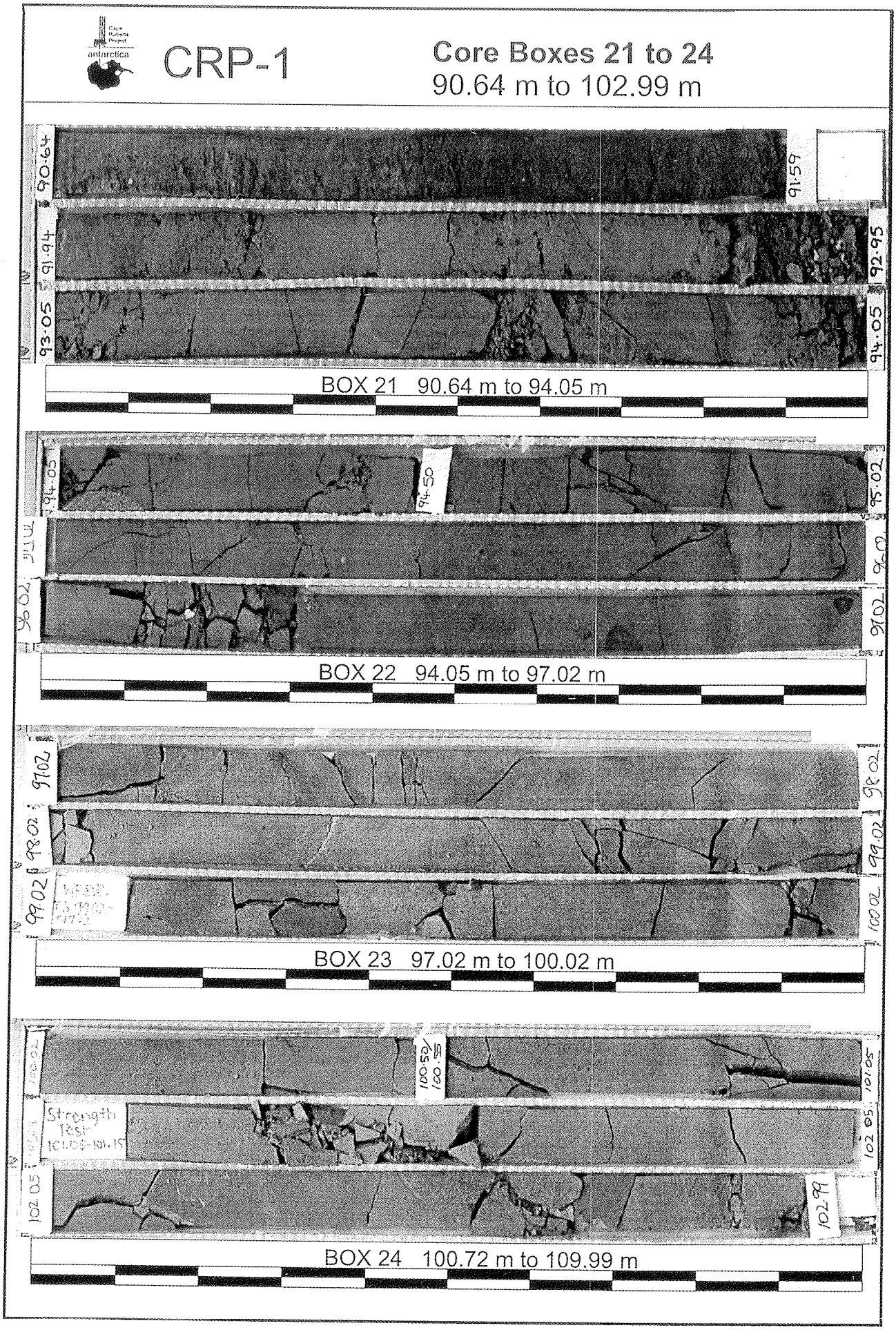
CRP-1
Core Boxes 21 to 24
90.64 m to 102.99 m
BOX 21 90.64 m to 94.05 m
BOX 22 94.05 m to 97.02 m
BOX 23 97.02 m to 100.02 m
BOX 24 100.72 m to 109.99 m

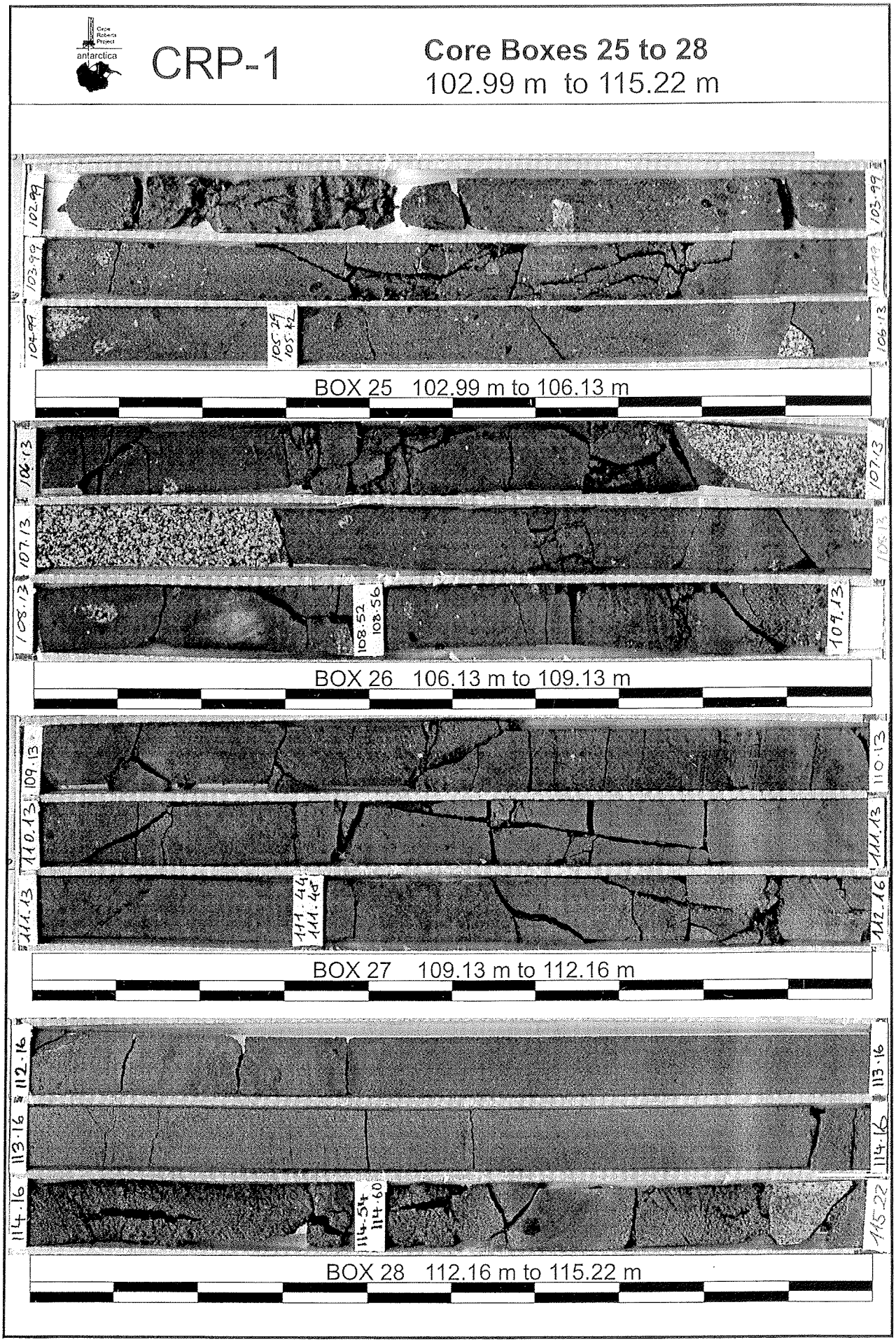
CRP-1
Core Boxes 25 to 28
102.99 m to 115.22 m
BOX 25 102.99 m to 106.13 m
BOX 26 106.13 m to 109.13 m
BOX 27 109.13 m to 112.16 m
BOX 28 112.16 m to 115.22 m

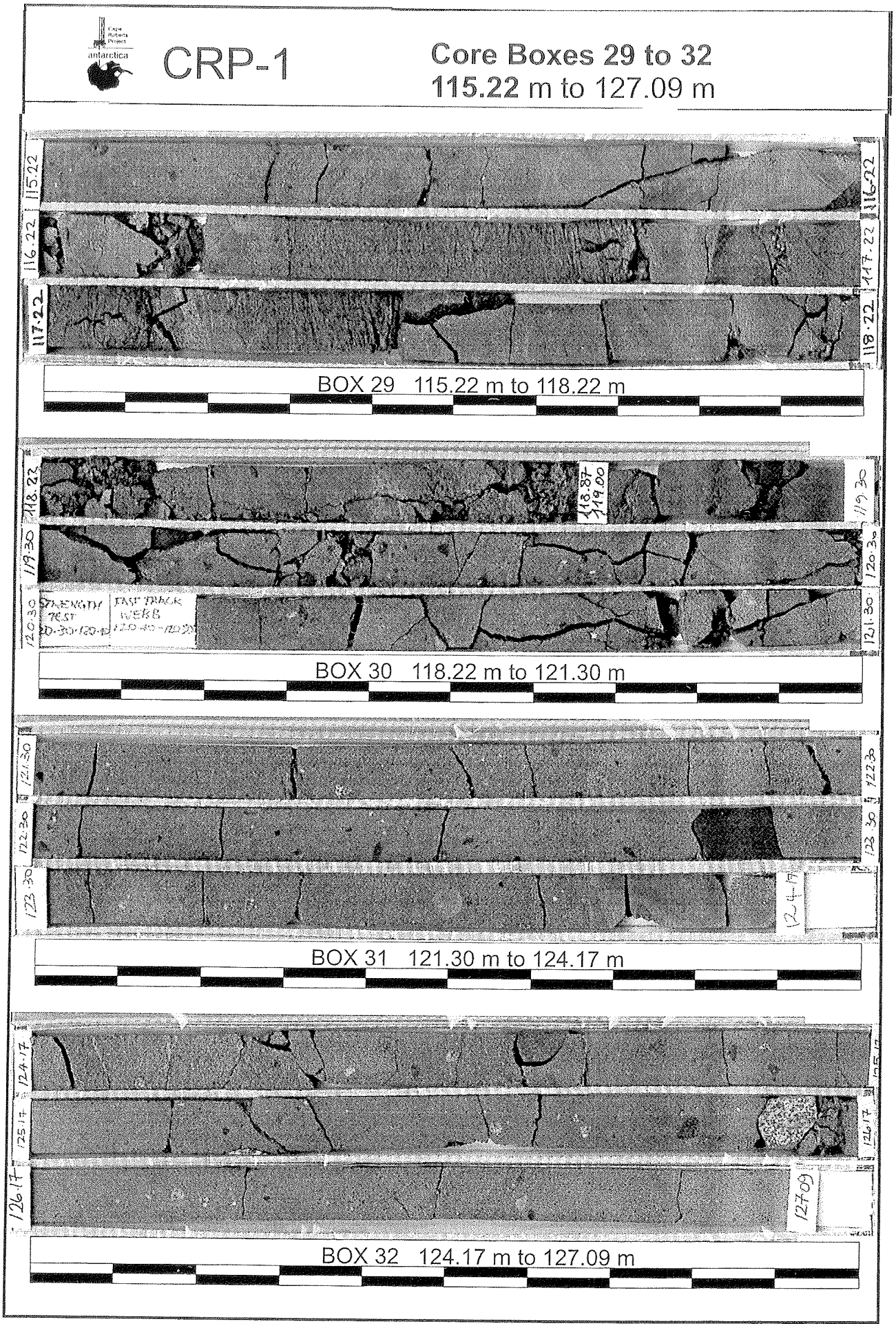
CRP-1
Core Boxes 29 to 32
115.22 m to 127.09 m
BOX 29 115.22 m to 118.22 m
BOX 30 118.22 m to 121.30 m
BOX 31 121.30 m to 124.17 m
BOX 32 124.17 m to 127.09 m

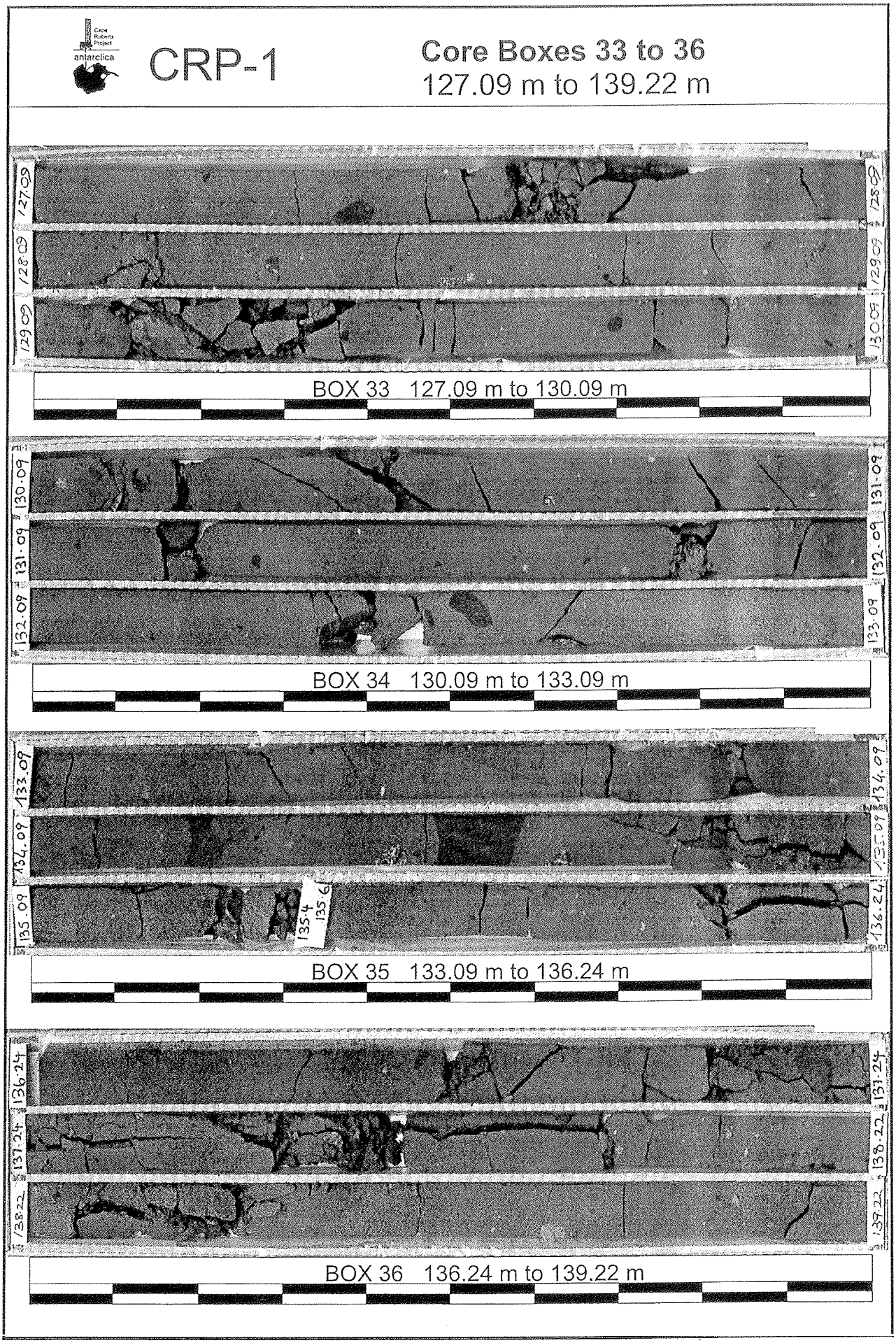
CRP-1
Core Boxes 33 to 36
127.09 m to 139.22 m
BOX 33 127.09 m to 130.09 m
BOX 34 130.09 m to 133.09 m
BOX 35 133.09 m to 136.24 m
BOX 36 136.24 m to 139.22 m

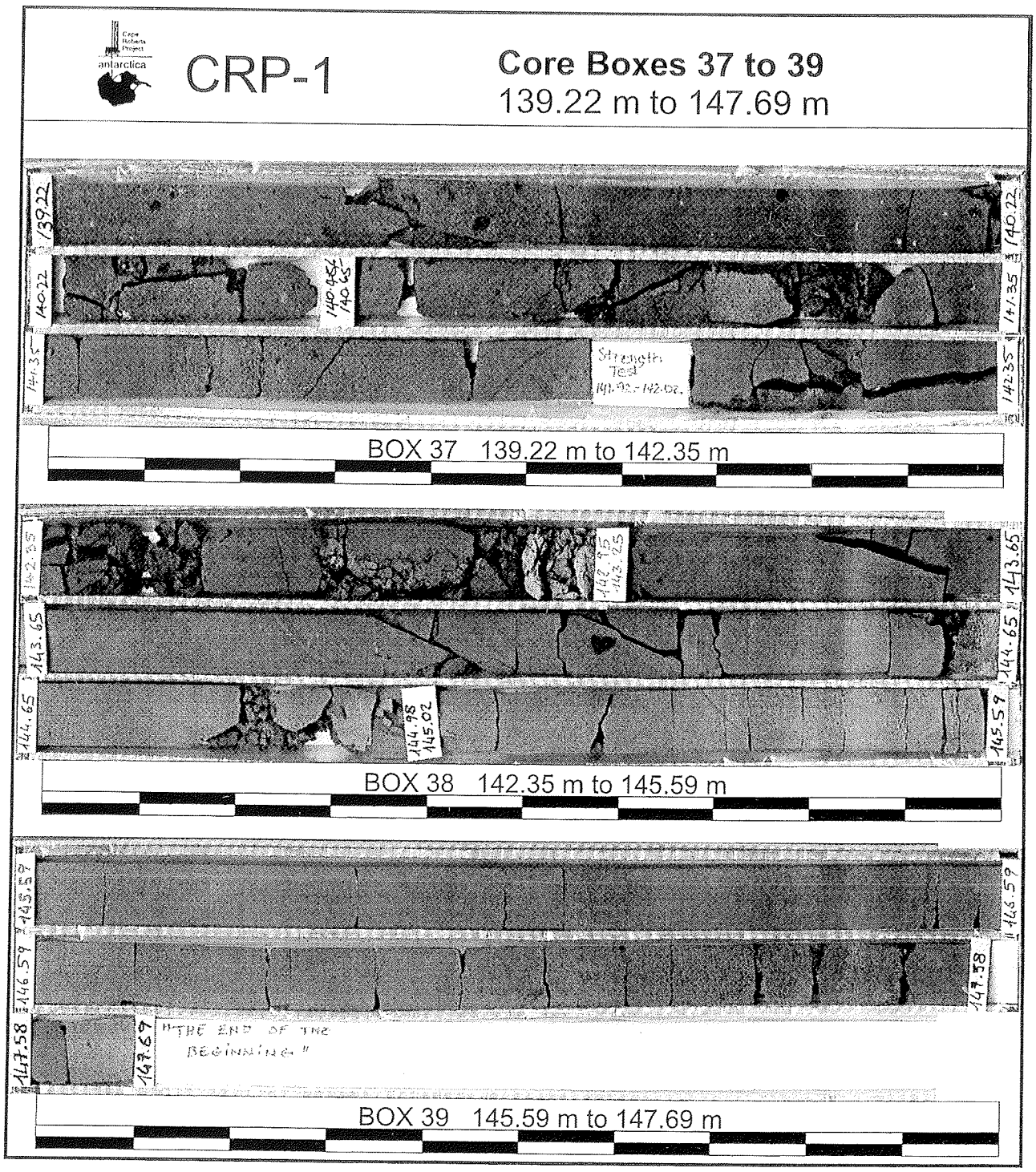
CRP-1
Core Boxes 37 to 39
139.22 m to 147.69 m
BOX 37 139.22 m to 142.35 m
BOX 38 142.35 m to 145.59 m
BOX 39 145.59 m to 147.69 m